The Skin Injury Device: A Tribological Analysis of Rugby Turf to Enhance Player Welfare

A thesis presented for the degree of

Doctor of Philosophy

MAXWELL JAMES MACFARLANE

Medical Engineering Research Group, Cardiff University, United Kingdom

January 2024

Abstract

Artificial turf offers a consistent and durable playing surface, minimising maintenance requirements and enhancing accessibility to sports in diverse environments. However, players' perception of increased injury risk on these surfaces significantly limits widespread acceptance. Sporting governing bodies have turf quality programmes that assess performance characteristics over a product's lifespan, but despite this, there is a continued prevalence of skin injuries. To ensure the integrity of sport and the safety of players is maintained, there is an urgent and crucial need for a new comprehensive test method.

Traditional test methods often fail to replicate realistic player-surface interactions. The Skin Injury Device (SID) has emerged as a pioneering solution to fill this void. SID's development, a testament to World Rugby's commitment to player safety, is rooted in a deep understanding of biomechanics and player experiences. Acknowledging that the tackle poses the highest risk, the device was meticulously designed to simulate knee-turf contact, replicating an authentic impact and subsequent protracted slide.

SID is an electro-mechanical apparatus designed to simulate realistic player-surface interactions during gameplay. The impactor, 3D printed using anthropometric knee data, is encased in Lorica Soft, a synthetic leather renowned for mirroring frictional responses akin to natural skin. The device uses similar technology found in roller coasters to generate a horizontal velocity of 5 m/s. Meanwhile, the 36 kg impactor free falls to generate a vertical velocity of 3 m/s.

The aetiology of 'turf burns' is not yet fully understood; therefore, evaluating the abrasive nature of turf and heat profiles provides insights into the potential injury mechanisms. The Maxwell Tribo Index (MTI) is a multi-faceted classification system that combines these results with kinematic data to enhance understanding of impact mechanics and sliding characteristics. This diagnostic tool facilitates in-depth analysis of artificial turf, enabling manufacturers to optimise their products, ultimately improving player safety.

Keywords: Artificial Turf, Abrasions, Turf Burns, Skin Injuries, Test Method, Biomechanical Analysis, Player-Surface Interaction, Player Welfare.

Acknowledgements

There are several people that I would like to thank for their support throughout my PhD research period.

Firstly, I'd like to thank my supervisor Dr Peter Theobald for his unlimited support and advice throughout my time at Cardiff University and whose expertise has guided my research philosophy and many other research papers.

Secondly, thank you to Marc Douglas, Neale Lees, and Eric Harrison from World Rugby, as well as Eric O'Donnel, Richard Nixon, and the Sports Labs I&D Department, for their sponsorship and unwavering support throughout this period.

I extend my gratitude to Robin Wallace for his exceptional skills and invaluable assistance in constructing the test device.

A tribute to my Papa, whose unwavering support, boundless enthusiasm, and inspiring spirit guided me through all my engineering endeavours.

I am grateful to my family for their encouragement and guidance in fulfilling my ambitions, and to Charlotte for her patience and always being there for me throughout this journey.

Table of Contents

List of Figures

List of Tables

Key terms, definitions, and abbreviations

For the purposes of this thesis, the following terms and definitions apply.

SID: The Skin Injury Device (SID) developed during this thesis was designed to assess the risk of skin injury on sports surfaces.

Skin Simulant: The skin simulant - Lorica Soft (LS 2930) – which covers the Knee Form.

Knee Form: The impactor which is interacting with the surface.

Impact Zone: The initial point of contact with the surface which generates the greatest magnitudes of vertical and horizontal forces.

Sliding Phase: The phase of the interaction characterised by the most prolonged linear movement while maintaining continuous contact with the surface.

Kinematic Injury Metrics (KIM):

Performance indicators are employed to forecast the potential risk of skin injury for the test specimen. The following three parameters are derived by processing accelerometer data to quantify the turf's dynamic characteristics during the Impact Zone and Sliding Phase.

i. Impact Resistance (R_i) [m/s^2]

This measurement helps us understand how quickly something slows down during the Impact Zone. Faster decelerations are important for predicting the chance of a player getting a skin injury.

ii. Slide Resistance (R_s) [m/s^2]

This measurement helps us understand how things slow down during the Sliding Phase. A higher average deceleration in the Sliding Phase suggests a greater potential for injury.

i. Actual Sliding Distance (d_E) [m]

This measurement determines the overall displacement during the Sliding Phase.

ii. Expected Sliding Distance (d_E) [m]

This measurement predicts how far the simulated player will slide before stopping.

Potential Injury Metric (PIM):

These test results (Abrasion Severity Index and Heat Profiles) offer insights into the mechanisms that cause damage to the skin.

i. Abrasion Severity Index (ASI) [dimensionless]

An imaging method that measures the extent of skin damage by quantifying the area then forecasts the severity for the *expected* sliding distance.

ii. Heat Profile [°C]

Thermal camera data which independently monitors the Impact Zone and Sliding Phase to identify the simulation event where the greatest temperature is generated.

Maxwell Tribo Index (MTI):

A diagnostic tool that simplifies the classification of sports surfaces by integrating PIM and KIM. It serves as the overall test outcome for assessing skin injury risk.

1G: First Generation Artificial Turf

2G: Second Generation Artificial Turf

3G: Third Generation Artificial Turf

COF: Coefficient of Friction

SDASI: Skin Damage and Severity Index

CHAPTER 1

Defining the Problem

SKIN INJURIES

Through interactions during game play in rugby

1.1 General

The game of rugby, a thrilling global sport, is supported by a diverse range of nations. As a close-contact, physically demanding game, World Rugby, the sport's governing body, is deeply committed to promoting global participation and has a dedicated focus on player welfare, including injury prevention, to make the game as safe as possible at all levels. While head injuries causing concussions are key safety issues, the lesser recognised but more immediate concern is the issue of inconvenient skin injuries. As Jack Nowell, an English Rugby Union player, emotively illustrates his view on new third-generation (3G) artificial pitches:

"It's all about cuts. Anyone who doesn't like them (pitches) puts pictures of their cuts up. The cuts are brutal. It's crazy. Players aren't able to train because their wounds are so badly opened and they're not healing, and they're infected. It's horrible."

My deep interest in researching the topic of skin injuries is not just academic, but personal. It stems from my own experiences as an U20 Scottish Rugby Union Internationalist. The pride of playing and training with the squad on 3G pitches at national sports venues was marred only by the discomfort from turf burns caused by sliding interactions during tackles, jackals, and scoring tries on the artificial turf. An ambition for the outcomes of my thesis is the global adoption of the Maxwell Tribo Index (MTI), an innovative skin injury risk classification system. In combination, the MTI and the enhanced bio-fidelity of the Skin Injury Device will contribute to improvements in sports performance testing and potentially revolutionise player welfare, ultimately producing safer playing surfaces in the future.

Professionalism in rugby has led to the introduction of sports science, significantly improving playing performance on the pitch by increasing player body mass, speed, and power. The late Doddie Weir (Figure 1-1), a Scottish second-row and captain with a 10-year playing career evenly spanned across both the amateur and professional era, was 6′ 6′′ and 114kg. Meanwhile, his current-day positional equivalent, Eben Etzebeth, is significantly bigger at 6′ 8′′ and weighs 120kg. With the height and mass of forwards reported as crucial team performance indicators, players are becoming bigger, faster, and stronger.

Figure 1-1: Comparison of player characteristics pre (a) and post (b) professional era in rugby.

Innovations aimed to improve player safety focus on designing equipment to mitigate against injury, e.g. scrum caps, mouthguards, and shoulder pads to help reduce the risk of head injuries, dental injuries, and shoulder injuries. In recent years, amendments to the laws of the rugby game to promote player safety, e.g. reducing dangerous tackles and improving scrummaging engagement techniques to reduce the biomechanical loadings experienced by the front row, have been effective in enhancing player safety and reducing injuries.

The need for essential biomechanical data describing the epidemiology of skin injuries on artificial turf was attributed to the underreporting of minor injuries such as turf burns. In combination with the fear of injury, the underreporting of injuries contributes to a noticeable disparity between player perception and injury incidence rates [1]. The faster speed and higher mass of current-day players increase the forces acting in interactions with other players and with the playing environment. Consequently, elite players are perceived to be more vulnerable to skin injuries from artificial turfs.

As early adopters of artificial grass surfaces as an alternative to natural grass, World Rugby has developed Rugby Turf Performance Specifications (Regulation 22) to ensure a safe quality playing environment [2]. However, with the power of social media, elite players with large followings can promote negative messages associated with skin injuries and effectively suppress the widespread popularity of artificial turf. Despite extensive World Rugby testing of artificial turf, the continued prevalence of turf burns implies that the current test method for assessing skin friction needs to be improved. This limitation is associated with the interaction not representing a player's forces in motion. Additionally, the current test methodology analyses the Coefficient of Friction, which appears to be a poor indicator of skin abrasion. In combination, these issues impact the validity of current testing results, highlighting the need for a new test device.

The frictional response of a rugby turf is complex, and understanding the behaviour is critical to improving players' risk of skin injuries. This thesis aims to design and develop a new test device to represent a player in motion better, addressing the limitations of current testing methodologies. Standardised test conditions will help develop insightful perspectives on factors contributing to skin injury risk. By incorporating many aspects of injurious interaction into the discussion, this research will enhance the understanding of player-surface interactions and identify the most significant factors contributing to skin injury risk. These findings ultimately assisted the development of the Maxwell Tribo Index, a novel classification system for evaluating skin injury risk on synthetic sports surfaces.

1.2 Aims and Objectives

The principal aim of this thesis was to improve the current testing methodology for evaluating the potential skin injury risk associated with artificial turf. This objective was achieved by developing a novel test apparatus that simulates realistic player-surface interactions. A secondary aim was to develop a new classification system to enhance understanding of the factors contributing to skin injury risk. This analytical tool should provide turf manufacturers with a test methodology for optimising artificial turf to ensure player safety.

A list of objectives was created to achieve these aims:

1. Obtain an extensive understanding of skin properties and identify factors contributing to injury risk.
2. Review the literature on artificial turf developments and associated test methodologies to understand current knowledge and identify gaps that must be addressed comprehensively.
3. Develop a set of realistic simulation characteristics describing injurious interactions. This prerequisite will contribute to knowledge gaps in the existing literature, thereby facilitating data-driven rationale and providing confidence in the simulation's motion profile.
4. Develop and critically analyse a series of potential concepts against the desired design specification.
5. Assimilate knowledge from Objectives 1, 2 and 3 to create an injury prediction model.
6. Improve player welfare as a consequence of enhanced understanding of player surface interactions and associated skin injury risk.

1.3 Thesis Structure

Below is an outline of the thesis structure and a summary of each chapter. Figure 1-2 visually depicts the thesis flow, emphasising the connections between chapters and objectives.

Chapter 1 – Introduction

Chapter one serves as an introduction to the thesis, offering a synopsis of the background knowledge within the research area, elucidating the thesis's aims and objectives, and outlining its structure.

Chapter 2 – Literature Review

This review thoroughly investigates the literature on skin and the associated injury risks on artificial turf, focusing on four key domains:

1. Assimilate insights from studies on skin and tribology to enhance understanding of managing tribology for improved skin performance in sport.
2. Research the background of artificial turf, introduce World Rugby's protocols for assessing the safety of artificial pitches, and explore properties of the latest generation that could contribute to skin injury risk.
3. Investigating injury rates and biomechanics in rugby gameplay and exploring methodologies for assessing the risk of skin injuries will help us better understand the requirements for the new test method.
4. Identify a suitable skin simulant for the new test method.

Chapter 3 – Establishing Design Parameters

This chapter delved into aspects identified in the literature review that were previously underexplored, aiming to enhance the design parameters for the new test method. The exploration focused on the following key areas:

1. Understand the true extent of skin injuries on artificial turf by capturing players' perceptions and quantifying the incidence rates and severity index of skin injuries on rugby turf.
2. Establish appropriate loading conditions during the sliding phase to simulate real-world scenarios accurately.
3. Investigate Lorica Soft's mechanical and thermal properties to understand its behaviour under various conditions.

Chapter 4 – The Skin Injury Device (SID): Design, Development and Manufacturing

This chapter comprehensively explores potential design concepts to ensure a robust and thorough planning phase. The project systematically categorises the components into propulsion, gantry, and impactor. By critically analysing and evaluating various alternative solutions, valuable lessons were gained from conceptual failures, ultimately leading to an improved prototype design.

Chapter 5 – The Maxwell Tribo Index (MTI): Developing an Injury Prevention Model

The design specification articulated the necessity for the new test method to precisely quantify two fundamental aspects: the abrasive properties of turf and the temperature fluctuations arising from the interaction. These metrics were deemed crucial in comprehending the underlying injury mechanisms. Moreover, in pursuit of a comprehensive injury risk assessment, additional kinematic data derived from accelerometer readings were analysed to delineate the Impact Zone and Sliding Phase dynamics.

These four key parameters were integrated into an algorithm, yielding an enhanced understanding of the intricate interplay between players and the playing surface. This novel classification system, the Maxwell Tribo Index, represents a significant advancement in accurately characterising the player-surface interaction, which should facilitate more informed decisions in injury prevention and surface design.

Chapter 6 - Skin Injury Risk Associated with Different Turfs

The previous chapters have culminated in developing a novel test apparatus and classification system for assessing skin injury risk. This chapter will explore the interplay between each element and consider their individual and collective impact on the severity of potential injuries. The objectives of this chapter were three-fold:

1. Evaluate 3G surface components' contribution to skin injury risk.
2. Investigate skin injury risk on alternative sports surfaces.
3. Assess the repeatability of inter-operator variation.

Chapter 7 – Conclusions and Future Work

This section addresses the aims and objectives detailed in Chapter 1 concerning each chapter's findings. It reinforces the critical research findings and outlines areas for future work.

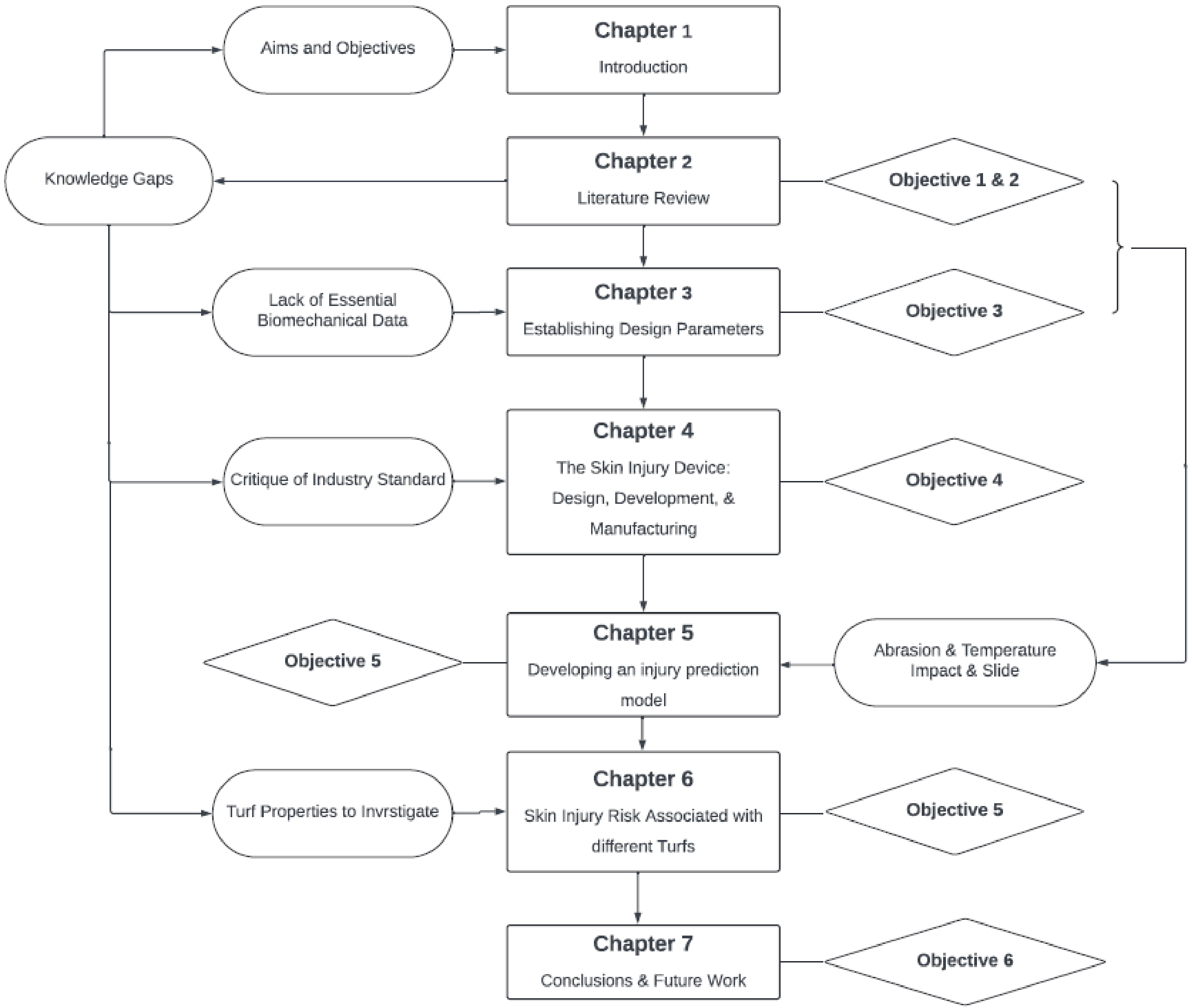

Figure 1-2: - Flow diagram showing thesis structure and objectives addressed.

CHAPTER 2

Literature Review

SKIN INJURIES

Through interactions during game play in rugby

2.1 Introduction

This chapter presents a comprehensive review of the available literature, beginning with exploring skin and tribology themes and culminating in strategies to manage tribology for enhanced skin performance. The section on artificial turf provides insights into the product's evolution and describes the current state-of-the-art surfaces. Despite extensive surface performance testing mandated by sporting governing bodies to ensure quality and safety, there is a notable disparity between players' perceptions and the actual incidence rate of skin injuries. A review of the gold standard for measuring friction and skin wear on artificial turf reveals significant limitations of the current device. These limitations and the persistent prevalence of skin injuries underscore the need for a new test device. The development of a new methodology that better represents a player in motion will offer turf manufacturers a more effective tool for optimising the skin-friendliness of artificial turf.

2.2 Human Skin

2.2.1 Anatomy

The body's largest organ is the integumentary system, consisting of skin and appendages (hair, nails, and exocrine glands). It accounts for 16% of the body mass and varies in thickness with anatomical location and across individuals [3]. The integumentary system is a multifunctional organ that works with the nervous system to provide a sense of touch, helps regulate heat and forms a protective barrier from the outside world [4]. The skin consists of three main layers: the subcutis, the dermis, and the epidermis, as illustrated in Figure 2-1

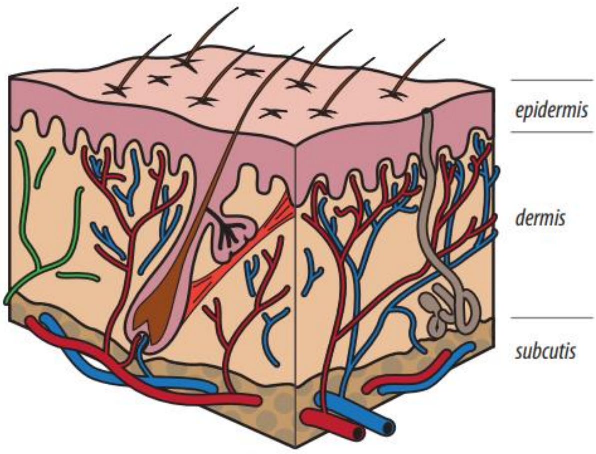

Figure 2-1: Illustration of the layers and structures in the skin [5].

Subcutis:

The subcutis, also known as the fascia, is the deepest layer of the skin, protecting the body from low-energy impacts [6]. The deep fascia is a strong and tough layer consisting of a dense network of connective tissue which attaches to other structures beneath the skin, such as muscles, tendons, blood vessels, and bones. The orientation varies across anatomical locations to improve strength in different directions. The superficial fascia, which consists of areolar and adipose tissue, is immediately below the dermis. The areolar connective tissue consists of loosely arranged elastin and collagen fibres, which allow the skin to stretch and move independently of its underlying structures. The fatty adipose tissue traps heat produced by the muscles, aiding thermoregulation.

Dermis:

The dermis is the skin's thickest layer and consists of two sublayers: the reticular layer and the papillary dermis [4]. The deeper layer of the dermis, the reticular dermis, is made up of dense irregular connective tissue containing thick bundles of collagen and stretchy elastin fibres that provide the skin with strength and flexibility. The papillary dermis, the more superficial layer that borders the epidermis, is a thinner layer of finger-like projections containing blood capillaries and nerve endings. The increased surface area these projections provide creates an excellent interface for exchanging nutrients, heightening the senses of touch, pain, and temperature. The sizeable vascular network throughout the dermis is vital in wound healing.

Additionally, several specialised cells (fibroblasts and mast cells) and structures (sweat glands, hair follicles, and lymphatics) are scattered throughout the dermis. An extracellular matrix surrounds these appendages, a viscous gel that lubricates the network of collagen and elastic fibres [7]. The viscous nature of this gel also provides shock-absorbing properties to cushion the deeper structures from mechanical stress.

Epidermis:

The most superficial layer of the skin, the epidermis consists of terminally differentiated keratinocytes that progressively move through the following sublayers [3]:

Stratum basale - the base layer of the epidermis, is typically one cell thick and is responsible for the proliferation of basal cells into keratinocytes. The 'floor' of the epidermis is the basement membrane (Figure 2-2), forming an adhesive interface with the underlying dermis. As the epidermis is avascular, this interface is essential for delivering nutrients and removing waste products.

Stratum spinosum - is the thickest layer of the epidermis and contains irregular polyhedral cells with spines that contact neighbouring cells via an adhesive protein complex called desmosomes. The asymmetrical shapes and adhesive binding are partly responsible for the skin's strength and flexibility.

When keratinocytes migrate from the *stratum spinosum* into the *stratum granulosum*, they undergo keratinisation, producing a structural protein, keratin, which makes skin waterproof and highly durable. During this process, the cells discharge their lipid component into the intercellular space, which is vital in barrier function and intercellular cohesion within the stratum corneum. A by-product of this process is the conversion of keratinocytes to corneocytes, which are flat, brittle cells with no nuclei.

The *stratum lucidum* is a thin, clear layer of dead keratinocytes that is only found in areas with thick skin, such as the palms of the hands and soles of the feet.

The most superficial layer of the skin, the *stratum corneum*, consists of corneocytes that are constantly shedding. A skin cell's lifespan is about 28 days from when a basal cell divides into a keratinocyte to pass through the different skin layers and eventually shed. These dead cells provide skin resistance to abrasion and penetration [8].

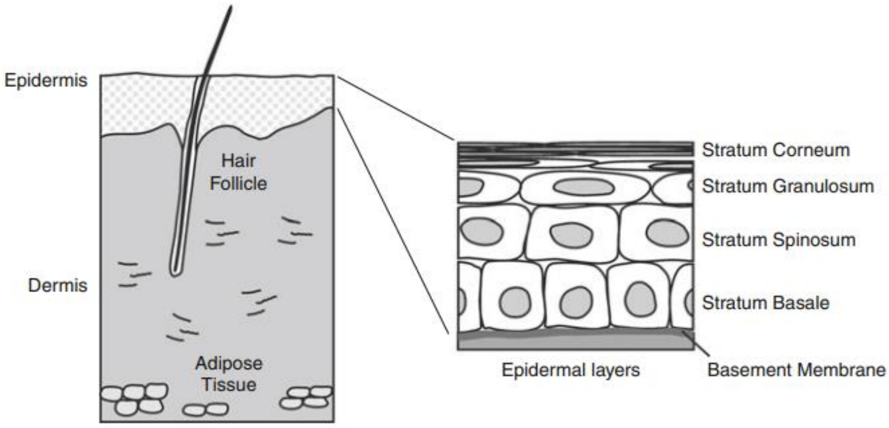

Figure 2-2: Illustration of skin's layers with the epidermis magnified. New cells form near the basement membrane, flatten, harden, and move towards the stratum corneum as they age. [9]

2.2.2 Friction & Measurement Techniques

Skin friction is governed by two main mechanisms: adhesion and deformation [10], [11]. At the contact between skin and material, van der Waals bonds are formed between asperities, creating a sliding resistance due to adhesion. Skin's soft and elastic behaviour means it will conform around the counteracting surface, requiring a force (Ft) to deform the skin during relative movement (V), as illustrated in Table 2-3. Importantly, an individual's unique skin properties play a significant role in influencing both factors, along with the loading conditions (Fn and V), contact material and environmental conditions [5].

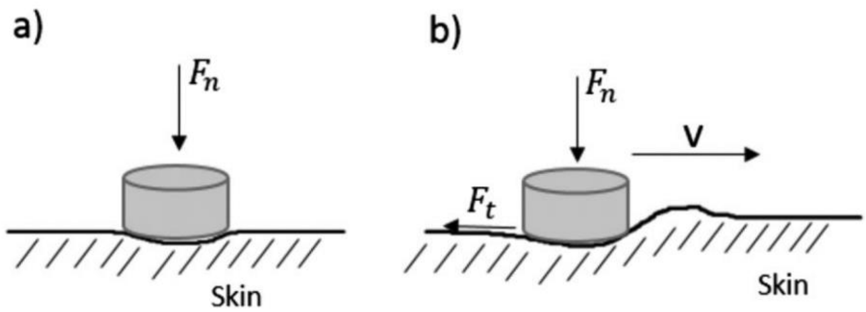

Figure 2-3: Schematic of skin deformation (a) static conditions (b) under sliding conditions. [12]

Skin friction testing involves the measurement of normal load and resistive force as skin slides relative to a contact material. The most common devices apply a constant normal load, monitoring the resistive force of a testing probe that moves with linear or rotational motion across the skin, as illustrated in Figure 2-4. The constant normal load can be regulated using spring load [5], static load [13], or servomechanisms [14]. The rotational testing consists of two categories: the rotational axis lies parallel (rotating disk) or perpendicular (revolving wheel) to the skin plane. The variation in velocity across the rotating disk is the main limitation of the parallel methodology [i.e. between the inside and outside of the test material as it traverses the skin]. The perpendicular methodology requires minimal surface area, consistent velocity and normal load when measuring.

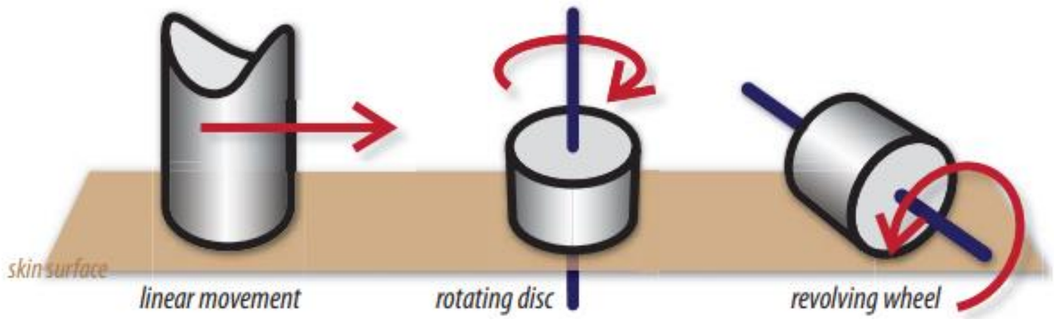

Figure 2-4: Schematic diagram of movement types to monitor skin friction [5].

With human *in vivo* testing, the main limitations are ethical constraints on repeated number of tests and the inherent variability between individuals. Therefore, tests on human or animal *ex vivo* samples are performed in research requiring an extensive database. The results from such preliminary experiments can then be compared to *in vivo* results and used to make informed decisions based on the research context. Additionally, numerical models can simulate various contact parameters for interactions between skin and rigid bodies to provide insight into the global frictional response [15]. Furthermore, synthetic stimulants offer a more consistent test material, providing insight into the behavioural response and skin friction, which will be discussed more extensively in Section 2.7.3.

2.2.3 Mechanical Properties

Skin is bio-mechanically complex due to its anisotropic, non-linear elastic, and viscoelastic behaviours [16]. Skin generally remains taut against the body frame due to the constant tension created by the arrangement and orientation of collagen fibres in the dermis. The geometry of the maximum skin tension over the entire body is known as Langer's Lines. The collagen fibres that lie parallel to Langer's Lines are in greater tension, providing a stiffer response than when perpendicularly loaded, so producing anisotropic behaviour [17]; hence, the interaction orientation will determine the skin deformation characteristics and, thus, the frictional response.

Skin can dissipate energy and contribute to friction [10], with each layer having unique mechanical properties contributing to the combined highly non-linear response [16]. The basement membrane, a microstructural network at the epidermal and dermal junction, is an essential structure for the frictional properties of skin. This subsurface structure combines individual layers that influence global deformation [15], [17]

At low strains (I - Figure 2-5), under uniaxial tension, collagen fibres are slack and non-load bearing; therefore, the skin's structural response is dictated by the elastin components, making skin relatively soft. As strain levels increase, the skin rapidly stiffens due to the recruitment of collagen fibres (II - Figure 2-5). Once the fibres have fully aligned, the behavioural response progresses from non-linear to linear, elastic, where the skin exhibits its highest stiffness (III - Figure 2-5). Combining these responses allows the skin to change shape and recover during biomechanical movements [18]. Skin is also viscoelastic, caused by the dermis' extracellular matrix, a viscous gel that biomechanically serves as a time-dependent energy absorber that protects skin from mechanical failure [19].

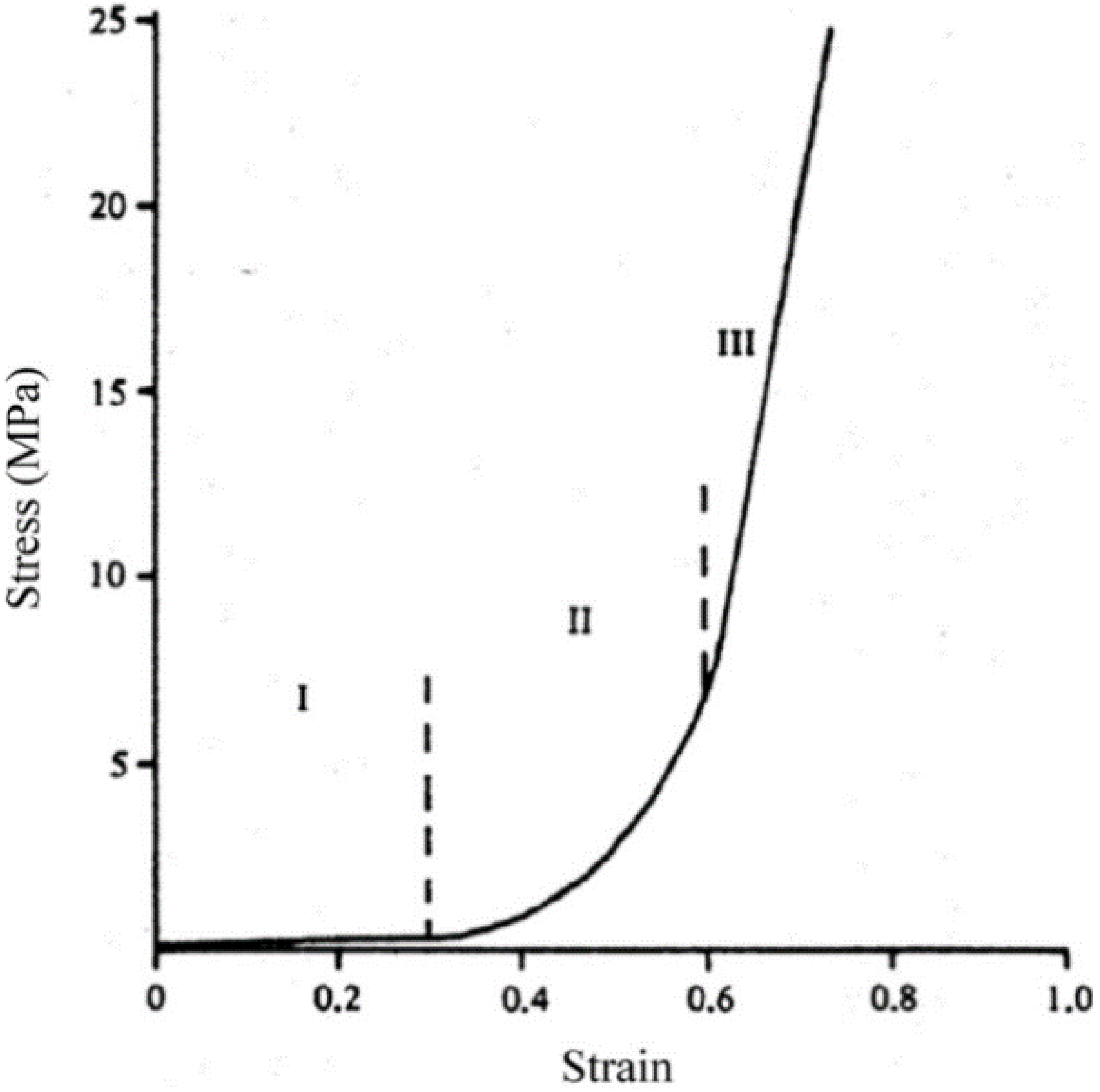

Figure 2-5: Stress–strain diagram for skin highlighting its biomechanically complex behaviour. Stage I: collagen fibres are still wavy, and elastin fibres are the load-bearing components; Stage II: collagen fibres are gradually getting aligned and contribute to load-bearing; Stage III: all the collagen fibres are aligned, and the tissue has its highest stiffness. [16].

These complex bio-mechanical behaviours mean skin does not conform to Amontons' Laws. Instead, the contact area increases with increasing pressure, with skin deforming around the asperities of the opposing surface until maximum contact. These conditions will also dictate the predominant wear regime: abrasive wear with a rough, hard surface or adhesive wear with smooth and soft surfaces.

Anatomical location affects friction due to the variations in skin hydration, thickness, hair, and composition of the surface hydrolipid film. Hydration influences the elastic modulus.

Hydrated skin increases compliance and contact area, increasing adhesion and deformation [20]. Once fully saturated, however, a fluid film forms on the skin, acting as a lubricant, which reduces resistance [21], [22], [23], [24], [25]. Additionally, when skin is hydrated, the greater water content may increase the viscoelastic effects of energy dissipation, potentially hindering elastic recoil and increasing friction. Skin can thin when over-extended [26]. However, the stratum corneum can also gradually thicken due to repeated mechanical loading, typically on the hands and feet [27]. This response can increase abrasion resistance, reduce elasticity, and increase friction [28].

The primary function of body hair is protection, temperature regulation, and contribution to the sensory function of the skin; however, it also influences skin friction. The presence of hair acts as an intermediate layer between the skin and the contact material, reducing friction's adhesion component. The hydrolipid film found on the skin's surface is an emulsion of sweat and sebum. Sebum is a naturally produced mixture of lipids, wax esters, and triglycerides. The thickness of the sebum layer has negligible effects on the frictional behaviour of the skin; however, the composition of sebum varies between individuals, contributing to significant differences in frictional responses [29].

2.2.4 Failure

Skin strength is the summation of collagen fibril strength and the collagen-matrix interaction [16]. At low strain rates, the bonds between the collagen fibrils and the matrix fail as the fibrils deform along the loading axis. Therefore, the strength depends on the crosslinks between collagen fibrils. The ultimate tensile strength increases at high strain rates due to the viscous shearing between the collagen and extracellular support matrix. The mechanical behaviour of the skin produces a positive relationship between the ultimate tensile strength and strain rate; however, as the strain rate increases, the failure strain decreases [16]. Additionally, the bundled arrangement of collagen fibres along Langer's lines produces the highest ultimate tensile strength. Skin is stiffer when exposed to an external force parallel to the fibre alignment instead of a perpendicular interaction [26]. Langer's line symmetry around the spine means there should be an equal response on the left and right sides of the body.

2.2.5 Injuries

Skin provides a protective barrier against external environmental threats; however, it is still susceptible to traumatic injury when exposed to energy that exceeds the inherent mechanical properties, including stiffness and strength [30], [31]. The precise injury mechanism is influenced by factors such as the magnitude of load, orientation, and velocity, with acute wounds including blisters, lacerations, and contusions [32], [33], [34], [35], [36]. This section provides an overview of different types of injury which may be sustained during rugby, as illustrated in Figure 2-6. At the end of this section, Table 2-1 summarises each definition and clinical appearance.

Load	Orientation	Wound	Depth	Repear time [weeks]	Clinical appearance
Shear	In-plane	Abrasion	Epidermal	1-3	
Shear	In-plane	Blister	Dermal-epidermal	1-2	
Shear	Out-of-plane	Punture	Hypodermal	2-3	
Shear	Out-of-plane	Laceration/cut	Hypodermal	2-3	
Tension	In-plane	Tear	Hypodermal	3-4	
Compression	Out-of-plane	Contusion	Hypodermal	2-3	

Figure 2-6: Overview showing the relation between mechanical load, type of wound, depth, repair time and corresponding typical clinical appearance [37].

Skin, especially that covering the hands and feet, is in frequent contact with its surroundings, meaning it will experience friction as it slides over another surface. Using a pen, a grab-rail or holding a glass are everyday examples of the skin interacting with an opposing surface to achieve a desired function. Too little friction and the design of these objects would have to be revised to ensure enhanced functionality, whilst excessive friction will likely cause the user to cease the task or identify a different object to enable successful completion. In a sporting environment, however, increasing contact loads and velocities, a task-based mindset, and an environment that competitors influence can lead to an entirely different friction scenario that may cause acute or chronic skin injury.

The healing process for skin injuries is complex and dynamic, involving inflammation, proliferation, and remodelling throughout this period [38]. The progression of the healing process typically differentiates acute and chronic wounds. Acute wounds tend to recover efficiently and timely, and the recovery period will vary depending on the depth and extent of the injury, sometimes lasting up to three weeks. In contrast, chronic wounds exhibit a delayed progression through the healing stages, often extending beyond the typical timeframe of three months. These injuries usually remain in the inflammatory stage and may never heal, resulting in the patients suffering from persistent pain.

An *abrasion* is an acute injury caused by removing the superficial skin layer. This injury is most likely when sliding over a rough surface [32], for example, when falling during road cycling ("road rash") or when performing a sliding stop on a bare, dry cricket outfield. Such injuries are generally considered minor and typically have minimal bleeding, though painful due to the exposed nerve endings [39]. *Abrasions* can be prevented by covering vulnerable body parts, with cricketers now using elasticated bandaging to protect their elbows when fielding. While these materials should be scaled up (e.g., making them thicker and denser) for interactions with potentially higher speeds or greater loads, such precautions are often overlooked to avoid impinging on athlete performance (e.g., in cycling). Lubricants can also be beneficial in minimising abrasion, though re-application is needed, especially in frequent contact with the same skin region. Some sports can benefit from this approach, with the repeated 'time-outs' in boxing providing an ideal opportunity for the ring-side support team to reapply petroleum jelly around the eye, reducing abrasive injury risk [40].

In contrast to the acute nature of *abrasive* injuries, chronic damage can occur with repeated rubbing against clothes or other skin regions. *Chafing* is identified by irritated, red skin, which can be exacerbated by prolonged exposure and/or abrasive fabrics [32]. Skin with relatively high hydration generally exhibits a higher frictional coefficient, making it more susceptible to chafing. Relatively high 'normal' (i.e., perpendicular) and/or 'shear' (i.e., parallel) loading on the skin also increases chafing. Such factors can manifest in inner thigh chafing caused by skin-to-skin rubbing. This chaffing is especially prevalent in those athletes with increased lower limb muscle mass and those who perform repeated cycles. Overlying fabrics can also influence chafing. Clothing folds and seams are design features that typically increase fabric friction, meaning skin may become irritated and red in regions, including the neck/collar interaction. The repeated sliding of a runner's vest relative to the areola tissue causes *jogger's nipple*, ultimately leading to skin swelling, bleeding, or crusting. Innovative technologies now produce an overlying fabric that remains dry and lightweight, two essential attributes to minimise friction [41], [42]. The tissue, however, will become moist with sweat, increasing the frictional coefficient. The dynamic nature of the activity and the localised tissue mass will determine the magnitude and frequency of tissue displacement, a significant contributor to chafing risk. Indeed, the constraining effect of a sports bra means *jogger's nipple* is less common in female athletes [43] To reduce risk, Athletes may also create a barrier between the skin and fabric by using adhesive plaster or petroleum jelly.

Repeated friction with high loading may cause skin blistering. Like chafing, these rarely prevent athlete participation; however, they typically cause greater discomfort and are more likely to influence performance negatively [44]. *Blisters* can be identified as tender, fluid-filled vesicles commonly found on the hands and feet. These structures should be preserved, as they provide natural infection control; however, the repetitive nature of sporting tasks means the epidermal roof is frequently detached. Blisters can be prevented by keeping the skin dry and eliminating sources of rubbing. Athletes may mitigate risk by changing equipment or technique or introducing cushioned grips and gloves; however, in some instances, these are insufficient, leading to thick and hard calluses that locally reinforce the skin. *Calluses* are typically asymptomatic, commonly developing over the distal metacarpal heads or under the plantar metatarsal prominences. They lack nerve innervation, allowing removal by filing or with a scalpel.

Skin *burns* are a significant health concern primarily caused by heat or radiation, electricity, friction, or chemical contact. The most common is a thermal (heat) injury where the tissue is destroyed by hot liquids (scalds), hot solids (contact burns), or flames. The severity of thermal burns is typically identified by the depth of the injury, a model known as the time-temperature relationship, first proposed by Moritz and Henriques (1947) [45]. Despite being extensively cited throughout the literature, this relationship needs to be more accurate, leading to misleading information being incorporated into a wide range of industrial standards and burn prevention literature. Understanding and clarifying this relationship is crucial for effective burn prevention and treatment.

Martin and Falder (2017) [46] conducted a comprehensive literature review in response to misinterpreting the time-temperature relationship. This paper evaluates the robustness of the literature, exploring research from experimental burn damage and bioheat transfer models. The review of superficial burns reported consensus across in vitro and in vivo studies; however, limited clinical evidence exists for time-temperature relationships in deep or subdermal burns. Several studies have reported that pain perception in adult human skin occurs just above 43°C [47], [48], [49], [50]. While irreversible damage to the uppermost dermis is sustained when the basal layer of the epidermis reaches 44°C [51]. The rate of tissue damage increases logarithmically with temperature, with rapid damage beyond 70°C [52]. While factors such as skin thickness, blood flow, and post-injury cooling influence burn depth [53]. While the relationship between pain and superficial dermal burns in adults is well-supported, caution is warranted when applying it to other burn types, especially in children. Bioheat transfer models show potential but are currently of limited practical use.

Rugby, a physically demanding sport, often leads to *lacerations* and *contusions*. *Lacerations*, which are cuts or tears in the skin, are typically caused by direct impact with opponents' body parts or contact with equipment such as studs or sharp objects on the field. These injuries can range from minor cuts requiring basic wound care to more serious wounds necessitating medical attention. On the other hand, *contusions*, commonly known as *bruises*, occur when blood vessels beneath the skin rupture due to blunt force trauma.

In rugby, players frequently collide with each other during tackles, scrums, and rucks, increasing the likelihood of sustaining contusions. The forceful impacts and collisions inherent in the game can lead to contusions on various body parts, particularly areas exposed to contact, such as the limbs and torso.

The aetiology of burn-related skin friction injuries is not yet fully understood. Friction burns appear different to thermal burns by damage to the superficial skin only [37], whilst other burn-related injuries include abrasion and dermal removal [32], [54]. While athletes do anecdotally report injuries consistent with thermal burns, such events lack corroborating data demonstrating the required temperature increase. Cyclists falling in a velodrome appear to be the most likely athletes to experience a thermal-like friction burn. Unlike falling onto asphalt, velodromes are typically smooth, wooden surfaces and present a low risk of abrasive injury. However, this enables the athlete to slide relatively long distances with a significant contact area [55]. These conditions create an environment that can generate considerable thermal energy with minimal dissipation, meaning a heat-related burn may be plausible. Artificial turfs appear to provide a slightly more sympathetic environment as, despite generally enabling longer slides than natural turfs, players typically sustain only a part-abrasion, part-burn injury [56], [57].

Further research is required to understand thermal energy generation through friction. A new test device is required to perform such investigations, which simulate realistic loadings that players would experience when interacting with turf [58]. Additionally, the skin simulant for the Securisport, the current industry standard for assessing skin friendliness of artificial turfs, has limited suitability for this testing as its frictional performance is significantly different to *ex vivo* human skin samples; therefore, an alternative skin simulant is required [59].

Table 2-1: Summary of definitions and clinical appearance of skin injuries sustained during rugby.

Skin Injury	Reference	Definition	Appearance
Abrasion	Basler et al. (2004) [32] Shrestha et al. (2020) [39]	Superficial layers of the skin are removed. Typically sustained when sliding over a rough surface.	Irregularly denuded epidermis and an exposed upper dermis. Resulting in exposed nerve endings, tissue exudate, and bleeding.
Chafing	Deu et al. (2020) [60]	A superficial inflammatory dermatitis results from skin rubbing against skin or clothing.	A painful, inflamed, oozing lesion.
Blister	Hsieh and Tsai (2023) [61]	Detachment of the epidermal roof due to repeated rubbing.	Tender, fluid-filled vesicles, commonly found on the hands and feet
Burn	Martin and Falder (2017) [46] Warby and Maani (2023) [62]	Irreversible damage to the uppermost dermis when the skin is exposed to heat.	**1st Degree:** Skin is dry and exhibits a pink to red colour without a blister. **2nd Degree:** Unroofed blister will exhibit a homogeneous red or pink colour, which blanches under pressure.
Contusion	Urakov (2020) [63]	Result of direct contact or blunt force without the skin being broken	Blood-stained area of skin that impairs its aesthetic appearance. If deep, a hematoma will develop within the affected tissue
Laceration	Deu et al. (2020) [60]	Disruption of the epidermis and dermis caused by blunt trauma. In a sporting context, they are likely to occur from blows from equipment (studs) or player-player contacts.	A cut or tear of the skin - unlike an abrasion, none of the skin is missing.
Turf Burn	Basler et al. (2004) [32]	An injury that is part abrasion and part burn due to the friction heat as a result of a sliding contact of uncovered areas with artificially surfaced fields	Irregularly denuded epidermis and an exposed upper dermis with a pink or red colour. Bleeding or tissue exudation may occur.

2.2.6 Infections

In addition to concerns about musculoskeletal injuries, there are also fears regarding chemical contamination from materials used in constructing artificial sports surfaces, which can result in the presence of carcinogenic substances. Media outlets have voiced concerns for human health due to the possibility of players developing skin infections [64], [65]. Studies have reported that microorganisms may grow more prevalently in the conducive environment of synthetic sports surfaces [66]. However, a more recent study reported conflicting conclusions. Out of 20 synthetic surfaces surveyed, no bacteria were found on any field [67]. Despite this finding, microbial colonies were detected on the accessory equipment.

Methicillin-resistant Staphylococcus aureus (MRSA) is a pathogenic bacterium resistant to many antibiotics. Although it is relatively harmless on the skin's surface when in contact with open wounds, it can cause more severe infections [68]. The likelihood of exposure to infectious bacteria on synthetic surfaces appears minimal [69]. However, the higher propensity of artificial turf to produce skin abrasions may increase the possibility compared to natural turf.

2.3 Artificial Turf

2.3.1 History of Artificial Turf

In sports, artificial turfs consistently perform in all weather conditions and are durable for high-intensity usage. While some traditionalists may prefer playing sports on natural grass, artificial turf enables accessibility to sports participation in areas where maintaining natural grass is challenging. There are four generations of artificial turfs. Better technology and enhanced understanding of turf design surfaces have advanced to improve performance characteristics. A "next generation" has been created, and significant development has occurred.

A short-pile fibre (12-15 mm) system without any infill is the first generation (1G) of synthetic pitches. In 1964, a product called ChemGrass was the first large-scale installation of artificial turf as a recreational area for a school in Rhode Island. However, it was not until later that first-generation surfaces became more popular. In 1965, the Houston Astro baseball team built the world's first domed stadium, where the roofed structure restricted light, making a grass surface unrealistic. Consequently, Houston Astro installed artificial turf, which would be later named, and forever known as, 'AstroTurf' as a homage to its beginnings in the Astrodome. The yarn fibres were typically made from nylon, a hardwearing and durable material, which gave the surface a reputation for being hard, hot, and abrasive [70], [71], [72], [73]

In the early 1970s, artificial turfs came under scrutiny due to their surface deterioration, thereby influencing the playing experience and increasing the incidence of injuries. Increased fibre length and adding infills aim to reduce skin injury risk and enhance synthetic turfs' performance characteristics. Multi-use Games Areas (MUGAs) are recognised as the second generation (2G) of artificial turf systems and consist of a short (20-25mm) dense carpet with a sand layer. This sand layer aims to keep the fibres upright to help improve ball roll, traction, and drainage. Heat build-up was also reduced; however, the abrasive nature of sand continued to present an injury risk [74].

In the late 1990s, the next evolution of artificial turfs (3G) was designed to significantly increase the length of fibres (40-60mm) and incorporate an additional performance infill with an optional shock-absorbing base layer. The shock pad base layer was introduced to provide the surface with a cushioning effect, whilst the increased fibre length was designed to accommodate the additional infill, which helped with traction and stability. On top of further improving the performance characteristics of turf, the performance infill provided more comfort for the player as it was softer and less abrasive than sand. In isolation, the infill can represent the dynamics of fluid and acts as a lubricant, which in theory should reduce the forces experienced by a player; however, when it is incorporated into the lattice matrix of yarn fibres in the carpet, the frictional response becomes more complex than initially thought; therefore, the risk of skin injuries is not entirely reduced. These design improvements to synthetic pitches mean they are now regarded as a genuine alternative for a natural turf pitch; however, apart from the transition from the harsh and unforgiving nylon yarns to softer polyolefin monofilaments, there has been little innovation or development to synthetic turfs to improve skin-friendliness.

There is a common misconception that fourth-generation (4G) surfaces are the most technologically advanced infilled surfaces. In contrast, the latest iteration of artificial pitches consists of non-filled systems that are being developed to help with the upcoming ban on microplastics, which will be further discussed in Section 2.3.2. These systems typically consist of a longer filament yarn embedded into a thatched sublayer with a crimpled structure designed to provide the surface with the necessary traction and stability. The filament yarn typically protrudes out of the thatch, and its soft and smooth nature makes it more forgiving on the skin than in earlier generations. Due to the lack of infill, these systems require a shock pad to provide adequate shock-absorbing properties. However, they have yet to be approved to be played on competitively by World Rugby or FIFA [75].

2.3.2 Properties of Rugby Turf

Developing a new test device necessitates a comprehensive understanding of the turf system and the properties of its components that will influence skin injury risk. Impact attenuation studies have reported natural turf to be fundamentally non-linear [76], [77]. Rugby Turf (Figure 2-7) is the most complex artificial turf system due to the multiple components within its construction compared to the other generations of artificial surfaces. Rugby Turf is expected also to exhibit non-linearities.

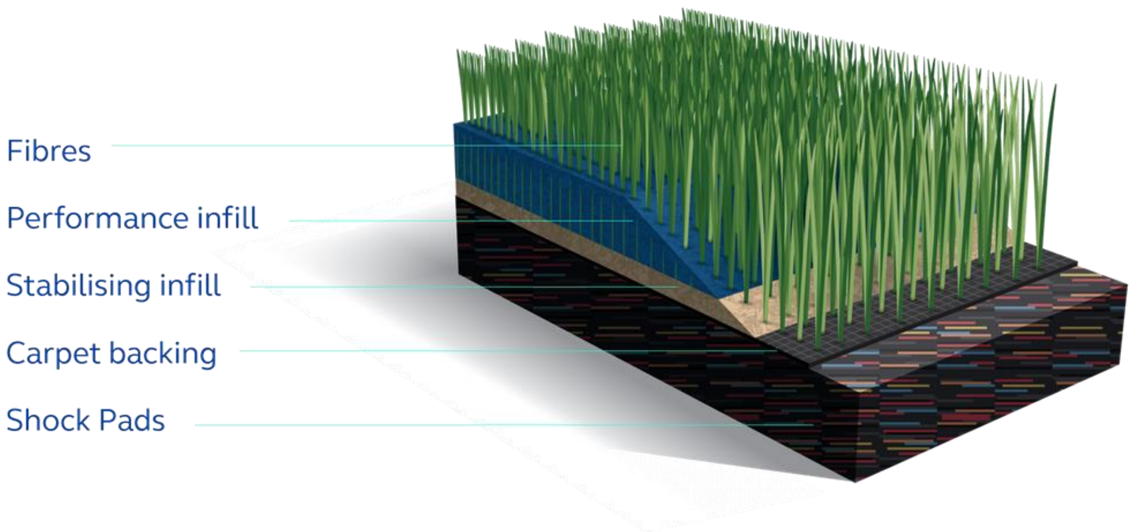

Figure 2-7: Properties of a Third Generation (3G) Artificial Pitch

Shock Pad

Shock-absorbing padding is recommended to cushion and reduce injury risk if a person falls from a height, such as on a sports field. This recommendation is particularly relevant for the head injury criterion and must be present in engineered rugby turf [78]. A thicker shock pad will be required on surfaces without a performance infill to compensate for the reduced shock-absorbing properties. This safety feature ultimately ensures that the overall performance characteristics are maintained.

Shock pads can be made from various materials such as rubber, foam, cork, or recycled shoes. These materials have different properties, such as density, elasticity, durability, and environmental impact. The shock pad is the deepest component within a turf system; therefore, it was unsurprising that the effects of shock pads on skin injury risk have yet to be published. However, a more rigid surface would transfer more force onto the player, increasing their risk of injury. Consequently, the use of a shock pad should reduce skin injury risk.

Carpet Backing

Initial turf generations had the yarn knitted together to produce a woven backing similar to cloth. Newer technology has developed a tufting process wherein it loops the yarn through a non-woven material and then cuts the loop, forming two separate strands collectively called piles. Unsurprisingly, the effects of carpet backing on skin injury risk have yet to be published. Although woven or non-woven carpet backings will have inherently different mechanical properties, their respective contribution to skin injury risk was considered negligible compared to other turf properties.

Stabilising Infill

Silica sand (size 0.2–1.2 mm) acts as a ballast to weigh the grass down, preventing dimensional movement such as rippling [79]. Sand is virtually incompressible and has limited air void space, which improves the shock-absorbing properties of 2G surfaces compared to 1G [80]. However, abrasion remained a player welfare issue, leading to the development of performance infill and the advent of 3G surfaces. In 3G systems, the stabilising infill layer is typically 10-20 mm evenly spread across the surface.

Performance Infill

Performance infill is a granular material that helps artificial grass mimic the performance characteristics of natural grass by improving shock absorption to provide a more natural response [81]. When the stabilising and performance infill are incorporated into the system, the infill depth is typically two-thirds of the pile height. [82]. The infill accommodates stud penetration to improve traction while allowing the foot to slide to reduce the risk of major injuries.

The widespread use of Styrene-Butadiene Rubber (SBR) as a performance infill is due to its commendable performance characteristics and durability. Moreover, it's a sustainable choice as it repurposes a product that has reached its end of life. In fact, around 20% of recycled tyres find a new life in artificial pitch design and construction [83], [84]. The process of converting car tyres to rubber crumb involves two techniques. The more cost-effective method is mechanical shredding in a cracker mill. Alternatively, the rubber can be cryogenically frozen and shattered into small, smooth-edged particles. The milling process produces a more jagged granule, which increases the risk of skin injury due to the higher asperities.

The particle size of SBR can range from 0.5 – 4.0 mm [85], whilst air void percentage ranges from 50-70% [80], depending on the level of compaction. The mobility of these tiny particles is recognised as providing a "ball bearing" phenomenon within a turf system. The combination of the elastic nature of rubber, the ball-bearing effects, and the presence of air voids reduce skin injury risk compared to 2G surfaces. During manufacturing, SBR can be encapsulated in a cross-link across-linkable coating. Coated SBRs can provide an additional aesthetic appeal by changing the colour to match the yarn. Alternatively, the coating can be a light colour to reflect temperature in geographically hot regions to reduce the overall surface temperature, which could help mitigate skin injury risk [86].

Another factor that is expected to influence skin injury risk is the ratio of sand and performance infill. Increasing the volume of sand stiffens the system, reduces surface deformations, and increases the force returned to the player. This latter factor is associated with an increased risk of injury. This postulation should only be applied to surfaces with the same performance infill as the relationship between surface stiffness and injury risk is currently unknown for cross-comparisons of infill material. The physical properties (surface roughness and specific heat capacity) are expected to significantly affect skin injury risk, which might dominate the influence of surface stiffness.

Although tyres are primarily made of rubber, a natural material, their processing involves the use of other chemicals. This treatment results in the small particle size of SBR, which is less than 5mm, placing it in the microplastic category [87], [88]. Evidence shows that SBR can leach or leak into the environment, contributing to microplastic pollution [84], [89]. The European Chemicals Agency (ECHA) has taken steps to regulate the use of SBR and other synthetic performance infills [90]. As a result, alternative products are being explored to serve as performance infill while adhering to environmental regulations. These alternatives fall into four main categories based on their composition:

- Organic – living and found in nature (cork, coconut husks, olive pits, wood chips). Benefits include moisture retention and cooler overall temperatures in hot climates.
- Inorganic – Non-living but found in nature.
- Synthetic – Chemically derived.
- Biobased – Biodegradable plastics.

Identifying new alternative infill materials with the potential to replace SBR is a crucial task. It's important to ensure that the mechanical characteristics and response of the turf remain uncompromised. Additionally, when choosing a biodegradable infill, the life expectancy of a pitch should be evaluated. The speed of biodegradation and the replacement life of infills to maintain integrity could significantly impact the lifespan of the playing surface. The choice of infill for future pitch development is a complex topic requiring extensive research and development to ensure the system is optimised from ethical, financial, and performance perspectives.

Fibres

There are two types of artificial turf fibres: fibrillated and monofilament (Figure 2-8). In 2015, FIFA introduced the groundbreaking Lisport XL testing, a method that accelerates wear in a laboratory to produce an artificial end-of-life product. This testing proved crucial as it revealed that the fibrillated yarns, which lacked a strong core structure, failed to stay upright. This outcome adversely affected the performance testing, specifically the ball roll. Consequently, these systems started to fail post-wear performance testing. As a result, monofilament fibres have come to dominate the market. However, it's important to note that the flattening of yarn fibres produces a larger fibre-skin contact area and reduces the infill's ball-bearing effects, corresponding to an increased risk of skin injury, a safety concern that should not be overlooked.

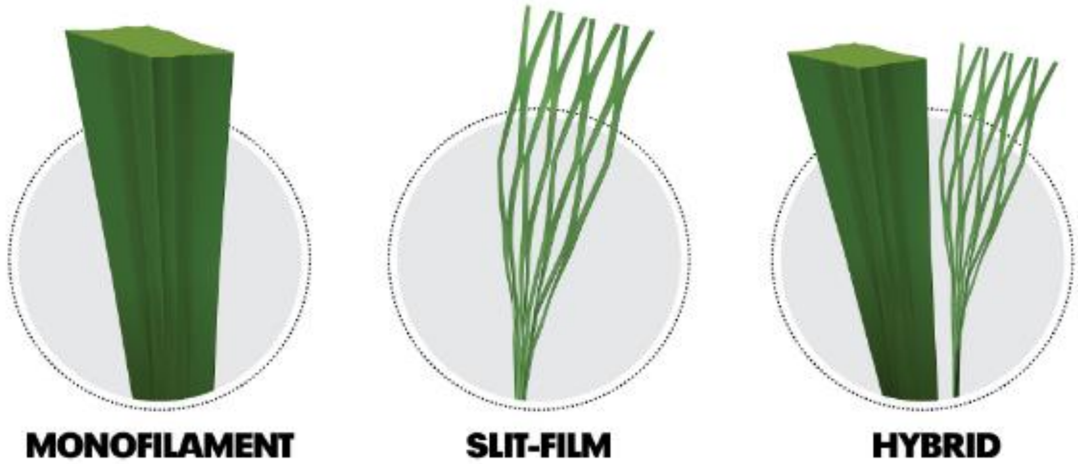

Figure 2-8: Illustration of different fibre types [91]

The woven or tufting process, a key step in the production of artificial turf, plays a crucial role in determining the direction in which the fibres lie, known as the grain. This grain has been found to influence the distance a hockey ball would roll across a 2G surface [92]. McLaren et al., (2014) [93] further supported this finding, noting that the grain had less effect on the ball roll when the fibres were upright. They also concluded that the free pile height, representing the part of the fibre extending above the infill, was inversely proportional to the ball roll distance. This implies that increased contact with the fibres results in the ball experiencing greater resistive force and not travelling as far. Applying this theory to a player-surface interaction, it could be assumed that increasing free pile height increases frictional behaviour, which agrees with Tay et al. (2015) [94]. Therefore, the grain should not affect the skin injury risk of newly installed surfaces; however, if turfs are not maintained and the fibres begin to flatten, an interaction against the grain could produce an increased frictional response associated with a greater risk of injury.

Turf density is determined by the number of tufts per square meter, influenced by two key factors: the stitch gauge and the stitch rate. The stitch gauge measures the number of rows per meter, while the stitch rate counts the number of stitches per meter (Figure 2-9). Both metrics collectively define the overall density of the turf. A higher turf density means the fibres are tightly packed, enhancing the surface's ability to cope with intense usage while providing a cushioned feel underfoot.

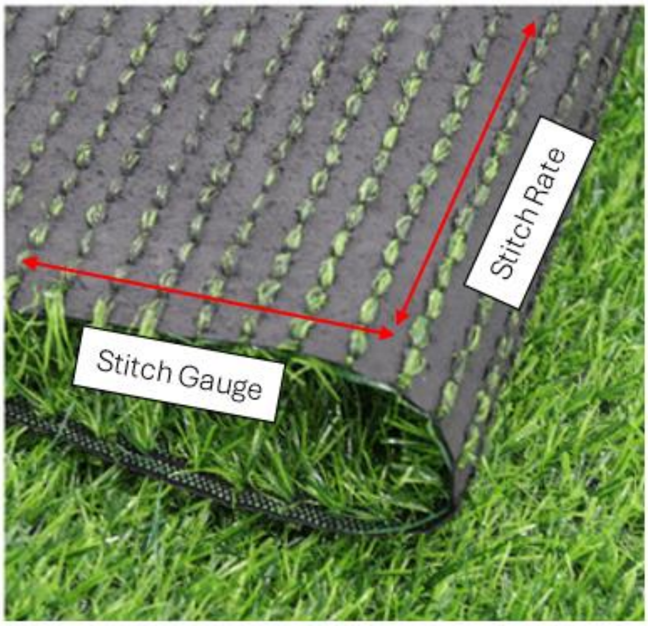

Figure 2-9: Explanation of Turf Density - Stitch gauge and rate

While little has been published on the effects of carpet density, Tay et al. (2015) [94] reported that longer free pile height produced higher COF. This effect implies that an interaction with high surface area contact with the yarn will produce more significant frictional responses. Consequently, it could be hypothesised that the Securisport would report higher COF on carpets with larger turf densities. However, it should be noted that Tay et al. (2015) [94] concluded that COF is not indicative of skin injury risk. Therefore, further investigation is required to assess the effect of tuft density, which could have significant implications for turf design and maintenance.

A lubricating spin oil substance is applied to yarn fibres during the tufting process to improve manufacturing efficiency. Spin oil has been found to influence the performance characteristics, explicitly producing favourable results for the Securisport to pass noncompliant surfaces. Consequently, the FIFA Technical Advisory Group has validated a washing method, making it compulsory to remove excess spin oil before testing [95].

2.4 Biotribology

Tribology is a term which refers to the science and engineering of materials that interact with relative motion [96]. This technical discipline traditionally centres on studying and applying friction, wear, and lubrication of engineering systems; however, it has recently extended its application to biomaterials such as human skin. In daily life, skin is in constant contact with its environment, which provides various research topics ranging from skin cancer research to investigating the effects of cosmetic skin care products on skin conditions. Whilst mechanical systems have well-established theories to control and mitigate friction, knowledge gaps remain in understanding skin tribology and injury epidemiology. Such an understanding is particularly important in sports, where external factors can vary the interactions between an athlete's skin and their surroundings (e.g. equipment, playing surface), potentially influencing performance and competition; however, such demands must be balanced against injury risk. Some sports strive to optimise skin friction to maximise performance, such as applying chalk to increase grip in elite shot-put. Others seek maximum friction by adopting intermediary materials, such as golf gloves. Managing skin friction, directly and indirectly, influences playing performance [97].

2.4.1 Friction

The COF defines the resistance of one surface when sliding over another with an applied load. Three laws define dry friction, with Amontons' first and second stating that frictional force is proportional to the normal load and is independent of the apparent contact area. The third law, introduced by Coulomb, states that kinetic friction is independent of sliding speed. COF is a dimensionless unit, denoted by the symbol μ, which typically ranges between 0-1. The COF of two surfaces manifests in two distinct forms. The kinetic COF (μk) represents the ratio between the resistive force and normal load during constant relative motion between the two surfaces. Concurrently, the static COF (μs) denotes the ratio between the two loads when there is no relative motion. The frictional forces for a static object are greater than those of a moving object, as inertial forces have a more considerable influence. Therefore, the static COF will be greater than the kinetic COF. Equation 1 defines the calculation for the COF, where F_f is the force of friction, and F_n is the normal load.

Equation 1

$$\mu = \frac{F_f}{F_n}$$

Understanding the COF is crucial in various fields, especially in engineering and physics. There are two main forms of friction, sliding and rolling, which can be identified by the mechanisms in which the two bodies move in relative motion. Typically, rolling friction reduces the frictional response, compared to sliding friction, due to the smaller surface area and larger normal forces generated at the point loads through the circumference of the rolling object. Friction is a system property where the COF depends on multiple factors [98]. For instance, in mechanical engineering, the COF is a key parameter in designing efficient machines and reducing energy loss due to friction. Skin friction, on the other hand, refers to a system between *in vivo* skin and a surface. Due to skin's unique properties, skin friction is complex and does not directly conform to the laws of friction [5], [13].

2.4.2 Wear

Wear is a process resulting in the progressive material loss between two contacting surfaces in relative motion. Surface deterioration occurs due to the mechanical failure of highly stressed contacting asperities, where environmental conditions often influence the failure mode. There are three main mechanical wear mechanisms: adhesive, abrasive, and fatigue wear, as illustrated in Figure 2-10 [99], [100]. Solid-solid interfaces typically produce these; however, materials can also degrade when subjected to high-velocity impacts by fluids, known as fluid erosion [101]. Chemical wear is the most complex mechanism, combining mechanical and chemical action [100]. This two-part process involves a corrosive attack on a surface, which produces a reaction layer on the superficial surface of the material, followed by the wearing of the corroded surface. The chemical reaction itself does not constitute wear; however, when accompanied by mechanical action, such as friction, chemical wear occurs via removing the reaction layer. The chemical wear rate depends on the reaction layer's growth and removal rates. Rapid chemical wear can occur if the reaction layer is harder and more brittle than the original surface, which can result in the total thickness of the reaction layer flaking off.

Adhesive Wear

Adhesion or *cohesion* refers to the atomic attraction between two surfaces in intimate contact that holds them together [96]. If these surfaces move with relative motion, they will experience shear forces due to the formation and rupturing of asperity junctions, which can be along the interface or within the asperities. Sufficient shear forces within asperities of the weaker material can transfer material from the softer to the more rigid body. However, the reverse is also possible. These fragments can be transferred to the original surface but usually break off to form loose wear particles.

Abrasive Wear

Abrasive wear is the resultant loss of material when a more rigid material slides across a soft surface in an interaction dominated by a plastic deformation mechanism [96]. A protrusion from the contacting surface or hard, loose particles contaminating the sliding system may cause the deformation. These loose particles may come in the form of grit or airborne dust or be a contribution from the loose wear particles generated from adhesive wear. Despite these contaminants not producing as much wear as the protrusions, they can potentially damage both surfaces.

Fatigue Wear

Fatigue wear is a cyclic loading process that generates surface or subsurface cracks and can result in severe plastic deformation, as demonstrated by large fragments breaking off the surface [96]. This wear mechanism is more prominent in rolling contacts than in sliding conditions due to high stresses and small slips. The cyclic frequency and type of deformation identify the two fatigue mechanisms. In high-cycle fatigue, the surface is exposed to repeated elastic strain under a high number of load cycles before failure. After the critical number of cycles, the accumulation of plastic strain around pre-existing micro defects within the material can generate a crack. In contrast, low-cyclic fatigue is characterised by repeated plastic deformation, which produces wear particles and provides the component with a relatively short lifespan.

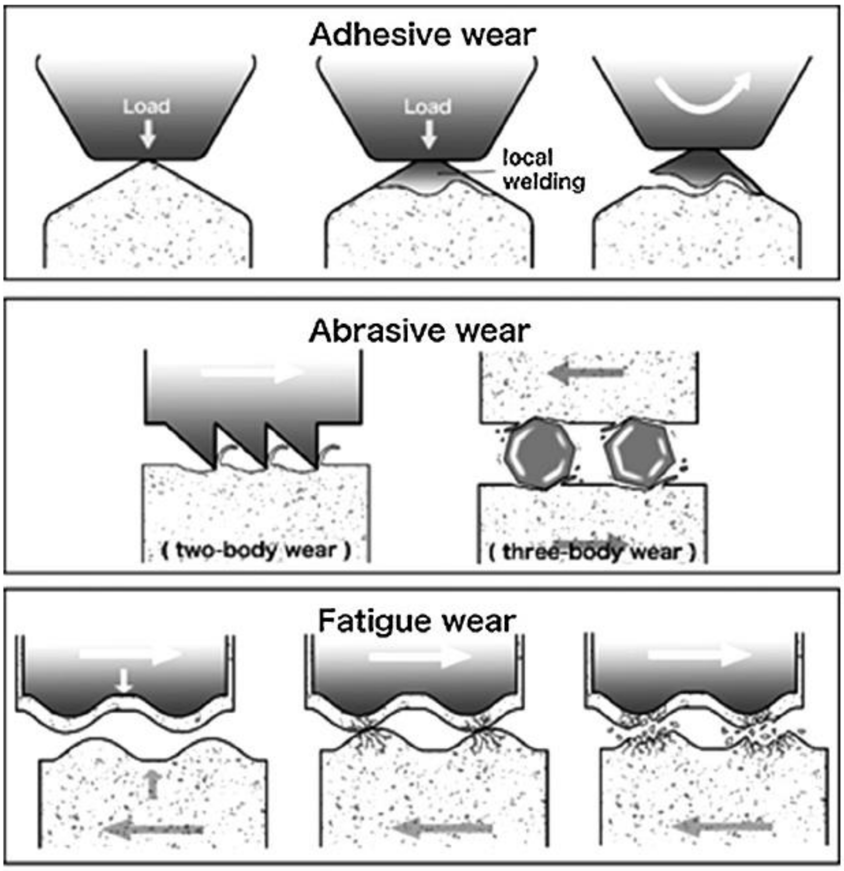

Figure 2-10: Illustration of wear mechanisms: Adhesive, Abrasive and Fatigue Wear. [102]

2.4.3 Lubrication

In tribology, lubricants enhance performance, efficiency, and durability. Lubrication is the addition of a medium between two surfaces in motion to reduce friction, thereby improving performance. In general, lubricants excel at dissipating heat, thus reducing the energy lost as heat due to friction. Hence, the efficiency of the machine is improved. When applied, lubricants fill uneven surfaces to provide a consistent surface during force transfer and provide a dampening effect for components under high stress. Lubricants also provide a protective layer to limit corrosive and mechanical wear, reducing downtime and extending the machinery's life. Hersey (1949) [103] reported that the coefficient of friction of a lubricated system depends on the viscosity (μ), speed (n) and load (p) which he simplified into one single variable known as the Hersey Number – Equation 2.

Equation 2

$$Hersey\ Number = \frac{\mu\, n}{p}$$

Lubrication is the practical application of a substance, which works under three different regimes, to modify friction and limit wear by aid bearing load and reduce shear strength between contacting surfaces, as presented in Figure 2-11.

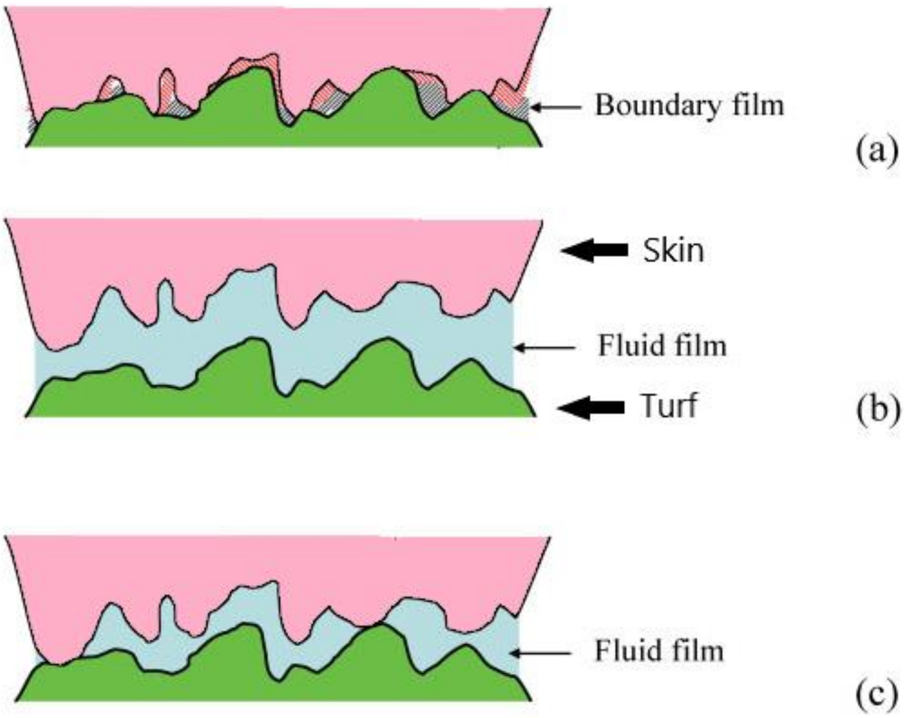

Figure 2-11: Lubrication regimes: (a) boundary lubrication, (b) hydrodynamic lubrication, and (c) mixed lubrication.

Boundary lubrication

A complete fluid film cannot be formed when surfaces roll or slide over each other with high loads or at low speeds. Therefore, a boundary film is generated. This thin film separates the contacting bodies; however, the frictional response is dominated by the solid asperities, which are the microscopic high points or roughness on the surface. The boundary film is easily sheared, which minimises adhesive and chemical wear compared to a dry interaction [104].

Hydrodynamic lubrication

Hydrodynamic lubrication, a highly efficient regime, involves the separation of two surfaces by a thick fluid film. This film supports the applied load and reduces shear strength between the contacting bodies, effectively eliminating asperity contacts and any measurable wear.

The reduction in physical contact between the two bodies results in the frictional response being dominated by the lubricant's viscosity, and frictional losses are minimal under hydrodynamic lubrication. This regime, therefore, offers significant benefits in terms of reducing wear and improving system efficiency, making it a key concept for engineers and lubrication specialists to grasp.

Mixed lubrication

Mixed lubrication, a regime that combines the characteristics of both boundary and hydrodynamic lubrication, is a dynamic and complex phenomenon. It typically occurs when the viscosity and speed increase during the transition between low and high speeds. As the fluid film thickens, it creates a greater separation between the surfaces in motion, reducing the potential for asperity contact and diminishing the load experienced. This dynamic transition is marked by a dramatic drop in the coefficient of friction, as illustrated by the red line on the Stribeck curve (Figure 2-12). Understanding this regime requires a deep understanding of both boundary and hydrodynamic lubrication, making it a challenging but essential concept for engineers and lubrication specialists to master.

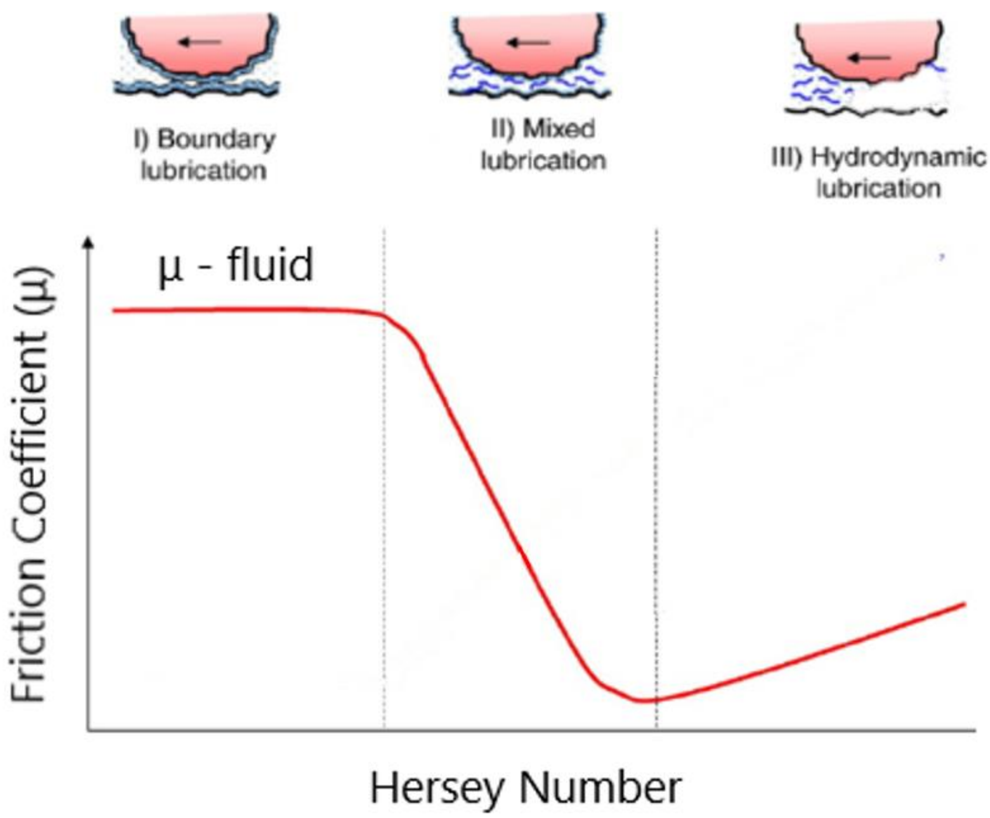

Figure 2-12: Stribeck Curve – an example of the frictional response of a fluid [105]

2.4.4 Biotribology of Artificial Turf

Biotribology of artificial turf involves the study of friction, lubrication, and wear as they relate to the interactions between an athlete's skin and synthetic surfaces used in sports. This field focuses on understanding how the physical properties of artificial turf impact athlete safety and performance. Artificial turf consists of granular material integrated into a network of synthetic fibres to provide cushioning and stability. Comparing 2G and 3G artificial turfs highlights the advancements in performance infill. 2G turf primarily uses sand as an infill material, which offers less cushioning and higher friction. This results in a harder surface with increased wear and tear on both the turf and players. Conversely, 3G turf incorporates a mix of rubber granules and sand, which acts more like ball bearings. The rubber granules enhance shock absorption and reduce friction, providing a softer, more player-friendly surface. This innovation in 3G turf leads to improved performance, reduced injury risk, and better durability, ensuring a safer and more consistent playing experience compared to 2G systems.

Artificial turf is a complex material that experiences concurrent rolling and sliding friction phenomena. Performance infill operates akin to ball bearings, improving efficiency and diminishing surface resistance through enhanced rolling friction. The infill facilitates smoother interactions by reducing direct contact between players and turf fibres, resembling how ball bearings transform sliding into rolling motion. This notably decreases friction, with rolling friction being markedly lower than sliding friction [106]. Moreover, the infill evenly distributes loads across the surface, mitigating stress on individual points, thereby minimising wear and lowering injury risks.

If the rubber infill resembles a fluid, the frictional response of a 3G pitch was expected to be similar to the red line on the Stribeck Curve (Figure 2-12). Take the example of a car driving through a deep puddle. At slow speeds, the tyre would be in complete contact with the tarmac and experience all the forces of friction. Then, as the speed increases, the fluid will become stiffer, and the contact between the tyres and the road will reduce, so the friction decreases. In cases where a car is moving so fast, it starts to aquaplane, and the only contact is between the water and the road, the friction rises again. Figure 2-13 illustrates this analogy in the context of a rugby player interacting with 3G turf at varying velocities.

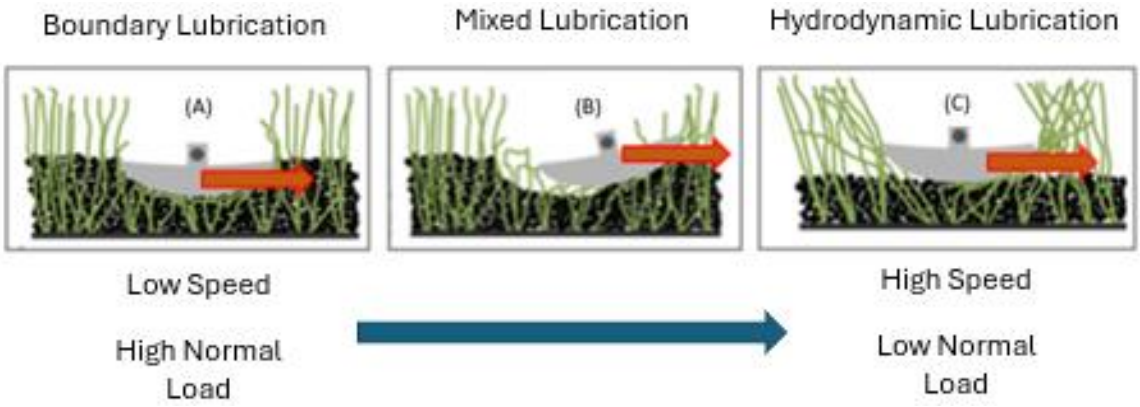

Figure 2-13: Comparison of 3G turf's frictional response with increasing velocity or decreasing load [94].

Figure 2-13A represents the frictional response for a rugby player in complete contact with the turf, where the deformation of the infill dictates the resistive force. Figure 2-13B illustrates that the rugby player is reducing the infill penetration so there is less rubber crumb to plough through. Therefore, the friction should decrease. Finally, in Figure 2-13C, where the rugby player is only in contact with the turf fibres, the overall frictional response is expected to be lower than the starting value as there is less drag from the infill.

The fibres protruding from the infill, however, make 3G turf a more complex medium than a simple fluid. Therefore, it was postulated that 3G turf is more likely to exhibit an inverse response of what is expected of a fluid. During low-speed interactions, the infill behaves like ball bearings at the boundary film, providing a lower frictional response than initially thought. With increasing sliding speed, the infill becomes stiffer, reducing the player's penetration. The reduced ploughing effects are expected to reduce friction. However, the player experiences more adhesive forces from the fibre, increasing the friction during an interaction where the player essentially slides across flattened yarns resembling a polymer sheet. There would be no interaction with the infill, resulting in the greatest frictional forces exposing the player to the highest risk of injury.

In summary, the frictional force combines the forces required to displace the infill and the adhesion between the skin and the turf fibres. Therefore, the COF would increase with low loads or high speeds while interacting with artificial turf. This observation implies that 3G turf is a complex non-linear system which will not conform to the fundamental laws of friction.

2.4.5 Contact Mechanics

Hertzian contact theory [107] is a widely accepted method for illustrating localised stress fields between two objects and can be applied to the contact between a knee and artificial turf. The theory makes several assumptions:

- The two bodies in contact are homogenous,
- Both surfaces are assumed to be relatively hard and non-conforming,
- The interaction of the two involved bodies is perfectly elastic,
- The interaction is frictionless.

Artificial turf, which will be discussed further in Section 2.3, is a system which combines granular infill and yarn fibres; therefore, it is considered heterogeneous. The granular content of turf produces a material that is soft and conformal. At the same time, the dynamic nature of a player-surface contact will permanently displace the infill. Further, the interaction is not perfectly elastic, and the theories of elasticity cannot be applied. Additionally, tangential loadings produce friction as the player traverses across the surface. When considering the knee on artificial turf, it fails to meet any of the criteria of the Hertzian contact theory. Consequently, this theory was deemed irrelevant to the context of this project.

2.5 Managing Tribology to Enhance Skin Performance

Managing the friction and wear between skin and equipment is a focus in many sports. In some instances, participants seek to increase friction even in dry contact as they strive for enhanced grip, whereas others try to minimise friction to enhance performance. Other adaptations become apparent when climatic conditions lead to sub-optimal playing performances. When aiming to improve skin performance in sports, it is crucial to consider the parameters detailed in Figure 2-14.

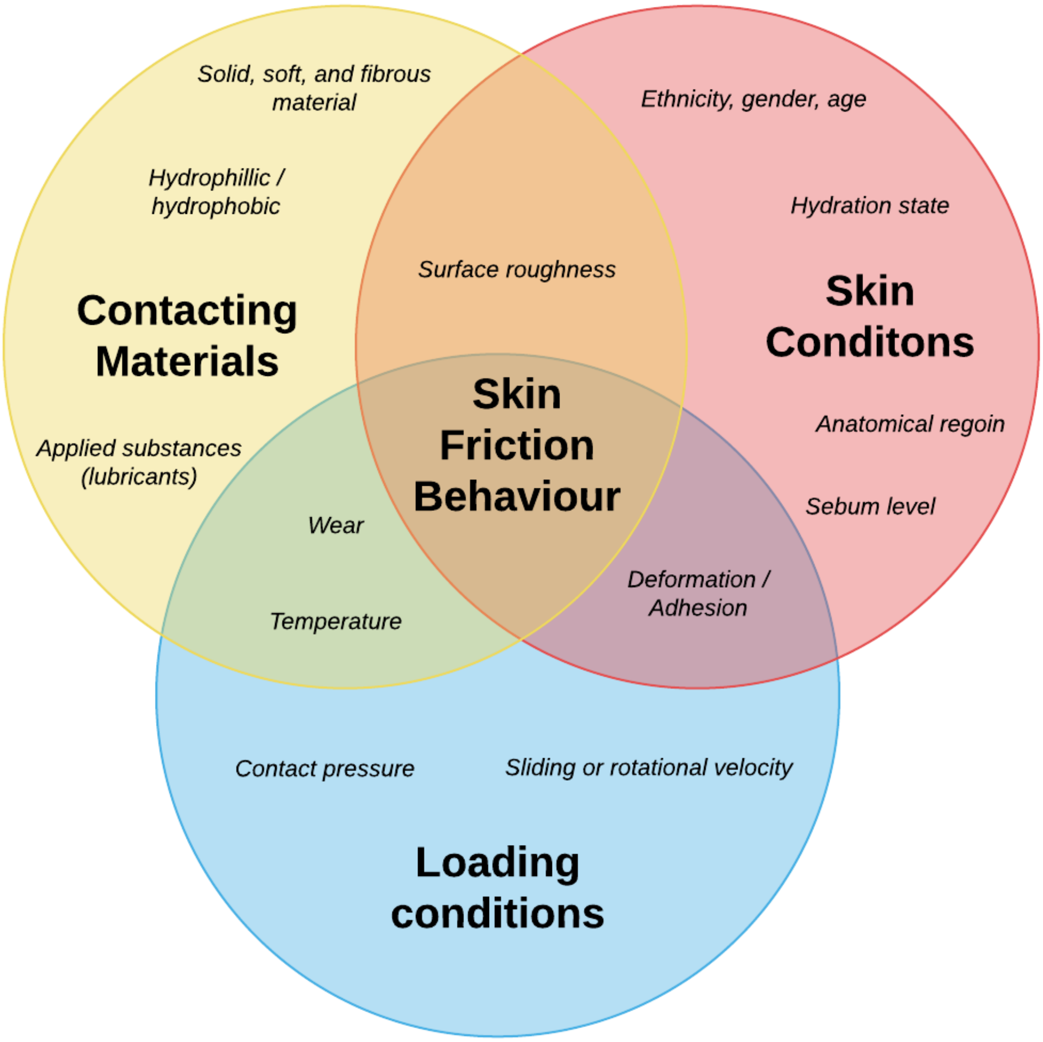

Figure 2-14: Important factors to consider when attempting to enhance skin performance.

2.5.1 Enhancing Skin Friction

Weightlifting, climbing, gymnastics, and javelin are just some sports where athletes attempt to influence the skin-equipment COF despite already possessing dry contact (the only potential exception is javelin due to its being performed outdoors). Agents are ordinarily applied to dry skin to increase friction with equipment, displacing the natural oils that provide an element of boundary lubrication. A secondary aim may be to absorb sweat. Carre et al. (2012) [108] evaluated four agents (Powdered and liquid Chalk, Rosin, and Venice Turpentine) applied to the finger and ran against a polished steel surface alongside a clean finger, representing a ground truth. In dry conditions, Venice Turpentine, a tacky resin, was the only intervention that increased (doubled) COF. Using powdered chalk and Rosin reduced the frictional coefficient, adhering to the skin and acting as a solid lubricant, reducing the skin-equipment contact area. Similar effects were observed when Rosin powder was applied to the skin when simulating baseball pitching. The chalk hindered performance by limiting the shear force imparted on the ball; however, it achieved a more consistent frictional behaviour, an important attribute when developing repeatable techniques in elite sports [109]. Chalk in suspension (“liquid chalk”) ensures more precise and controlled application, with alcohol evaporation quickly leaving a chalk residual covering the skin; however, it provided a similar frictional coefficient to dry, natural skin.

2.5.2 Mitigating Climatic Conditions

Additives for optimising skin-equipment friction are only viable in sports that require a short, concerted effort. Rugby players rely on sufficient skin friction when throwing a pass, as it is necessary to impart spin to achieve the desired ball flight. A smooth, dry ball produces the highest COF, with the flat surface maximising contact and so the abundance of locally ‘welded’ asperity junctions. In wet conditions, it is impractical to apply an additive before passing; hence, the ball surface is designed with a texture and roughness to optimise COF, with pimples the most effective patterning [110]. Players have also trialled semi-permanent interventions, including applying finger tape and wearing gloves. Lewis et al. (2013) [111] reported that synthetic leather mitts provided the best handling performance, with a design optimised to interlock with the specific ball surface texture. Mitts with a more generic fabric performed more consistently when considered across a range of ball textures.

The use of gloves to increase friction with equipment is now commonplace in golf, with Sorbie et al. (2017) [112] reporting that players could generate significantly greater club head and ball speed. The increased friction translated to improved hitting distance and accuracy, though only for those shots using the longer clubs. Gloves are also used in wheelchair-based sports, enabling athletes to increase their acceleration and agility significantly [113] . The most problematic combination of environments involves wet sports equipment and wet skin, with both surfaces having surface coatings that may, depending on conditions, achieve hydrodynamic lubrication during dynamic events, leading to minimal friction [59]. For example, a rower’s grip may fail, and the oar may slip during stroking [114]. Whilst powdered chalk and Rosin offer an opportunity to absorb excess moisture and so increase COF, practical application is inherently constrained to specific sports and environments. Venice Turpentine does not influence friction in wet conditions, as it is insoluble and so unable to bond to skin. Whilst damp skin absorbs moisture and slightly swells, it still causes an overall reduction in friction compared to dry skin on a dry surface.

2.5.3 Innovative Approaches

Some sporting interactions benefit from lower skin friction coefficients. The once-infamous cauliflower ear in rugby was, in some instances, caused by repeated abrasion against a neighbouring player during the scrummage [115]. Mitigating solutions have had a significant impact, including using tape to cover the ear, reducing friction and wear during repeated sliding and using petroleum jelly to create a thick boundary lubricant layer. Indeed, the latter material has also been used surreptitiously, with players coating their legs to hinder an opponent's attempt to perform a successful tackle [116]. Rugby attire has also been designed to influence friction. For the 2011 Rugby World Cup, Scotland released an innovative shirt with the 'backs' having low friction material to help them slip out of tackles. The 'forwards' had higher friction to aid scrum binding and ball carrying [117]. The lack of uptake indicates that this technology did not achieve the desired goals. Reducing skin friction has been more successful when considering innovative pitch constructs, with the latest generation artificial playing surfaces benefitting from rubber granules designed to facilitate player sliding [118]. The latest surfaces are a marked improvement on earlier versions, with the abrasive injuries synonymous with sand-based composition now a distant memory for the most part.

2.6 Rugby

2.6.1 Injury Incidence in Rugby

Artificial turf offers consistent playing conditions and enhanced durability with intense usage compared to natural grass. Sports clubs and schools installing artificial turf have the added benefit of a potential revenue stream from renting out the facilities. These benefits have resulted in the proliferation of artificial surfaces globally. The impact of the widespread adoption of artificial turf fields only became evident in the late 2000s, coinciding with a surge in published studies comparing injury rates between natural grass and 3G artificial turf surfaces, as illustrated in Figure 2-15.

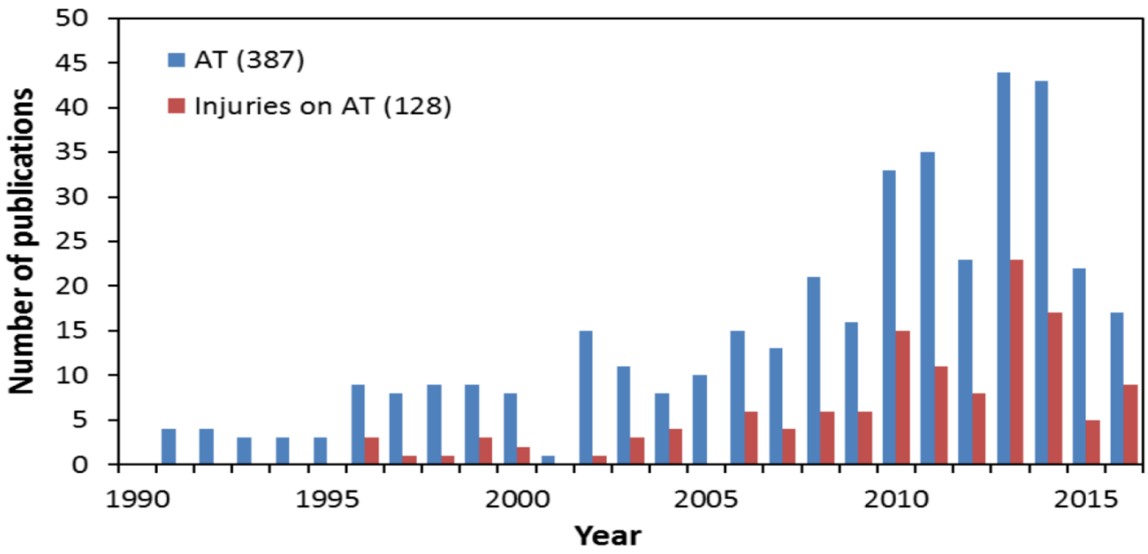

Figure 2-15: Number of literature publications, from 1990 to 2016, on artificial turf surfaces and related epidemiological studies. "Artificial Turf" is abbreviated as "AT" in the figure. [118]

World Rugby's 'Player Welfare' strategy, with its focus on expanding and supporting injury surveillance across all ages and levels of rugby, is a testament to their commitment to player safety. The Year in Review: 2021 [119] provided key findings that approximately three injuries occur per match in elite men's rugby and almost two per match in the women's game. Within amateur rugby, injury frequency varied with age, but there was no real trend for time-loss injuries. This injury definition represents when a player is unavailable for seven days or more. In terms of concussions, the incidence rates were much lower for younger age groups (U13 = 1 in 14 matches) compared to older age groups (U18 = 1 in 7 matches). At the senior level, concussions occurred on average every five matches for females and six for men. In youth rugby, concussions were associated with 27-29 days of missed time, while adults were typically out for 29-30 days. These statistics demonstrate the effectiveness of World Rugby's 'return to play' protocol as the time out is significantly higher than the guidelines that recommended six days of rest. This trend is encouraging as it hopefully prevents long-term damage and recurring injuries.

Due to the increased physicality and frequency of contacts [120]. In elite rugby, there are more injuries than in amateur rugby. The significant increase in injury incidence in the professional era (74/1000 hours) compared to amateur rugby (47/1000 hours) highlights this discrepancy [121]. In elite rugby, the injury incidence rate was significantly higher during matches (91/1000 hours) compared to training (2.8/1000 hours) [122]. These match injury rates are high in comparison to most other team sports. Meanwhile, training injury rates are comparable to other sports [123], [124]. Whilst each phase of rugby has its inherent risks, the tackle contributes to about half of all injuries to either the tackler or ball carrier due to the tackle being the most frequently occurring event [119, 120, 123].

An increasing number of elite clubs (e.g., Cardiff Blues, Glasgow Warriors, and Racing Metro) have installed artificial surfaces. With the power of social media, elite players can share experiences, often unfavourably portraying artificial turf, to their large followers. This propaganda creates preconceptions of increased risk of injury compared to natural turf and limits universal approval. There is, however, no clear consensus defining if there is a difference between the surfaces.

Gould et al. (2023) [126] conducted a systematic review comparing the incidence of lower extremity injuries playing on artificial turf versus natural grass across all sports. The review evaluated many articles (n = 53) published between 1972 and 2020, providing a robust basis for conclusions. The extensive coverage of literature and inclusion of various sports at different competition levels offer a thorough examination of injury rates. However, the broad scope also introduces complexity due to the variability in factors influencing injury rates. Consequently, the researchers refrained from aggregating risk ratios across individual studies to produce an overarching effect size estimate, acknowledging the study divergences. Over half of these papers reported no difference in overall injury rates between new-generation artificial surfaces and natural grass. Almost 40% reported that artificial turf was more injurious. However, most of these adverse reports were due to the influence of older-generation surfaces. Only three of the reports suggested that natural grass was more injurious. However, the author cast doubt over these findings as they implied that funding from industry could have created biased results. When considering the anatomical location of the injuries, there were higher reports of foot and ankle injuries on artificial turf. While there were similar rates for knee and hip for amateur footballers, elite players had a higher propensity for knee injuries on artificial turf than on natural grass. Studies on American football, however, suggest that the increased biomechanical stresses at the shoe-surface interface result in a higher risk of knee and ankle injuries on artificial turf [127].

Most of those studies focused on comparing surface type's influence on major injuries that result in significant absence from participating in the sport. Peppelman et al. (2013) [128]

were the first to investigate minor injuries and were interested in the mechanism behind skin injuries. They performed tests on *in vivo* skin after participants slid on artificial and natural grass under various environmental conditions. They reported that artificial and dry grass generated more abrasions, while natural grass produced more erythema (skin redness). However, skin injuries can be effectively reduced by playing on an irrigated surface, using protective base layers, and applying skin lubricants [129].

Despite the advancements in new-generation artificial surfaces, many people still have preconceptions associated with an increased risk of abrasion on previous generations of turf. There is, however, an apparent disparity between perceptions of skin injury risk and the incident rates that are reported [130]. In rugby and football, there are relatively low reports of abrasion rates (2 - 6%) [131], [132], [133], [134]. This result is due to the varying definitions of injury, which generally consider time loss or the requirement for medical attention. Skin injuries are typically considered minor inconveniences and generally do not prevent players from participating; therefore, they are often not included in major injury studies.

More consistent injury definitions and detailed reporting are essential to appreciate the full extent of sports-related skin injuries. To prevent inconsistencies in reported data and improve the reliability of interstudy comparisons, the International Rugby Board (IRB), now rebranded as World Rugby, established a consensus statement on injury definitions and data collection procedures for injuries in rugby [131]. The paper presented the following definitions:

> *"Any physical complaint, which was caused by a transfer of energy that exceeded the body's ability to maintain its structural and/or functional integrity, that was sustained by a player during a rugby match or rugby training, irrespective of the need for medical attention or time-loss from rugby activities. An injury that results in a player receiving medical attention is referred to as a 'medical-attention' injury and an injury that results in a player being unable to take a full part in future rugby training or match play as a 'time-loss' injury."*

In 2015, a study investigated injury risk in elite rugby (English Premiership and National Cup), primarily focusing on muscle soreness and abrasions [135]. The study contributes to a better understanding of the safety and performance implications of playing on artificial turf, with a specific focus on rugby. The prospective cohort design facilitated the longitudinal assessment of one team for one and a half seasons, comprising 40 matches. Researchers conducted the primary study throughout the 2013/2014 season. They compared home games played on artificial turf against away games on natural grass. The second half of the previous season (13 matches) was used as a pilot study to evaluate the suitability of the data collection methodology and injury definitions (primary – time loss, secondary - any physical complaint). Visiting players accustomed to natural grass were sampled to assess their perception of muscle soreness over four days following a match.

Over two consecutive weeks, players in this sample self-reported, with an equal number of responses from those who played on artificial turf first and those who played on natural grass to mitigate bias related to fixture timing within the season. Incorporating the pilot study into the research design and mitigating bias from player responses enhances the reliability and rigor of the study, thereby contributing to increased validity of the findings. Additionally, combining objective and subjective measures enhances the comprehensiveness of the collected data.

Throughout the investigation, the difference in time-loss injury rates for artificial (66/1000 hours) and natural (73/1000 hours) grass was determined to be trivial. Results suggested that muscle soreness was consistently higher over the four days after playing on artificial, although the magnitude of this effect was small. They agreed with the consensus that there was no real increased risk on either surface. Abrasions were considerably more common on artificial (119/1000 hours) than natural grass (15/1000 hours). The abrasion rates correlate to an incident ratio almost eight times greater when using natural grass as a reference category. On average, the damaged surface area was 12 cm^2. Wingers, centres, and flankers had the highest propensity of sustaining an abrasion, with the knee being the most vulnerable anatomical location. Out of the 123 abrasions, only two resulted in time loss, which provides insights into the magnitude of unreported skin injuries.

A subsequent study by Twomey (2019) [1] significantly enriched the understanding of the prevalence and severity of abrasion injuries on artificial turf. The review confirms a discrepancy between players' perceptions of abrasion injuries and the evidence of injury risk on artificial turf. Developing an extensive scope that included a wide range of sports and competitive levels was a significant advantage of this review. The authors ensured that the reviewed research selection was thorough and objective by following the established guidelines. They strengthened the credibility of the compiled evidence by enforcing strict inclusion and exclusion standards. The methodical process of choosing, evaluating, and screening literature highlights how rigorous the methodology is.

Furthermore, the moderate sample size of the review (n = 25) strengthens the conclusions and gives confidence in the validity of the results. The review gathers data to show how artificial surfaces impact athletes in various situations. To reliably estimate the incidence of abrasion injuries, the authors emphasise the necessity for more precise surface specifications and injury classifications. This comment was surprising given that a consensus statement on injury definitions and data collection procedures of injuries was developed more than ten years before this review [131]. Such improvements are necessary for the perceived risk to continue to impede the adoption of artificial surfaces.

In a previous study, Lenehan and Twomey (2016) [58] reviewed the current testing procedures for quantifying skin friction and wear on artificial turf. They emphasised that a new test device should accurately replicate the player's interaction with the surface, which is crucial to reducing the risk of skin injuries. However, the limited biomechanical data describing injurious interactions during gameplay in rugby indicate a pressing need for further research. This comment underscores the necessity of accurate data for effective injury prevention.

2.6.2 Biomechanics in Rugby Gameplay

Rugby is a dynamic and physically demanding sport where players exert themselves while rucking, scrumming, and changing direction to complete or evade a tackle. Player-surface interactions are critical aspects that influence players' performance and safety during these game elements. Traction, stability, and biomechanical loading are essential player-surface interactions to gain a competitive advantage whilst avoiding injury due to excessive force transmission or slips.

The rotational resistance generated when a player's studs interact with a penetrable surface such as natural or artificial grass, is termed *traction*. In general, increased traction forces improve player movement performance, such as changes in speed or direction [136]. However, when players reach a critical threshold, traction no longer influences their performance [137]. Injury studies have associated higher shoe-surface traction with an increased likelihood of injury and should, therefore, be kept low to minimise risk [138]. Artificial surfaces have an advantage over natural grass, as turf components can be altered during construction to enhance biomechanical loading, optimising performance while mitigating the risk of injury. Surface stability during scrummaging is also a critical shoe-surface interaction to prevent slippage. Rugby Turf (60mm) is generally longer than Football Turf (40mm) to facilitate additional infill. Longer turf enables forwards, who scrummage, to wear longer studs, improving their grip. Concurrently, turf engineered with high traction combined with longer studs could elevate the likelihood of injuries by extending the lever arm, particularly during mediolateral movements [139].

The inherent variability among natural turfs, influenced by the construction and environmental conditions, leads to challenges in research when trying to identify optimal field characteristics. In contrast, artificial pitches are more consistent across the whole surface. Despite this benefit, players still prefer natural pitches due to the perceived increased risk of injury [140]. This negative preconception may psychologically influence their behaviour, resulting in a play style change. For instance, a player may not go to the ground to retrieve a loose ball due to fear of a skin injury. Skin injuries typically occur during an abrasive sliding interaction, which removes the first layer of the skin. Currently, no biomechanical data describing injurious interactions during gameplay in rugby exists. Therefore, comparisons with other sports, such as baseball, softball, and football, will be required. Biomechanical analysis of sliding interactions has described the interaction in three phases: a free drop, an impact zone, and a sliding phase [141], [142], [143]. Despite variations in the fundamental motion profiles of tackles between rugby and football, these key stages remain consistent during player-surface interactions.

In rugby, the tackle, the most frequent [120] and dangerous [132] phase of play, carries the most significant risk of injury. Considering injury risks for the ball carrier and the tackler is essential. A successful tackle, where the tackler wraps their arms around the ball carrier, usually results in both players going to the ground with their knees on the playing surface as their immediate point of contact. The uncontrolled way their respective knees contact the turf generates a unique loading profile for each interaction. The magnitude of the forces experienced during this point loading makes the knee the most vulnerable anatomical location during the impact zone. This vulnerability is also valid for the second most common contact sites, the elbows, and forearms.

Elite rugby players are known to exceed 100 kg in weight [144], with some capable of reaching speeds of 10 m/s during play [145]. However, it is unrealistic to expect the skin to interact with the surface at such high speeds during player-surface interactions, as players are no longer propelling themselves when airborne. The lack of biomechanical data describing injurious interactions complicates the determination of accurate impact velocities, necessitating certain assumptions in defining simulation characteristics. Given the uniqueness of each interaction, it is anticipated that skin injuries may occur across a range of velocities. To address this, the speed was conservatively reduced to 5 m/s, aligning with the suggested speeds during the development of a modification of the Securisport by Lenehan and Twomey (2016) [58]. This speed was based on velocities expected during a football slide tackle. Therefore, further research is needed to validate this assumption in rugby. The vertical component was estimated using fundamental equations of motion to calculate the impact velocity of a free-falling object. For instance, the 95th percentile popliteal height, representing the knee height of an elite male rugby player, was selected [146]. This height suggests a fall of approximately 0.5 meters during a tackle, with the tibial shank generally horizontal to the surface upon impact. Accordingly, this free-fall distance corresponds to a vertical impact velocity of 3.1 m/s.

Instrumented shoulder pads record tacklers experiencing impact loads approximating 1 kN [147]. Limited data exists describing the biomechanics of the player-surface interaction during tackling, given the ethical challenges of integrating pain-free sensing. However, estimates can drawn from other sports with a more prescribed landing zone, enabling the use of embedded force plates. Soccer goalkeepers experienced 4-9 times their body weight (3-8 kN) during hip impacts when landing from a dive, while soccer tackles produced peak ground reaction forces of 2.3 kN for the knee and 4.9 kN for the hip (3-6.5 times body weight) [148]. Peak horizontal forces were 1.4 kN and 1.8 kN for the knee and hip [149]. Combined with tackling being the most frequent phase of play and the predominant activity where players may aim to contact the ground, these magnitudes explain why it is also associated with the most significant risk of skin injury.

In rugby, the tackle is the most frequent and dangerous aspect of gameplay, presenting the highest potential for injury. Within a player-surface interaction during a tackle, two pivotal stages emerge - an impact zone and a sliding phase. Although comprehensive biomechanical data on player-surface interactions during tackles is lacking, the knee was anticipated to be the initial point of contact, rendering it particularly susceptible to injury. Estimates drawn from parallels in other sports suggest that the knee may endure impact forces ranging from 3-4kN. Elite rugby players typically weigh 100 kg, serving as the basis for determining the carriage mass. The horizontal (5 m/s) and vertical (3.1 m/s) impact velocities were derived from assumptions and theoretical calculations. Therefore, additional research is needed to validate these values. These conclusions mark the starting point for developing the simulation characteristics outlined in the product design specifications in Table 2-2.

Table 2-2: Design Specification of Desired Simulation Characteristics

<table>
<tr><th>ID</th><th>User Requirement</th><th>Criteria ID</th><th>Design Criteria</th><th>Desired Output</th></tr>
<tr><td rowspan="2">1</td><td rowspan="2">Motion profile</td><td>1.1</td><td>Impact zone</td><td>Greatest magnitude of forces</td></tr>
<tr><td>1.2</td><td>Sliding phase</td><td>Constant contact</td></tr>
<tr><td>2</td><td>Impactor possessing good biofidelity</td><td>2.1</td><td>Impactor geometry</td><td>Knee</td></tr>
<tr><td rowspan="4">3</td><td rowspan="4">Realistic interaction conditions</td><td>3.1</td><td>Impactor force</td><td>3-4 kN</td></tr>
<tr><td>3.2</td><td>Carriage mass</td><td>100 kg</td></tr>
<tr><td>3.3</td><td>Vertical velocity</td><td>5 m/s</td></tr>
<tr><td>3.4</td><td>Horizontal velocity</td><td>3 m/s</td></tr>
</table>

2.7 Assessing the Safety of Rugby Turf Through Performance Testing

With the evolution of technology in the sports industry, new artificial surfaces are more advanced than ever. Manufacturers are continually adjusting the properties of their artificial turf to produce a system equivalent to natural grass. When installing a pitch, clients are often constrained by scope, time, and cost, which could potentially compromise the condition of the surface. However, it's important to note that Regulation 22, a stringent safety standard, ensures all turfs are safe for use in rugby, providing clients with the reassurance they need for their investment.

A synthetic surface must possess the playing characteristics the sport demands to provide the comfort and protection players require when running, falling, and sliding on the surface. World Rugby produced the Rugby Turf Performance Specification to establish a minimum standard and specify the testing procedures to follow when installing artificial playing surfaces. Regulation 22 requires completing laboratory and field tests for accreditation of the surface. Accordingly, only World Rugby-approved synthetic surfaces, referred to as Rugby Turf, will be permitted for use in rugby. The laboratory testing was designed to evaluate products' ball surface interaction, player surface interaction, and environmental resistance. The products are then exposed to simulated wear and retested to assess the ability of the surface to perform over its lifespan. The field testing repeats the ball and player interaction tests whilst also assessing the construction of the surface.

One of the biggest misconceptions about artificial turfs' perceived benefits is that they are maintenance-free [150]. Although they do not need as much attention as natural grass, they still need to be looked after. The client acquiring the Rugby Turf is responsible for maintenance and must demonstrate that the surface still conforms to the requirements periodically (at least every two years). This regular maintenance is crucial to ensure the longevity and performance of the turf. Artificial turfs are typically very durable; however, over time, they are subjected to high use and impacts from environmental exposure, which can result in a flattening of fibres, reduction of infill quantity, and damage at seams [70], [151]. Reducing infill quantity will influence performance characteristics, and flattening of fibres increases turf surface area during contact. Both are undesirable as they can increase the risk of injury [152], [153]. Consequently, groundskeepers should regularly rake surfaces to maintain fibre structure, periodically check infill quantities, and top them up when necessary, emphasising the importance of their role in the maintenance process.

2.7.1 Current Methods of Measuring Friction and Wear of Skin

A review of injury risk among athletes on artificial turf suggests no increased risk of injury when playing on artificial or natural grass [127]. However, artificial surfaces have a negative stigma due to the perceived increased risk of skin injuries in all sports [1]. This perception is interesting, given that testing standards are implemented to ensure the rate of those injuries is limited. Section 2.6.1 highlighted that the full extent of skin injury incidence is unknown due to underreporting. Consequently, further research on the device's validity in measuring skin friction and wear is required.

The Securisport is the current industry standard test device for calculating skin-surface friction and is used to predict skin injury risk. The apparatus consists of a motor, a pneumatic system, and a test foot with silicone attached to represent skin. The test begins by applying a 100N vertical force through the test foot via the pneumatic system. The motor rotates the test foot (radius 0.2 m) continuously in a sweeping motion at 40 rpm, which correlates to a linear velocity of 0.84 m/s [154]. The test consists of five complete rotations, which equates to a sliding displacement of 0.63 m. A torque transducer installed on the motor (Figure 2-16a) captures rotational resistance, while a pressure gauge (Figure 2-16b) attached to the test foot (Figure 2-16c) measures the normal load. The torque transducer and pressure gauge readings are combined to calculate the COF. This data is sampled at 40 Hz, providing detailed insights into the frictional interaction between the test foot and the surface. This process is repeated three times, with a new silicone skin attached to the test foot for each test. The test is concluded by evaluating the skin condition and comparing the results to the condition prior to testing – Equation 3. This assessment determines the force required to pull the skin along the metal plate over a sliding distance of 100mm at a speed of 500 ± 10mm/min. According to the requirements in the Rugby Turf Performance Specification, a product must produce a coefficient of friction between 0.35–0.75 and a skin abrasion value of ±30%. There appears to be no justification determined for the thresholds for performance requirements [155]. Insufficient critical and robust evaluation of the surface’s condition could contribute to high skin injury rates.

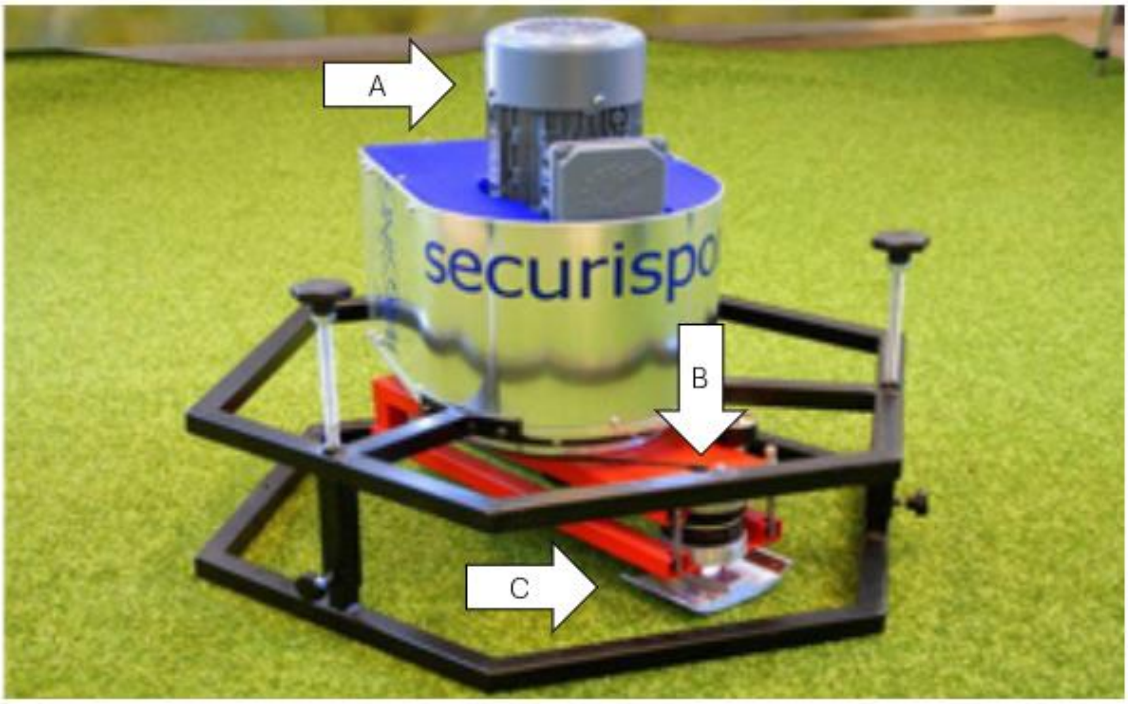

Figure 2-16: Main components of the Securisport: (a) motor, (b) air pressure tank and (c) test foot attachment.

Equation 3

$$Skin\ Abrasion\ (\%) = \left(\frac{F_{new\ skin} - F_{tested\ skin}}{F_{new\ skin}}\right) \times 100$$

Despite its widespread use as a standard FIFA test instrument, limited research on the efficacy of the Securisport exists. The continued prevalence of skin injuries means the device's validity is doubtful. Fundamental limitations are the inability to represent a player in motion by not accurately simulating an authentic impact and slide at realistic speeds [94], [129]. Initially designed to assess hard surfaces, the Securisport does not translate well to the dynamic nature of artificial pitches. Additionally, the repetitive circular sweeping action creates a trough in the infill, quickly influencing the surface condition as Figure 2-17 demonstrates. Consequently, the results are not representative of the specified turf system.

Figure 2-18 illustrates the low bio-fidelity of the current test device, which uses a generic impactor and a simple silicone skin to represent a player. Reports indicate that the surrogate materials do not mimic the natural skin response [156]. These deficiencies, in combination, highlight the potential for low-quality Rugby Turfs to gain accreditation and cause preventable skin injuries, posing a significant risk to players.

Figure 2-17: Example of a trough generated on the sample surface by repetitive circular sweeping action. [94]

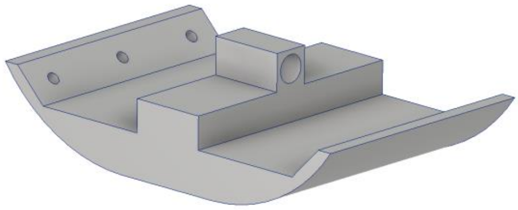

Figure 2-18: Model of Securisport Impactor

Tay et al. (2017) [157] evaluated the efficacy of the Securisport while investigating a range of different turf properties. This study aimed to enhance the understanding of its ability to assess skin injury risk. The study employs a laboratory-based experimental design enabling systematic investigation of skin friction behaviour under standardised conditions. Two carpets with different yarn types (monofilament vs fibrillated) and fibre lengths (40- vs 60 mm) were filled with varying infill rates of sand or SBR to influence the free pile height. The study assessed five surface systems for each carpet type:

- Carpet only.
- Carpet semi-filled with sand or SBR to achieve a 20 mm free pile height.
- Carpet overfilled with sand or SBR to achieve a 0 mm free pile height.

The adherence to the FIFA handbook of test methods in sample preparation and testing procedures enhanced confidence in the reliability and reproducibility of the data. However, the systems constructed in this study would fail Regulation 22 testing due to the absence of a shock pad. Consequently, the results do not entirely indicate injury risk during rugby gameplay. Finally, the methodology states inconsistent results for the skin abrasion scores during preliminary testing. To address this limitation, Tay et al. (2017) [157] conducted separate, independent assessments of surface roughness using optical microscopy and 3D scanning techniques. This supplementary testing significantly bolsters the robustness of the study. Overall, the thoroughness and attention to detail suggest that the study was rigorous in its design and execution.

The analysis provides detailed COF profiles for every turf system, highlighting the sharp increase in COF at first, followed by an equilibrium stage. Extending the analysis to include static, maximum, and steady-state COF values rather than just reporting steady-state COF, as required by Regulation 22, makes a more comprehensive appreciation of frictional qualities over time possible. This thorough analysis aids in understanding the dynamic friction behaviour of various surfaces.

The device's COF measurements and skin surface roughness varied significantly when assessing different combinations of 3G carpet and infill. The findings revealed that systems with no infill, especially those with fibrillated yarn, exhibited the highest friction. Conversely, overfilled systems produced comparably low levels of friction. According to the study, the skin simulant's initial surface roughness was higher than the surface roughness of every post-test sample, indicating that the surface had a polishing effect during testing. Sand consistently proved to be more abrasive than SBR, with the unfilled and over-filled samples being more abrasive than the semi-filled samples. The overfilled samples showed lower maximum and steady-state COF values, although they produced more abrasion than the semi-filled samples. These findings underscore the importance of skin and surface roughness characteristics in predicting the likelihood of damage, which has significant implications for the safety of sports surfaces.

Additionally, this result suggests that the Securisport COF measurements did not accurately reflect the damage inflicted on the skin during testing, questioning its validity as an industry standard. Wear imposed on a skin simulant may be a more appropriate assessment parameter. Upon further inspection of Equation 4, representing Archard's (1980) wear equation [99], no association was found between COF and skin damage. This lack of correlation implies that there could be more convenient indicative injury metrics than COF.

Equation 4

$$Wear\ Volume = K \text{ x } F \text{ x } s$$

Where: K = wear factor (mm^3/Nm) | F = Normal Load (N) | s = sliding distance (m)

Tay et al. (2017) [157] conclude the discussion by suggesting adjustments to the device's functionality, emphasising the need to enhance the realism of the motion profile. This modification includes monitoring frictional behaviour during controlled deceleration. To guarantee consistent friction assessments on diverse surfaces, the researchers recommended using a more appropriate skin surrogate with more realistic surface roughness. This study's conclusion is consistent with another study showing that surrogate materials do not replicate the skin's natural response [156]. Consequently, these features were integrated into the design specification. Comparing the design criteria of the new simulation characteristics against the features of the Securisport reveals that the device needs to be improved to represent a player in motion. Since the only parameter meeting the criteria is an acceptable sliding phase (Table 2-3).

Table 2-3: Comparison of Securisport's features with the design specification.

ID	User Requirement	Criteria ID	Design Criteria	Desired Output	Critical Analysis
1	Motion profile	1.1	Impact zone	Greatest magnitude of forces	Failed
		1.2	Sliding phase	Constant contact	Passed
		1.3	Measurement phase	Natural deceleration	Failed
2	Impactor possessing good biofidelity	2.1	Impactor geometry	Knee	Failed
		2.2	Skin Simulant	Realistic surface roughness	Failed
3	Realistic interaction conditions	3.1	Impactor force	3-4 kN	Failed
		3.2	Carriage mass	100 kg	Failed
		3.3	Horizontal velocity	5 m/s	Failed
		3.4	Vertical velocity	3 m/s	Failed

2.7.2 Alternative Methods of Measuring Friction and Wear of Skin

While players continue to express discontent regarding the perceived increased risk of skin injuries, a new test device is necessary. This section aims to explore different methods for measuring friction and skin wear. The goals of this review are:

- To examine current alternative test methods and give a detailed overview.
- Analyse these methods critically and establish whether they meet the requirements outlined in the design specifications.

ASTM F1015 - "Relative Abrasiveness of Synthetic Turf Playing Surface"

A technique for measuring the "Relative Abrasiveness of Synthetic Turf Playing Surfaces" is offered by the American Society for Testing and Materials (ASTM). This technique allows researchers to assess the risk of skin injuries by tracking the mass loss that occurs when they drag an instrument across the surface. The test material consisted of four friable foam blocks, as illustrated in Figure 2-19a, with an overall mass of ~9 kg, consistent with the normal force produced by Securisport. A pulley system was connected to a foot restraint to ensure the horizontal force applied to the instrument was parallel to the surface. This process is repeated across four directions, as in Figure 2-19b demonstrates, to ensure comprehensive testing. According to ASTM F1015, an Abrasiveness Index (AI) is computed by dividing the weight loss in grammes for each set of four blocks by 0.0606. However, the technique does not compare the AI score with an acceptable level of injury, which undermines the robustness of the test method.

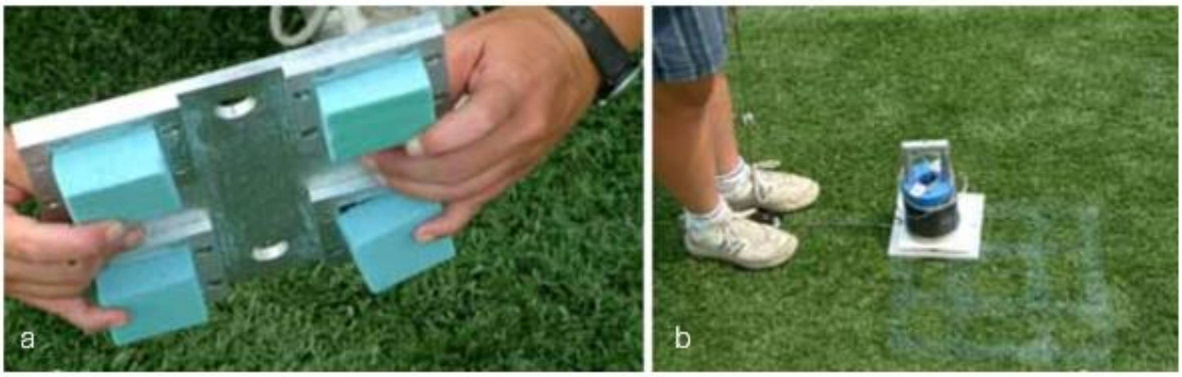

Figure 2-19 a) Picture of test instrument with four friable blocks b) Demonstrating envelope of the testing area.

The validity of this test is doubtful because the foam blocks do not accurately replicate human skin. Additionally, the technique does not simulate a genuine player's impact forces, sliding displacement and velocity. Despite this, McNitt et al. (2007) [158] reported that third-generation artificial grass systems typically have an AI score roughly half that of conventional second-generation artificial turf when using the ASTM technique. This finding is consistent with injury surveillance studies [126].

Modified Securisport

Lenehan and Twomey (2016) [58] modified the Securisport to generate a linear interaction that better represents a player in motion, specifically a football slide tackle. The primary aim of this study was to determine whether a more biofidelic interaction influenced the abrasion experienced by the skin simulant. The modified device, presented in Figure 2-20, adjusted the motion profile by producing a linear sliding speed of 5 m/s while retaining the vertical load (100±10N) exerted by the Securisport, accomplished by affixing a dead mass equivalent to 10kg to the impactor. An additional alteration was incorporated, increasing the sliding distance to 4m to mimic a slide tackle, as identified by Ingham (2013) [154].

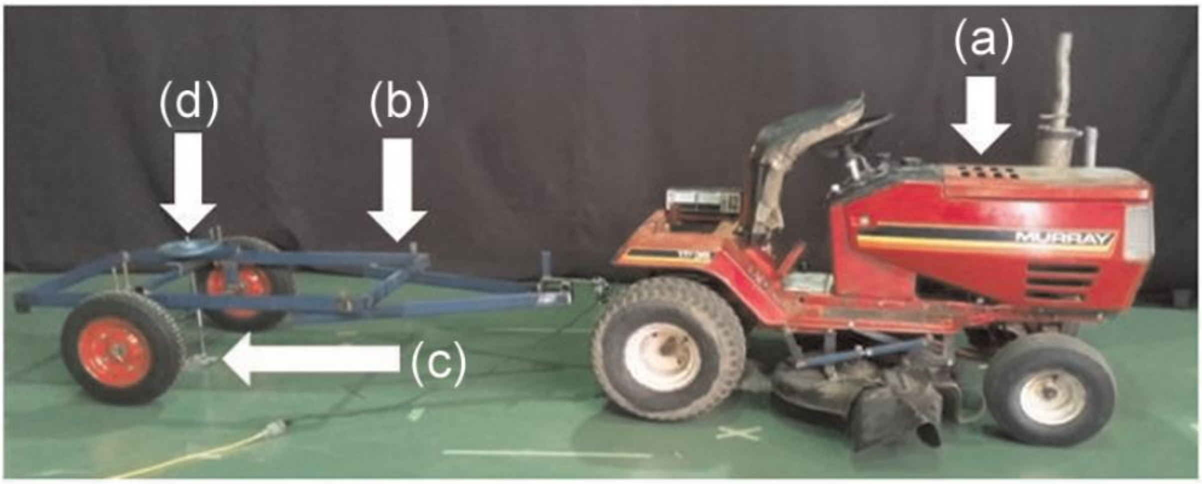

Figure 2-20: Main components of the modified device: (a) ride-on mower, (b) cart stabilising the test foot, (c) test foot attachment and (d) applied weight. [58].

Three systems, each comprising a 63 mm polyethylene carpet, were filled with different sand and SBR ratios; each device tested each surface three times. The first sample had 16 mm of sand, the second had 14 mm of SBR added to create a lower rubber content with a total infill depth of 30 mm, and the third had additional SBR to achieve a higher rubber content with an overall infill depth of 38 mm. According to the study, there was a considerable variation in the modified device's abrasion scores among the three systems, suggesting that the outcome was influenced by speed, direction, or both variables. The study's results, however small (n = 18 trials), were troubling because both the modified device (34.5%) and the Securisport (86.2%) failed to meet the existing abrasion standards of less than 30%. The author suggests readers interpret these results cautiously, as the new methods were not fully validated. However, this exposes the shortcomings of the existing test apparatus and provides more evidence for the necessity of creating a new test apparatus to enhance the safety standards of artificial pitches.

The scope of the study was appropriate for addressing the research question; however, a broader investigation into different turf parameters could enhance the comprehensiveness of the research. The study exhibits a rigorous testing approach, adhering to established protocols for the Securisport. However, strengthening the methodological robustness could offer a more comprehensive explanation of how the test foot contacted the surface at the desired speed. Moreover, while the authors stated using a radar gun to confirm a peak speed of 5 m/s, they omitted details regarding whether this speed was maintained constantly or if a natural deceleration was simulated, a recommendation later introduced by Tay et al. (2017) [157]. Another limitation of the study is the need for more clarity addressing sliding distances between each device, a key factor significantly influencing wear [99]. Overall, the study lacks rigour in certain aspects of its approach; however, addressing these limitations could further strengthen the validity and generality of the findings.

Despite the shortcomings of this study, it represents progress, if somewhat limited, towards developing a more biofidelic apparatus. It offers justification for the new device's sliding displacement, orientation, and speed, albeit within a football context. Validation of these findings in rugby is warranted. The proposed test device aims to replace repetitive sweeping with linear sliding initiated by genuine impacts at realistic speeds and loads. A comparison between the new device's design criteria and the features of the Modified Securisport suggests it is better suited for simulating player motion. However, further enhancements are needed for authentic impacts (Table 2-4).

Table 2-4: Comparison of the Modified Securisport's features with the design specification.

ID	User Requirement	Criteria ID	Design Criteria	Desired Output	Critical Analysis
1	Motion profile	1.1	Impact zone	Greatest magnitude of forces	Failed
		1.2	Sliding phase	Constant contact	Passed
		1.3	Measurement phase	Natural deceleration	Doubtful
		1.4	Orientation	Linear	Passed
2	Impactor possessing good biofidelity	2.1	Impactor geometry	Knee	Failed
		2.2	Skin Simulant	Realistic surface roughness	Failed
3	Realistic interaction conditions	3.1	Impactor force	3-4 kN	Failed
		3.2	Carriage mass	100 kg	Failed
		3.3	Horizontal velocity	5 m/s	Passed
		3.4	Vertical velocity	3 m/s	Failed

Ramp and Sliding Tester

Environmentalists disapprove of irrigated hockey surfaces due to the excessive water volumes required to prepare the surfaces, especially in regions where drought is an issue. This criticism continues to be prevalent at the time of writing, which has resulted in HIF, hockey's governing body, banning water-based surfaces after the 2024 Olympics [159]. Sliding is a standard task hockey players perform to control a fast-moving ball or attempt a tackle. This movement often results in the player interacting with the surface, which can result in the player sustaining a skin injury.

This issue motivated Verhelst et al. (2009) [56] to develop a sliding tester to monitor rising temperatures via thermocouples to assess skin injury risk during an interaction with artificial sports surfaces. The apparatus consisted of a sledge and a ramp, as illustrated in Figure 2-21. The sledge, ranging from 15–30kg, had a polymeric skin simulant on the interaction face, which was selected based on its fractional and thermal properties. However, the lack of sufficient information on the properties of artificial skin and how they compare to human skin casts doubt over its validity. The ramp had an adjustable release height, which could generate horizontal speeds up to 22 km/h (6.1m/s). The method indirectly calculates the COF using the sliding distance, but the study did not report these results. Additionally, the study lacks clarity by not mentioning the method for quantifying abrasion despite discussing the abrasive nature of each surface.

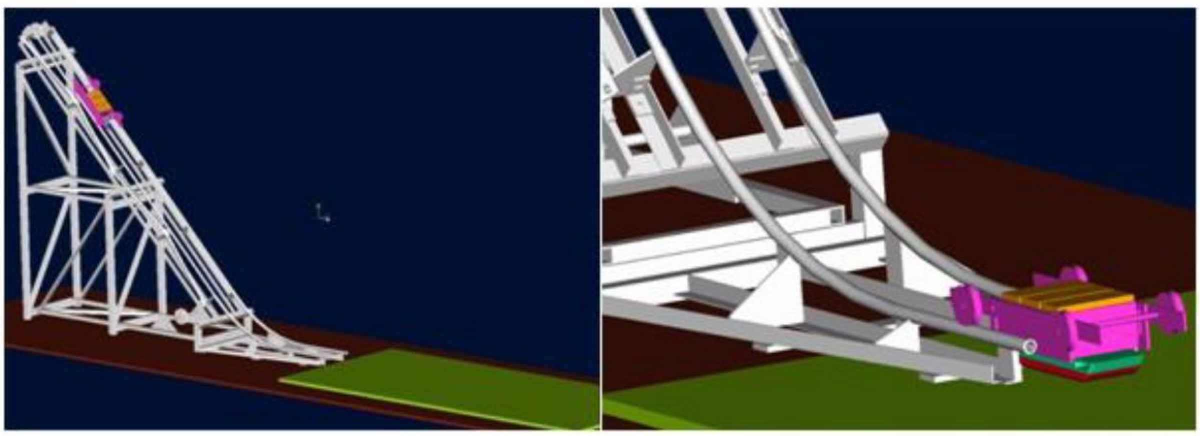

Figure 2-21: Schematic diagram of the Slide Tester [56].

This study investigated how three artificial turf types affected temperature rise during a sliding interaction: a sand-based hockey surface, a water-based hockey surface, and a typical 3G football surface. This study evaluated all surfaces under dry and wet conditions to simulate real-world scenarios. However, there needed to be an indication of several test repeats or statistical analysis, which questions the reliability of the data. To prevent the slope from influencing the results, researchers prepared the surfaces accordingly, ensuring that the overall length was 9m to guarantee that the slider had ample sliding distance in all tests. This foresight demonstrates that the experimental design was, to a degree, robust.

The study presents precise temperature profiles for each turf system, showcasing the initial rapid rise in temperature followed by a slow relaxation period. This simple illustration lets readers quickly assimilate that the three surfaces exhibit different thermal profiles. Understanding these temperature changes during sliding provided insights into the thermal properties of artificial turf and potential implications for player safety. However, the results section should be more explicit to help identify each surface rather than using arbitrary letters as a reference code. A dry water-based surface registered the highest peak temperature (12°C) in dry conditions, indicating that friction-induced temperature occurs in the yarns. Conversely, the sand-based surface exhibited the highest level of abrasion. This result agrees with Tay et al. (2017) [157], who reported that sand systems were more abrasive than SBR. Concurrently, the 3G system generated peak temperature rises of 8°C. The maximum temperatures recorded were insufficient to induce burns; therefore, skin injuries sustained on artificial surfaces are mechanical abrasions rather than thermal damage. The study conducted all tests at a constant ambient temperature of 20.2°C, which does not accurately represent global playing conditions. Therefore, there is scope for future research in this area, as results might differ significantly at higher temperatures. Despite its shortcomings, the study makes valuable contributions toward improving player safety by providing insights into the thermal profiles during a sliding interaction with artificial turf.

Upon further inspection of Figure 2-21, it appears that once the impactor contacts the surface, there is no mechanism to ensure it remains in constant contact. Consequently, if the surface is not perfectly level or the impactor does not exit the ramp smoothly, the interaction could resemble a bounce rather than a slide. This condition could negatively impact the test results by either decreasing the wear on the skin simulant or artificially increasing the sliding distance, potentially lowering the coefficient of friction (COF). Both outcomes are undesirable, as they would infer a lower risk of injury. Despite these limitations, this design feature allows the test method to monitor the natural deceleration of the impactor as it slides across the surface, representing a step towards developing a more biofidelic apparatus. Comparing the new device's design criteria with the features of the ramp and sledge suggests it is better suited for simulating player motion. However, further enhancements are needed to replicate authentic impacts (Table 2-5).

Table 2-5: Comparison of the Ramp and Sledge's features with the design specification.

ID	User Requirement	Criteria ID	Design Criteria	Desired Output	Critical Analysis
1	Motion profile	1.1	Impact zone	Greatest magnitude of forces	Failed
		1.2	Sliding phase	Constant contact	Passed
		1.3	Measurement phase	Natural deceleration	Passed
		1.4	Orientation	Linear	Passed
2	Impactor possessing good biofidelity	2.1	Impactor geometry	Knee	Failed
		2.2	Skin Simulant	Realistic surface roughness	Doubtful
3	Realistic interaction conditions	3.1	Impactor force	3-4 kN	Failed
		3.2	Carriage mass	100 kg	Failed
		3.3	Horizontal velocity	5 m/s	Passed
		3.4	Vertical velocity	3 m/s	Failed

Biaxial Load Applicator

Eijnde et al. (2017) investigated the biomechanical loading of a football slide tackle to better understand the mechanisms underlying acute skin injuries. The main goal of this study group was to evaluate the risk of injury by combining qualitative skin damage studies with mechanical stress. This study demonstrated the importance of the initial impact's peak pressures in causing skin injury. These results suggest that reducing peak shear stresses may be a crucial first step towards preventing injuries.

Recognising the limitations of the Securisport and ASTM methods, they developed a novel biaxial load applicator and ex-vivo model. This innovative approach allowed for more accurate and comprehensive biomechanical testing. The study design allows for controlled testing of skin injuries under various impact conditions, enhancing the reliability of the findings. The device's design involved launching an impact body onto a surface with vertical and horizontal velocity components. The apparatus includes:

- Adjustable horizontal and vertical rails,
- A mass-spring configuration to mimic human body impact and
- A clamping system for ex-vivo skin samples.

The impact body's vertical and horizontal velocities can reach 3.0±0.2 m/s and 1.9±0.2 m/s, respectively. Accelerometers were integrated into the impactor to monitor biaxial forces, and an acceptable accuracy (within 10%) was confirmed through a force plate validation. This level of accuracy ensures that the measurements of the biaxial forces are reliable and valid, providing a solid foundation for the study's findings. Testing involved natural grass and third-generation artificial turf, both dry and wet, under controlled lab conditions. Researchers employed ex-vivo rabbit ear skin samples for morphological evaluation, which they examined under a microscope using ImageJ software. They used Pearson correlation coefficients to explore the connection between mechanical characteristics and stratum corneum thickness.

The study successfully addressed a significant gap in the field: the need for biomechanical data on skin tolerance to impact sports surfaces. It used a novel biaxial load applicator and an ex-vivo rabbit ear skin model. Visual examination of skin samples revealed distinct patterns of grooves and pits on both dry and wet artificial turf, predominantly aligned with the sliding direction. Following numerous runs on both artificial turf kinds, skin damage was seen, with infill material remaining on the skin. On natural grass, the grooves were less noticeable, and after several runs, there was only slight damage. Peak shear and normal stress levels varied from 18 N/cm^2 to 150 N/cm^2 due to different combinations of horizontal and vertical impact velocities caused by different impact situations. Skin breakdown occurred at lower impact velocities on dry artificial turf compared to wet conditions and natural grass. Stratum corneum thickness strongly correlated with various mechanical parameters on dry artificial turf, whereas only moderate correlations were observed on wet artificial turf. No meaningful relationships were discovered on natural grass. The results reveal that skin injury on dry artificial turf is less tolerant to impact load magnitude than on natural grass and wet conditions. This result underscores the significance of surface qualities in injury prevention and is consistent with player views and clinical observations [128].

The study's quantitative and qualitative analysis provide invaluable insights into the mechanisms of skin damage on different surfaces. The research's real-world applications for surface design and safety regulations are a significant discovery that underscores the relevance and importance of this research. If integrated into Regulation 22 testing, the test method could present challenges due to the study's reliance on ex-vivo skin models and histological examination. Future studies could investigate other skin models and automated analysis methods to improve efficiency and accuracy.

In summary, this study developed an innovative approach that enabled comprehensive biomechanical testing, under realistic conditions, of artificial turf by generating a biaxial load and utilising an ex vivo skin simulant. When considering the design specification, the limitations were not achieving the desired horizontal velocities, a carriage mass representing a player, and the absence of an impact geometry resembling a knee. Overall, this test device represents the best alignment to the desired design criteria so far; however, there is still room for improvement, as demonstrated in Table 2-6.

Table 2-6: Comparison of the biaxial load applicator's features with the design specification.

ID	User Requirement	Criteria ID	Design Criteria	Desired Output	Critical Analysis
1	Motion profile	1.1	Impact zone	Greatest magnitude of forces	Passed
		1.2	Sliding phase	Constant contact	Passed
		1.3	Measurement phase	Natural deceleration	Passed
		1.4	Orientation	Linear	Passed
2	Impactor possessing good biofidelity	2.1	Impactor geometry	Knee	Failed
		2.2	Skin Simulant	Realistic surface roughness	Passed
3	Realistic interaction conditions	3.1	Impactor force	3-4 kN	Passed
		3.2	Carriage mass	100 kg	Failed
		3.3	Horizontal velocity	5 m/s	Failed
		3.4	Vertical velocity	3 m/s	Passed

Skin Friction Test

Labosport has addressed the issue of skin injuries on artificial sports surfaces by introducing the 'Skin Friction Test' device. This device can simulate athletes weighing 25 to 150 kg while sliding at speeds up to 5 m/s, all within a compact dimension of 5m x 0.4m [160]. The device's design aims to replicate the impact of a fall; however, specific data quantifying this impact is not provided. Additionally, the motion profile during the interaction lacks clarity; however, further investigation established that the device operates at a constant speed during the sliding phase, which is undesirable. The COF is monitored using a 6-axis load cell, and the temperature elevation is recorded using thermocouples. Using COF as a metric is described as a unique technical solution [160], albeit one that contradicts the findings of Tay et al. (2017) [157], who argued that COF is not a reliable indicator of skin damage.

In 2018, the device was used during a comparative study to evaluate the influence of infill material, shock pad, and humidity on skin injury risk. For this study, the researchers prepared thirteen samples using standard infill quantities to represent systems in the market, marking an improvement over the samples assessed by Tay et al. (2017) [157]. In this study, the simulated athlete has a mass of 75 kg and generates a sliding at a speed of 5 m/s. The primary limitation of this study is the utilisation of a generic-geometry impactor, reminiscent of the Securisport as depicted in Figure 2-22, without detailed information on the skin simulant. Additionally, the study fails to consider the mechanical abrasion of skin during interaction despite acknowledging in their report the potential for player-surface interactions to cause abrasions.

Figure 2-22: Photo of the Skin Friction Test’s impactor.

The study investigated the impact of various factors on the friction temperature of synthetic playing surfaces. A shock pad did not significantly affect friction temperature on fibrillated and monofilament turf. As expected, a humid (wet) surface significantly decreased friction temperature for wood chips on both types of turf. As the volume of wood chip infill increased, the temperature generated by friction conversely decreased. This finding suggests that temperature generation occurs within the carpet yarns, aligning with conclusions made by Verhelst et al. (2009) [56]. Dry wood chips exhibited lower friction temperature than dry crumb rubber, which was lower than cork. Furthermore, on fibrillated yarns, as opposed to monofilament turf, dry wood chips produced lower friction temperatures; however, this tendency was reversed with humid wood chips. These results offer insight into the likelihood of skin injuries associated with various turf characteristics. However, their value could be enhanced by conducting a more thorough examination of skin injury risk by considering the broader implications of their findings, such as including information on COF and abrasion.

The FIFA turf quality programme plays a crucial role in evaluating the consistency of the polymers within the yarns. Part of this assessment measures melting points via differential scanning calorimetry (DSC) [161]. Sports Labs laboratory tests report DSC melting points between 105°C and 130°C for high-density polyethylene in a similar temperature range recorded for three samples. This outcome indicates a potential that the yarns could have melted. However, this seems unrealistic for a player-surface interaction in standard laboratory conditions, raising questions about the credibility and accuracy of the interaction's biofidelity. It is important to note that the device has not been peer-reviewed, which introduces uncertainty regarding the reported data.

In summary, Labosport has developed another biaxial load applicator which overcomes the limitations Eijnde et al. (2017) [149] encountered trying to achieve the desired horizontal velocity (5 m/s). One of the key objectives of this research is to ensure that the applicator mimics player movements as accurately as possible. Therefore, it is crucial to address the fact that the impactor geometry does not represent a player, and the sliding phase does not exhibit a natural deceleration, which is undesirable. These design criteria are compared to the desired outputs of the design specification, as presented in Table 2-7.

Table 2-7: Comparison of the Skin Friction Test's features with the design specification.

ID	User Requirement	Criteria ID	Design Criteria	Desired Output	Critical Analysis
1	Motion profile	1.1	Impact zone	Greatest magnitude of forces	Doubtful
		1.2	Sliding phase	Constant contact	Passed
		1.3	Measurement phase	Natural deceleration	Failed
		1.4	Orientation	Linear	Passed
2	Impactor possessing good biofidelity	2.1	Impactor geometry	Knee	Failed
		2.2	Skin Simulant	Realistic surface roughness	Failed
3	Realistic interaction conditions	3.1	Impactor force	3-4 kN	Doubtful
		3.2	Carriage mass	100 kg	Passed
		3.3	Horizontal velocity	5 m/s	Passed
		3.4	Vertical velocity	3 m/s	Doubtful

Summary of Alternative Methods for Assessing Skin Injury Risk

This section provided a detailed overview by examining various current alternative test methods. The review highlighted various testing methods developed to assess synthetic turf playing surfaces' abrasiveness and injury risks. These methods include ASTM F1015, Modified Securisport, Ramp and Sliding Tester, Biaxial Load Applicator, and Skin Friction Test. Each technique was critically analysed based on criteria such as accuracy, repeatability, and relevance to real-world conditions to establish whether they met the requirements outlined in the design specifications. Below is a summary of each method and how its features align with the needs of the new test apparatus.

The ASTM F1015 method measures the *"Relative Abrasiveness of Synthetic Turf Playing Surfaces"* by tracking mass loss as an instrument is dragged across the surface. McNitt et al. (2007) [158] found that third-generation artificial grass systems typically have an Abrasiveness Index (AI) score roughly half that of conventional second-generation artificial turf when using this technique. However, the method needs comparability with an acceptable level of injury, which is a standard or threshold that determines whether a surface is safe for play. This standard is crucial for ensuring the reliability and consistency of the testing results. Its validity is also questioned due to the foam blocks not accurately replicating human skin.

Lenehan and Twomey [58] modified the Securisport to better represent a player in motion during a football slide tackle. The new test device replaced the repetitive sweeping motion with linear sliding; however, they did not address the impactor geometry and skin simulant issues. They found significant variation in abrasion scores among different turf systems, which suggests that the choice of turf system could significantly affect the risk of player injury. This finding underscores the need for more accurate and reliable testing methods with the modified device and the Securisport failing to meet existing abrasion standards. Despite the authors' acknowledgement that the new techniques still need to be fully validated, no subsequent studies have been published to elaborate on this research.

Verhelst et al. (2009) [56] developed a ramp and sliding tester to assess skin injury risk during interactions with artificial sports surfaces. They observed distinct temperature profiles for different surfaces during sliding interactions. A dry water-based surface registered the highest peak temperature (12°C) in dry conditions, indicating that friction-induced temperature occurs in the yarns. Conversely, the sand-based surface exhibited the highest level of abrasion. The temperatures reported were insufficient for players to sustain burns, which implies that a *turf burn* is more a mechanical abrasion rather than thermal damage. However, this study did not investigate the effects of different turf temperatures; therefore, burns still have the potential to occur at higher surface temperatures. This apparatus generated the desired horizontal velocity and a natural deceleration during the sliding phase. However, the limitations consisted of not representing an authentic contact with a realistic impactor.

Eijnde et al. (2017) [149] developed a biaxial load applicator and ex-vivo model to evaluate skin tolerance to impact sports surfaces. They found skin injury on dry artificial turf is less tolerant to impact load magnitude than on natural grass and wet conditions. This finding suggests that players may be at a higher risk of injury on dry artificial turf, which could have significant implications for designing and maintaining such surfaces. This study's innovative approach enabled comprehensive biomechanical testing under realistic conditions; however, they did not achieve the desired horizontal velocities. Additionally, integrating the test method into Regulation 22 could present challenges due to the reliance on ex-vivo skin models and histological examination.

Labosport introduced the 'Skin Friction Test' device, which simulates athletes sliding on artificial sports surfaces. Results from this study emphasised that temperature build-up was generated in the yarn, corroborating the conclusions drawn by Verhelst et al. (2009) [56]. This outcome indicates a potential that the yarns could have melted, which could significantly affect the surface's performance and safety. However, this seems unrealistic for a player-surface interaction in standard laboratory conditions, raising questions about the credibility and accuracy of the interaction's biofidelity. It is important to note that the device has yet to be peer-reviewed, which introduces uncertainty regarding the reported data.

Overall, the biaxial load applicator and the skin friction test devices show promise in aligning with the desired design criteria. This review highlights a positive direction for the future of synthetic turf testing, although there is still room for improvement. For example, there is still a need to develop an impactor that resembles a human body part and identify a suitable synthetic skin simulant.

2.7.3 Skin Simulants

The literature review highlighted that skin is a bio-mechanically complex material that exhibits large inter- and intra-subject variability [162]. The proposed testing will generate a high-energy interaction with artificial turf; hence, working with human skin poses ethical challenges. Ex-vivo samples are not suitable either, as it is impossible to obtain identical samples as properties change rapidly with time [163]. Animal skin, including that of mice, rats, and rabbits, has been extensively researched in the literature. However, regarding anatomical and physiological structures, porcine skin is deemed the closest match to human skin [164]. A skin surrogate is preferred for improved repeatability and reduced variability in testing to overcome these limitations and ethical concerns relating to animal welfare. This section will review a range of available skin simulants and assess whether they are suitable for the proposed test method.

Skin simulants have been widely applied in clinical settings, such as surgical, pharmaceutical, and cosmetic healthcare studies. They are particularly crucial in managing and reconstructing acute burns [165]. The pharmaceutical industry uses skin simulants to monitor permeability and absorption rates during drug therapy, providing insights into the product's performance quality before human trials [166]. In developing cosmetic skin care devices, such as electric razors, skin friction and deformation are key to determining comfort during use. However, the development of skin surrogates has primarily focused on replicating the biological or histological aspects of human skin, often neglecting the importance of mechanical and textural similarities [167], [168], [169]. While these surrogates serve their purpose in biological testing, they often fall short in mechanical experiments. Explorative studies have developed skin simulants to explore tribomechanical behaviour, but limitations exist when simulating the full range of skin conditions [10], [14], [17], [170].

A review of the relevant literature highlighted the skin simulants that mimic the mechanical and textural properties of skin, typically consisting of silicone elastomers or polyurethanes [163], [171], [172], [173], [174], [175]. While numerous skin simulants have been developed, they are typically research field-specific, making them difficult to transfer to different applications [176]. In the current test method of assessing skin injuries on artificial pitches, FIFA utilises silicone skin (L7350) based on the overall mechanical properties. This approach, however, has questioned the validity of this skin simulant. Doubt exists regarding whether mechanical properties alone can assess sliding safety or offer insights into further optimisations to enhance the perceived comfort of artificial turf [59]. Another disadvantage of the silicone skin is its hydrophobic properties. Hydration significantly influences the tribological behaviour of human skin [17], [21], [177]. For example, in everyday life, the friction of a moist finger on a touch screen is greater than when the finger is dry. Therefore, hydrophobic material is unsuitable because it forms a fluid film between the silicone and the artificial turf in moist conditions. Consequently, the frictional response generated is lower than expected [174]. These limitations, in combination with the limited availability of the material referenced in the current test method, imply that an alternative skin simulant is required.

SynDaver [178] has developed an advanced skin simulant, SynTissue®, consisting of multiple discrete layers with a natural wear layer at the surface to provide a realistic texture. SynTissue consists of salt, water, and fibre to produce a skin simulant with the "most realistic tactility", which similarly responds to stimulus in vivo. The patented product was designed for medical device design verification and possesses relevant skin properties from tests on living tissue. When selecting a skin simulant, one must consider how it responds to dry and wet moist conditions. The highly porous nature of SynTissue is detrimental to its potential use as a viable skin simulant in friction testing. The pressure applied to the skin in such tests results in the fluid being squeezed out of the porous structure, forming a lubricating film. The barrier function of the stratum corneum prevents fluid loss under applied loads. Therefore, the frictional behaviour of SynTissue will be lower than in vivo in dry conditions [175].

Lorica is a Latin word that directly translates to 'body armour'; therefore, Lorica Soft is a felicitous name for a skin simulant. Several studies have investigated the use of Lorica Soft, a synthetic leather, as a viable option for a tribological skin simulant [163], [179], [180], [181], [182]. The polyurethane-coated polyamide microfibre fleece (14.93µm) possesses a similar surface roughness to *in vivo* skin [180], [182], [183], [184]. Even though *in vivo* skin exhibited a more significant number of strongly defined furrows compared to the smooth edges of Lorica Soft, a topographic analysis of both surfaces reported that the two specimens had comparable textures [185].

Derler et al. (2007) [182] conducted a pioneering study that delved into the frictional behaviour of *in vivo* and skin equivalents against textiles. This research not only aimed to enhance the comprehension of the variables influencing skin-textile friction but also sought to devise more precise skin models for textile property testing, with a specific focus on sports and medical applications. What sets this study apart from others is its unique approach of comparing i*n vivo* against various skin simulants, providing a detailed comparison to establish which material exhibited the best correspondence with human skin. The researchers also delved into the influence of different hydration levels, a factor known to influence skin friction, further adding to the robustness of the conclusions.

The study employed a robust methodology to measure normal and tangential forces using a triaxial force place. Twelve subjects, evenly distributed between males and females, rubbed their index fingers against a textile affixed to the measurement system. Human skin models, made of various silicone and polyurethane materials, were tested using a device that oscillated the skin simulant under the textile. All experiments were conducted under consistent environmental conditions (heat and humidity). Furthermore, the participants underwent an acclimatisation period, which further enhanced the repeatability and reliability of the results. It is worth noting that the participants' skin was untreated, providing an accurate representation of *in vivo skin*, albeit with potential inter-subject variation. This approach was expected to yield a broader range of results compared to testing with clean skin.

In participant testing, normal loads varied from 0.2 N up to 15 N to monitor the influence of contact pressure. Observations from this testing guided the device's setup for assessing the skin simulants, configuring it to apply a normal load of 3 N with a stroke length of 20 mm at a frequency of 1.25 Hz. Throughout this study, a standardised wool fabric, as specified in the Martindale abrasion test [ASTM D4966-98(2004)], served as a reference textile. Since skin hydration and lipid content vary significantly between individuals, COF varied dramatically, ranging from 0.27 to 0.71. The polyurethane-coated polyamide fleece (Lorica® Soft) corresponded best with human skin in dry conditions as Figure 2-23 illustrates. Supplementary testing consisted of applying defined volumes of water to the interface between the Lorica Soft and the textile. The results indicated that COF increased with moisture content before stabilising at a certain threshold, corresponding to the response exhibited by *in vivo* skin [25]. This result aligns with the findings from Tang et al. (2018) [180], who developed an instrument for evaluating the stickiness of textiles under wet skin surface conditions.

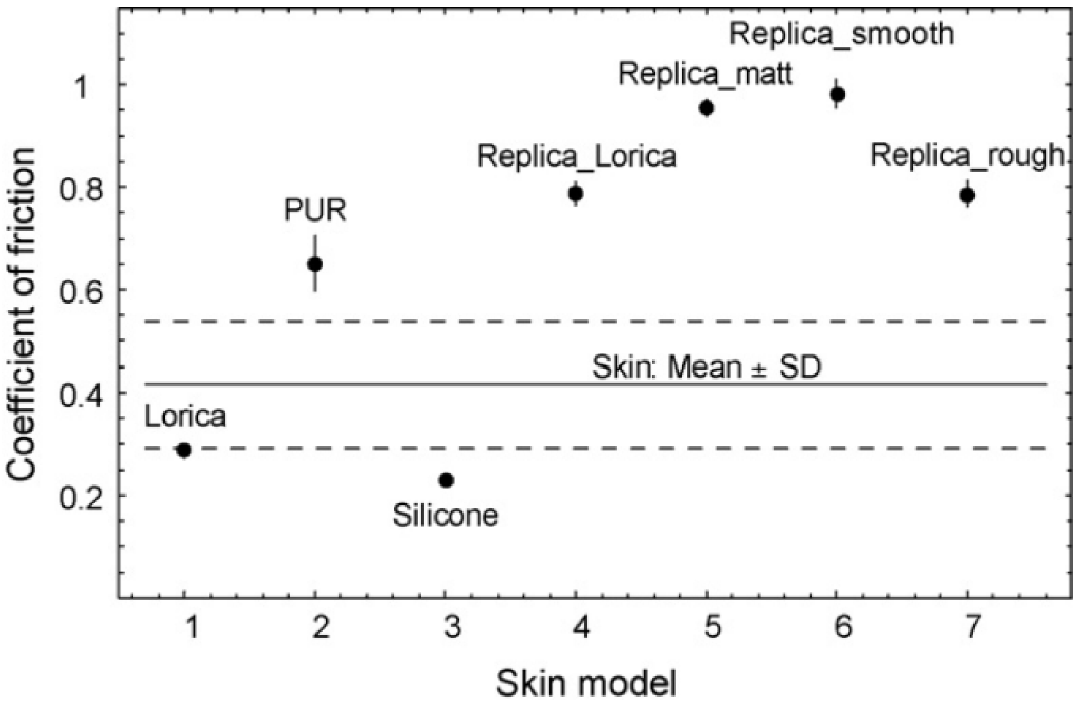

Figure 2-23: The reference fabric's friction coefficients (mean value ± S.D.) against seven skin models measured on the friction test device. The horizontal lines represent the mean value (0.415) ± 1 S.D. (0.124) of the friction coefficients found in touch experiments with 12 subjects. [182]

Klaassen et al. (2019) [185] also reported that the reduced Young's modulus of the Lorica Soft (1.8 MPa) was determined to be equivalent to the elastic modulus of the epidermis (1.5 MPa) [186]. However, the properties of *in vivo* skin are known to change with penetration depth. Therefore, an additional elastic sublayer may be required. The choice of skin simulant is influenced by the fact that no single material can perfectly replicate all the properties of human skin. Instead, the selection depends on the specific properties that need to be simulated. One approach is to combine Lorica soft with a silicone sublayer to achieve the desired mechanical response. However, this combination must accurately represent the homogenous layer of natural skin and introduce additional variables. Moreover, the elasticity of silicone is influenced by environmental conditions, meaning that different times of the year could affect its response. In the analysis of contact mechanics, it was observed that the deformation of the soft material primarily governs the frictional response between a hard and soft material. Considering that artificial turf is a compliant material, the deformation of the turf would take precedence over the deformation of the skin. Consequently, a silicone sublayer was deemed surplus to requirement.

2.8 Purpose of the Present Work

This chapter provides an extensive overview of the literature, exploring skin and tribology themes to offer insights into managing techniques for improved skin function in sports. The comprehensive review of skin provided insights into anatomy, skin friction and measurement techniques, mechanical properties, failure conditions, types of friction injuries, and skin infections. This review highlighted that skin is bio-mechanically complex due to its anisotropic, non-linear elastic, and viscoelastic behaviours. This review also highlighted that rugby turf is a non-Hertzian material, meaning it does not adhere to the fundamental principles of Hertzian contact mechanics, a theory that describes the deformation of solids under contact. Instead, rugby turf exhibits non-linear behaviours due to integrating a mobile granular infill into a lattice network of yarn fibres. Consequently, the skin and Rugby Turf should not be regarded as adhering to the fundamental principles of friction.

The section on artificial turf unveils its evolution and advantageous characteristics compared to natural grass. Despite the proliferation of synthetic turf in amateur and elite rugby, universal player approval is limited, to an extent, due to the perceived increased fear of injury compared to natural turf. This view was attributed to preconceptions associated with earlier turf generations and the influence of elite players revealing negative assessments. There is, however, no clear consensus defining any difference in injury risk between the surfaces due to conflicting reports throughout the current literature. Skin injuries, referred to as *Turf Burns*, are typically considered a minor inconvenience. They do not often prevent players from participating; therefore, major injury studies do not regularly include them. This omission contributes to the disparity between perceptions of skin injury risk and reported incident rates.

World Rugby's Player Welfare strategy, a testament to their commitment to player safety, prioritises ensuring that surfaces and equipment are safe. Regulation 22 sets a minimum standard for turf quality and performance characteristics. Only World Rugby-approved synthetic surfaces, referred to as Rugby Turf, will be permitted for use in rugby. The Securisport, a widely used test device in the sports industry, is the current industry standard for calculating skin-surface friction. Despite its widespread use as a standard FIFA test instrument, limited research has been published on its efficacy. The continued prevalence of skin injuries suggests that the device's validity may be in doubt. The combination of the deficiencies, highlighted in Section 2.7, underscores the potential for low-quality Rugby Turfs to gain accreditation and the possibility of causing preventable skin injuries, a matter of serious concern.

As players express their concerns about the perceived higher risk of sustaining skin injuries, the need for a new test device becomes not just a necessity but an urgent priority. This device should replicate a better player surface interaction, addressing the current limitations of existing test devices. The modifications include replacing the repetitive sweeping action with a linear sliding interaction initiated by an authentic impact with subsequent a natural declaration at realistic speeds and loadings. Additionally, an impactor should be designed using anthropometric data and wrapped in an improved skin simulant. Lorica Soft emerged as the skin simulant that best resembled the textural and frictional properties of in vivo skin, which will be adopted for use during the development of this test method. This innovative approach is crucial for advancing the understanding of skin injuries in sports and developing effective preventive measures.

The combination of high-velocity movements and abrupt changes in direction during player-surface interactions often causes skin injuries. To ensure the safety of players and the integrity of the sport is maintained, there is a pressing need for a comprehensive testing method that meticulously replicates realistic gameplay scenarios on artificial pitches. In rugby, tackling is frequent and perilous, with the knee being the most vulnerable anatomical area. Biomechanical analysis of sliding motions involved in the tackle process reveals three phases: free drop, impact, and sliding. While limited injury data exists, estimates suggest typical knee impact forces of 3-4 times body weight, often exceeding 3-4 kN for elite athletes weighing over 100 kg. Effective testing should assess the impact and sliding phases separately, necessitating further research for sliding phase loading conditions. While elite players can reach speeds of 10 m/s, realistic interaction speeds with the turf are estimated to be around 5 m/s. This estimate was derived from slide tackles in football. Therefore, further research is required to establish impact velocities and corresponding sliding distances for rugby.

Despite this in-depth review, the aetiology of burn-related skin friction injuries still needs to be fully understood. Accordingly, the proposed test method should quantify the abrasive nature of turf and the temperature rise, providing a more comprehensive understanding of the injury mechanism in operation when players sustain turf burns. Currently, the COF serves as the metric for predicting injuries; nonetheless, developing novel kinematic injury metrics becomes essential, given that both skin and Rugby Turf deviate from conventional friction principles and the absence of a correlation between COF and wear. These new metrics will offer a comprehensive approach to evaluating the risk of skin injuries and developing safer surfaces. Existing test methods should be considered during the design and development stages to ensure their seamless adoption into Regulation 22. FIFA Test Method 15 emerged as the most relevant test to consider as it provides details for determining wear on artificial turf, which will be beneficial for predicting skin injury risk on an end-of-life product. Consequently, the device's dimensions should accommodate integration into the Lisport XL. The desired simulation characteristics (Table 2-8) will ensure the new test method's effectiveness in replicating realistic player-surface interactions.

Table 2-8: Summary of Desired Simulation Characteristics

ID	User Requirement	Criteria ID	Design Criteria	Desired Output
1	Motion profile	1.1	Impact zone	Greatest magnitude of forces
		1.2	Sliding phase	Constant contact
		1.3	Measurement phase	Natural deceleration
2	Impactor possessing good biofidelity	2.1	Impactor geometry	Based on real anthropometric data
		2.2	Skin simulant	Lorica Soft
3	Realistic interaction conditions	3.1	Impactor force	3-4 kN
		3.2	Carriage mass	100 kg
		3.3	Horizontal velocity	5 m/s
		3.4	Vertical velocity	3 m/s
		3.5	Sliding distance	TBD
4	Assessing skin injury risk	4.1	Abrasion	Surface roughness
		4.2	Temperature	Thermocouple
		4.3	COF	μ
		4.4	Gantry dimensions to fit within Lisport XL	1.1 – 1.34 m
		4.5	Additional metrics to inform on skin injury risk	TBD

CHAPTER 3

Establishing Design Parameters

SKIN INJURIES

Through interactions during game play in rugby

3.1 Introduction

The literature review has established the current state of the art for the most advanced artificial pitches and delved into the current testing procedures. The necessity for a novel test apparatus to assess the potential risk of skin injuries on artificial turfs is underscored by the continued prevalence of injuries and the evident disparity between players' perceptions and reported incidence rates. The literature review has also brought to light a significant gap in essential biomechanical data about injurious interactions, which is a crucial factor hindering the development of a robust test method replicating an in-game scenario. Therefore, this chapter introduces a conceptual framework of experimental studies, a pivotal step towards addressing this gap. These preliminary studies aimed to establish a comprehensive rationale for refining the undefined design specifications of the new test method. This initiative was accomplished by delving into the principles underlying each experimental approach and justifying how these approaches align with the objectives outlined within the scope of the thesis.

The framework encompasses macro-scale and micro-scale studies, which are designed to investigate the following key areas thoroughly. These studies are aimed at enhancing the understanding of injury mechanisms and informing the development of standardised test methods, ensuring the validity and reliability of this research. The aims of this chapter are:

1. Capture players' perceptions to understand the skin injury problem on artificial turf comprehensively.
2. Quantify the incidence rates and severity of skin injuries on rugby turf to build upon the insights gained from players' perceptions.
3. Utilise video analysis of injurious interactions to derive data-driven biomechanical simulation characteristics based on the injury incidence and severity study findings.
4. Establish accurate loading conditions during the sliding phase to realistically simulate real-world scenarios on artificial turf.
5. Investigate the mechanical and thermal properties of Lorica Soft to understand its behaviour under various conditions and its potential impact on skin injuries.

Figure 3-1 visually depicts the flow of the conceptual framework, emphasising the connections between studies and objectives.

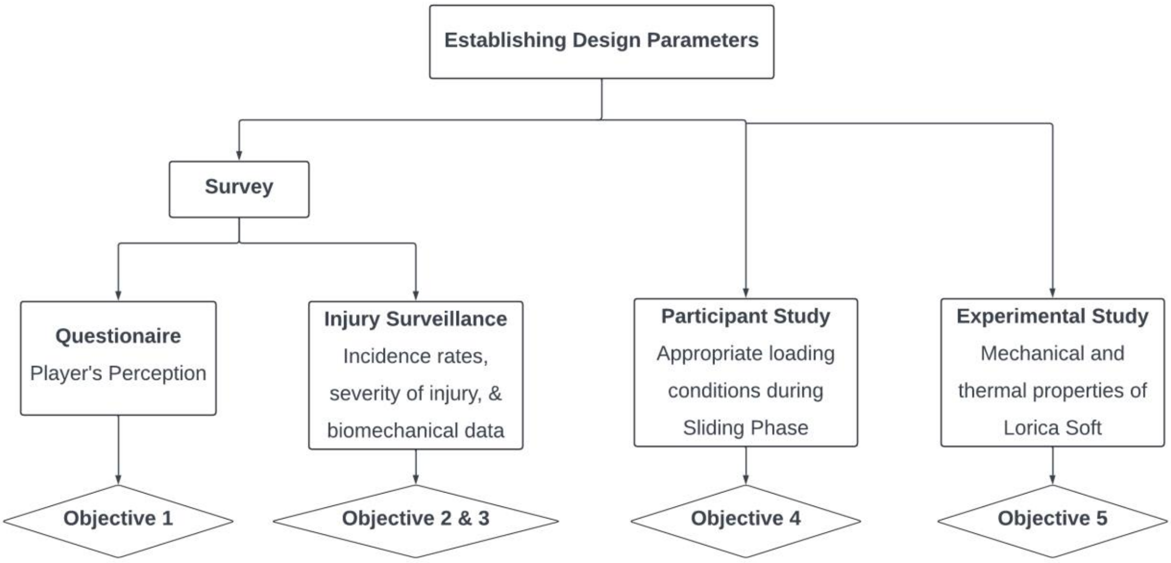

Figure 3-1: Illustration of the framework for establishing the design parameters

3.2 Background

3.2.1 Questionnaires

A *survey*, a crucial primary research tool, collects data from a group of people, providing invaluable insights into trends within the population. At the onset of a research project, surveys are cost-effective and easy to perform, yet they yield substantial information that aids in comprehending the reviewed literature. Depending on the survey type, qualitative and quantitative data can be recorded through various question types – multiple choice, dropdowns, ranking, Likert scale, open-ended, and more – all of which can be customised to meet the researcher's requirements.

Survey questions consist of three categories: descriptive, casual, and exploratory research. Descriptive research collects quantitative data to infer information about a population statistically. This research typically utilises structured questions, such as multiple choice or rank, to define a group's opinions, attitudes, or behaviours. Meanwhile, causal research also collects quantitative data, investigates cause-and-effect relationships, and requires experimental design to explain the relationship between variables. On the other hand, exploratory research discovers insights and ideas, often through probing open-ended questions, to fully understand the problem or determine the reasons behind an outcome.

This qualitative data provides valuable information for understanding perceptions better. However, data collection and analysis require more time than the quantitative methods. Understanding these research methods is essential for designing effective surveys for their specific purposes.

Survey questions, when crafted with clear and concise language, ensure that respondents grasp the intended meaning, while avoiding leading questions that could sway the answer. Vague or ambiguous questions can lead to different interpretations, resulting in diverse answers. The order and structure of the questions are also crucial for obtaining meaningful data. The initial questions should engage the respondents, providing context for the subsequent ones. Moreover, questions should gauge the respondents' experience level to assess the validity and reliability of the answers. The survey length should be considered to prevent rushed or incomplete responses. Despite the apparent simplicity of a survey, the accuracy of the data can vary if participants are not forthcoming due to the anonymity when submitting answers. The survey should also adhere to ethical considerations, such as obtaining informed consent, ensuring confidentiality, and allowing respondents to withdraw.

3.2.2 Observational Studies

An observational study is a different research survey that collects facts and figures obtained through visual inspection. This type of study should capture the subject's natural behaviours whilst focusing on minimising the influence of artificial settings. The data collected is typically qualitative since the researchers merely observe and record what naturally unfolds. However, quantitative data can still be gathered. The qualitative data would consist of descriptions of participant patterns and interpretations of observed behaviours. In this case, quantitative data will be collected, including incidence rates and injury severity.

Injury surveillance studies have associated earlier generations of artificial turf with an increased risk of skin injuries due to their abrasive characteristics [187], [188]. Despite design improvements incorporating longer fibres and softer performance infill to mimic natural grass better. A persistent fear of injury is associated with 3G surfaces.

To prevent inconsistencies in reported data and improve the reliability of interstudy comparisons, the International Rugby Board (IRB), now rebranded as World Rugby, established a consensus statement on injury definitions and data collection procedures of injuries in rugby [3]. The paper presented the following definitions:

> *"Any physical complaint, which was caused by a transfer of energy that exceeded the body's ability to maintain its structural and/or functional integrity, that was sustained by a player during a rugby match or rugby training, irrespective of the need for medical attention or time-loss from rugby activities. An injury that results in a player receiving medical attention is referred to as a 'medical-attention' injury and an injury that results in a player being unable to take a full part in future rugby training or match play as a 'time-loss' injury."*

Skin injuries are minor; therefore, they are regularly not accounted for in major injury studies that adopt 'time-loss' or 'requires medical attention' injury definitions. The omission of 'any physical harm' as an injury definition contributes to underreporting skin injuries [4]. Due to the game's physical nature, the Rugby Injury Consensus Group (RICG) anticipated that most rugby studies would record time-loss injuries. During this study, however, '*any physical complaint*' was the selected injury definition due to the high number of minor skin injuries that would not be recorded by the '*time-loss'* criteria.

Due to the game's physical nature, the Rugby Injury Consensus Group (RICG) anticipated that most rugby studies would record time-loss injuries. During this study, however, '*any physical complaint*' was the selected injury definition due to a high number of minor skin injuries that the 'time-loss' criteria would not record.

The RICG guidelines recommend that injury surveillance studies follow more than one team for at least one year or during a major tournament. At the same time, they advise that any study should not use mixed definitions to simplify any retrospective analysis comparisons. In sports, injury incidence rates are typically reported as the number of injuries (n_i) per 1000 hours of player exposure (E) (Equation 5). Where total exposure time is expressed as the product of the number of matches (M), the number of players on the pitch (P), and the duration of the match (D – hours) (Equation 6).

Equation 5: Injury Incidence Rate (IIR)

$$\mathrm{IIR} = \frac{\mathrm{n_i}}{\mathrm{E}} \times 1000$$

Equation 6: Total Exposure (E)

$$E = M \times P \times D$$

The available literature which adopted appropriate injury definitions was typically limited to football, where the overall injury rates were lower than expected, ranging from 1.0 – 3.11 per 1000 hours of player exposure [130], [134]. However, Williams et al. (2015) [7] conducted a season-long study in the English Rugby Premiership to investigate the influence of playing surface on injury rates. They concluded that skin injury risk was almost eight times higher on artificial turf (119 per 1000 hours of player exposure) than on natural grass (15 per 1000 hours of player exposure). These findings shed light on the extent of the skin injury problem in rugby. However, further research is required to understand better the notable gap between the perception of skin injury risk and the documented incident rates.

3.2.3 Skin Damage and Severity Index (SDASI)

Eijnde et al. (2014) [156] developed a non-invasive dermatological tool for evaluating a skin lesion. An involved area score complemented the sum of three clinical parameters to quantify damage and severity (Equation 7).

Equation 7: Skin Damage and Severity Index (SDASI)

$$SDASI = (A + E + TE) \times I_A$$

Where - A: abrasion; E = erythema; TE = type of exudation; I_A: involved area.

The paper provided a visual reference scale to rank the individual damage characteristics independently. Both abrasion and erythema were rated from 0 (no damage) to 4 (very severe) whilst the type of exudation was assessed by selecting one of the following weightings: dry skin (0), transparent fluid (1), blood (2). The involved area was represented as a percentage of coverage over a 60 cm^2 area (Equation 8). A transparent sheet containing a grid (1 cm x 1 cm) was used to count the number (n) of grid boxes covered by the lesion.

Equation 8: Involved area calculation.

$$I_A = \frac{n}{60\ cm^2} \times 100\%$$

The following numerical value is given to the relative involved area and applied to Equation 7 to calculate the overall SDASI [0 = no involvement, 1 ≤ 10%, 2 ≥ 10% but < 30%, 3 ≥ 30% but < 50%, 4 ≥ 50% but < 70%, 5 ≥ 70% but < 90% and 6 ≥ 90%].

3.3 Materials and Methods

In this section, the framework was divided into four separate studies, and each focused on investigating and establishing:

1. Players' perception of the skin injury problem on Rugby Turf
2. The true extent of the skin injury problem on Rugby Turf
3. Appropriate loading conditions during the Sliding Phase
4. Mechanical and thermal properties of Lorica Soft

3.3.1 Players' perception of the skin injury problem on Rugby Turf

This study, which consisted of a questionnaire, aimed to contribute to the current literature by capturing the opinions of amateur and elite rugby players towards skin injuries on Rugby Turf. The theoretical aspects of a survey, discussed in Section 3.2.1, highlighted that this study should primarily focus on descriptive research intertwined with several casual and exploratory questions. This combination would provide sufficient data to understand better players' perceptions of interactions resulting in skin injuries during match play. This information will be vital for providing rationale when selecting the desirable characteristics to simulate a potentially injurious interaction. The first eight questions, presented in Table 3-1, were designed to capture data describing player status and playing experience. The following six questions explored skin injury history, perceived traits of injurious player-turf interactions and properties. The questionnaire concluded with a free text question, encouraging participants to describe interactions they think are most injurious. This study was approved by Cardiff University's School of Engineering Ethical Approval Committee. The questionnaire was then circulated as a Google survey via the Scottish Rugby Union's social media channels.

Table 3-1: Questions Exploring Player's Perceptions of Rugby Turf

1. Gender
i) Female ii) Male iii) Other
2. Age
i) 18 – 22 ii) 23 – 27 iii) 28 – 32 iv) > 32
3. Height
i) < 159 ii) 160 – 169 iii) 170 – 179 iv) 180 – 189 v) 190 – 199 vi) > 200
4. Weight
i) < 59 ii) 60 – 69 iii) 70 – 79 iv) 80 – 89 v) 90 – 99 vi) 100 – 109 vii) 110 – 119 viii) > 120
5. Position
i) Front Row ii) Second Row iii) Back Row iv) 9 / 10 v) Centre vi) Wing vii) Fullback
6. Club
* Short Answer Text *
7. How often do you play/train a week?
i) Monthly ii) Fortnightly iii) Weekly iv) Twice a week v) Three times a week vi) > Three times a week
8. What percentage of training/games do you play on artificial pitches?
i) 0% ii) 0 - 25% iii) 25 – 50 % iv) 50 – 75 % v) > 75 %
9. What surface do you think is more likely to produce a skin injury?
i) Artificial Grass ii) Natural Grass
10. Which artificial turf property do you think produces skin injuries?
i) Polymer Grass Fibre ii) Rubber Infill iii) Surface Temperature iv) Not Sure
11. Which body part do you think is most susceptible to receiving skin injuries? Choose one or more:
i) Elbow ii) Knee iii) Face iv) Forearm v) Thigh vi) Shin vii) Other
12. Choose an interaction that you think is most likely to produce a skin injury?
i) Ruck ii) Maul iii) Tackling iv) Tackled v) Sliding for a try vi) Going to ground to collect a loose ball vi) Other
13. Which of the following environmental conditions do you think are more likely to produce a skin injury? Choose one or more:
i) Dry ii) Wet iii) Cold iv) Hot v) Other
14. Which of the following term(s) do you think best describes any injuries you have experienced? Choose one or more:
i) Abrasion ii) Blister iii) Burn iv) Contusion v) Laceration vi) No injury vii) Other
15. Briefly describe the interaction with the surface which you think results in a skin injury?
* Long Answer Test *

3.3.2 True extent of the skin injury problem on Rugby Turf

The injury surveillance study was conducted at a major British 7s tournament providing the advantage of a high number of games throughout the day, combined with personal observations of high injury rates from the previous year, indicating a significant need for this research. The men's straight knockout tournament consisted of 24 teams, who played 23 games. The women's tournament was a round-robin format where each team played each other once for three games. Participants were recruited by collectively asking the teams after each game if they had "*any physical complaints*" regarding skin injuries. After each game, all consenting players were assigned an anonymous player ID. Each skin injury was photographed with the grid for the SDASI assessment. Additional information was collected to develop a player profile to help identify them during the games by completing a questionnaire (Appendix 1). This data included the specific match in which the injury occurred, the player's shirt number, their position on the field, and how they sustained the injury. Their role was specified if a tackle was identified as an injurious event (whether they were tackled or performing the tackle). At the same time, basic biomechanical data such as height and weight were recorded with a stadiometer (SECA) and electric scales (SECA), respectively.

Throughout the tournament, the surface temperature at the halfway line where the players enter the field was recorded every hour with a FLIR thermal camera. The broadcast footage from the tournament was used for video analysis to characterise the injury's motion profile and quantify the number of participants utilising preventative measures to mitigate skin injury risk, such as wearing leggings or Hypafix. Cardiff University's School of Engineering Ethical Approval Committee approved this study.

Pitch Condition Report

Within the last six months of the tournament, the Sports Labs field department recently performed a field test report as part of the mandatory retesting every two years to ensure pitches are still compliant with Regulation 22. The turf system consisted of a mix of sand and SBR within a 60 mm carpet with a shock pad base layer. The results from the field testing, presented in Table 3-2, demonstrated that the pitch complied with FIFA Quality Pro requirements, representing a state-of-the-art surface. The report commented that the pitch was in good condition overall despite some areas becoming flat. Additionally, there were concerns about the Head Impact Test as there were a few locations where the result met the minimum criteria.

Table 3-2: Field Test Report

Performance Characteristic	Test Result	Requirements
Free Pile Height (mm)	17	For information
Infill Depth (mm)	39	For information
Shock Absorption (%)	66 ± 0.2	60% - 70 %
Vertical Deformation (mm)	8.9 ±0.1	4 mm – 10 mm
Rotational Resistance (Nm)	30.8 ± 0.7	30 Nm – 45 Nm
Vertical Ball Rebound (m)	0.88 ± 0.02	60 cm – 85 cm
Ball Roll (m)	7.3 ± 0.1	4 m – 8 m
Head Impact Test (m)	1.30	≥ 1.3 m

Video Analysis Protocol: Identifying Injurious Interactions

Kinovea, a sports analysis software, was used to evaluate interaction conditions and better understand the injury. The pitch dimensions from the field test report, presented in Table 3-3, will be helpful during video analysis to establish distances covered by players.

Table 3-3: Pitch dimensions from observational study monitoring skin injury incidence rate

Parameter	Result	Units
Carpet Length	122.00	m
Carpet Width	78.00	m
Field of Play Length	100.00	m
Field of Play Width	68.00	m
In-Goal Length	6.00	m

Injurious interactions were identified by meticulously following each player and clipping every event where the player interacted with the turf. For each clip, three essential time indexes were identified: T1 – beginning of acceleration, T2 – initial contact with the surface, and T3 – end of the interaction. Clips for video analysis were only included if they had consistent footage from one camera angle between T1 and T3 and unobstructed views between T2 and T3. Appendix 2 - Appendix 22 contains screenshots of T1, T2, and T3, a diagram depicting these three locations on the pitch, and a photo of the injury for the interactions that met these criteria.

Video Analysis Protocol: Analysing Injurious Interactions

Time, distance, and speed were identified as the three main components required to provide quantitative insights into the characteristics of injurious interactions.

Time

To calculate the duration of T1 – T2 and T2 – T3, the number of frames between the interaction events was divided by 30 frames per second (FPS) since the footage was filmed at that rate.

Distance

Autodesk Inventor was used to create a 1:1 scale model of the pitch. Markers were placed at T1, T2, and T3 for each clip to generate a player's motion profile. This enabled the distance travelled by the players between the essential time indexes to be established.

Speed

By approximating distances travelled and calculating the duration between the essential time indexes, the player's speed was quantified using simple equations of motion (Equation 9).

Equation 9. Speed, Distance, Time

$$Speed = \frac{Distance}{Time}$$

Causative Factors Contributing to Skin Injury Risk

Further qualitative analysis generated interaction criteria to understand better causative factors contributing to skin injury risk. These criteria consisted of describing the dynamics of the interaction through an assessment of the player's level of control; inspecting the abrupt or fluid nature of the interaction; monitoring dissipation of energy; evaluating the angle of the joint at impact; assessing the position of the centre of mass (COM); and determination of the proportion of body weight through the injured location.

Situational Control

Being in control was qualitatively evaluated by establishing whether the player intentionally brought themselves to the ground in a controlled manner, such as exerting dominance in the tackle, scoring a try, or going down on a loose ball. In contrast, being out of control was classified as being dominated in the tackle or a consequence of altering their positioning, and the player finds themselves in a vulnerable or susceptible situation whilst attempting to complete a tackle.

Smooth or Abrupt Interactions

Injurious interactions were classified as either 'Smooth' or 'Abrupt'. A smooth interaction occurred when the player slid freely across the surface. In contrast, an abrupt interaction occurred when the player jolted due to experiencing a significant force on impact.

Angle of the Joint at Impact

If the anatomical location injured was a joint, the angle was recorded at T2. Kinovea's angle analysis tool was utilised to quantify the knee angle using the ankle and hip, while the wrist and shoulder served as reference points for the elbow.

Mass Distribution at Impact

The centre of mass, in relation to the impact at T2, was divided into three categories: in front, above, or behind.

Percentage of Body Weight during Impact

Calculating the percentage of body weight transmitted through the impact joint involved analysis of the points of contact with the turf during the impact. The value was a rough estimate used to improve the overall understanding of the interaction with the reader. An interaction with 100% of the body weight was identified if the injury location was the only part of the player in contact with the surface at T2. If two clear points of contact with the ground or the player supported themselves via another player during a tackle, it was deemed 50%. If there were three points of contact, it was deemed 33%, and if there were four clear points of contact, it was 25%. When a second player's weight was applied through the impact joint, it was deemed 125%.

3.3.3 Appropriate Loading Conditions during the Sliding Phase

This study was performed in Cardiff University's medical engineering Trauma Lab. A turf sample, 300 x 400 mm, was constructed on a 10 mm shock pad and a 60 mm carpet was filled with sand (15 mm) and SBR (25 mm) to produce a free pile height of 20mm. A force plate was located beneath the turf to monitor the loading conditions the player applied to the turf. Participants were requested to simulate a tackle technique whilst kneeling on the turf sample and utilising a Zimmer frame for stability, as illustrated in Figure 3-2. The force through the participant's knee was measured one at a time; therefore, foam blocks provided comfort whilst also making up the difference in height between the ground and the turf. During the measurement phase, participants were instructed to focus on equal weight distribution between both knees. Tests were performed three times on each knee, after which the surface was prepared. The Cardiff University's School of Engineering Ethical Approval Committee approved this study and recruited participants from the University's men's and women's rugby teams.

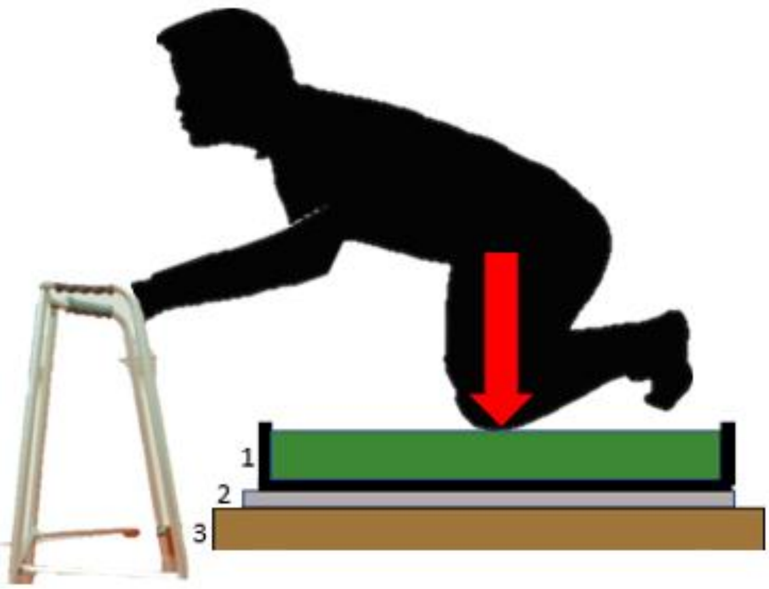

Figure 3-2: Schematic of Participant Testing Setup 1) Turf sample 2) Force Plate 3) Floor

3.3.4 Mechanical and Thermal Properties of Lorica Soft

Lorica Soft, obtained from the German wholesaler Ehrlich Leder, is a polyamide fleece with a polyurethane coating pressed with a template to produce a repeatable texture. Bruker's Contour Optical Profilometer assessed an untested sample to quantify the surface roughness of the material. Three samples were tested in three locations to assess how the surface roughness varied across the roll of material.

The dynamic nature of the skin injury risk assessment means that the skin will experience high shear forces. This force could stretch the skin, adversely affecting the kinematic data collected during the simulation. Tensile tests were performed to understand better the material properties, such as strength and strain. The skin was cut into dumbbell shapes where the narrowest section was 50 mm long and 26 mm wide, as presented in Figure 3-3. Five tests were performed on the machined and cross-direction of the fabric roll at 100 mm/min. The clamps were positioned at the top and bottom of the tested area, separating them by 50 mm, which was considered the *"zero"* point to measure the extension of the sample.

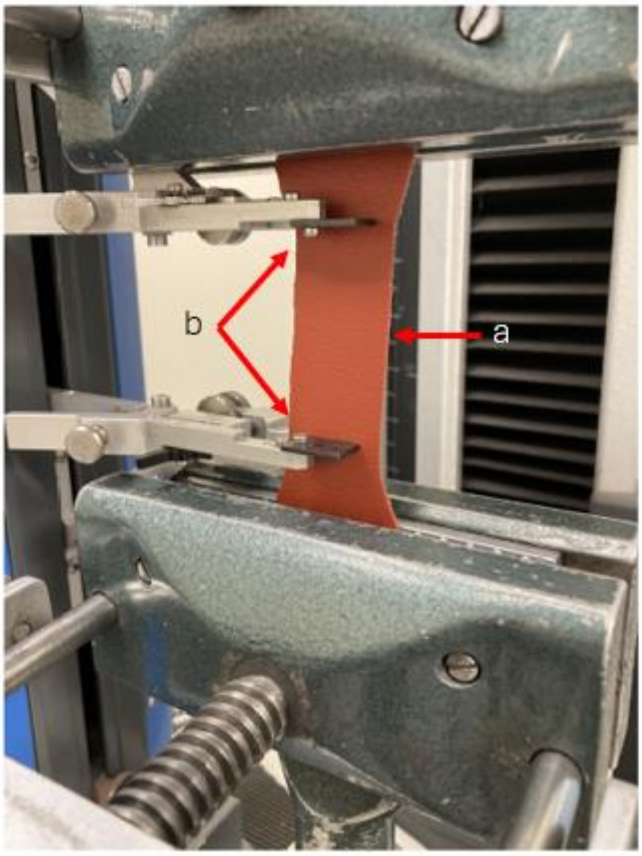

Figure 3-3: Tensile Testing on the Skin Simulant a) dumbbell shaped Lorica Soft b) clamps

Finally, the thermal conductance of the skin was analysed to assess how well heat transferred through the material. This investigation aimed to establish if heat transfer would be fast enough and to be of sufficient magnitude for thermocouples to provide suitable sensitivity when measuring temperature changes. The testing consisted of a sheet of Lorica Soft suspended in the middle of the lab. The polyamide coating of the skin will be the external test surface during the skin injury risk assessment. Therefore, a heat gun was directed at this side of the material for 90 seconds. The surface temperature was monitored on both the front (heated) and back (not heated) with two Micro-Epsilon thermal cameras equally positioned 1m away. The thermal camera recorded data at 60 Hz. Testing was repeated five times in a dark room to mitigate surface reflectiveness influencing results. TIMconnect software was used to monitor the infrared data by analysing two sections: the centre of the sheet (80 x 80 pixels) and a peak tracer (10 x 10 pixels), which followed the maximum temperature.

Statistical Analysis

T-tests were conducted to establish significantly different results for surface roughness and tensile test measurements. All statistical analyses were performed with Excel, adopting a significance threshold of $p < 0.05$.

3.4 Results

3.4.1 Players' perception of the skin injury problem on Rugby Turf

The questionnaire received responses from 430 participants (377 male), including 58 elite male players. Eighty-nine per cent trained/played at least twice a week, which provides confidence in the robustness of the collected data. Most participants (97.4%) perceived artificial grass as more injurious than natural grass, which agrees with previous literature [140], [190], [191]. The most common perceived injuries were abrasions (67.4%) or burns (74.2%). The majority (90.2%) identified that a dry environment was more conducive to producing a skin injury. This perception agrees with fundamental tribo-mechanical theories that mechanical abrasion and thermal build-up will increase without a lubricant. Despite most participants suggesting they had experienced burns, only 38.6% thought a hot environment would increase the likelihood of sustaining a skin injury. The ambiguity of the term ‘Turf Burn’, a common term used to describe injury in the rugby and football community, was attributed to this lack of consensus. Accordingly, the simulation should aim to better understand the mechanisms behind the injury by quantifying the mechanical abrasion and thermal induction experienced by the simulated player.

No consensus existed on which turf property was most likely to cause skin injuries; however, participants agreed that prominent bony joints were the anatomical location most susceptible to skin damage (elbows—69.8% & knees—92.1%). Williams et al. (2015) [7] reported incident rates of the knee (74%) and elbow (7%) abrasion injuries, confirming the perception of the knee being the most vulnerable body part. The majority (70.2%) identified that a situation involving a tackle would most likely produce a skin injury, whilst others thought sliding to score (12.1%) or when going to the ground to collect a loose ball (14.0%). This perception agrees with injury incident rates from a meta-analysis study suggesting that the tackle was the most dangerous phase of play [12]. Their study was not specific to skin injuries; however, utilising the time loss injury definition, they reported that the ball carrier was at higher risk than the tackler. In contrast, this survey reported that almost half of the participants (47.4%) thought the tackler would be more susceptible to sustaining skin injuries whilst tackling rather than being tackled (22.8%). Analysis of the qualitative data from the final question highlighted that the most likely causative player-turf interactions were “sliding”, “tackling”, and “tackled”, which agreed with the data from Question 12.

When forming conclusions from these results, player-player interactions must be considered. In rugby, the ball carrier is usually in control of the contact. The tackler will, therefore, need to respond to the ball carrier’s footwork when trying to evade the tackle. This movement can compromise the tackler’s technique, resulting in them reaching out or jumping to complete the tackle (Figure 3-4). Once the player commits to the tackle in a compromised position, they will no longer entirely control their legs until they contact the surface again. With the tackler’s arms involved in the tackle, their lower limbs are likely to be the first point of contact. The knee is a hinge joint, meaning that when it starts to flex, the skin becomes taut and closer to its failure limit. In combination with high pressures on a point load during a high-speed interaction, can explain why this anatomical location is most vulnerable. In contrast, being tackled was associated with more time-loss injuries. The high forces the ball carrier experiences during a dominant tackle or the result of the tackler landing on top of them could contribute to the more severe injuries reported.

Figure 3-4: Illustration of tacklers in compromised position, which increases chances of sustaining skin injuries - a) tackler airborne which could result in a point loading on the knee b) tackler being dragged by ball carrier resulting in a protracted slide [13].

In summary, this survey has successfully captured the opinions of amateur and elite rugby players towards skin injuries on Rugby Turf. As expected, most participants preferred natural grass; however, no consensus existed on identifying the artificial turf property most likely to cause skin injuries. The tackle was deemed the most dangerous phase of play, with the knee being the most vulnerable anatomical region. There were conflicting perceptions when comparing the type of injury acquired and environmental conditions conducive to sustaining a skin injury. This conflict highlights the term 'Turf Burn' ambiguity and warrants further investigation into the mechanisms behind the injury. In conclusion, the new test device should simulate a knee-turf contact and generate the forces a body would experience during a tackle whilst monitoring temperature rises and the abrasive nature of turf.

3.4.2 True extent of the skin injury problem on Rugby Turf

Ambient temperatures throughout the day were 12±1°C with a maximum surface temperature of 37°C at 2 pm. A total of 270 players competed in the tournament (240 male and 30 female). The average male was 183.5±0.9 cm with a body mass of 91.2±1.3 kg. The average female was 170.6±1.9 cm with a body mass of 68.9±2.2 kg. Of the 270 players, 1.5% wore leggings, 18.1% used Hypafix, a skin-friendly adhesive tape (Figure 3-5), and many used Vaseline to prevent skin injuries. Despite efforts to mitigate the risk of skin injury, 87 skin injuries (81 male | 6 female) were recorded during the tournament. This result equates to an injury incidence of 1078 and 612 per 1000 hours of player exposure for males and females, respectively. Skin injuries were most commonly experienced on the knee (65.5%), shin (10.3%), elbow (6.9%) and forearm (6.9%). The remaining 12.6% of injuries occurred on the hip, thigh, wrist, nose, and buttock.

Figure 3-5: Effectiveness of Hypafix as a protective layer to prevent skin injury risk
a) knee covered in Hypafix b) area of skin damage significantly reduced due to protective layer

Following the general data protection regulations guidelines, three male players with nose injuries were excluded from the SDASI analysis to protect their anonymity and privacy. From the remaining 84 incidents, SDASI scores ranged from 3 to 42, where the average was 18.7±1.1 and 17.2±3.7 for males and females, respectively. Unfortunately, technical issues with the live stream prevented some game analysis. Consequently, only 25 interactions complied with the inclusion criteria for video analysis (Appendix 2 - Appendix 22). All the eligible participants were male, and the average SDASI was 23.9±1.9. Appendix 23 presents all reported skin injuries and the corresponding SDASI scores.

Most (92%) of the analysed injurious interactions occurred during a tackle and were deemed out of control. The two incidences that were in control occurred while scoring a try. This result, combined with the knee being the more vulnerable anatomical location, agrees with the results from Part 1 of the survey. Results from the video analysis reported an average impact velocity of 5.65±0.20 m/s. The linear regression analysis indicates that the severity of damage increases by a factor of 4.2 with respect to velocity (Figure 3-6).

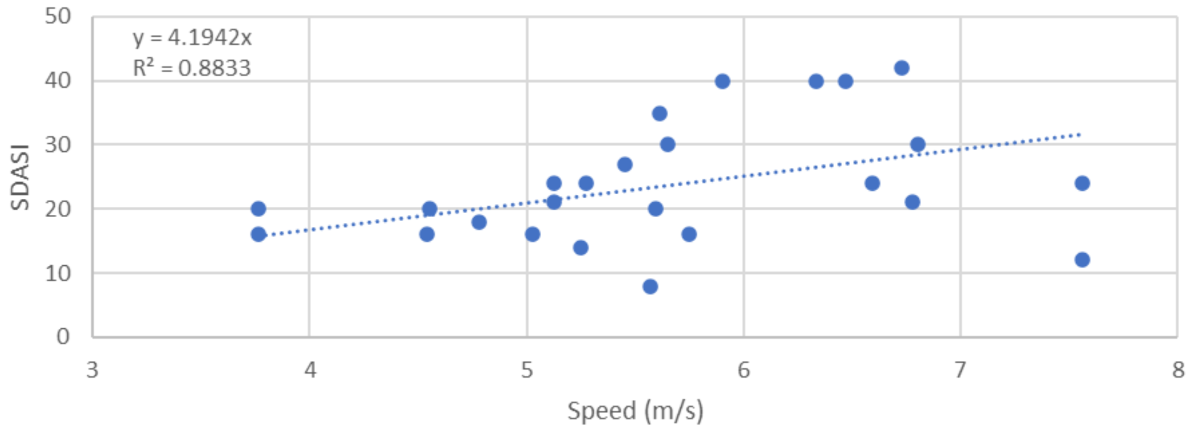

Figure 3-6: Relationship between impact velocity and SDAS where the linear regression through the origin indicates that severity of injury increases by a factor of 4.2 with respect to velocity.

The average sliding distance was 1.9±0.3m. No apparent trends were identified when analysing the linear regression of sliding distance and SDASI scores (Figure 3-7).

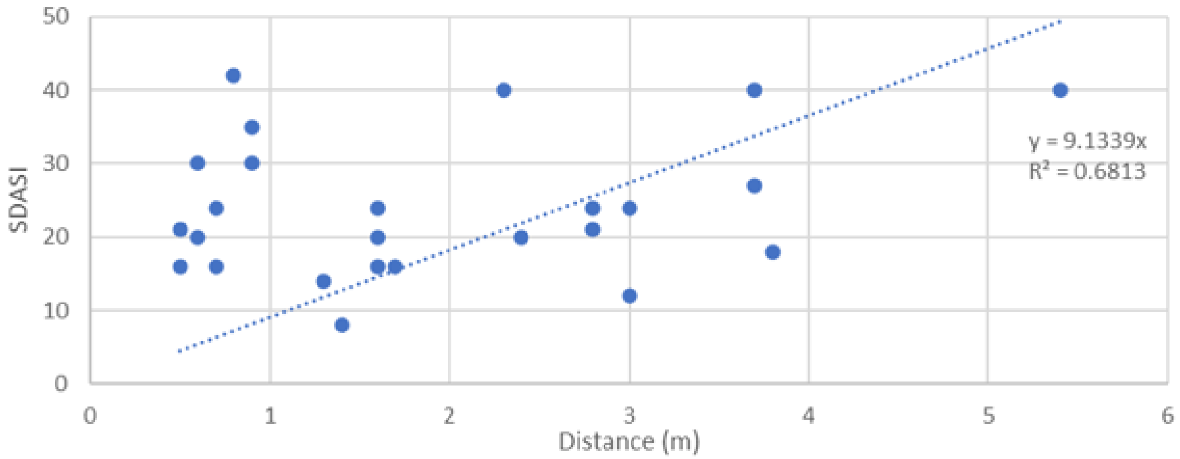

Figure 3-7: Relationship between sliding distance and SDASI where the linear regression is applied through the origin.

However, when contrasting the outcomes of abrupt and smooth interactions with varying sliding distances, a noticeable disparity in the rate at which the SDASI increased became apparent (Figure 3-8). The abrupt and smooth interactions produced average sliding distances of 0.7±0.1m and 2.6±0.3m, respectively, with corresponding SDASI scores of 26.0±3.0 and 22.8±2.5. The linear regression analysis indicates that the severity of damage increases by a factor of 37.8 concerning sliding distance for abrupt interactions compared to a factor of 8.1 for smooth interactions.

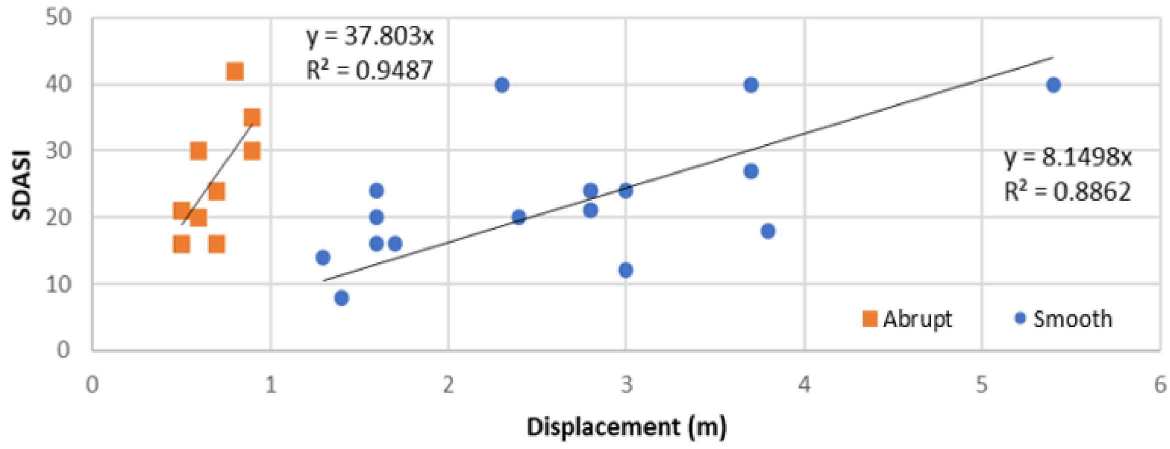

Figure 3-8: Monitoring the influence of interaction dynamics on SDASI. Where Abrupt interaction exhibit a more rapid increase in SDASI compared to Smooth interactions.

Four participants were excluded from the joint angle analysis since the view was as if the injured area was not a joint or the view was obstructed during impact. No clear trend was identified during the analysis of the joint angle at impact (Figure 3-9). Further analysis separated the joint angle into two categories: acute (<90°) and obtuse (>90°). The average impact angle was 59±5° and 135±7° for the acute and obtuse categories, respectively. On average, acute impact angles generated greater SDASI (24.0±28) than obtuse impact angles (21.1±2.4). Despite no statistical significance to the result, a visual inspection reported that the acute injuries appeared more severe.

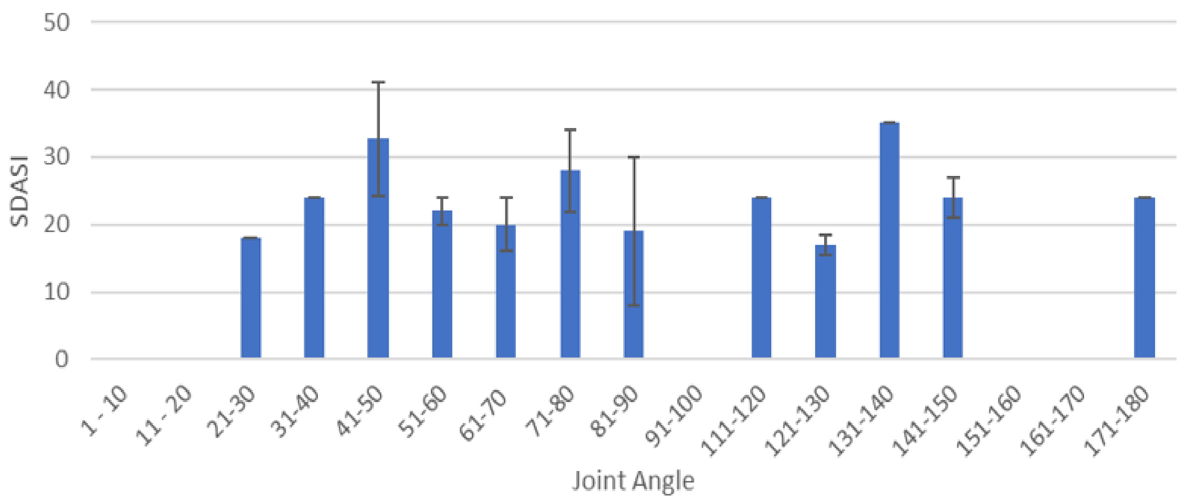

Figure 3-9: Monitoring the influence of joint angle during impact on SDASI.

Figure 3-10 presents a box plot of the SDASI scores for three different distributions of COM. The boxes indicate the interquartile range and median, with X indicating the average. The T-bars at both ends of the box represent the maximum and minimum scores. Skin injuries (68%) commonly occurred when the COM was perceived to be above the injured area. This type of interaction produced the greatest range of SDASI scores (8 to 42). Interactions where the COM was in front of the injured player were less common (24%). These injuries were associated with players reaching to complete a tackle. There were two interactions (8%) where the COM was behind the point of contact associated with elbow injuries.

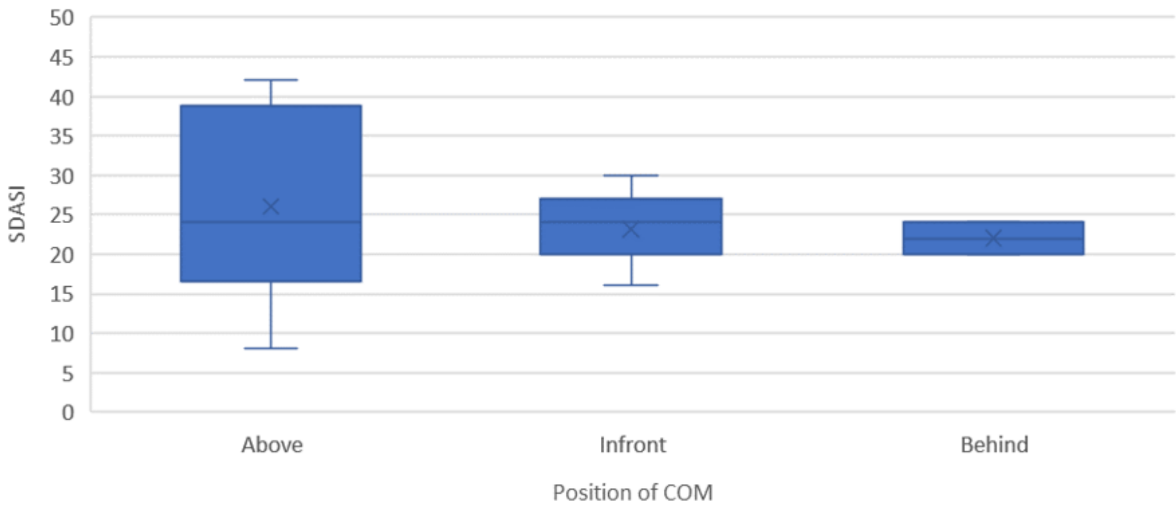

Figure 3-10: Monitoring the influence of mass distribution on SDASI.

A distinct trend was observed, demonstrating that an increasing percentage of body weight applied through the injured area corresponded to greater SDASI scores (Figure 3-11).

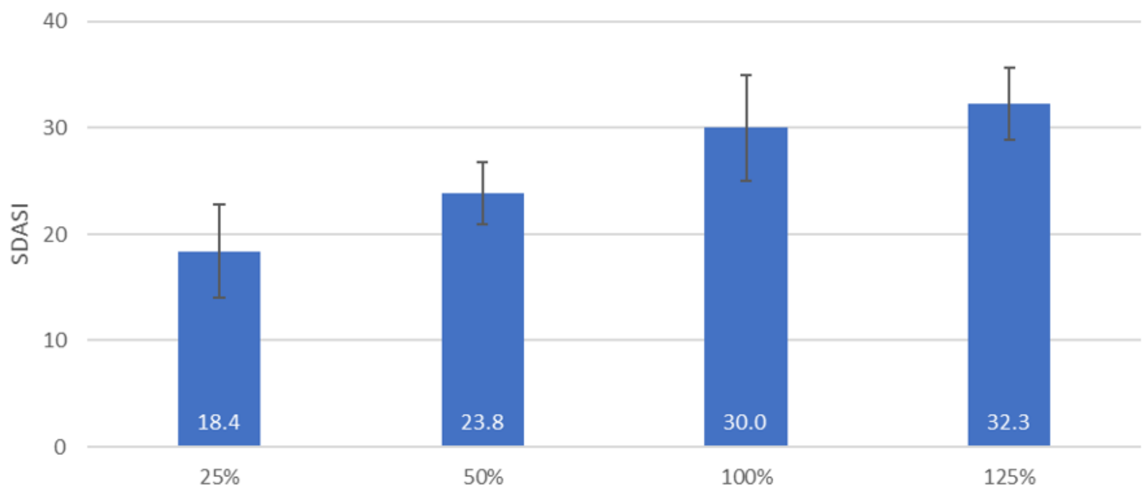

Figure 3-11: Influence of Percentage of Body Weight applied during Impact on SDASI.

3.4.3 Establishing Realistic Loading Conditions during the Sliding Phase

There were 76 participants with an average age of 21 ± 0.21, ranging from 19 to 31. The average height and weight of the 55 male participants were 1.81 ± 0.01 m and 82.7 ± 1.8 kg, respectively. The average female was 1.66 ± 0.02 m and 64.4 kg, respectively. Most participants were right-foot dominant, while 9% of males and 5% of females were left-footed. The average body-weight ratio applied to the turf was 31.8% while simulating a tackle. Both male and female participants applied a more significant percentage of their body weight through the right knee (Figure 3-12).

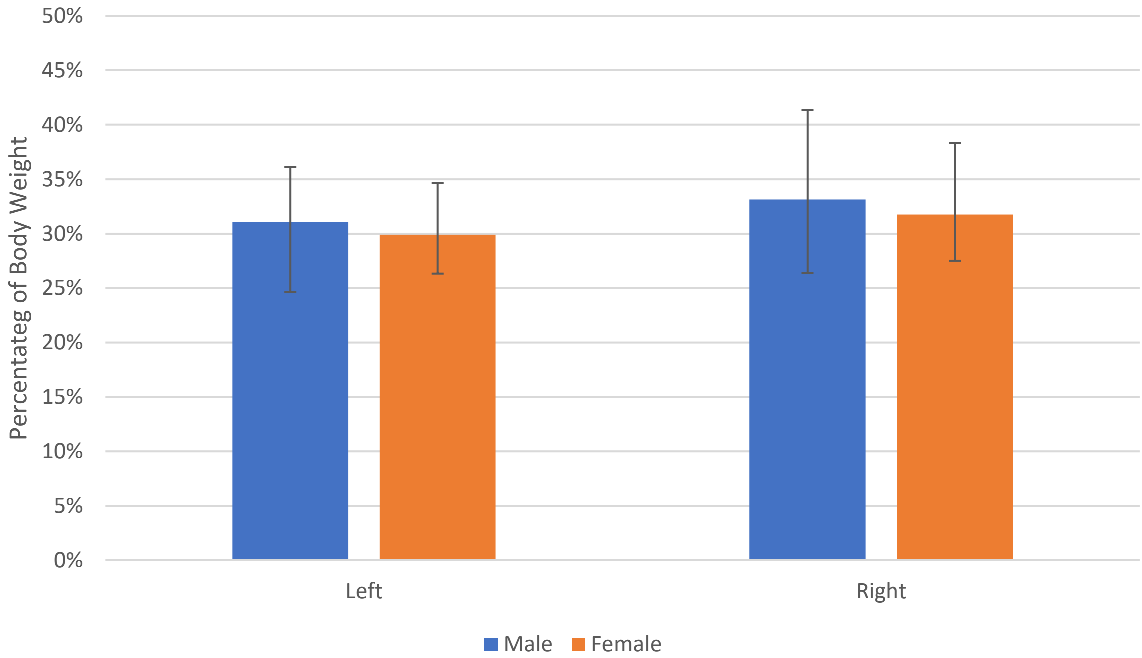

Figure 3-12: Comparison of percentage body weight applied through left and right knee during a simulated tackle with maximum and minimum error bars.

3.4.4 Investigating the mechanical and thermal properties of Lorica Soft

Bruker's Contour Optical Profilometer created a 3D profile of the skin (Figure 3-13). The analysis reported a mean surface roughness of 10.55±1.62μm for the untested area of skin (5.2x6.1 mm). The three samples had no statistical significance ($p > 0.05$), confirming that the surface roughness is consistent across the roll of material.

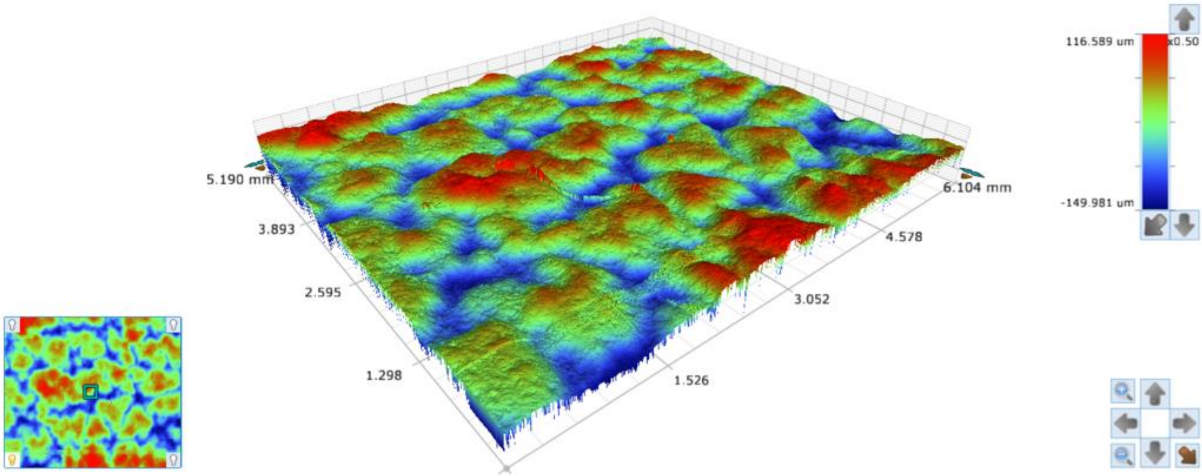

Figure 3-13: Surface Roughness Assessment of Lorica Soft

The tensile strength of Lorica Soft showed a significant increase ($p < 0.05$) in the machined direction (446.4 ± 8.2 N) compared to the cross direction (371.6 ± 8.8 N). This substantial difference in strength is a key finding of this study. Similarly, the strain, reported as elongation percentage, significantly decreased ($p < 0.05$) in the machined direction (124.4±3.2%) compared to the cross direction (146.1±8.9%). These results underscore the importance of considering the machining direction in the material's performance.

Figure 3-14 presents a novel observation of the thermal behaviour of the Lorica Soft sample. It illustrates the typical thermal build-up between the sample's front (heated) and back (not heated). The initial surface temperature for all samples was 24.8±0.2°C. After 90s heat exposure, the average maximum temperature on the front of the sample was 40.5±1.3°C. Interestingly, the maximum temperature (37.6±0.8°C) monitored on the back of the sample peaked at 93±0.6s, indicating a thermal gradient within the material. This outcome corresponds to a 7.7% lower peak temperature than the front, a significant difference that warrants further investigation.

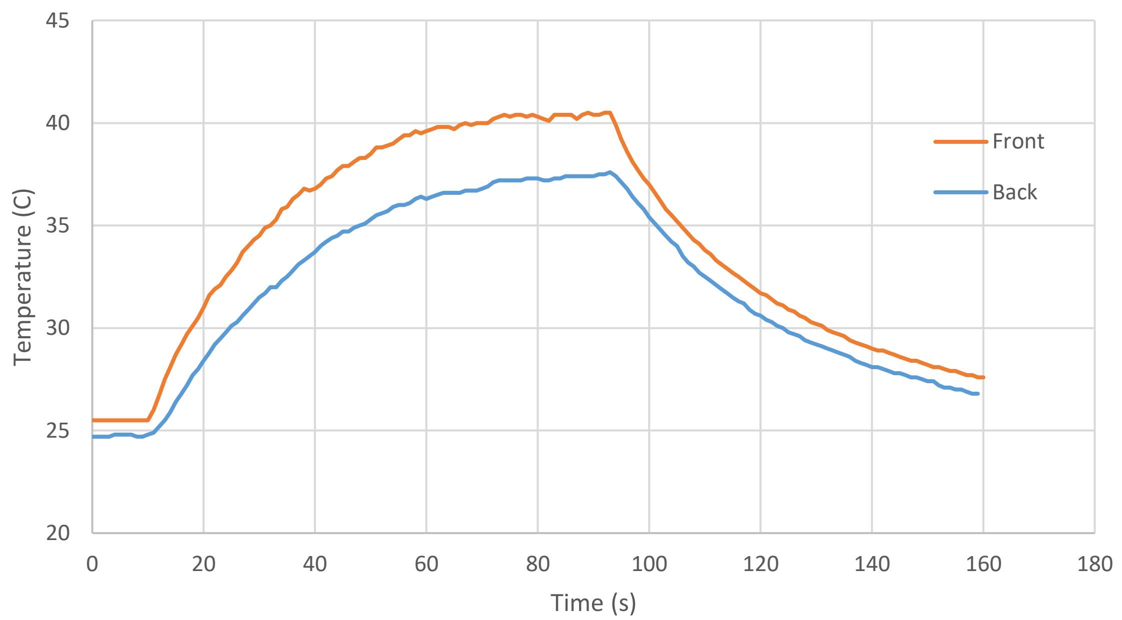

Figure 3-14: Assessing thermal conductivity of Lorica Soft, where the peak temperature was 40.5°C and 37.6°C for the front and back, respectively.

3.5 Discussion

3.5.1 True extent of skin injury problem on Rugby Turf

This study reported higher injury incidence rates than previous studies [187], [188]. This outcome was attributed to the differences in rugby codes. The combination of reduced team size and a faster-paced game, in 7s compared to 15s, resulted in more frequent interactions with turf at high speed [194], [195]. Additionally, the increased defensive responsibilities in 7s, which demand players to cover more ground, occasionally placed them in situations where they had to compromise control to complete tackles. Furthermore, the high intensity of the games would stimulate physiological responses to increase skin hydration [196], [197], contributing to higher skin friction [13], [21], [198], [199], [200], [201]. However, it was postulated that the low ambient temperatures would not promote excessive sweating. Hydrated yet unprotected skin (lacking sweat as a lubricant) could make players more susceptible to injury in this unique scenario.

Figure 3-5 highlights the benefits of utilising protective layers as a preventative method to reduce skin injury risk significantly. Almost 1 in 5 players wore Hypafix, meaning the skin injury incidence rates could have been higher if those players had not worn the protective layer. Hypafix, an adhesive tape, is typically used as an anchor when strapping injured body parts to prevent the tape from slipping off sweaty skin. Players used it to cover susceptible areas like elbows and knees to prevent skin injuries. Alternatively, medical staff applied it to provide a sterile environment by keeping dressings in place, reducing the risk of infection in previously injured areas. Quantifying the total number of players applying Vaseline from the video analysis was impossible. However, it was assumed from visual observations during interviews that most players were applying a topical lubricant to minimise the risk of injury. One team even applied cow udder cream. Their physio's rationale for this was that the cream contained Linalool. This natural terpene compound has soothing and anti-inflammatory properties, which may alleviate redness and discomfort [24].

The video analysis reported that skin injuries occurred over a range of velocities from 3.75 m/s – 7.56 m/s. However, no specific parameter directly linked to the severity of the injury was identified. Therefore, it was assumed each injury was unique and occurred due to a combination of various factors. Applying the average SDASI score of 24.4±1.9 to the linear regression through the origin in Figure 3-6 suggested that the ideal conditions to simulate an injurious interaction in a standardised test method would be 5.35 m/s – 6.26 m/s. Until now, literature quantifying the impact velocities of injurious interactions in rugby has yet to be published. Therefore, this unprecedented data significantly contributes to a better understanding of the conditions in which skin injuries occur.

A player will interact with the surface during a tackle or intentionally ground themselves to collect a loose ball or score a try. In all scenarios, their speed will be significantly reduced upon impact due to the collision of the tackle, or they will no longer be propelling themselves when airborne. Therefore, it is unrealistic for the player to interact with the turf at maximum velocity. During the development of the SID, the desired simulated horizontal impact velocity was reasonably reduced to 5 m/s. Although the range identified in this study was slightly higher, it was concluded that a velocity of 5 m/s remained within the acceptable range.

The video analysis identified abrupt and smooth interactions as two motion profiles when players sustained skin injuries (Figure 3-8). Abrupt interactions resulted in the player visibly jolting on initial contact, which was attributed to higher impact decelerations. In contrast, smooth interactions were associated with longer contact time, exposing the player to a more significant accumulation of resistive forces, ultimately increasing the risk of injury. The contrast in the rate of change of the SDASI, concerning sliding distance, between abrupt and smooth interactions implies two distinct injury mechanisms in operation. Abrupt is an interaction with a high rate of energy transfer. In contrast, smooth interactions were associated with a protracted slide, describing it as an interaction with a high impulse. The new standardised test device should evaluate the magnitude of impact decelerations and quantify sliding dynamics, such as slide resistance and resulting displacements, to provide a comprehensive assessment.

No clear trend for a specific joint angle that generated the greatest SDASI scores was identified (Figure 3-9). Acute joint angles (<90°) were more prevalent, accounting for 60% of the cases, and typically yielded higher SDASI scores (24±2.8) compared to obtuse angles (>90°) (21.3±2.4). The result's significance was trivial, which was attributed to the small sample size. The skin will be taut across the knee during an acute impact angle, making it less malleable. Tighter skin will require less strain for the tissue to reach its failure point [25]. Therefore, it was expected that acute joint angles to be more susceptible to injury.

The majority of harmful interactions (64%) occurred when the player's centre of mass was situated above them (Figure 3-9). A detailed analysis compared joint angles and mass distribution, which revealed a significant correlation. Specifically, acute angles were linked with the centre of mass situated above, potentially increasing the severity of injuries. Conversely, obtuse angles were associated with a centre of mass in front of the player, a circumstance in which the player's momentum heightens the risk of skin injuries.

Further qualitative analysis for this dataset involved an examination of the motion profiles observed when players sustained skin injuries. In each instance, the motion profile was simplified into three distinct events: 1) attaining velocity, 2) experiencing an Impact Zone, and 3) entering a Sliding Phase. This categorisation aligns with the findings from previous literature [141], [142], [143]. The four interactions that generated SDASI scores exceeding 40 were further scrutinised to better understand the kinematics of a severe injury.

Incident 1 (Appendix 2) corresponds to the SDASI with a sliding distance of 0.8 m (Figure 3-8). During this interaction, the player attempts a tap tackle, which results in his entire body weight loaded through his knee. This high-force contact, combined with a short sliding distance, indicates that the body has experienced a significant and abrupt deceleration, resulting in a severe skin injury.

Incident 3 (Appendix 3) corresponds to the SDASI with a sliding distance of 5.4 m (Figure 3-8). During this interaction, the ball carrier receives the ball in open space and accelerates down the wing. The defender is running back to make a cover tackle. With both players running at speed in the same direction, their momentum generates a long, protracted slide with the knee in constant contact with the surfaces. Consequently, the considerable sliding distance contributes to a large wear volume.

Incident 4 (Appendix 4) corresponds to the SDASI with a sliding distance of 2.3 m (Figure 3-8). During this interaction, the player attempts a tackle from behind, preventing the player from progressing up the pitch. With the tackler's arms around the ball carrier's waist, he stops running and looks for an offload. To bring the effectively static ball carrier to the ground, the tackler pivots around him with his knee/shin in contact with the surface. By performing this task, the player generates an acceleration during the Sliding Phase, applying most of his body weight through a small area to create a severe injury.

Incident 5 (Appendix 5) corresponds to the SDASI with a sliding distance of 3.7 m (Figure 3-8). During this interaction, the ball carrier runs across the pitch whilst being chased by the covering defender. As the ball carrier tries to evade the tackle, he lands on top of the tackler but remains in a position where he can run. With the defender committed to the tackle, he maintained a tight hold on the ball carrier, dragging himself across the surface. The combination of a force greater than body weight and being dragged across the surface resulted in a severe injury.

In Incidents 4 and 5, unique interaction characteristics were observed as the only players to experience an extra horizontal force in addition to their momentum during the Sliding Phase. This phenomenon resulted in severe injuries. However, the limited sample size hinders the development of a standardised test to assess skin injury risk and provide a quantifiable rationale for defining the magnitude and timing of the additional force generated during the sliding phase.

Most of these injuries occurred during a natural deceleration, aligning with the recommendations by Tay et al. (2017) [28] for developing a new test method to assess skin injury risk. Additionally, a distinct trend demonstrated that a more significant proportion of the player's body weight applied through a small area would be associated with greater SDASI scores (Figure 3-11). As a result, the standardised test method should be designed to simulate a situation involving the momentum of two players with a natural deceleration.

It is essential to acknowledge the limitations of this study, which include data collection and analysis techniques. The sample size of analysed interactions compared to incidence rates was low due to technical issues experienced whilst broadcasting the tournament. Intermittent glitches occurring during specific segments of the games have compromised the integrity of the analysis, rendering it ineffective for drawing meaningful conclusions. Despite best efforts to obtain the raw video footage from each camera angle, the tournament organisers only supplied the broadcast footage, which consisted of one continuous film with changes in camera angle. Altering the perspective is undesirable during video analysis as the footage is not guaranteed to sync. Consequently, the player's position may vary during the transition between camera angles, influencing the velocity calculations. The velocities calculated represented the player's average speed over the distance travelled. Future work should calculate instantaneous velocities better to understand the player's motion profile throughout the interaction.

In summary, the study attributes the high incidence rates of skin injuries in rugby 7s to increased defensive responsibilities and the game's fast pace. Protective clothing can help mitigate skin injury risk. Impact velocities ranging from 3.75 to 7.56 m/s resulted in SDASI scores from 3 to 42, with each interaction being unique. Regression analysis recommends a simulated impact velocity of 5.35 – 6.26 m/s. Although 5 m/s was deemed acceptable for the new test method. The findings offer valuable insights into injury mechanisms, identifying the Impact Zone and Sliding Phase as critical. Interactions involving the momentum of two players tended to yield higher SDASI scores, suggesting simulation of these scenarios in the new test method. These findings underscore the need for further research to advance injury prevention and player safety in rugby 7s and 15s.

3.5.2 Appropriate Loading Conditions during the Sliding Phase

In this study, the participants consistently applied a greater body weight ratio on their right knee than the left. It was assumed that this variation was due to the biomechanical tendency to favour the dominant foot. The smaller error bars associated with female participants on Figure 3-12, indicates a higher degree of consistency with the pressure they applied. This finding suggests that female players had a more uniform weight distribution during the simulated tackle. The most extreme body weight ratios, 24.6% and 41.3%, were observed on a male participant's left and right knee, respectively.

Given the limited data available to define the forces and phases of an injurious player-surface interaction, the simulation needed to represent a worst-case scenario. The dynamic nature of the Impact Zone was expected to generate vertical forces significantly more than the player's body weight. In contrast, the Sliding Phase was anticipated to generate the most significant sliding distance - both factors known to contribute to wear volume due to the short duration of the Impact Zone, which is a function of the turf system in use, and the protracted measurement period characterising the Sliding Phase. This approach was necessary to ensure that the forces generated during the Sliding Phase closely mirrored real-world conditions, thus facilitating the worst-case scenario simulation.

Considering the current test method predicts skin injury risk by calculating COF, the impactor must maintain constant contact with the turf during the Sliding Phase. This requirement was designed to ensure the vertical loading was greater than zero, as this condition would invalidate the COF calculation. As a result, it was anticipated that the vertical loading during the Sliding Phase would be equivalent to the impactor's mass. When translating the loading conditions recorded during the simulated tackle to an elite player (108.0 kg & 187.6 cm) [29]. The impactor's mass would be 26.6-44.6kg. This information provides a practical understanding of the forces involved in player-surface interaction.

3.5.3 Mechanical and Thermal Properties of Lorica Soft

In a recent study, Maiti et al. (2020) [30] observed that the surface roughness of *in vivo* skin varied with anatomical location. Ranging from 2.7 to 3.3 μm for load-bearing areas and 2 to 5 μm for non-load-bearing regions. The outcomes obtained from Bruker's surface roughness assessment (10.55±0.27 μm) concurred with findings by Derler et al. (2007) [31]. Who recorded an average surface roughness of 14.93±1.73 μm using a laser profilometer (Altisurf 500, Cotec). These results closely resemble the characteristics of *in vivo* skin, confirming that Lorica Soft is a suitable skin simulator due to its analogous surface texture.

The tensile strength of non-woven materials is typically more robust in the machined direction than in the cross-direction [32]. Results from the tensile test suggest that Lorica Soft is more robust and less susceptible to strain in the machined direction. A higher tensile strength is desirable for testing the skin to ensure it can withstand the high forces. Consequently, the skin template will be cut, ensuring the testing orientation runs parallel to the machined direction.

Non-woven fabrics are typically poor conductors of heat, as demonstrated in Figure 3-14. As expected, the side of the skin targeted by the heat gun raised the temperature at a much greater rate. When the heating element was removed, the temperature on both sides of the sample reduced at a similar rate. The delays and differences in peak temperature between the front and back of the sample raise concerns about the ability to accurately monitor changes in temperature by thermocouples located on the internal skin surface. Despite this concern, the low percentage difference in peak temperature between the front and back was deemed to have an acceptable level of heat transfer that will be detectable for thermocouples during testing in this project. Consequently, thermocouples should be integrated into the impactor design; however, they need to be validated against a thermal camera that monitors the temperature of the rugby turf.

3.5.4 Summary of Simulation Design Parameters and Constraints

This section will comprehensively outline the design constraints that have been meticulously identified while defining the simulation characteristics. The information provided in this section will be succinctly summarised and presented as a design specification with precise and well-defined limits. There will be no acceptable range for instances where the design criteria are non-negotiable, ensuring a clear and unambiguous understanding of the project's requirements.

Motion Profile

The central focus of this project was to develop a simulation that accurately represents a player in motion. The extensive video analysis underscored the crucial role of two distinct phases in a player-surface interaction, each playing a significant part in the overall simulation:

(i) The *'Impact Zone'* represents the initial contact where significant energy absorption occurs due to the typically nominal rebound height.
(ii) The *'Sliding Phase'* involves the translation of the knee in constant contact along the turf.

The planning stage was marked by a strong commitment to designing an authentic and organic interaction. It was a fundamental principle that no external forces should have influenced the measurement system during either interaction phase. This prerequisite was deemed essential for monitoring the natural deceleration and providing unbiased insights on the surface's injury risk, thereby ensuring the highest level of realism in the simulation.

In rugby, tackle is the most frequent [33] and dangerous phase of play [34], which agrees with the conclusions from the questionnaire and injury surveillance survey in this chapter. A tackle is an unpredictable interaction where the tackler engages with the ball carrier to bring them to the ground. A player may experience linear or rotational motion across the turf's surface during a tackle. The limitations of implementing a repetitive circular sweeping motion have already been established as it quickly compromises the surface condition. However, incorporating an authentic impact while generating and maintaining a rotational interaction with a natural deceleration would be challenging. The new test method should generate a linear interaction consisting of a knee striking the turf with an appropriate Impact Zone and Sliding Phase.

Considering that the apparatus must be incorporated into a laboratory setting, it was designed ergonomically to ensure the specific dimensions fit. Since the device could not be infinitely long, the first constraint identified was a quick transition between the Impact Zone and the Sliding Phase. Defining how quickly the impactor would enter the Sliding Phase was impossible without performing tests. Therefore, it was established that a quick transition phase between the Impact Zone and the Sliding Phase was required to ensure sufficient data collection for the Sliding Phase. A fast transition period ensures that each test iteration will interact with the sample over similar distances. Inevitably, the repeatability of the abrasion generated on the skin will improve. To ensure the transition is quick, the desirable displacement during the transition zone should be less than 10% of the overall gantry length, whilst an acceptable level would be no more than 20%.

Impactor Possessing Good Bio-fidelity.

The critical review of Securisport highlighted that the impactor's generic geometry and the use of a simple silicon skin were significant limitations of the current test method. Consequently, a new impactor should be designed based on real anthropometric data and wrapped in Lorica Soft, a skin simulant comparable to in vivo skin, to ensure the simulation possesses good biofidelity — as discussed in Chapter 2.

Realistic Interaction Conditions

While monitoring loading conditions during a simulated tackle, participants applied 24.6 – 41.3% of their body weight through one knee. The desirable impactor mass based on the average mass across all positions of professional players was 108 kg, which equates to 26.6 -44.6kg. This dataset was collected during static single-player loadings; therefore, the forces applied through the player onto the surface could be different during a dynamic tackle. When considering the player at the bottom of the interaction, the force applied would combine both players. On the other hand, the player above could experience a buoyancy effect, which would produce lower loads. Subsequently, an acceptable limit of 5 – 50 kg was selected. Concurrently, the acceptable carriage mass independently represented the average of the backs and forwards (95.9 - 116.5 kg). The desirable range of 130 - 200 kg was selected to represent the combined mass of two players, as discussed in Section 2.

Elite athletes can achieve sprint velocities up to 10 m/s; however, it is unrealistic for the knee to interact with the turf at this speed. The collision between two players during a tackle means the player's velocity will significantly reduce upon contact. Therefore, the desired simulated horizontal impact velocity was reasonably reduced to 5 m/s. Although the range of impact velocities identified in Section 3.4.2 exhibited a slightly higher magnitude, it was ultimately concluded that a velocity of 5 m/s remained within the acceptable range. The vertical loading condition was theoretically established by calculating the impact velocity from a mass free-falling from knee height. A rugby player's knee is typically 500-600 mm from the ground, representing an impact velocity of 3.1-3.4 m/s. In an ideal scenario, the knee form will free fall without any resistance; however, due to the dynamic nature of the interaction, friction within the bearings may increase due to the thrust generated by the propulsion system. The acceptable upper limit for the release height was increased to 1m to ensure the desired impact velocity was achievable. If higher speeds were required, this limit was double the desirable height for future testing. If these speeds were not possible, a lower limit of 3 m/s for the horizontal component and 2 m/s for the vertical component was deemed acceptable. The sliding distance of the simulation will be a direct function of the achievable horizontal speed and displacement during the transition zone. The video analysis reported an average sliding distance of 1.9m and 2.6m of the entire dataset and smooth interactions, respectively. Therefore, the desired and acceptable distances were set at >2 m and 1-2 m, respectively.

Assessing Skin Injury Risk

Survey 1 highlighted that the new test method should assess the abrasive nature of turf whilst monitoring the temperature rises generated during the interaction. Survey 2 highlighted that the Impact Zone and Sliding Phase dynamics should also be quantified. The skin simulant is a synthetic material with a consistent texture. Therefore, quantifying changes in surface roughness would be the most desirable assessment technique. The best way to monitor surface roughness is via 3D topography. However, the accuracy of this technique makes the equipment expensive. If this method is not financially feasible, quantifying the damaged area is deemed an acceptable alternative. In terms of monitoring temperature, thermocouples or thermal cameras will be suitable for directly (desired) or indirectly (acceptable) monitoring heat generation.

To evaluate the potential for a surface to harm a player the current test method calculates COF; however, the literature review highlighted no correlation between COF and abrasion. This insight suggests that additional metrics will be required to enhance understanding of interaction events linked to skin injury risk. Both load cells and accelerometers would be suitable transducers for this application.

The final design constraint identified was the ability to assess skin injury potential over the lifespan of a turf sample. FIFA Test Method 15 describes the procedure for determining wear on artificial turf. According to this method, a test sample must provide a uniformly conditioned area of at least 2.5m by 0.9m to facilitate the necessary performance measurements. The Lisport XL, the FIFA Test Method 15 device, has an internal free space of 1.34 m. Therefore, the gantry should be 1.1 – 1.34m wide.

In summary, the new test method holds promise in applying a holistic approach to measuring skin injuries on Rugby Turf. It aims to predict injury potential by generating realistic vertical and horizontal impact velocities (3 & 5 m/s) and developing an impactor with good bio-fidelity. The design of this method is intended to generate a linear interaction with natural deceleration, consisting of an Impact Zone and Sliding Phase where the impactor is in constant contact with the surface. The gantry frame is designed to fit within the dimensions of the Lisport XL, enabling a comparison of the interaction dynamics, the abrasive nature of turf, and the changes in temperature between a fresh sample and a simulated end-of-life product. This new device is expected to demonstrate improved validity compared to Securisport, potentially revolutionising the field of sports injury prevention and testing. The simulation criteria and constraints, referred to as the essential design specifications, are summarised in Table 3-4. The factor column represents the importance of each design criterion, which will be used during the critical evaluation of potential design concepts. A score of 5 denotes an important parameter, whereas a score of 10 signifies that the design criteria are non-negotiable.

Table 3-4: Design specifications

ID	User Requirement	Criteria ID	Factor	Design Criteria	Desired Output	Acceptable Output
1	Motion Profile	1.1	10	Impact zone	Greatest magnitude of forces	-
		1.2	5	Transition zone	10 % of gantry length	20 % of gantry length
		1.3	10	Sliding phase	Constant contact	-
		1.4	10	Measurement phase	Natural deceleration	-
		1.5	10	Orientation	Linear	-
2	Impactor Possessing Good Biofidelity	2.1	10	Impactor geometry	Based on real anthropometric data	-
		2.2	10	Skin simulant	Lorica Soft	-
3	Realistic Interaction Conditions	3.1	5	Impactor mass	25.5 - 40.5 kg	5 - 25 kg
		3.2	5	Carriage mass	120 - 200 kg	95.9 - 116.5 kg
		3.3	5	Release height	0.5 - 0.6 m	0.5 - 1 m
		3.4	5	Vertical Velocity	3.1-3.4 m/s	2 - 3.1 m/s
		3.5	5	Horizontal Velocity	4.9 - 5.1 m/s	3 - 4.9 m/s
		3.6	5	Sliding distance	>2 m	1-2 m
4	Assessing Skin Injury Risk	4.1	10	Abrasion	Surface Roughness	Damaged Area
		4.2	10	Temperature	Thermocouple	Thermal Camera
		4.3	5	COF	μ	-
		4.4	5	Gantry dimensions to fit within Lisport XL	1.1 – 1.34 m	-
		4.5	N/a	Additional metrics to inform on skin injury risk	TBC	-

CHAPTER 4

Design, Development, and Manufacturing

SKIN INJURIES

Through interactions during game play in rugby

4.1 Introduction

This section outlines potential design concepts to ensure the planning phase was robust and thorough. Systems thinking is a holistic approach to analysis that breaks down a complex and intricate process into smaller, more manageable stages [188]. In this case, the project was streamlined into three categories: propulsion, gantry, and impactor. Applying a systems thinking approach while critically analysing and evaluating several alternative solutions, lessons were learned from conceptual failures, leading to an enhanced prototype design.

4.2 Potential Design Concepts

The critical analysis consisted of ranking the design concepts based on their quality and ability to achieve each criterion independently. The quality value was then multiplied by the factors presented in Chapter 3 to produce a weighted score. The sum of all weighted scores, represented as a percentage of the ideal design, provides insights into the success of the design concept. The quality ranking scores (Q) are detailed below:

- 0 - Unknown (i.e., further testing required)
- 1 – Low
- 3 – Medium
- 5 – High

4.2.1 Design Concept 1: Propulsion System – Turf or Impactor

Eisenhower's (2023) urgent principle, a productivity theory of paramount importance, guides us in identifying and tackling the most crucial assignments to ensure the objectives are achieved. In the realm of sports equipment design, this principle is particularly relevant. For instance, the most challenging target to accomplish from the design specifications was a horizontal impact velocity of 5 m/s. Initial considerations of propulsion mechanisms proposed two options: accelerate the impactor and interact with a static turf or vice versa.

This concept and all subsequent designs will incorporate a knee form (Q=5) with the desired mass (Q = 5) wrapped in Lorica Soft (Q=5). This integration ensures that all designs are high quality, guaranteeing good biofidelity, which, in turn, instils confidence in their effectiveness.

A pendulum connected to a trolly via an inextensible cable through a pulley system containing a turf sample could rapidly accelerate the turf in a linear orientation (Q = 5), as illustrated in Figure 4-1. Generating an impact zone (Q=5) is highly achievable by manufacturing a dropping column which releases the impactor as the turf passes underneath it. The dropping column would be static and easy to design; therefore, generating the desired vertical velocity (Q = 5) from the release height (Q=5) should be relatively straightforward. There would, however, be no carriage mass (Q = 1) to represent the player’s body weight. Consequently, the momentum behind the interaction would not be representative of the realistic forces experienced by a player. The primary limitation of this critical analysis is the uncertainty in generating a quick transition zone. Preliminary testing is necessary to evaluate the impactor's effectiveness in moving from the Impact Zone to the Sliding Phase. As a result, this analysis, along with all subsequent assessments, will assume a transition zone with Q = 0.

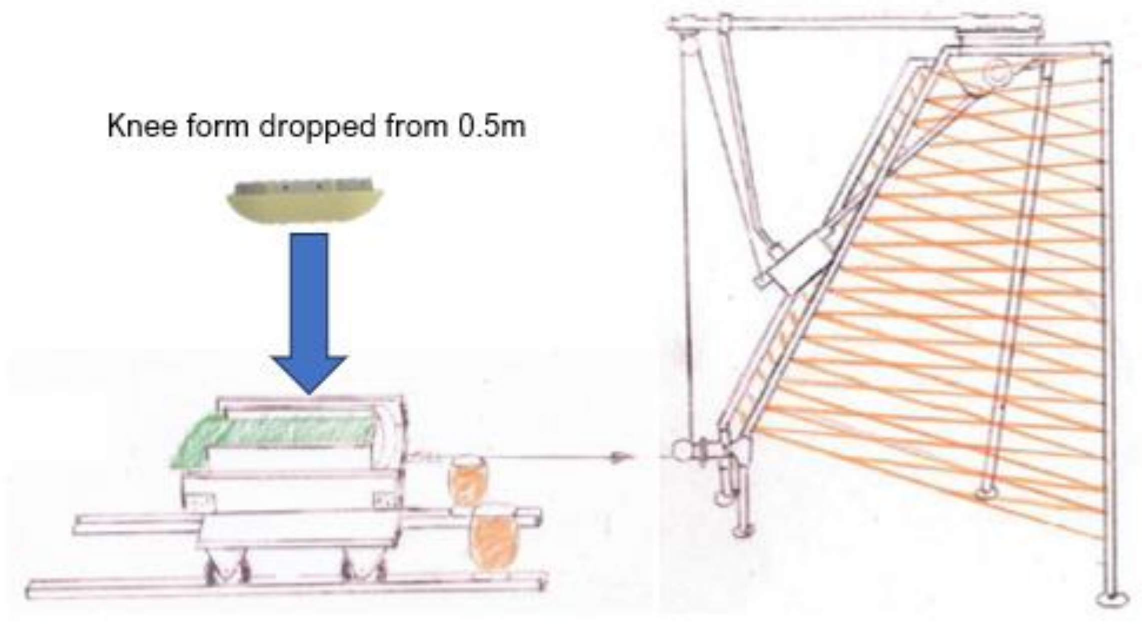

Figure 4-1: Design Concept 1 – Accelerating Turf

The horizontal velocity would be generated by converting rotational acceleration from the pendulum into linear acceleration via the pulley system. Once the inextensible cable becomes taut, motion would be initiated; however, achieving a consistent velocity (Q = 1) would be difficult as the system's mass will vary with different fibre lengths and infill types. If the impact velocity varies, then the sliding phase (Q = 1) will not be consistent, which will influence the assessment of skin injury risk (Q = 1), which is not acceptable.

Another concern with this technique was that the turf moves in relation to the player, making the interaction unrealistic. Therefore, a Lisport XL sample could not be tested (Q = 1). Furthermore, on impact, the unconstrained infill would maintain its momentum, propelling it forward. The sample condition would quickly become compromised and not represent the specified system for the sliding phase (Q = 1). Additional complications would arise with repeated testing as the samples constantly require preparation before each test iteration. Due to these concerns, it was accepted that the impactor/carriage would need to be accelerated.

The critical analysis produced a weighted score of 54.4%, a summary presented in Table 4-1, which implies that this concept would not sufficiently match the design specifications.

Table 4-1: Critical Analysis Summary of Design Concept 1.

ID	User Requirement	Criteria ID	Factor	Design Criteria	Quality	Weighted Score
1	Motion Profile	1.1	10	Impact zone	5	50
		1.2	5	Transition zone	0	0
		1.3	10	Sliding phase	1	10
		1.4	10	Measurement phase	1	10
		1.5	10	Orientation	5	50
2	Impactor Possessing Good Biofidelity	2.1	10	Impactor geometry	5	50
		2.2	10	Skin simulant	5	50
3	Realistic Interaction Conditions	3.1	5	Impactor mass	5	25
		3.2	5	Carriage mass	1	5
		3.3	5	Release height	5	25
		3.4	5	Vertical Velocity	5	25
		3.5	5	Horizontal Velocity	1	5
		3.6	5	Sliding distance	1	5
4	Assessing Skin Injury Risk	4.1	10	Abrasion	1	10
		4.2	10	Temperature	1	10
		4.3	5	COF	1	5
		4.4	5	Gantry dimensions to fit within Lisport XL	1	5
					Total Score	54.4%

4.2.2 Design Concept 2: Pendulum

The next propulsion concept drew inspiration from a current EN Standard, the pendulum test, which assesses the slip resistance of a surface. The device transfers rotational acceleration into a linear interaction (Q = 5), which would generate a measurement phase without any external forces (Q = 5). Meanwhile. The compact nature would enable testing of pre and post Lisport samples (Q = 5). The release height of the impactor can be determined to achieve an impact velocity of 5 m/s, as presented in Equation 10.

Equation 10

$$h = \frac{v^2}{2g}$$

A release height (Q = 1) of 1.27m would be required to achieve a horizontal velocity (Q = 5) of 5 m/s. However, the slip resistance test was designed for the impactor to slide across the surface and for the pendulum to continue along its swinging arc in a linear orientation (Q = 5). In this design concept, the impact zone and sliding phase co-occur, which is undesirable. Therefore, the sliding phase (Q = 1) would be limited to the length of the impactor, which does not meet the desired sliding distance. During this player-surface simulation, there is no vertical velocity (Q = 1) at the bottom of the swing.

Consequently, the magnitude of the vertical force will not be sufficient. Therefore, the impact zone does not meet desirable criteria (Q = 3). Again, there would be no additional carriage mass (Q = 1) representing the player’s body weight, producing an unrealistic interaction.

Accelerometers or loadcells could be integrated into the impactor to monitor COF and provide a means to develop ancillary injury metrics. This method has the potential to abrade the skin and generate temperature during the interaction. However, the lack of a distinctive impact zone and sliding phase implies that the interaction does not represent a player in motion. Therefore, they have been provided with a quality score of 3.

The critical analysis produced a weighted score of 67.2%, a summary presented in Table 4-2, which implies that this concept would not sufficiently match the design specifications.

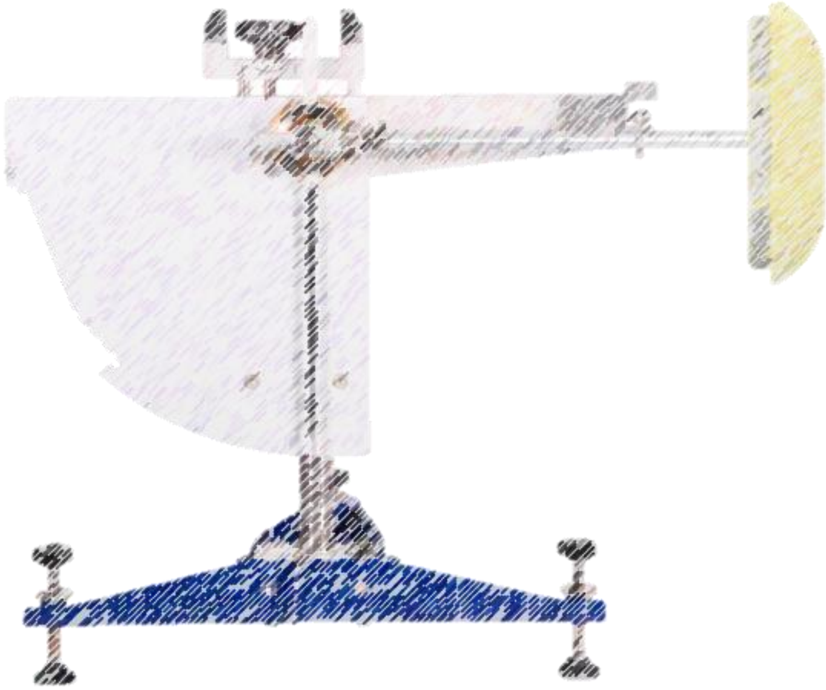

Figure 4-2: Design Concept 2 – The Pendulum

Table 4-2: Critical Analysis Summary of Design Concept 2 – The Pendulum

ID	User Requirement	Criteria ID	Factor	Design Criteria	Quality	Weighted Score
1	Motion Profile	1.1	10	Impact zone	3	30
		1.2	5	Transition zone	0	0
		1.3	10	Sliding phase	1	10
		1.4	10	Measurement phase	5	50
		1.5	10	Orientation	5	50
2	Impactor Possessing Good Biofidelity	2.1	10	Impactor geometry	5	50
		2.2	10	Skin simulant	5	50
3	Realistic Interaction Conditions	3.1	5	Impactor mass	5	25
		3.2	5	Carriage mass	1	5
		3.3	5	Release height	1	5
		3.4	5	Vertical Velocity	1	5
		3.5	5	Horizontal Velocity	5	25
		3.6	5	Sliding distance	1	5
4	Assessing Skin Injury Risk	4.1	10	Abrasion	3	30
		4.2	10	Temperature	3	30
		4.3	5	COF	5	25
		4.4	5	Gantry dimensions to fit within Lisport XL	5	25
					Total Score	67.2%

4.2.3 Design Concept 3: Ramp

Again, the following approach used gravity to achieve a horizontal impact velocity via a ramp, as illustrated in Figure 4-3. Once the impactor/carriage leaves the ramp, it can slide across the surface without external forces, resulting in a linear natural deceleration (Q = 5).

Figure 4-3 Design Concept 3 – The Ramp

Similarly, the release height would be 1.27m for a pendulum set-up if there was no friction. There is, however, a non-conservative force acting on the carriage rolling down a ramp, as illustrated in Figure 4-4, which makes the calculation more complicated. The kinetic energy, Equation 11, is equivalent to the potential energy minus the force of friction times the displacement. As the ramp is at an angle, the normal load (Fn) is perpendicular to the surface, which can be explained in basic trig as the cosine of the ramp's angle (ϴ) times the object's weight. The frictional force (Ff) is calculated and substituted into Equation 12 which can be rearranged to determine the impact velocity, as presented in Equation 13.

Equation 11

$$\frac{1}{2}mv^2 = mgh - F_f.d$$

Equation 12

$$\frac{1}{2}mv^2 = mgh - \mu mgcos\Theta d$$

Equation 13

$$v = \sqrt{2g(h - \mu cos\Theta d)}$$

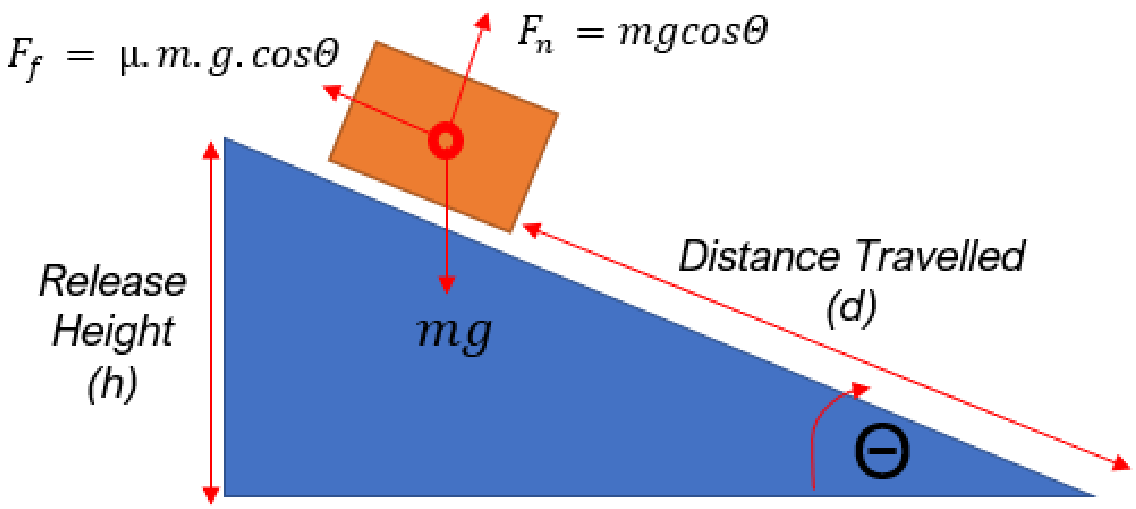

Figure 4-4: Evaluating ramp conditions to generate 5 m/s impact speed.

To ensure consistency across all design concepts, the angle of incidence should remain constant. Through basic trigonometry, by applying the inverse tangent to the ratio of the vertical (3.1 m/s) and horizontal velocities (5 m/s), the angle of incidence was calculated as 31.8°. Incorporating Automotion Components' linear guide rails and bearings into the ramp design would produce a COF of 0.01. With all the unknowns established and assuming the distance travelled was two metres (d = 2), Equation 13 can be rearranged to calculate the required release height to achieve the desired impact velocity, as presented in Equation 14.

Equation 14

$$h = \frac{v^2}{2g} + \mu cos\Theta d$$

Despite achieving the desired horizontal impact velocity from a relatively safe working height (h = 1.29 m | Q = 1), the nature of the ramp would dampen the vertical velocity (Q = 1) as the impactor is unable to free fall. Consequently, the magnitude of the vertical force will not be sufficient, and the impact zone will not fulfil the desirable criteria (Q = 3). A development of this design concept could be to integrate a dropping mechanism within the ramp. The linear guide rails would need to be supported along the entire length of the turf sample at an increased height to accommodate the dropping mechanism, which could potentially put the apparatus above head height, which would be a safety concern.

Since the carriage will be free to move across the surface once it leaves the ramp therefore the impactor may not be in constant contact throughout the Sliding Phase (Q = 3).

Additionally, the carriage must be returned to the release height. A winch mechanism that reels the carriage is not an option, as this would compromise the surface condition and contribute to further abrasion on the skin. Ideally, this test method would only require one operator; therefore, the carriage mass must be considered for ease of repeated testing. Accordingly, it is unlikely that the desired carriage mass (Q = 3) will be achieved. Subsequently, the extent of skin abrasion (Q = 3) and thermal (Q = 3) build-up might be less than what would be produced during an interaction that generates a realistic impact with the appropriate loadings. However, the device would be relatively narrow, therefore, it would be suitable for assessing Lisport XL samples (Q = 5).

This design is a step in the right direction as it would enable additional metrics (Q = 5) to be generated from accelerometers during a natural deceleration, highlighted by the increased weighted score of 73.6%, a summary of the critical analysis presented in Table 4-3. Due to the lack of an authentic impact, this concept would not adequately match the design specifications.

Table 4-3: Critical Analysis Summary of Design Concept 3 – The Ramp

ID	User Requirement	Criteria ID	Factor	Design Criteria	Quality	Weighted Score
1	Motion Profile	1.1	10	Impact zone	3	30
		1.2	5	Transition zone	0	0
		1.3	10	Sliding phase	3	30
		1.4	10	Measurement phase	5	50
		1.5	10	Orientation	5	50
2	Impactor Possessing Good Biofidelity	2.1	10	Impactor geometry	5	50
		2.2	10	Skin simulant	5	50
3	Realistic Interaction Conditions	3.1	5	Impactor mass	5	25
		3.2	5	Carriage mass	3	15
		3.3	5	Release height	1	5
		3.4	5	Vertical Velocity	1	5
		3.5	5	Horizontal Velocity	5	25
		3.6	5	Sliding distance	3	15
4	Assessing Skin Injury Risk	4.1	10	Abrasion	3	30
		4.2	10	Temperature	3	30
		4.3	5	COF	5	25
		4.4	5	Gantry dimensions to fit within Lisport XL	5	25
					Total Score	73.6%

4.2.4 Design Concept 4: Linear Gantry

The critical analysis of the previous design concepts has established that propulsion systems that convert rotational/angular acceleration into linear motion are unsuitable due to the reduced vertical velocity on impact. Alternative designs should focus on developing a linear gantry frame with an independent dropping mechanism.

A monorail, which is used in many high-speed trains and rollercoasters, was the inspiration for the next potential design concept. The dropping mechanism was constructed by creating a right-angled triangle where the impactor would free-fall along two parallel linear rails on the vertical axis, as presented in Figure 4-5. The hypotenuse provided beneficial support to limit deflections on the vertical column during impacts. The horizontal component would be integrated into the monorail as Figure 4-6 illustrates.

Figure 4-5: Design Concept 4 – The Dropping Column

Figure 4-6: Design Concept 4 – The Monorail

This design has the potential to generate an impact zone (Q = 5) and sliding phase (Q = 5) that generates a linear measurement phase with no external forces (Q = 5) if an acceptable propulsion system is identified. The carriage design could be optimised to achieve the desired release height (Q = 5), corresponding vertical velocity (Q = 5), and carriage mass (Q = 5). The main limitation of this design was the nature of the monorail, which would make it difficult to test multiple test locations without compromising the durability and stability of the frame. This limitation prompted further research into alternative gantry concepts before exploring options for accelerating the carriage. A suitable propulsion system has yet to be identified. Therefore, this concept cannot achieve horizontal velocity (Q = 1), and the skin injury risk assessment (Q = 1) cannot be performed over a suitable sliding distance (Q = 1)

This design performed less well in the critical analysis (64.2%) than the ramp concept (72.3%). However, it was the first concept to generate the desired impact zone and sliding phase. Therefore, further investigation is required to create a design that can perform the surface evaluation on multiple test locations.

By incorporating a lead screw into the dropping column, the impactor will have an additional degree of freedom within the apparatus, which will provide the ability to test multiple locations on the sample, as presented in Figure 4-7. An armature plate would set the release height with a quick-release mechanism to lock it in place. Free fall would be initiated by activating the release of a magnet located on the impactor. To accommodate the new carriage design, the monorail was converted into a cuboid with linear rails on the top and bottom of the upper length, as presented in Figure 4-8. By facilitating multiple testing locations and designing a gantry frame to fit within the Lisport dimensions (Q = 5), the weighted score increases to 70.9%, a summary of the critical analysis presented in Table 4-4.

The design specification defines a desired vertical impact velocity of 2.8 – 3.1 m/s, which can be achieved by using hydraulics, pneumatics, or spring loading on the impactor to reduce the drop height. Emphasis was placed on designing an interaction that was as organic as possible, which would allow the impactor to move freely during the sliding phase; therefore, a hydraulic or pneumatic piston that would lock at full extension and not allow the impactor to move freely over the surface, which was not desirable. Spring loading the impactor was viable due to the lower release height benefit. The simplicity of a free-falling impactor, a better representation of a player, was more appealing. Therefore, spring loading the impactor was avoided.

The vertical impact velocity was achieved by allowing the impactor to free fall from the desired height down a linear guide rail. Two options to ensure friction was kept to a minimum: bearings or bushings. Bearings are designed for low friction movement between two moving objects and can support both axial and radial loads at high speeds. This mechanical component consists of a series of recirculating balls within a plastic sleeve, allowing for a smooth, low-friction movement. In contrast, bushings are designed to reduce friction when a shaft rotates within a bore; however, they cannot withstand high radial loadings perpendicular to the shaft's axis. Due to the nature of the simulation's motion profile, it is apparent that bearings will perform better than bushings.

In summary, this design is the most promising concept; however, an acceptable propulsion system still needs to be identified.

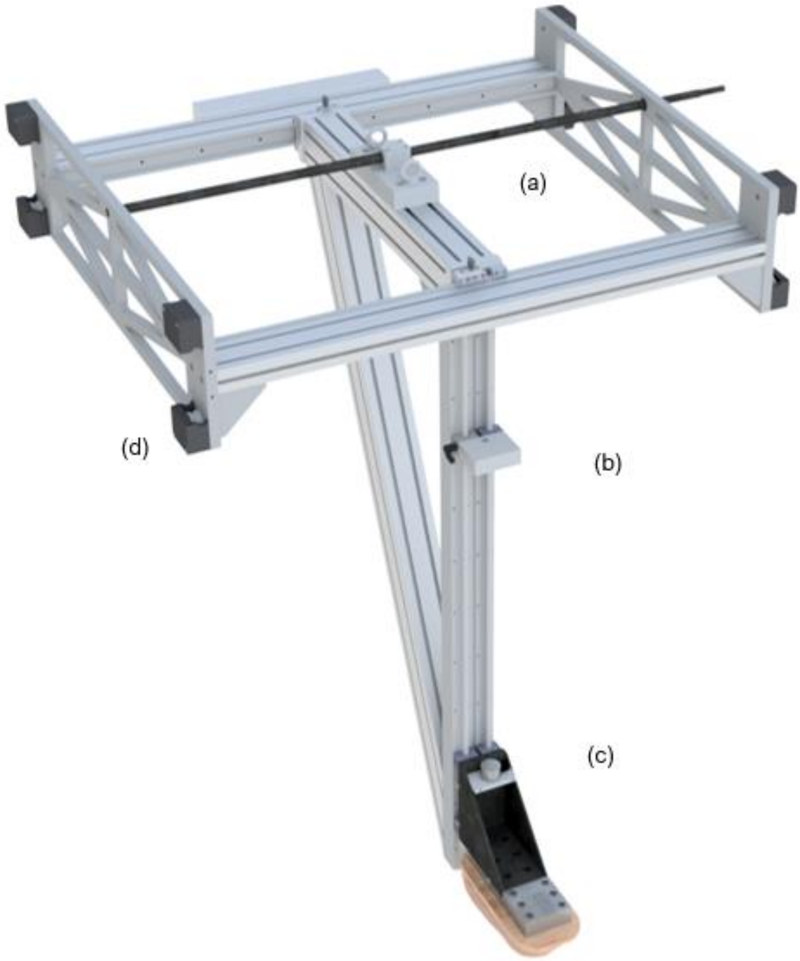

Figure 4-7: Design Concept 4 – Dropping Column incorporated into a carriage with three degrees of freedom. (a) lead screw (b) armature plate (c) release magnet (d) roller bearings

Figure 4-8: Design Concept 4 – Adaptation to Monorail to incorporate new carriage.

The critical analysis, summary presented in Table 4-4, implies this design concept (70.4%) performed worse than the ramp (73.6%). This disparity highlights the questionable durability and safety concerns discussed above. However, redesigning to a more compact frame would boost the weighted score closer to the ideal 100%.

Table 4-4: Critical Analysis Summary of Design Concept 4 – The Gantry

ID	User Requirement	Criteria ID	Factor	Design Criteria	Quality	Weighted Score
1	Motion Profile	1.1	10	Impact zone	5	50
		1.2	5	Transition zone	0	0
		1.3	10	Sliding phase	5	50
		1.4	10	Measurement phase	5	50
		1.5	10	Orientation	5	50
2	Impactor Possessing Good Biofidelity	2.1	10	Impactor geometry	5	50
		2.2	10	Skin simulant	5	50
3	Realistic Interaction Conditions	3.1	5	Impactor mass	5	25
		3.2	5	Carriage mass	5	25
		3.3	5	Release height	5	25
		3.4	5	Vertical Velocity	5	25
		3.5	5	Horizontal Velocity	1	5
		3.6	5	Sliding distance	1	5
4	Assessing Skin Injury Risk	4.1	10	Abrasion	1	10
		4.2	10	Temperature	1	10
		4.3	5	COF	1	5
		4.4	5	Gantry dimensions to fit within Lisport XL	1	5
					Total Score	70.4%

4.2.5 Design Concept 5: Propulsion System - Hydraulics & Pneumatics

Hydraulics and pneumatics are linear actuators which exploit the mechanical advantages of pressurising fluids to apply a load [190]. Hydraulics systems use liquids, such as oil or water, while pneumatic systems use compressed air or other gases as the fluid. Gases are described as compressible because they can be tightly packed into smaller spaces. Consequently, compared to hydraulic systems, they can generate greater accelerations to achieve higher top speeds when the built-up pressure is released. The volume of a gas is dependent on the pressure within the container; therefore, gases are more challenging to contain, contributing to leakage issues within pneumatic systems. Due to their incompressible nature, liquids maintain a consistent volume when pressurised, which means hydraulics can transfer more power per unit of volume. Pneumatic systems are generally considered safer than hydraulic systems because compressed air is not flammable or toxic, while hydraulic fluids can be flammable or toxic. Hydraulics are typically implemented on heavy-duty industrial equipment and construction machinery due to the higher output forces. While the faster top speeds generated by pneumatics are more appropriate for application in this project, the mass of the carriage was a concern for manufacturers as they could not guarantee speeds above 2 m/s, which was unacceptable. As a result, the critical analysis did not improve from the score provided in Table 4-4.

4.2.6 Design Concept 6: Propulsion System - Winch

Propulsion is the generation of force by pushing or pulling an object. Most of these potential solutions have attempted to propel the impactor by driving it. Therefore, methods of pulling the carriage were investigated. A *pulley system* is a mechanism composed of a wheel and rope used to lift heavy objects via mechanical advantage, which results in a trade-off between force and distance. Effectively, what you benefit in terms of force requires additional distance to be travelled. A pulley system is, therefore, not an appropriate application to rapidly accelerate the impactor. Equally, winches can be used to move heavy objects weighing up to several tonnes. However, their line speed is typically meters per minute, which is insufficient for this application. Again, the critical analysis did not improve from the score calculated in Table 4-4.

4.2.7 Design Concept 7: Propulsion System - Servomotor

Servomotors are primarily designed to generate rotary motion; however, they can be modified to generate linear motion by utilising mechanical components such as gears, screws, or belts. The feedback on the rotary servomotor provides precise control of angular position, which would generate a consistent impact velocity [191].

A lead screw consists of a threaded rod that engages with a nut [192]. As the motor drives the rod, the nut moves along the screw generating linear displacement. At the same time, racks and pinions operate similarly, with a pinion gear engaging with the teeth on a rack to generate displacement [193]. Both systems are unsuitable for high-speed applications due to the limitations of thread pitch. The thread pitch is the distance between adjacent teeth. Larger thread pitches offer a greater mechanical advantage by producing more extended displacements per revolution. However, this advantage comes at the cost of linear speed, as the driving motor must rotate more to cover a given linear distance. Conversely, smaller thread pitches enable faster linear speeds but sacrifice the mechanical advantage provided by larger pitches. The torque requirements of the driving motor are influenced by the thread pitch, with larger pitches demanding higher torque to overcome resistance and generate axial force. Additionally, motor limitations, including maximum rotational speed, can restrict the achievable linear speed.

Since high-speed linear motion is required, belt and pulley systems are more suitable applications for converting rotational speed to linear motion. In this arrangement, a belt is wrapped around a pulley connected to the servomotor shaft, and another pulley is attached to the load. As the servomotor rotates, the belt moves, causing the load to move linearly. They provide excellent power transmission and can generate the desired velocity by selecting the appropriate pulley diameter [194]. According to the principles of rotational motion and the conservation of angular momentum, the linear speed of the belt is directly proportional to the circumference of the pulley. Since the circumference of a circle is determined by its diameter, a larger pulley diameter results in a greater circumference and, therefore, a higher linear speed. These systems are easy to maintain and replace, offering corrosion resistance and versatility for various load capacities. Belt and pulley systems offer an economical, efficient, and adaptable solution for power transmission needs.

The main limitation of this concept would be the constant speed through the measurement phase (Q = 1), which is not representative of a player in motion. Consequently, the skin injury risk assessment results may vary on different surfaces (Q = 3). For example, it is expected that infill, acting as a ball bearing, should reduce forces experienced by the simulated player sliding along the surface. Since there is more infill in rugby (60 mm) systems compared to football (40 mm), ploughing effects may be increased due to the larger volume of infill. In comparison, minimal ploughing would occur during an interaction on non-filled systems.

Consequently, the constant speed may amplify the ploughing effects when comparing filled and non-filled systems, suggesting that non-filled systems are safer than filled systems. Non-filled systems are yet to be accredited for use in rugby [65]. Therefore, little data is available to provide insights into skin injury incidence rates on these surfaces. Additionally, the constant speed does not represent an authentic interaction and could misrepresent the abrasiveness of turf (Q = 3) and temperatures (Q = 3) generated during gameplay. It is, therefore, essential to simulate a realistic interaction with natural deceleration to produce consistent data across all potential surfaces.

To accommodate this power, the motor could be removed, and the momentum of the carriage provides linear motion during the sliding phase. However, this was not recommended by suppliers as applying excessive force may cause damage to the internal gears or other servo motor components. If the motor needs to be moved manually, it is generally best to do so gently and smoothly when not powered. At the same time, avoiding force on the motor beyond its normal range of motion or causing any sudden movements. Alternatively, a clutch could be implemented to disengage the belt when 5 m/s was achieved. Considering the advantages of the propulsion system, presented in Section 4.2.8, this setup was deemed too engineering intensive with potential complications whilst operating at such high speeds. Therefore, this approach was also discounted.

In conclusion, a belt and pulley system are the best method to incorporate a servomotor into the design. The lack of a natural deceleration, however, is the main limitation due to the knock-on effects this has on the validity of the test results across different generations of turf. Consequently, the critical analysis of this potential design produced a weighted score of 83.2%, a summary presented in Table 4-5.

Table 4-5: Critical Analysis Summary of Design Concept 7 - Servomotors

ID	User Requirement	Criteria ID	Factor	Design Criteria	Quality	Weighted Score
1	Motion Profile	1.1	10	Impact zone	5	50
		1.2	5	Transition zone	0	0
		1.3	10	Sliding phase	5	50
		1.4	10	Measurement phase	1	10
		1.5	10	Orientation	5	50
2	Impactor Possessing Good Biofidelity	2.1	10	Impactor geometry	5	50
		2.2	10	Skin simulant	5	50
3	Realistic Interaction Conditions	3.1	5	Impactor mass	5	25
		3.2	5	Carriage mass	5	25
		3.3	5	Release height	5	25
		3.4	5	Vertical Velocity	5	25
		3.5	5	Horizontal Velocity	5	25
		3.6	5	Sliding distance	5	25
4	Assessing Skin Injury Risk	4.1	10	Abrasion	3	30
		4.2	10	Temperature	3	30
		4.3	5	COF	5	25
		4.4	5	Gantry dimensions to fit within Lisport XL	5	25
					Total Score	83.2%

4.2.8 Design Concept 8: Propulsion System - Linear Induction Motor

Generating the desired horizontal impact velocity of a heavy carriage over a short distance appeared to be on the boundary of physically impossible following the extensive research focused on identifying a suitable propulsion system. By adopting rollercoaster technology, a highly innovative solution was developed that utilises electromagnetic induction to produce rapid linear accelerations [195]. Linear induction motors (LIM) offer several advantages compared to traditional motors, as they produce acceleration without needing mechanical conversion from rotational to linear motion. They provide high acceleration rates and can achieve rapid speeds without mechanical contact between components, reducing wear and maintenance requirements. However, the complexity of their design and control systems results in higher manufacturing and installation costs.

A LIM operates on the same principles as a traditional rotary induction motor but is configured linearly. The basic construction of a linear induction motor consists of a primary stator, referred to as the LIM housing, and a secondary mover, referred to as the reaction fin. A series of three-phase windings within the LIM housing create an electromagnetic field (EMF) when energised by an AC power source. The reaction fin is typically made of a conductive metal, a 3 mm copper plate. When the EMF extends across a small air gap, the reaction fin currents are induced within the copper, known as Eddy currents, which create their own EMF perpendicular to the LIM housing. These EMFs repel each other, generating a push-pull effect known as a Lorentz force, which can be used to drive a load (Seal & Sengupta, 2022; The Editors of Encyclopaedia Britannica, 2023).

Overall, linear induction motors provide a direct and efficient means of generating linear motion, offering speed, acceleration, and maintenance advantages. Once the reaction fin leaves the LIM housing, the carriage will no longer be accelerated, which provides the means to monitor the natural deceleration of the simulated player (Q = 5). Improving the consistency of results from the skin injury risk assessment (Q = 5) across different generations of artificial surfaces. Consequently, the critical analysis produced a weighted score of 98.4%, summarised in Table 4-6.

Table 4-6: Critical Analysis Summary of Propulsion Systems – Linear Induction Motor

ID	User Requirement	Criteria ID	Factor	Design Criteria	Quality	Weighted Score
1	Motion Profile	1.1	10	Impact zone	5	50
		1.2	5	Transition zone	5	25
		1.3	10	Sliding phase	5	50
		1.4	10	leasurement phas	5	50
		1.5	10	Orientation	5	50
2	Impactor Possessing Good Biofidelity	2.1	10	Impactor geometry	5	50
		2.2	10	Skin simulant	5	50
3	Realistic Interaction Conditions	3.1	5	Impactor mass	5	25
		3.2	5	Carriage mass	5	25
		3.3	5	Release height	5	25
		3.4	5	Vertical Velocity	5	25
		3.5	5	Horizontal Velocity	5	25
		3.6	5	Sliding distance	5	25
4	Assessing Skin Injury Risk	4.1	10	Abrasion	5	50
		4.2	10	Temperature	5	50
		4.3	5	COF	5	25
		4.4	5	Gantry dimensions to fit within Lisport XL	3	15
					Total Score	98.4%

4.2.9 Potential Design Concept 9: Impactor

The surveys from Chapter 3 reported that prominent bony parts are the most vulnerable anatomical locations, with the elbows and knees being the most susceptible to sustaining injuries. An alternative impactor could be designed based on the elbow. There is a massive variation in the elbow's geometry (Q = 1) between full flexion and extension. When the arm is fully extended, the skin around the elbow becomes loose and malleable, reducing skin injury risk. When the elbow is at full flexion, the skin is stretched over a small area. Therefore, the point loading would be much more significant, increasing the risk of injury. The knee, however, is closer to the ground; therefore, there is expected to be a higher incidence of initial contacts where the magnitude of forces experienced will be much greater than secondary contacts that the elbow would experience.

While it would be interesting to assess skin injury risk on the elbow, there is a convincing rationale to maintain the knee as the primary focus. Being closer to the ground, the knee is more likely to experience initial contacts with much greater forces than secondary contacts that the elbow would experience, making it a more practical area to prioritise in injury prevention and impact biomechanics research. Consequently, the critical analysis score generated a score of 88.0%, as presented in Table 4-7.

Table 4-7: Critical Analysis Summary of Design Concept 8 – Impactor Geometry

ID	User Requirement	Criteria ID	Factor	Design Criteria	Quality	Weighted Score
1	Motion Profile	1.1	10	Impact zone	5	50
		1.2	5	Transition zone	0	0
		1.3	10	Sliding phase	5	50
		1.4	10	leasurement phas	5	50
		1.5	10	Orientation	5	50
2	Impactor Possessing Good Biofidelity	2.1	10	Impactor geometry	1	10
		2.2	10	Skin simulant	5	50
3	Realistic Interaction Conditions	3.1	5	Impactor mass	5	25
		3.2	5	Carriage mass	5	25
		3.3	5	Release height	5	25
		3.4	5	Vertical Velocity	5	25
		3.5	5	Horizontal Velocity	5	25
		3.6	5	Sliding distance	5	25
4	Assessing Skin Injury Risk	4.1	10	Abrasion	5	50
		4.2	10	Temperature	5	50
		4.3	5	COF	5	25
		4.4	5	Gantry dimensions to fit within Lisport XL	3	15
					Total Score	88.0%

4.2.10 Summary of Potential Design Concepts

In summary, considering alternative solutions is essential while developing a new test device to ensure an enhanced final product. A comparison of the weighted scores produced during critical analysis (Figure 4-9) suggests that concept 8 is the best approach for meeting the design specification requirements.

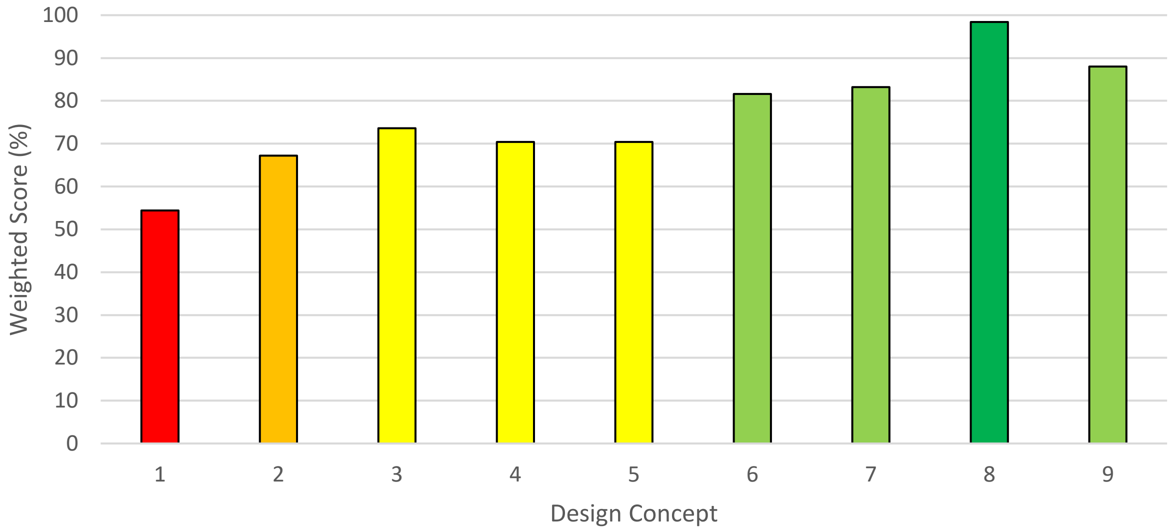

Figure 4-9: Critical Analysis: A comparison of potential design concepts.

The analysis of initial design concepts revealed that propulsion systems using gravity to convert rotational acceleration into linear motion were unsuitable due to the reduced vertical velocity upon impact. Consequently, a linear gantry frame and dropping mechanism will be combined to independently generate the horizontal and vertical velocities. A cuboid gantry frame will be designed to fit within the dimensions of the Lisport XL to enable comparison of new and end-of-life products. A lead screw will be incorporated into the carriage to provide the ability to test multiple test locations. Throughout this process, it was apparent that an advanced propulsion system was required to generate 5 m/s; however, a revelation occurred by evaluating different design concepts for the gantry. The monorail sparked an interest in investigating how high-speed trains and rollercoasters achieve their top speeds, ultimately leading to the discovery of the LIM as an ideal propulsion system. Additionally, this section highlighted further work that could be completed by assessing skin injury risk on other body parts.

4.3 Initial Prototype Design

Several design iterations were developed throughout the progression of this project before the final product was completed. This section will outline the initial prototypes used to provide confidence in the functionality of the apparatus by proving basic principles. This step was essential before committing to significant financial investment whilst procuring the LIM propulsion system. Furthermore, any noteworthy insights will be analysed to provide a better understanding and illustrate how they helped improve the next iteration.

4.3.1 Gantry & Surface Dimensions

The design specification recommended that the gantry frame fit within the Lisport XL's dimensions to enable skin injury risk assessment on an end-of-life product [147]. The Lisport XL has an internal free space of 1.34m, which the gantry for the new test method must fit within. FIFA Test Method 15 specified that the test specimen should have a uniformly conditioned area of at least 2.5m by 0.9m. For this project, the specified width of the sample will be adopted. However, the length will be increased to 4m to ensure an acceptable sliding distance. Additional space was required for the impactor to be accelerated. Therefore, a suitable dimension for the gantry frame was 6m long. The impactor required at least 1m to free fall from to generate the desired impact velocities. While ensuring no moving parts were above head height, the maximum gantry height was determined to be 1.5m. The initial gantry external dimensions were finalised as 6 m x 1.28 m x 1.50 m (LxWxH). All members were made from versatile MiniTec aluminium extrusions for fast and easy construction whilst accommodating any necessary design amendments. The 12 edges of the cuboid shape consisted of 90x90mm members, while the support struts in the middle were 45x90mm, placed on the outside of the main frame to allow the carriage to pass freely, as presented in Figure 4-10. To facilitate the carriage traversing along the gantry, linear guide rails are installed on the top and bottom of the upper lengths. These guide rails are made of hardened steel with a diameter of 16 mm and are positioned 130 mm apart. They are designed to ensure smooth and precise movement of the carriage along the gantry.

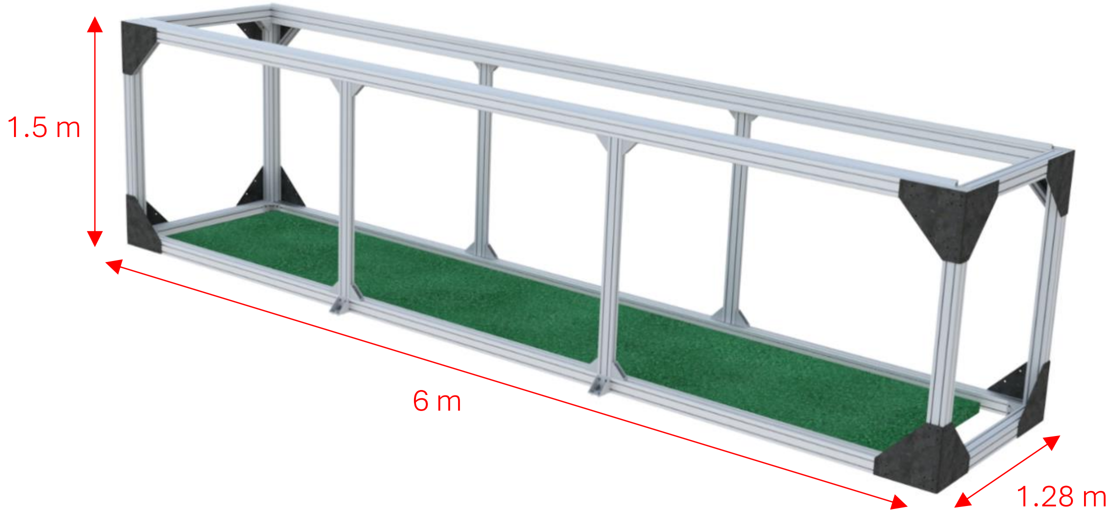

Figure 4-10: Initial Gantry Frame

The high energy interaction generated required a robust and sturdy gantry frame to tolerate the forceful impacts. Therefore, support struts and steel brackets were used to reinforce the structure. The number of vertical support struts was selected via an iterative finite element analysis process where the maximum deflection of the top section was monitored as the number of support struts was increased. The maximum load capacity for the carriage's bearings was 7kN, the force selected for the finite element analysis, as illustrated in Figure 4-11.

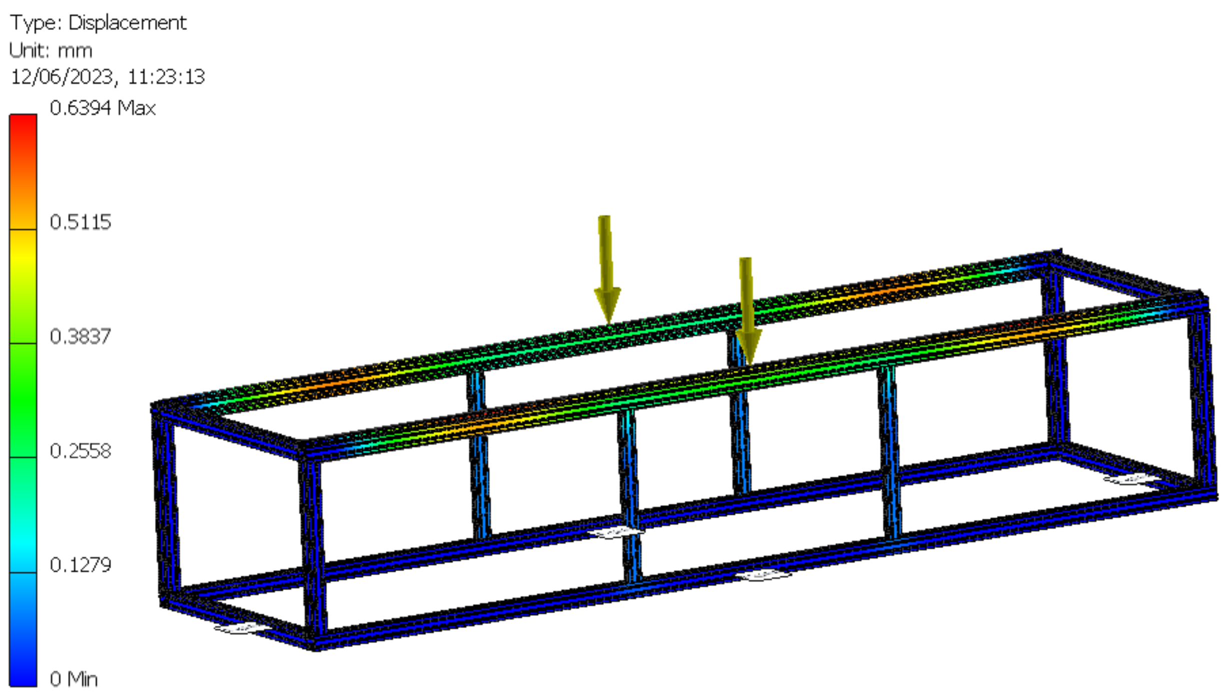

Figure 4-11: Finite Element Analysis: Optimal Gantry Frame

The optimum design was selected with rigidity and budget in mind. Increasing the number of struts will decrease the maximum deflection, which is associated with increased cost. The analysis reported that the best gantry design consisted of two support struts evenly spaced along both lengths of the horizontal axis. This setup produced a maximum deflection of 0.64 mm compared to 0.47 mm with three supports. The minor variation in maximum deflection did not warrant the additional support struts.

4.3.2 Carriage

The carriage, as shown in Figure 4-12, was designed to bear the player's weight while allowing the impactor to move within the gantry. The carriage's design can be simplified into two key features that embody the desired motions: horizontal and vertical. The horizontal aspect was crafted with two bespoke rollers, maintained in parallel by two aluminium extrusions. These rollers, inspired by a MiniTec standard part (LR16-90), were redesigned to perfectly suit the needs of this carriage. A 900mm length was chosen to ensure stability without compromising on interaction space. To achieve an optimal horizontal velocity, the initial carriage's weight was reduced by strategically removing material from the sliders. The vertical component, known as 'the dropping column', was designed as a right-angled triangle, with the hypotenuse serving as a structural support to limit deflection.

Figure 4-12: Initial Carriage Design (a) roller bearings (b) lead screw (c) Impactor for attaching knee form. (d) armature plate

The initial prototype was designed to enable three degrees of freedom: X – horizontal, Y – lateral, and Z – vertical. Eight wheels enabled the horizontal motion, and nuts were repurposed from the MiniTec roller. The bottom four wheels had eccentric nuts, which provided control over the rolling resistance of the carriage along the linear rails, Figure 4-18a. Lateral motion was incorporated into the design to provide the ability to assess multiple test locations. This movement was facilitated by operating a lead screw, Figure 4-18b, to move the dropping column along another set of linear guide rails integrated into the extrusions keeping the rollers parallel. The dropping column enabled vertical motion via a set of parallel spindle rails that ran the extrusion's length. The spindle guide rails required open bearings, as illustrated in Figure 4-18c, which were recessed into the vertical face of the impactor to ensure consistent alignment. The horizontal component was supported with steel plates to form a right-angled triangle to ensure the knee form was parallel with the surface throughout the interaction. An armature plate would set the drop height, Figure 4-18d, with a quick-release mechanism to lock it in place, and free-fall would be initiated by the release of the magnet mounted on the impactor.

4.3.3 Impactor

The University of Michigan Transportation Research Institute developed a realistic framework model, HumanShape [214], which produces a manikin based on actual anthropometric data from high-resolution laser scans of men, women, and children. The software generates the 3D model using the following minimal parameters: gender, height, body mass index (BMI), age, and seated stature ratio. The model comes in two formats: seating or standing. The seated model was selected as the bent knee better represented the knee geometry during a realistic player-surface interaction. The average male player who stands at a height of 1.87m and weighs 108 kg would be considered obese as their BMI would be 30.8. Elite athletes typically have a lot of muscle mass, which makes them heavier; therefore, BMI is considered a poor metric for determining body composition.

Consequently, the BMI was dropped to 24 to represent a healthy individual to ensure the model mimicked an elite rugby player. A range of ages was tested to assess its effects on the model. As the age increased, the model became more hunchbacked and appeared less athletic. The average age of senior players is typically between 25-27 [199]; therefore, the younger age was selected to ensure the model represented an athletic player. Finally, the seated stature ratio represented the model's height proportion above and below the waist, ranging from 0.4 – 0.6. There was no data to suggest which ratio should be applied. Therefore, the midpoint of 0.5 was selected. The model was generated with all the values for the input parameters established, as presented in Figure 4-13.

Figure 4-13: Full body manikin to represent the simulated player.

The model required alterations to produce a product which could be utilised in testing. Superfluous body parts were removed, and further refinements were made until the remaining object resembled the desired geometry. The model generated by the software was highly faceted. It was predicted that these features would be transferred onto the external surface when the knee was wrapped in the skin. These features were undesirable as edge effects could influence wear and kinematic data. Accordingly, the node size of the '.stl' file was altered to reduce the magnitude of the undesirable features. During the smoothing process, a trial and error process was applied to changing the mesh node sizes to achieve a knee form that was sufficiently smoothed but still maintained the integrity of possessing good bio-fidelity. An additional design feature was incorporated to provide a surface for the attachment mechanism to clamp the skin simulant against, as presented in Figure 4-14. This model was then turned into a shell and 3D printed. To reinforce the shell, it was filled with epoxy, and M8 holes were tapped to enable attachment to the dropping mechanism. Despite the knee form appearing relatively smooth on CAD the 3D printed surface was still relatively faceted which could be observed through the skin, as observed in Figure 4-15.

Figure 4-14: Initial knee form design.

Figure 4-15: Highlighting the projection of the surface facets through the skin simulant.

This feature was deemed unacceptable as the edges between the mesh nodes do not represent a person and could influence the abrasion sustained during the interaction. Although the knee form possesses good bio-fidelity, the asymmetrical geometry was also considered a concern for laboratory testing as edge effects could produce inconsistent data during the interaction. Therefore, further refinement of the geometry was required. Another improvement identified during the preliminary test was that a significant skin area was untested in the first two iterations. Therefore, the overall height was reduced from 115 mm to 77.5mm. Whilst maintaining a width of 130 mm, the length was reduced from 340 mm to 290mm. The third impactor was entirely created in CAD software, starting from scratch, utilizing the built-in loft feature. This feature was manually fine-tuned through continuous visual comparisons until the geometry aligned with the original model. This process produced the ideal balance between a sufficiently smooth and symmetrical surface, closely conformed to the original human shape model.

During a workflow efficiency analysis, the attachment of the skin to the knee was identified as a bottleneck. The current attachment method only had one point of contact; therefore, if the tension was released at any point, the process would have to start again. The focus during the redesign of the impactor was creating a new attachment method that clamped the skin in multiple places to allow fine adjustment.

Additionally, the tapped holes in the epoxy started deteriorating after repeatedly attaching and removing the impactor from the dropping mechanism. Aluminium components were, therefore, incorporated into the shell to provide a robust attachment method. These inserts were T-shaped (Figure 4-16), slotted into locating features within the shell to ensure accurate placement. The T-shape was adopted to provide a maximum surface area within the epoxy to ensure the inserts were secured well. Aluminium semicircles were also inserted at the bow and stern of the shell for additional attachment points to distribute the forces experienced by the attachment mechanism during impact over the full length of the impactor. The T-slots had M6 tapped holes on the lateral faces while the semicircles had three tapped holes, where one was centrally located, and the other was offset by 45°, to help clamp the skin to the impactor, as illustrated in Figure 4-17.

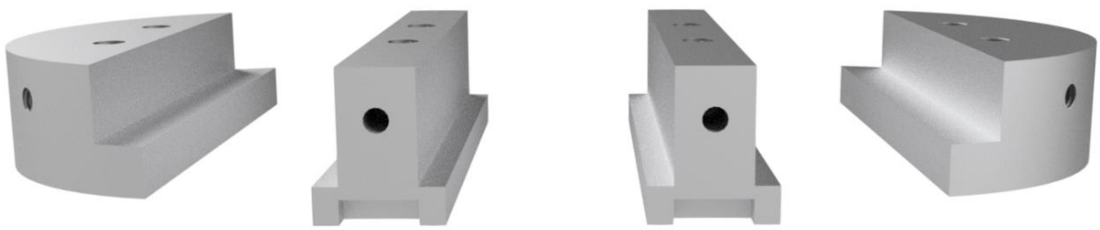

Figure 4-16: Aluminium components for robust attachment mechanism.

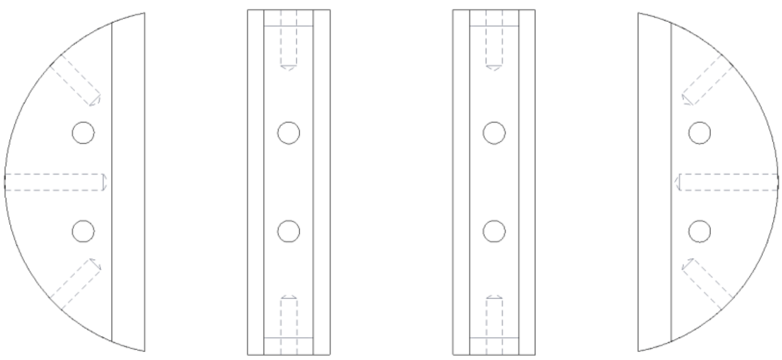

Figure 4-17: Schematic of Aluminium components highlighting angle of tapped holes for attachment mechanism.

Following testing with the second impactor it was apparent that consistent thermocouple placement was an issue, therefore, the impactor was designed to incorporate built-in thermocouples, as presented in Figure 4-18.

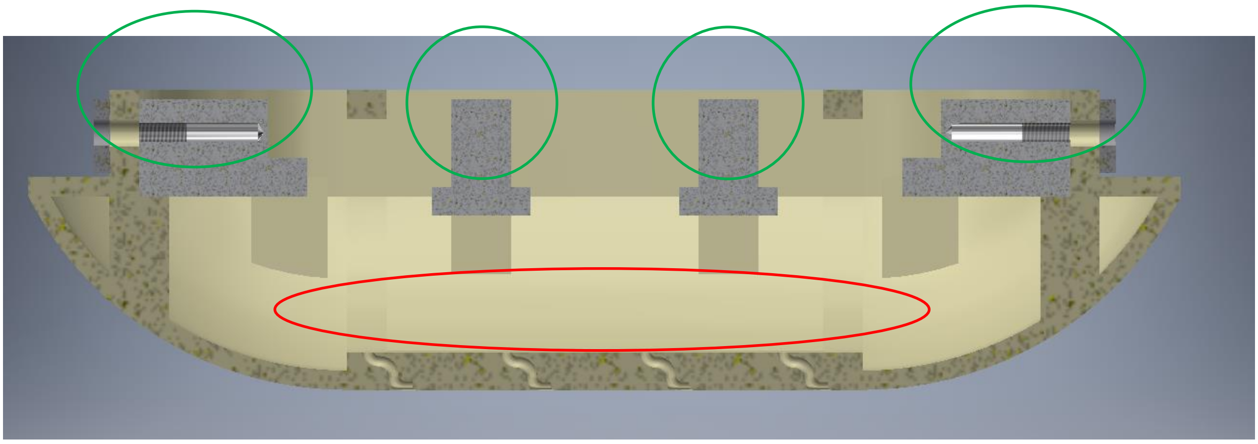

Figure 4-18: Half View Schematic of Third Impactor Design: Green – Aluminium Inserts for attachment to dropping mechanism and clamping the skin simulant |. Red – Thermocouple channels.

The final improvement for the impactor was established when analysing the abrasion on the skin, which predominantly occurs on the nose of the impactor, which ploughs through the surface. From the temperature data collected in the preliminary studies, the maximum rise in temperature was only eight °C, which was suspiciously low for such a high-speed interaction. Therefore, thermocouple channels were integrated into the nose to better represent temperature during the interaction, Figure 4-19. Additionally, during the abrasion analysis of a severely damaged sample, there were four red circles, as observed in Figure 4-20, which were attributed to the thermocouple channels. Therefore, the size of the holes was reduced so that their influence on the abrasion score was minimised.

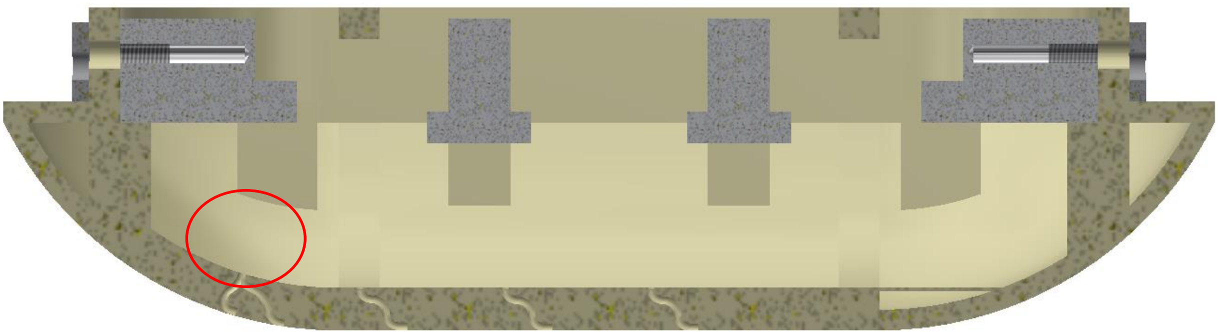

Figure 4-19: Half View Schematic of Third Impactor Design – highlighting amendments to thermocouple locations.

Figure 4-20: Skin simulant sample, which highlights undamaged area due to thermocouple holes.

Evaluating previous design iterations identified that creating a template, presented in Figure 4-21, for preparing the skin, which samples focused on eliminating the folds and wrinkles around the apex of the knee, was essential. All these design improvements were considered and implemented into the final knee form, as presented in Figure 4-22.

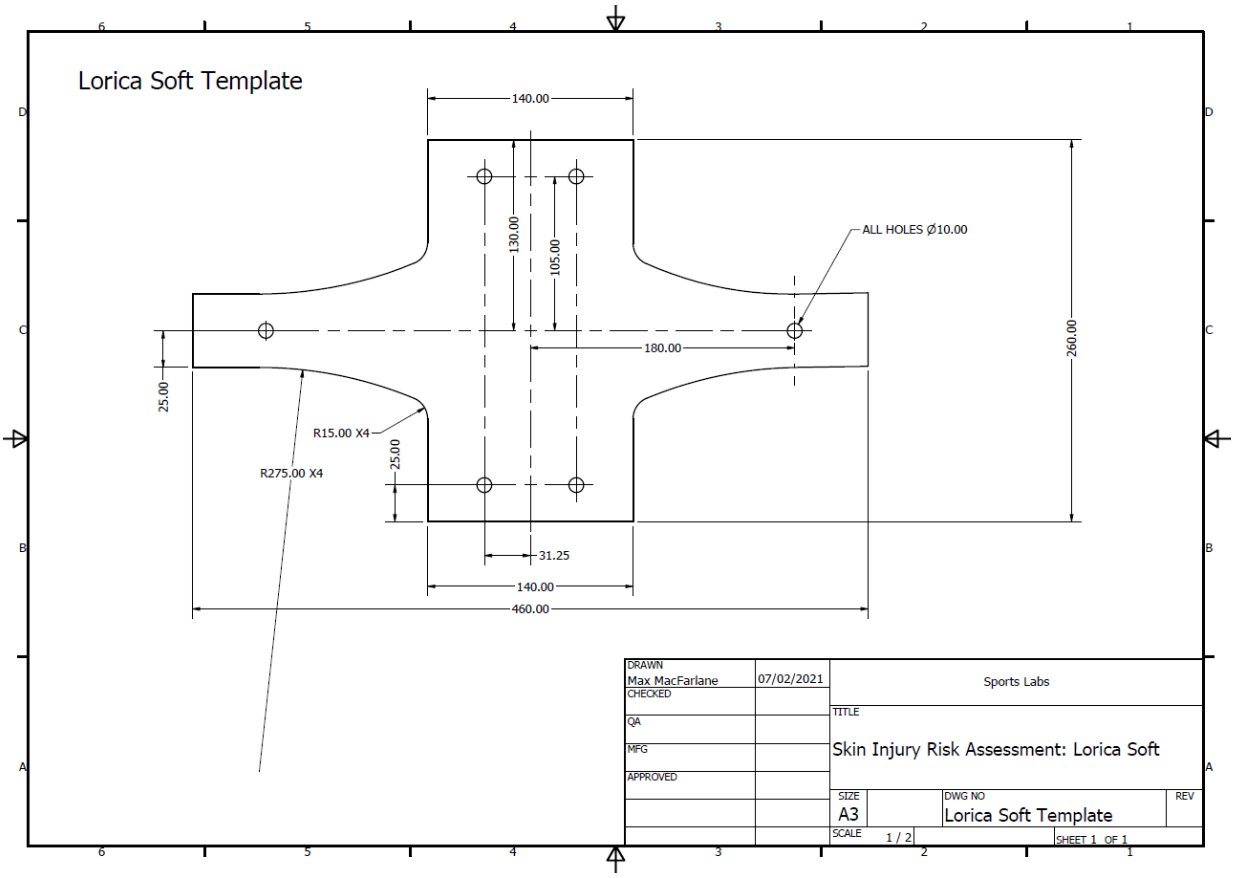

Figure 4-21: Skin Template

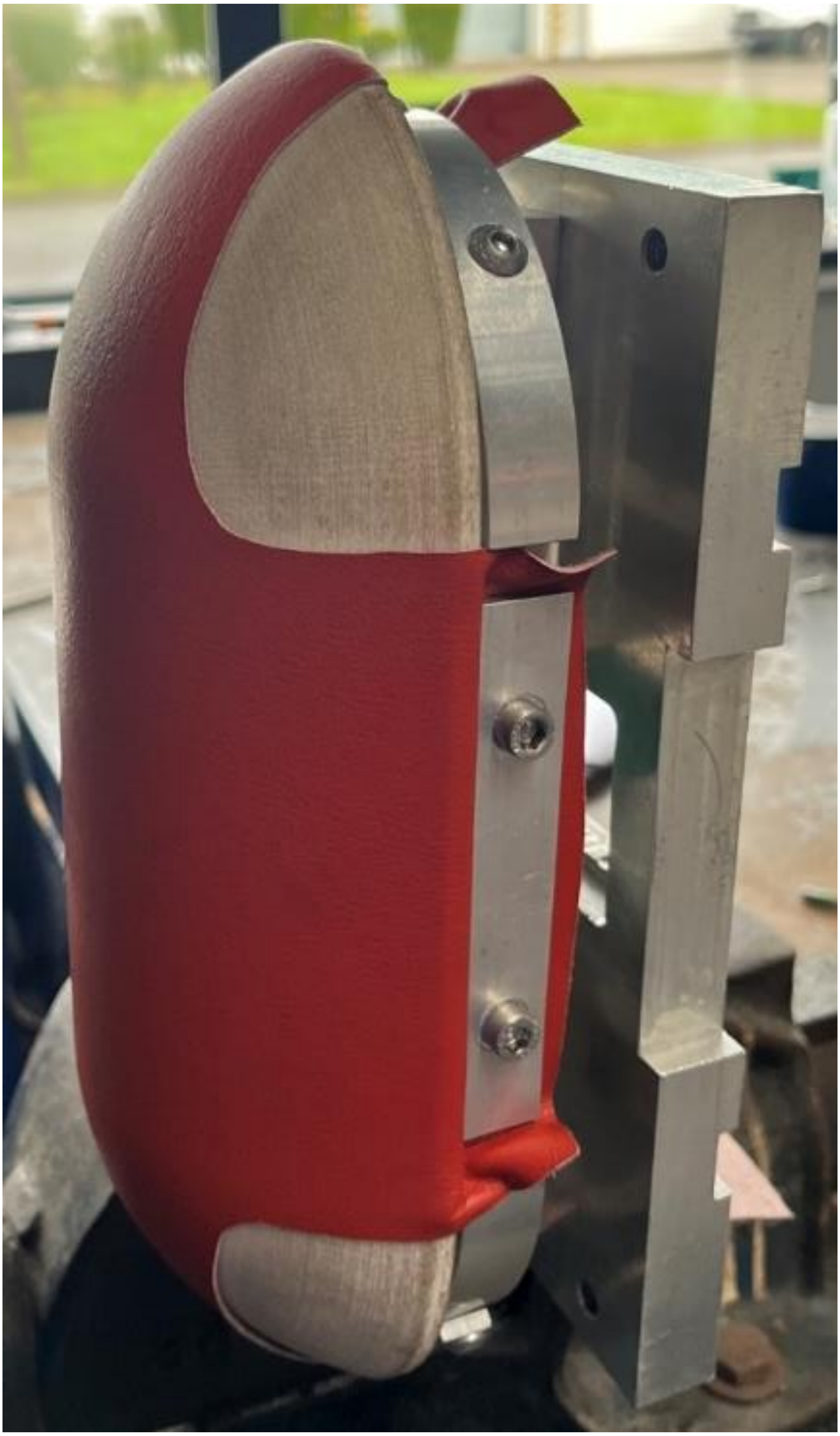

Figure 4-22: Final Impactor Design

4.3.4 Propulsion Mechanism - Generating Horizontal & Vertical Velocity

The investigation into propulsion methods for high-speed trains and rollercoasters highlighted that a linear induction motor was a viable option for achieving 5 m/s over a short distance; however, a significant financial investment comes with this advanced technology. Therefore, a cheap and simplistic solution was designed and developed to prove the basic principles of the device. The preliminary testing was performed with a spring propulsion system, Figure 4-23, manufactured from a repurposed kit available in the workshop. The carriage was accelerated by compressing the springs via hydraulics and released by electromagnetics on the end of the pistons. The compression of the springs, which had an overall length of 770 mm, was limited to the stroke length of the hydraulic pistons, which was 127 mm.

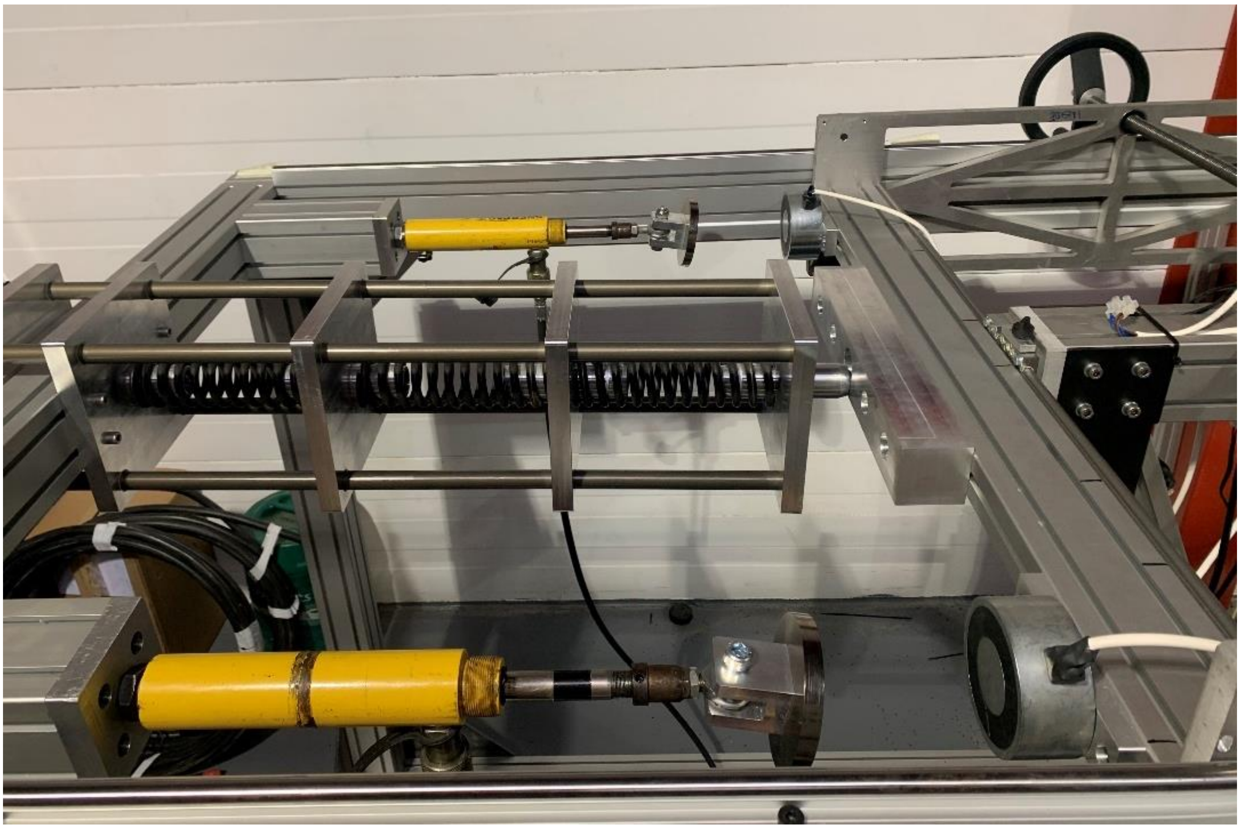

Figure 4-23: Spring Propulsion System

When springs are configured in series, as they are above, the system is equivalent to a single spring of spring constant k_T, as presented in Equation 15 [200]. Each identical spring had a rate of 57.27 N/mm, which equated to a theoretical spring constant of 19.09 N/mm.

Equation 15

$$\frac{1}{k_T} = \frac{1}{k_1} + \frac{1}{k_2} + \frac{1}{k_3}$$

The potential energy of a spring is related to the compressive deformation (x) of the spring from its equilibrium position and the spring constant (k) which is a measure of stiffness, as presented in Equation 16.

Equation 16

$$P_E = \frac{1}{2}kx^2$$

The main constraint of this design was the stroke length of the hydraulic piston which limited the compressive deformation to 127 mm. Consequently, this system had a maximum potential energy of 154 J. The maximum carriage velocity can be calculated by equating potential energy and kinetic energy and then rearranging to find v, as presented in Equation 17.

Equation 17

$$v = \sqrt{\frac{2P_E}{m}}$$

Figure 4-24 presents the full assembly of the carriage, dropping column, and impactor which has a total mass of 87.2kg. Applying this mass to Equation 17 the maximum launch velocity was 1.88 m/s, which was deemed sufficient for performing preliminary testing.

Figure 4-24: Dropping Mechanism

4.3.5 Operation and Measurement Systems

Initially, this prototype was controlled by physically hardwired components to simplify troubleshooting, unlike a wireless or software-based operation system. The spring system hydraulics and electromagnets were controlled manually to ensure the launch was safe; however, preliminary testing established that the dropping mechanism electromagnet required a time delay to allow the carriage to reach full speed before release. This time delay was integrated using a National Instruments USB-6212 and DAQExpress software. The DAQ collected accelerometer data on the vertical and horizontal axis to provide information on velocities and displacements and help validate the basic principles.

4.4 Prototype Testing and Subsequent Design Improvements

The final device developed during this project will ultimately be adopted by World Rugby and enrolled in their Rugby Turf Performance Specifications programme; therefore, the protocol must be optimised for laboratory tests [201]. This section will provide an overview of observations noted that would help improve the performance and user-friendliness of the device. The main aim of the preliminary testing was to demonstrate that the device would function as desired and establish if the design specification requirements could be achieved. The preliminary testing consisted of three studies which focused on providing insights into the capacity and functionality of the apparatus. The typical horizontal and vertical accelerometer waveforms generated during an interaction, which have been integrated to calculate velocity and displacement, are presented in Figure 4-25. This data will be analysed to discover any undesirable features, vital information to help improve the prototype for the next design iteration.

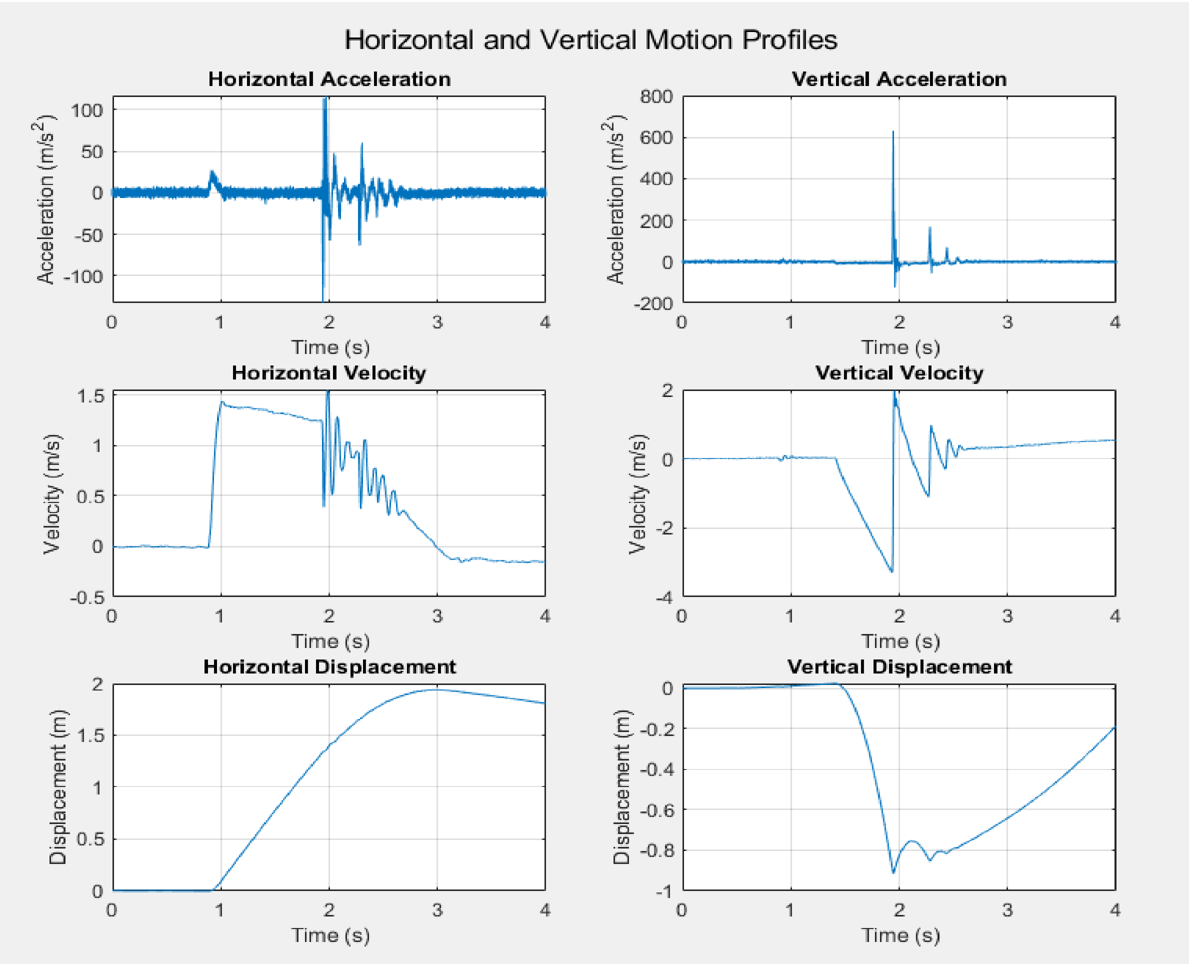

Figure 4-25: Typical horizontal and vertical accelerometer wave form generated during an interaction.

4.4.1 Study 1: Identification of Accelerometer Range & Evaluating the Impactor's Ability to Free Fall

Introduction

The magnitudes of horizontal and vertical forces experienced were expected to differ during the impact zone and sliding phase significantly. This study aimed to establish a suitable accelerometer measurement range for each interaction event.

Materials and Methods

The surface was a standard Rugby Turf spec, which consisted of a 60mm carpet on a 20mm shock pad. There were equal rates (15 kg/m^2) of stabilising and performance infill to produce a system with a free pile height of 15 mm. The testing consisted of four release heights and five different speeds, which were achieved by varying the compression of the spring system, each with 3 test repeats where the impactor was centrally located within the carriage. Accelerometer data was recorded at 20 kHz via the NI DAQ to monitor the vertical and horizontal axis.

Around 1s, an initial peak can be observed in Figure 4-26a, which represents the release of the spring system, which accelerates the carriage. This positive peak represents forward propulsion; any negative values can be considered a resistive force. The horizontal impact G force was calculated by dividing the minimum acceleration by 9.81 m/s^2. Around 1.4s, a negative vertical acceleration is highlighted, representing the impactor's release, which begins to free fall. The same calculation was performed on the maximum vertical acceleration to determine the vertical impact G force.

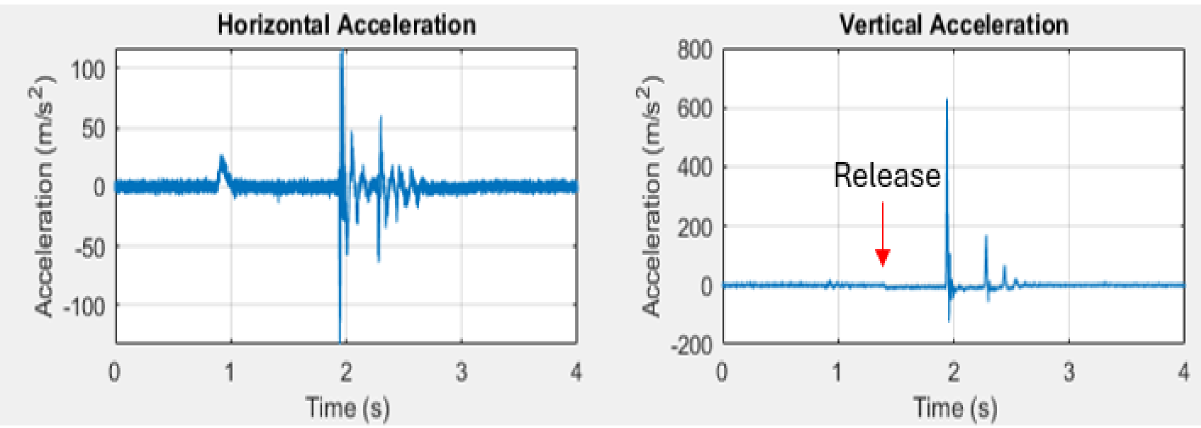

Figure 4-26: Typical acceleration waveforms a) Horizontal b) Vertical

It was impossible to define the horizontal and vertical sliding phase velocities in the design specification as they would be a function of the turf properties. Therefore, assumptions had to be made to establish suitable values. The impact zone produced the highest deceleration rate, and the sliding phase commenced when the impactor reached equilibrium in the vertical direction; therefore, the desired horizontal velocity was half the impact speed (2.5 m/s), and the vertical velocity was limited to 1 m/s. To evaluate the G forces of the sliding phase, the next interaction with the turf after the impact zone was analysed, representing the second peak in Figure 4-26b.

To evaluate the impactor's ability to free fall, the theoretical impact velocity (Equation 18) was calculated from the release height. By analysing the vertical motion profile of the impactor, it can be observed that the initial peak on the acceleration waveform represents the minimum experimental impact velocity and displacement, as presented in Figure 4-25. The release height was equivalent to the displacement at the time index for the maximum acceleration.

Equation 18

$$v = \sqrt{2gh}$$

Results

Figure 4-27 and Figure 4-28 present the horizontal and vertical impact G forces and corresponding velocities recorded during Study 1. The design specification defined a desired upper output value of 5.1 and 3.4 m/s for horizontal and vertical impact velocities, respectively. By extrapolating this data to meet the criteria of the design specification, it was demonstrated that realistic impact values would be 40.9G and 73.8G for the horizontal and vertical axes, respectively.

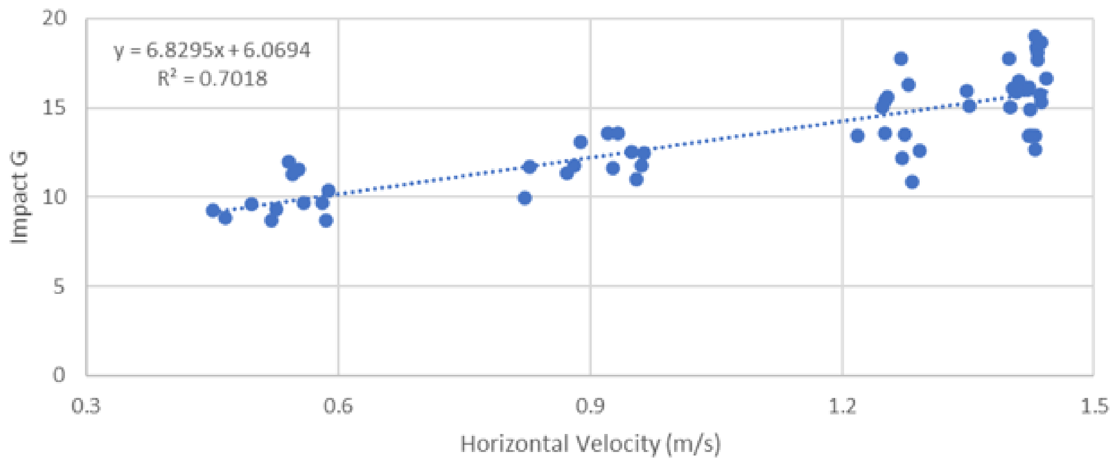

Figure 4-27: Extrapolating horizontal impact data to establish a suitable accelerometer measurement range.

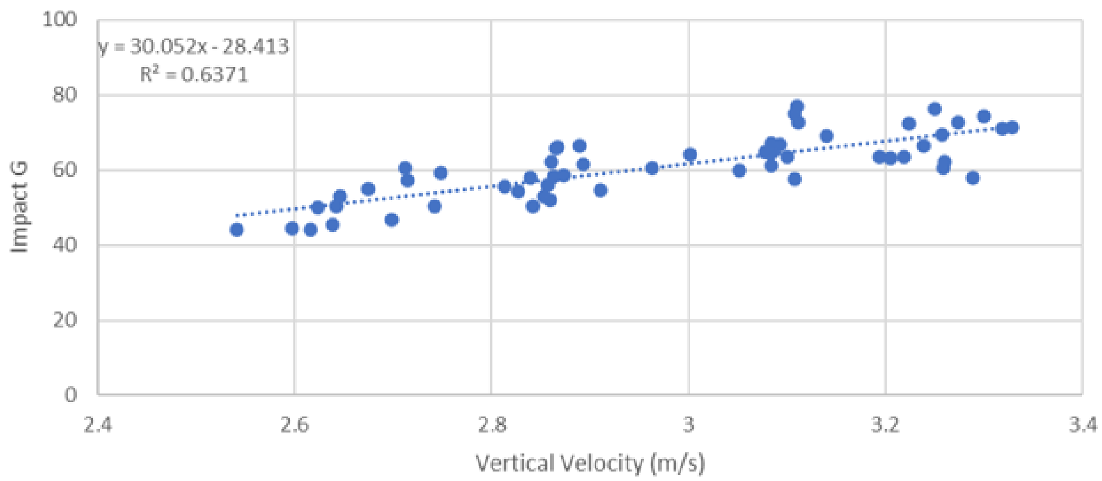

Figure 4-28: Extrapolating vertical impact data to establish a suitable accelerometer measurement range.

The vertical and horizontal sliding phase G forces and corresponding velocities are presented in Figure 4-29 and Figure 4-30. Extrapolating this data set to find the G forces at the assumed sliding phase conditions demonstrated that forces at the start of the sliding phase would be 10.7G and 8.7G for the horizontal and vertical axes, respectively.

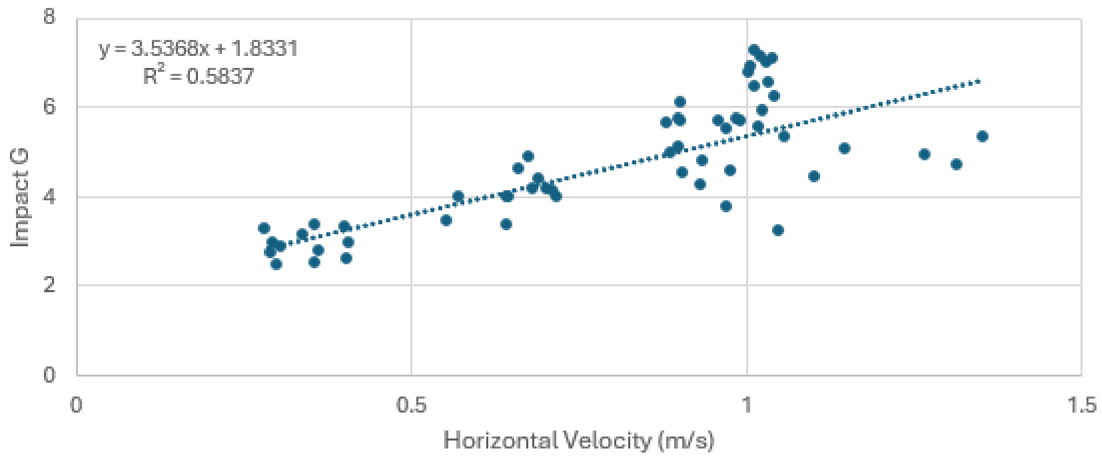

Figure 4-29: Extrapolating horizontal sliding data to establish a suitable accelerometer measurement range.

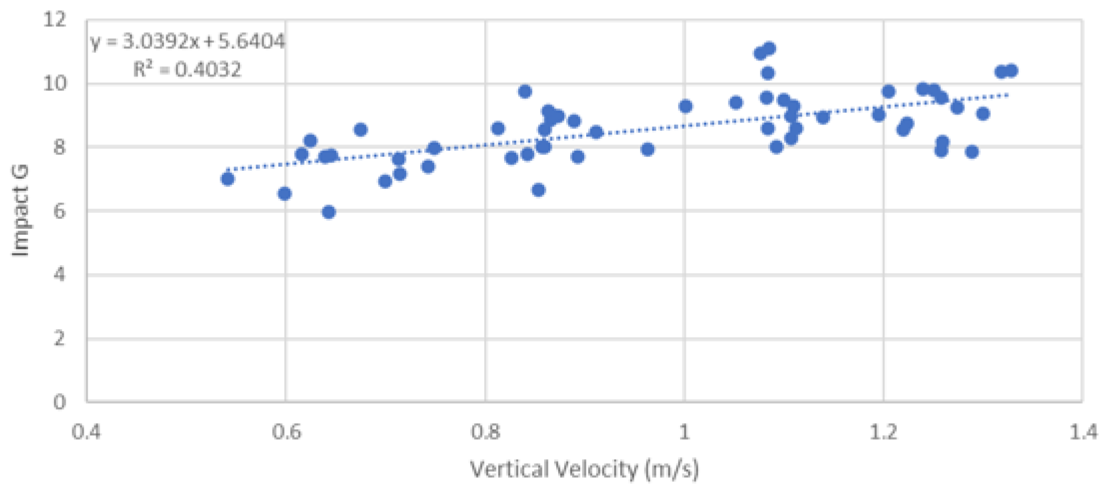

Figure 4-30: Extrapolating vertical sliding data to establish a suitable accelerometer measurement range.

The comparison of the experimental and theoretical impact velocities in relation to their corresponding release heights can be observed in Figure 4-31. Standard error bars were added to each data point; however, they were so small that the marker size was disguised. This low standard error (SE < 0.01) implies that the dropping mechanism had good repeatability of generating consistent vertical impact velocities across a range of drop heights.

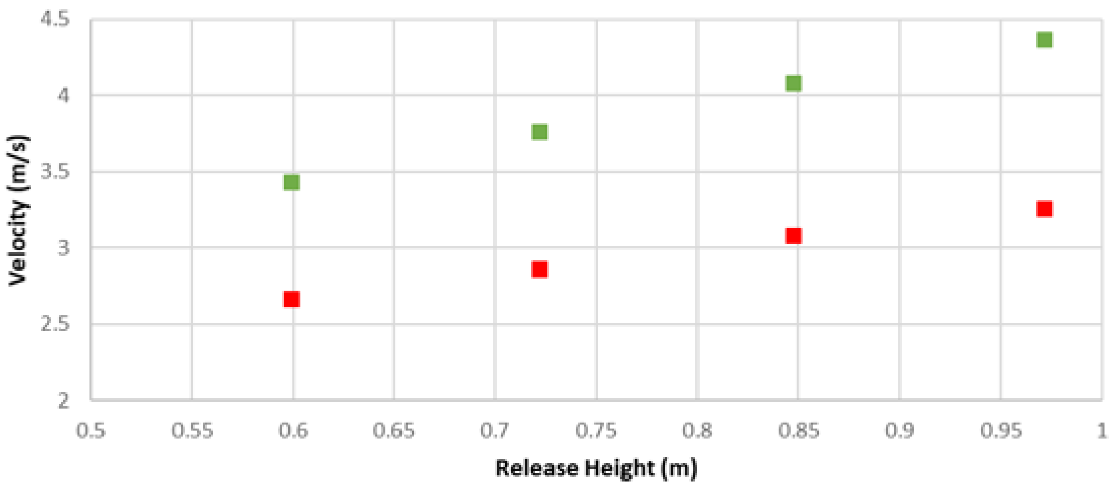

Figure 4-31: Comparison of Theoretical (green) and Experimental (red) Vertical Impact Velocities (error bars disguised by marker)

Discussion

This testing, crucially, was only performed on one standard surface, resulting in a relatively small sample size. It's important to note that different surface constructs (infill rates and infill type) could produce varying forces. To account for this, the values were doubled to ensure a suitable measuring range that could assess any surface. The impact zone accelerometers were 200G and 100G for the vertical and horizontal axis, respectively, while the sliding phase accelerometers were 20G each.

With the increase in release height, significant differences between experimental and theoretical velocities became apparent in Figure 4-31. The escalating percentage error indicates the impactor's encounter with unwanted resistive forces during the fall. This unacceptable error was attributed to the impactor's eccentric loading as it traversed the vertical linear guide rails. This loading profile generates a moment on the two bearings, increasing friction. Therefore, it is imperative to redesign the dropping mechanism to ensure it falls through its centre of mass, thereby reducing resistance.

The final consideration from this study was the impactor's bouncing nature, which can be observed in Figure 4-26. Three distinct vertical peaks correspond to discrete contact with the surface. The final peak corresponds to the time index, where the horizontal acceleration flat lines suggest no sliding phase. This, however, requires further investigation once higher horizontal speeds are achieved, emphasizing the ongoing nature of this study.

4.4.2 Study 2: High-Speeded Camera Analysis of Horizontal Motion

Introduction

During Study 1, a reoccurring feature in the horizontal velocity after the impact, highlighted in red in Figure 4-32, was greater than the launch velocity. This feature was concerning as it meant the impactor was accelerating after the impact, which does not represent a player in motion.

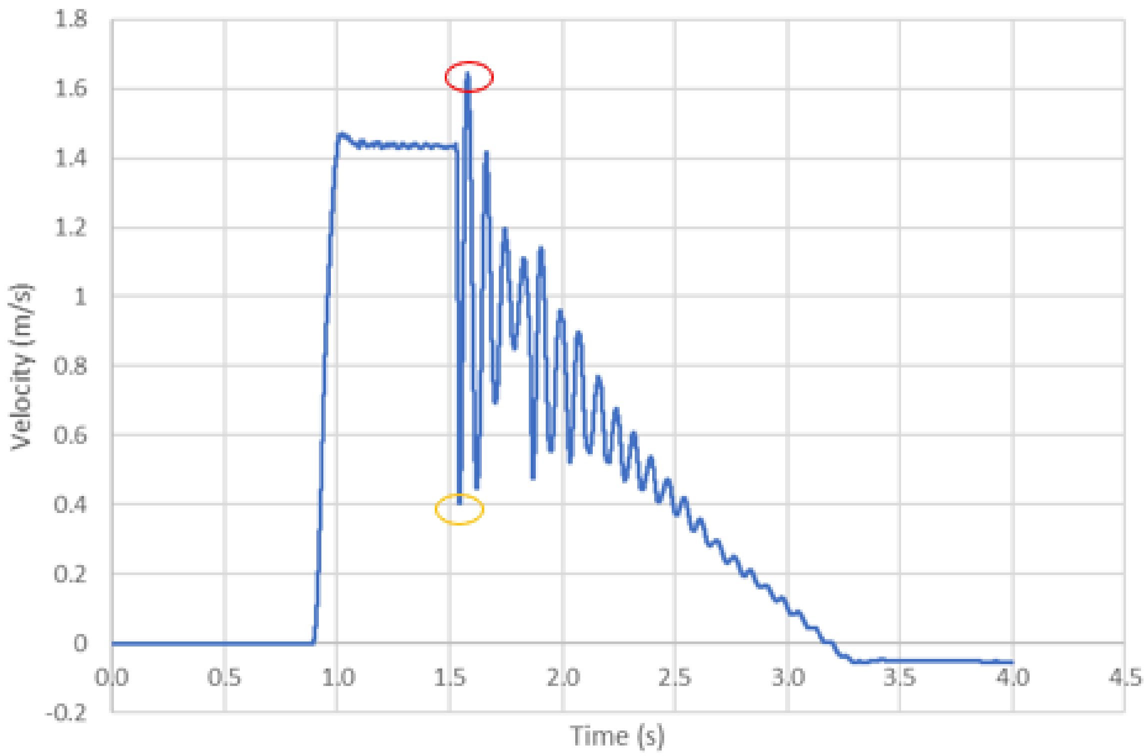

Figure 4-32: Highlighting potential deflection of the dropping column.

On further inspection (Figure 4-33), the time delay is a fraction of a second (0.034s); however, the accelerometer data was recorded at 20kHz, corresponding to 680 samples. This duration was sufficient to conclude that the artefact was not anomalous. This finding warranted further investigation and provided motivation to perform a high-speed camera analysis of the impact zone to monitor the motion profile of the knee form.

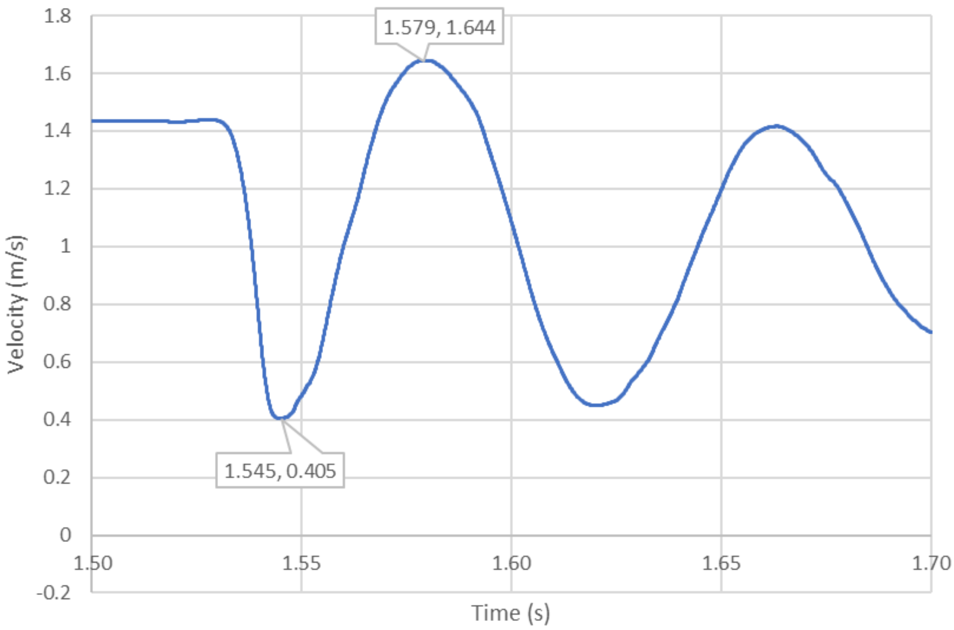

Figure 4-33: Focusing on reoccurring artifacts in horizontal velocity.

Materials & Methods

The surface was a standard Rugby Turf spec, which consisted of a 60mm carpet on a 20mm shock pad. There were equal rates (15 kg/m^2) of stabilising and performance infill to produce a system with a free pile height of 15 mm.

Dartfish software was used to analyse high-speed camera footage, as presented in Figure 4-34. In the reference frame, Figure 4-34a, a grid overlapped on the images to ensure the vertical member was perpendicular to the ground. The linear guide rails were held in place on the dropping column via nuts and bolts, which can be observed in the images. The nut at the top of the vertical member was used as a reference point for measuring deflection. Then, a known length of 0.05 m was used to calibrate the software to calculate the length (L = 0.71 m) from the reference point to the base of the dropping column. A frame-by-frame analysis of the impact was performed to determine the maximum and minimum deflection of the dropping column. Basic trigonometry was applied to the deflections to calculate the horizontal displacement, as presented in Equation 19 – where L is the length of the flexed member, and θ is the deflection angle.

Equation 19

$$x = \mathrm{L}.\sin(\theta)$$

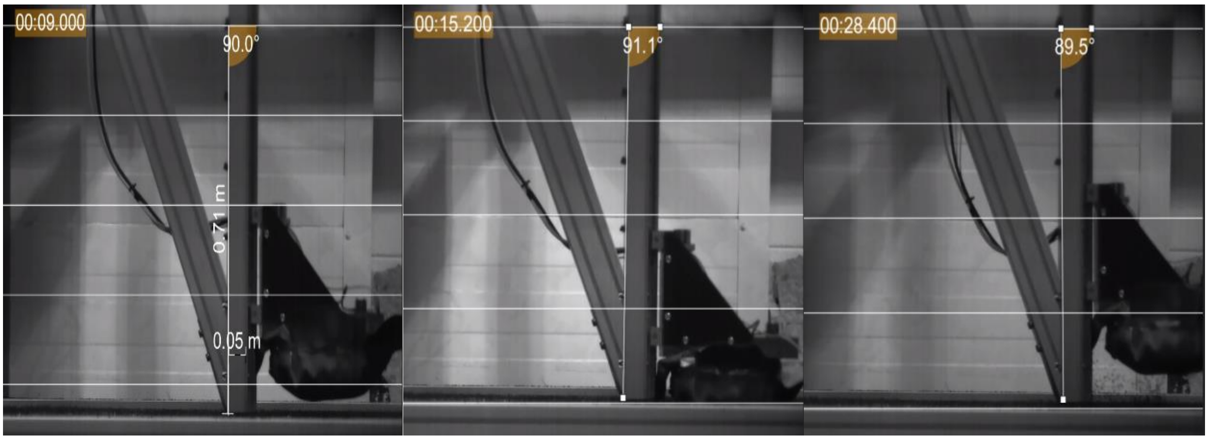

Figure 4-34: High-speed camera analysis of dropping column deflection during impact zone a) Preimpact neutral reference point b) Maximum posterior deflection c) Maximum anterior deflection.

Results

During contact with the ground, the surface grips the impactor, causing it to significantly reduce its speed to around 0.4 m/s, as highlighted in Figure 4-33. However, during the impactor's deceleration, the carriage's momentum continues to drive it along the guide rails, resulting in posterior deflection of the dropping column, as presented in Figure 4-34b. A frame-by-frame analysis of the impact determined that the impact generated a maximum deflection of 1.1°, which correlated to a horizontal displacement of 13.6 mm.

As the impactor rebounded off the surface, the force generating the deflection was released, and the impactor shot forward past the neutral reference point, which resulted in an anterior deflection of 0.5°, as presented in Figure 4-34c. Applying this deflection to Equation 16, a horizontal displacement of 6.2 mm was calculated. This out-of-phase movement in relation to the carriage generated a maximum velocity greater than the launch velocity after the impact.

Discussion

The results of the high-speed camera analysis suggested that the artefact was attributed to the dropping column deflecting on impact. The desired measurement axis for the horizontal and vertical accelerometers was parallel and perpendicular to the surface, respectively. The unwanted deflection, however, forces the measurement axis along an unpredictable arc, a function of the turf properties. For example, a stiffer turf would produce a more significant deflection than a softer system. The deflection of the dropping column may amplify decelerations, making skin injury risk assessment challenging to predict because the resultant forces will differ for each surface.

Consequently, the dropping mechanism should be redesigned to minimise deflection and maintain a consistent measurement axis throughout the interaction. This modification could be achieved by reducing the length between the anchoring point on the carriage and the point of contact with the surface. This design change will be beneficial as the carriage's centre of mass will be closer to the surface, making momentum forces behind the interaction more realistic than what a player would experience.

4.4.3 Study 3: Investigating Influence of Multiple Testing Locations

Introduction

The potential design concepts section suggested that a lead screw would be suitable for enabling multiple test locations across a sample. This study was designed to evaluate the functionality of the lead screw and establish if the impactor location within the carriage had any influence on the results.

Materials & Methods

The surface was a standard Rugby Turf spec, which consisted of a 60mm carpet on a 20mm shock pad. There were equal rates (15 kg/m^2) of stabilising and performance infill to produce a system with a free pile height of 15 mm. The testing consisted of centrally located locations, and the other two positions were offset by 300 mm left and right. Testing consisted of 10 iterations where the hydraulic piston was fully contracted, and the release height was set to 850 mm to achieve the desired vertical velocity. Accelerometer data was recorded at 20 kHz via the NI DAQ to monitor the vertical and horizontal axis.

Results

The horizontal launch velocities, presented in Figure 4-35, illustrate that eccentrically positioning the impactor within the carriage to assess a different impact location resulted in a reduced launch velocity compared to a centrally located test. The low standard error bars imply that the spring system could generate consistent launch velocities.

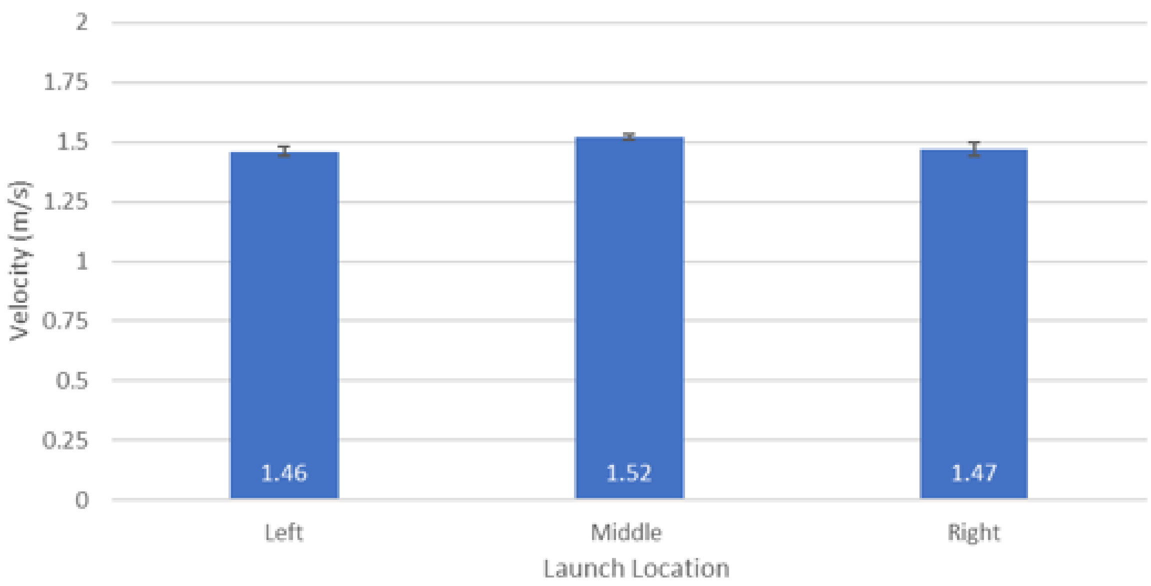

Figure 4-35: Comparison of launch velocities when varying impact locations.

Discussion

Despite generating consistent velocities at each launch location, the system has losses. This setup could only achieve 1.52 m/s, 19.1% less than the theoretical maximum (1.88 m/s). During testing, where the impactor was not centrally located, the carriage would rattle, which was attributed to the eccentric loading. At these low speeds, there did not appear to be any damage; however, at the desired 5 m/s, the frame might not support repeated testing. Therefore, the gantry should be redesigned to move across the surface to assess multiple test locations. Making the gantry more compact will make the design more robust, and the rattling should be eliminated.

The main limitation of this initial prototype was the ability to generate a horizontal impact velocity of 5m/s. The overall length of the spring system is an additional concern as it consumes a proportion of the interaction length. Therefore, the new propulsion system should accelerate the carriage outside the gantry to ensure the largest area can be tested.

4.4.4 Summary of Design Improvements

Several improvements have been identified for the redesign of the testing apparatus. Firstly, the gantry should be made more compact to minimise the moment on the dropping column and offer increased support, thereby preventing deflection. This modification will also ensure that the accelerometer axis remains parallel and perpendicular to the surface, ultimately improving the assessment of skin injury risks. Furthermore, this modification makes the interaction more realistic by better representing the centre of mass and momentum forces. The dropping column should also be modified to fall through the centre of mass, enhancing its free-falling capability to reduce the percentage error between theoretical and experimental impact velocities.

Another enhancement involves eliminating the lead screw and incorporating the capability to move the gantry across the sample, enabling multiple test locations. Furthermore, the impactor should be redesigned to enhance skin attachment, making it more manageable for a single person. Tensile testing performed on the skin reported that the skin was much stronger when tested along the length of the roll. Skin samples should, therefore, be prepared in this orientation whilst using the template to remove unwanted wrinkles. Thermocouples should be integrated into the knee form and positioned on the impactor's nose to obtain the most accurate temperature measurements.

Given the dynamic nature of the testing process, effective cable management would be crucial to prevent wire damage. Initially, there was concern that the power cable connected to the magnet could trap them during the free fall. To address this issue, the position of the magnet and armature plate should be reversed. Another potential hazard was posed by the accelerometer cables, which should be guided out of the back of the new impactor design and secured using a cable gland. This measure will safeguard the transducers from sudden cable jerks and ensure optimal performance.

4.5 Skin Injury Device: Final Design and Technical Specification

Preliminary testing provided valuable information, which significantly enhanced the final product. Considering all the design recommendations, this project has delivered a new machine capable of representing realistic velocities that a player would experience during gameplay, enabling accurate simulations of potentially injurious rugby scenarios. This section will outline the features and technical specifications of the research device used in the following chapters.

4.5.1 Impactor

The main limitation of the dropping column was the eccentric loading of the impactor along the linear guide rails, which prevented it from free falling. Therefore, the impactor was redesigned to fall through its centre of mass. This modification was achieved by incorporating two laterally located linear bearings, as presented in Figure 4-36. Each housing unit contained two closed bushings capable of supporting high loads. Alignment of the bearings was essential; therefore, they were recessed into an aluminium block that formed the main body of the impactor. The magnet's armature plate was centrally located on the top, and a cavity was created on the bottom to house the measurement system. The cable gland was attached via a tapped keyhole shape. This geometry was required to allow the accelerometer cables to be safely installed or removed without removing the transducer's plugs.

The accelerometer mount was T-shaped for easy attachment to the plate below, with fillets on each edge to prevent sharp edges from fraying the cables. There were two attachment plates: 1 – to contain the accelerometer mount within the cavity and 2 – to allow the impactor to be removed quickly. Alignment of the accelerometer mount was essential; therefore, several recesses were created on the attachment plates. The first recess was in the centre of the plate to maintain the accelerometer mount's position. This plate was made longer than the main body of the impactor to create a recess for mating the block and the plate. Two parallel extrusions were created on the bottom face of plate 1, which required corresponding recesses on the plate below. Plate 2 had a hole created in the middle to provide access to insert thermocouple plugs into the sockets within the knee form.

Additionally, spacers were inserted between plate 2 and the knee form to provide access to thermocouple wires.

Part of the validation process required comparing the accelerometers and the load cell. Therefore, the design also included an attachment method to incorporate a load cell, as presented in Figure 4-36.

Figure 4-36: New Impactor Design: a) Top view exploded b) bottom view exploded.

4.5.2 Carriage

To accommodate the new linear bearings, two 30 mm steel reinforced shafts were required, as presented in Figure 4-37. The next design upgrade focused on mitigating the dropping column's deflection on impact. Lowering the carriage's centre of mass will reduce the moment around the anchoring points. Additionally, support struts were placed on the vertical and horizontal aluminium extrusions, forming a hypotenuse, to provide reinforcement. The supports were anchored at the back of the carriage, on the horizontal component, to provide the longest support strut possible. The lower support struts were attached to the dropping column where the impactor's centre of mass would be during the impact zone. Ideally, these support struts would be symmetrical on the upper section; however, they had to be lower due to space constraints within the LIM housing. Lowering the centre of mass and providing multiple support struts should limit deflection experienced by the dropping column during an impact.

The next design consideration was attaching the reaction fin to the carriage. Through collaboration with Force Engineering Ltd., a concept for the LIM system was developed, which recommended a 1.5m reaction fin to generate the desired impact velocity. With the redesign of the dropping column, the impactor would now be located within the rollers of the carriage, which consumes space to attach the reaction. Therefore, the rollers were increased to 1m to provide extra stability whilst anchoring. The reaction fin was attached to a 1.5m extrusion and secured to the lateral extrusions within the carriage via Minitec's cross-connector 45.

Another consideration identified during the preliminary testing was swapping the magnet and armature plate to mitigate the risk of trapping any power cables. This redesign required further attention to develop a method for setting the release height. Additionally, the increased impactor mass was now too heavy for a single-person lift. Therefore, the release height was automated through a worm-geared hoist and motor. The worm gear was identified as a desirable feature as it would prevent the impactor from dropping as the gear can only move in one direction without being driven. Finally, the magnet was connected to the hoist via a Dyneema rope, the world's strongest man-made fibre, to ensure the repeated lifting of the impactor wouldn't cause the rope to fail.

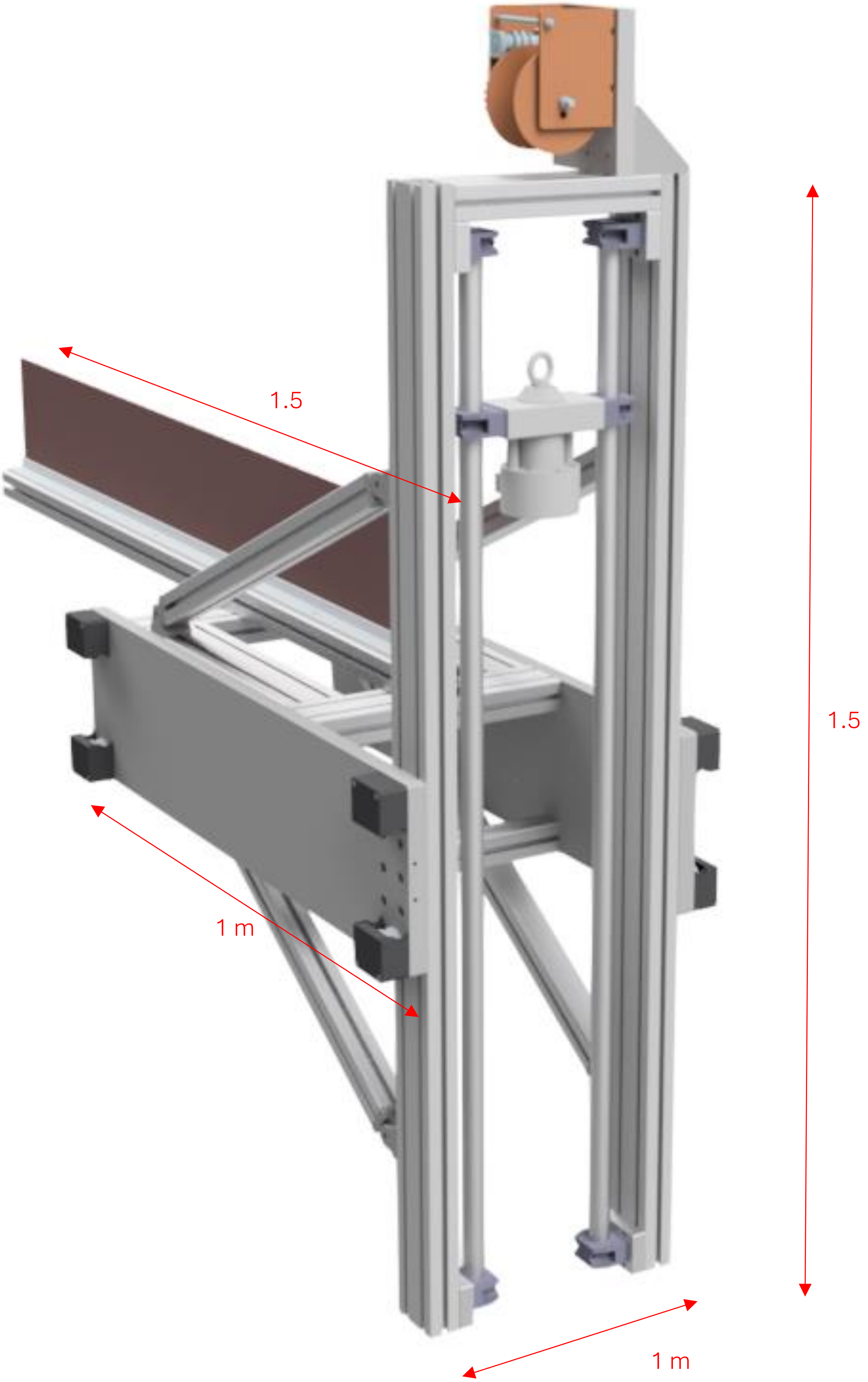

Figure 4-37: New carriage design which allows impactor to fall through its centre of mass and incorporates reaction fin for propulsion system.

4.5.3 Gantry

The gantry was reduced to a 0.62 x 0.62 x 6 mm frame to accommodate the new carriage design. The second design development improved the ability to assess multiple test locations, as the eccentric loading within the carriage could damage the apparatus at higher speeds. This modification was enabled by eight unidirectional castors, as presented in Figure 4-38. The maximum height of a typical surface would be around 90-100mm; therefore, the castors were positioned to provide a clearance of 125 mm to allow the frame to move freely across the surface. An additional structure was created to support the LIM housing. Finally, shock absorbers were installed at the end of the gantry to prevent the carriage from damaging the frame.

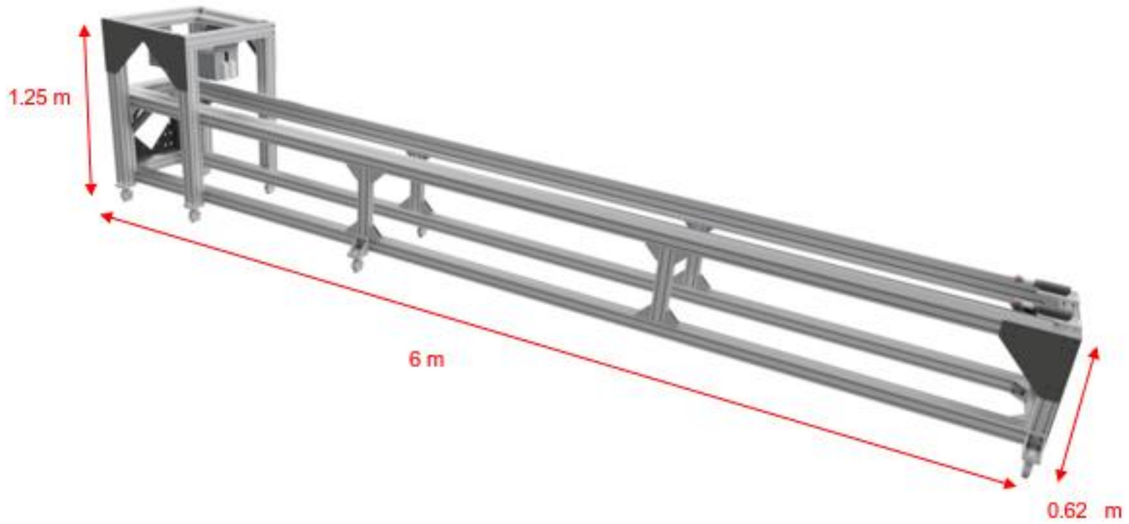

Figure 4-38: Redesigned gantry which incorporates LIM housing.

4.5.4 Propulsion System

The LIM is powered by a Ni-dec M700 driver, which supplies a three-phase primary voltage through a VFD output filter. The launch speed of the carriage can be controlled by three variables: thrust, frequency, or time. The time represented the duration of the EMF pulse, which was kept constant at 0.4 seconds. The thrust represents the wave's amplitude, and the frequency is the number of waves that pass a fixed point in unit time. Both these parameters are controlled by an analogue output channel from the DAQ; therefore, they will be varied by the voltage supplied to them (0 – 10V). A short study was developed to understand better how these variables influence the launch velocity, which consisted of iteratively increasing the frequency from 0.5V to 2.5V whilst keeping the thrust constant. The average of three launches at thrust values of 1V and 1.5V are presented in Figure 4-39.

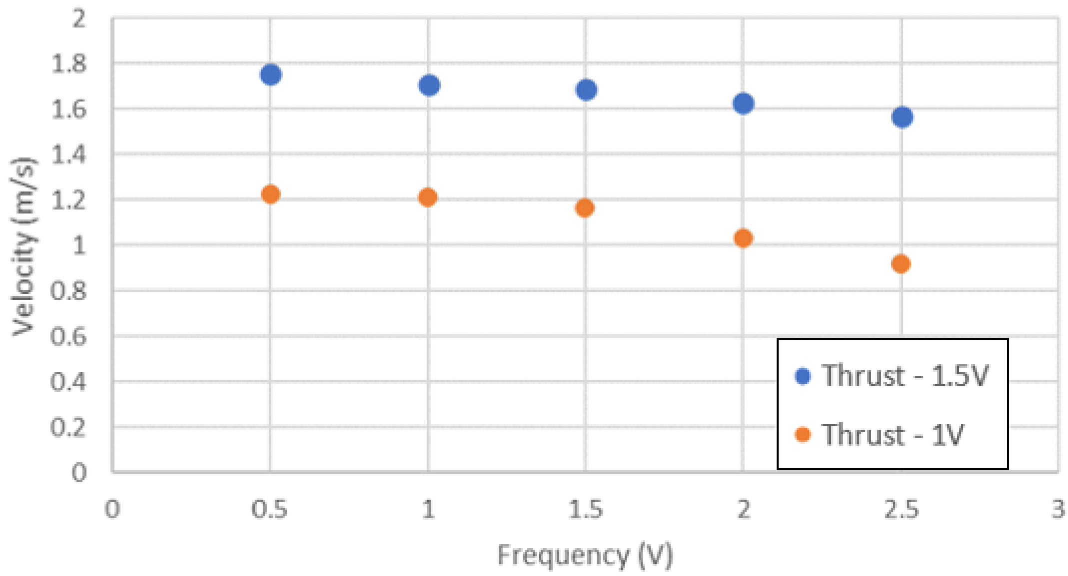

Figure 4-39: Investigating the effects of thrust and frequency on launch velocity.

These results suggest that thrust and frequency are the coarse and fine-tuned adjustments for the launch velocity. As expected, the greater the thrust, the faster the launch velocity; however, the frequency had an inverse relationship with velocity, which was surprising. Further investigation established that this relationship was associated with variations in the synchronous speed with different frequencies.

4.5.5 Dampening Mechanism

The final consideration from Study 1 highlighted concerns over the bouncing nature of the impactor. These concerns were amplified when further testing was performed with this new design at higher speeds. After the impact, the knee form acted like a stone skimming across the water. Therefore, the simulation never entered the desired sliding phase. Despite an initial emphasis on designing an organic interaction that experienced no external forces during the measurement phase. It became apparent that this issue needed to be resolved by developing a dampening mechanism. Time was of the essence to ensure sufficient data could be collected with the final design; therefore, the sprint design methodology was applied to find suitable solutions.

Dead Blow Hammer

Initial design concepts to limit the rebound were inspired by a dead blow hammer, with a hollow head filled with loose pellets [202]. As the hammer is driven onto the striking surface, the pellets fill the back of the hollow head. On impact, the pellets maintain their momentum and travel towards the striking surface, which continues to absorb energy from the pellets, preventing the rebound of the hammerhead. A limitation of this concept is the increased striking force due to the reduced rebound. Despite concerns about amplifying impact forces, a temporary solution was devised to prove basic principles by attaching hollow containers half-filled with sand to the front and back of the impactor, as presented in Figure 4-40. During high-speed camera analysis, it was observed that the sand would free-fall at the same rate as the impactor. Therefore, there was no delay between the impactor and the pellets (sand) striking the surface. For this system to work, the knee form must be driven from the release height into the sample to displace the pellets (sand) to the back of the hollow chamber. The combination of greater impact forces and the lack of free fall required to potentially dampen the rebound deviated too much from the design specification. Therefore, this method was abandoned.

Figure 4-40: Investigating the dead blow hammer as potential concept to limit rebound.

Clamping Brake

The next potential solution explored the feasibility of applying a brake on the vertical linear rails to limit the impactor's rebound. The timing of the brake application would be essential to creating a repeatable dampening mechanism across a range of artificial systems. The best solution would be to trigger the brake through feedback from the accelerometer data. However, it would be challenging to learn how to implement the Control Design and Simulation Module, which is required for live feedback in the LabVIEW programme, while integrating the electronics into the control box and developing the specifications for the brake system whilst maintaining the desired weight.

An alternative solution would be utilising the ground reaction force to compress a clamp on the vertical shafts mechanically. This operation could be achieved by incorporating an RCK 19 clamping element, Figure 4-41, into a bespoke assembly. The clamping element comprised two discs with a tapered bore and an open-slotted ring. The ring is wider in the middle and tapered to the ends to match the geometry of the discs. When the assembly is compressed, the diameter of the ring reduces, increasing friction on the shaft, which goes through the bores to act as a clamping mechanism. Unfortunately, the RCK 19 was not available with a 30 mm bore. Therefore, an Automation Components nylon bushing was modified to become open-slotted and was inserted as a spacer. The bespoke assembly involves attaching the RCK 19 to the linear bearings with a small mass above to apply the force required to compress the clamp. The evolution of the dampening mechanism is presented in Figure 4-42.

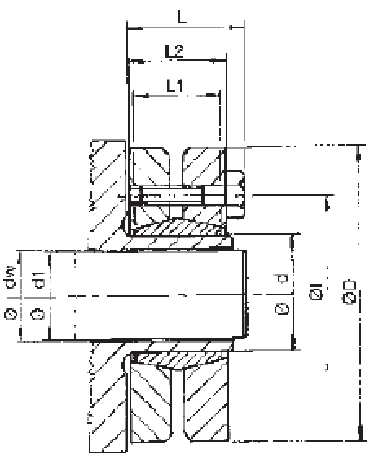

Figure 4-41: Clamping Element Exploded

Figure 4-42: Dampening Mechanism Assembly

The dampening mechanism consisted of a collar to align the RCK 19 with a dead weight above the clamp to generate compressive forces during the impact. For the initial design, Figure 4-42a, the mass above was made of aluminium. However, this made the overall height of the dampening mechanism longer, which affected the release height mechanism. To make the design more ergonomic, the material was changed to steel, a denser material, which reduced the overall height. To prevent the mass above from rebounding off the clamp and generating unwanted features in the accelerometer data, the mass was connected to the collar via shoulder bolts in the second design iteration. To ensure consistent pressure across the dampening mechanism, the shoulder bolts were torqued to 8.8 Nm, per the supplier's technical recommendations. In the first design, the mass above impacted straight onto the nylon, so a counterbore was created to protect the spacer.

During the validation testing, when the load cell (9kg) was included, this setup produced repeatable transition zone displacements, which was encouraging. In subsequent testing, when the load cell was removed as presented in Figure 4-43. The dampening mechanism's repeatability was reduced across a range of turf systems.

Figure 4-43: Impactor set up for preliminary testing without loadcell.

To assess the repeatability of the dampening mechanism across a range of systems with different shock-absorbing properties, a 60 mm carpet was filled with various infill rates. On stiffer systems, such as an underfilled system, one prominent peak could be observed, Figure 4-44a, representing the impact zone followed by one smaller peak. After the second peak, the impactor was in constant contact with the surface, representing the sliding phase. On softer systems with high rates of performance infill, multiple peaks on the vertical axis could be observed, Figure 4-44b. Suggesting that the simulation never entered the sliding phase because the dampening mechanism was not operating effectively. This was attributed to lower ground reaction forces on softer systems, reducing the clamp's compressive forces.

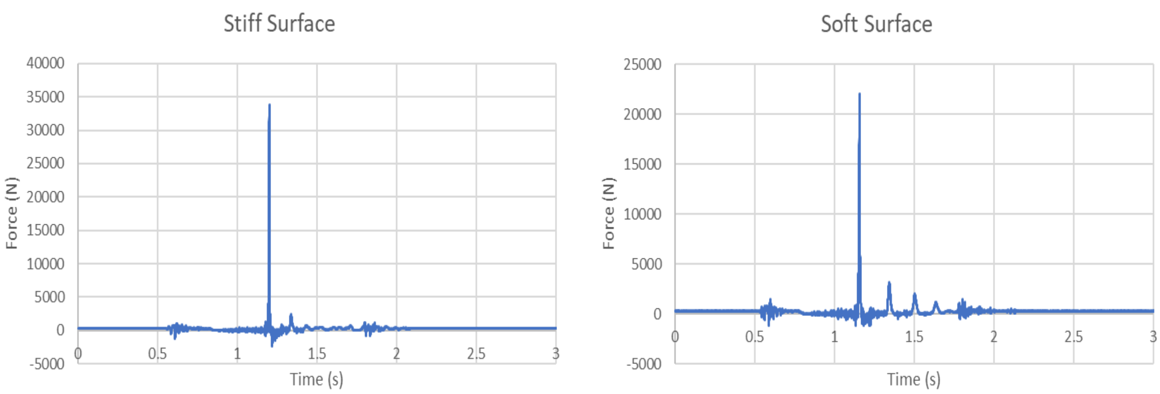

Figure 4-44: Effectiveness of dampening mechanism on (a) stiff and (b) soft surfaces.

The dead weight was increased from 1 kg to 2 kg to increase the compressive forces. However, this had knock-on effects on the dampening mechanism's durability. The higher weight resulted in the open slotted ring seizing inside the tapered discs, which locked the brake and prevented the impactor from moving freely during the sliding phase. To prevent this from occurring, a rubber O-ring was placed between the two discs. This intervention helped prevent the dampening mechanism from seizing. However, repeatability issues were still concerning compared to the set-up when the load cell was used. This design was persisted with by testing several design iterations where torque settings varied to alter the preloading conditions; however, this was unsuccessful enough to warrant continuing with this design. Another issue, with respect to durability, was highlighted by the nylon bushing fatiguing with repeated testing, as presented in Figure 4-45. Consequently, this design was abandoned, and a new dampening mechanism was required.

Figure 4-45: Fatigued Open Slotted Bushing

Bump and Rebound

The next design concept was inspired by technology used in world rally cars [203] and mountain bikes [204]. During racing events over rough and undulating terrain, cars, and bikes, moving at high speeds, can become airborne as they cross a track's peak. They require high-performance shock absorbers to provide smooth transitions on landing whilst maintaining control and stability on impact. Regular suspension systems dampen impacts during compression; however, cars or bikes experience high kickback forces during the extension. Resulting in the diver losing control by bouncing off the track.

To compensate for this, dual action shock absorbers, known as bump and rebound, have been developed, which employ separate operating mechanisms for handling compression (bump) and extension (rebound). Both phases involve a piston moving inside a cylinder filled with hydraulic fluid. As the piston moves, it forces the hydraulic fluid through small valves within the shock, creating resistance to slow down the motion, which softens the impact and prevents excessive bouncing. These high-performance shocks have adjustable dampening settings, allowing drivers to fine-tune the shocks for personal preference in different conditions.

While reviewing the market for bump and rebound shocks, it became apparent that there were several options with different features at various prices. The forces experienced by a car suspension would be significantly higher than those experienced by a bike; therefore, this review focused on bike shocks. Manufacturers produce both front and rear shocks, which have different types of springs, mounting options, travel lengths, and levels of adjustability.

Front shocks, designed like a fork to fit the front wheel, have longer stroke lengths to help handle bumps and obstacles on a track. Rear shocks, integrated into the frame to complement the front shock, are typically more compact. Considering the height of the new impactor design, the compact nature of the rear shock is more desirable.

Springs are also incorporated into bump and rebound shocks to provide support by evenly distributing the rider's weight to deliver a balanced suspension response. Shock springs are available as standard coils or advanced air systems. The performance of a coil spring, dictated by the thickness and diameter of the coil, will be linear over the stroke length. In comparison, the performance of an air spring is determined by the air pressure, which makes it more progressive over the stroke length. As pressure builds up, with decreasing volume, the response is more sensitive during the initial stroke for minor bumps and provides improved support for larger impacts. Despite heavier coil springs, they are more durable and not susceptible to pressure losses for air leakage. Considering these variables, an air spring is more desirable for this application as it is lighter and adjustable.

Rear shocks can be attached to bikes via eyelets or trunnions. The eyelet design is a more traditional mounting option, where a bolt passes through the bore to attach to the frame. Trunnions have recently been incorporated into shocks to increase travel length for a given shock size, which enables designers to optimise frame layout. Trunnion mountings also provide more rigid and robust connections, improving structural integrity. The compact nature and robust mounting option make trunnions more desirable.

The travel length of shocks can range from 40 – 200 mm, depending on the type of shock and the rider's weight. Since the compressive mass is a fraction of a person's body weight, the lower end of the range is expected to be required.

Increased adjustability is associated with greater costs. Therefore, the required adjustability should be considered when selecting an appropriate shock. During the compression period, the shock should have limited influence on the impact. The extension phase requires dampening; therefore, more adjustability would be required when fine-tuning the shock's performance. Adjustability of the compression phase is not essential; however, a small sensitivity is required for the extension period.

The ideal shock would be a rear shock with an air spring system with trunnion mounting features and a relatively short travel length with high adjustability for rebound settings. Based on market research, the Fox Float DPS (dual piston system) met all these criteria. The selected shock has three compression settings (open, medium, firm), 12 rebound settings, and Fox's EVOL air spring. The EVOL air sleeve increases the size of the negative air chamber, which helps reduce forces that initiate travel and provides added sensitivity and better small bump compliance.

To limit the influence of the shock during impact and provide the greatest rebound dampening, the compression and extension settings were set to open and closed, respectively. The air spring was also set to the lowest recommended pressure (50 PSI). Lower pressures provide softer responses during the impact and produce a more linear feel throughout the stroke. The eyelet at the bottom of the shock was incorporated into the design via custom clevis, which utilised the existing tapped hole to secure the armature plate. A thin-walled spacer was inserted to provide a tight fit and to protect a 15 mm eyelet from the thread on an M12 fastener. The trunnion was secured to the dampening mass via another clevis, as presented in Figure 4-46. The dampening mass was created by repurposing the alignment plates from the spring propulsion system, which allowed the mass to be altered during validation testing. The bottom plate, with the clevis attachment, had four tapped holes; the rest had through holes, which matched the pattern of the tapped holes. Six plates, which equated to 12kg, provided the best dampening response while minimising the additional mass. Pillow bushings were attached to the top and bottom plate to support and align the dampening mass during the free fall, as presented in Figure 4-47. With the new dampening mechanism incorporated, the impactor's mass increased to 36.66 kg, which increased the carriage mass to 163 kg, both of which are still within the desired masses as stated in the design specifications.

The final impactor design, presented in Figure 4-48, significantly improved the previous dampening mechanism. This was highlighted by (Figure 4-49a & b) the bump and rebound having a shorter delay between peaks 1 and 2 during vertical loading on a soft sample, compared to the clamping mechanism on a stiff system. After the second peak, in Figure 4-49b, the impactor is in constant contact with the surface as desired, providing sufficient data to be collected to analyse the sliding phase.

Figure 4-46: Incorporating bump and rebound shock onto the impactor.

Figure 4-47: Alignment and structural support for dampening mass.

Figure 4-48: New Impactor Design

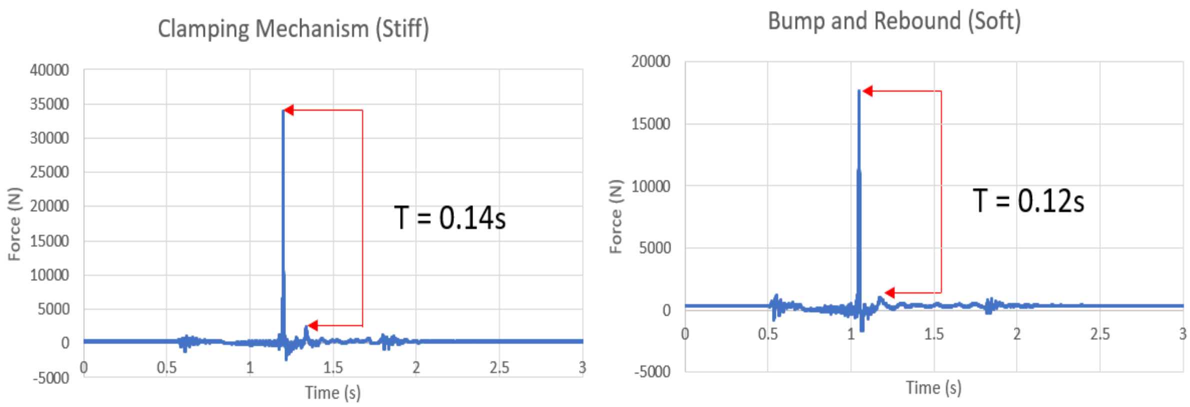

Figure 4-49: Comparison of Dampening Mechanisms: Clamp versus Bump & Rebound.

4.5.6 Transit System

An optimisation process was undertaken to streamline testing procedures and prepare the apparatus for rollout as a new World Rugby Test Method for Regulation 22. The critical bottleneck identified was apparatus preparation for different testing locations, which consumed time and introduced potential errors. Implementing a transit system eliminated human error and enhanced efficiency.

Using the robust and reliable design of Sports Labs' LisportXL [205], a transit system with specially designed tracks and trolleys was developed (Figure 4-50). This system reduced the time and effort required for skin injury risk assessment and provided an anchoring mechanism that enhanced stability, reduced vibrations and improved test result reliability. Consequently, the research became more robust and dependable, improving the overall quality and credibility of the findings.

4.5.7 Operation and Measurement

A bespoke LabVIEW program was developed to operate the electrical components manually, provide a timing sequence to perform the launch and record accelerometer data. The software also processed the data to produce meaningful parameters that will provide insights into skin injury risk, as discussed in Chapter 5. As a safety feature, two-way authentication was incorporated to perform launches safely. This system consists of a physical push button to enable the LIM for launch, followed by a Boolean switch on the LabVIEW program.

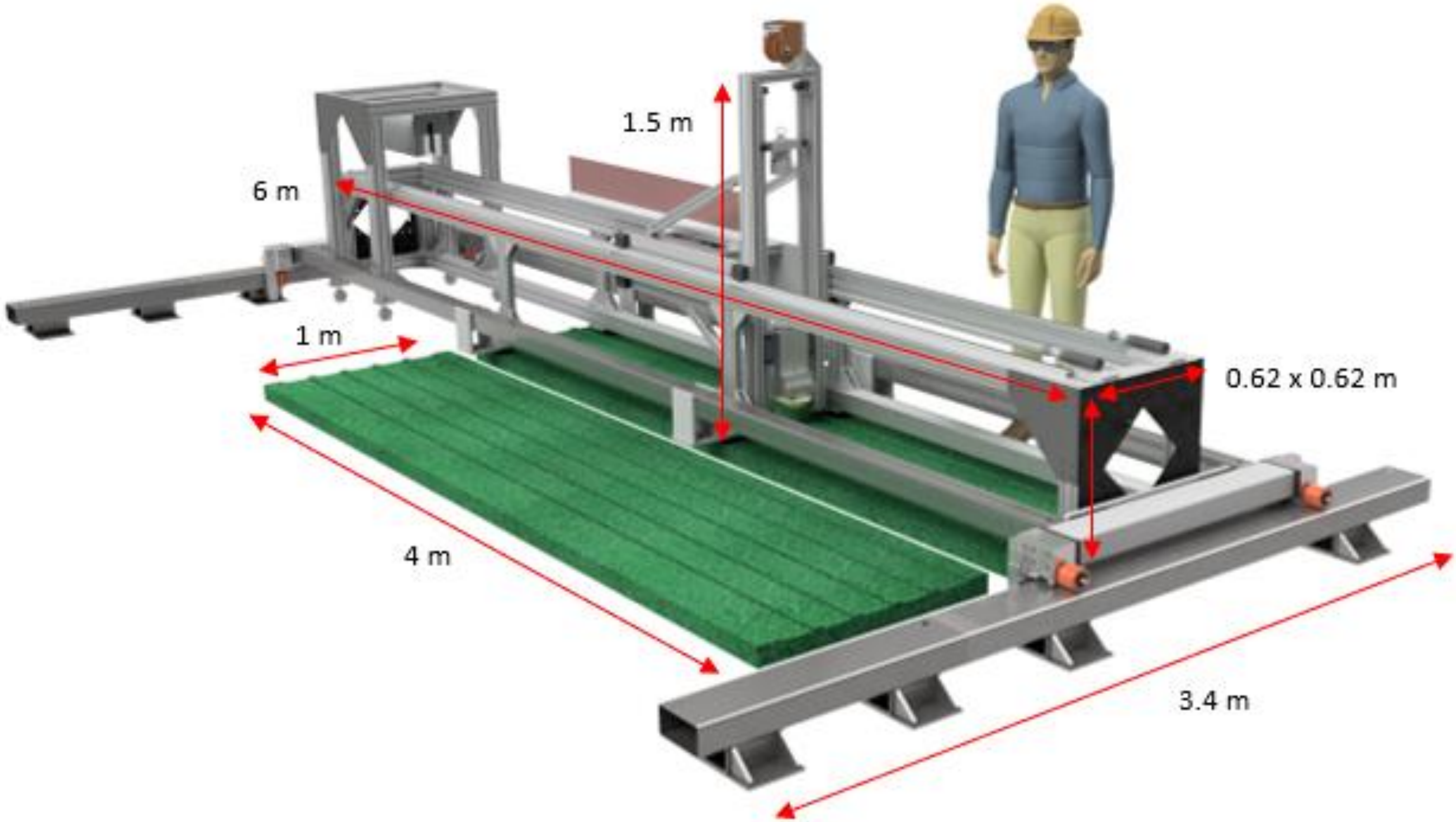

Figure 4-50: Final CAD model incorporating the transit system to complete The Skin Injury Device

CHAPTER 5

Developing an Injury Prediction Model

SKIN INJURIES

Through interactions during game play in rugby

5.1 Introduction

In sports injury prevention, the performance characteristics of sports surfaces are continually evaluated to ensure they comply with the accreditation regulations (World Rugby, 2016b). However, the continued prevalence of high skin injury incidences cast doubt over the validity of the current test method. World Rugby's player welfare strategy prioritises player safety, motivating research to investigate methods to improve injury prevention strategies (World Rugby, 2023c). Skin injury risk can be mitigated by wearing protective clothing or applying a lubricant, such as Vaseline, to reduce the energy the skin experiences during contact with turf. These solutions, however, are only temporary fixes. To create real change, the artificial grass's skin injury issue must be tackled at the root of the problem – the pitch itself.

The development of a test apparatus which simulates a realistic player-surface interaction during gameplay facilitates experimental studies on artificial pitches under standard operating conditions. To effectively improve injury prevention strategies, novel metrics for the newly designed device tailored to assess skin injury risk on rugby turf are required. The literature review highlighted a lack of correlation between COF and abrasion, which casts doubt over the traditional injury assessment method [143]. A pressing need, therefore, exists to develop a more accurate and reliable approach to measure the potential for skin injury during gameplay on rugby turf [51].

This chapter aims to explore, develop, and evaluate parameters encompassing various measurement techniques to comprehensively assess the simulated interaction. Developing these output metrics will enhance the understanding of the underlying factors contributing to skin injuries on rugby turf. Additionally, providing objective data-driven insights will enable turf manufacturers to optimise their turf systems. Ultimately improving injury prevention strategies by creating safer surfaces.

Skin injuries on Rugby Turf are often referred to as 'Turf Burns'; however, it is unclear whether the damage generated is from mechanical abrasion or induced via thermal damage [208]. This section will present methods to reverse engineer the problem by developing the potential injury metrics (PIM), which quantify the abrasive nature of turf and heat profiles generated during the simulation. These parameters will be supplemented by developing kinematic injury metrics (KIM) designed to enhance understanding of impact mechanics and sliding characteristics. Each method will be analysed to establish the most suitable technique to be incorporated into a laboratory test method. Finally, these output variables will be combined into one metric, thereby allowing categorisation of their relative skin-friendliness.

5.2 Heat Profiles

5.2.1 Background

Microscopic asperity contacts continuously form and break during a sliding interaction [209]. When these junctions are broken, kinetic energy is converted to thermal energy. Under the conservation of energy laws, this energy transfer resists relative motion. Therefore, faster decelerations should generate more heat. The magnitude of temperature rise generated during the interaction will be influenced by the material properties of the two surfaces in contact, loading conditions such as applied load and sliding speed, and duration of the slide.

Thermal energy can be monitored directly via thermocouples and thermistors or indirectly via infrared sensors and pyrometers. Thermocouples are robust transducers which can monitor a wide range of temperatures with a fast response time [210]. However, the junction type can significantly influence the behavioural response. For instance, K-types tend to exhibit a linear response across the valuable operating range, whereas J-type thermocouples are inherently non-linear [211]. While thermistors offer better accuracy than thermocouples, they have a more limited temperature range, slower response times, and are vulnerable to self-healing. Infrared sensors, such as thermal cameras [212], and pyrometers operate by detecting thermal radiation emitted by an object [213]. Pyrometers provide single-point measurements from spectral analysis of radiation wavelengths emitted from high-temperature industrial equipment, such as furnaces. Thermal cameras capture two-dimensional temperature profiles across the surface, enabling hotspot identification and visualising temperature gradients.

The design specification states that the desired and acceptable techniques for monitoring temperature to provide insights into thermal energy experienced by the simulated player would be direct and indirect measurements, respectively. The dynamic nature of the interaction requires linear and fast responses; therefore, k-type thermocouples were preferred over thermistors. Preliminary testing (Section 3.4) highlighted concerns over thermocouples' ability to accurately monitor peak temperatures through the skin simulant. Therefore, a preliminary study was conducted to establish the most suitable transducer.

5.2.2 Materials & Methods

To enhance opportunities for participation, World Rugby has recently approved 50 mm carpets as a Rugby Turf system [214]. World Rugby has promoted projects by Cardiff Metropolitan University and Sports Labs suggesting there is no increased risk playing on 50 mm surfaces; however, the document providing the rationale for this change in policy did not specify types of injury [215]. While developing the output metrics to assess skin injury risk, 50mm and 60mm systems were evaluated.

Two Rugby Turf samples were prepared by securing the carpet (4x1m) to a prefabricated foam 14 mm shock pad. Both carpets, made of polyethylene monofilament fibres with a stitch gauge of 63.5 per meter, differed in stitch rates: the 50 mm carpet had 178.3 tufts per meter, while the 60 mm carpet had 155.5 tufts per meter. The 50 mm carpet was filled with 12.5 kg/m^2 of sand and 12.5 kg/m^2 of SBR. While the 60 mm carpet was filled with 15 kg/m^2 of sand followed by 15 kg/m^2 of SBR. Testing involved five launches at fresh impact locations as the gantry moved laterally across the sample. After five iterations, the skin was replaced, and samples were prepared. Each sample was tested twice, totalling 20 impacts.

A Mircro-Epsilon thermoIMAGER was secured to the gantry and aimed at the turf. TIMconnect software captured temperature profiles at the maximum sampling rate of 120Hz. The three areas of interest were centrally aligned and stacked vertically (Figure 5-1). Area 1 (10x10 pixels) evaluates the initial surface temperature. Area 2 (10 x 40 pixels) evaluates the Impact Zone. Area 3 (10 x 60 pixels) assesses the Sliding Phase. The NI USB-6212 DAQ acquires data (10 kHz) from three k-type thermocouples. T-tests were conducted to establish whether any systems produced a significantly different result. All statistical analyses were performed with SPSS, adopting a significance threshold of $p < 0.05$.

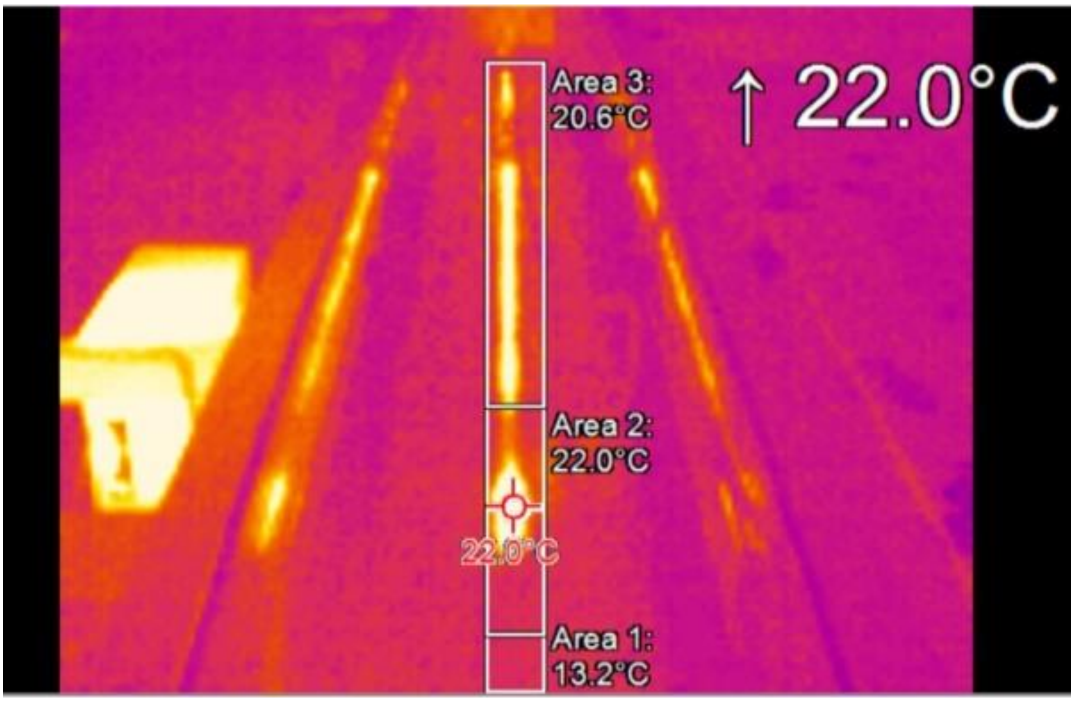

Figure 5-1: Typical temperature profile from the thermal camera.

5.2.3 Results

Figure 5-2 presents the typical temperature profiles from the thermal camera. The average surface temperature was 14.5±0.2°C and 14.7±0.2°C for 50 mm and 60 mm, respectively. The greatest thermal energies were recorded in the Impact Zone, where 50 mm (25.6±0.4°C) generated significantly greater temperatures compared to 60 mm (22.5±0.3°C). The same significant trend was observed during the Sliding Phase, where 50 mm (25.2±0.2°C) generated greater temperatures compared to 60 mm (21.1±0.5°C). Both results were statistically significant, with p-values of 1.21x10-5 and 6.61x10-5 for the Impact Zone and Sliding Phase, respectively, underscoring the importance of these findings.

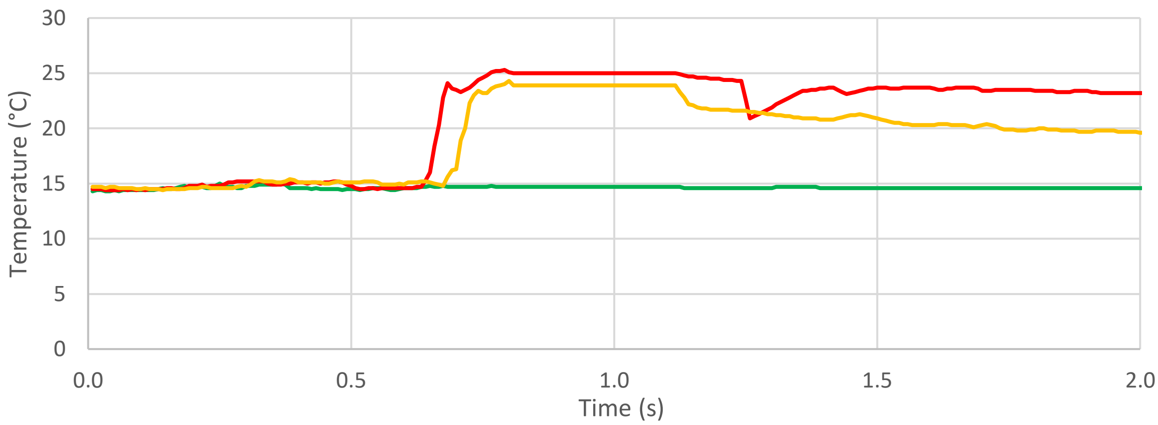

Figure 5-2: Example of thermal camera Heat Profile highlighting: Surface Temperature (green), Impact Zone (red), and Sliding Phase (orange).

Across five test repeats the initial temperatures recorded by the thermocouples increases implying that the skin retains heat from the previous test iterations (Figure 5-3). Despite this elevation in baseline readings, the delta between initial and maximum temperature was identified the most suitable parameter to validate the transducers.

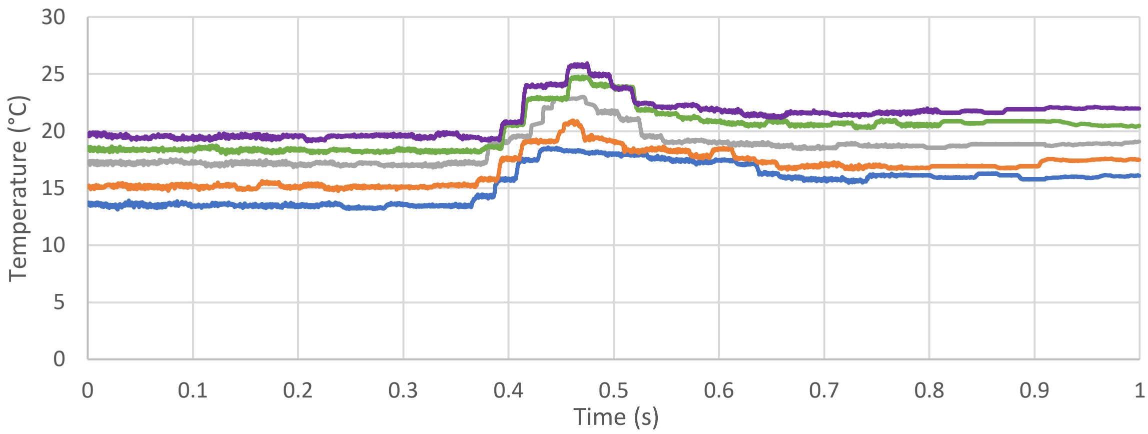

Figure 5-3: The influence of repeated testing on the thermocouple profile. Test iterations 1 to 5 are represented by blue, orange, grey, green, and purple profiles, respectively.

The comparison of temperature delta (Figure 5-4) highlighted that 50 mm yielded greater temperature deltas than 60 mm for all three measurement techniques. Despite all measurement techniques producing statistically significant results (Impact Zone $p = 0.001$ | Sliding Phase $p = 3.87 \times 10^{-5}$ | Thermocouple $p = 0.02$), the thermal camera was more sensitive for monitoring the Heat Profiles. Confirming concerns from Chapter 3 that thermocouples may be inadequate for recording peak temperatures. No statistical significance ($p > 0.05$) existed between the repeated tests on each surface, highlighting the result's consistency.

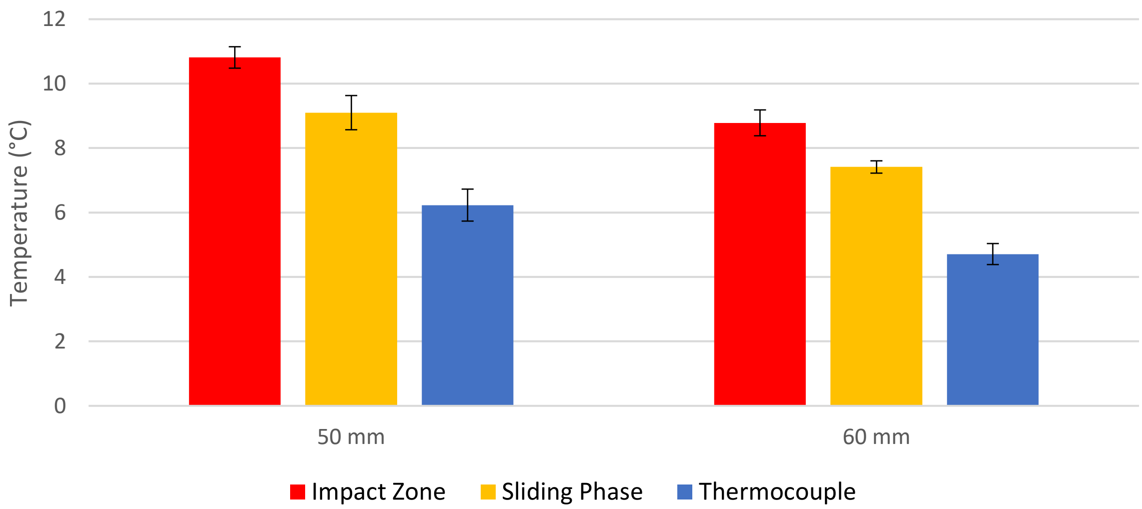

Figure 5-4: Comparison of temperature change monitored by the thermal camera

5.2.4 Discussion

This study aimed to establish the most suitable transducer for monitoring Heat Profiles and provide a better understanding of the mechanism contributing to skin injuries in rugby turf. Literature on Heat Profiles during simulated player-turf interactions is limited and conflicting. Verhelst et al. (2009) [56] reported changes in temperature around 8°C for an SBR system, consistent with the data collected by the thermal camera in this project. In contrast, BrockFIll (a wood chip infill) advocated their product as a safer alternative to SBR and cork, highlighting a unique selling point of lower temperatures generated during a simulated player-surface interaction. An independent test institute reported BrockFILL (184°F/84.7°C), SBR (198°F/92.4°C) and cork (244°F/117.6°C) all generated significantly higher temperatures in comparison to the results from this study [216]. It should be acknowledged that the study was never published in a journal. Consequently, a degree of uncertainty exists regarding the reported data.

Similarities in motion profile characteristics identified between the current project and Verhelst et al., (2009) consisted of high horizontal velocities (5 v 6 m/s), vertical loading (36 v 30 kg) during the sliding phase and monitoring the natural deceleration of the sliding interaction. The paper reports the utilisation of polymer skin simulant with similar frictional and thermal properties of in vivo skin. However, further details still needed to be provided on the material. The main differences were a low bio-fidelity impactor geometry (similar to the test foot used in the Securisport but on a larger scale) and the lack of an authentic impact as the horizontal velocities were generated by launching the sledge down a ram.

Limited data was publicly available on the testing procedures for comparing the three infill materials. The apparatus description alludes to generating an authentic impact by simulating a fall; however, no data quantifies the loadings or velocities [146]. However, by contacting Brock, it was established that the interaction consisted of a constant sliding speed of 5 m/s with a dropping mass of 75kg. The impactor appeared to adopt a similar geometry as the Securisport and the skin simulant was selected based on its thermal properties. This method would provide insights into the potential for burns; however, it did not facilitate the assessment of abrasion. Again, no further information regarding specific material properties was provided. The combination of higher normal loads and a constant velocity were attributed to the significant differences in temperature [217].

The FIFA turf quality programme evaluates the consistency of the polymers within the yarns by measuring melting points via differential scanning calorimetry (DSC) [147]. Sports Labs laboratory tests report DSC melting points between 105°C and 130°C for high-density polyethylene, which is in a similar temperature range recorded during the assessment of cork. Consequently, there is a potential that the yarns could have melted. This outcome seems unrealistic for a player-surface interaction in standard laboratory conditions. Therefore, the credibility and accuracy of the interaction's biofidelity are questioned.

Analysis of the thermocouple profiles presented by Verhelst et al.,(2009) highlighted a smooth and rapid build to the peak, after which the temperature gradually reduces. The peak temperature represented total energy dissipation as the sledge was reported to come to rest at this time index. In contrast, the thermocouple profile from SID exhibited a stepped response where the peak temperature occurred before the simulated player came to rest (Figure 5-3). The stepped response was attributed to the low thermal conductivity of the skin simulant. The early measurement of peak temperature implied that the highest temperatures were generated during the Impact Zone. This result was attributed to the rapid deceleration of the simulated player, which resulted in the greatest transfer of kinetic to thermal energy. This combination of limiting factors implied that thermocouples were inadequate for accurately measuring the Heat Profiles.

Flash temperatures are a localised phenomenon at the micro-asperity level, where intense heat is concentrated for a short duration [218]. It is recognised that the indirect measurement technique of utilising thermal cameras would be unable to monitor flash temperatures. It was deemed an acceptable method due to the consistency with the data reported by Verhelst et al., (2009) and the greater statistical significance between the two surfaces. A thermal camera's added benefit is the ability to monitor the Impact Zone and Sliding Phase independently.

Figure 5-4 highlights consistent surface temperatures during the Impact Zone and Sliding Phase for 60 mm surface. In comparison, there was a greater difference between the two interaction events generated on the 50 mm surface. With the potential ban on SBR, alternative infills will populate the market, and non-filled systems may regain accreditation. By removing the granular infill, which provides a ball-bearing effect, it is predicted that higher temperatures will be generated, potentially exposing players to a higher risk of burns. However, the temperature magnitude is insufficient for thermal damage on these surfaces. This analysis will be essential for accrediting novel infill materials or non-filled systems.

In summary, the Heat Profiles recorded during this study were consistent with literature during a naturally decelerating interaction. The limited thermal conductivity of Lorica Soft adversely affects the sensitivity of thermocouples. Therefore, thermal cameras should be utilised to provide independent insights into the heat profiles of the impact zone and sliding phase.

5.3 The Abrasive Nature of Turf

5.3.1 Quantifying an Abrasion

An abrasion, a common skin injury, involves the removal of superficial skin layers due to friction with rough surfaces [219]. The severity of abrasion can vary, from light grazes to deeper scratches that expose the underlying tissue. In all cases, the surface profile of the skin is altered. Quantifying the extent of these abrasions is crucial, and the most common method is monitoring surface roughness and damage area. Surface roughness, which refers to irregularities and deviations in the material, is characterised by parameters such as average roughness, maximum height of roughness, root mean square roughness, and total roughness. The area of damage, which quantifies the size of the injury, can be estimated by measuring the height and width of the injury. W. van den Eijnde, (2017) developed a more accurate method for quantifying the area of damage using a grid, as demonstrated in their skin damage and severity index (SDASI) tool.

Contact Measurement Techniques

Traditional surface profilometers, which employ contact measurement techniques, are limited in their ability to monitor surface texture. The Taylor Hobson surface roughness machine, for instance, is a minimally invasive metrology instrument that assesses fine scale deviations by recording the vertical position of the stylus probe as it traverses across the surface [221]. While it offers high precision and accuracy, its measurement range is confined to a short distance along a single plane. This limitation necessitates multiple readings, which can introduce operator errors if the sample is misaligned between different test iterations. Atomic Force Microscopy (AFM), on the other hand, can characterise 3D profiles by raster scanning a fine probe across the sample [222]. Despite its nanoscale resolution, the limited field of view makes it impractical for certain projects. Furthermore, the contact force from the stylus can cause soft materials to deform easily, generating ripples and leading to inaccurate measurements. Therefore, these metrology devices, such as Lorica Soft, are unsuitable for measuring delicate materials.

Non-Contact Measurement Techniques

With technological advancements, non-contact techniques have emerged as alternative methods to monitor surface roughness. These techniques, such as electron microscopy and optical profilometry, do not physically touch the material, eliminating the risk of compromising the surface or introducing measurement artefacts such as rippling. Moreover, data acquisition is significantly faster, making analysis more efficient than contact techniques.

The targeted sample must be conductive or semiconductive for scanning electron microscopy (SEM) to work effectively [222]. Insulating materials, such as Lorica Soft, can build up charge from the beam of electrons, creating distortions and poor-quality images. To compensate for this, samples can be prepared by coating them with a thin layer of conductive material. However, this method is expensive and destroys the sample, which can be undesirable. *Optical profilometry* is a powerful metrology technique that analyses patterns of light interference to produce high-resolution images on a nanometre scale [223]. This technique is sensitive when measuring surfaces that are highly reflective or exhibit large vertical variations (greater than a few cm); however, this would not be an issue in the context of this project. The main concern is finding a suitable measurement range, as there is often a trade-off between the field of view and the price of the apparatus. The total length of the impactor is 390 mm; therefore, multiple measurements would be required to evaluate the full sample with cost-effective devices. Complex post-processing would be required to identify and match the individual assessments to create one detailed 3D profile.

In summary, the higher precision, resolution, and fast data acquisition make non-contact methods superior for quantifying surface roughness compared to invasive contact techniques. The Taylor Hobson machine and AFM are unsuitable for assessing Lorica Soft as direct contact generates ripples that adversely affect the results. The challenge with implementing advanced metrology devices is establishing the correct balance between time and cost associated with complex post-processing analysis and financial price. A suitable trade-off could not be achieved despite the design specification stating that the desirable output would analyse surface roughness. Consequently, further investigation would be required to establish a robust protocol for quantifying the acceptable output from the design specification - the area of damage.

5.3.1 Digital Image Processing Techniques

The SDASI evaluated the extent of skin damage using a 10 x 10 mm grid to quantify the area of the injury. Although this provides a rough gauge of the size of the injury, the large grid size could lead to subjective variation in the number of affected boxes counted. This technique led to controversy regarding the final value reported by different researchers. To compensate for this, the grid size could be reduced to create a more refined assessment; however, this could become a tedious task for technicians if the scale was too small. Repetitive and monotonous tasks, providing little stimulation, can lead to inattention errors [224]. Therefore, automating this task via digital image processing would increase efficiency and reduce human error. The area of damaged skin identified and visualised by this image-processing technique will be referred to as the Abrasion Zone.

Any image can be described as an m-by-n-by-3 data array where each pixel combines red, blue, and green intensities. This RBG image is stored as a 24-bit image, where red, blue, and green are 8 bits each. These combinations can generate over 16 million colours, leading to the nickname '*truecolour image*' given the precision with which real-life images can be replicated [225]. A greyscale image is a simplified version of an RBG image where each pixel is the average intensity of the three colour channels. Since each colour is stored in 8 bits

(28), the range of a grayscale image is from 0 – 255, where a pixel value of 0 represents black and 255 represents white.

Image segmentation is an analysis technique that divides images into subgroups to reduce the complexity of an image or enable enhanced processing on the area of interest. In digital image processing, thresholding is the simplest type of image segmentation. This technique converts a greyscale image into a binary image by assessing each pixel and comparing the value to a threshold. If the pixel value is above or below the threshold, the pixel value is amended to 0 or 1, which generates an image that is only black or white. This technique is utilised in the current FIFA Test Method 16 to determine the quantity of infill splash. This procedure provides quantitative and qualitative data analysis that complies with the acceptable outcome of the design specification. Subsequently, this technique was further investigated to establish if it would be viable for quantifying the damaged area.

5.3.2 Exploring the Feasibility of an Open-Source Imaging Software

ImageJ, a Java-based image processing programme, offers a wide array of tools and functionalities. Its extensive use across various scientific fields for image analysis, measurement, and visualisation underscores its versatility. The intuitive design, coupled with comprehensive documentation outlining step-by-step protocols, ensures that users can quickly grasp its functions and features without the need for extensive training.

The feasibility study began with preliminary testing, identifying five skin samples with significant variations in Abrasion Zones' characteristics. Shadows were initially observed on the skin during scanning, a feature attributed to the plastic deformation of the synthetic material. These random shadows, resulting from the distorted skin, were ironed out to eliminate inconsistencies and produce a smoother surface (Figure 5-5). This process is crucial for analysing all damaged skins, enhancing the repeatability of the thresholding technique.

Figure 5-5a: Cork Turf System – Original Skin

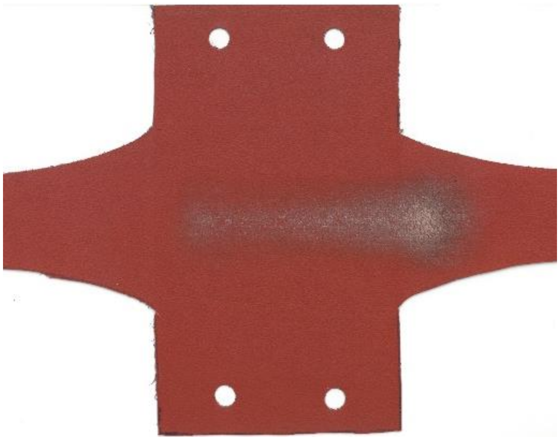

Figure 5-5b: Cork Turf System – Ironed Skin

To improve the resolution of the image processing, an area of interest (4500 x 1500 pixels) was selected to focus on the Abrasion Zone, as presented in Figure 5-6. At the front of the abrasion, the corners of the target area should be close to the arc of the skin template. At the same time, the back of the target area should be parallel to the lateral flaps on the skin template. Additionally, any white pixels from the scanner's background should not be included in the area of interest as they would adversely affect the area calculation during the thresholding technique.

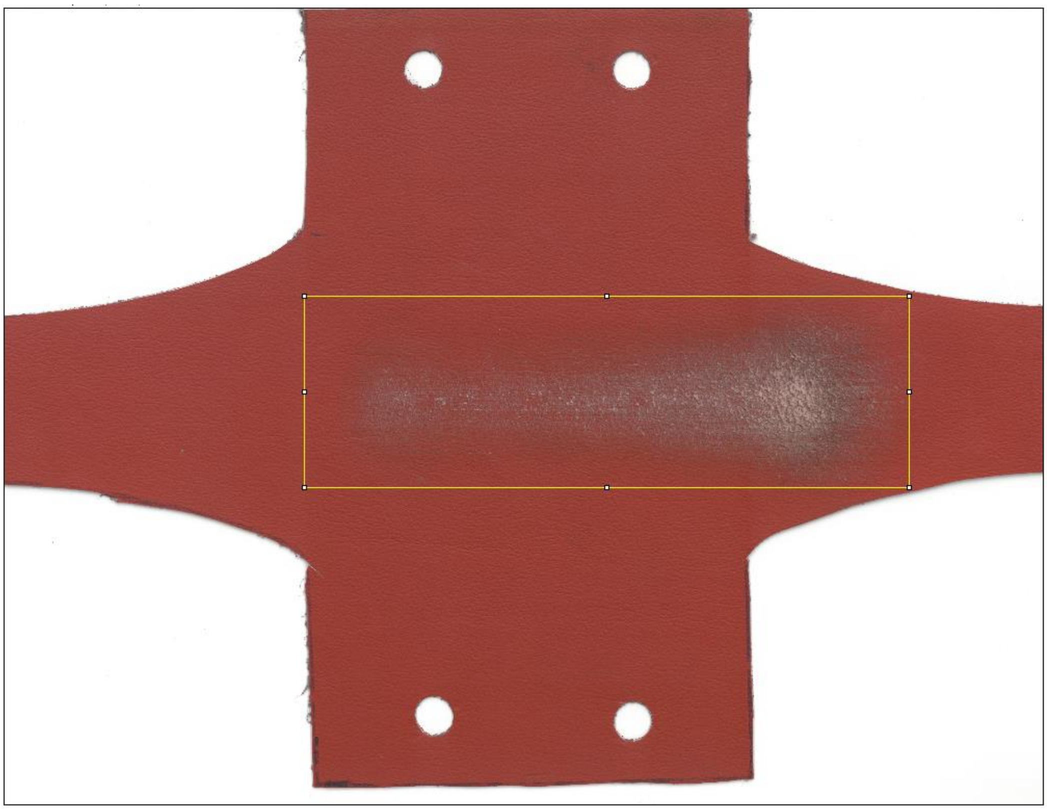

Figure 5-6: Identifying areas of interest in damaged skin.

The area of interest was then converted to greyscale, as presented in Figure 5-7, and threshold parameters were selected, as presented in Table 5-1.

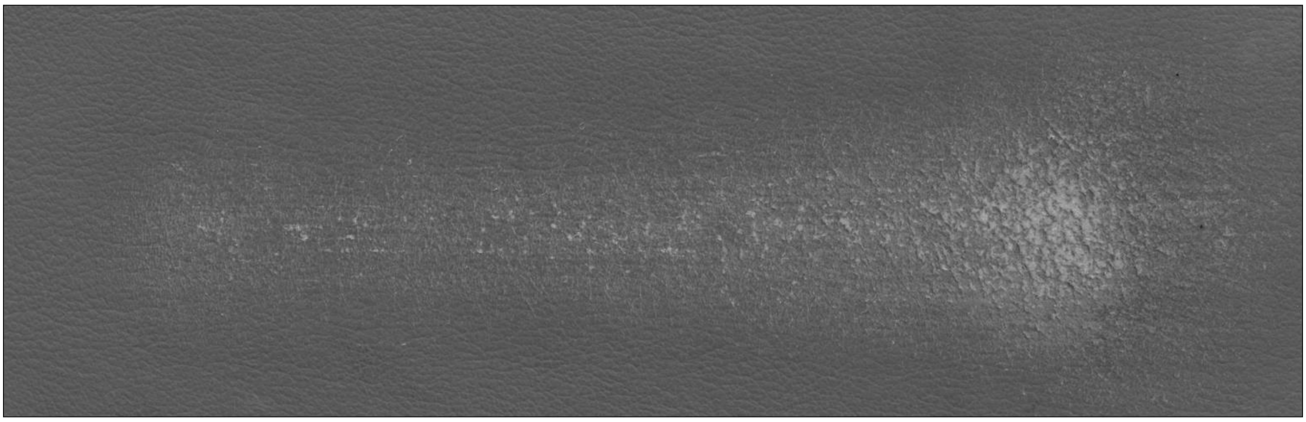

Figure 5-7: Converting area of interest to greyscale.

The histogram at the top of Figure 5-8 represents the magnitude of different greyscale intensities. The peak should, therefore, represent the red colour of the skin as that is the majority colour in interest. The red box illustrates the thresholding boundary conditions, a key technique in image processing that separates objects from the background based on their intensity values. These conditions can be manually set by adjusting the sliders below the histogram. Alternatively, an option from the drop-down menu of pre-set techniques can be selected to apply different algorithms to establish the threshold value based on the data. The five skins with extreme variations in Abrasion Zone characteristics and their respective greyscale intensity histograms are presented in Table 5-1.

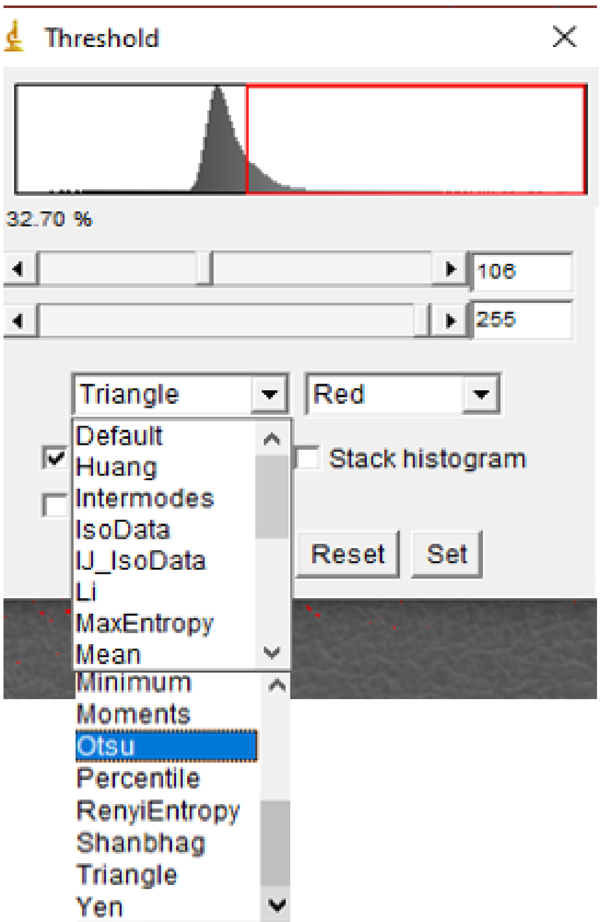

Figure 5-8: Selecting Thresholding Parameters

Table 5-1: Comparison of different infills on abrasion profiles.

Sample	Abrasion Zone	Grayscale Intensity Histogram
SBR (1)		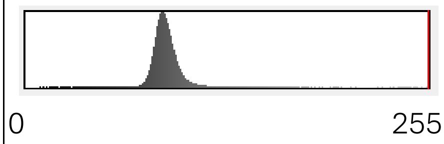
SBR (2)		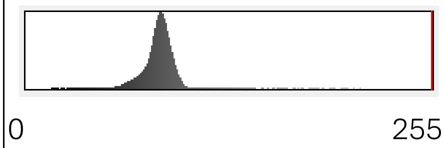
Cork		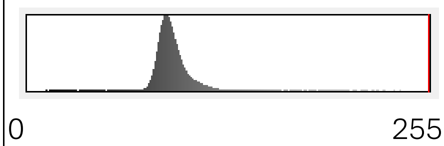
Wood	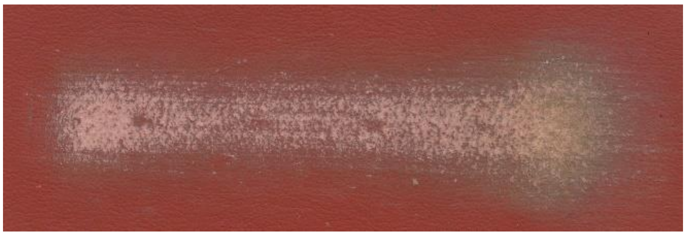	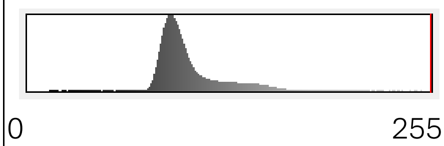
Non-fill		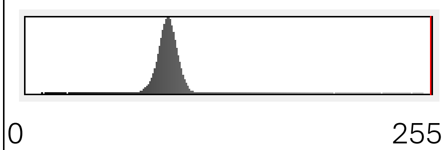

While examining the Abrasion Zones, distinct characteristics from each turf sample can be observed. Point loading forces generate the damage on SBR (1) on the nose of the impactor as the impactor ploughs through the turf during the impact zone and sliding phase. This interaction abrades the polyamide surface, exposing the grey microfibre fleece underneath. Hints of material transfer from the SBR can be observed at the leading edge of the abrasion. The main observation from SBR (2) is the significant increase in material transfer from the SBR with minor scratches at the nose of the knee form. Cork produced a similar point loading at the nose of the impactor whilst generating additional scratches towards the tail. Wood generated an abrasion that maintained a relatively consistent width along the length.

Interestingly, the only damage generated on the non-filled sample was at the nose of the impactor. These observations suggest that the infill material will have the most significant impact on the severity of the abrasion. Where organics seem more abrasive than polymeric infills, this observation agrees with the initial hypothesis formed from anecdotal reports. Four Sports Labs employees were asked to visually inspect the samples and rank the skin damage from highest to lowest severity. The unanimous decision ranked them in the following order: Wood, Cork, SBR (1), SBR (2), and non-fill.

The characteristics identified above can be observed when examining the histogram waveforms. The skin is a dark red, and the texture will produce lighter and darker areas. Therefore, the histogram takes the shape of a bell-shaped curve rather than an independent spike. A relatively sharp build-up to the peak was noticed on SBR (1), Cork and Wood. However, the build-up to the peak is more gradual on SBR (2) and non-fill. This result was attributed to the absence and presence of darker areas on the skin. Different patterns were observed as the intensities diminished from the peak. From the visual inspection, the larger area after the peak corresponded to a larger area of skin damage, which encourages this technique to progress as a viable option for quantifying skin injury risk.

The next step was establishing an appropriate threshold to convert the grayscale to binary images. The pre-set options on the drop-down menus were trialled across a range of skins with different abrasion zone profiles; however, there was no repeatability or consistency across different infill types. To address this, a LabVIEW programme, a widely used software platform for data acquisition and analysis, was designed and developed to mimic ImageJ's processes. By designing custom software, more profound insights into the operation of the software were developed, fostering a comprehensive understanding of the analysis tool. This, in turn, facilitated the implementation of additional tools for evaluating histograms, such as monitoring the rate of change of greyscale intensity, a capability not readily accessible within the ImageJ software.

5.3.3 Investigating Extent of Skin Damage of Abrasion Zone Different Characteristics.

Before determining the appropriate thresholds for image processing, a preliminary analysis was carried out to differentiate between the light and dark lesions formed during the interaction. The purpose of this analysis was to investigate the extent of damage within both the lighter and darker areas of the Abrasion Zone through microscopic examination. To achieve this, a microscope was utilised, providing a precise magnification of 200x, as displayed Figure 5-9 & Figure 5-10.

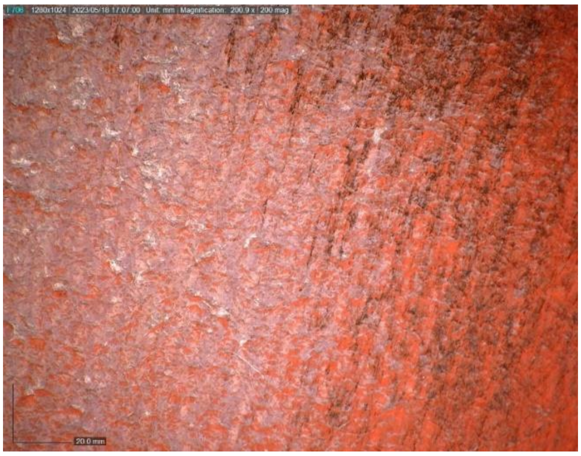

Figure 5-9: Monitoring the Abrasion Zone at the nose of the knee form.

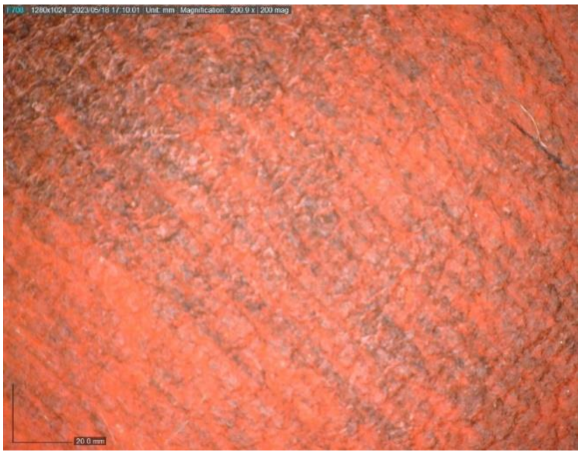

Figure 5-10: Monitoring material transfer along the length of the Abrasion Zone.

The material loss experienced on the nose of the geometry appears to be more intense than the damage created along the length of the knee form when comparing Figure 5-9 and Figure 5-10. The red polyurethane coating on the nose of the impactor appears to have been removed, exposing the grey microfibre fleece. In the areas where the polyurethane coating remains, there is a noticeable height difference, increasing surface roughness. In some areas, the damage has resulted in the fleece breaking into strands of fibres. The combination of significant variations between peaks and troughs and the fibrous nature of the skin represents a high risk of injury.

In comparison, dark areas in Figure 5-10 seem to have reduced skin texture due to surface polishing during material transfer. A player would still experience pain in this area despite the surface roughness potentially reducing. Consequently, the lighter and fibrous areas should be considered more extreme damage than the darker polished areas.

5.3.4 Establishing Suitable Thresholds for the LabVIEW Programme

The purpose of the thresholding technique was to attenuate the skin's original colour to accentuate the abrasive zone. While exploring the feasibility of ImageJ, visual analysis identified that different Abrasion Zone characteristics were noticeable in the histogram profile of the greyscale image. Subsequently, testing was conducted to establish the greyscale properties of four untested skin samples. Each sample was scanned three times to create twelve data points. Figure 5-11 illustrates the typical bell-shaped curve of an untested sample, demonstrating consistency on either side of the peak. The range of greyscale intensities was more condensed compared to Table 5-1, which was attributed to a consistent colour range within the untested sample.

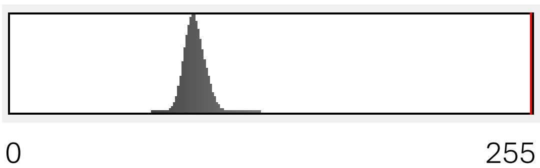

Figure 5-11: Example histogram profile of untested skin samples.

A stopband filter was applied to remove red, and the thresholds were identified by evaluating fresh skin simulant samples. The grayscale histogram, forwards and backwards from the peak, was evaluated to establish the intensity index when the gradient was less than the initial index and to define upper and lower thresholds. The initial gradients were relatively flat, then steadily became steeper until they reached a pinnacle, after which they began to flatten out as the intensity approached the end of the range. An iterative method was employed to determine the intensity index when the rate of change fell below the initial gradient. This procedure was conducted before and after the peak to define the lower and upper boundary limits encompassing most of the original colour. The peak intensity across the twelve measurements on the untested samples was 90±0.1, while the lower and upper boundary limits were 75±0.5 and 107±0.4, respectively.

When evaluating tested samples, the peak intensity exhibited more variation. This observation was attributed to the different colour profiles of the Abrasion Zones. During the validation of this diagnostic tool, a static and dynamic threshold was evaluated. The static threshold represented the upper and lower boundary limits, and the dynamic threshold was established by applying an offset to the peak intensity of the tested samples. The lower (15) and upper (17) offsets were selected by calculating the deviation of the boundary limits from the untested peak intensity.

The final step of the thresholding technique involved quantifying the area of the damaged skin. This technique converted the greyscale image into a binary image by assessing each pixel and comparing the value to a threshold. If the pixel value is above or below the threshold, the pixel value is amended to 0 or 1, generating an image that is only black or white, as illustrated on Figure 5-12. This procedure was separately executed for the lower and upper thresholds to ascertain the pixel count within the area of interest. By calibrating the number of pixels per millimetre within the software, the area of interest could be calculated by comparing the pixel count to the total area.

Skin damage assessment from preliminary testing highlighted that peak intensity varied with infill material. A high-pass filter (threshold = peak grayscale intensity + 17) defined the abraded area (‘A_1’), before a second low-pass filter (threshold = peak grayscale intensity − 15) defined the darkened area associated with material transfer (‘A_2’). This darkened perimeter was consistent with skin injuries and was generally associated with less severe trauma; hence, A_2 was given half the weight of A_1 - Equation 20.

Equation 20: Abrasion Zone

$$Abrasion\ Zone\ (AZ) = A_1 + \frac{A_2}{2}$$

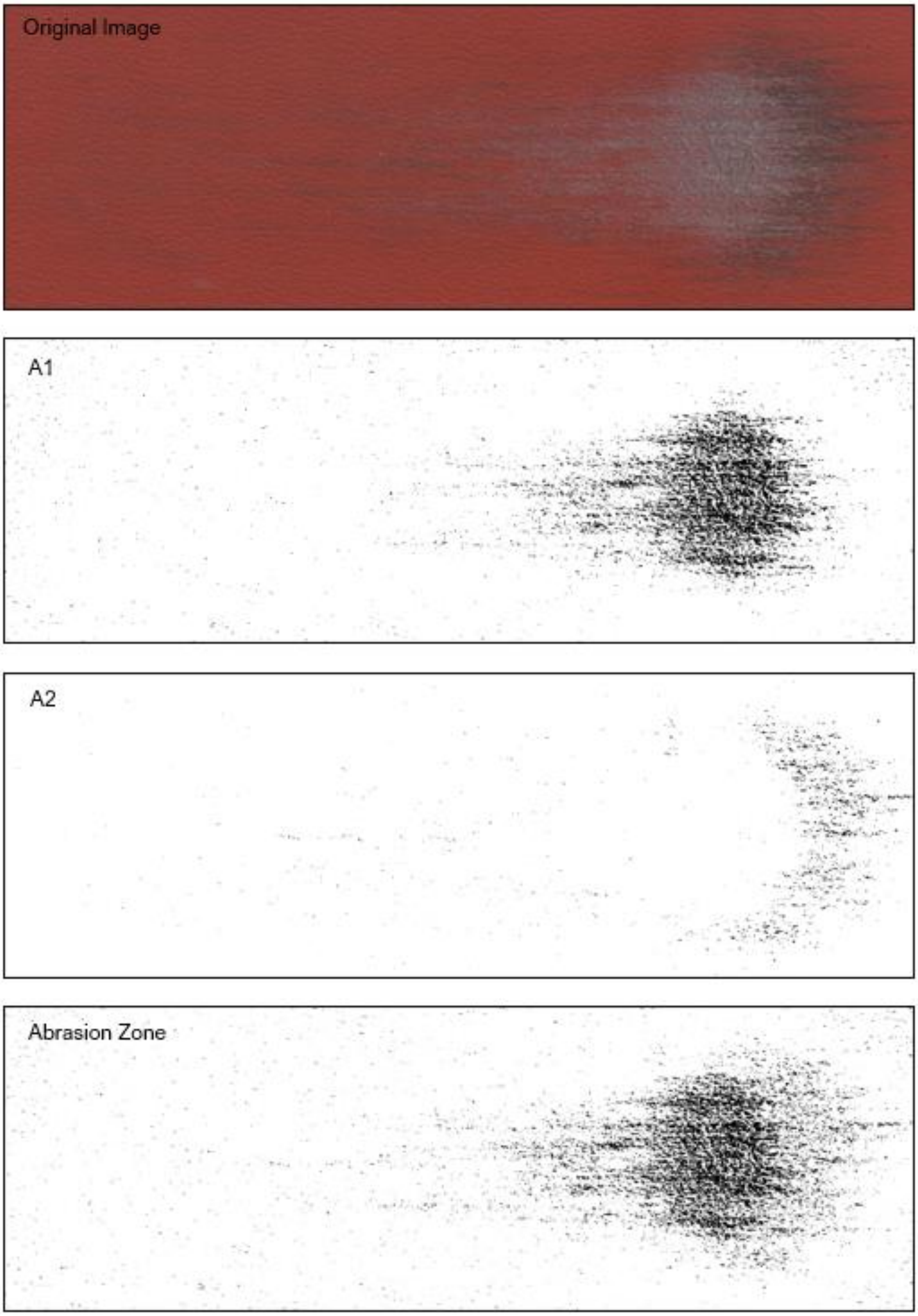

Figure 5-12: Example of Generating Abrasion Zone Image

5.3.5 Generating and Validating Abrasion Zone Results

The skin damages (Table 5-1) processed using the static and dynamic thresholds, and the corresponding Abrasion Zones (AZ) are presented in Table 5-2 and Table 5-3, respectively. By applying the static thresholds, the Abrasion Zone images exhibited more dark speckles in areas that were not damaged, creating a poor visual representation of the skin damage, which inflated the quantitative output (Table 5-2).

Table 5-2: Comparison of Abrasion Zone for different infills utilising the Static Thresholds

Sample	Original Image	Abrasion Zone Image	AZ (mm^2)
SBR (1)		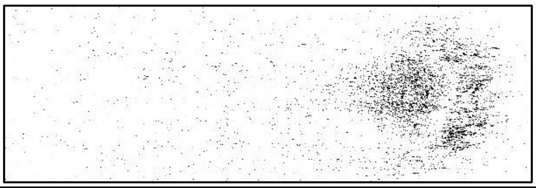	293
SBR (2)		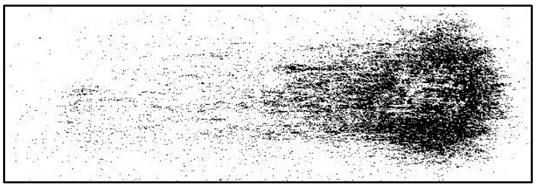	1032
Cork		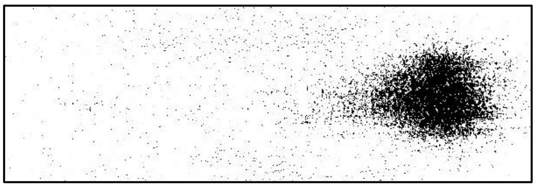	1428
Wood		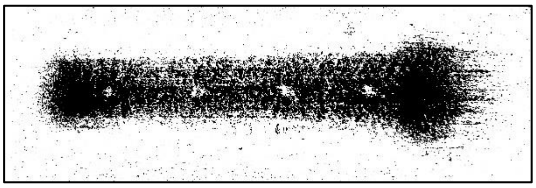	3446
Non-fill		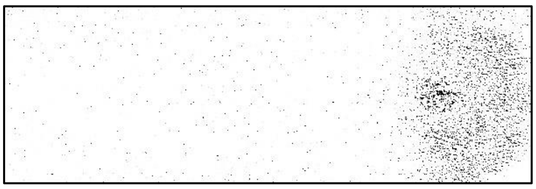	189

When applying the dynamic thresholds, the Abrasion Zone images (Table 5-3) provide a better visual representation of the skin damage. Additionally, the quantitative Abrasion Zone scores aligned with the predictions made during the visual inspection. This agreement significantly enhances the confidence and applicability of this diagnostic tool in forecasting the risk of skin injury.

Table 5-3: Comparison of Abrasion Zone for different infills utilising the Dynamic Thresholds

Sample	Original Image	Inverted Image	AZ (mm^2)
SBR (1)		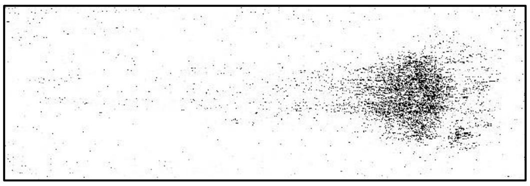	428
SBR (2)		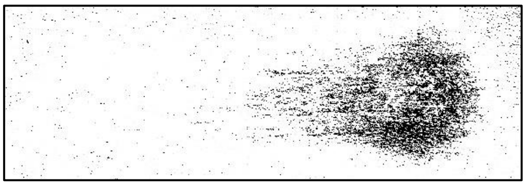	552
Cork		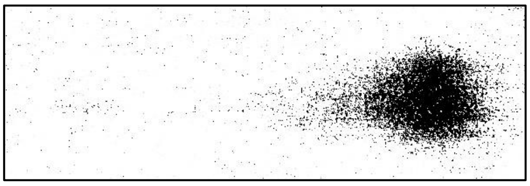	1404
Wood		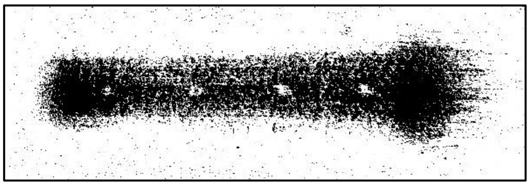	3312
Non-fill		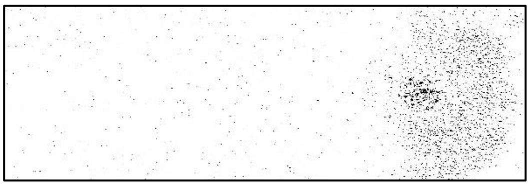	154

The final step of this section was to evaluate the repeatability of this analysis tool which consisted of analysing the skins from the temperature validation study, as presented in Table 5-4: Assessing repeatability of the Abrasion Zone method to quantify the abrasive nature of turf..

Test	Skin Damage	Abrasion Zone Image	AZ (mm^2)
50 mm (1)			620
50 mm (2)	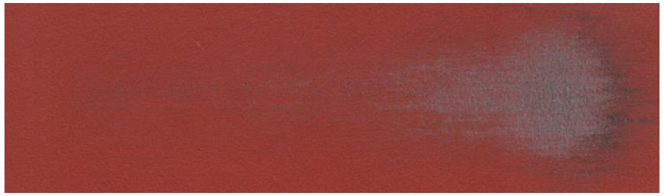	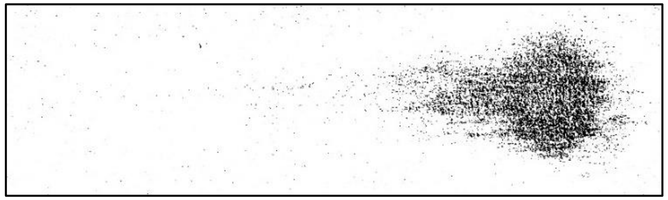	661
60 mm (1)			452
60 mm (2)			426

Table 5-4: Assessing repeatability of the Abrasion Zone method to quantify the abrasive nature of turf.

5.4 Filtering and Data Processing Procedures

Prior to the development of the KIMs, appropriate filtering and data processing techniques were established. *Signal filtering* is a major pre-processing step which attenuates noise and accentuates the signal of interest. The accelerometer data collected during this study was a discrete, non-linear, non-stationary time series. The waveform information can provide insights into the compressive and shear forces the simulated player would experience during the Impact Zone and Sliding Phase. Additionally, the accelerometer data can be manipulated to calculate velocities and displacements, which will assist in categorising the surface's skin injury risk index. Analysis of this data requires proper determination of the morphological and interval aspects of the recorded signal, which are susceptible to various kinds of predominant noises such as channel noise (additive white Gaussian noise) and instrumentation noise, which come in the form of electromagnetic interference generated by the LIM and apparatus motion due to the dynamic nature of the interaction. This section will explore filtering processes currently used in other turf test methods and present alternative options. Once a suitable filter has been identified, selecting appropriate cut-off frequencies is discussed.

5.4.1 Background on Filtering

Selecting the optimal filter type requires a comprehensive knowledge of filtering processes and an understanding the desired outcome. Filtering impact attenuation data requires high passband fidelity with suitable roll-off steepness and phase linearity [226]. These filter characteristics, combined with suitable cut-off frequencies identified through Fourier analysis, should attenuate unwanted data while maintaining the signal of interest. In contrast, the Sliding Phase will not produce magnitudes as extreme as the Impact Zone; however, apparatus-induced noise from the high-energy impact may be more apparent. Consequently, each interaction event will require different filtering processes.

In the field of signal processing, four fundamental principles can be adopted to smooth features in a waveform by removing unwanted frequency components [227]. A low-pass filter preserves low frequencies and attenuates high frequencies. Alternatively, a high-pass filter can eliminate lower frequencies while maintaining higher frequencies. These filters can create band-pass or band-stop filters, which preserve or attenuate a specific range of frequencies.

There are five main types of filter responses which can be utilised: Bessel, Butterworth, Chebyshev type I and type II, and Elliptic [228]. Each has its advantages and disadvantages, as presented in Table 5-5. The Bessel filter provides the best signal preservation due to the high phase linearity. However, the slow roll-off speed will not adequately attenuate unwanted noise. To compensate for this limitation Chebyshev or Elliptic filters could be more suitable. Chebyshev filters have a relatively fast roll. However, the rippling distortions were undesirable characteristics for the context of this project. Elliptic filters are the most complex, requiring iterative design processes to optimise the desired response. Since Rugby Turf is a complex and non-classical friction system, there were concerns that optimising the response for one system may not be suitable for another system. The Butterworth filter was the most desirable due to its simplicity of smoothest transition without ripples. Initial concerns of phase distortion can be minimised by using low-order filters combined with forward and backwards processing of the filter [229].

Table 5-5: Summary of Filter Type Advantages and Disadvantages

Filter Type	Advantages	Disadvantages
Bessel	· Smoothest Curve · No ripples · No time delay	· The slowest roll off speed of all filters
Butterworth	· Smoothest Curve · No ripples	· Very slow roll off speed · Would require a very large order number · Time delay
Chebyshev I	· Faster roll off speed than Butterworth · Ripples can be minimised to 0.01dB	· Ripples in the pass band · Large time delay
Chebyshev II	· Faster roll off speed than Butterworth · Ripples can be minimised to 0.01dB	· Ripples in the stop band
Elliptic	· Fastest roll off speed of all filters	· Ripples in both stop and pass bands · Largest time delay

5.4.2 Filtering Processes Adopted in Current Test Methods.

The governing bodies utilise a wide range of apparatus to assess the performance of artificial pitches; however, the only apparatus which implements a filtering process is the Advanced Artificial Athlete (AAA) [147]. The AAA test device characterises the responses between athlete/surface interaction during a run, stop or cut. Due to the complex biomechanics involved in these player movements, the apparatus has been simplified to generate a discrete and repeatable interaction [230]. The test method quantifies surface hardness via an accelerometer by performing a drop test with a spring-mass system to simulate the body's ability to absorb impact. The motion profile generated by the AAA is similar to a static drop from the apparatus presented in this project; therefore, this filtering process should be investigated further to establish if it will be suitable for this application. The filtering involves applying a 2nd order low-pass Butterworth filter with a cut-off frequency of 600 Hz [147]. The duration of a AAA impact is typically less than 50ms [231]. By implementing the Nyquist frequency theory, the minimum sampling frequency should be 40Hz, which is relatively low and confirms why a low-pass filter was applied to remove noise.

5.4.3 Fourier Analysis

Fourier analysis is a mathematical technique which breaks down complex signals to highlight the inherent frequency characteristics. This analysis provides detailed information which was utilised when establishing cutoff frequencies. The first step of Fourier analysis consists of trimming the data to represent the area of interest. The Impact Zone was established by identifying the peaks of the vertical and horizontal accelerations and then working forward and backward to the x-axis. The sliding phase was established by finding the end of the interaction and working backwards until the impactor was no longer in contact with the surface. The magnitude of forces experienced by the simulated player was expected to be significantly different during the Impact Zone and Sliding Phase. Accordingly, four accelerometers with suitable sensitivity were selected to evaluate the vertical and horizontal axis. They all require independent filtering to provide a smooth waveform with removed unwanted frequency components. The fast Fourier transforms for the vertical and horizontal axis during both the Impact Zone and Sliding Phase are presented in Figure 5-13 - Figure 5-16.

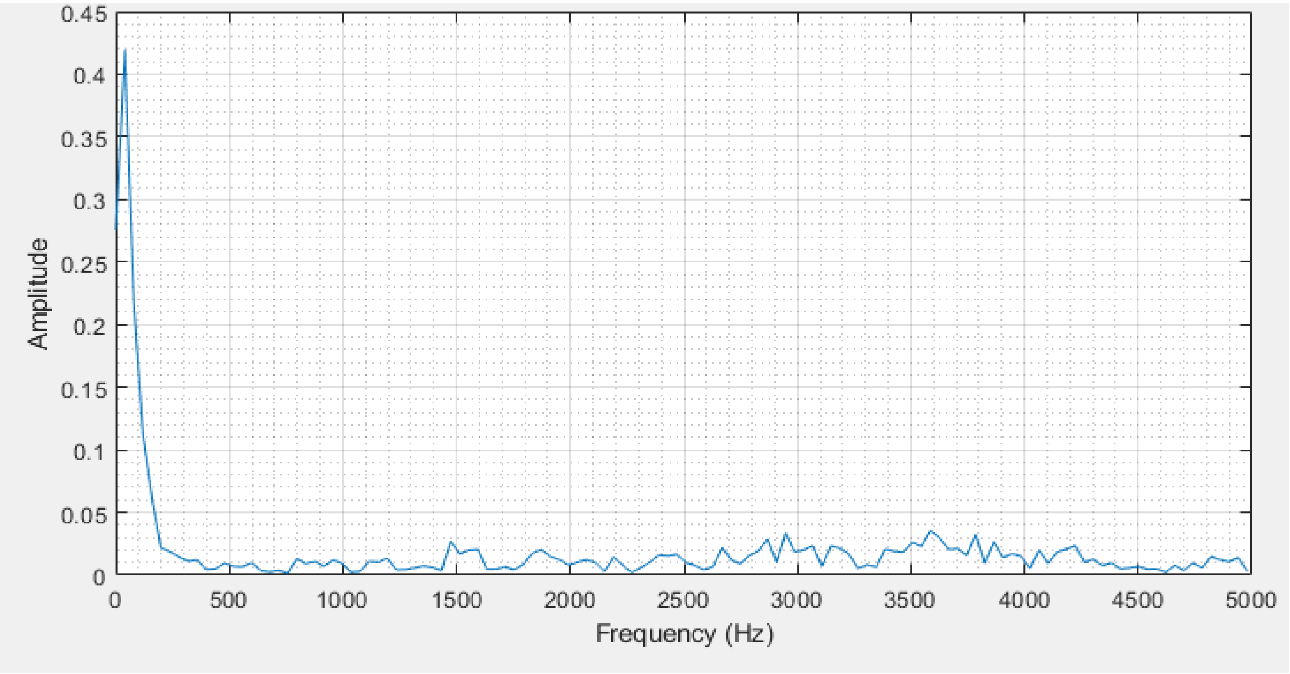

Figure 5-13: Fourier Analysis: Example of raw vertical Impact Zone data with the greatest magnitude of frequency components in the low-frequency zone. (<600Hz).

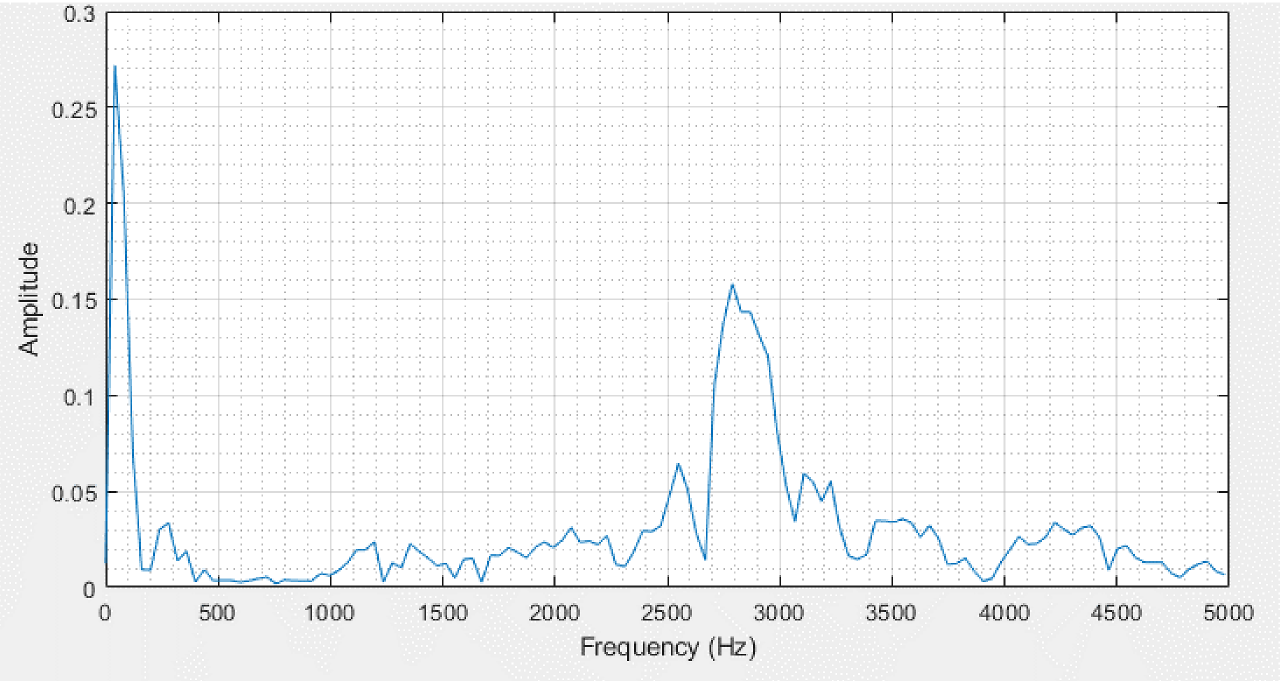

Figure 5-14: Fourier Analysis: Example of raw horizontal Impact Zone data with the greatest magnitude of frequency components in the low-frequency zone and a secondary spike between 2500 – 3000Hz.

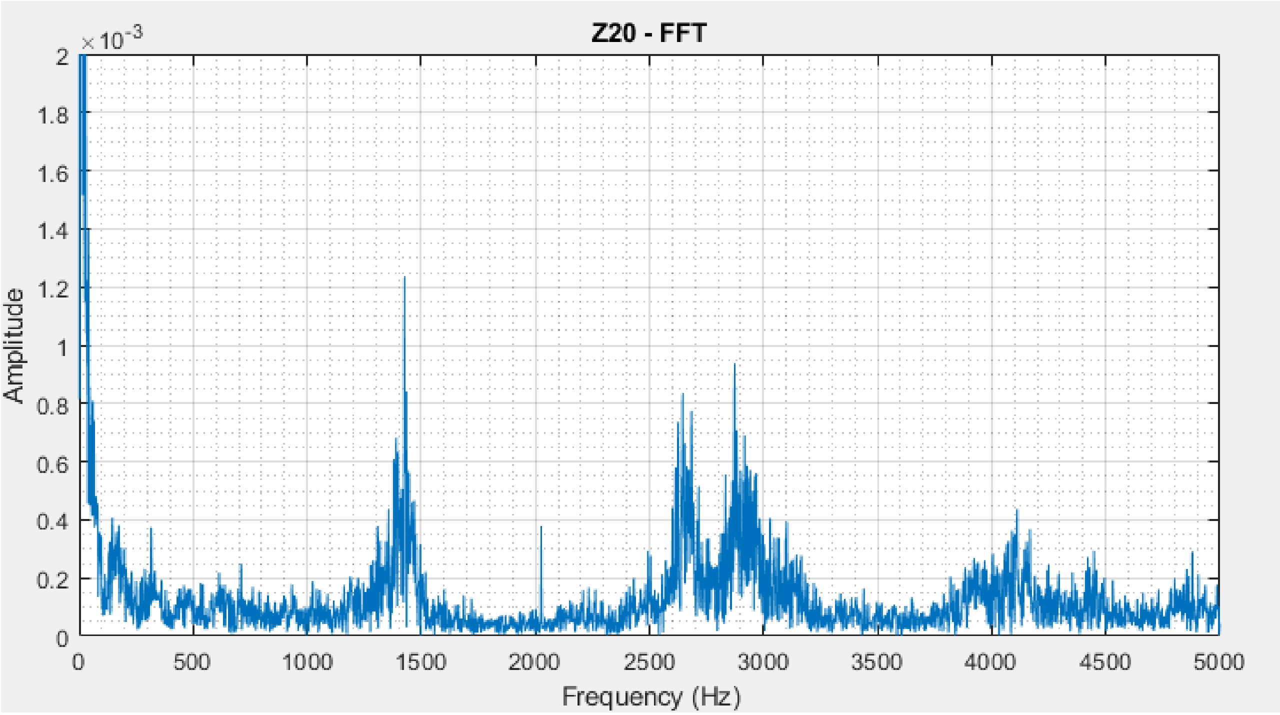

Figure 5-15: Fourier Analysis: Example of raw vertical Sliding Phase data with the greatest magnitude of frequency components in the low-frequency zone. Additional frequency components are present around 1500Hz and between 2500 - 3000Hz.

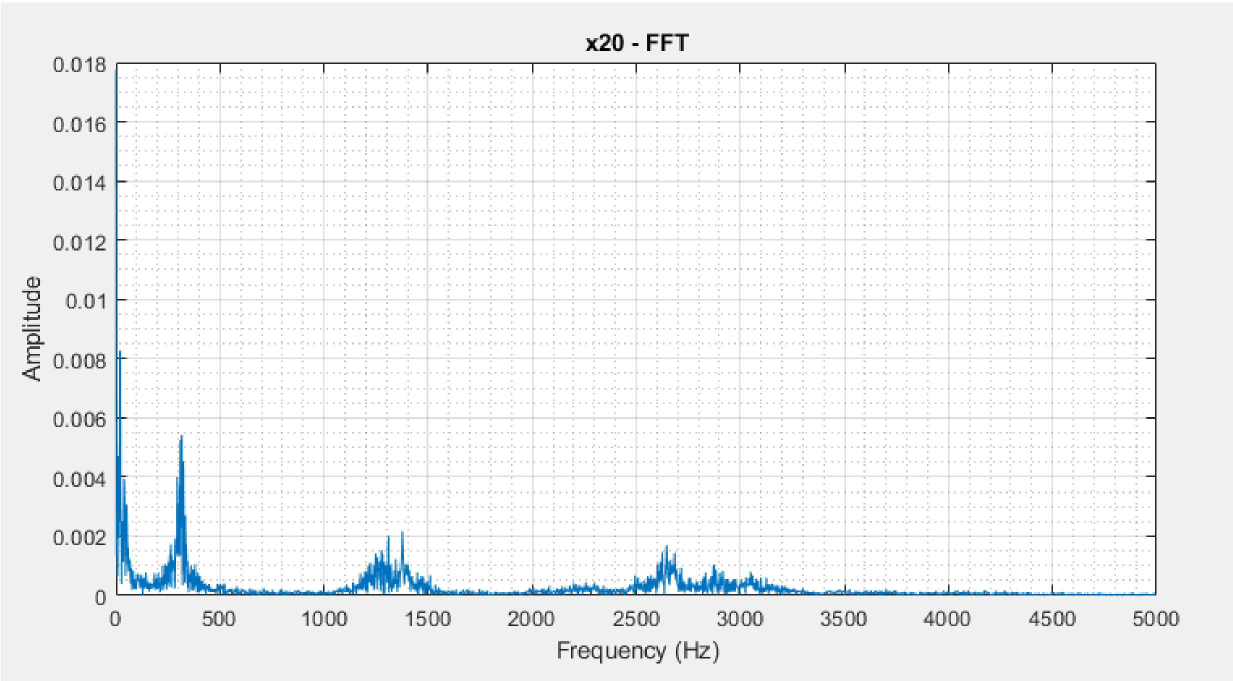

Figure 5-16: Fourier Analysis: Example of raw horizontal Sliding Phase data with the greatest magnitude of frequency components in the low-frequency zone. Additional frequency components are present around 300Hz, 1300Hz, and 2600Hz.

The biggest magnitudes of frequency components observed during the Impact Zone (Figure 5-13 & Figure 5-14) culminated in the low-frequency range. After the initial peaks, both waveforms remained relatively low at 1000 Hz. The frequency components on the vertical axis remained at this magnitude. However, a secondary peak was observed on the horizontal axis, which reached a maximum of around 2800 Hz. The sliding phase had more volatile frequency components, attributed to apparatus-induced noise from the impact and the increased duration. Again, the greatest magnitude of frequency components was observed in the low-frequency range during the Sliding Phase (Figure 5-15 & Figure 5-16). A single peak around 1500 Hz and a double peak between 2500 – 3000 Hz could be observed on the vertical axis. While the horizontal axis did not exhibit the same magnitude of frequency components, there were spikes around 300, 1200 and 2600 Hz. These frequency components were evaluated through trial and error to establish their influence on the signal. Table 5-6 presents a summary of the final filtering processes applied to each accelerometer.

Table 5-6: Summary of Filtering Process

Accelerometer	Impact Zone		Sliding Phase	
	Vertical	Horizontal	Vertical	Horizontal
Measuring Range	200G	100G	20G	20G
Sample Rate	Minimum 10kHz			
Filter Type	Low-pass Butterworth Filter			
Cut-off Frequency	600 Hz	1000 Hz	200 Hz	150 Hz
Order	2	4	2	4

A 2nd order low pass filter (Fc 600 Hz) was applied to the vertical Impact Zone to remain consistent with the existing AAA method. From visual inspection, a steeper roll-off created a smoother signal on the horizontal axis. Therefore, a 4th-order low pass filter (Fc – 1000 Hz) was applied. In the sliding phase, the vertical and horizontal data were significantly noisier than the Impact Zone. Subsequently, lower cut-off frequencies were applied with the same order low pass filters. Examples of the raw and filtered data generated during the Impact Zone and Sliding Phase are presented in Figure 5-17 - Figure 5-20.

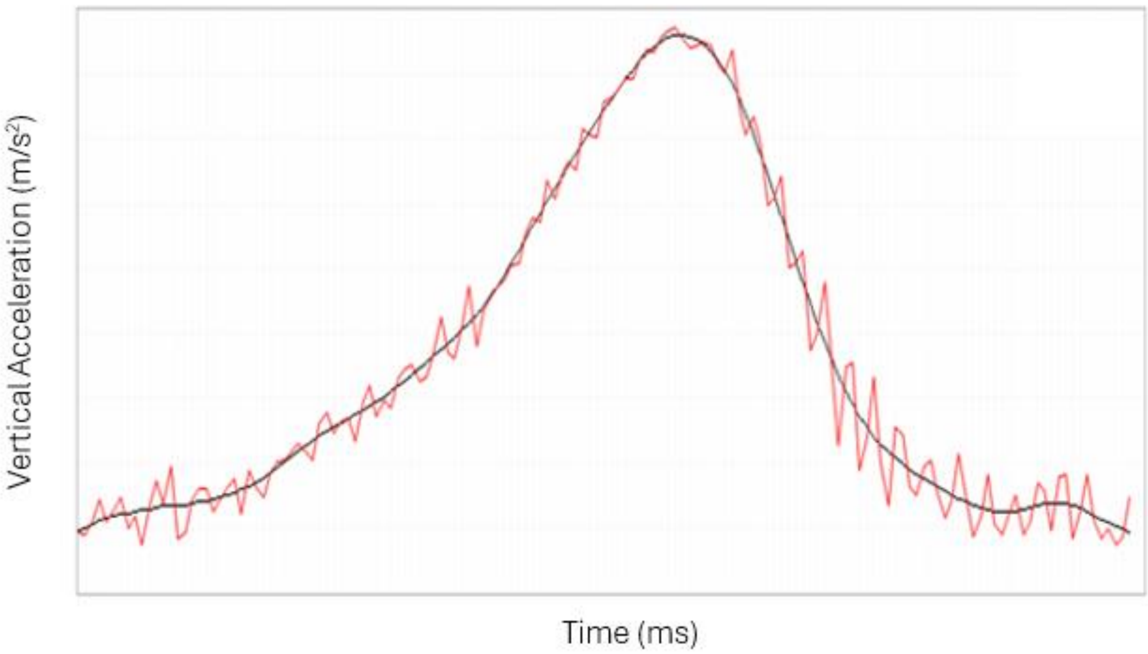

Figure 5-17: Comparison of filtered (black) and unfiltered (red) vertical Impact Zone data.

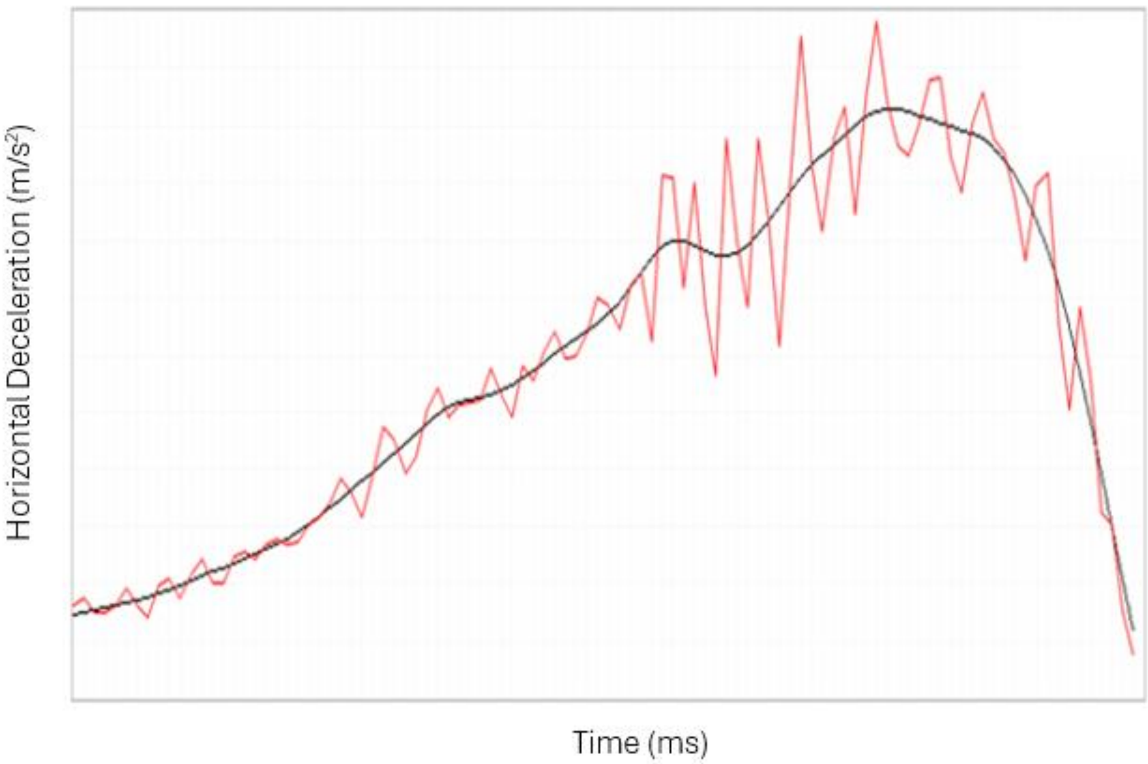

Figure 5-18: Comparison of filtered (black) and unfiltered (red) horizontal Impact Zone data.

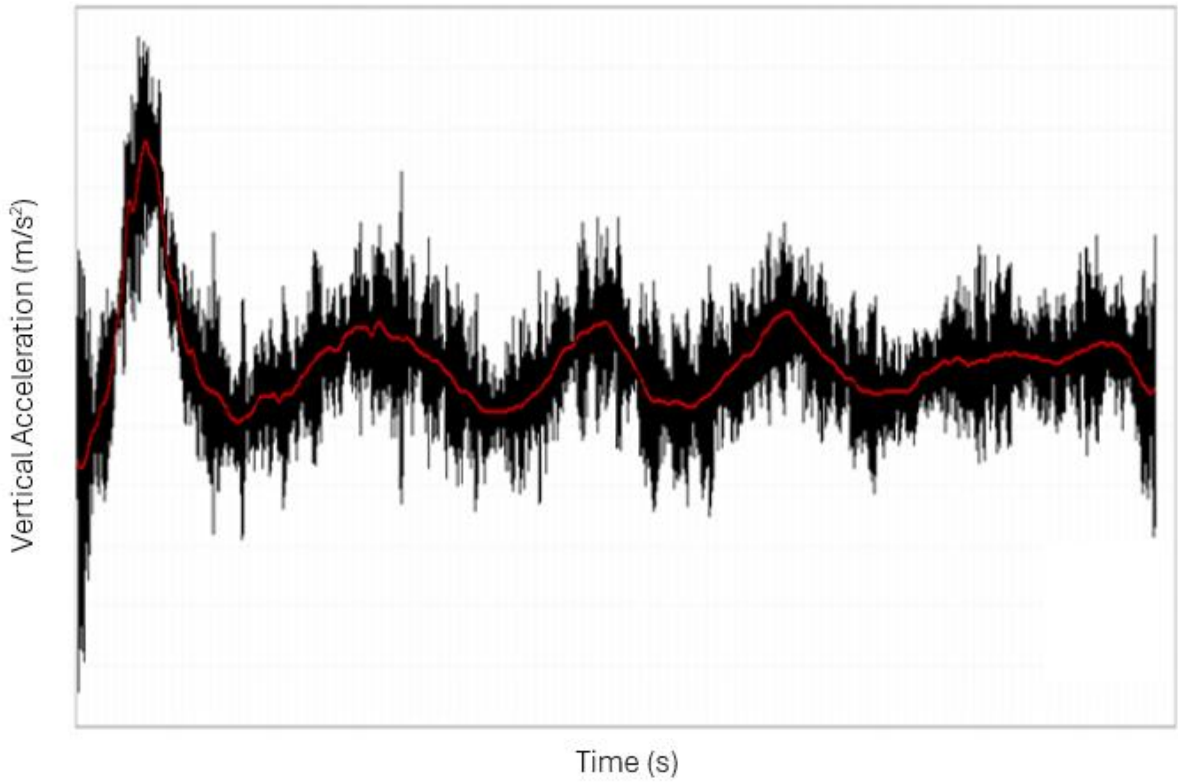

Figure 5-19: Comparison of filtered (red) and unfiltered (black) vertical Sliding Phase data.

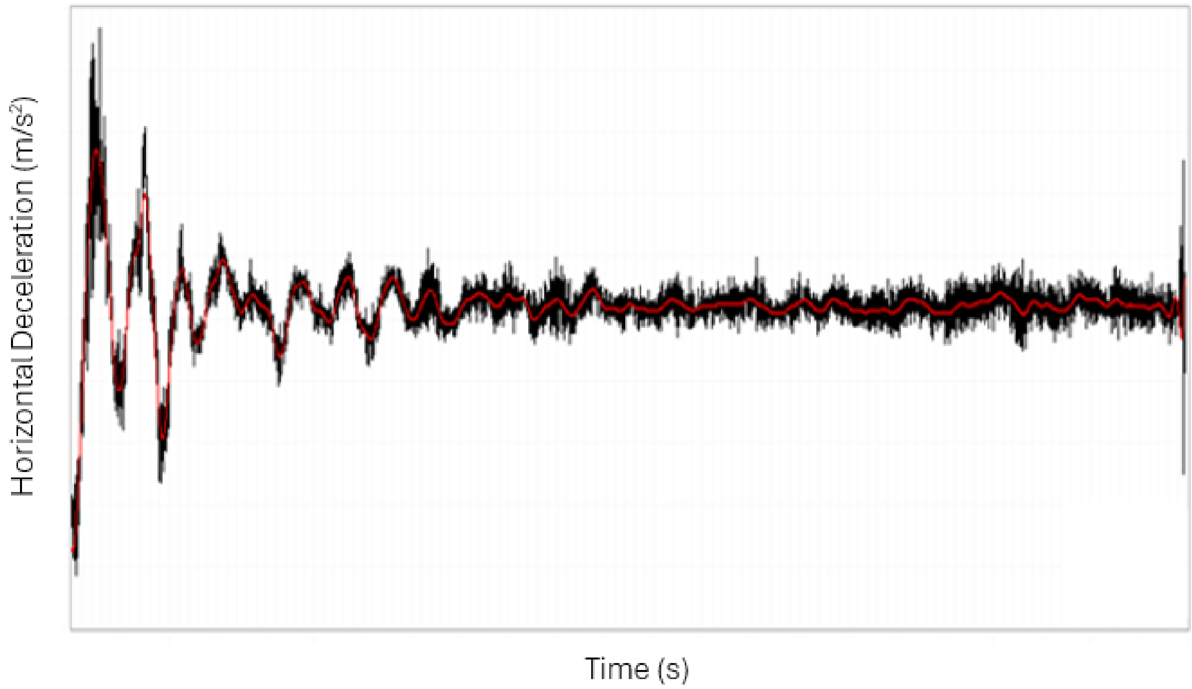

Figure 5-20: Comparison of filtered (red) and unfiltered (black) horizontal Sliding Phase data.

The final filtering process on the vertical Impact Zone (Figure 5-17) demonstrates a smooth profile with minimal attenuation of peak acceleration and no phase shift. The profile generated on the horizontal axis (Figure 5-18) exhibits a positive peak followed by a negative peak. This was attributed to the dropping column experiencing strain as the vertical load increased. Resulting in the rapid deceleration of the simulated player. As the impactor rebounds, the strain reduces, causing the dropping mechanism to return to its original position. Generating an acceleration (negative peak). The dynamic nature of this axis generates more noise than the vertical axis, which was attributed to instrumentation vibrations. Consequently, a more aggressive filter was implemented to yield a refined signal that effectively serves as a line of best fit through the signal.

The design specification stated that the knee should constantly contact the surface throughout the Sliding Phase. As desired, the lowest vertical acceleration occurs at the beginning of the vertical accelerometer profile (Figure 5-19). This demonstrates that the dampening mechanism has successfully attenuated the rebound to produce a protracted slide with the knee in constant contact. However, the instrumentation noise generated by the Impact Zone continues to manifest within the signal as the Sliding Phase commences. Newton's third law states that for every action, there is an equal and opposite reaction. This principle applies to the analysis of vibrations as visually depicted by the 'trumpet' shaped profile (Figure 5-20). With the evolution of the Sliding Phase, these forces are quickly attenuated. This culminates in a state of equilibrium, during which the knee undergoes sliding motion unaffected by the presence of noise or external disturbances. Consequently, the timeframe preceding the attainment of equilibrium should be omitted during the analysis of the Sliding Phase.

The requirement for four accelerometers was assessed during an optimisation process for turning the prototype into a commercial kit. Through further investigation, it was established that all accelerometers are calibrated at 1G. Therefore, the larger G accelerometers dedicated to the Impact Zone could be sensitive to monitoring the Sliding Phase. In this retrospective analysis, the smaller G accelerometers were compared to the larger G transducers with different filtering parameters (Figure 5-21 & Figure 5-22). The filter type (Butterworth) and order (n) remained constant during this analysis, as defined in Table 20, while the cutoff frequency varied. The red profile represents the initial Sliding Phase signal from the 20G accelerometer. The black and green profiles represented the signals from the larger G accelerometer with the Sliding Phase and Impact Zone cutoff frequencies applied, respectively. Both graphs show that the green trace, which represents the Impact Zone filtering process, is much noisier than the other two traces with lower cut-off frequencies.

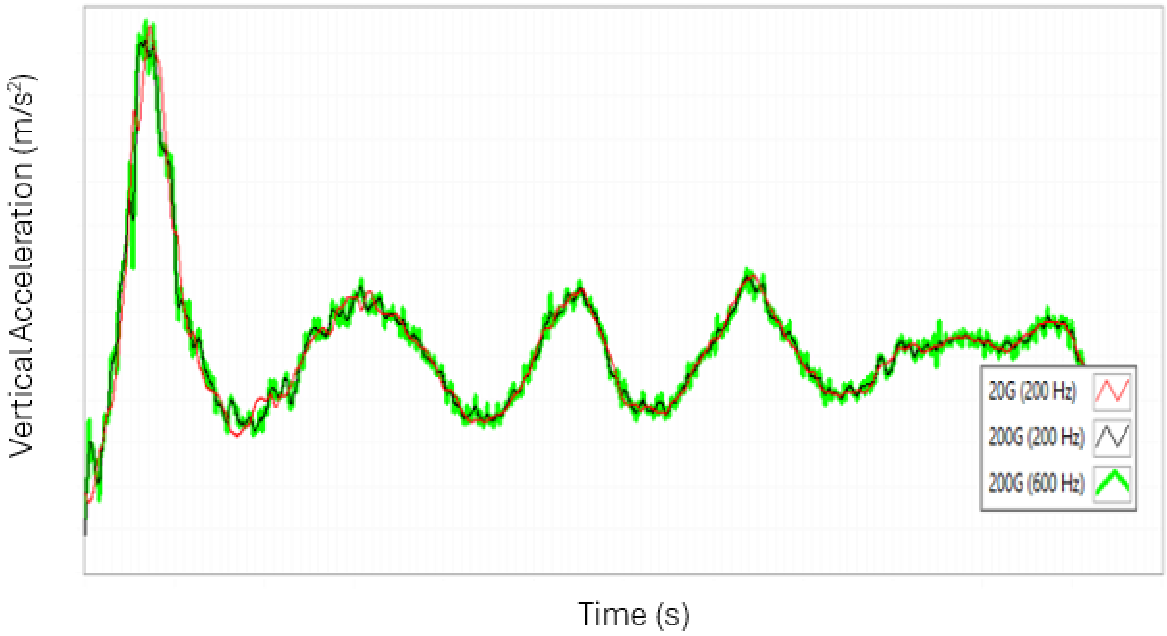

Figure 5-21: Comparison of 200G and 20G Vertical Accelerometer Data During Sliding Phase

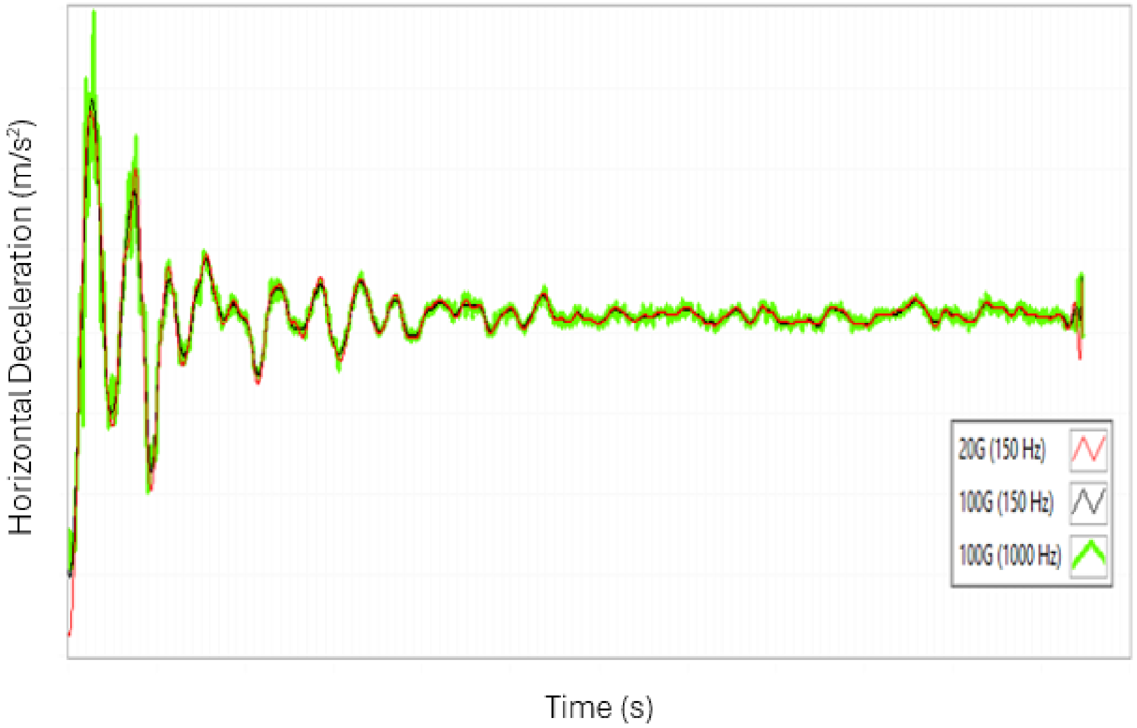

Figure 5-22: Comparison of 100G and 20G Horizontal Accelerometer Data During Sliding Phase

To establish when the Sliding Phase achieved equilibrium, an iterative procedure was implemented on the 20G data collected during the thermocouple validation to monitor the standard deviation of the profile in 0.05-second increments, as presented in Table 5-7.

Table 5-7: Evaluating standard deviation of the Sliding Phase to establish the time index when equilibrium is achieved.

Sample	Time Increment (s)							
	0.05	0.1	0.15	0.2	0.25	0.3	0.35	0.4
SBR50(1)	12.7 ± 2.6	5.6 ± 0.3	3.0 ± 0.4	0.8 ± 0.0	0.7 ± 0.1	0.8 ± 0.1	0.7 ± 0.1	0.7 ± 0.1
SBR50(2)	10.7 ± 1.8	6.1 ± 0.8	4.4 ± 1.8	1.1 ± 0.2	0.9 ± 0.5	0.9 ± 0.3	0.8 ± 0.2	0.8 ± 0.2
SBR60(1)	16.3 ±3.9	4.8 ± 1.5	3.4 ± 0.6	0.9 ± 0.2	0.6 ± 0.2	0.7 ± 0.0	0.7 ± 0.1	0.7 ± 0.1
SBR60(2)	11.8 ± 5.6	6.2 ± 0.9	3.5 ± 0.7	1.2 ± 0.5	0.9 ± 0.3	0.8 ± 0.2	0.7 ± 0.2	0.7 ± 0.2
Total	12.9 ± 4.1	5.7 ± 1.1	3.6 ± 1.1	1.1 ± 0.6	0.8 ± 0.3	0.8 ± 0.2	0.7 ± 0.1	0.7 ± 0.1

These results numerically describe the ‘trumpet’ shape identified during the visual inspections, highlighting the noticeable trend in which the standard deviation started at an elevated level and subsequently reduced. The average sliding duration throughout these tests was 0.60±0.04s. A consistent standard deviation was observed from 0.2s until the end of the interaction, implying that equilibrium had been achieved. Consequently, this time index was selected as an acceptable starting point for Sliding Phase analysis. A consistent duration of 0.3s should also be implemented to compare equal datasets fairly. Finally, an ANOVA test was conducted on the three filter setups with these boundary conditions, highlighting no statistical significance ($p > 0.05$) between the averages. Despite the lack of differences between the filtering parameters, the lower cutoff frequency for the Sliding Phase was more desirable as it yielded a more refined signal. Consequently, all proceeding data presented will represent the large G accelerometers, which have been processed using the final filter parameters detailed in Table 5-6.

5.5 Data Processing Techniques

5.5.1 Identifying repeatable features in the accelerometer data

To better understand the interaction and optimise data processing, the motion profiles were morphologically analysed to identify repeatable components of the waveforms and provide time stamps for interaction events. Six essential features were identified: beginning of interaction (T1), release of the impactor to initiate free fall (T2), point of contact (T3), end of initial contact (T4), beginning of sliding phase (T5), and end of the interaction (T6).

5.5.2 Defining the Beginning and End of the Interaction [T1 & T6]

When analysing the horizontal acceleration, *Figure 5-23*, two distinct positive peaks can be observed representing the initial contact and the end of the interaction. The flatline at the beginning of the waveform represented a half-second delay, which was utilised to calibrate an offset to zero the accelerometers. The beginning of the interaction [T1] was defined at the point where the horizontal axis deviated from zero G. The initial significant deviation, signifying forward movement from this static reference point, exhibited a negative direction. Consequently, the positive axis indicates decelerations within this project's context. The end of the interaction was defined by identifying the second peak and working back to establish a threshold where the simulated player was still in motion. This threshold was calculated by an offset of minus 0.02 seconds from the second peak. Then, taking an average of the previous 0.3s, as illustrated in Figure 5-24.

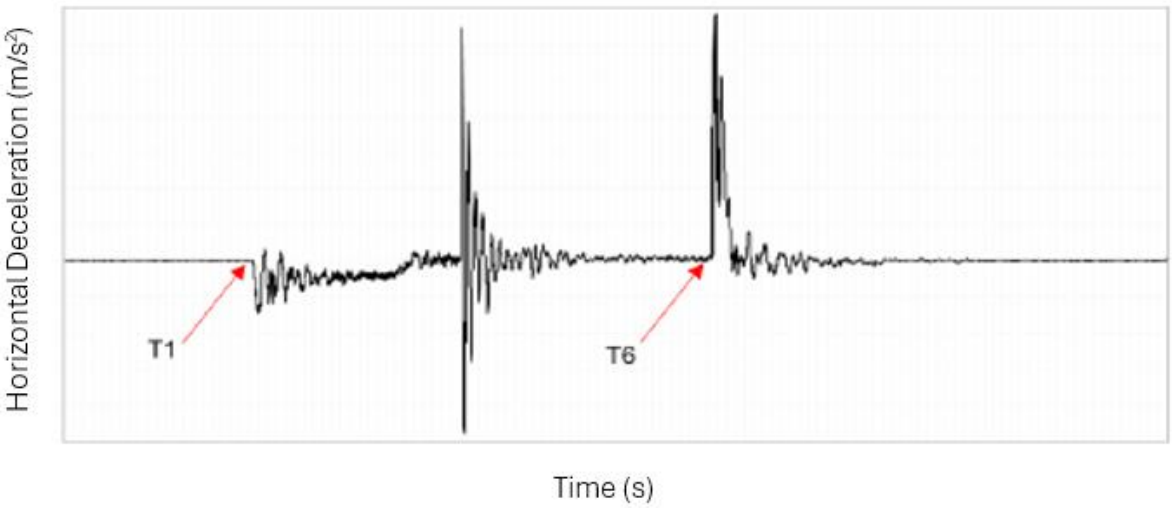

Figure 5-23: X-axis motion profile highlighting essential time index. Where the positive axis represents decelerations which represents resistive forces.

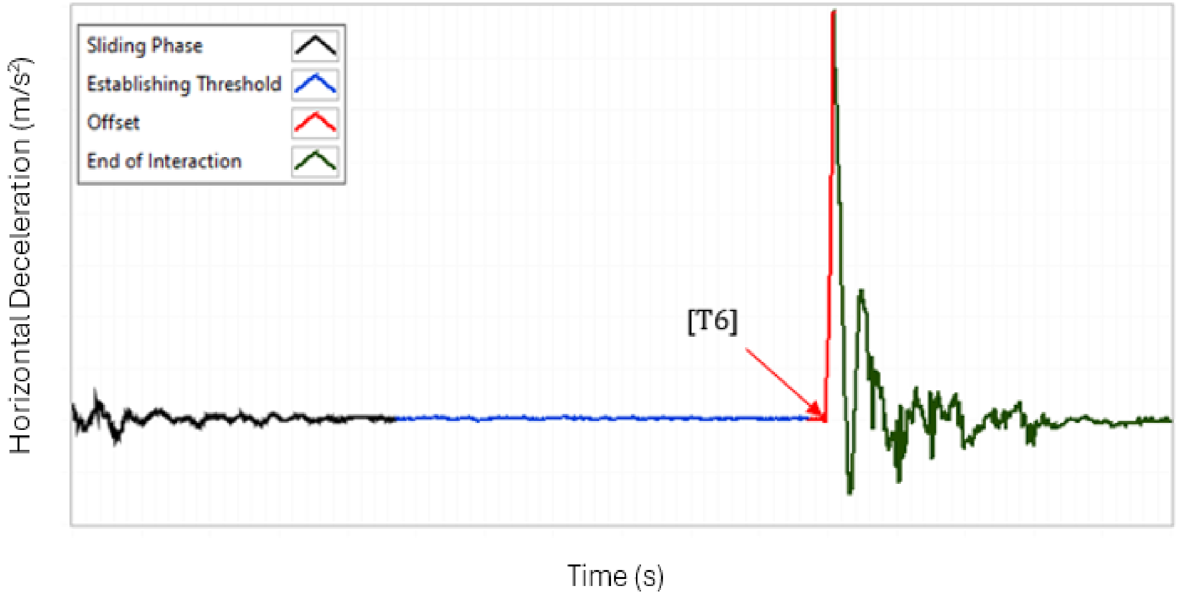

Figure 5-24: Defining protocol to establish the end of interaction where the red arrow represents the 0.02s offset and green represents the data, which is averaged to calculate the threshold.

5.5.3 Establishing the Release of Impactor to Initiate Free Fall [T2]

When examining the vertical accelerations (*Figure 5-25*) the signal becomes noisy before the release of the knee, which was attributed to the horizontal acceleration of the carriage. This noise prevented identifying the impactor's release using the same principles as T1, therefore, a new approach had to be created.

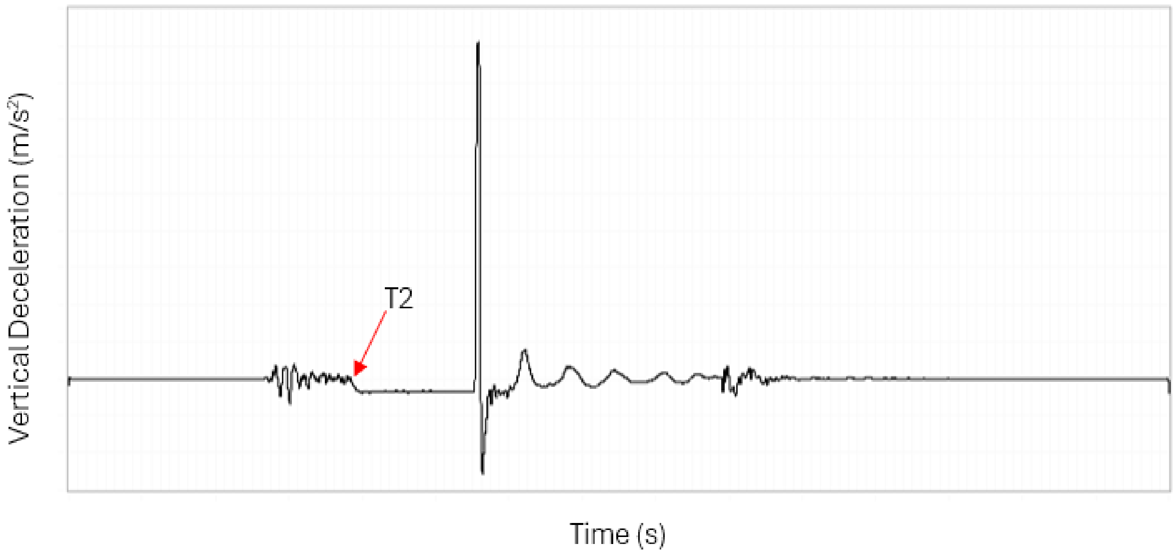

Figure 5-25: Z-axis motion profile highlighting essential time index - negative axis represents downwards travel.

Free fall was initiated by de-energising the magnet, resulting in the knee accelerating towards the sample at a rate close to gravity. The negative drop-off and flatline around 9.81 m/s^2 represent the free fall, which illustrates that negative values are down and positive values are up (*Figure 5-25*). The release point was determined by identifying the time index of the peak acceleration and then applying a 50ms offset, the typical duration of the AAA contact, to establish a time index between the release and point of contact [231]. The time index of T2 was established by reverse processing this dataset to determine when the free fall started, represented by zero-G on the vertical acceleration graph.

5.5.4 Establishing the Contact Period of the Impact Zone [T3 & T4]

In a recent study, Cole et al., (2020) evaluated the AAA and reported that the current algorithm did not accurately determine the point of contact. Consequently, the quality of the output metrics was influenced as the Vertical Deformation was underestimated. This limitation was attributed to the current test method utilising the minimum and maximum vertical velocities to define the start and end of the interaction. A better representation of initial contact is when the free-falling impactor decelerates before it achieves its minimum velocity. Subsequently, the new algorithm proposed established the point of contact by detecting the peak force and working forwards and backwards until the time index before the normal load crosses a threshold of 30N [231].

This protocol was adopted to keep data processing consistent with existing test methods; however, the threshold value was adjusted to accommodate for the variation in mass. The impactor mass for the AAA is 20kg; therefore, 30N represents 15% of the mass. This percentage was applied to the SID's 36kg impactor mass, which produced a threshold value of 55N, as presented in Figure 5-26. Ground reaction forces were calculated by transforming accelerometer data on the vertical axis to Newtons using the formula provided in FIFA Test Method 04a – Equation 21

Equation 21

$$F_V = m, g.G + m.g$$

Where:

- F_V – Vertical Force – expressed in Newtons (N).
- m – mass of impactor – expressed in kg.
- g – acceleration due to gravity (9.81 m/s^2).
- G – the acceleration during the interaction, expressed in g (1g = 9.81 m/s^2).

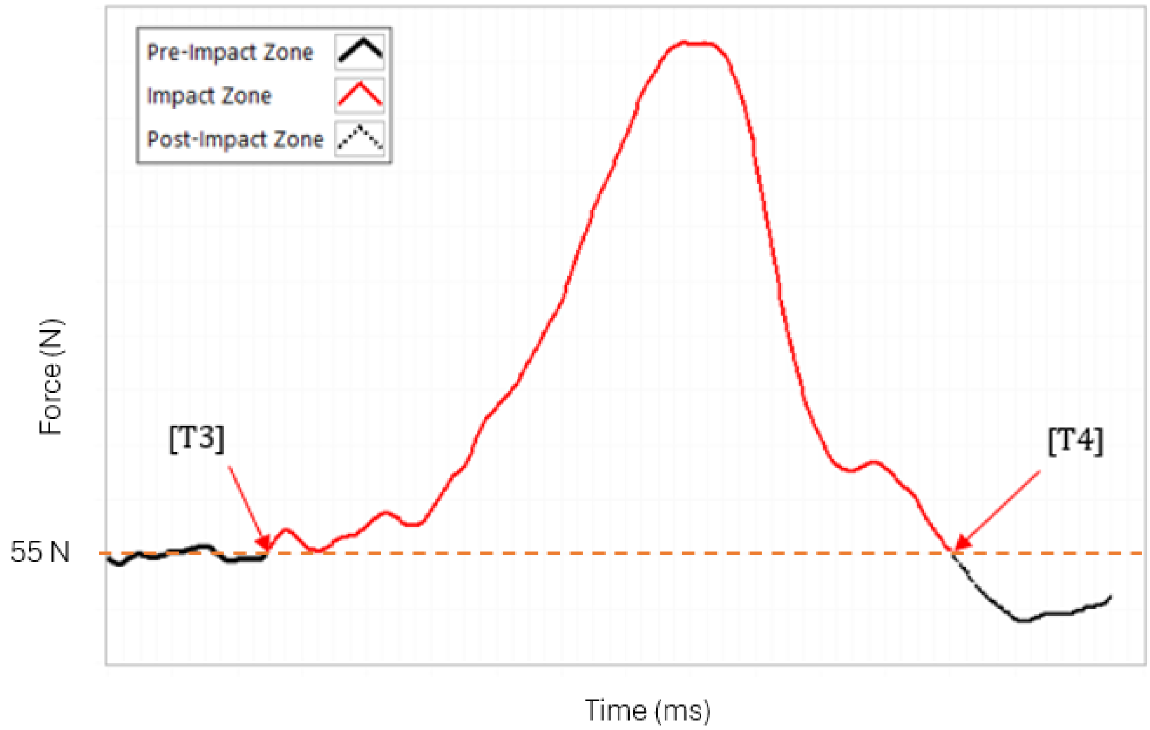

Figure 5-26: Example force-time profile from a single SID impact highlighting contact period.

5.5.5 Establishing the Beginning of the Sliding Phase

The design specification stated that the impactor must constantly contact the surface during the sliding phase. The beginning of the sliding phase was established by working back from T6 to find the last point before the vertical force crosses the 0N line (Figure 5-27).

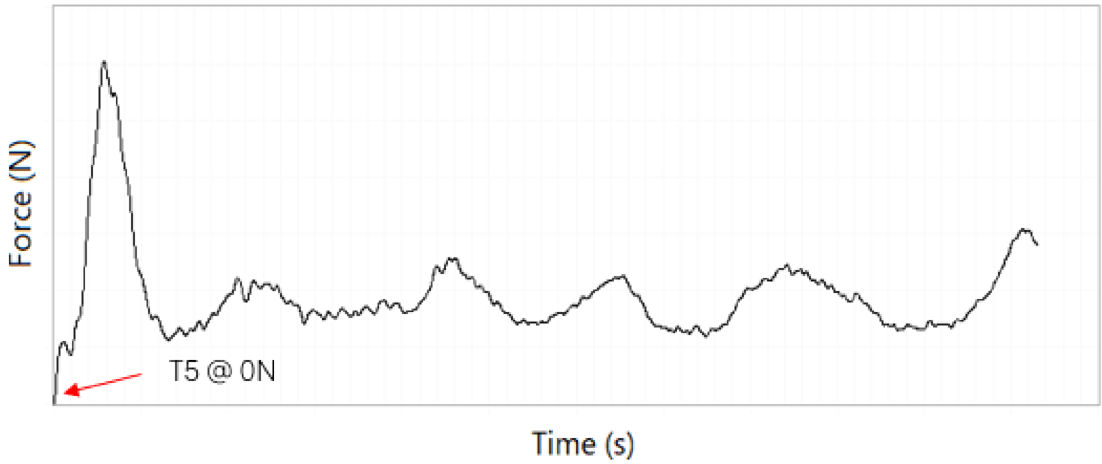

Figure 5-27: Example force-time profile from SID to establish starting time index for the Sliding Phase.

5.5.6 Summary of Essential Time Index

A summary of the essential time index is illustrated on the typical vertical motion profile generated during the simulation (Figure 5-28).

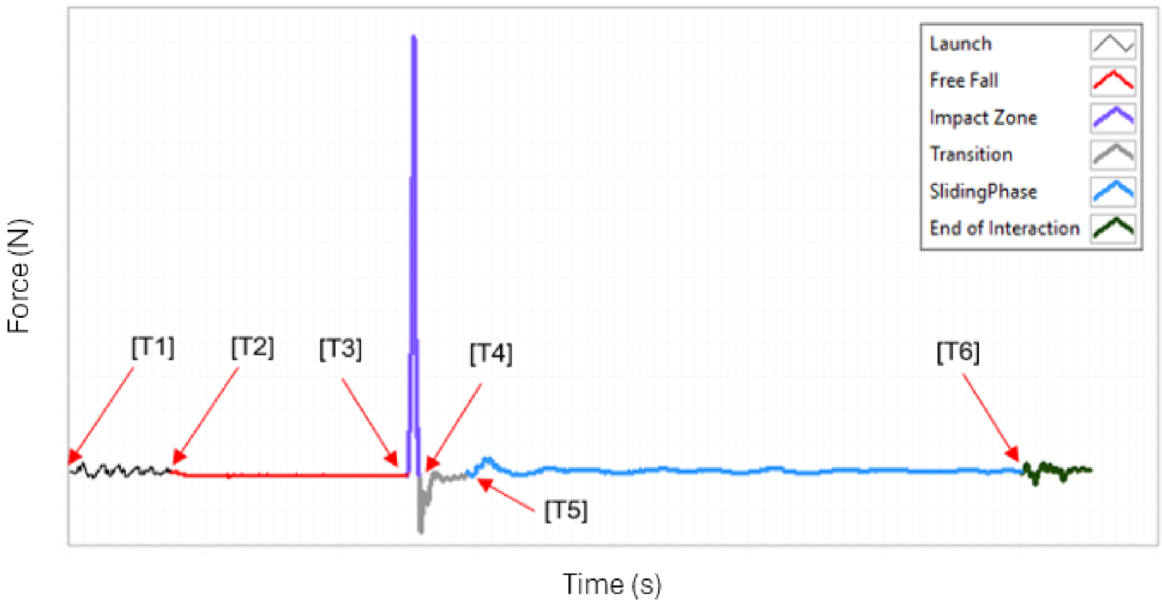

Figure 5-28: Example of vertical motion profile identifying essential time index – beginning of interaction (T1), release of the impactor to initiate free fall (T2), point of contact (T3), end of initial contact (T4), beginning of sliding phase (T5), and end of the interaction (T6).

5.5.7 Establishing protocols to derive velocity and displacement.

The subsequent data processing phase involved the computation of velocities and displacements through single and double integration. In all integration procedures, Simpson's Rule was employed due to its recognised accuracy [233]. This process should start as close to the beginning of motion to mitigate any compound errors in processing static accelerometer data. The horizontal accelerometers were integrated from T1 – T6, as presented in *Figure 5-27* (a, c, e). While the vertical impact accelerometers were integrated from T2 – T6, as presented in *Figure 5-27* (b, d, f). An offset of T2 minus T1 was applied to the vertical motion profiles to compensate for the delay between the launch and the impactor release to keep time stamps consistent on both axes.

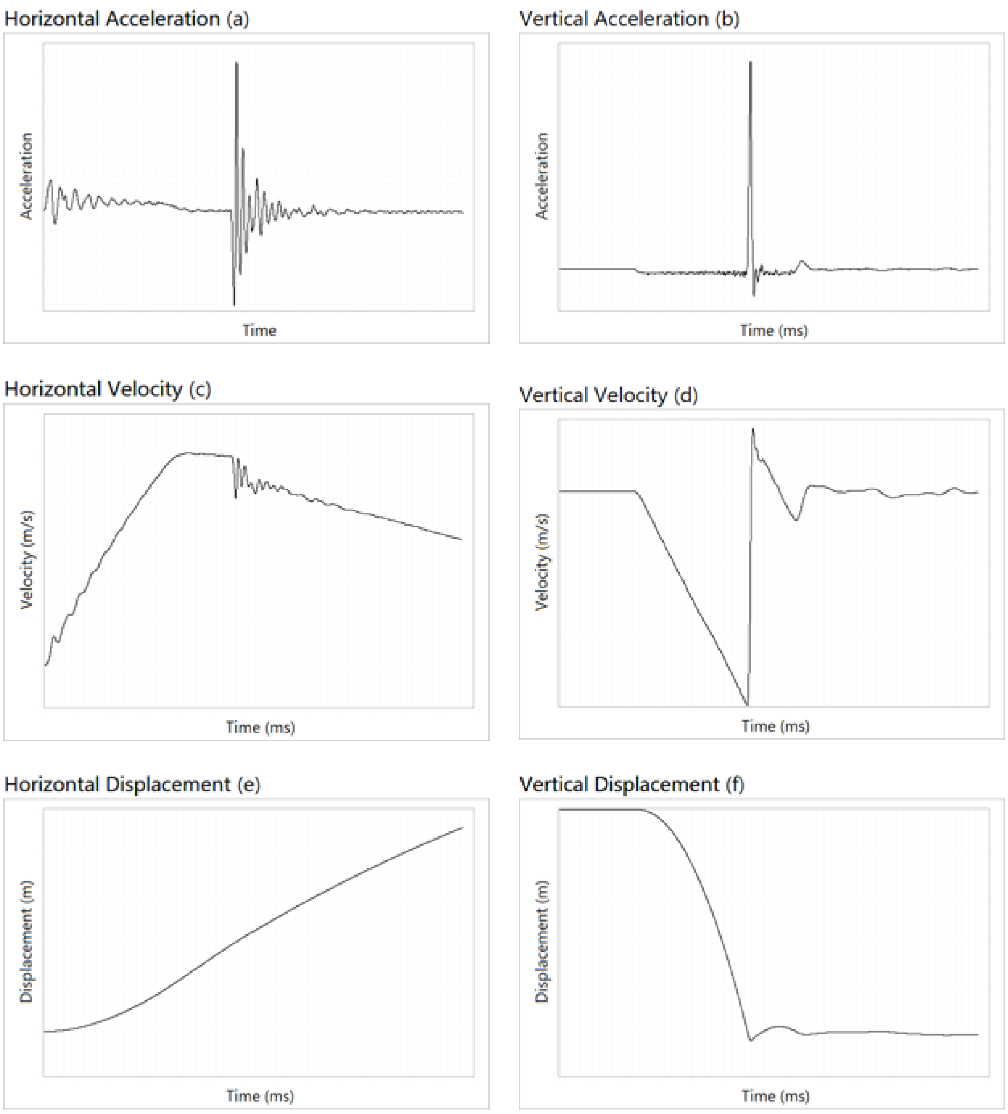

Figure 5-29: Motion Profile during Skin Injury Risk Assessment a) Horizontal Acceleration; b) Vertical Acceleration; c) Horizontal Velocity; d) Vertical Velocity; e) Horizontal Displacement; d) Vertical Displacement

The design specification stated that the test method should simulate realistic horizontal (5 m/s) and vertical (3.1 m/s) velocities. During the testing, as outlined in Section 5.2, the apparatus produced repeatable horizontal (4.99±0.01 m/s) and vertical (2.95±0.01 m/s) impact velocities (T3). Figure 5-30 illustrates deviation from the specified impact velocities in the form of percentage difference. This highlighted the vertical axis was lower than the desired velocity by 4.98±0.003%. Interestingly, the vertical impact velocity was much closer to the desired 3.1 m/s during static drops. No horizontal forces were acting on the impactor's bearings in a static drop. During a dynamic launch, the reduction in vertical velocity was attributed to the bearings experiencing thrust, which increased pressure between contacting surfaces, leading to higher friction and subsequent energy losses [234]The consistency of the vertical impact velocities was deemed acceptable; therefore, a consistent release height of 500 mm was maintained for all future testing. Consequently, 2.95 m/s was selected as the desired vertical impact velocity to accommodate additional internal friction during dynamic launches.

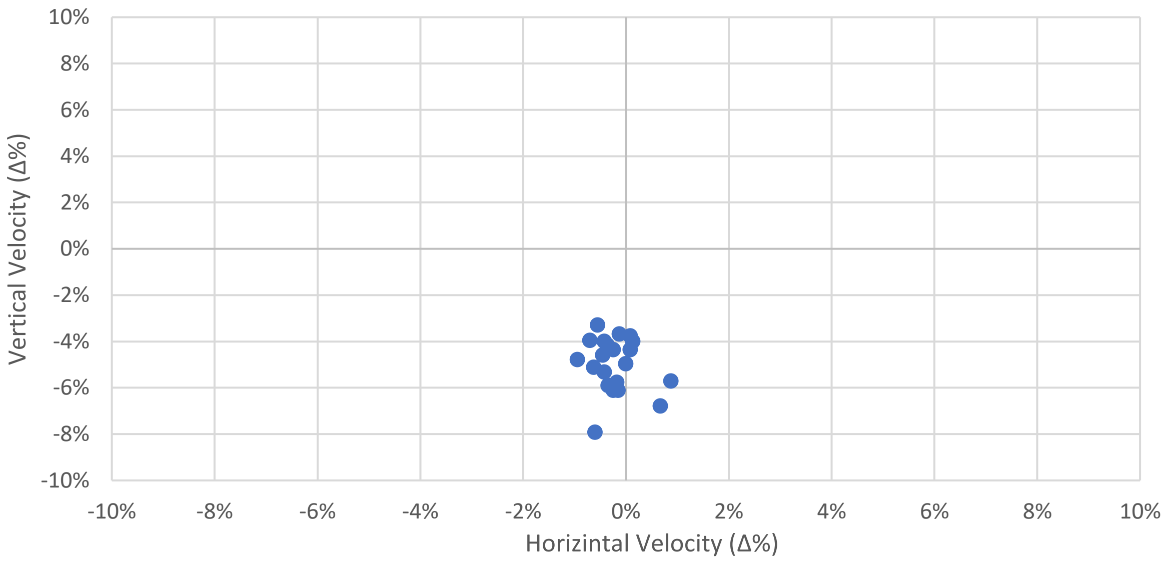

Figure 5-30: Illustrating deviation from desired impact velocities during thermocouple validation.

The next stipulation of the design specification was a quick transition zone from the Impact Zone to the Sliding Phase. The effectiveness of the dampening mechanism was unknown when this was defined. Therefore, desirable (<10%) and acceptable (10-20%) limits were defined in terms of a percentage of the overall length of the apparatus. The distance travelled during the transition zone was calculated by integrating the horizontal velocity from

T4 to T5. During the testing, as outlined in Section 5.2, there was no statistical difference ($p = 0.20$) between the 50 mm (0.37±0.01m) and 60 mm (0.40±0.02m) samples (Figure 5-31). This result met the requirements of the desirable limits, which equated to a transition zone of less than 0.6 m.

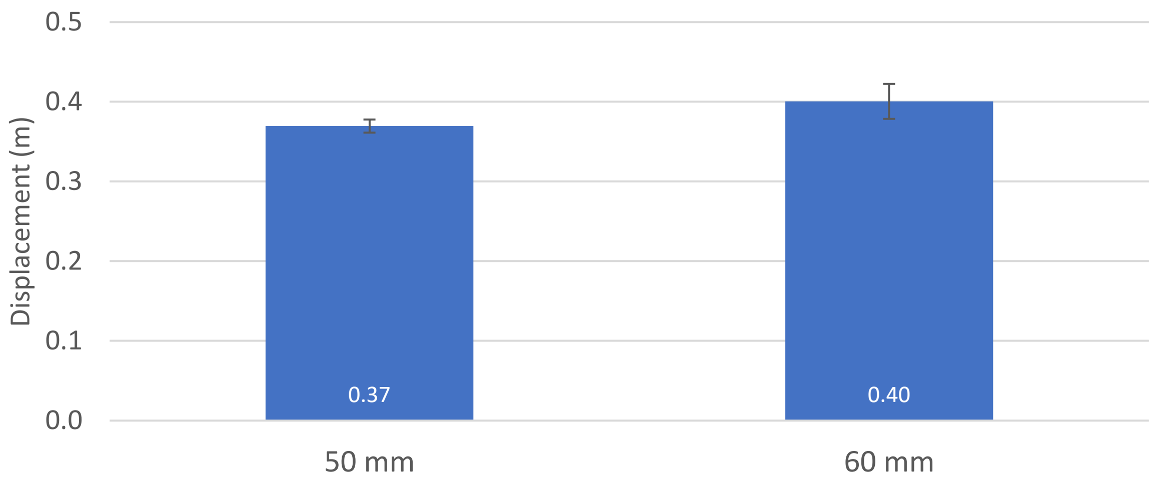

Figure 5-31: Comparison of transition zone displacements on a 50- and 60-mm sample.

The final prerequisite for the simulated player's motion profile was a Sliding Phase with the knee in constant contact with the surface. The desired (2m) and acceptable (1-2 m) sliding distances were based on data collected during the video analysis study in Chapter 3. Figure 5-32 This study compares the Sliding Phase displacements on a 50—and 60-mm sample, which indicates that the apparatus can consistently ($p = 0.64$) generate the desired motion profile.

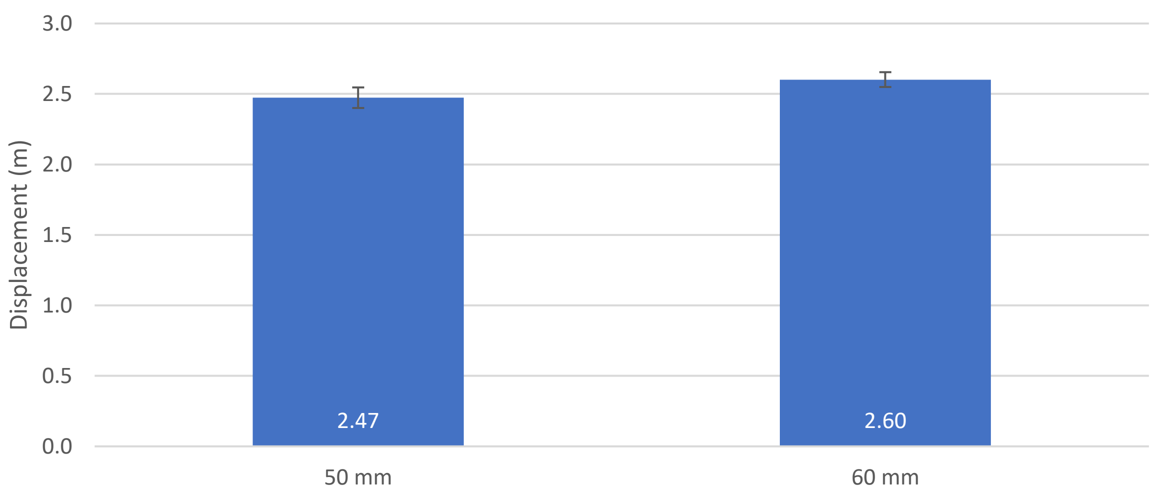

Figure 5-32: Comparison of Sliding Phase displacements on a 50- and 60-mm sample.

5.6 Kinematic Injury Metrics

The design specifications required including additional metrics, alongside monitoring the Heat Profiles and Abrasion Severity Index, to enhance the understanding of the impact mechanics and sliding characteristics. This section aimed to explore, develop, and evaluate various parameters generated by manipulating the accelerometer to quantify the turf's dynamic performance characteristics during the Impact Zone and Sliding Phase. These will be named Kinematic Injury Metrics (KIM), ancillary performance indicators to predict the test specimen's potential skin injury risk.

5.6.1 Coefficient of Friction

The first supplementary injury parameter explored was the coefficient of friction (COF), which aligned with the current test method. The parameter describes the relationship between the resistance of one surface sliding over another and the applied - Equation 22.

Equation 22

$$Coefficient\ of\ Friction\ [dimensionless] = \frac{Horizontal\ Force\ [N]}{Vertical\ Force\ [N]}$$

Section 5.5.4 stated that FIFA Test Method 04a was adopted to calculate the Vertical Forces. However, there is currently no test method for assessing Horizontal Forces. Equation 21was, therefore, further investigated to establish the correlation between g-force and Newtonian force. An object with zero-G can be described as static, therefore, when substituting zero G into Equation 21 the vertical force is equivalent to the object's weight. Since no forces act horizontally on a static object, this can be simplified to remove the body weight constant – Equation 23. This equation expresses g-forces in multiples of g, which can be further simplified to acceleration. Thus, the horizontal forces were calculated using Equation 24, a rigorous application of Newton's second law.

Equation 23

$$F = m.g.G$$

Equation 24

$$F_H = m \times a$$

Where:

- F_H – Horizontal Force – expressed in N.
- m – mass of impactor and carriage, expressed in kg.
- a – the acceleration during the interaction, expressed in m/s^2.

Impact Zone

The Impact Zone is the contact with the greatest magnitude of forces (Figure 5-33) from the point of contact (T3) through the peak vertical force and back to 55N (T4). The corresponding COF for the Impact Zone is presented in Figure 5-34. m/s^2

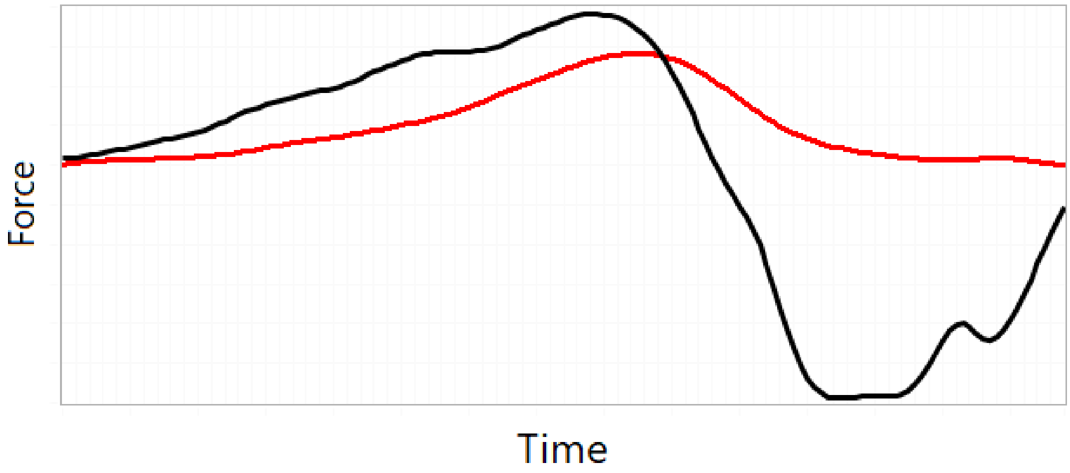

Figure 5-33: Comparison of horizontal and vertical forces during the Impact Zone. The red and black lines represent the vertical and horizontal forces, respectively.

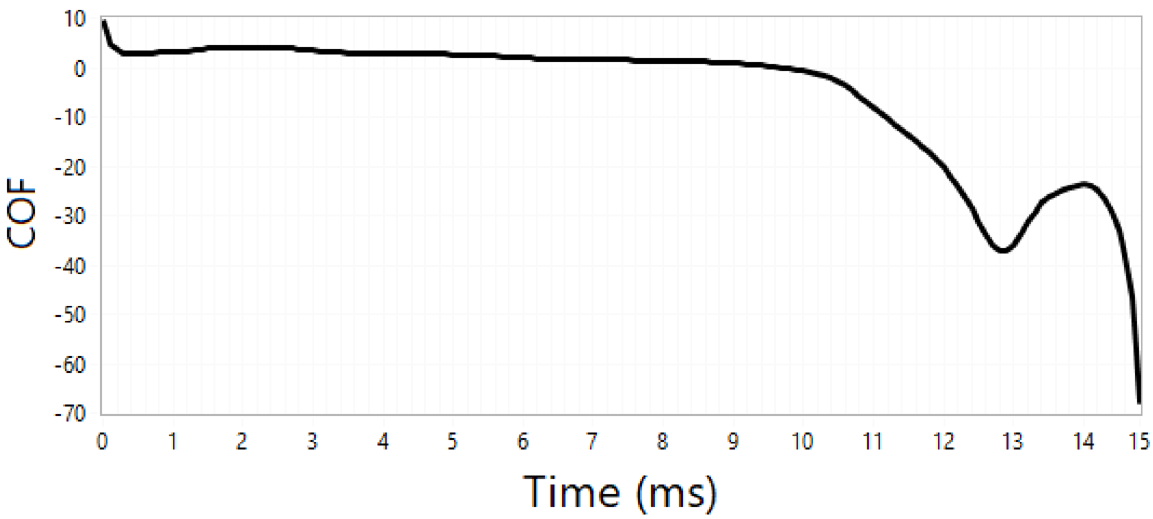

Figure 5-34: Corresponding Impact Zone COF from forces presented above.

COF typically ranges from 0-1 and is known to be sensitive during low vertical loading [235]. As expected, the vertical loads at the beginning of the interaction significantly influenced the COF by generating magnitudes that were unrealistic (Figure 5-34). Frictional forces can only oppose the direction of travel; therefore, any negative horizontal force cannot be considered a resistive force. Consequently, new boundary conditions must be applied to remove the undesirable sections of the signal. To mitigate the effects of low normal loads dominating the COF calculation, new boundary limits were established by identifying the peak vertical force and working back to 360N, equivalent to the impactor's weight. The end of the Impact Zone was defined by identifying the peak and establishing the time index before the horizontal force drops below 0N, as presented in Figure 5-35. The corresponding COF graph with the new boundary conditions is displayed in Figure 5-36.

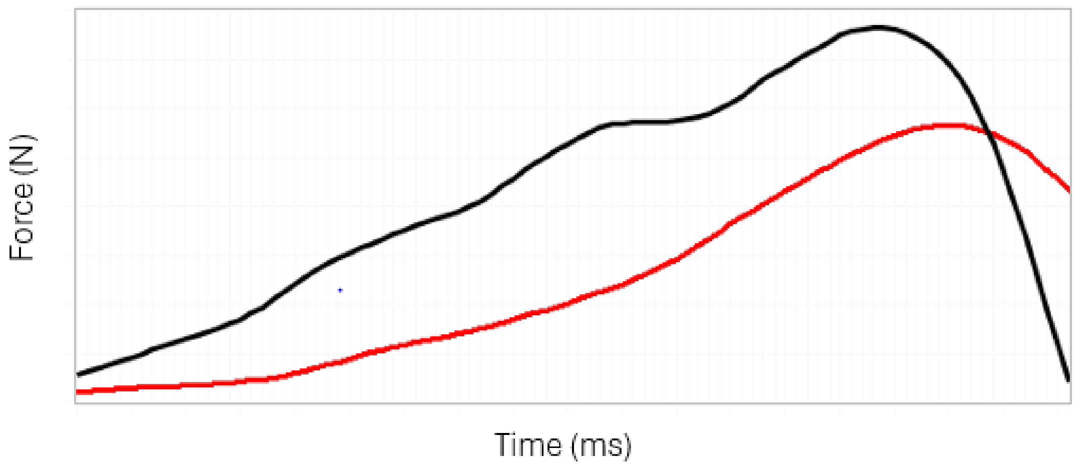

Figure 5-35: Impact Zone forces with new boundary conditions.

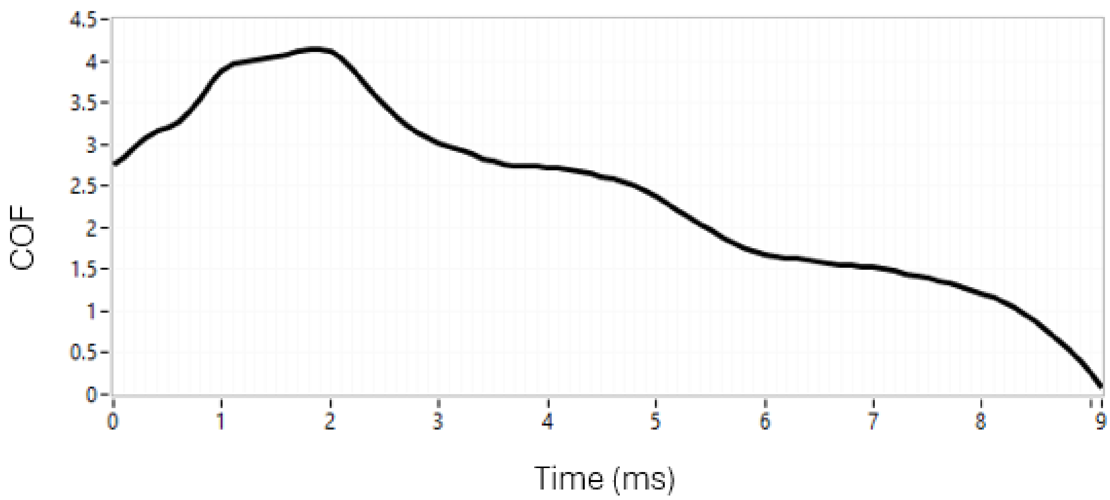

Figure 5-36: Impact Zone COF with new boundary conditions.

Sliding Phase

The Sliding Phase lasted significantly longer than the Impact Zone, with lower force magnitudes. Although the knee form was in constant contact between T5 and T6, an offset of 200ms was added to T5 to facilitate analysis of the Sliding Phase in equilibrium, as discussed in Section 5.4.3. Furthermore, a constant duration of 300ms was implemented to ensure that all datasets were of equal length during the analysis stage. The new boundary limits (red data) were applied to the vertical and horizontal forces, and the corresponding COF was calculated, as presented in Figure 5-37 -Figure 5-39. The oscillations in the vertical force were attributed to the impactor moving freely as it traversed across the sample (Figure 5-37). Confirming no external forces are acting on the impactor during the sliding phase is a desired output stated by the design specification.

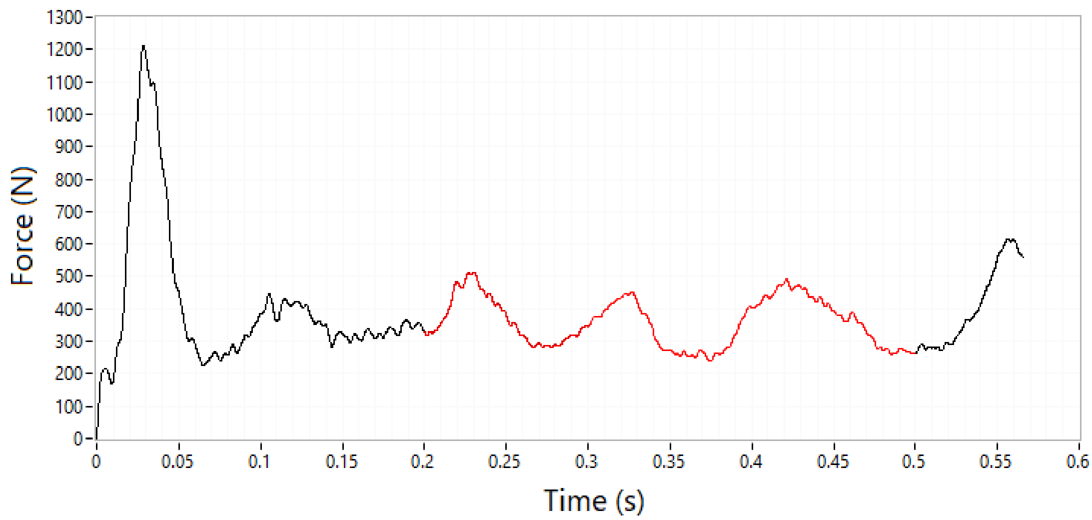

Figure 5-37: Vertical Forces during new Sliding Phase time index.

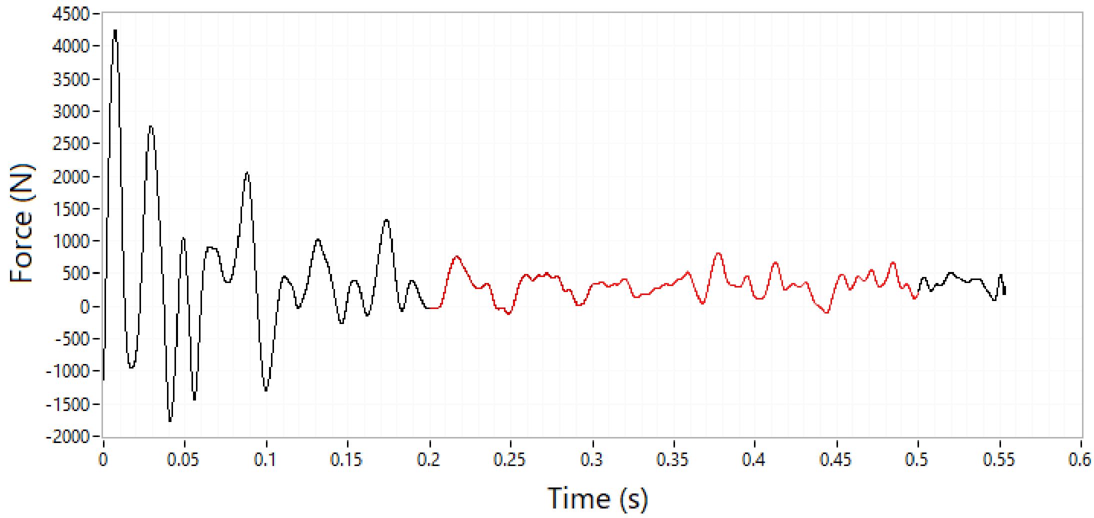

Figure 5-38: Horizontal Forces during new Sliding Phase time index.

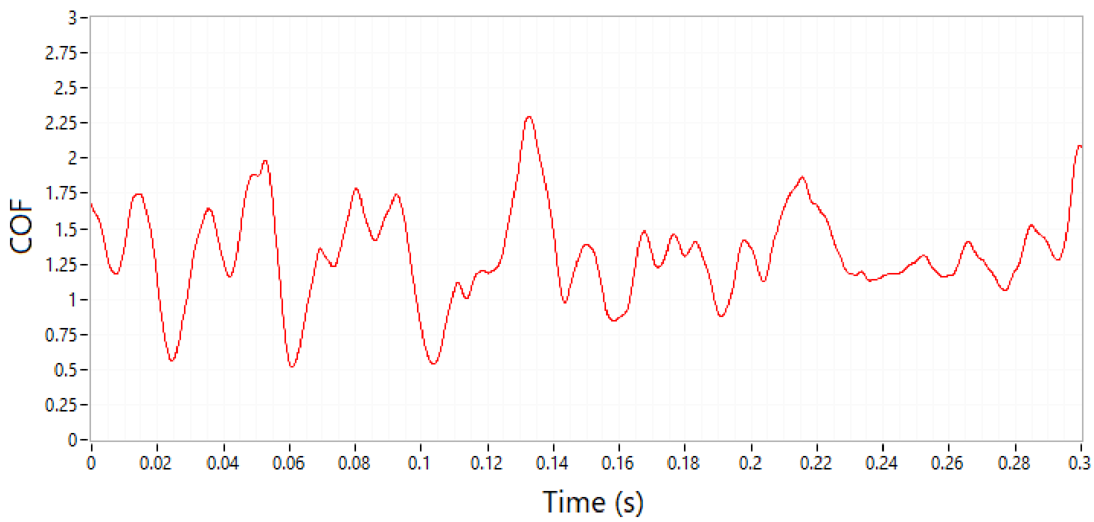

Figure 5-39: Coefficient of Friction during new Sliding Phase time index.

Results

During the Impact Zone, this novel apparatus generated an average force of 8005±179N and 7719±108N on Samples 1 and 2, respectively, equating to roughly 8 times the body weight of an elite rugby player. Analysis of the COF results highlighted the 50 mm sample exhibited an elevated Impact Zone COF (1.85 ± 0.02) compared to the 60 mm sample (1.83 ± 0.02); however, the result was not statistically different (p = 0.34).

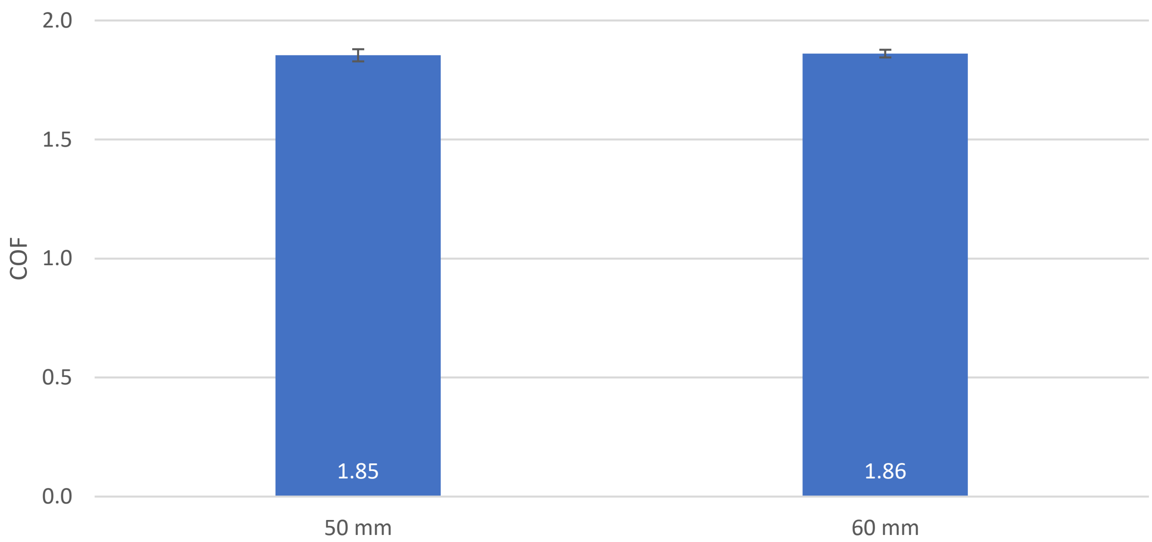

Figure 5-40: Investigating the influence of different turf constructions on Coefficient of Friction during the Impact Zone.

Throughout the Sliding Phase, the new device exerted an average force of 358.5±5.0N and 356.9±4.2N on Samples 1 and 2, respectively. This corresponded to the body weight of the impactor, which was within the desired limits of the design specification. Analysis of the COF results indicated that the 50 mm sample generated a higher Sliding COF (1.04 ± 0.04) than the 60 mm sample (0.98 ± 0.08). Again, the result had no statistical significance ($p = 0.39$).

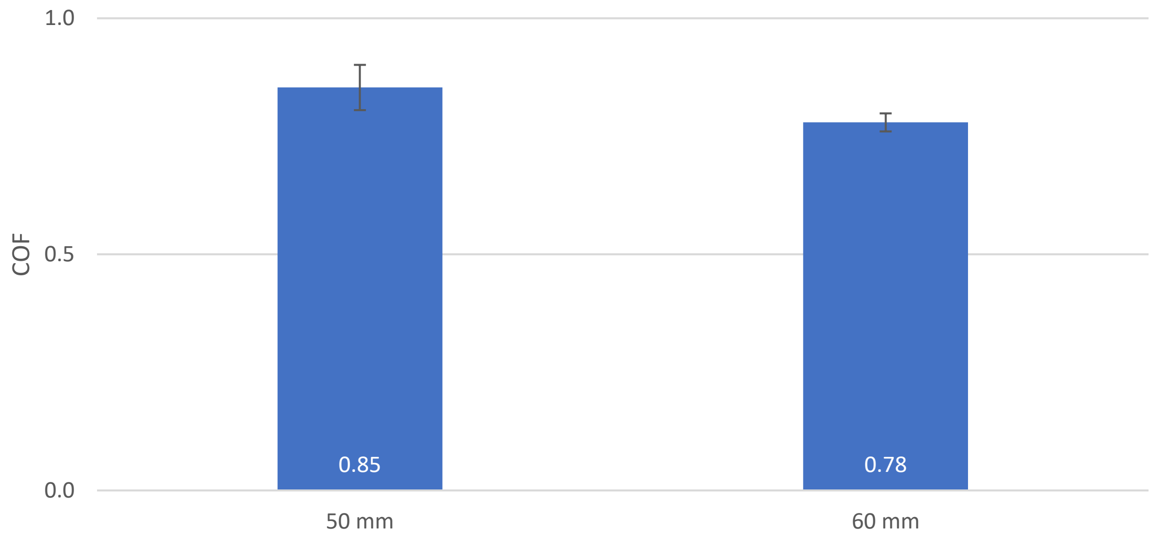

Figure 5-41: Investigating the influence of different turf constructions on COF during the Sliding Phase.

Discussion

This novel research device has generated unprecedented data on a realistic player-surface interaction. The apparatus produced an Impact Zone followed by a subsequent Sliding Phase. The literature lacks essential biomechanical data describing the forces a player would experience during rugby gameplay. However, studies have reported that footballers produce ground reaction forces of 3 – 6.5 times BW on the knee and hip, respectively [136]. The lack of data describing injurious interactions required a study (Chapter 3) to establish realistic loading conditions during the Sliding Phase. Based on the findings from this study, a 36 kg impactor was designed, which, when released from 500 mm, generated forces similar to what goalkeepers would experience when landing from a dive (4.2-8.6 BW) [135]. The motion profiles of a tackle in rugby and football are completely different. During football, the tackler is predominantly the more susceptible player to sustaining a skin injury, whereas, in rugby, both the ball carrier and tackler are vulnerable. A situation where the tackler lands on the ball carrier could generate significantly greater impact force than a footballer.

Additionally, rugby players are typically heavier than footballers, which would contribute to greater impact forces. Despite generating normal loads greater than the forces that would be experienced by the knee during a football slide tackle, the loading conditions were deemed acceptable. This determination was made based on the forces representing a worst-case scenario for rugby whilst concurrently providing realistic loading during the Sliding Phase.

Laboratory friction tests are typically performed between two solid surfaces in a controlled environment with a consistent normal load at constant velocity (N. K. Veijgen, 2013). During the Impact Zone, a significant vertical load was generated over a short horizontal distance where the simulated player experiences a rapid deceleration. Meanwhile, the Sliding Phase exhibits a natural deceleration during a protracted slide. In combination, these characteristics establish a divergence from conventional friction tests. The dynamic nature of the interaction results in the turf experiencing multi-dimensional deformations, which will influence the surface's behavioural response. Additionally, the dynamic nature of turf enables permanent infill displacement as the impactor interacts with the surface. Consequently, energy is lost from the system. Artificial turf may, therefore, not conform to Amonton's Laws of Friction, which state frictional forces are proportional to the normal load. This divergence is akin to findings in existing research that have identified artificial turf as inherently non-linear [71].

COF has been reported to be a poor indicator of skin injury risk [143]. Section 5.3.4 reported a higher Abrasion Zone score on the 50 mm samples (640.5±20.5) than on the 60 mm samples (439±13). Despite both the impact and slide COF indicating the 50-mm sample exhibited greater frictional responses, the results were not statistically different, which did not provide confidence in the correlation between COF and abrasiveness of turf. This aligns with the theories presented in the literature review, which analysed the wear Equation 25 to highlight there is no association between COF and skin damage. This combination of compounding negative features implies that COF is not the convenient indicative injury metric that should be used.

Equation 25

$$W = k.F.d$$

Although the COF may not initially appear to be a suitable KIM for providing insights on skin injury risk, the methods presented above for analysing the data are still valuable. Consequently, the time stamps established for analysing the Impact Zone and Sliding Phase will be adopted whilst developing future KIMs. An example of the simulation events and datasets which should be evaluated is illustrated in Figure 5-42.

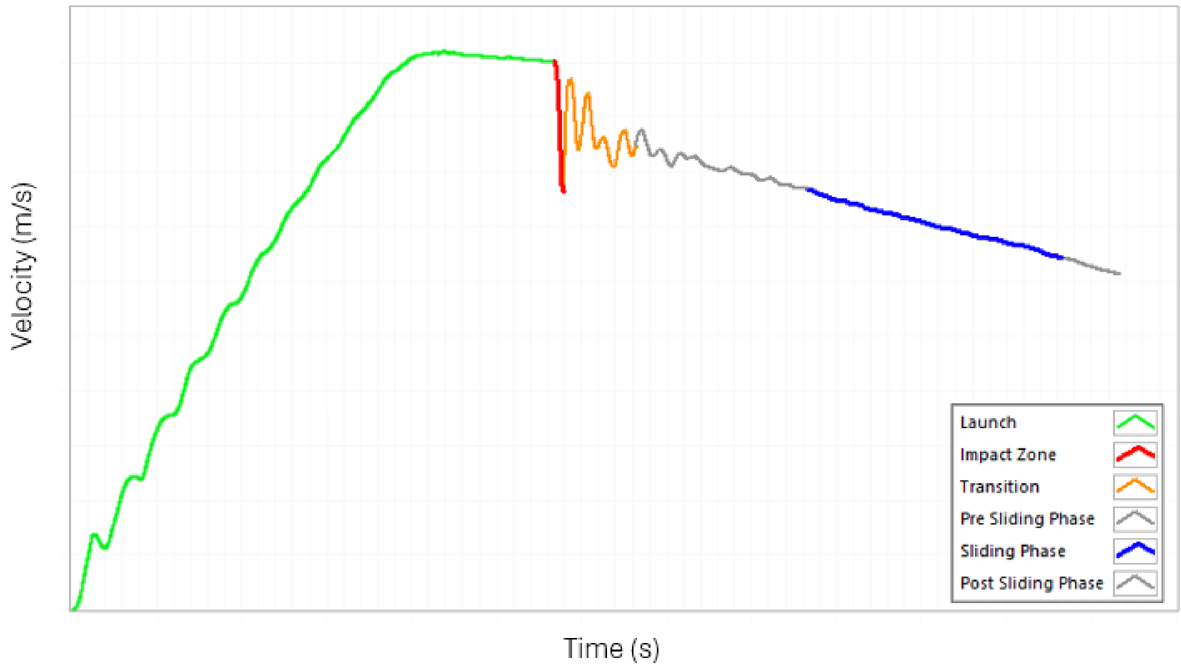

Figure 5-42: Example of simulation events during the horizontal velocity highlighting the Impact Zone & Sliding Phase

5.6.2 Deceleration

Acceleration, the rate of change in velocity, is a fundamental concept used to rate performance in a sporting environment. The ability to quickly achieve top speed or change direction can gain a competitive advantage over opponents. However, it's important to note that these rapid movements can also increase the risk of injury. Deceleration, the act of slowing down, is equally important in sports biomechanics as it enables fine control over the athlete's body to execute complex manoeuvres during high-energy interactions. These movements can place a high demand on the musculoskeletal system, making the athlete more susceptible to injury [236]. For example, accelerations are associated with a greater metabolic cost [237], while decelerations generate higher mechanical loads [238]. These interactions are likely attributed to elevated peak impact forces and loading rates [239], which have the potential to cause more substantial damage to soft-tissue structures, notably if these high forces cannot be efficiently attenuated [240].

Skin strength is a mechanical property that reflects the skin's ability to resist external forces. As the strain rate increases, there is a corresponding decrease in the skin's failure strain [16]. Skin damage will occur when the forces applied exceed the established failure strength of the skin. Although there is no player data indicating the forces required to generate skin injuries, deceleration could be used to predict the injury potential of the simulated player. This parameter will provide an indirect measure for monitoring resistance where a higher resistance indicates a greater risk of injury.

Impact Resistance

The initial point of contact with turf during a high-energy impact, such as the Impact Zone, generates sudden and intense forces that rapidly decelerate the player, as illustrated in Figure 5-43. This event produces the greatest magnitude of forces which can significantly impact skin injury risk.

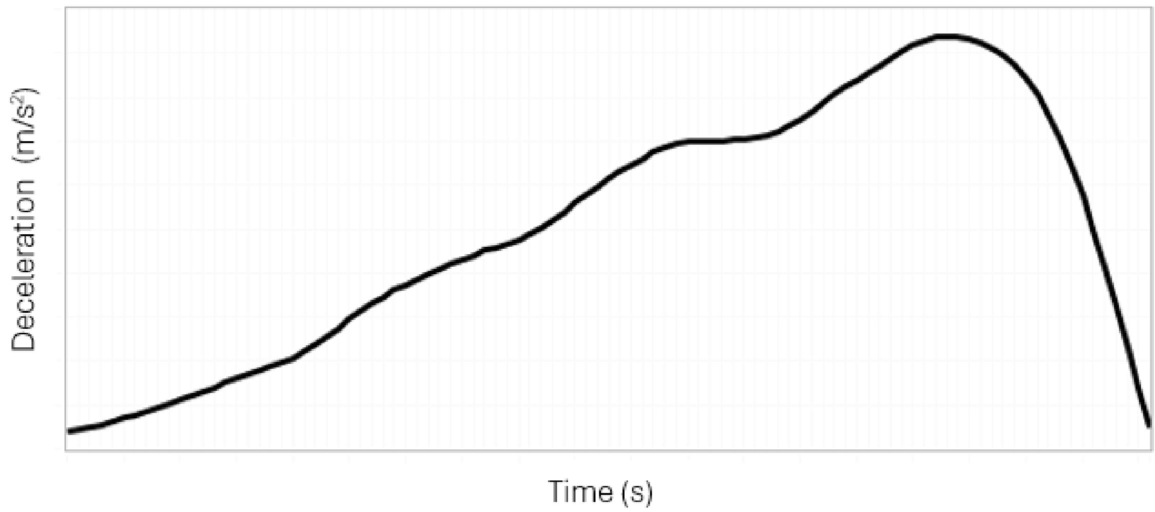

Figure 5-43: Example of Impact Zone Deceleration Profile

The lack of essential biomechanical data describing injurious interactions makes it extremely challenging to determine the KIM parameters' thresholds that would exceed the failure strength. Therefore, different methods were explored to quantify the deceleration experienced during the Impact Zone. Instinctively, the peak deceleration was the most logical analysis method to quantify the intensity of the interaction. At the same time, it is considered a fundamentally flawed methodology to employ data averaging when attempting to quantify the magnitude of an impact to gain insights into the severity of an injury. Consequently, this approach was promptly dismissed. Impact durations could also influence the skin's failure strength. The influence of an abrupt deceleration compared to a slower deceleration with a more extended impact duration is currently unknown. Head injury studies monitor the influence of this phenomenon by calculating the integral of an acceleration versus time curve [241]. Adopting this technique would quantify the overall reduction in horizontal velocity from the initial 5 m/s, which could provide insights into skin injury risk.

Slide Resistance

The Sliding Phase represents a protracted slide after the Impact Zone with the knee in constant contact with the surface. As previously discussed, an offset will be applied to analyse the data whilst the simulated player is sliding in equilibrium (Figure 5-44). Descriptive statistics, such as mean, median or mode, can be utilised to quantify the central tendency of this type of dataset. The mean is the most commonly adopted descriptive statistic, while the median and mode are limited [242]. Therefore, the dataset's average was the best tool for evaluating the Sliding Phase. Slide Resistance is a parameter that enhances the understanding of the sliding characteristics by quantifying the mean deceleration during a protracted slide. Intuitively, more significant decelerations during the Sliding Phase indicate higher injury potential.

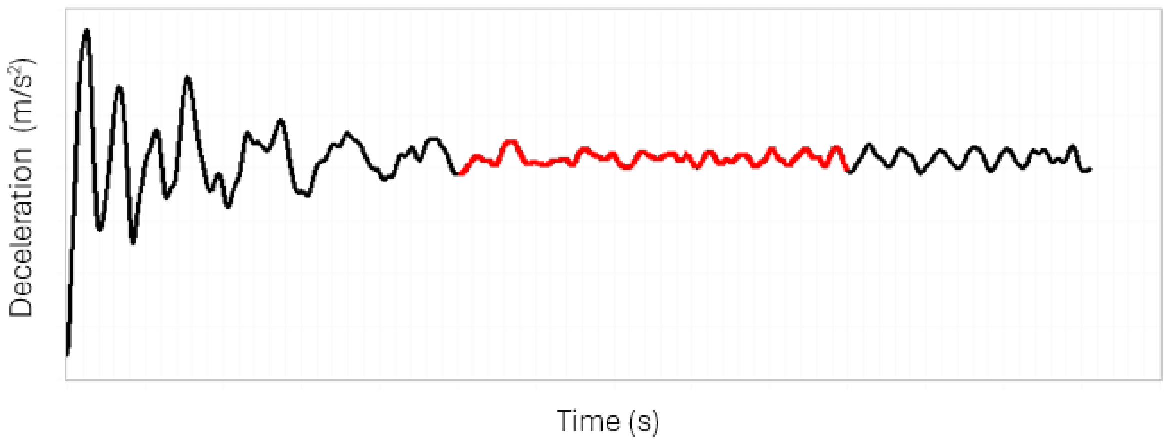

Figure 5-44: Example of Sliding Resistance Profile

Results

A deeper exploration of the data collected in this Chapter highlighted a strong linear trend ($R^2 = 0.97$) between the peak deceleration and the area under the curve (Figure 5-45). This correlation implies that peak deceleration is critical for monitoring speed reductions. The 50 mm sample generated statistically greater peak decelerations (125.1±1.6 m/s²) and reduction in speed (0.90±0.01 m/s), compared to the 60 mm sample (102.1±1.8 m/s² and 0.80±0.01 m/s). Figure 5-46 demonstrates that during the Sliding Phase, the 50 mm sample (1.82±0.04 m/s²) generated a statistically greater ($p < 0.01$) Slide Resistance compared to the 60 mm sample (1.69±0.01 m/s²).

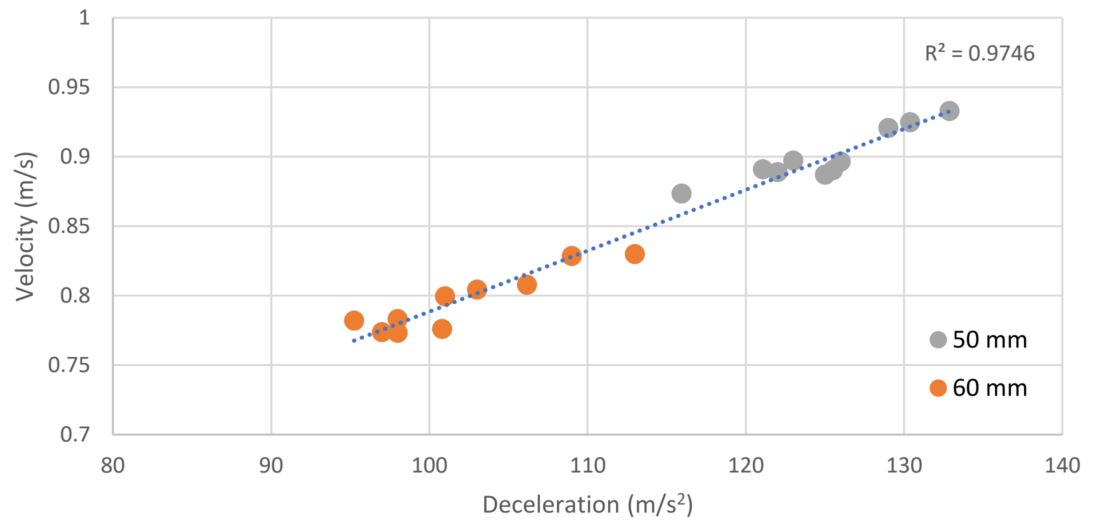

Figure 5-45: Comparison of peak deceleration and reduction in velocity

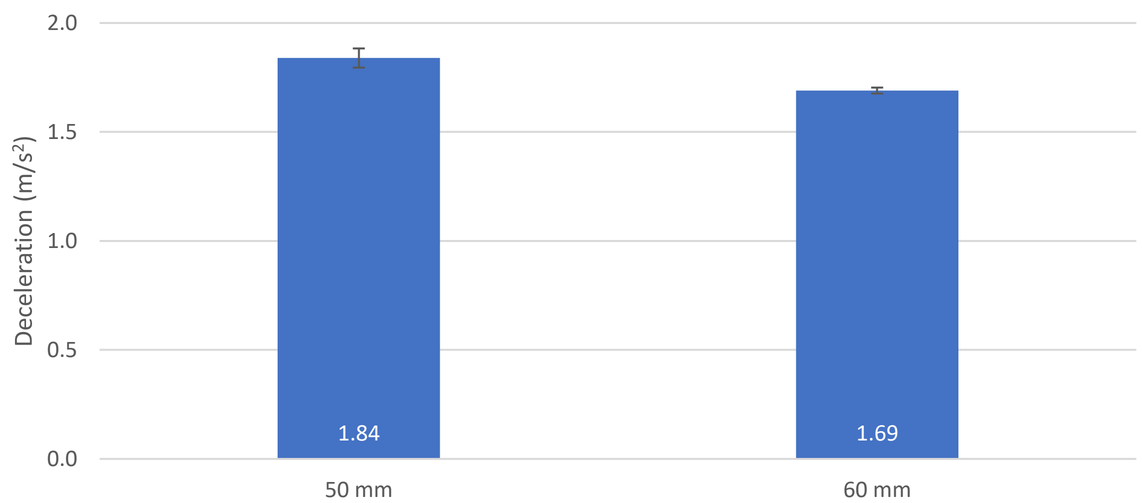

Figure 5-46: Comparison of Slide Resistance on a 50- and 60-mm sample.

Discussion

This research has revealed that both results reported statistical significance during the Impact Zone. However, the peak deceleration (22.5%) produced a more substantial percentage difference than the reduction in velocity (13%). This finding underscores the importance of the test method's high sensitivity, which enables the detection of subtle differences between samples. Importantly, peak deceleration, referred to as Impact Deceleration, has emerged as a more reliable metric for differentiating between Rugby Turfs and identifying their potential to induce skin injuries. This metric provides new and crucial insights into the impact mechanics during player-surface interactions on artificial turf.

Performance infill was incorporated into third-generation turfs to improve traction and impact attenuations [243]. The 50- and 60-mm samples were ratiometrically constructed to yield the same free pile height. The volume of performance infill in artificial turf has been reported to have a negative relationship with surface hardness (Forrester & Tsui, 2014; K. H. Dickson et al., 2022). If this theory is applied to the horizontal axis, the 60 mm sample should generate lower Impact Decelerations, which agrees with the results presented in Figure 5-45. During a sliding interaction, the granular nature of performance infill will act like a lubricant by providing a ball-bearing effect. This behaviour is anticipated to mitigate the forces experienced by the simulated player, thereby reducing the risk of potentially sustaining a skin injury. In combination, the higher turf density and reduced infill volume resulted in the 50 mm sample generating a higher Slide Resistance (Figure 5-46).

Section 5.3 highlighted that the 50 mm sample generated greater Abrasion Zone scores, implying that higher Impact Decelerations and Slide Resistances are associated with greater surface damage. With the European ban on intentionally added microplastics, the sports industry is faced with the challenge of finding a suitable replacement for SBR, the most popular performance infill [80]. This is a significant task as SBR has been widely used and appreciated for its performance. The most popular alternative infills, such as cork, wood, or coconut husk, have been anecdotally reported to be rougher than SBR. However, the moisture content of these organic materials may be more skin-friendly. Therefore, more research is required to establish the severity of skin injury risk on these surfaces. Non-filled systems could be a solution to overcome the potential problems associated with these organic infills. They still need to be considered suitable for gameplay in rugby or football because they do not meet all the quality requirements [246]. The lack of infill could also increase skin injury risk as the players will effectively slide over polymer sheets, potentially generating greater Heat Profiles and exacerbating the Turf Burn issue.

5.6.3 Velocity

The AAA assesses the performance characteristics of turf using vertical velocities before and after impact to calculate the energy of restitution which quantifies how much kinetic energy is restored following the collision – Equation 26 & Equation 27. Stiffer surfaces return a large proportion of the impact energy, which is desirable on running tracks to improve athletic performance [262], [263], [264]. In contrast, artificial surfaces, which host contact sports are optimised to provide suitable stiffness for running whilst cushioning player-surface interactions to reduce the risk of injury. In the context of skin injuries, landing on a stiffer surface is predicted to increase the risk of injury due to the player experiencing greater strains on their skin.

Equation 26

$$E = \frac{1}{2}mv^2$$

Equation 27

$$ER(\%) = \frac{E_2}{E_1} \times 100$$

Where: E_1 is minimum velocity; and E_2 is maximum velocity.

The efforts towards limiting the knee form's bounce on impact via the dampening mechanism will influence the rebound velocities. Therefore, the energy of restitution calculation would be adversely affected. Additionally, this performance assessment does not include horizontal velocity, which was deemed to be an important parameter. Ultimately, this analysis technique may have its limitations in quantifying skin injury risk; therefore, it was not considered a viable metric. Cole et al. (2020) proposed a new method for quantifying the energy of restitution by calculating the area under a force-displacement curve - this analysis technique will be further discussed in Section 5.6.5.

Alternatively, the interaction can be evaluated by implementing the laws of energy conservation, which states that energy can neither be created nor destroyed - only converted from one form of energy to another. The initial energy at the point of contact will be a combination of the horizontal kinetic energy (E_H) generated by the LIM and vertical potential energy (E_V) created by releasing the impactor from a set height. The resultant energy vector can be quantified by calculating the magnitude of these components – Equation 28.

Equation 28

$$E_C = \sqrt{{E_H}^2 + {E_V}^2}$$

The initial horizontal energy can be calculated by substituting the overall mass of the carriage and the velocity at the point of contact (T_3) into Equation 26. The initial vertical energy can be calculated by substituting the drop height (h) into Equation 29, where m is the mass of the impactor and g is the gravitational constant (9.81 m/s^2). The repeatable impact conditions should yield consistent vertical (~180J) and horizontal (~2040J) energies to generate a contact energy of 2048J.

Equation 29

$$E_V = m.g.h$$

Considering that the impactor was in constant contact with the surface during the sliding phase, it was assumed that the vertical velocity would be negligible when the energy was calculated at the end of the interaction. Therefore, the final energy was calculated by substituting the horizontal velocity at T6 into Equation 26. The energy dissipated during the interaction was quantified by taking the difference between the initial and final energy. A system that produces a lower final energy will have applied more resistance to the simulated player compared to a surface that generates a higher final energy. The energy dissipated during the interaction will, therefore, be greater, which suggests a higher risk of injury. This underscores the importance of the research in evaluating a method for assessing skin injury risk in a simulated player-surface interaction.

While the method initially seemed a reasonable approach for assessing skin injury risk, it is important to note its limitations. The technique shares the same constraints as the current energy used in restitution calculation. For instance, it only utilises two distinct time indices, leaving a significant portion of the data unexamined. Moreover, the parameter merely provides an output for the entire interaction, failing to differentiate between the Impact Zone and Sliding Phase as intended by the design specification. However, these limitations also present an opportunity for improvement, offering hope for a more suitable injury metric than velocity.

5.6.4 Displacement

The governing bodies set the requirements for the turf quality test methods to ensure that the artificial turf's performance aligns with natural grass's characteristics. On artificial turf, fibres permanently flatten due to intense usage and poor maintenance [69]. As a result, ball roll (FIFA Test Method 3) is generally one of the first surface criteria to fail during field tests on Football Turf. Due to spatial constraints within the laboratory, this test was not feasible. Therefore, FIFA Test Method 17 (reduced ball roll) was developed to theoretically estimate the displacement for the ball to come to rest. At slower speeds, a football does not experience linear deceleration. Therefore, the lab test releases the ball from four different heights to establish a correlation and help accurately determine the displacement on a field.

In the context of this project, the simulated player did not naturally slide to rest. Therefore, the reduced ball roll methodology inspired a new metric for assessing injury risk. While the Abrasion Zone was identified as a critical output metric, it was essential to maintain the desirable impact velocities to simulate a scenario with a high risk of injury. This prerequisite was imperative for inducing significant skin damage, enabling the differentiation between various turf samples. Therefore, the technique of varying sliding speed to predict the theoretical displacement was deemed undesirable as this would influence the abrasion scores and increase testing time. Under the assumption of linear deceleration, the Sliding Phase velocity was extrapolated to predict the displacement for the simulated player to slide to rest, as presented in Figure 5-47. The *actual* sliding distance (d_A) was calculated by integrating the velocity from T5 to T6, while the *theoretical* displacement (d_T) was calculated by manipulating the fundamental equations of motion. To establish the time index when the entire interaction energy had been dissipated, the extrapolated line of best fit, $y = mx + c$, was rearranged to calculate x when y was equal to zero. The displacement was then calculated by using Equation 30 where the initial velocity (u) had the time index T6, the final velocity (v) equalled zero m/s, and the time (t) represented the duration of the theoretical slide (T6 – x). The combination of *actual* and *theoretical* displacements was referred to as the *expected* displacement (d_E).

Equation 30

$$s = \frac{u + v}{2}t$$

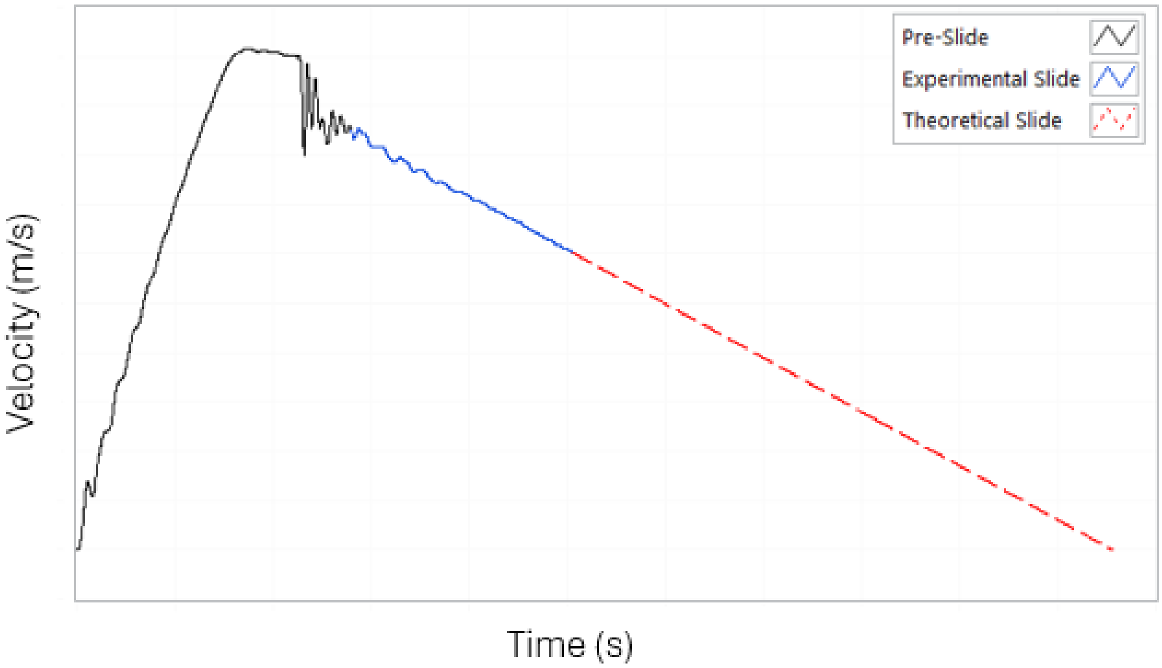

Figure 5-47: Estimating theoretical displacement for simulated player to come to rest.

Systems that generated short theoretical displacements would imply that high resistances were experienced, exposing the player to a higher risk of injury. Therefore, it was expected that the expected displacement would exhibit an inverse relationship with respect to Slide Resistance. This hypothesis agrees with the results presented in Figure 5-48 where the 50 mm sample generated a statistically shorter ($p < 0.05$) theoretical displacement.

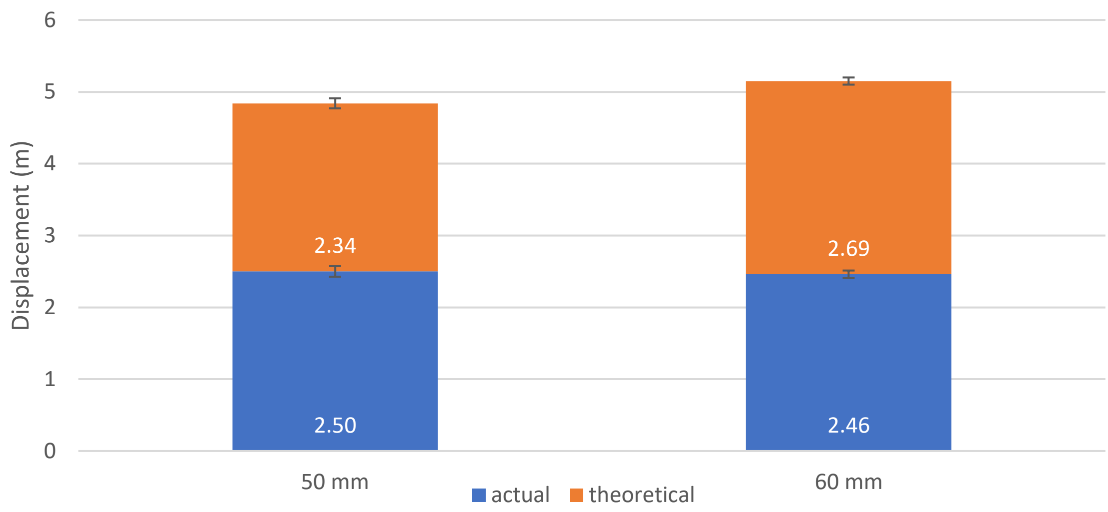

Figure 5-48: Comparison of actual and theoretical displacements on the 50- and 60-mm samples

5.6.5 Shear Energy

The new AAA method quantifies the Energy of Restitution (ER) by calculating the area under a force versus displacement curve. However, as discussed previously, the dampening mechanism was designed to attenuate the rebound of the impactor, which will negatively affect the energy returned and contribute to a lower ER. This limitation makes calculating the energy of restitution from this device an unsuitable metric for predicting skin injury risk, therefore, an alternative method is needed. This is where the adaption of this parameter to monitor the energy dissipated on the horizontal axis, Equation 31, comes into play. This could further develop the concept of interaction energy, presented in Section 5.6.3, enabling the Impact Zone and Sliding Phase to be assessed independently. The Impact Zone forces and displacements were calculated from T3 through peak horizontal deceleration to zero m/s^2. The force versus displacement curve representing the horizontal impact energy loss is presented in Figure 5-49.

Equation 31

$$Energy = Force \times Displacement$$

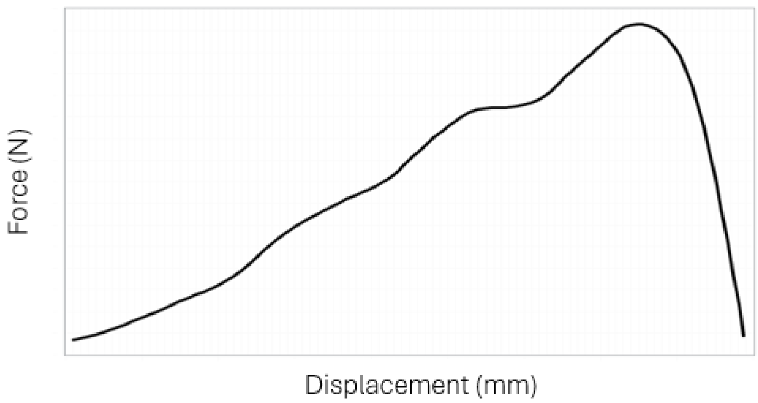

Figure 5-49: Example of force-displacement curve used to calculate horizontal energy loss during Impact Zone

When calculating the area under the force versus displacement curve for the Sliding Phase, there is a choice between adopting a constant time or displacement interval. A constant time interval will quantify the energy dissipation rate over time. This approach is suitable for analysing the dynamic nature of the Sliding Phase and understanding how quickly energy is lost. Conversely, employing a constant displacement interval will assist in quantifying the total energy loss over a specified distance. The process is valuable when assessing energy loss during a particular movement.

In many cases, combining both approaches may be necessary to comprehensively understand energy loss within a given physical system. Section 5.6.6 will explore the influence of the rate of energy. Therefore, a constant displacement interval was adopted when calculating the energy loss during the Sliding Phase. The start of the analysis section for the sliding phase was established as detailed in Section 5.5.5. From this point, the velocity was integrated to establish the time index when a displacement of 1m was achieved. As described in Section 5.5.4, force was calculated, and these exact boundary limits were applied, as presented in Figure 5-50.

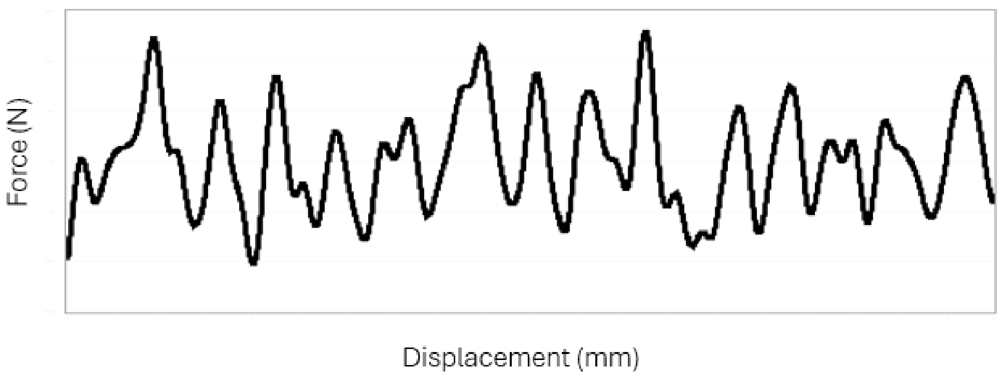

Figure 5-50: Example of force-displacement curve to calculate horizontal energy loss during Sliding Phase

In contrast to the deceleration results the Shear Energy yielded similar magnitude of results in both the Impact Zone (Figure 5-51) and Sliding Phase (Figure 5-52). The results followed the same trend as the deceleration where the 50 mm sample produced Impact (11%) and Slide (5.1%) Shear Energies greater than the 60 mm sample. Both results were statistically significant ($p < 0.05$). Deceleration was the purest form of the data which provided greater sensitivity when differentiating between the two samples for the Impact Zone (22.5%) and Sliding Phase (8.1%). Consequently, Impact Deceleration and Slide Resistance remained the most suitable metrics for predicting skin injury risk.

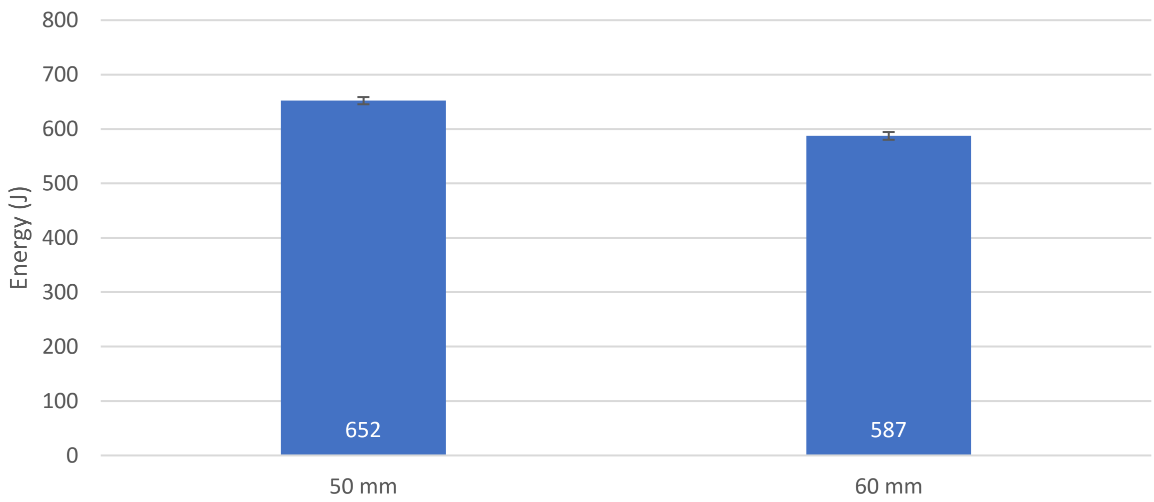

Figure 5-51: Comparison of Impact Shear Energy on a 50- and 60-mm sample.

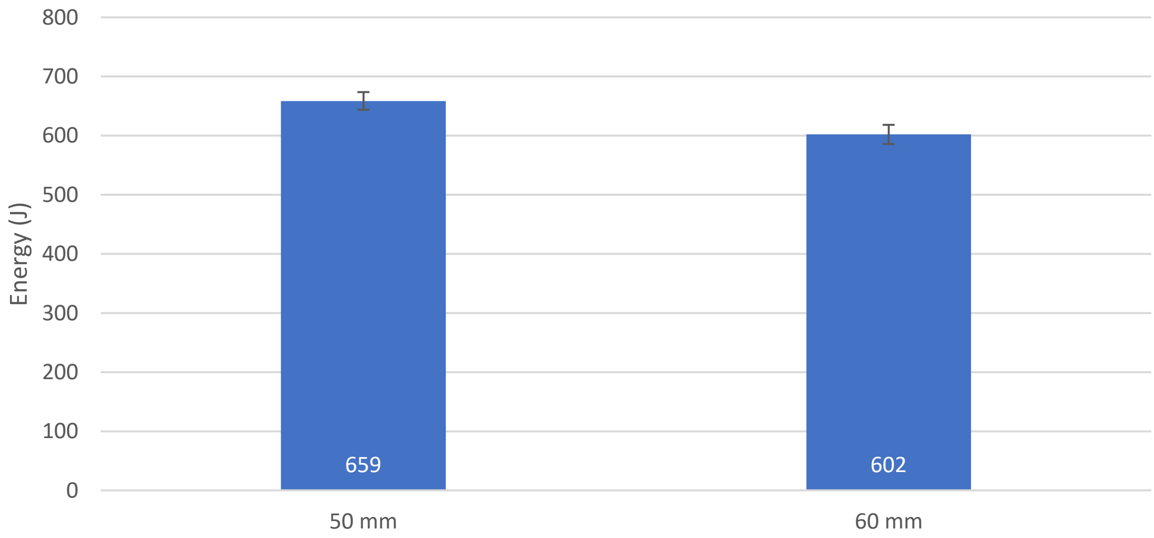

Figure 5-52: Comparison of Sliding Shear Energy on a 50- and 60-mm sample.

5.6.6 Rate of Shear Energy

When analysing preliminary data, it was observed that the duration of impact varied on different surfaces. The rate of energy dissipated could be used to predict skin injury risk to normalise this variation (Equation 32). When establishing correlations between the potential kinematic injury metrics, a linear relationship was observed between deceleration and the rate of Shear Energy, as highlighted by the $R^2 = 1$ in Figure 5-53. This linear relationship prompted a further investigation to establish why the parameters were equivalent.

Equation 32

$$Rate = \frac{Energy}{Time}$$

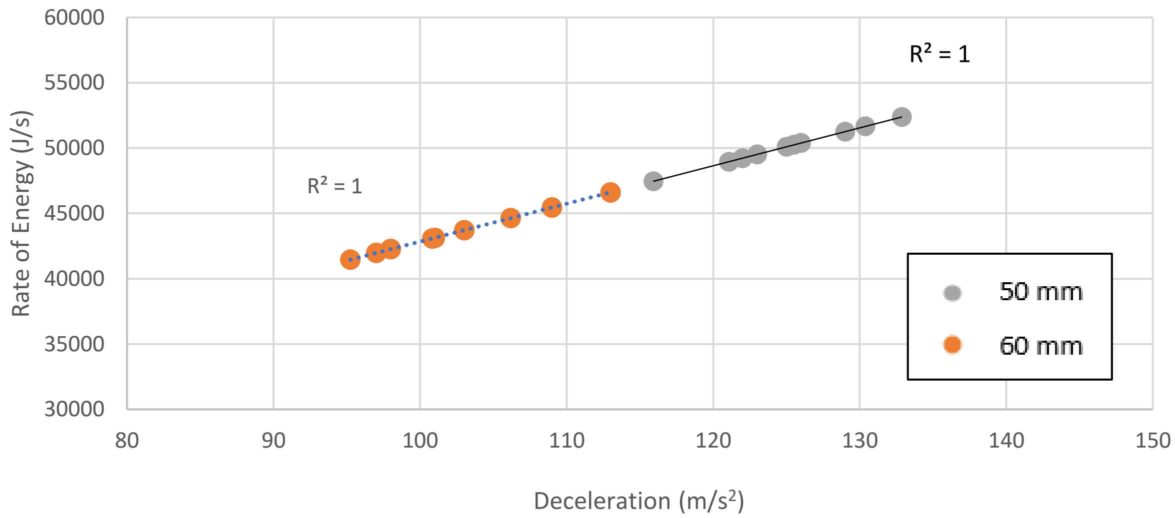

Figure 5-53: Linear relationship between rate of shear energy and deceleration.

Are shear energies and decelerations analogous?

The energy calculated can be represented as the product of force and displacement. While the force can be further expanded into mass times acceleration – as defined in Section 5.6.1. Subsequently, the rate is equivalent to the product of mass, acceleration and displacement divided by the duration of the interaction - Equation 33.

Equation 33

$$Rate = \frac{mass \times acceleration \times \text{displacement}}{time}$$

The S.I. units for the rate of energy dissipated, presented in Equation 34, will be rearranged and simplified to establish if the rate is equivalent to the deceleration.

Equation 34

$$Rate = \frac{[kg] \times \left[\frac{m}{s^2}\right] \times [\mathrm{m}]}{[s]}$$

The first step of simplifying the S.I. units was to establish if any of the parameters were constants which only acted as a scalar value to calculate the correct magnitude. Since the mass of the impactor and carriage remained the same for every interaction the derivation was simplified by removing kilograms (Equation 35). The fraction was then split to form two independent variables (Equation 36) and rewritten to simplify the complex fraction (Equation 37). The derivation can then be further simplified by multiplying the individual parameters as presented in Equation 38. Finally, the derivation was completed by square rooting the numerator and denominator to confirm that the rate of energy dissipated was equivalent to the deceleration (Equation 39). Consequently, there was no need to evaluate both the rate of shear energy and the deceleration. This discovery completes the analysis of accelerometer data on the horizontal axis, instilling confidence that the data has been meticulously examined.

Equation 35

$$Rate = \frac{\left[\frac{m}{s^2}\right] \times [\mathrm{m}]}{[s]}$$

Equation 36

$$Rate = \left[\frac{\frac{m}{s^2}}{s}\right] \times \left[\frac{m}{s}\right]$$

Equation 37

$$Rate = \left[\frac{m}{s^3}\right] \times \left[\frac{m}{s}\right]$$

Equation 38

$$Rate = \left[\frac{m^2}{s^4}\right]$$

Equation 39

$$Rate = \left[\frac{m}{s^2}\right] = Deceleration$$

5.6.7 Wear Volume

The next potential injury prediction model explored Archard's wear equation. This is a fundamental concept in tribology that combines normal load, sliding distance, and a wear coefficient to estimate the wear rate. Again, this technique would facilitate the independent analysis of the Impact Zone and Sliding Phase. By utilising the boundary conditions for the normal loads detailed in Section 5.5 the corresponding horizontal displacements could be calculated by double integrating the accelerometer data. Given that the vertical forces and horizontal displacement would vary as a function of the turf system during the Impact Zone. This parameter was expected to provide suitable sensitivity to differentiate between surfaces. However, earlier in this chapter, the apparatus was reported to generate consistent normal loads and displacements during the Sliding Phase. The consistency in results raised concerns about whether this technique would provide adequate sensitivity for evaluating this event. Although S2R was a theoretical calculation, it was assumed that the vertical forces would remain constant and could be applied to this injury prediction model.

The wear coefficient describes the propensity for a material to wear under specific conditions [250]. This parameter is a system property which considers various factors, including the type of material, surface finish, lubrication, and temperature. A system with a low wear coefficient indicates that the materials are robust and durable. A high wear coefficient implies that the materials will be susceptible to damage. Many EN or ASTM standards provide methods for calculating wear coefficients; however, each. However, it will vary depending on the materials of interest [250]. Typical tests represent a pin-on-disc or rotating drum format where the materials are exposed to a combination of torque and normal load for a set duration. The wear coefficient is then reported as the wear volume per unit meter per unit load (mm^3/Nm). Since Rugby Turf is a system, extensive testing would be required to establish the wear coefficient for a system with different infill rates alone. Subsequent testing with different infill materials and carpet properties would exponentially increase the required tests. It was, therefore, accepted that calculating wear volume would only be feasible with estimating the specific wear coefficient. Consequently, the parameter was avoided as an injury prediction model.

5.7 Skin Injury Classification System

The motivation for developing a new method for evaluating skin injury risk arose from the limitations of the existing method, which often failed to capture the complex interactions. This chapter has explored several injury metrics, providing insights into the potential for a turf system to cause harm under standard operating conditions. However, when considered individually, these metrics only offer a partial narrative of the overall context. Therefore, developing a novel classification system that integrates these vital parameters was imperative to provide a holistic overview of injury risk.

Developing new preventive measures to reduce sliding-induced skin injuries on artificial turf requires a thorough knowledge of the injury mechanisms [251]. Turf burns are a combination of mechanical abrasion and thermal damage [32]. Analysing the design specification also highlighted that one desired outcome was developing ancillary performance characteristics. The video analysis in Section 3.4.2, crucial for our understanding, highlighted two potential injury mechanisms: an abrupt impact or a protracted slide. To keep the new classification system straightforward, a single parameter was selected for each aspect: abrasions, heat, the Impact Zone, and the Sliding Phase.

This section introduces the new classification system while concurrently setting the stage for clear and concise results in the next chapter. This approach aims to help the reader comprehend how each parameter contributes to skin injury risk. The data presented throughout this chapter was used to establish the most suitable metrics indicative of injury risk and evaluate the potential of this single unified factor. The next chapter will further scrutinise the validity of this system, hopefully providing confidence in its ability to evaluate skin injury risk comprehensively.

5.7.1 Quantifying Heat Generation and Abrasive Nature of Turf

The thermal camera facilitates an independent evaluation of surface temperature during the Impact Zone and Sliding Phase. However, due to the relatively short duration of both events, the maximum temperature was identified as the most critical parameter for establishing if there is a potential for skin to burn. The Abrasion Zone (AZ) in its current form differentiates between light (A_1) and dark (A_2) lesions, which have been reported to represent different levels of severity. A current limitation of the interaction is that the simulated player does not naturally come to a complete rest. Despite monitoring the skin damage over a consistent actual displacement (D_A), AZ does not account for longer theoretical displacements. These protracted slides were anticipated to contribute to more significant skin damage, as per Archard's wear equation.

Consequently, expected sliding distance (D_E) emerged as a metric which could be combined with D_A and AZ to forecast the full extent of skin damage after the contact energy had completely dissipated (Equation 40). This new and enhanced injury metric for quantifying the true extent of skin damage will be referred to as the Abrasion Severity Index (ASI). Figure 5-54 compares the AZ (blue) and ASI (orange), where the 50- and 60-mm samples increased by 93.6% and 109.4%, respectively.

Equation 40

$$ASI = \frac{d_E}{d_A} \times \left(A_1 + \frac{A_2}{2}\right)$$

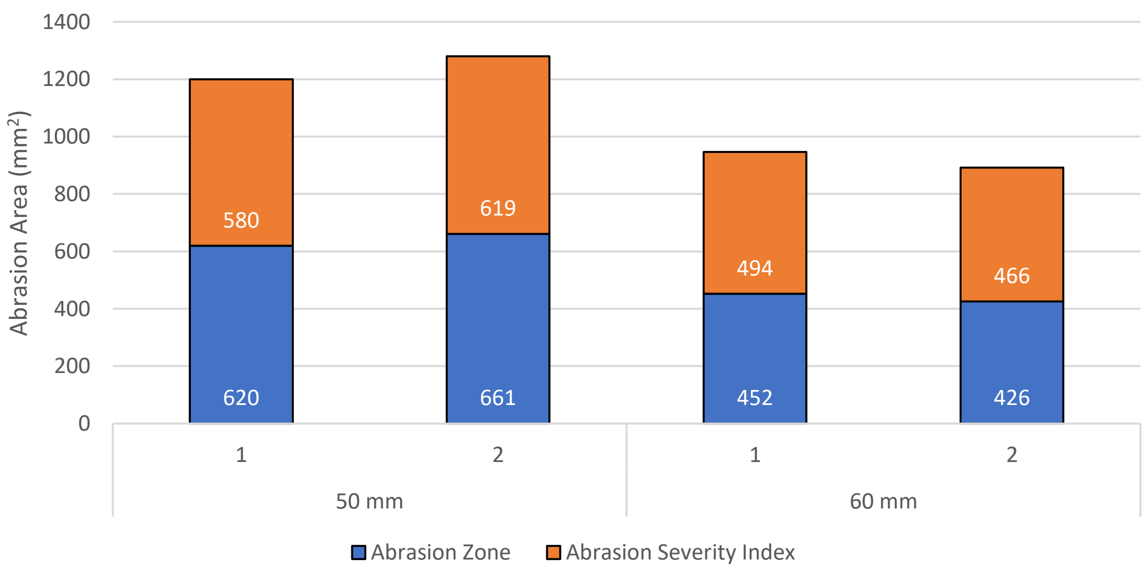

Figure 5-54: Comparison of Abrasion Severity Index on 50- and 60-mm samples

5.7.2 Establishing the best kinematic injury metric

The three main kinematic injury metrics discussed during this chapter were COF, deceleration, and shear energy. A critical review was conducted to establish the most appropriate parameter to be included in the classification system. Despite the limited sample size, there was a clear difference between the ASI scores for the 50- and 60-mm samples as Figure 5-54 illustrates. This section aimed to identify which kinematic injury metric exhibited the highest sensitivity and best correlation with the ASI.

In Section 5.6.1, the COF could not identify a significant difference between the Impact Zone or Sliding Phase surfaces. This result aligned with Tay et al. (2017) [157] findings that COF was not a convenient injury metric that correlated well with skin damage. Therefore, it was excluded from consideration. In sections 5.6.2 and 5.6.5, the 50mm sample produced higher test results for Deceleration and Shear Energy. As desired, these results corresponded to a higher ASI. Impact and Slide Resistance were deemed more sensitive than the corresponding Shear Energy values, as the percentage difference between the 50- and 60-mm samples was greater. Consequently, the four parameters that will be incorporated into the new classification system are Peak Temperature (T_P), Abrasion Severity Index (ASI), Impact Resistance (R_I), and Slide Resistance (R_S).

5.7.3 Maxwell Tribo Index

The Maxwell Tribo Index (MTI) is a new multifaceted analytical tool that integrates these four injury metrics. This system was created to encapsulate the fundamental properties of tribology, the study of friction, wear, and lubrication, while also considering the interaction events believed to contribute to the skin injury mechanism. Thus, it provides World Rugby with a novel classification system for assessing skin injury risk on artificial turf.

The magnitude of the selected parameters was expected to be significantly different. Therefore, the MTI utilised normalising coefficients to yield a standardised amplitude (Equation 41). This ratio was then squared to accentuate small differences between samples. Initially, each injury metric was considered to contribute an equal weighting to skin injury risk. The resulting sum was multiplied by 100 to provide a scale from 0 to 400 to rank skin injury risk.

Equation 41

$$MTI = \left(\left(\frac{T_P}{N_{T_P}}\right)^2 + \left(\frac{ASI}{N_{ASI}}\right)^2 + \left(\frac{R_I}{N_{R_I}}\right)^2 + \left(\frac{R_S}{N_{R_S}}\right)^2 \right) \times 100$$

Where:

- T_P – Peak Temperature
- ASI – Abrasion Severity Index
- R_I – Impact Resistance
- R_S – Slide Resistance
- N_x – normalising coefficient for the corresponding (x) injury metric.

The literature review highlighted that the severity of a burn is dependent on the duration of the contact, intensity of the heat, and thickness of the skin [46]. Burn injuries have been reported to occur when the basal layer of the skin reaches a critical level of 44°C. Subsequently, this value was selected as the normalising coefficient for temperature. The initial aim of this project was to establish an acceptable level of injury; however, the limited data on skin injuries makes it challenging to relate the ASI scores to the literature. To make artificial sports surfaces safer, this test method must classify abrasive surfaces as high-risk.

Consequently, the normalising coefficient was established by assessing the entire database of results collected by the device in its final iteration. The database consisted of 84 systems, which covered a range of surface types such as 3G (Rugby Turf and Football Turf), 2G (sand-dress/filled), non-fill, and hybrid. The normalising coefficient of 1750 was selected for ASI. This value was based on the mean of all ASI scores (Figure 5-55). This threshold was considered acceptable by labelling 50% of the tested systems as excessively abrasive. Adopting this strategy ensures that a satisfactory number of surfaces would not conform to the test method requirements, ultimately enhancing player safety without eliminating all market variations.

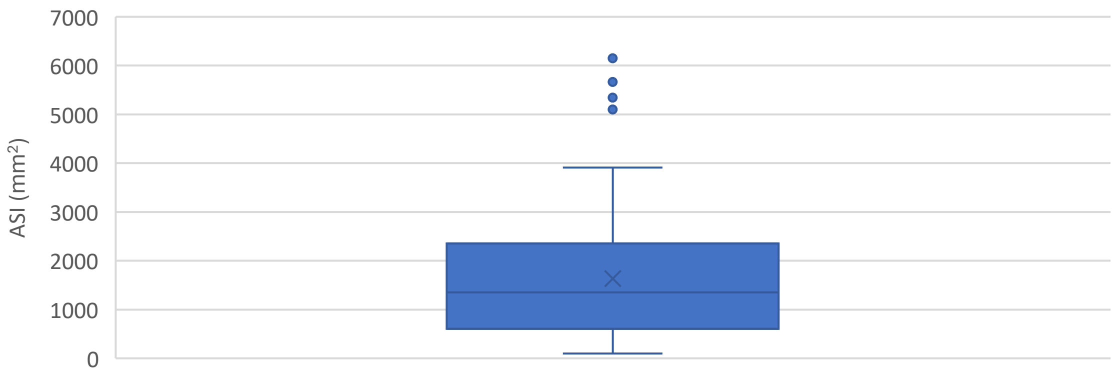

Figure 5-55: Box plot summary of ASI scores on various sports surfaces

The kinematic injury metrics provided a high level of sensitivity. As expected, the 2G surfaces generated the greatest Impact Resistance, significantly higher than any other sports surfaces (Figure 5-56). Therefore, only 3G surfaces were considered when establishing the normalising coefficients. Assessing 3G systems in isolation highlighted that the greatest Impact Resistance (291 m/s^2) occurred on a 45mm SBR sample. Despite not being a compliant Rugby Turf, this threshold represented a high risk of injury. To simplify the MTI calculation and incorporate a safety margin, the Impact Deceleration normalising coefficient was subsequently rounded up to 300 m/s^2. This threshold was carefully considered and deemed acceptable as the standardised amplitude would highlight surfaces approaching significant decelerations considered high risk, such as a 2G surface.

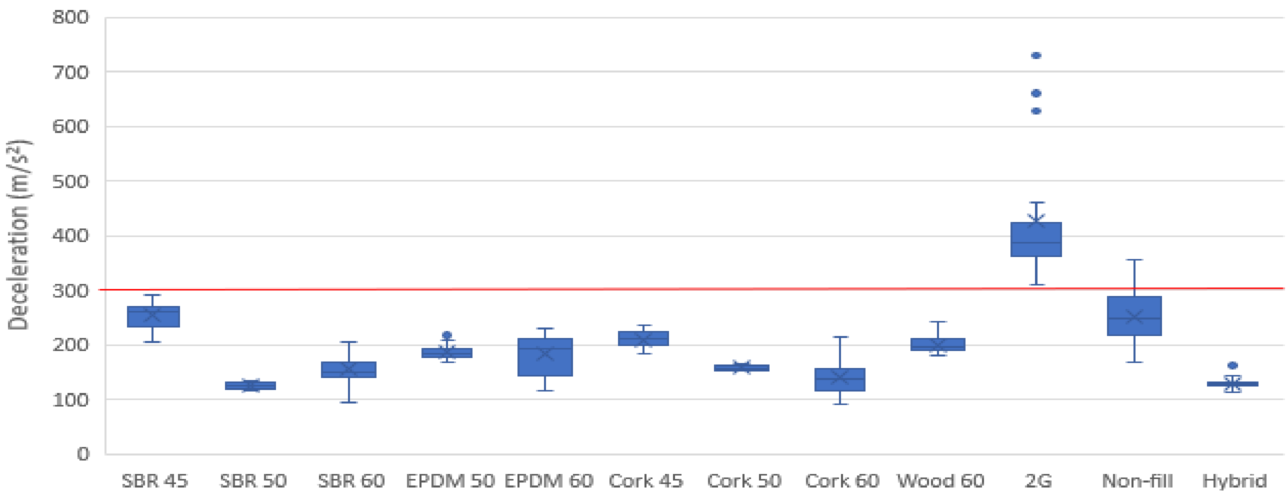

Figure 5-56: Comparison of Impact Deceleration on various surfaces – red line represents the normalising coefficient.

This exact process was employed again to establish the normalising coefficient to determine a suitable value for the Slide Resistance (Figure 5-57). Assessing 3G systems in isolation highlighted that the greatest Slide Resistance (2.56 m/s^2) occurred on a 50 mm EPDM sample. Once more, the value was rounded up to streamline the MTI calculation and include a safety buffer. The selected threshold (2.60 m/s^2) was deemed acceptable since a surface with a standardised amplitude approaching or surpassing one will exhibit a high resistance during the Sliding Phase. For instance, the non-filled system will be identified as high risk due to the lack of infill. This result was expected as a filled system will yield a smoother Sliding Phase because the infill acts like a lubricant.

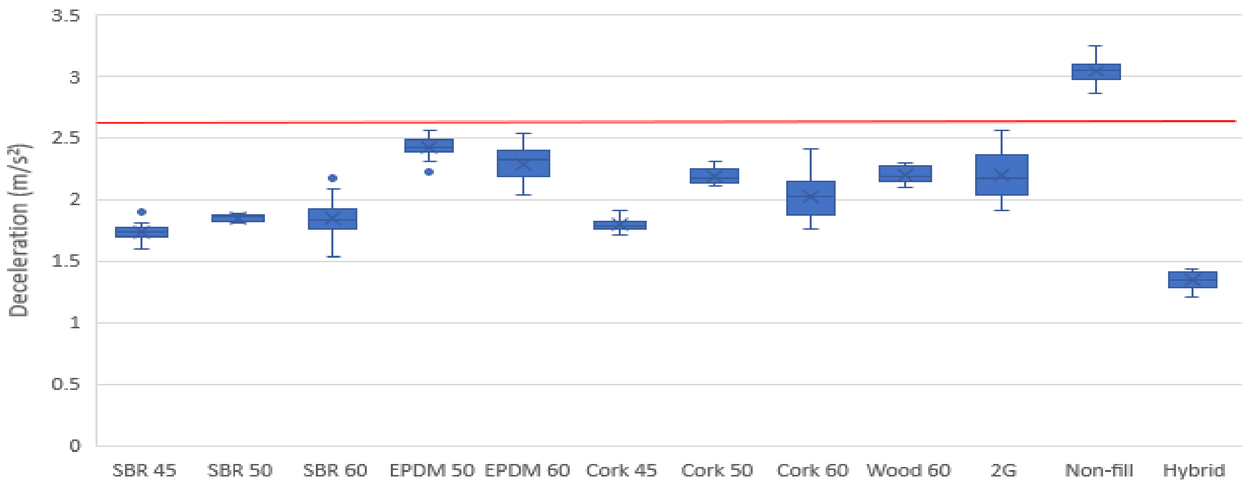

Figure 5-57: Comparison of Slide Resistance on a various surfaces – red line represents the normalising coefficient.

Now that the normalising coefficients have been established, the data collected in the validation study was collated and summarised in Table 5-8. At the same time, the corresponding MTI results were calculated and illustrated in Figure 5-58. Before testing, it was postulated that the 50 mm sample would pose a higher risk of injury than the 60 mm sample. This presumption was attributed to the reduced volume of performance infill. The MTI results followed the expected trend, which was encouraging. The consistent MTI scores across the two samples provided confidence in the sensitivity and repeatability of the new classification system. These findings imply that the 50 mm sample has a higher risk of injury; however, on further inspection, it was observed that most of the results collected in this study were significantly smaller than the normalising coefficients. This result was attributed to a thick shock pad (14 mm) and a relatively large depth of performance infill, effectively attenuating both surfaces' impact forces.

Table 5-8: Summary of Maxwell Tribo Index components for the validation study

Sample	Test	T (°C)	ASI	R_I (m/s^2)	Rs (m/s^2)
50 mm	1	26.1	1200	125.4	1.83
	2	26.4	1280	124.8	1.85
60 mm	1	22.1	946	102.1	1.68
	2	21.8	892	103.1	1.71
Normalising Coefficient		44	1750	300	2.60

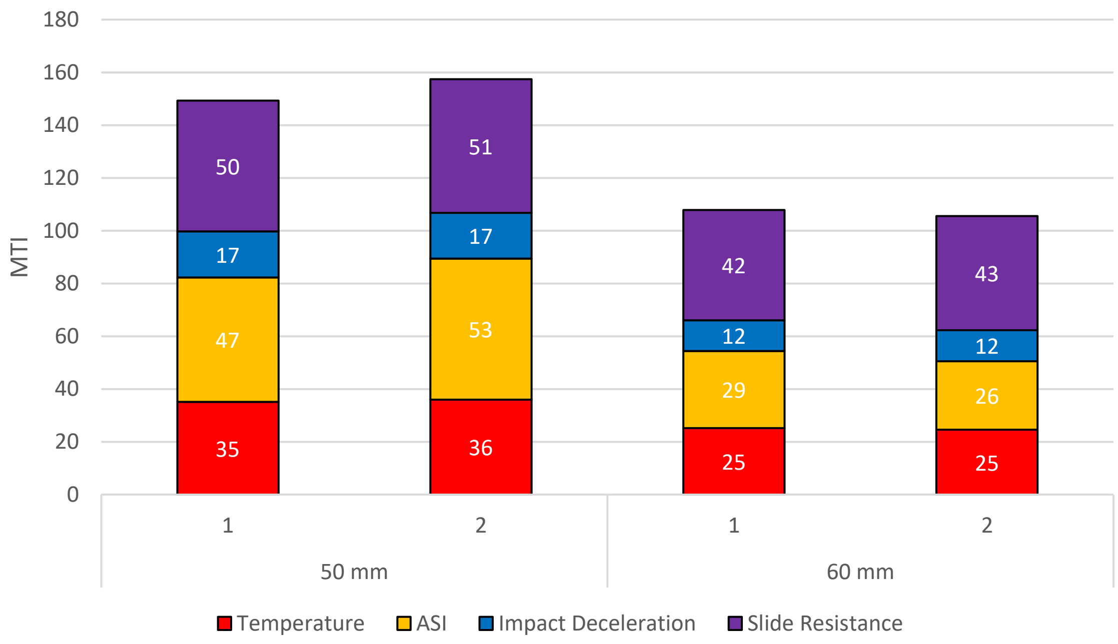

Figure 5-58: Comparison of Maxwell Tribo Index results for a 50- and 60-mm sample

Despite the current iteration of the MTI initially appearing to perform well as an injury prediction model, the equal weighting of each parameter warranted further consideration. Since turf burns are widely recognised as a combination of mechanical abrasion and thermal damage, it was essential to prioritise these metrics. Whilst reflecting on the outcomes from the video analysis, Section 3.4.2, it was acknowledged that an abrupt impact and a smooth, protracted slide did not coexist. Therefore, the reader may be sceptical that the impact and sliding resistance should possess the same weighting as the

ASI and T_P. Consequently, impact and sliding resistances were combined to produce a global representation of the surface's resistance during a player-surface interaction, as demonstrated in Equation 42. The revised MTI model is presented in Figure 5-59.

Equation 42

$$MTI = \left(\left(\frac{T_P}{44}\right)^2 + \left(\frac{ASI}{1750}\right)^2 + \frac{\left(\frac{R_I}{300}\right)^2 + \left(\frac{R_S}{2.6}\right)^2}{2} \right) \times 100$$

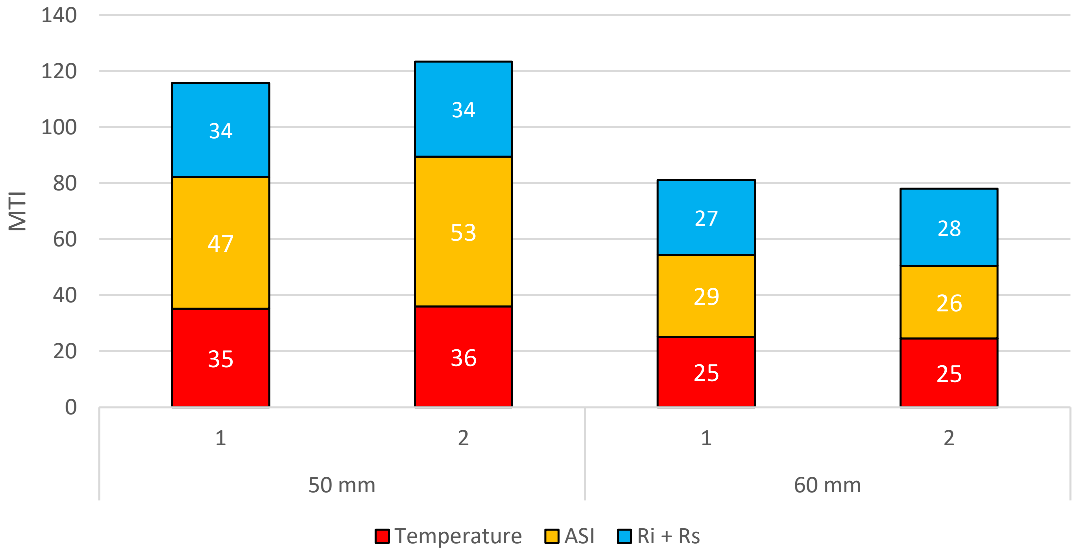

Figure 5-59: Comparison of the updated Maxwell Tribo Index results for a 50- and 60-mm sample

The two iterations of the MTI followed the same trends, highlighting that the 50 mm samples generated greater values for each parameter, indicating that a player would be exposed to a higher risk of injury than the 60 mm samples. The ultimate aim of this chapter was to provide World Rugby with a powerful tool for evaluating artificial turfs. The expected benefits include more accurate assessments of skin injury risk, leading to improved safety standards and injury prevention strategies on artificial turf. The success of this classification system will be pivotal in reducing skin injury risk on future turfs, as the MTI will be directly applied during the design, development, and optimisation of artificial turf. The initial results from the revised iteration, which emphasised the ASI and TP's influence, appear promising. Therefore, this iteration was selected as the new classification system, which will be further scrutinised in Chapter 6 to validate its effectiveness for predicting skin injury risk.

5.8 Conclusion

This chapter has successfully explored, developed, and evaluated a range of parameters to assess the simulated interaction comprehensively. The thermocouple validation study confirmed earlier concerns raised in Chapter 3, which identified possible issues with using thermocouples to record temperature directly through the skin simulant. To address this issue a thermal camera was integrated into the test method. This approach recorded temperatures which agreed with previous literature (Verhelst et al., 2009), marking a significant step forward in this research. A review of various approaches for quantifying surface roughness highlighted that contact and non-contact measurement techniques had limitations when evaluating the skin simulant.

Consequently, a bespoke greyscale image processing technique was developed to quantify the area of the damage. This injury metric was enhanced by predicting the potential damage if the simulation energy had dissipated entirely. The 50 mm sample generated greater maximum temperatures and ASI scores than the 60 mm sample. The maximum temperatures recorded were not sufficient to induce thermal damage. This finding implies that skin injuries should be described as mechanical abrasions instead of burns. More research will be required to establish if surface temperatures influence the potential for a player to sustain a burn.

The design specification also requested ancillary performance characteristics for the Impact Zone and Sliding Phase. The accelerometer data was morphologically analysed to establish the essential time indexes for these interaction events and facilitate the development of these injury metrics. The final output metric was selected based on a correlation with the ASI whilst providing suitable sensitivity between samples. COF is the current standard for predicting skin injury risk. However, comparing the results did not yield a significant difference between the two samples. Subsequent injury metrics were developed through a comprehensive and thorough review of the kinematic data by manipulating the accelerations by integration and other mathematical techniques. This technique culminated in the analysis going full circle as it was eventually demonstrated that the rate of shear energy was equivalent to the initial decelerations. A critical review of the parameters explored during this chapter highlighted that the Impact Deceleration and Slide Resistance positively correlated with the ASI scores while yielding acceptable sensitivity.

Examining abrasion, heat, impact deceleration, and slide resistance in isolation offers insights from different perspectives on factors contributing to the risk of skin injury. The MTI combined these four metrics to quantify the severity of player-surface interactions during rugby gameplay. This novel classification system for assessing skin injury risk represents a unique contribution to the field, underlining the originality and uniqueness of this research. The next chapter will evaluate a range of different surface properties to demonstrate the repeatability and validity of the MTI.

CHAPTER 6

Skin Injury Risk Associated with Different Turfs

SKIN INJURIES

Through interactions during game play in rugby

6.1 Introduction

3G artificial surfaces consist of stabilising and performance infills incorporated into a lattice network of yarn fibres secured to an inherently non-linear shock pad. This combination makes rugby turf a dynamic and complex system (Anderson et al., 2006;X. Wang et al., 2012; Leiva-Molano et al., 2022).Each component of artificial turf has unique physical and mechanical properties; however, the aggregate of the turf system will have the biggest influence on the system's potential to induce skin injuries.

Turf manufacturers develop unique product selling points; therefore, many surface constructions exist within the market. The performance of these surfaces depends on several factors, such as quality of materials, intensity of usage, age, and maintenance [270]. The fibre type, infill material, and infill rates have been identified as the key structural components that contribute to abrasion-type injuries [157]. However, there is a lack of literature exploring how shock pads and turf density affect the risk of injury. Throughout the lifespan of artificial turf, fibres flatten, fibrillation occurs, and infill compacts, resulting in greater surface areas of exposed yarn and systems hardening. Despite mechanical and environmental degradation adversely affecting performance characteristics, the effects of surface deterioration on skin injury risk are still unknown (N. McLaren et al., 2012; P. R. Fleming et al., 2015; Sánchez-Sánchez et al., 2018;D. M. Twomey et al., 2019).

The previous chapters have culminated in developing a novel test apparatus and classification system for assessing skin injury risk. This chapter will explore the interplay between each element and consider their individual and collective impact on the severity of potential injuries. The objectives of this chapter are outlined below:

1. Evaluate 3G surface components' contribution to skin injury risk.
2. Investigate skin injury risk on alternative sports surfaces.
3. Assess the repeatability of inter-operator variation.

6.2 Investigating the Influence of Turf Properties on Skin Injury Risk

The design features of artificial turf have significantly improved through the evolution of each generation. The continuous advancements of these surfaces have culminated in systems that closely replicate the characteristics of natural grass. Despite these developments, skin injuries continue to be prevalent; therefore, manufacturers constantly strive to improve performance and safety by developing novel turf products (Felipe et al., 2013; Burillo et al., 2014; Tay et al., 2017). The carpet stands out as the primary turf component with the greatest degree of freedom for the manufacturers to customise. For instance, the following properties can be varied independently: type of yarn, shape, colour, weight, and density (Dixon et al., 2015; P. Fleming et al., 2016). However, apart from the transition from tough and unforgiving nylon yarns to softer polyolefin yarns, there has been little innovation or development to synthetic turfs to improve skin friendliness [273].

The surface area of exposed yarn has been identified as a characteristic influencing skin injury risk. Tay et al. (2015) [94] reported that greater free pile height increased the frictional properties of artificial turf. The free pile height is a function of fibre length and the infill depth; however, the exposed surface area can also be influenced by the carpet's density and the yarns' flatness. Turf density measures the number of tufts per meter square and is determined by the stitch gauge and rate. A higher turf density means the fibres are tightly packed, enhancing the surface's ability to cope with intense usage while providing a cushioned feel underfoot. To the best of knowledge, no literature investigates the influence of turf density on skin injury risk.

The latest development of Rugby Turf is the approval of 50 mm carpets [230]. Despite World Rugby strongly advising the utilisation of a 60 mm carpet, which has demonstrated a proven track record in delivering high-quality surfaces for rugby. They will now consider carpets with fibre lengths between 50 and 60 mm to enhance opportunities for participation in the sport. However, these surfaces will be limited to multi-sport community-based fields. World Rugby has promoted projects by Cardiff Metropolitan University and Sports Labs, suggesting no increased risk of playing on 50 mm surfaces [231]. The document providing a rationale for this policy change did not specify types of injury. However, further investigation established that the study was focused on scrummaging injuries.

In summary, manufacturers can tailor turf properties to optimise the playing surface. The exposed surface area of the yarn was identified as the turf property most likely to contribute to skin injury risk. Therefore, free pile height and turf density will be investigated. However, it is important to note that further research is required to establish how the new Rugby Turfs will affect skin injury risk, underscoring the ongoing need for research in this area.

6.1.1 Materials and Methods

Four Rugby Turf systems were constructed to explore the effects of fibre length, free pile height, and turf density. The carpets were cut to size (4 x 1m), drainage holes were sealed to prevent infill leakage and secured to a prefabricated foam 14 mm shock pad. A summary of each system filled with sand (0.63 - 1.0 mm) and EPDM (1.25 - 3.15 mm) is presented in Table 6-1 and illustrated on Figure 6-1.

Table 6-1: Summary of turf construction

Sample	Fibre length (mm)	Free Pile Height (mm)	Stitch Gauge	Stitch Rate	Tuft Density (tufts/m^2)	Sand (kg/m^3)	EPDM (kg/m^3)
1	50	15	63.5	178	11,303	18	10
2	60	15	63.5	155	9,842	22	12
3	60	20	63.5	120	7,620	30	9
4	60	20	63.5	150	9,525	30	9

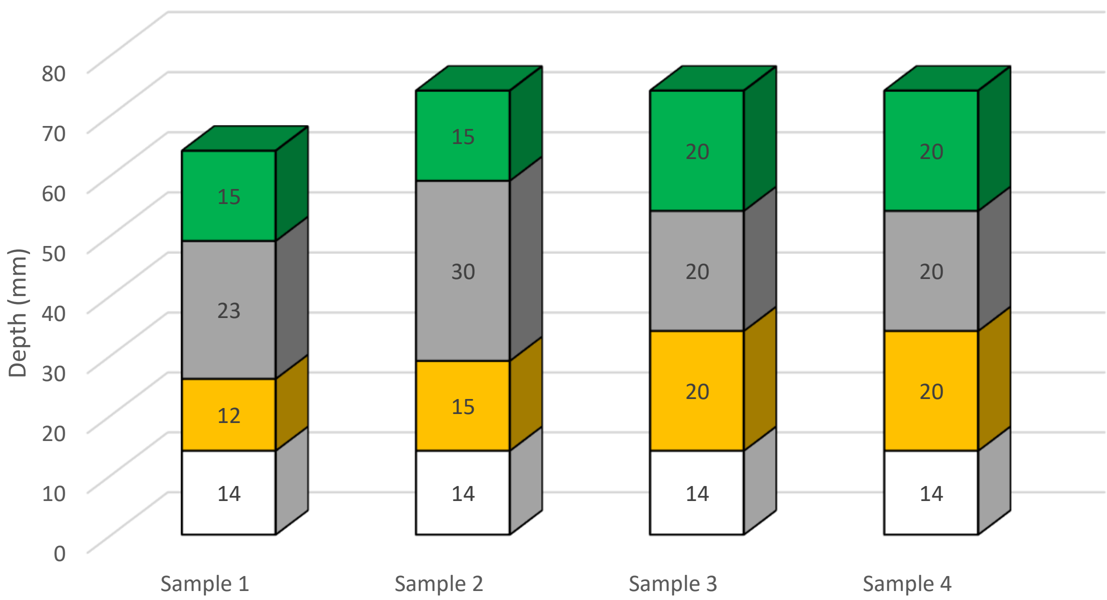

Figure 6-1: Illustration of tested surfaces: Shock Pad (white) | Sand (yellow) | EPDM (grey) | Free Pile Height (green)

The skin injury risk assessment consisted of five test iterations, each on a fresh impact location with the same skin. By releasing the knee from 0.5 m, a vertical impact velocity of 3 m/s was achieved. The linear induction motor generated a horizontal impact velocity of 5 m/s. After testing the sample, the system was dismantled and reassembled to verify the device's repeatability. Four tests were conducted on each sample, generating a database of 80 results.

A LabVIEW programme processed the accelerometer data during each launch to calculate the Kinematic Injury Metrics (KIMs). This study was conducted using an early iteration of the knee form where there were issues with the thermocouples. Additionally, the thermal camera had not been incorporated into the testing protocol at this stage. Therefore, no data was collected to provide insights into the Heat Profiles. Retrospective analysis digitised the wear pattern of the skin, differentiating between areas of severe abrasions ('A_1'), areas of less-severe disruption ('A_2'), and no abrasion. The Abrasion Severity Index (ASI) was then calculated to forecast the extent of damage when the simulated player slides to rest (Equation 43). The process to determine the *actual* and *expected* sliding displacements was outlined in Chapter 5.

Equation 43: Abrasion Severity Index (ASI)

$$ASI = \frac{D_E}{D_A} \times \left(A_1 + \frac{A_2}{2}\right)$$

Statistical Analysis

One-way analysis of variance (ANOVA) tests was conducted to assess the consistency of the accelerometer data. Post-hoc t-tests were performed to establish whether any systems produced a significantly different result. All statistical analyses were performed with SPSS, adopting a significance threshold of $p < 0.05$.

6.1.2 Results

The apparatus demonstrated satisfactory repeatability in producing horizontal (5.00 ± 0.003 m/s) and vertical (2.89 ± 0.006 m/s) impact velocities and subsequent Sliding Phase displacements (2.63 ± 0.02m). Figure 6-2 depicts the percentage difference between the experimental results and the target horizontal (5 m/s) and vertical (2.95 m/s) impact velocities. All recorded values fell within ±2.08% and ±4.27% of the mean for horizontal and vertical impact velocities, respectively. There were no statistical differences ($p = 0.49$, $F = 0.81$) between the experimental sliding displacements across the four systems (Figure 6-3). In contrast, there was a statistical difference ($p < 0.01$, $F = 18.69$) between the theoretical displacements. The post-hoc t-tests highlighted that all expected displacements were statistically different except from Samples 1 and 4. Further analysis assessed the consistency of repeated testing on the four systems. The ANOVA tests highlighted there were occasionally significant differences ($p < 0.05$) for both the experimental and theoretical displacements (Table 6-2). Despite these differences, the consistency of the motion profile during the Sliding Phase and predicted Slide to Rest was deemed acceptable and suitably sensitive.

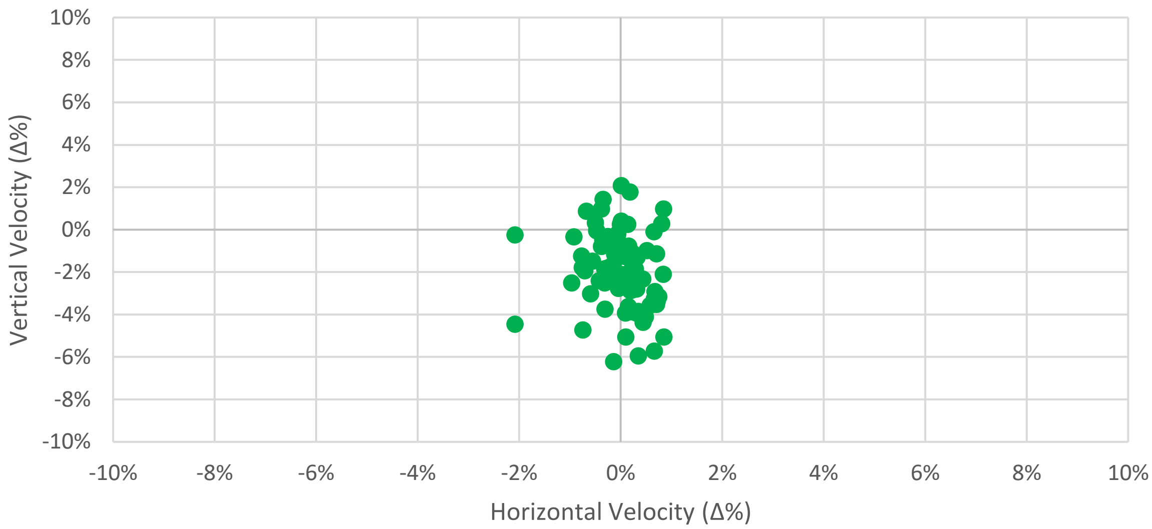

Figure 6-2: Illustrating consistency of impact velocity deviation from the desired horizontal (5 m/s) and vertical (2.95 m/s) values when assessing various turf properties.

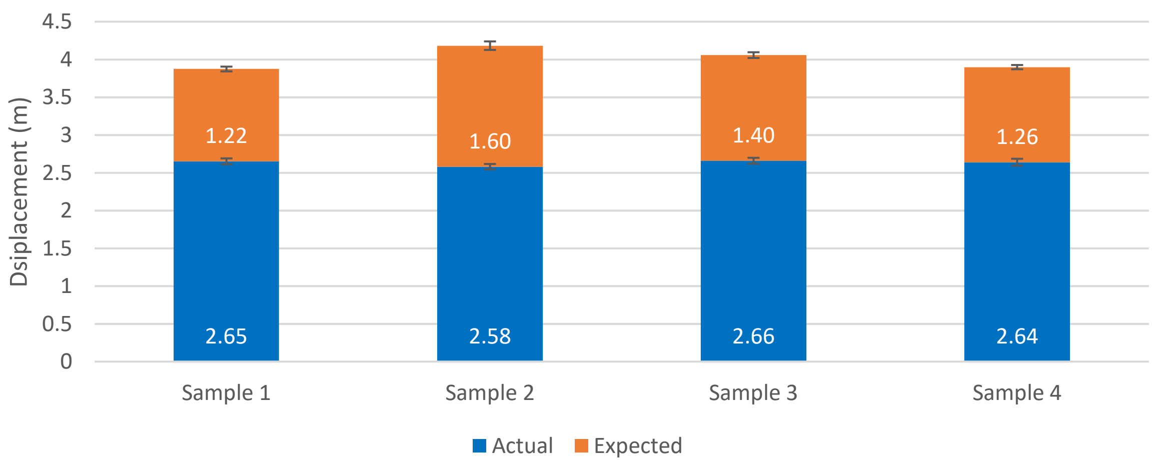

Figure 6-3: Comparison of Actual and Expected displacements when assessing various turf properties.

Visual inspection of the Abrasion Zone highlighted that EPDM produced different characteristics of skin damage compared to the infills used during the development of the greyscale imaging technique (Appendix 24 - Appendix 27). The typical point loading at the apex of the knee was consistent. However, the geometry of the skin damage was elongated, and the colour change was much less severe. Figure 6-4 presents a comparison of the ASI ranked the samples in the following order from most to least abrasive: 1,3,4,2.

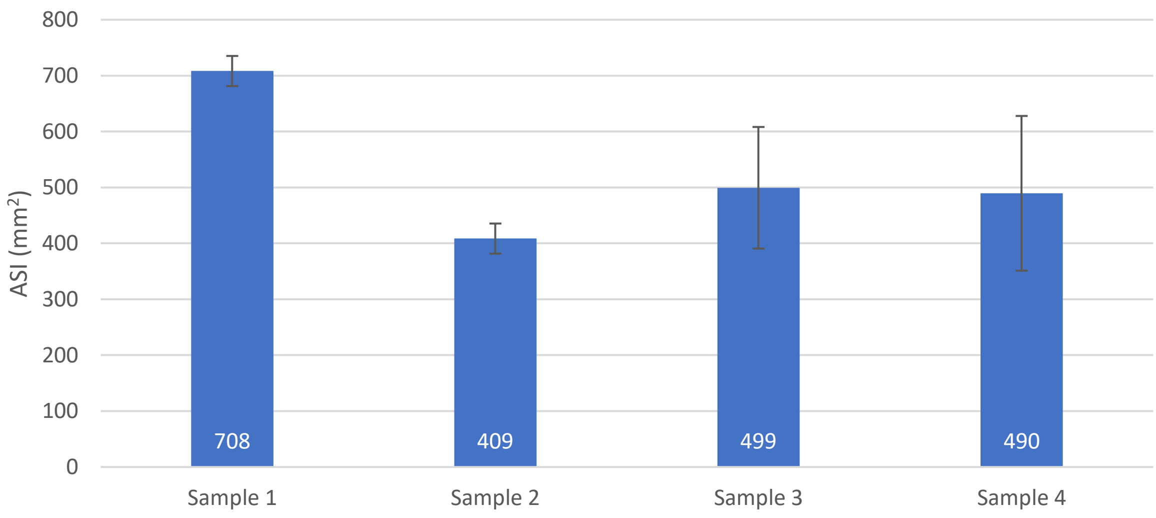

Figure 6-4: Comparison of turf properties on ASI scores

Impact Resistance (Figure 6-5) detected statistical differences ($p < 0.05$) across all samples where the following order ranked them from highest to lowest risk: 4, 3, 1, 2. The ANOVA results analysing repeated testing on each surface highlighted some statistical differences which were attributed to sample preparation (Table 6-3).

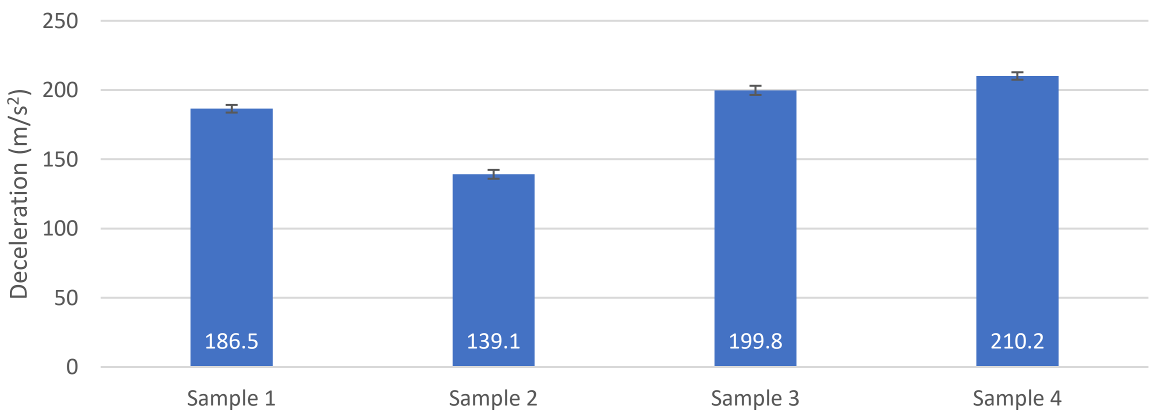

Figure 6-5: Impact Resistance: Comparison of different fibre lengths and turf densities on Skin Injury Risk

Sample 1: 50 mm | Sample 2: 60 mm Sample 3: 60mm (low density) | Sample 4: 60mm (high density)

Slide Resistance (Figure 6-6) ranked the surfaces from highest to lowest risk in the following order: 1, 4, 3, 2. All results reported statistical differences ($p < 0.05$) between all samples except for Samples 1 and 4. The ANOVA results highlighted some statistical differences during repeated testing. Again, this was attributed to sample preparation (Table 6-3).

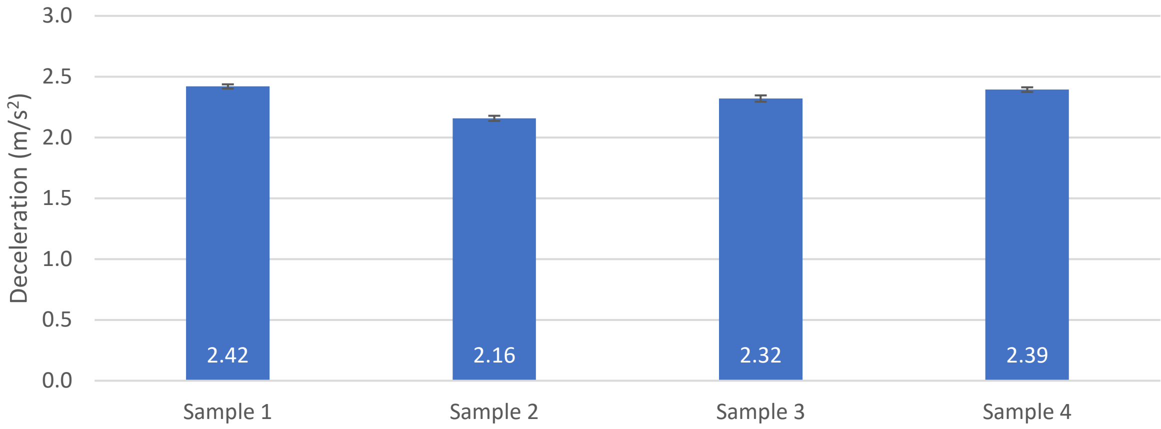

Figure 6-6: Slide Resistance: Comparison of different fibre lengths and turf densities on Skin Injury Risk Sample 1: 50 mm | Sample 2: 60 mm | Sample 3: 60mm (low density) | Sample 4: 60mm (high density)

Unfortunately, no temperature data was collected during this study; therefore, to calculate the MTI, the temperature was assumed to be 25°C. This assumption was based on the total database collected during this project, where 3G systems generated temperatures between 18.3°C and 32.7°C. Figure 6-7 presents the corresponding MTI scores, which ranked skin injury risk as highest to lowest in the following order: 4, 1, 3, 2. Significant differences in results ($p < 0.05$) were observed among all surfaces, with the exception being the comparison between sample 1 and samples 3 and 4.

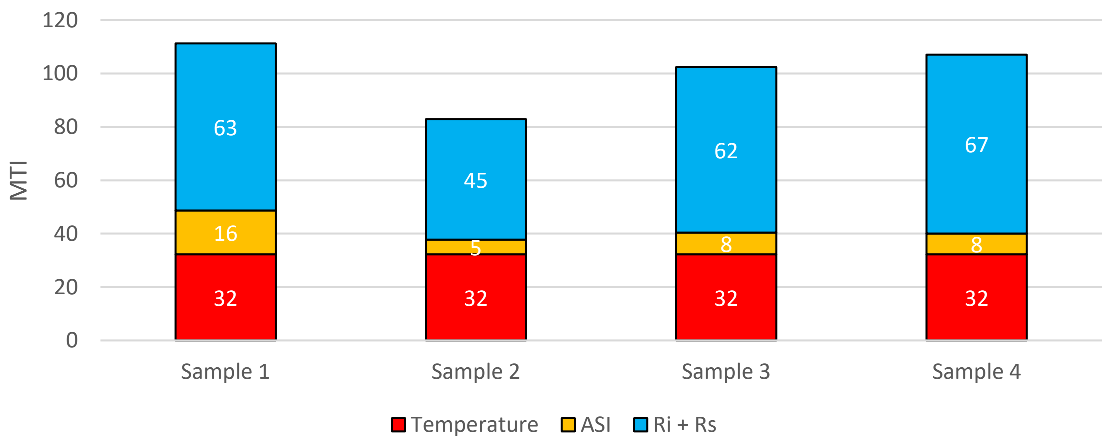

Figure 6-7: Comparison of MTI scores when evaluating different turf properties

Table 6-2: Analysis of variance results highlighting consistency of the impact conditions and subsequent sliding phase displacements (mean ± SE)

Parameter	System	Test Iteration				Statistics		
		1 (n=5)	2 (n=5)	3 (n=5)	4 (n=5)	F	p	
Horizontal Velocity (m/s)	1	5.00 ± 0.06	5.02 ± 0.01	5.01 ± 0.02	5.01 ± 0.01	0.29	0.83	-
	2	5.02 ± 0.02	5.00 ± 0.02	5.00 ± 0.04	5.00 ± 0.01	0.90	0.47	-
	3	5.00 ± 0.02	4.98 ± 0.01	5.01 ± 0.02	5.00 ± 0.02	1.86	0.18	2/3
	4	4.99 ± 0.02	4.96 ± 0.04	5.01 ± 0.03	5.00 ± 0.01	3.06	0.06	2/3
Vertical Velocity (m/s)	1	2.92 ± 0.08	2.90 ± 0.04	2.87 ± 0.03	2.88 ± 0.04	0.64	0.60	-
	2	2.90 ± 0.07	2.93 ± 0.05	2.88 ± 0.05	2.91 ± 0.03	0.96	0.44	-
	3	2.83 ± 0.05	2.92 ± 0.07	2.88 ± 0.08	2.87 ± 0.05	1.24	0.33	-
	4	2.90 ± 0.05	2.88 ± 0.05	2.91 ± 0.06	2.91 ± 0.05	0.28	0.84	-
Actual Displacement (m)	1	2.65 ± 0.18	2.70 ± 0.03	2.70 ± 0.20	2.56 ± 0.24	0.71	0.56	-
	2	2.56 ± 0.05	2.63 ± 0.15	2.64 ± 0.20	2.49 ± 0.19	0.89	0.47	-
	3	2.62 ± 0.09	2.52 ± 0.18	2.77 ± 0.02	2.72 ± 0.21	2.63	0.09	1/3, 2/3
	4	2.70 ± 0.04	2.45 ± 0.22	2.77 ± 0.20	2.64 ± 0.19	2.94	0.06	1/2, 2/3
Expected Displacement (m)	1	3.94 ± 0.27	4.01 ± 0.11	3.81 ± 0.13	3.74 ± 0.18	2.23	0.12	2/3
	2	4.35 ± 0.24	4.28 ± 0.20	4.09 ± 0.15	4.01 ± 0.13	3.68	0.03	1/3
	3	4.05 ± 0.07	4.08 ± 0.19	4.14 ± 0.06	3.96 ± 0.18	1.38	0.29	2/3, 2/4
	4	3.91 ± 0.06	3.77 ± 0.23	4.00 ± 0.04	3.91 ± 0.21	1.77	0.19	-

Table 6-3: Turf Properties Testing - Analysis of variance results of the Impact Resistance, Slide Resistance and MTI (mean ± SE). Where (/) represents a significant difference and (-) represents an insignificant difference.

Parameter	System	Test Iteration				Statistics		
		1 (n=5)	2 (n=5)	3 (n=5)	4 (n=5)	F	p	
Impact Resistance [m/s^2]	1	192.5 ± 11.3	197.2 ± 12.4	179.5 ± 7.0	176.9 ± 6.1	5.27	0.01	1/4, 3/2/4
	2	142.6 ± 18.2	144.4 ± 21.4	132.3 ± 7.0	137.3 ± 5.2	0.69	0.57	-
	3	202.8 ± 13.4	201.7 ± 13.7	196.7 ± 15.2	198.6 ± 18.8	0.15	0.93	-
	4	219.3 ± 9.10	211.4 ± 12.2	204.3 ± 5.7	205.7 ± 16.0	1.79	0.19	1/3
Slide Resistance [m/s^2]	1	2.41 ± 0.07	2.35 ± 0.10	2.43 ± 0.03	2.48 ± 0.06	3.02	0.06	2/4
	2	2.13 ± 0.09	2.21 ± 0.13	2.20 ± 0.05	2.09 ± 0.07	2.10	0.14	3/4
	3	2.37 ± 0.07	2.30 ± 0.17	2.27 ± 0.10	2.35 ± 0.09	0.74	0.55	-
	4	2.40 ± 0.08	2.45 ± 0.05	2.31 ± 0.08	2.41 ± 0.09	2.83	0.07	2/3
MTI	1	126.0	116.5	108.4	100.0	14.5	2.07×10^{-4}	1/3/4
	2	77.8	80.9	81.3	81.0			
	3	111.2	108.4	98.8	96.4			
	4	103.0	108.3	119.7	104.5			

6.1.3 Discussion

The consistent impact conditions depicted in Figure 6-2, provide confidence in the repeatability of the apparatus and conclusions formed from the rest of the results. Two outliers could be observed on the horizontal velocity. Further investigation established that the initial contact occurred as the simulated player reached maximum velocity. The launch conditions and time delays should be altered to ensure this was not an issue in future testing. In future testing, a consistent impact condition was achieved by generating a maximum launch velocity greater than 5 m/s and then allowing the carriage to coast briefly before impacting the surface at the desired velocity. Additional analysis highlighted that the vertical impact velocity was lower than the desired value. This discrepancy could be attributed to two factors. During a dynamic launch, the bearing housings experience thrust, increasing the internal resistance on the recirculating bearings. Alternatively, the release height protocol was unsuitable during this testing block. Therefore, the setup time was prolonged. Static loading for an extended time will deform the surface. Therefore, the position of the release height will be lower than desired, contributing to lower impact velocities. A 60-second set-up time limit should be implemented in future testing to ensure it does not occur again. A new impact location will be selected if setup takes longer than this threshold.

The experiment slide displacement was consistent throughout this study, demonstrating that the dampening mechanism generated a quick and repeatable transition from the Impact Zone to the Sliding Phase (Figure 6-3). Slide to Rest is a function of the Impact Resistance, dampening mechanism, and Slide Resistance. The magnitude of the Impact Resistance and the dampening mechanism's efficiency will dictate the sliding phase's initial speed. This velocity and the Slide Resistance will then influence the calculation of the theoretical displacement. It was reassuring to observe that the expected displacement demonstrated the anticipated capability to distinguish between various samples. For instance, when free pile height was consistent, the sample with the higher turf density yielded a lower Slide to Rest. This result aligns with the results that would be generated during a ball roll assessment [93].

This study investigated how fibre length, free pile height and turf density influenced skin injury risk. When comparing the ASI scores, a consistent trend was observed with the data collected in Chapter 5, where Sample 1 (50 mm) generated greater skin damage than Sample 2 (60 mm). Interestingly, the ASI scores were consistent in Samples 3 and 4, which suggests that turf density does not influence the ASI score. The skin damage generated by EMPD resulted in less discolouration and appeared smoother than SBR samples. EPDM and SBR are both synthetic rubbers [276]. SBR found in artificial turf is typically sourced by recycling old car tyres. EPDM is made from virgin materials, so it is free from debris. EPDM is reported to be more elastic than SBR [276]. A granular infill that is more malleable under compression will reduce sharp asperities interacting with the skin to generate an abrasion. When filling the samples, it was observed that the EPDM was covered in fine dust, which could assist the infill in sliding over the skin. This sliding action could reduce asperity interactions and minimise the severity of the abrasion. The geometry of the Abrasion Zone exhibited an extended length of damaged skin compared to SBR. This elongation could be attributed to the increased Slide Resistance observed in Figure 6-6 compared to the results from Chapter 5, where the 50- and 60-mm samples yielded a Slide Resistance of 1.84 and 1.69 m/s2, respectively.

The stiffness of an artificial turf can be effectively manipulated by adjusting the ratio of infill rates for the stabilising and performance infill. For instance, by increasing the sand content while maintaining a constant free pile height, the overall system can be made firmer. This, in turn, leads to less deformation during player-surface interactions. As a surface deforms, potential energy is stored and then transferred back to the athlete upon leaving the surface. On running tracks, all the energy is ideally returned; however, this is not possible as some energy will be lost as heat, sound, and vibration [277]. In contrast, artificial surfaces designed for contact sports are intended to attenuate impacts. By cushioning the landing during player-surface contacts, the energy returned to the player is decreased, thereby reducing the risk of injury [278].

The analysis of Impact Resistance (Figure 6-5) implies that incorporating sand enhances surface stiffness while higher quantities of performance infill accentuated impact attenuation. This outcome aligns with Cole (2020), who reported that the ratio of stabilising infill to performance infill will influence the stiffness of a surface. Despite samples 3 and 4 exhibiting the same infill depths and free pile height, sample 4 yielded a significantly greater Impact Resistance. This variation was attributed to the difference in turf density, which influenced the surface's stiffness. Incorporating performance infill into artificial turf creates a system that can be described as a lattice network. In isolation, infill can be considered a fluid. However, the behavioural response becomes more complex when interacting with the yarn fibres. Higher turf densities reduce the mobility of the infill by creating closer boundary limits [275]. Consequently, the surface becomes stiffer, which increases the risk of injury.

The surface area of exposed yarn has been identified as a characteristic influencing skin injury risk. When turf density remained constant, the longer free pile height produced a higher Slide Resistance. Concurrently, when free pile height was kept consistent, a higher turf density increased the Slide Resistance. Interestingly, the highest and lowest Slide Resistance occurred on the shortest free pile height. This finding contradicts Tay et al., (2015), who reported that longer free pile heights increased friction. Therefore, rugby turf's behavioural response is more complex than initially thought.

It was hypothesised that greater sand content, lower performance infill rates, longer free pile heights, and higher turf densities would contribute to a higher risk of injury. Therefore, it was reassuring to find that Sample 4, fulfilling all these criteria, was identified as posing the greatest risk of injury out of the 60 mm samples, according to the MTI. In contrast, Sample 2 did not fulfil any criteria and was identified as the safest surface. These results provide confidence in the repeatability of the simulation impact conditions and sensitivity of the parameters that contribute to the MTI calculation. They also highlight that under certain conditions a 50-mm sample does not pose a higher risk, compared to 60-mm surfaces.

6.1.4 Conclusion

This study demonstrated consistent impact conditions, enhancing confidence in the apparatus's repeatability and the results' validity. Two horizontal velocity outliers were attributed to initial contact at maximum velocity, suggesting adjustments in launch conditions and time delays for future tests. Lower vertical impact velocities were linked to internal resistance within the bearing housings due to thrust or prolonged setup times, causing surface deformation. To address the latter, future testing should adopt a 60-second setup time limit to mitigate this issue.

The consistency of the actual displacement highlighted the dampening mechanism's effectiveness. Theoretical displacements, influenced by Impact Resistance, dampening efficiency, and Slide Resistance, successfully distinguished between samples, with higher turf density yielding lower expected displacements, aligning with ball roll assessments.

ASI scores indicated that 50 mm samples caused more skin damage than 60 mm samples. EPDM samples caused less discolouration and smoother skin damage than SBR samples, likely due to EPDM's elasticity and fine dust coating. The extended length of damaged skin in the Abrasion Zone was linked to increased Slide Resistance.

Surface stiffness was manipulated by adjusting infill ratios. Higher sand content created firmer surfaces with less deformation, while performance infill enhanced impact attenuation. This suggests that the choice of infill material and its ratio can significantly affect the surface stiffness and, consequently, the impact attenuation properties of the surface. Increased turf density led to greater Impact Resistance due to reduced infill mobility, aligning with previous research.

The conclusions drawn from this research are importance as they challenge previous assumptions. The relationship between free pile height and turf density exhibited varying Slide Resistance, suggesting a more complex turf response than Tay et al. (2015) proposed. Out of the 60 mm samples, the surface, with higher sand content, lower performance infill rates, longer free pile heights, and higher turf densities, posed the greatest injury risk per the MTI. Sample 2 was the safest, validating the sensitivity of the simulation's repeatability and MTI parameters. These findings also highlight that a 50-mm sample may not always pose a higher risk than a 60-mm sample, which has significant implications for future testing and injury prevention.

6.3 Investigating the Influence of Shock Pad on Skin Injury Risk

In sports, optimising surface stiffness has been reported to improve athletic performance and reduce the risk of injury (McMahon & Greene, 1978; McMahon & Greene, 1979; Kerdok et al., 2002;Arampatzis et al., 2004; Firminger et al., 2019). The stiffness of an artificial turf can be manipulated by incorporating a shock pad or as reported in the previous study, by altering the ratio of infill rates for the stabilising and performance infill. In 2015, World Rugby increased the minimum head injury criteria requirement to 1.3m (World Rugby, 2023d). Given the current state of the art, surfaces are optimised to produce ideal traction and shock-absorbing properties. This stipulation ultimately necessitates the integration of a shock pad for a surface to be considered a Rugby Turf whilst complying with the other requirements of Regulation 22. The main reason for this alteration was to minimise the risk of concussion. However, World Rugby advocates integrating shock pads due to their additional benefits. Not only does the shock pad facilitate the fulfilment of other performance characteristics, but it also increases the durability of the surface. With proper maintenance, using a shock pad can extend the lifespan of a carpet before it needs to be replaced (World Rugby, 2023d). Despite improving impact attenuation, shock pads' influence on skin injury risk remains unknown [281]. This study, therefore, aims to evaluate how the density of a shock pad contributes to skin injury risk on different infill materials.

6.2.1 Materials and Methods

Three pad densities were selected to monitor the influence of the shock pad on skin injury risk while maintaining a constant thickness (12 mm). The three prefabricated foam pads with varying densities were selected to vary the force reduction (FR) properties of the pad: 39%, 45%, and 55%, respectively. Three 60-mm monofilament carpets with a stitch gauge and rate of 70 and 140, respectively, were then filled with sand (0.63 - 1.00 mm @ 15 kg/m^2) followed by SBR (1.0 - 2.5 mm @ 15 kg/m^2) to produce a free pile height of 15 mm. The apparatus was configured to increase the delay before releasing the knee, as recommended by the previous study, to ensure the desired horizontal impact velocity was achieved. Each system was tested three times each test. Before retesting, the skin was replaced, and the sample was prepared with a rake and a studded roller in accordance with FIFA's installation specification.

Statistical Analysis

One-way analysis of variance (ANOVA) tests was conducted to assess the consistency of the accelerometer data. Post-hoc t-tests were performed to establish whether any systems produced a significantly different result. All statistical analyses were performed with SPSS, adopting a significance threshold of $p < 0.05$.

6.2.2 Results

This study investigated the skin injury risk on three different shock pads tested thrice to create a total dataset of 45 test results. The consistency of impact velocities and sliding dynamics are presented in Figure 6-8 and Figure 6-9. The ANOVA analysis highlighted that the repeatability of the Sliding Phase dynamics had improved (Table 6-4).

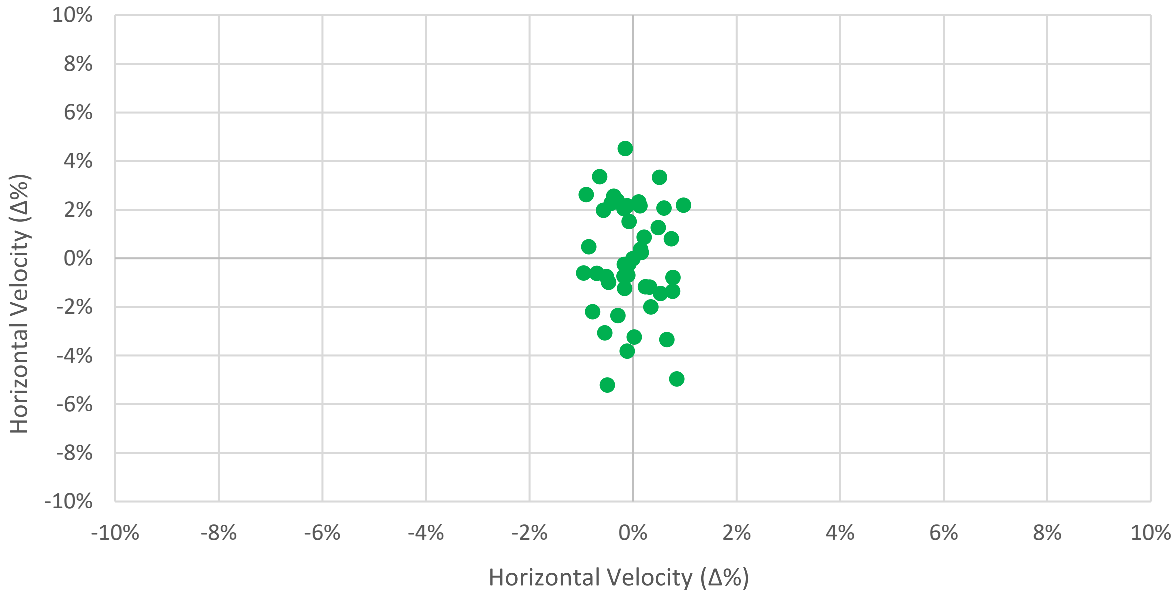

Figure 6-8: Illustration of the deviation of impact velocities from the desired horizontal (5 m/s) and vertical (2.95 m/s) values during shock pad testing.

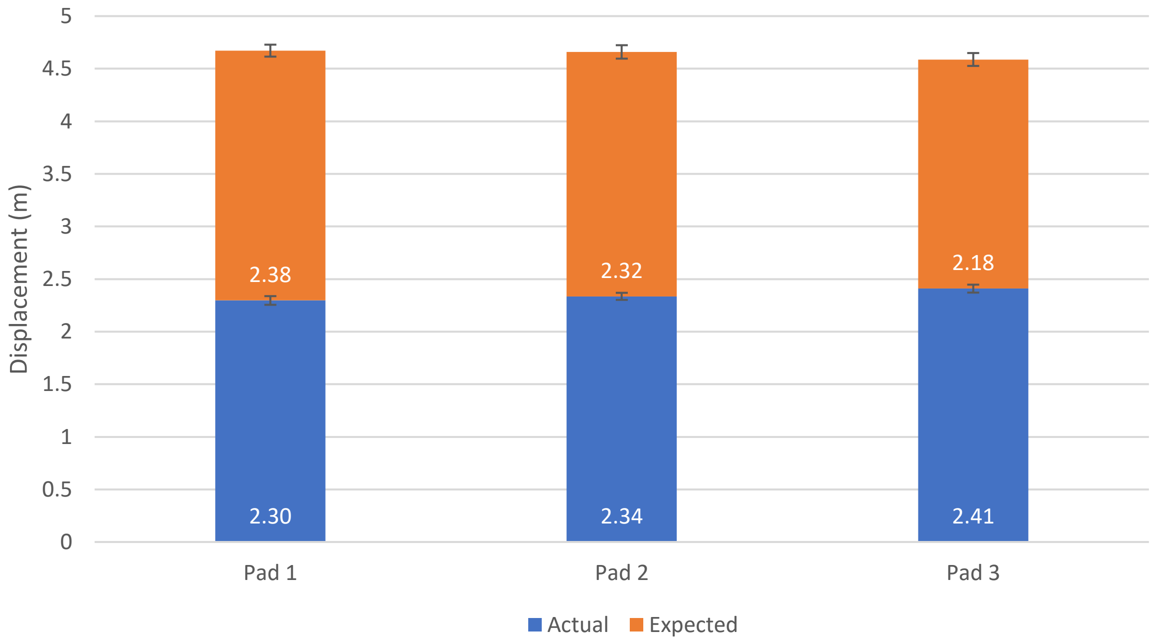

Figure 6-9: Comparison of Actual and Expected displacements during shock pad testing.

There were trivial differences between the ASI scores when assessing the influence of a shock pad on skin injury risk (Figure 6-10). Visual inspection of the Abrasion Zone highlighted consistent geometries around the apex of the knee (Appendix 28 - Appendix 31). The length of the profile was much shorter than in the previous study. These characteristics were consistent with the skin damage assessed in Chapter 5.

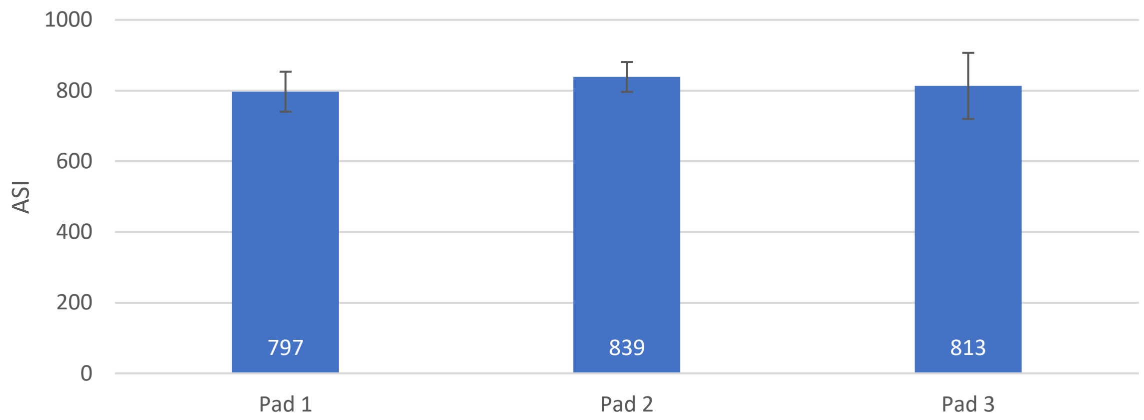

Figure 6-10: Comparison of ASI score when evaluating the influence of a shock pad on skin injury risk.

Analysis of the Impact Resistance (Figure 6-11) implied that shock pads with lower force reduction contributed to produce stiffer surfaces, however, a statistical difference ($p < 0.05$) was only detected between the stiffest (Pad 3: FR - 39%) and softest (Pad 1: FR - 55%) shock pad systems. Again, the ANOVA results highlighted improvements in the consistency of repeated testing (Table 6-5).

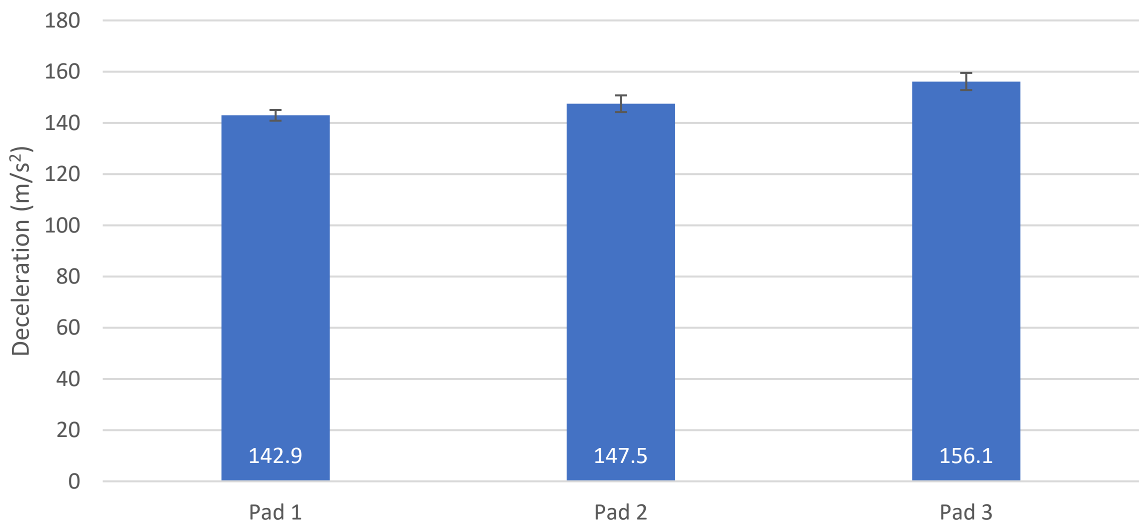

Figure 6-11: Impact Resistance: Comparison of different shock pads on Skin Injury Risk

Analysis of the Sliding Phase demonstrated a consistent magnitude for Slide Resistance (Figure 6-12). Statistical analysis reported trivial differences across the three systems expect when comparing the pads 2 and 3 ($p = 0.03$). The ANOVA analysis highlighted there was no differences for Slide Resistance between repeated testing results (Table 6-5).

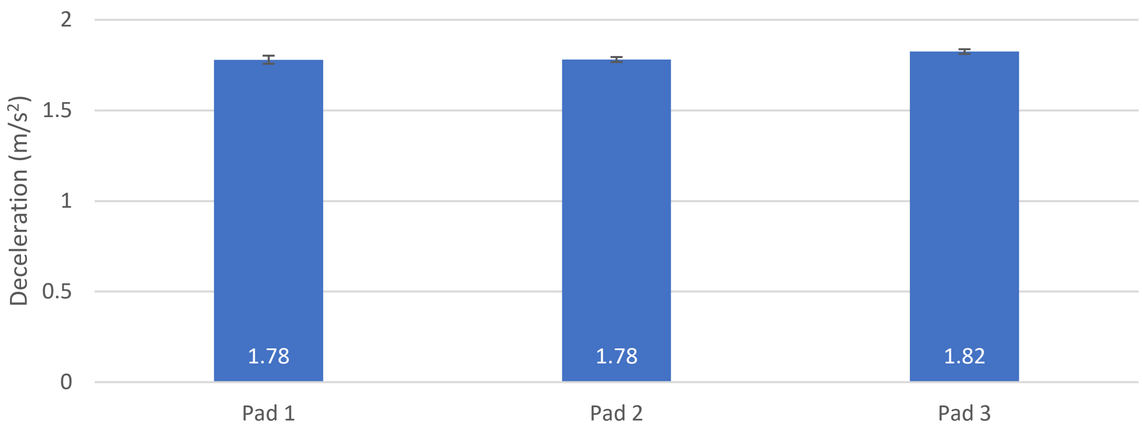

Figure 6-12: Slide Resistance: Comparison of different shock pads on Skin Injury Risk

Again, no temperature data was collected during this study; therefore, the temperature was assumed to be 25°C to calculate the MTI. Figure 6-13 presents the corresponding MTI scores, which implies that stiffer shock pads contribute to a higher risk of skin injury. However, these results are trivial as there was no significance ($p > 0.05$).

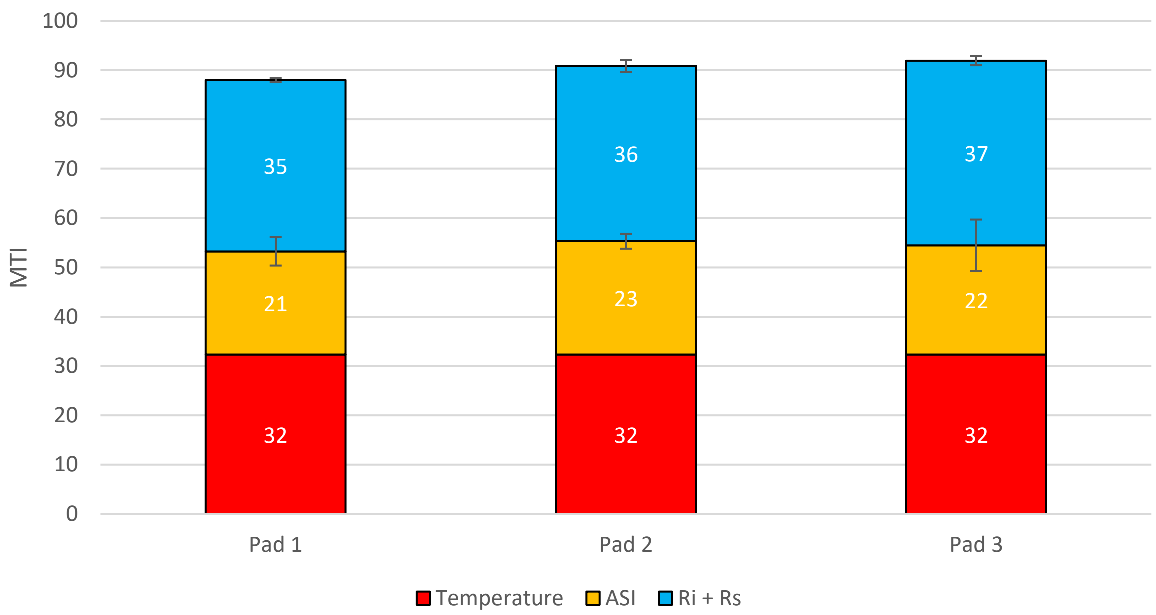

Figure 6-13: Comparison of MTI scores when evaluating the effects of different shock pads on skin injury risk

Table 6-4: Analysis of variance results highlighting consistency of the impact conditions and subsequent sliding phase displacements (mean ± SE)

Parameter	Pad	Test Iteration			Statistics		
		1 (n=5)	2 (n=5)	3 (n=5)	F	p	
Horizontal Velocity (m/s)	1	5.01 ± 0.01	5.02 ± 0.01	4.99 ± 0.01	1.61	0.24	-
	2	4.99 ± 0.01	4.99 ± 0.00	4.99 ± 0.01	0.21	0.82	-
	3	5.00 ± 0.01	5.01 ± 0.01	5.00 ± 0.01	1.42	0.28	-
Vertical Velocity (m/s)	1	2.98 ± 0.02	2.97 ± 0.04	2.97 ± 0.03	0.10	0.90	-
	2	2.93 ± 0.02	2.96 ± 0.03	2.95 ± 0.05	0.27	0.77	-
	3	2.93 ± 0.03	2.92 ± 0.03	2.98 ± 0.03	0.98	0.40	-
Actual Displacement (m)	1	2.32 ± 0.06	2.26 ± 0.11	2.31 ± 0.04	0.19	0.83	-
	2	2.35 ± 0.06	2.38 ± 0.09	2.39 ± 0.06	0.08	0.92	-
	3	2.46 ± 0.09	2.39 ± 0.06	2.38 ± 0.04	0.39	0.69	-
Expected Displacement (m)	1	4.68 ± 0.13	4.62 ± 0.11	4.71 ± 0.05	0.24	0.79	-
	2	4.92 ± 0.07	4.58 ± 0.06	4.57 ± 0.07	8.46	0.01	1/2, 1/3
	3	4.56 ± 0.10	4.71 ± 0.11	4.50 ± 0.12	1.04	0.38	-

Table 6-5: Shock Pad Testing - Analysis of variance results of the Impact Resistance, Slide Resistance and MTI (mean ± SE). Where (/) represents a significant difference and (-) represents an insignificant difference.

Parameter	Pad	Test Iteration			Statistics		
		1 (n=5)	2 (n=5)	3 (n=5)	F	p	
Impact Resistance [m/s^2]	1	138.6 ± 3.02	144.1 ± 2.30	146.1 ± 4.94	1.17	0.34	-
	2	144.6 ± 8.15	158.8 ± 2.65	148.5 ± 2.70	0.2	0.83	-
	3	163.1 ± 2.96	157.5 ± 8.22	147.8 ± 3.40	2.04	0.17	1/3
Slide Resistance [m/s^2]	1	1.79 ± 0.03	1.76 ± 0.05	1.79 ± 0.03	0.24	0.79	-
	2	1.80 ± 0.03	1.77 ± 0.01	1.76 ± 0.01	0.48	0.63	-
	3	1.82 ± 0.01	1.82 ± 0.01	1.84 ± 0.04	0.27	0.76	-
MTI	1	82.1	89.0	93.0	0.35	0.71	-
	2	92.6	92.7	87.5			
	3	89.2	100.9	85.6			

6.2.3 Discussion

The previous study recommended that the launch conditions be altered to improve the consistency of the impact velocities. A comparison of Figure 6-2 and Figure 6-8 clearly demonstrates the success of these amendments, instilling confidence in the research methodology. This success has paved the way for the development of this apparatus into a future test method. As a result of changing the launch conditions, the experimental sliding distance decreased by ~0.3m. This reduction, which still falls within the limits of the desirable outputs, further affirms the acceptability and benefits of the amendments for the consistency of the apparatus.

This study was crucial in understanding the impact of shock absorbing properties of the pad on skin injury risk. As the previous study indicated, stiffer surfaces can heighten the risk of injury. Therefore, it was hypothesised that there would be a direct correlation between force reduction of the shock pad and skin injury risk. The analysis of the impact resistances (Figure 6-11) validated this hypothesis; however, the significance of the outcome became evident only when comparing shock pads with a large variation in force reduction.

The Sliding Phase can be described as a superficial interaction with the turf. Consequently, the shock pad was anticipated to have minimal influence on the Slide Resistance results. Despite generating a consistent magnitude of results, one comparison highlighted statistical significance. This variation could be attributed to surface preparation, a crucial aspect that the outlier may have overlooked by having a slightly longer free pile height. The increased yarn exposure could contribute to the elevated Slide Resistance. Comparison of Table 6-3 and Table 6-4 highlights improved consistency of the kinematic injury metrics, which was attributed to proper surface conditioning prior to testing. This theory of increased yarn exposure, combined with improved consistency of results, underlines the paramount importance of sample preparation in our research.

The shock pad, being the lowest layer of a turf system, naturally has a minimal impact on the ASI scores. However, it was encouraging to note that the apparatus consistently generated Abrasion Zones with similar characteristics on comparable surfaces. The results contributing to the MTI suggested that stiffer surfaces may pose a higher risk of injury, although the significance of this result was not established.

This study's limitation was that it only used continuous prefabricated shock pads from one supplier. This limitation underscores the need for future research to explore the potential of varying the manufacturer and thickness of the pad or incorporating in situ pads. Preliminary testing on tiled in situ pads highlighted repeatability issues when impacting the boundary between two pads. Therefore, this variation should be considered when installing the surface to ensure the Impact Zone is in the middle of a tiled shock pad.

6.3.1 Conclusion

This study addressed previous recommendations to enhance launch conditions, achieving more consistent impact velocities and increasing the apparatus's reliability for future testing. Despite this improvement, sliding displacements were reduced; however, this was deemed acceptable as the distance exceeded the desirable threshold. This research indicated that the shock absorbing properties of the pad did not significantly impact skin injury risk. It is more probable that the combination of infill materials and turf properties plays a more substantial role in determining the potential for a player to sustain a skin injury. Despite the lack of variation in shock pad characteristics being identified as a limitation, it was reassuring that comparable surfaces produced similar results in all factors contributing to the MTI.

6.4 Investigating the Skin Injury Risk on Alternative Turfs

This chapter has so far provided insights into skin injury risks associated with 3G surfaces. The following studies will broaden this perspective by examining alternative turfs, specifically 2G, hybrid, and non-fill surfaces. These investigations will offer a nuanced understanding of skin injury risks and help establish acceptable pass-fail thresholds for the MTI, aiding World Rugby in adopting this test method under Regulation 22.

The negative connotations associated with artificial turf stem from preconceptions about 2G surfaces, which have historically been very abrasive (Fuller, Dick, et al., 2007; Steffen et al., 2007; Williams et al., 2011). Poorly maintained community surfaces can exhibit areas of turf that are either overfilled or underfilled. Therefore, three sand infill rates will be evaluated to understand how skin injury risk varies on an underfilled, overfilled, and standard surface.

In contrast, elite hockey is typically played on water-based surfaces. With sustainability a hot topic in the sports industry, hockey's governing body (FIH - Fédération Internationale de Hockey) has banned water-based surfaces in global competitions after the 2024 Olympics [159]. When surfaces are heavily irrigated, the risk of skin injury is reduced. Therefore, this ban will mean FIH must consider player welfare as skin injuries will become prominent again. The combination of 2G's historical association with skin injuries and FIH's potential interest provides a rationale for evaluating the validity of the MTI against some surfaces known to cause injuries.

Skin injury incidence on artificial has been reported to be almost eight times higher than on natural grass [135]. Environmental conditions will influence severity of injury as dry grass has been reported to be more abrasive than natural grass [128]. In a laboratory setting, it would be challenging to obtain natural grass; therefore, hybrid turf was the best alternative [134], [135], [283], [135], [284]. Hybrid turfs were designed by reinforcing natural grass with artificial fibres. This innovation aimed to combine the desirable characteristics to develop a superior surface. The benefits of this turf include facilitating longer playing hours, enhanced quality, consistent all year round, and faster recovery.

Innovation in the sports industry has developed non-filled systems; however, they have yet to gain accreditation to be considered Football or Rugby Turf [75]. Unsurprisingly, no literature has been published reporting skin injury incidence rates on non-filled systems. FIFA and World Rugby may change their stance on non-filled systems as potential replacements for SBR systems when the ECHA ban on intentionally added microplastics is enforced [90]. The combination of a lack of incidence rates and the potential for these systems to become accredited highlights a gap in the literature that warrants further investigation.

6.4.1 Materials and Methods

This section outlines the methodology used to evaluate skin injury risk across three distinct surface types: second-generation (2G), Hybrid, and Non-fill. Each surface type was prepared and tested under various conditions to assess their impact on skin injury potential.

Second Generation (2G) surfaces included sand-filled and water-based hockey carpets. The sand-filled carpet, with a 10 mm pile height, was secured to a 12 mm prefabricated foam shock pad and tested at three different infill rates (3, 5, and 7 kg/m^2). The water-based carpet, with a 13 mm pile height, was tested dry and irrigated with 1.25 L/m^2 of water. Each condition was subjected to five tests, except for the irrigated system, which was tested three times to avoid damaging the device due to the high velocity at the end of the gantry.

Hybrid surfaces involved a 55-mm tufted grass system arranged in 1m x 1m tiles. Two variations were evaluated: one with four tiles pressed together without a sublayer and another with an artificial root zone constructed from a wooden frame filled with 50 mm of sand. Both variations were left outside overnight before testing, with surface moisture and impact attenuation monitored using a time-domain reflectometry (TDR) sensor and the Advanced Artificial Athlete (AAA). Each hybrid system was tested three times, with the impacted tile replaced after each test to provide a fresh impact location.

Non-fill surfaces comprised a 28 mm carpet with a texturised thatch attached to a 14 mm prefabricated foam shock pad. Due to the lack of infill, acting as a ballast, significant double-sided tape was used to secure the carpet to the pad. The carpet's stitched backing required testing in both directions to evaluate the influence of fibre orientation, with each direction tested twice. An assistant was used to lay and flip the carpet to prevent the researcher from knowing the grain orientation. This procedure aimed to determine if the device was sensitive enough to detect differences in grain direction.

These comprehensive evaluations aim to understand the risk of skin injury associated with different artificial turf systems, guiding improvements in turf design and player safety.

Statistical Analysis

T-tests were conducted to establish whether any systems produced a significantly different result. All statistical analyses were performed with SPSS, adopting a significance threshold of $p < 0.05$.

6.4.2 Results

This section presents a comprehensive analysis of alternative synthetic sports surfaces.

Second Generation

Mean Peak Temperature, T_p

A positive correlation between free pile height and peak temperature with significant differences ($p < 0.05$) between each surface condition (Figure 6-14). As expected, irrigating the surface produced the lowest peak temperature. Meanwhile, the highest temperature (39.5°C) was recorded on the dry water-based surface.

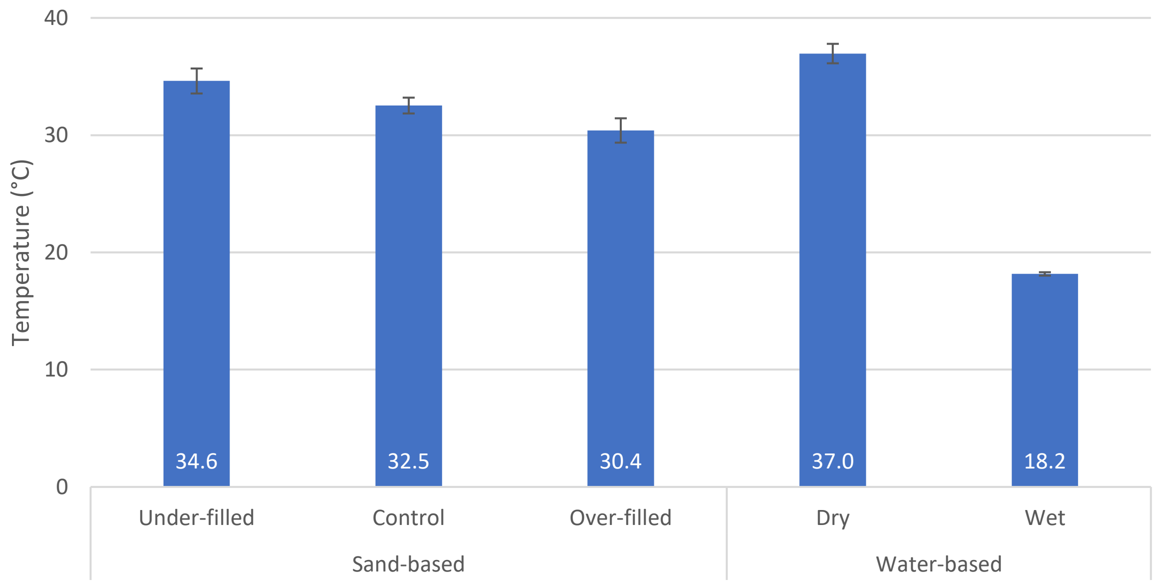

Figure 6-14: Comparison of Maximum Temperature whilst evaluating Skin Injury Risk on variations of Hockey Surfaces

Abrasion Severity Index, ASI

A positive correlation between infill level and skin damage on sand-filled surfaces was observed on Figure 6-15. When analysing the damage in Appendix 32 it was apparent that the abrasion was so severe that a hole was torn in the skin. Meanwhile, the water-based surface exhibited lower ASI scores, which implies that the infill generates skin damage.

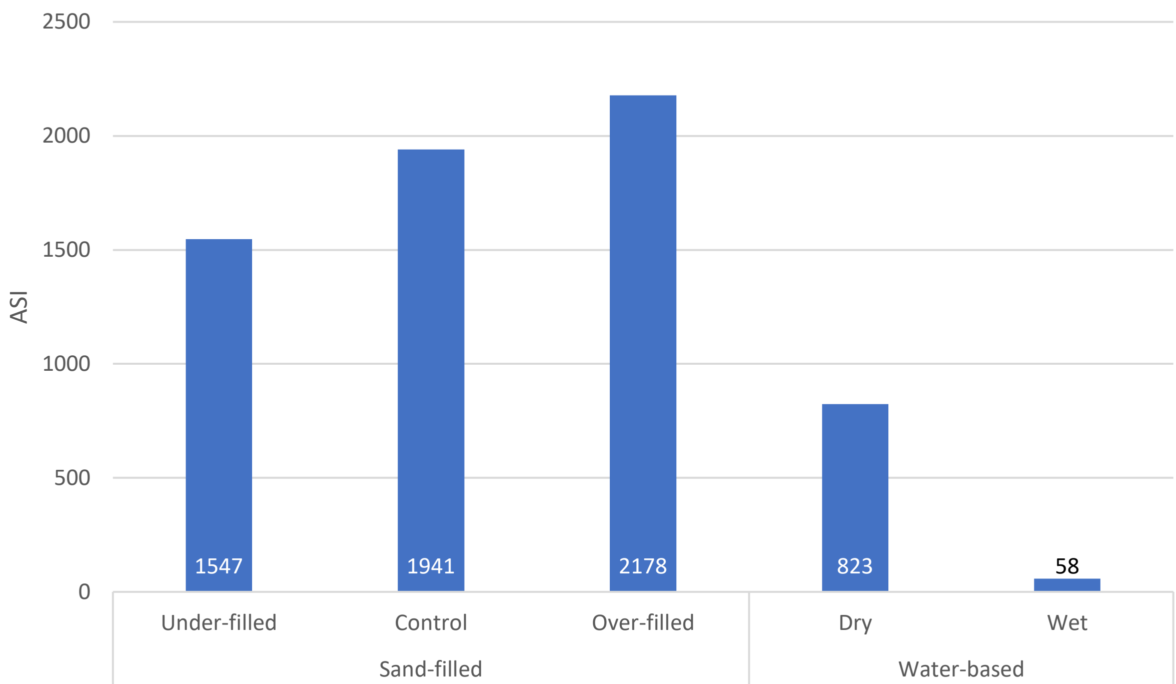

Figure 6-15: Comparison of ASI scores: Evaluating Skin Injury Risk on variations of Hockey Surfaces

Surface Resistance during Impact, Ri

The under-filled sample generated significantly lower ($p < 0.05$) Impact Resistances than the control and overfilled sample (Figure 6-16). Irrigating the surface significantly ($p < 0.05$) reduced the result compared to the dry surface; however, the introduction of water on the surface increased the variation in data.

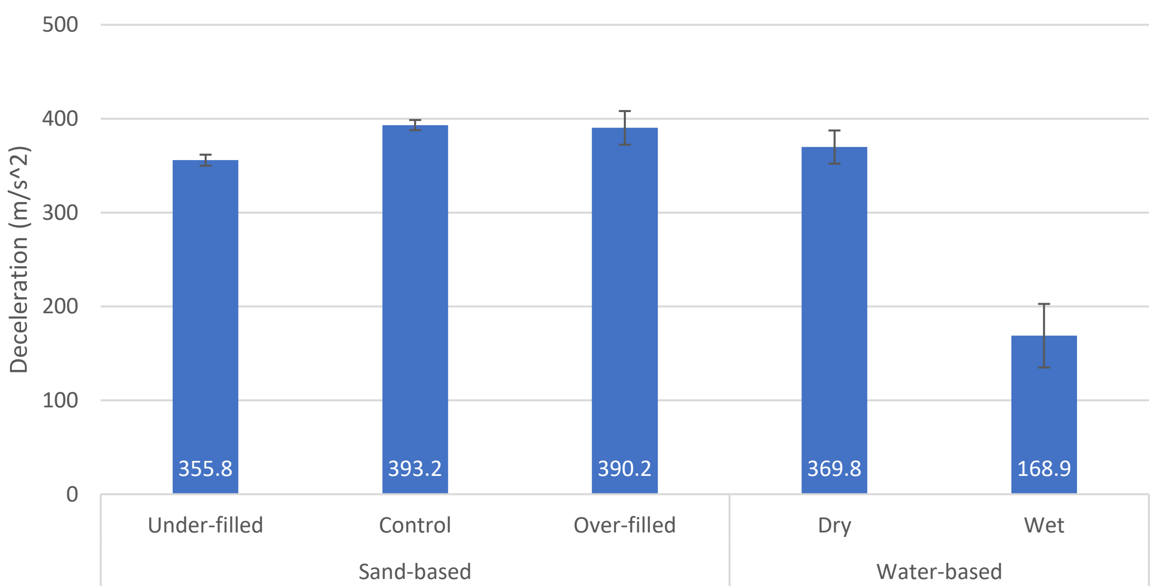

Figure 6-16: Impact Resistance: Evaluating Skin Injury Risk on Variations of Hockey Surfaces

Surface Resistance during Sliding, Rs

A significant ($p < 0.05$) negative correlation between Slide Resistance and infill rate was observed on Figure 6-17. As expected, the greatest and smallest results were produced on the dry and wet water-based surface.

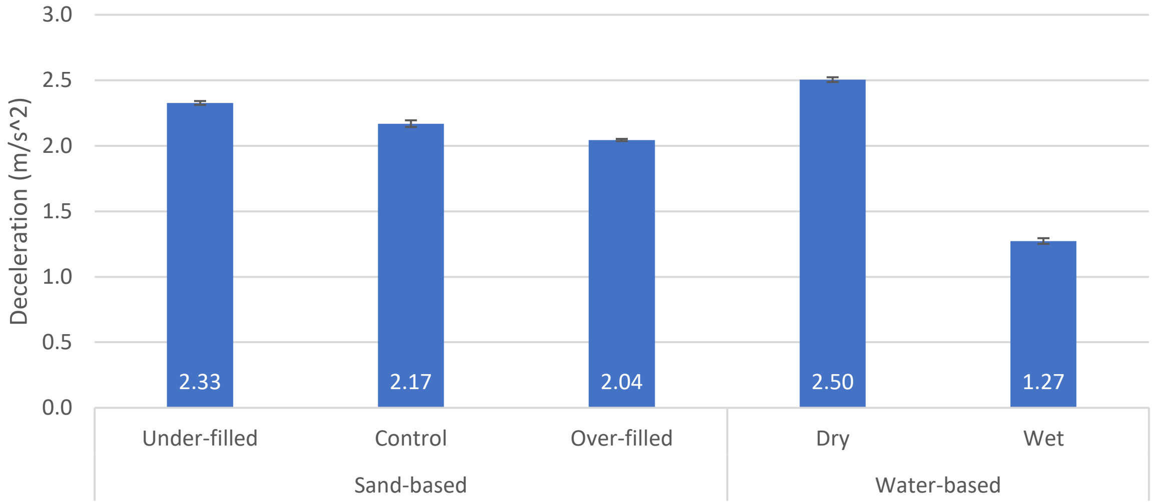

Figure 6-17: Slide Resistance: Evaluating Skin Injury Risk on Variations of Hockey Surfaces

Maxwell Tribo Index, MTI

As expected, the irrigated system generated the smallest MTI score (Figure 6-18). It was predicted that the overfilled sample would exhibit the highest risk of injury. However, the difference from the control was trivial. As the infill rates increased, the surface became stiffer, which increased the Impact Resistance. This outcome agrees with the results from Section 6.2.

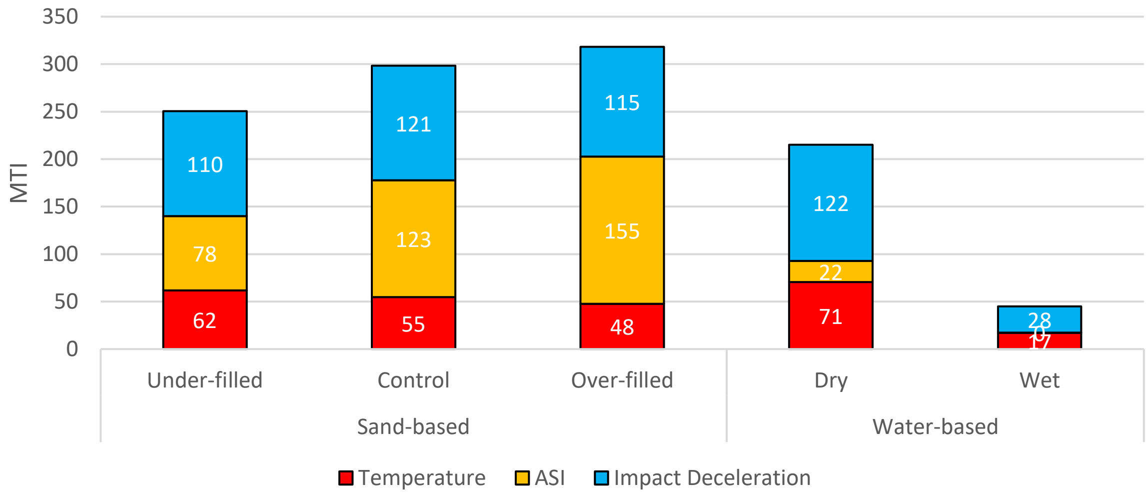

Figure 6-18: Comparison of MTI scores: Evaluating Skin Injury Risk on Variations of Hockey Surfaces

Hybrid

Results from the TDR data reported surface moisture levels of 8.3±1.4% and 20.2±1.8% for Sample 1 and 2, respectively. Integrating the artificial rootzone and increased moisture content resulted in the force reduction values from the AAA increasing from 39.2±1.2% to 55.4±1.4%.

Mean Peak Temperature, T_p.

Sample 1 generated a range of temperatures from 24.8-31.6°C. Meanwhile, Sample 2 generated a range of temperatures from 23.4-28.5°C. The dry and firm surface (Sample 1) generated statistically greater ($p < 0.05$) temperatures compared to the softer surface (Figure 6-19).

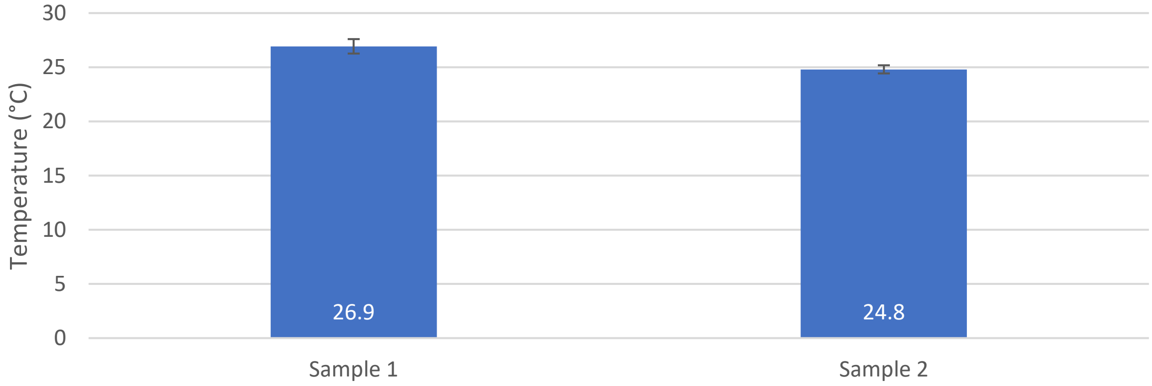

Figure 6-19: Comparison of Peak Temperature whilst evaluating Skin Injury Risk on Two Hybrid Surfaces

Abrasion Severity Index, ASI

Both hybrid surfaces experienced minimal skin damage. However, the dry and stiff surface produced statistically greater ASI scores compared to the softer surface (Figure 6-20).

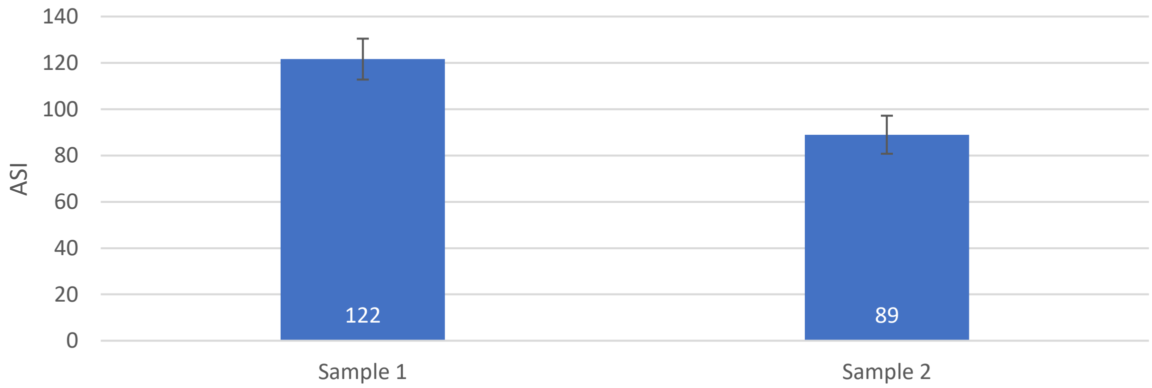

Figure 6-20: Comparison of ASI whilst evaluating Skin Injury Risk on Two Hybrid Surfaces

Surface Resistance during Impact, Ri

Impact Resistance had an inverse relationship with surface moisture and force reduction (Figure 6-21). The hybrid surfaces exhibited larger error bars compared to artificial systems, which was attributed to the inherent variation within the natural component of the hybrid turf.

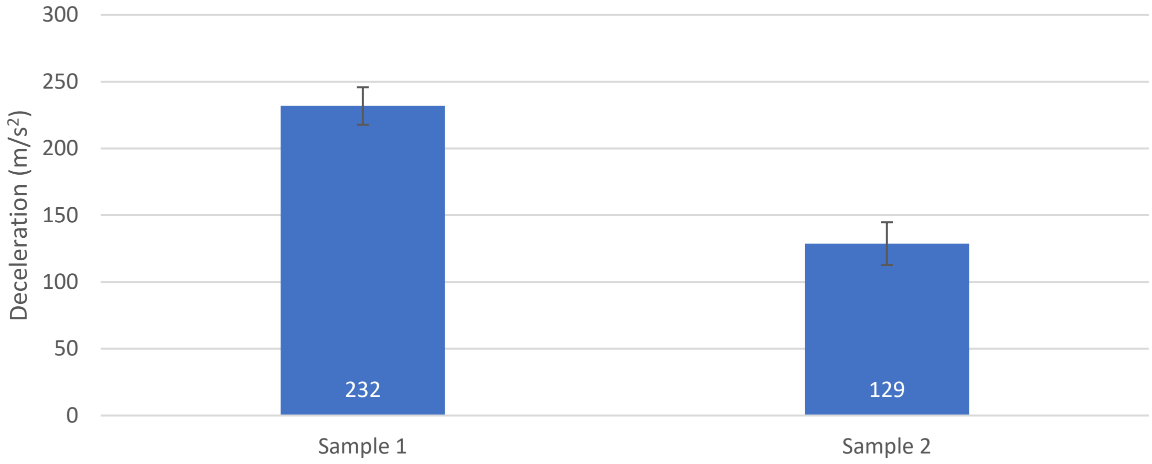

Figure 6-21: Impact Resistance: Assessing Risk of Skin Injuries on Hybrid Systems.

Surface Resistance during Sliding, Rs

Similarly, Slide Resistance had an inverse relationship with surface moisture and force reduction (Figure 6-22). However, the magnitude of the error bars was more consistent with those of previously tested artificial systems. This observation was attributed to the sliding phase representing a superficial interaction with the surface; therefore, underlying structural anomalies have less influence on the outcome.

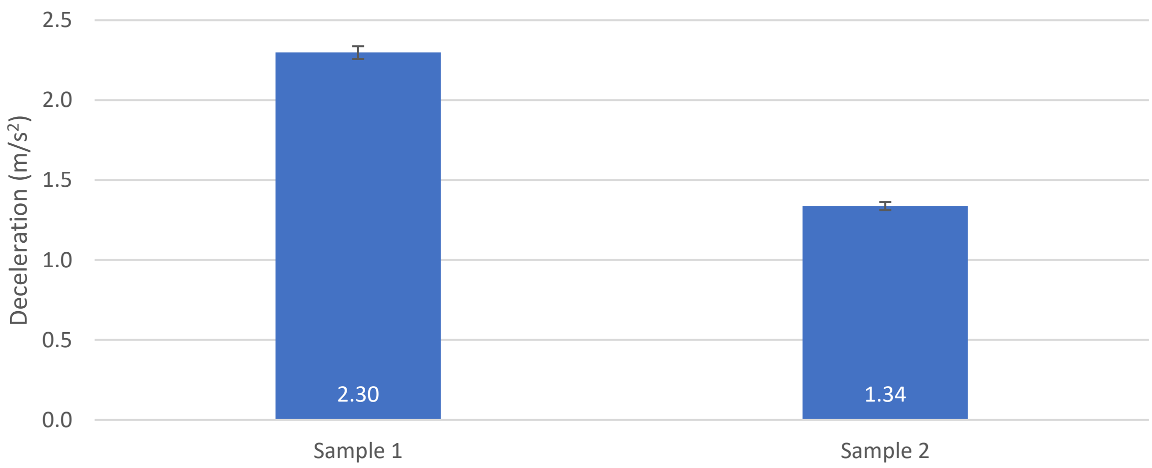

Figure 6-22: Slide Resistance: Assessing Risk of Skin Injuries on Hybrid systems.

Maxwell Tribo Index, MTI

When analysing the MTI scores (Figure 6-23) it was apparent that the contribution of the ASI was missing. This was due to the minimal damage generated by both samples (Appendix 33-Appendix 34). Compared to sand-based or dry 2G surfaces (Figure 6-18), the MTI scores for hybrid surfaces were less than half. Meanwhile, the wet 2G and soft hybrid surfaces exhibited similar scores.

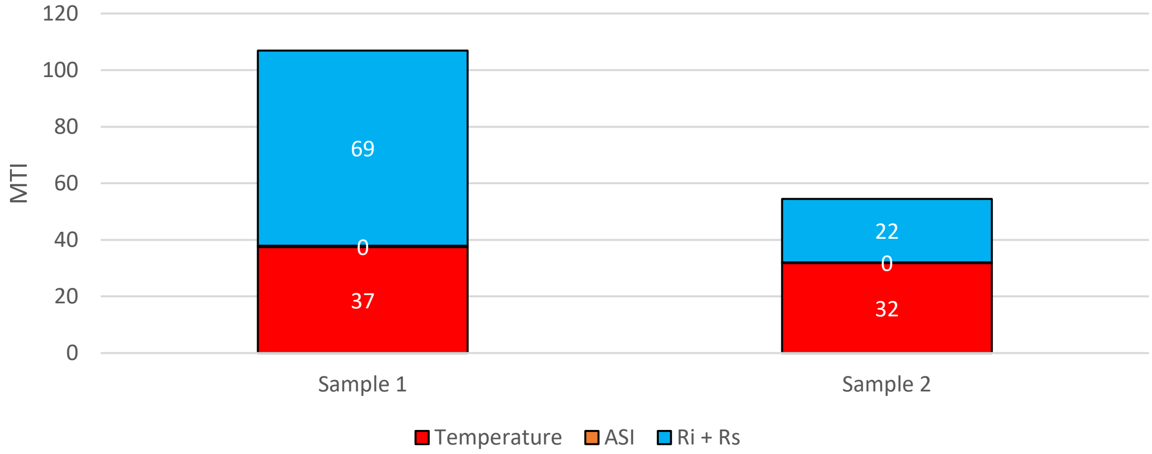

Figure 6-23: MTI: Assessing Risk of Skin Injuries on Hybrid Systems.

Non-fill

Mean Peak Temperature, T_p.

The orientation of the non-fill did not affect the temperature generated during the interaction (Figure 6-24). The peak temperatures generated ranged from 30.7-34.1°C.

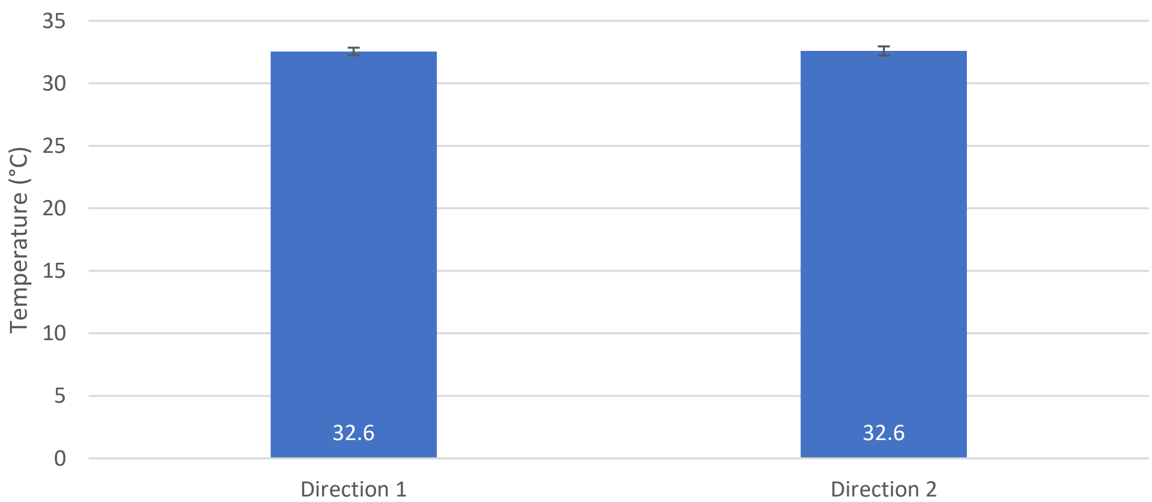

Figure 6-24: Comparison of Peak Temperature whilst evaluating the orientation of a non-fill system

Abrasion Severity Index, ASI

Direction 1 generated statistically greater ASI scores; however, the results were relatively low in both directions (Figure 6-25, Appendix 35).

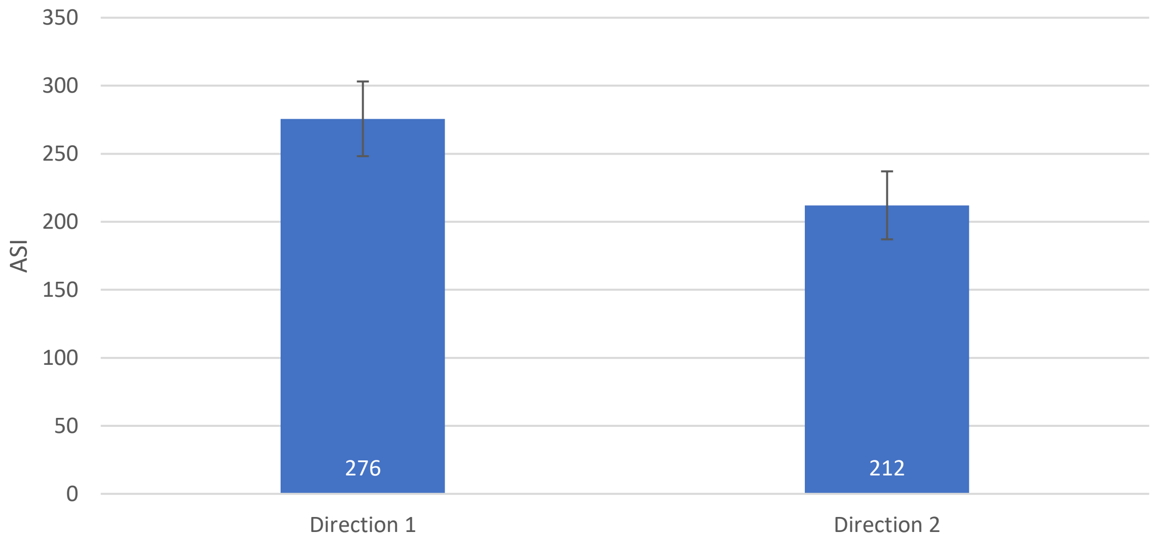

Figure 6-25: Comparison of ASI scores whilst evaluating the orientation of a non-fill system.

Surface Resistance during Impact, Ri

In contrast to the ASI, Direction 1 generated a statistically smaller Impact Resistance when conducting an antiparallel test on the non-filled carpet (Figure 6-26).

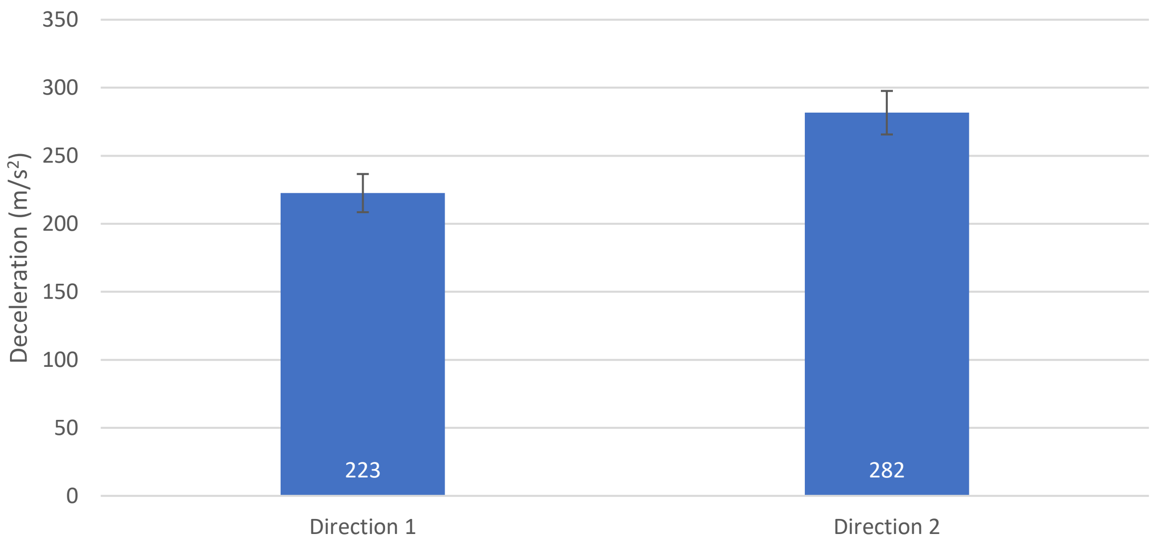

Figure 6-26: Impact Resistance: Evaluating Skin Injury Risk on Non-filled Systems.

Surface Resistance during Sliding, Rs

Similarly, Direction 1 generated a statistically smaller Slide Resistance when conducting an antiparallel test on the non-filled carpet (Figure 6-27). Despite generating greater impact and slide resistances in the second direction, this did not correspond to an increase in temperature, which was consistent in both directions (32.6±0.3 and 32.6±0.4).

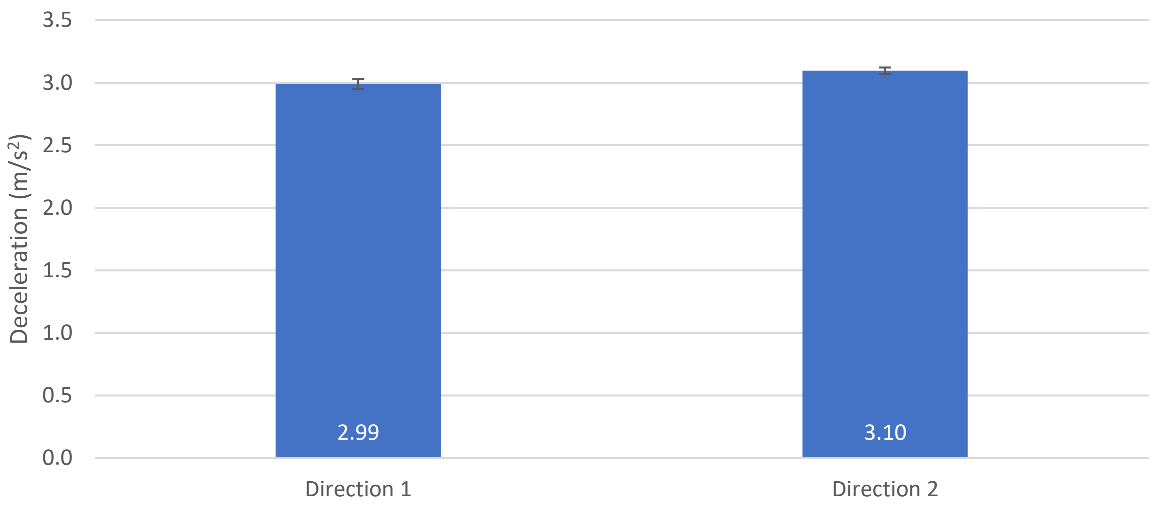

Figure 6-27: Slide Resistance: Evaluating Skin Injury Risk on Non-filled Systems.

Maxwell Tribo Index, MTI

Despite the lack of abrasion, the combination of high decelerations and corresponding peak temperatures contribute to the MTI score (Figure 6-29). The magnitude of the MTI scores was higher than the 3G surfaces tested in Sections 6.2 and 6.3, implying non-fills are high risk.

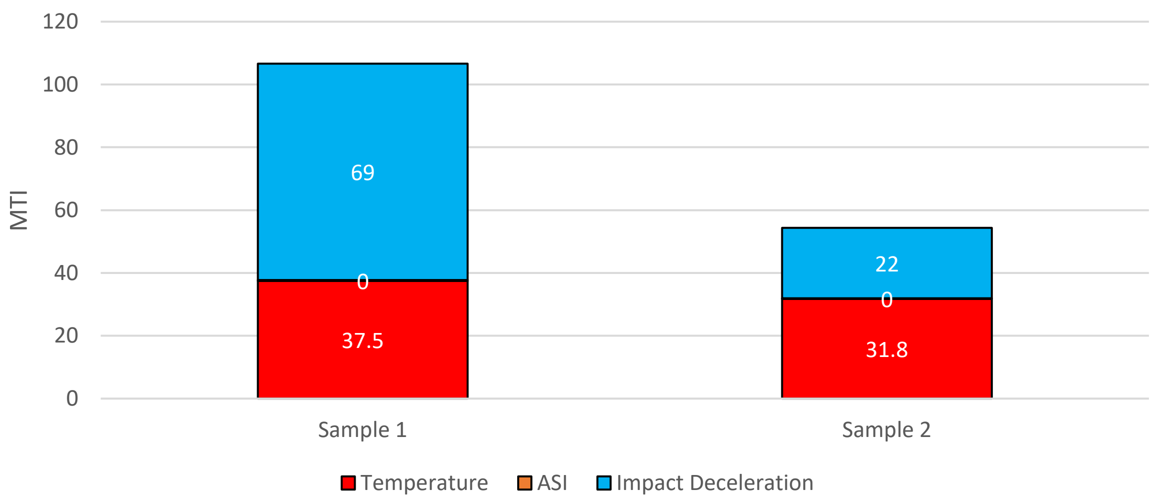

Figure 6-28: MTI: Assessing Risk of Skin Injuries on Non-filled Systems.

Figure 6-29 presents an overview of all surfaces tested in this section with the dashed lines representing the upper and lower boundaries of the 3G systems evaluated in the previous sections. The only MTI score which falls between the upper and lower boundaries was the dry and firm hybrid.

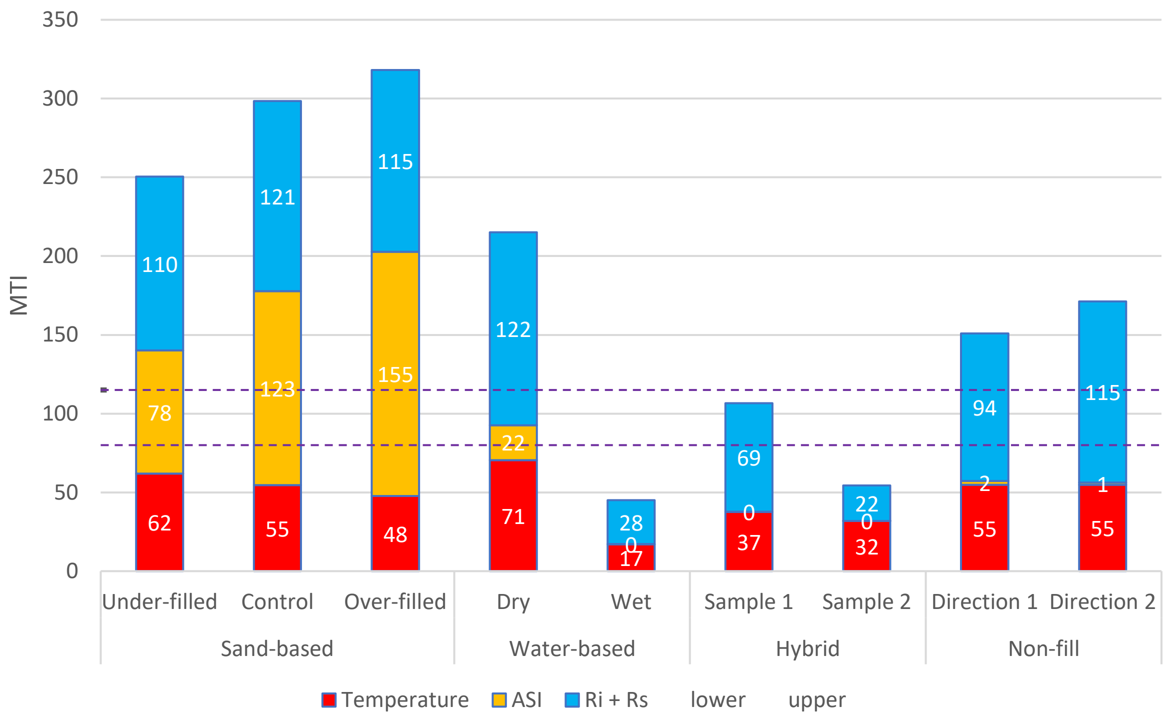

Figure 6-29: Overview of skin injury risk on alternative sports surfaces.

6.4.3 Discussion

Second Generation

The findings on the sand-based 2G surface are significant. The ASI (Figure 6-15) showed a clear positive relationship with infill quantity, while temperature (Figure 6-14) demonstrated an inverse relationship. This means that larger quantities of infill material led to more severe abrasions. The lower rate increased the area of exposed yarn, thereby increasing the temperature. The observation of temperature increasing with exposed free pile height was attributed to the variation in kinetic energy. Infill is mobile and free to move; any force it experiences will be transferred to kinetic energy. In contrast, the yarn is rooted within the carpet backing; therefore, any kinetic energy absorbed will be transferred to heat. The results from the water-based surface support this observation, as no sand generated the lowest ASI whilst generating the highest temperatures.

Additional stabilising infill makes the surface stiffer, which was predicted to increase the Impact Resistance. This expected trend was observed when comparing the underfilled sample to the control and overfilled sample (Figure 6-16). However, the Impact Resistance decreased when comparing the control to the overfilled system. This outcome was attributed to the lack of free pile height and loose infill at the top of the sample, which enabled the impactor to slide with the granular infill rolling underneath it. This combination of sliding and rolling reduced the consistency of the impact, as highlighted by the larger error bars. The influence of additional infill was also observed in the Slide Resistance (Figure 6-17), as the sliding and rolling could be described as a ball-bearing effect. The phenomenon, combined with reduced surface contact area with the constrained yarns, decreases the slide resistance. Both trends observed in Impact and Slide Resistance agree with the findings from Section 6.2. Furthermore, the infill rolling under the knee form could produce greater shear forces at the microscopic asperity level, which explains the increased ASI scores with additional infill.

Hybrid

Speaking to colleagues working for ProPitch, a natural grass consulting company, highlighted that TDR results for Sample 1 (8.3±1.4%) were lower than the desired 15-25% (Kennelly, 2015). A review of the AAA results also highlighted that the force reduction (39.2±1.2%) results were lower than the desired requirements set by FIFA [161]. The firmness of this surface was attributed to the low moisture content and lack of root zone that would be found in situ. Therefore, retrospective testing was conducted with an artificial root zone, which consisted of a 50 mm sand layer retained by a wooden frame. The function of the wooden frame was to prevent sand from displacing under pressure from the hybrid or forces during impact. The second sample was going to be irrigated on the morning of testing to address the issues of surface moisture. However, overnight rainfall negated this need as Sample 2 exhibited higher moisture levels (20.2±1.8%). The higher moisture content and artificial root zone reduced the surface's stiffness (force reduction - 55.4±1.4%).

The distinct differences in surface moisture levels and impact absorption capabilities between the two hybrid turf samples translated well to the Impact and Slide Resistances (Figure 6-21and Figure 6-22). As expected, the firmer surface generated higher impact decelerations, while the surface with the higher moisture content reduced slide resistance. Meanwhile, the dryer surface produced the highest peak temperatures.

Peppelman et al. (2013) [128] reported a higher risk of injury on dry grass compared to natural turf, a finding that aligns with the MTI scores (Figure 6-23). Despite the dryer and firmer surface generating a statistically greater ASI score, the skin damage on both surfaces was minimal. The lack of skin damage could be attributed to the natural properties of grass, which will assist in reducing skin injury risk. On impact, the structure of the grass fibres could be compromised, resulting in moisture released from the insides, forming a boundary lubrication layer. Additionally, natural grass fibres are not constrained within the system as strongly as artificial fibres. Therefore, if they experience a significant force, they will be pulled out of the surface without much resistance. This theory was apparent on some tests when the impactor was lifted to return the carriage to the launch position, and a clump of grass would fall off the impactor. These observations further contribute to the theory that the infill material influences skin abrasion most.

Non-fill

Tay et al. (2015) [94] reported that peaks and troughs on the Securisport waveform were attributed to the impactor sliding against and with the grain. Analysis of the Impact Resistance and Slide Resistance would imply that the second direction was against the grain. This finding agrees with the order in which the assistant laid the carpet, which implies that the device has suitable sensitivity for detecting the orientation of the yarn. Against the grain produced statistically greater impact and slide resistances, which was attributed to the orientation of the fibre interlocking with the texture of the skin and resisting the motion of the simulated player as it folded over on itself. In contrast, the fibre collapses when sliding with the grain, reducing the resistance. Overall, the non-filled systems produced the greatest slide resistance. This result was attributed to the lack of infill; therefore, the knee effectively slid across a polymer sheet. This outcome implies that the infill enhances sliding conditions by providing a mobile interface between the knee and the constrained fibres.

Interestingly, the orientation of the carpet did not influence the peak temperatures generated during the interaction. This result was attributed to the lack of infill, which would not be displaced. Therefore, there was a consistent temperature build-up in both directions. Greater peak temperatures were observed on the dry 2G (Figure 6-14), compared to the non-fill (Figure 6-24). This result was attributed to the thatch. The thatch acts as a sponge to assist impact attenuation. However, the air within the thatch will act as an insulator. Additionally, the thatch will compress as the simulated player slides over the surface. Therefore, kinetic energy is dissipated as the thatch compresses and returns to its original position. In combination the insulating air and kinetic energy dissipation reduces the peak temperatures.

Again, the lack of a significant Abrasion Zone contributes to the theory that the infill material is more abrasive than the smooth yarn fibres. Despite the apparent lack of abrasion, the MTI still ranks non-fill surfaces relatively high. This rating was attributed to the highest Slide Resistances and associated temperatures. During a player-surface interaction on non-fill, the player may be more susceptible to sustaining a burn than mechanical abrasion.

6.4.4 Conclusion

The results from this section contribute to our understanding of skin injury risk across a range of alternative sports surfaces. As anticipated, the sand-based and dry 2G systems yielded MTI scores significantly higher than those of a 3G system. A soft hybrid system, however, produced similar MTI scores to the irrigated hockey surface, indicating a low injury risk. Non-filled systems fell between 2G and 3G in MTI scores, suggesting further innovation is required before they can be considered skin-friendly alternative sports surfaces. Dry grass has been reported in the literature to be more harmful than natural turf, a finding that aligns with our MTI scores. The minimal skin damage observed on the hybrid and non-filled systems suggests that Lorica Soft is very durable. However, the MTI compensates for this by including a global assessment of surface resistance. This is a crucial factor as without it, the wet 2G, hybrid, and non-filled surfaces would yield significantly smaller MTI scores (Figure 6-29), emphasising the importance of considering surface resistance to effectively evaluate skin injury risk on artificial turf.

6.5 Evaluating the Repeatability of Inter-Operator Variation

In 2025, World Rugby plans to update its turf performance specifications, Regulation 22, the result will be the inclusion of SID into the quality testing programme. To ensure industry acceptance and approval of the new test method, the key stakeholders were regularly updated on the project's progress and offered multiple opportunities to provide feedback. This study aimed to provide the Accredited Test Institutes (ATI) with hands-on access to evaluate and scrutinise the device while assessing the repeatability of the procedures performed to complete the skin injury risk assessment across different operators. Given the inevitable ban of SBR [90], this study also aimed to evaluate the risk of skin injury on cork, a popular alternative infill, to establish the possible knock-on effects of banning SBR.

6.5.1 Materials and Methods

World Rugby selected four ATIs (University of Ghent, Institute of Biomechanics Valencia (IBV), Labosport, and Sports Labs) to participate in this repeatability study. Each ATI completed the skin injury risk assessment on four turf systems throughout the two-day study. These surfaces were designed to explore the effects of fibre length (45 vs 60 mm) and infill type (SBR vs Cork).

Before the event commenced, all carpets were cut to size (4 x 1 m). Drainage holes on the carpet backing were sealed to prevent infill leakage. To compare the influence of filling techniques, Sports Labs' technicians prepared eight 60 mm samples with a stitch gauge of 63 and a stitch rate of 128 per meter, using SBR (1.0-2.5mm) and Cork (1.25-2.5mm) for all four ATIs. Concurrently, each ATI prepared their own 45 mm samples with a stitch gauge of 63 and a stitch rate of 140 per meter. All carpets were secured to a 10mm prefabricated foam shock pad. The 60 mm samples were filled with 30 kg/m^2 of sand, followed by 11 kg/m^2 and 4 kg/m^2 for SBR and Cork, respectively. In comparison, the 45 mm samples were filled with 22.5 kg/m^2 of sand, followed by 8 kg/m^2 and 3 kg/m^2 for SBR and Cork, respectively.

Once filled with sand, infill depths were recorded at three evenly spaced locations across the width of the sample. Recordings were repeated six times (0.5m apart) along the length to create 18 measurements. Once filled with performance infill, the samples were conditioned cycled five times with a 90kg studded roller following FIFA Test Method 15.

Then, infill depths and free pile heights were recorded at the same locations. Figure 6-30 illustrates the tested surfaces' average infill depths and free pile heights. Following system construction, performance test results were collected with Sports Labs' lightweight impact attenuation device (3 drops on 6 locations) - Table 6-6.

Table 6-6: Impact Attenuation Results from the Field Marshal

AVG	SBR (60)	SBR (45)	Cork (60)	Cork (45)
FR	69.16 ± 0.22	66.78 ± 0.12	70.54 ± 0.30	69.00 ± 0.20
VD	10.47 ± 0.11	9.38 ± 0.03	10.23 ± 0.11	9.64 ± 0.05
ER	35.16 ± 0.21	37.71 ± 0.27	24.07 ± 0.29	27.11 ± 0.19

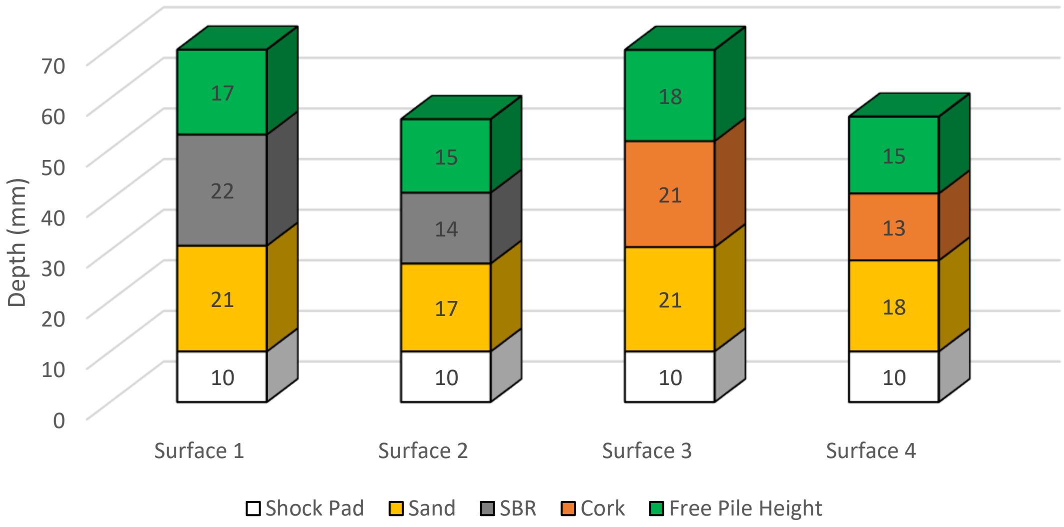

Figure 6-30: Illustration of samples tested during repeatability study.

Before testing, the thermal camera position was calibrated by placing two thermally reflective items on the turf. The first location was centrally located within the gantry 1m from the front of the turf sample, and the second item was placed 2m from the first location. The first item was used to locate the impact zone, and the second was used to ensure that the camera was square with the frame to monitor the sliding phase, ensuring the full heat profile was recorded by the thermal camera.

The skin injury risk assessment consisted of five launches, and each test was performed on a fresh impact location. The first impact location was 100 mm from the edge of the turf, and subsequent test locations were established by moving the frame laterally across the sample to a minimum of 150 mm. The knee form was released from 0.5 m to achieve a vertical impact velocity of ~ 3 m/s. The impactor was placed on the impact zone to set the release height, and a calibrated set length was used to offset an electromagnet. Rollercoaster technology, in the form of a linear induction motor, was utilised to generate a horizontal impact velocity of 5 m/s. A bespoke LabVIEW programme processed the accelerometer data during each launch to calculate the Kinematic Injury Metrics (KIM). After five launches, the skin was removed, and the Abrasion Zone was evaluated as described in Section 6.1.1.

The investigation into MTI validity was carried out by a panel of ten highly experienced synthetic surface experts. These experts, each with at least five years of experience within the 3G synthetic surface sector, were presented with the technical specifications and photographs of the four compositions. They were asked to rank them based on the likely skin injury risk. The experts were blinded to each other and to the data from the apparatus. The final ranked order was determined by calculating the mean score for each surface.

Statistical Analysis

Statistical analysis assessed repeatability across the 4 teams and then across the 4 samples. A Shapiro–Wilk test was conducted to assess the normal distribution of each metric. Based on these results, either a parametric test (one-way analysis of variance (ANOVA)) or a non-parametric test (Kruskal–Wallis test) was chosen. Post hoc Tukey's t-tests were conducted after the ANOVA test for further analysis. All statistical analyses were performed using SPSS, adopting a significance threshold of $p < 0.05$.

6.5.2 Results

Five tests were performed on all 3G (i.e., SBR and cork) samples. A total of 80 datasets were recorded, though twelve were excluded as they were from tests that exceeded the tolerance for vertical (four) and horizontal (eight) velocities (5.0 ± 2% m/s and 2.9.5 ± 5% m/s, respectively). Five files were found to be corrupted, leaving a total of 63 valid datasets. The consistency of the impact conditions was demonstrated in Figure 6-31, where the origin represents the desired velocities. Once anomalous data was removed, ANOVA tests were performed independently on the horizontal and vertical axis, highlighting no statistical differences ($p > 0.05$) between the five samples.

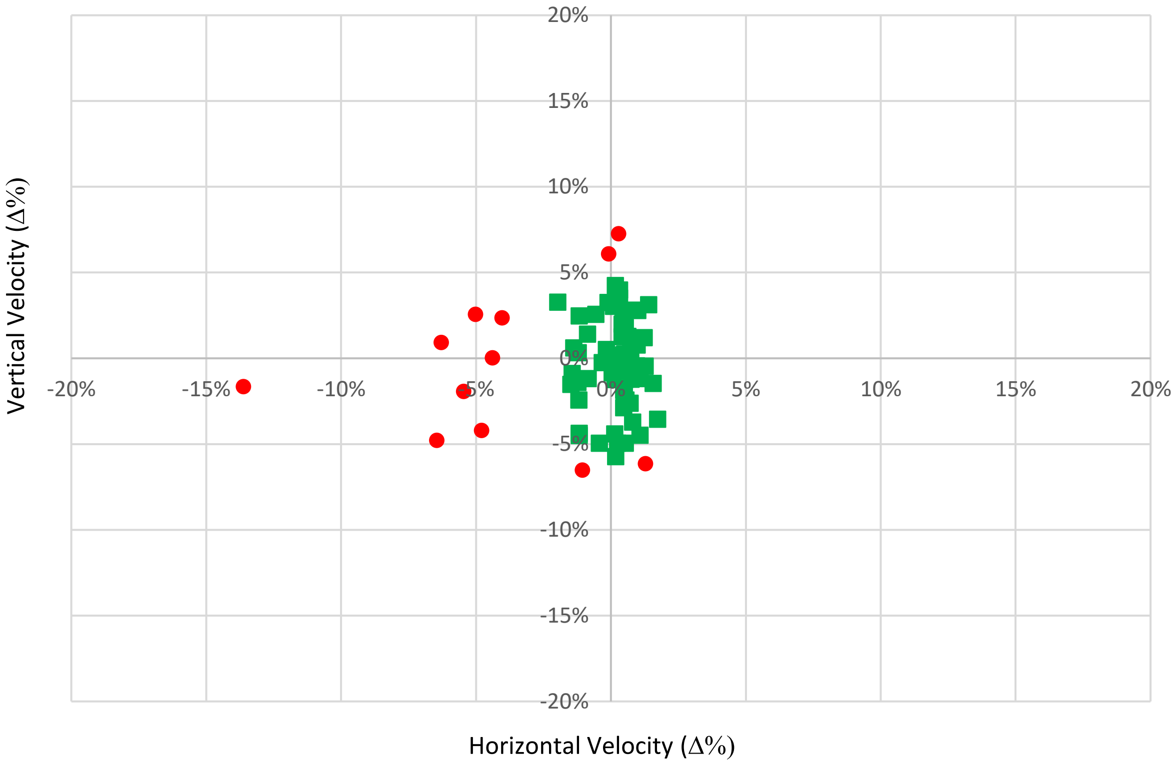

Figure 6-31: Illustration of the deviation of impact velocities from the desired horizontal (5 m/s) and vertical (2.95 m/s) values during shock pad testing.

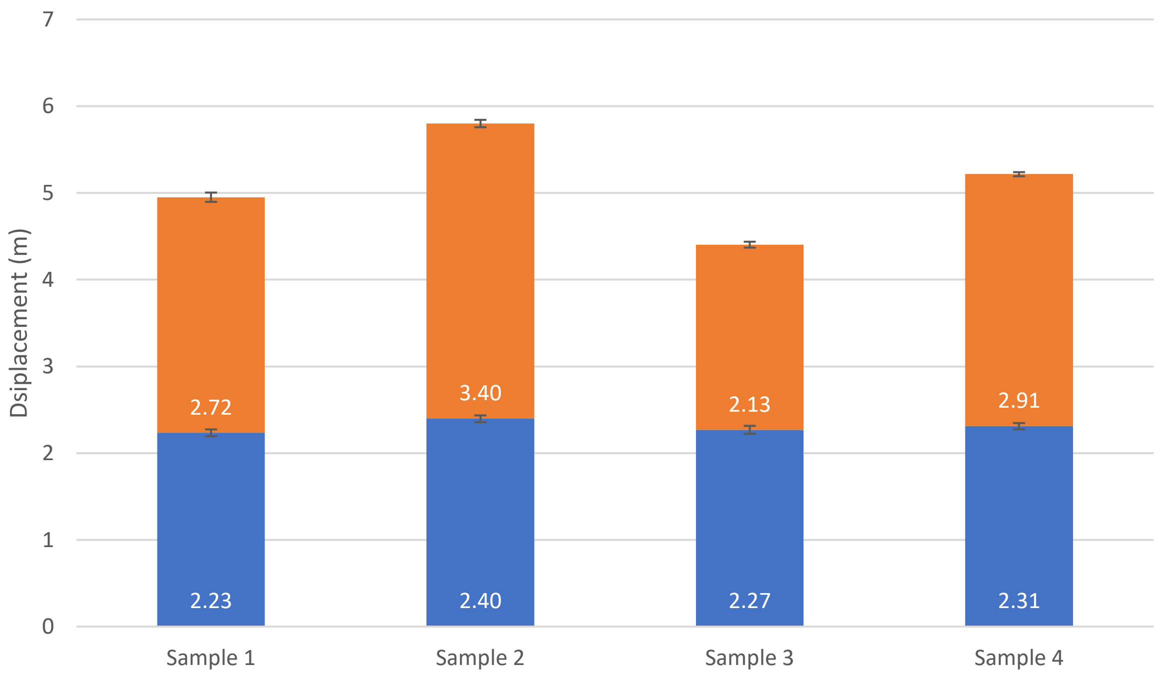

Figure 6-32: Comparison of Slide to Rest (blue – experimental | orange – theoretical) during shock pad testing.

Table 6-7: Analysis of variance results highlighting consistency of the impact conditions and subsequent sliding phase displacements (mean ± S

Parameter	System	Test Iteration				Statistics		
		1 (n=5)	2 (n=5)	3 (n=5)	4 (n=5)	F	p	
Horizontal Velocity (m/s)	1	4.93 ± 0.01	5.03 ± 0.01	4.98 ± 0.03	4.95 ± 0.01	5.28	0.02	1/2, 2/4
	2	5.02 ± 0.01	5.04 ± 0.01	5.01 ± 0.00	5.01 ± 0.01	1.26	0.32	-
	3	5.04 ± 0.01	5.03 ± 0.02	5.02 ± 0.01	4.95 ± 0.01	10.70	0.00	2/4, 3/4
	4	5.03 ± 0.02	5.01 ± 0.00	5.03 ± 0.01	5.03 ± 0.01	0.38	0.77	-
Vertical Velocity (m/s)	1	2.91 ± 0.04	2.90 ± 0.03	2.93 ± 0.03	2.90 ± 0.01	0.38	0.77	-
	2	2.86 ± 0.05	2.84 ± 0.02	2.98 ± 0.07	2.96 ± 0.04	2.49	0.10	2/4
	3	2.86 ± 0.03	2.86 ± 0.07	2.93 ± 0.02	2.79 ± 0.02	2.49	0.11	3/4
	4	2.85 ± 0.04	2.93 ± 0.04	2.86 ± 0.04	2.90 ± 0.06	0.71	0.56	-
Actual Displacement (m)	1	2.20 ± 0.05	2.19 ± 0.03	2.16 ± 0.03	2.38 ± 0.11	2.21	0.14	-
	2	2.32 ± 0.12	2.49 ± 0.06	2.44 ± 0.00	2.36 ± 0.04	1.02	0.41	-
	3	2.17 ± 0.04	2.31 ± 0.14	2.30 ± 0.09	2.29 ± 0.09	0.48	0.70	-
	4	2.35 ± 0.07	2.19 ± 0.01	2.34 ± 0.09	2.39 ± 0.07	2.04	0.16	2/4
Expected Displacement (m)	1	4.90 ± 0.11	5.01 ± 0.12	4.96 ± 0.07	4.95 ± 0.02	0.29	0.83	-
	2	5.85 ± 0.10	5.81 ± 0.07	5.98 ± 0.08	5.63 ± 0.06	2.64	0.09	3/4
	3	4.32 ± 0.09	4.53 ± 0.18	4.36 ± 0.08	4.41 ± 0.09	0.67	0.58	-
	4	5.25 ± 0.05	5.14 ± 0.02	5.22 ± 0.10	5.27 ± 0.04	1.21	0.34	-

Mean Peak Temperature, T_{p}.

The temperature measurements were acquired by a mounted thermal camera, collecting data along the length of travel. The median temperatures range from 24 °C to 28 °C across the four surfaces (Figure 6-33). The 60 mm pile carpet recorded the highest median value, whilst the shortest recorded the greatest variation in all surfaces. A Shapiro–Wilk test confirmed a non-normal distribution ($p < 0.05$), and a Kruskal–Wallis test assessed repeatability (the same surface measured by different teams) and validity (when combined to form the MTI, as compared to the expert panel). Table 6-9 describes strong repeatability across all measures, and Table 6-10 highlights a statistical difference between surfaces.

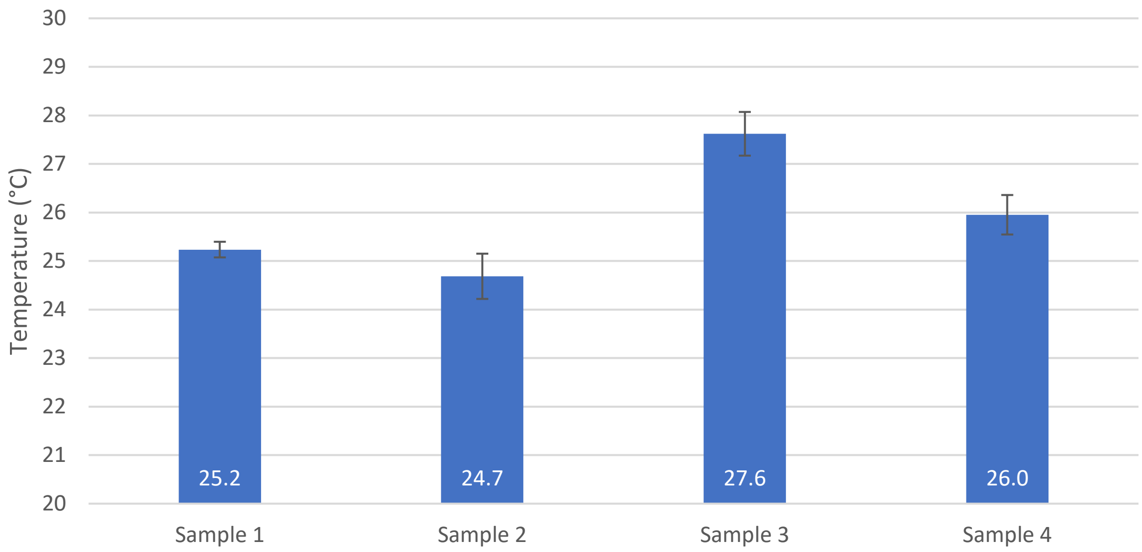

Figure 6-33: T_p reported from 20 tests on each surface. The median temperature ranged from 24–28 °C across the four surfaces, with the error bars greatest for the surfaces using cork infill (Surfaces 3 and 4). All surfaces were statistically different except for Surface 1 and 4.

Abrasion Severity Index, ASI:

The ASI is calculated as per Equation 43, combining the abrasive wear on the Lorica Soft sample with areas of infill material transfer. The ASI magnitudes were significantly different between the cork (Surfaces 3 and 4) and SBR (Surfaces 1 and 2) surfaces (Figure 6-34). The variation in data was minimal, except for the long-pile cork surface. The lack of outlying data does, however, indicate relatively high repeatability across each of the 20 tests. The ASI score per surface represents the wear accumulated over five tests, though it limits statistical analysis (Figure 6-34). Table 6-10 demonstrates that cork infill yielded significantly higher ASI scores ($p < 0.05$) compared to SBR infill.

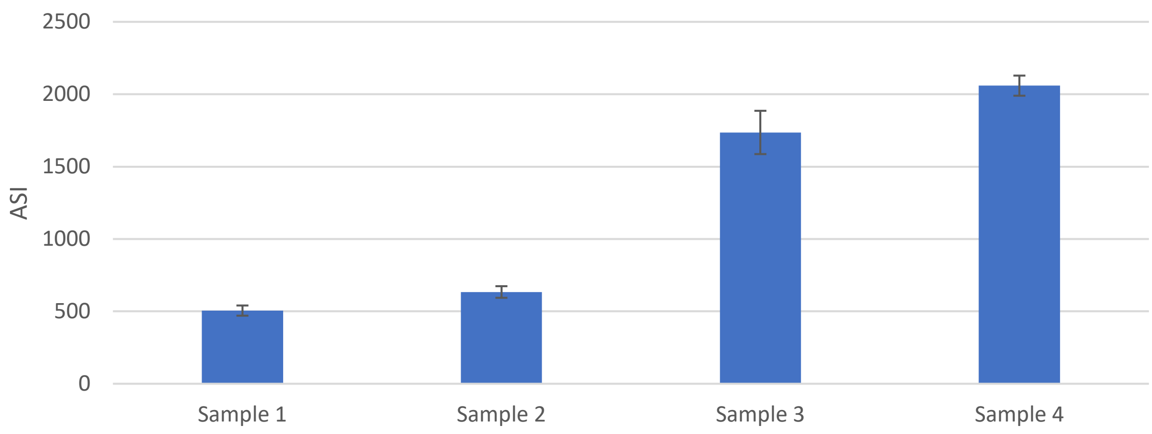

Figure 6-34: ASI reported from 20 tests on each surface. Magnitudes varied significantly between SBR (Surfaces 1 and 2) and cork (Surfaces 3 and 4).

Surface Resistance during Impact, R_i

The variation in R_i highlighted how the impactor experienced resistance to sliding during the initial contact (Figure 6-34). A Shapiro–Wilk test confirmed a normal distribution ($p > 0.05$). Consequently, an ANOVA test was conducted to assess repeatability among the teams and across the four surfaces. Table 6-10 shows that Team 3 produced less repeatable results; however, despite this variability, Tukey's post hoc tests detected significant differences across all surfaces. Surface 2 reported the greatest range in data, whilst the other short-pile carpet, Surface 4, had the greatest range among those with cork infill. This is possibly caused by the impactor penetrating the relatively thin layer of infill, engaging with the underlying sand and potentially causing it to 'plug' like a golf ball landing on soft ground, thus causing a more rapid deceleration.

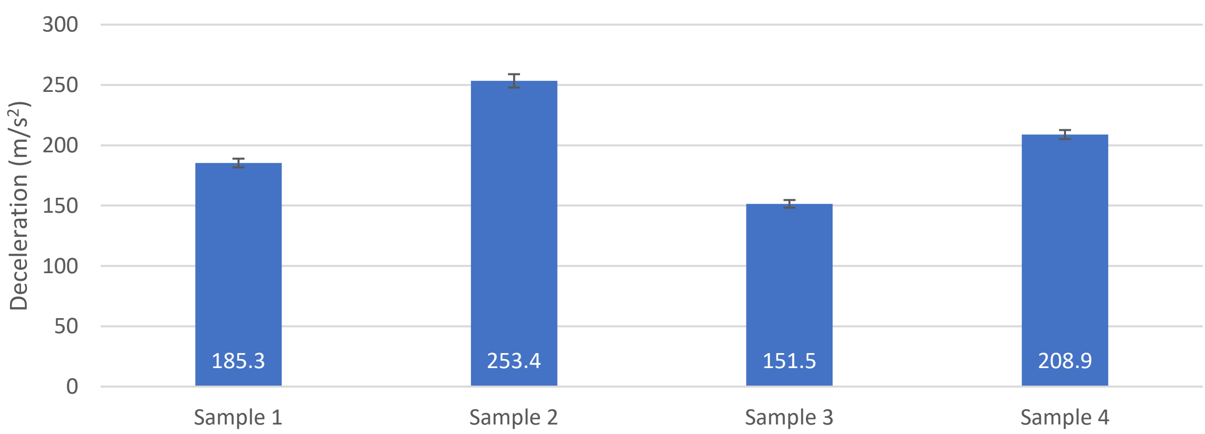

Figure 6-35: R_i reported from 20 tests on each surface. Cork (Surface 3 and 4) exhibited lower impact decelerations than SBR (Surface 1 and 2). Concurrently, additional performance infill (Surface 1 and 3) reduced surface resistance. All surfaces were statistically different.

Surface Resistance during Sliding, R_s

R_s is much lower than Ri, which is considered a positive attribute of 3G surfaces (Figure 6-36). High deceleration would indicate an abrasive interaction, potentially caused by a 'locked or bound' infill and carpet pile or when testing early-generation surfaces, which have a very thin infill layer, causing abrasion against the very short (~10 mm) carpet pile. The low standard error indicate that this method produced repeatable data, except for some outliers associated with the cork surfaces. A Shapiro–Wilks test confirmed a non-normal distribution ($p < 0.05$). Subsequently, a Kruskal–Wallis test was conducted to assess variation across the teams and surfaces. Table 6-9 demonstrates repeatable data were generated across most surfaces, whilst Table 6-10 again highlights statistical differences between surfaces.

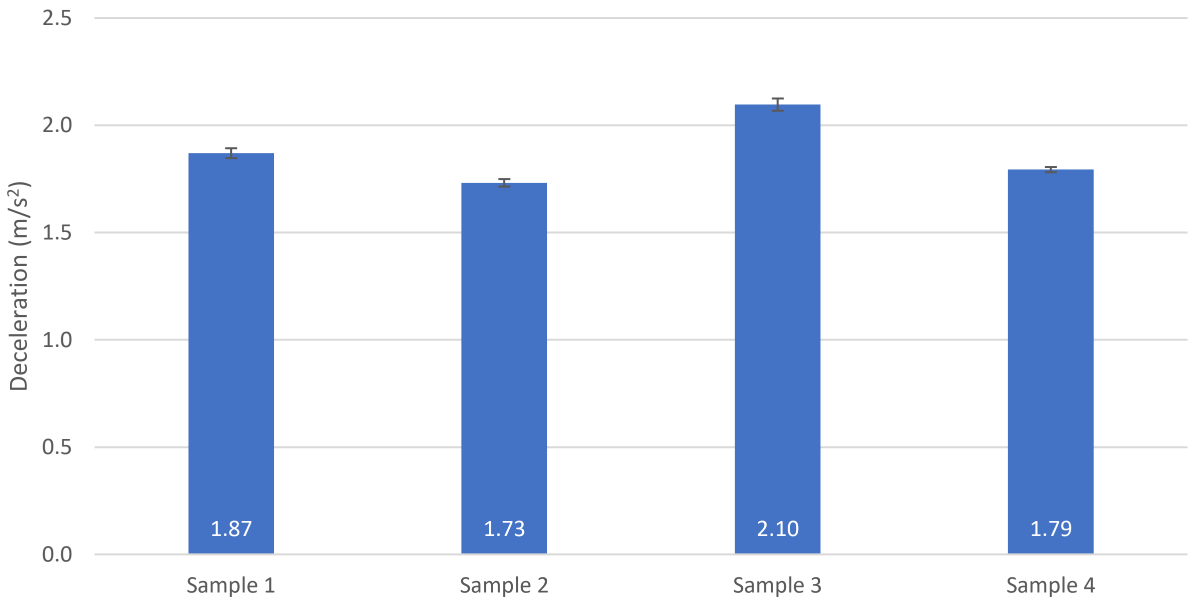

Figure 6-36: R_s reported from 20 tests on each surface. SBR (Surface 1 and 2) exhibited lower slide resistance than cork (Surface 3 and 4). Concurrently, additional performance infill (Surface 1 and 3) increased surface resistance. All surfaces were statistically different except for Surface 1 and 4.

Maxwell Tribo Index, MTI

The MTI weights and then summates the above parameters as per Equation (2), providing a single metric that describes relative injury risk. The composition of each MTI value is described in Figure 6-37. Surface 4—the shortest-pile, cork-filled surface—was identified as being the most likely to cause skin injury. Abrasion was considered the greatest contribution to this risk; indeed, both cork surfaces presented a far greater abrasion score than those filled with SBR, where it was reduced to a minor contribution. T_p was broadly common across all four surfaces and was always lower than the critical injury threshold. Surface 2 had the greatest R_i value, potentially due to plugging in the sand ballast, with this relatively high score reflected in a high R-value. The overall ranking for Surface 2 is still low; however, due to the small abrasion contribution. Surface 1, the 60 mm pile carpet filled with SBR and the traditional composition for Rugby Turf, is considered to represent the lowest skin injury risk.

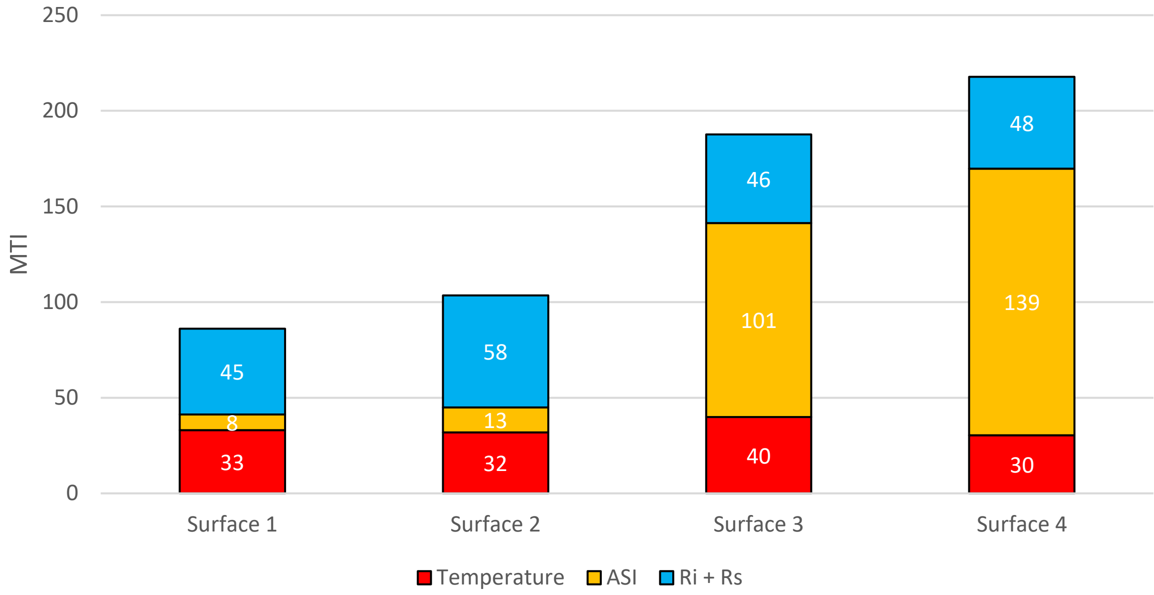

Figure 6-37: MTI reported from 20 tests on each surface. All surfaces were statistically different expect from Surface 3 and 4.

Expert Panel Survey

Ten Experts were recruited, with a combined 185 years' experience in synthetic surfaces. They ranked the 4 surfaces as per Table 6-8, with the mean values calculated to produce the overall ranking.

Table 6-8: Results from the Expert review panel, describing their individual assessment of injury risk for each synthetic turf composition. The final ranking was determined by calculating the mean score for each surface.

	Skin injury likelihood: least (1) to most (4) injurious			
	Surface 1	Surface 2	Surface 3	Surface 4
Expert 1	1	2	3	4
Expert 2	1	3	2	4
Expert 3	1	3	2	4
Expert 4	1	2	3	4
Expert 5	1	2	3	4
Expert 6	1	3	2	4
Expert 7	2	1	4	3
Expert 8	1	2	3	4
Expert 9	1	2	3	4
Expert 10	1	3	2	4
Mean score	1.1 ± 0.1	2.3 ± 0.2	2.7 ± 0.2	3.9 ± 0.1

MTI Validation

Directly comparing the blinded rankings of the Expert Panel with those of the MTI provided a route to exploring the validity of this new methodology. The direct correlation evident in

Figure 6-38 demonstrates successful validation, with those surfaces that the expert panel failed to rank unanimously also coinciding with relatively similar MTI values, indicating strong measurement sensitivity.

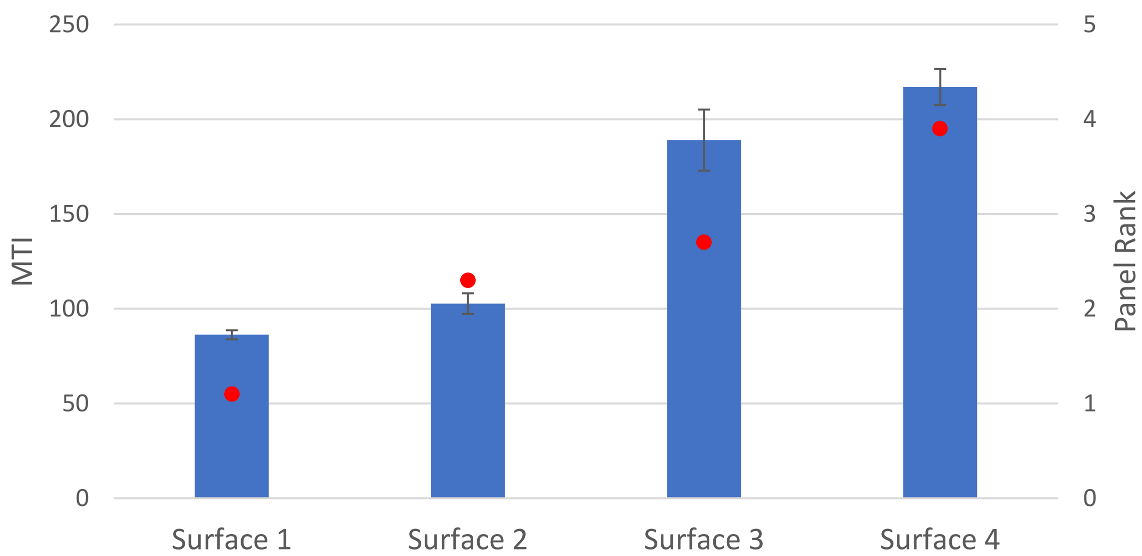

Figure 6-38: Demonstrating a positive correlation between the MTI and the Expert group rankings.

Table 6-9: Inter-operator Repeatability Testing - Statistical analysis demonstrating device repeatability across the 4 Teams (mean ± SE)

Parameter	Surface	Operator				Statistics		
		1 (n=5)	2 (n=5)	3 (n=5)	4 (n=5)	F	P	
Temperature [°C]	1	25.3 ± 0.2	25.0 ± 0.2	25.1 ± 0.1	25.6 ± 0.2	0.39	0.76	-
	2	23.7 ± 0.3	23.3 ± 0.2	24.5 ± 0.1	27.5 ± 0.8	3.31	0.05	2/4
	3	27.8 ± 2.1	28.4 ± 0.2	28.2 ± 0.3	26.8 ± 0.6	0.5	0.69	-
	4	24.6 ± 0.1	26.0 ±0.5	25.9 ± 0.6	27.2 ± 0.3	1.52	0.25	-
Abrasion Severity Index	1	591	493	452	516			
	2	713	653	522	647			
	3	1719	1318	2112	1733			
	4	1966	2136	2215	1921			
Impact Deceleration [m/s^2]	1	195.9 ± 3.1	196.6 ± 5.4	169.9 ± 4.6	181.8 ± 5.6	7.28	0.01	1/3, 2/3
	2	269.3 ± 10.1	242.6 ± 7.6	226.4 ± 11.5	264.7 ± 6.1	4.59	0.02	1/3, 3/4
	3	162.1 ± 3.2	143.9 ± 4.0	153.3 ± 4.3	146.2 ± 10.2	1.82	0.19	1/2
	4	207.6 ± 8.3	219.4 ± 4.0	201.3 ± 9.2	205.1 ± 7.7	1.16	0.36	-
Slide Resistance [m/s^2]	1	1.87 ± 0.04	1.94 ± 0.03	1.87 ± 0.06	1.81 ± 0.02	1.39	0.03	2/4
	2	1.70 ± 0.02	1.72 ± 0.03	1.75 ± 0.02	1.76 ± 0.05	0.69	0.57	-
	3	2.17 ± 0.03	1.97 ± 0.08	2.12 ± 0.02	2.13 ± 0.05	3.19	0.06	-
	4	1.80 ± 0.02	1.78 ± 0.01	1.78 ± 0.04	1.81 ± 0.04	0.48	0.7	-

Table 6-10: Inter-operator Repeatability Testing - Statistical analysis differentiation between synthetic surfaces

Parameter		Surface	1	2	3	4
	Surface	Average	25.3 ± 1.2	24.8 ± 0.7	27.8 ± 0.5	25.9 ± 0.4
Temperature [°C]	1	25.3 ± 1.2	-	-	-	-
	2	24.8 ± 0.7	**0.05**	-	-	-
	3	27.8 ± 0.5	**0.02**	**<0.01**	-	-
	4	25.9 ± 0.4	0.95	**0.04**	**0.02**	-
Abrasion Severity Index	Surface	Average	513 ± 29	634 ± 280	1721 ± 162	2060 ± 69
	1	513 ± 29	-	-	-	-
	2	634 ± 280	0.79	-	-	-
	3	1721 ± 162	**<0.01**	**<0.01**	-	-
	4	2060 ± 69	**<0.01**	**<0.01**	0.09	-
Impact Deceleration [m/s²]	Surface	Average	185.3 ± 3.5	253.4 ± 5.5	149.8 ± 3.4	204.4 ± 4.6
	1	185.3 ± 3.5	-	-	-	-
	2	253.4 ± 5.5	**<0.01**	-	-	-
	3	149.8 ± 3.4	**<0.01**	**<0.01**	-	-
	4	204.4 ± 4.6	**<0.01**	**<0.01**	**<0.01**	-
Slide Resistance [m/s²]	Surface	Average	1.87 ± 0.02	1.73 ± 0.02	2.10 ± 0.03	1.79 ± 0.01
	1	1.87 ± 0.02	-	-	-	-
	2	1.73 ± 0.02	**<0.01**	-	-	-
	3	2.10 ± 0.03	**<0.01**	**<0.01**	-	-
	4	1.79 ± 0.01	0.13	**0.05**	**<0.01**	-

6.5.3 Discussion

This study achieved consistent impact velocities across a range of surfaces (Figure 6-31). The central cluster of data points fell within the tolerances of 5.0 ± 2% m/s and 2.9 ± 5% m/s for the horizontal and vertical velocities, respectively. No test iterations generated a horizontal velocity greater than the desired values. However, there were eight tests which fell below 4.9 ms^{-1}. These outliers were attributed to a timing issue generated by new operators using the two-way authentication. To accommodate this observation, the timer's delay was increased to help achieve the desired impact velocity. This alteration, combined with the operators becoming more proficient at the test method, improved the repeatability of the launch conditions throughout this study. Once these anomalous tests were removed, no statistical differences were identified by an ANOVA test, which provided confidence in the horizontal propulsion system.

One of the main points of feedback from the ATIs was to improve the calibration of the release height, which has since been changed to incorporate a fine and coarse adjustment. Further testing will be required to establish if the 5% tolerance can be reduced to align with the smaller tolerance achieved by the LIM. The ANOVA (Table 6-9) highlights that testing was most repeatable on Surface 4. Weaker repeatability was evident across Surfaces 1–3. This may be caused by the lower-volume, lighter infill of Surface 4 (15 mm cork infill), meaning that surface preparation was easier and more consistent across the four testing teams. Conducting inferential statistics on the ASI scores was impossible, as each surface was tested only once. This is an area for future research.

The thermal camera detected significant differences across most of the 3G surfaces (Figure 6-33, Table 6-10), with cork-based infills typically generating higher temperatures, this agrees with data reported by Labosport [286]. ASI data showed good repeatability, with small standard deviations across most surfaces (Figure 6-34, Table 6-10). The variation in ASI and, indeed, the damage to the skin simulant varied significantly across the four surfaces and was particularly pronounced with the cork infill. The maximum temperature generated was 32.7°C. This magnitude was insufficient to induce thermal damage. Therefore, a skin injury on these surfaces in laboratory conditions is more likely to be a mechanical abrasion rather than a burn.

Visual inspection of the skin damage (Appendix 36 -Appendix 39) revealed intriguing findings. The characteristics of each lesion were consistent across the four repeated tests, instilling confidence in the test method's repeatability with different operators. Surface 1 exhibited typical light-coloured abrasions with SBR material transfer surrounding the leading and trailing edges. In contrast, Surface 2 presented a notably interesting feature where material transfer dominated the lesion. Despite both surfaces being filled from the same tonne bag, this phenomenon was attributed to the infill at the bottom of the bag being covered in more plasticiser dust than the fresh infill at the top. Although Surface 2 produced less intense abrasion, the affected surface area was larger, and the resultant polishing effect could still cause discomfort to a player. This observation underscored the need to quantify the difference between the dark and light regions on the lesion.

Surfaces 3 and 4 generated light-coloured abrasions at the apex of the knee geometry, with minimal trailing abrasion along the length of the knee. The lesion on Surface 4 appeared broader and longer than on Surface 3. A comparison of ASI scores and fibre length highlighted that more intense skin damage occurred on the short pile surfaces; however, no statistical difference was found (Figure 6-34). This result was unsurprising, given that the materials were consistent and the only surface variables were the fibre length and infill rates. The skin damage on the cork samples exhibited greater surface roughness compared to the SBR surfaces. The ASI statistically detected this difference, bolstering confidence in its ability to differentiate skin damage across different infill types.

The variability in the impact resistance results suggests Team 3 required additional training; however, the enhanced repeatability by the end of our study indicates that all teams became proficient in executing the test method (Table 6-9). Analysis of the impact and slide resistances highlighted that these injury metrics exhibited an inverse response when varying fibre length and infill type. For example, larger volumes of performance infill enhance impact attenuation, which reduces Impact Resistance (Figure 6-35). ASI scores were expected to increase with Impact Resistance; however, this theory holds true only when comparing surfaces with the same infill material. SBR, a synthetic material, is highly elastic and quickly recovers upon impact. In contrast, cork, a natural material with a complex cellular structure consisting of hollow chambers [287], exhibits lower compressibility and promotes internal dampening. This internal dissipation converts a proportion of kinetic energy into heat and vibration, resulting in the cork's lower Impact Resistance compared to SBR and explaining the increased temperature.

In contrast, the additional infill adversely affected the Slide Resistance (Figure 6-36). This outcome contradicts the findings from Sections 5.6.2 and 6.1.2, which reported that additional infill increased the ball-bearing effect to assist sliding. However, in those studies, the surface with shorter fibre length also had greater turf density, contributing to greater Slide Resistance. In contrast, this study evaluated four systems with similar turf densities. Despite attempting to construct systems with consistent free pile heights, the 60 mm surfaces were slightly longer. This variation elevated the Slide Resistance compared to the 45 mm surfaces. In combination, these observations of surface resistance confirm that artificial turf's behavioural response is complex; therefore, no single parameter is directly linked to skin damage.

An in-depth analysis of the properties of infill materials could elucidate the complex behavioural responses observed. Organic materials, such as cork, have smaller bulk densities and exhibit lower energy restitution than polymeric infills [288][258]. Lightweight granular infill with reduced energy restitution preserves less energy after a collision, reducing Impact Resistance. Momentum of the simulated player drives the impactor across the turf sample, this causes a pressure bulb to form at the leading edge of the knee form. The density of the infill influences how this force propagates through the sample and the extent of the resultant infill displacement.

Lower-density materials, such as cork (130 kg/m^3), generate more displacement as they are lighter and require less force to overcome inertia. Additionally, a material's elasticity affects infill displacement. SBR (400 kg/m^3) exhibits higher elasticity, leading to localised deformation before displacement begins. In contrast, the stiffer cork compresses less, resulting in immediate displacement that ripples into adjacent infill particles. This creates a path of least resistance for the knee form to travel through whilst in the Impact Zone, contributing to the cork's lower Impact Resistance.

The shape of the infill will also influence how it behaves as the knee slides over it. Sports Labs follows the British Standard EN 14955 to determine the particle shape for all infills used in product testing. The method quantifies the geometry (A—angular, B—irregular, C—round) and sphericity (1—high, 2—medium, 3—low). The SBR and cork used in this study were attributed to the shape of A2 and A3, respectively. Low sphericity implies that the shape is elongated and flat, making it difficult for the particles to roll over each other. The elongated shape could explain why the cork was more abrasive than the SBR, as the particles will be more likely to embed into the skin as they interact. Meanwhile, an angular shape is described as a developed face with sharp corners, large re-entrants, and numerous small re-entrants. The microtextured asperities will interact as the infill rolls over one another, increasing friction. The combination of an A3 particle will reduce the ball-bearing effect, contributing to the higher Slide Resistance.

This device captured surface temperature, skin abrasion, and surface resistance, values compiled to form the MTI, a single measure of injury risk. The MTI was then used to evaluate and rank four distinct 3G synthetic surfaces. Most of the panel suggested that Surface 1 had the lowest risk of injury while Surface 4 had the highest potential to cause harm. Surface 1 was perceived to be the most skin-friendly due to the additional infill, which was attributed to making the system softer. In contrast, Surface 4 was linked to being the most harmful due to the reduced infill, making the system firmer, and the “rougher” texture of cork, increasing the likelihood of an abrasion. Expert 7 was the only participant who disagreed with this statement, as they believed these systems had a higher risk of injury due to the additional infill with which the player could interact; therefore, there was a greater chance of injury. There were conflicting opinions concerning the differences between Surface 2 and 3. The lack of agreement arose from varying perceptions relating to the benefits of additional infill versus the texture of cork. However, the resultant ranking of the MTI aligns with the expert panel's consensus opinion, demonstrating this new methodology's validity. This congruity of the expert panel and the MTI scores provides confidence for incorporating this test method into Regulation 22; however, further work is required to define an acceptable level of injury.

6.5.4 Conclusion

In this study, consistent impact velocities were achieved across various surfaces, with most data points falling within the desired tolerances. Adjustments improved repeatability, and once anomalies were excluded, no statistical differences were observed in the horizontal propulsion system. Calibration improvements addressed vertical velocity variations. Overall, the ATI effectively adopted the test method, producing consistent impact conditions and test results across all four surfaces.

Thermal imaging revealed significant temperature differences across 3G surfaces, with cork-based infills generating highest temperatures, though not enough to cause thermal damage. ASI data showed good repeatability, with small standard deviations across most surfaces. The variation in ASI and the damage to the skin simulant varied significantly across the four surfaces, particularly pronounced with the cork infill, demonstrating the ASI's accuracy in quantifying these variations.

Quantifying surface resistance (Ri, Rs) provided additional insight into the deceleration profiles associated with each turf and each player–surface interaction. Ri describes the initial skin–surface contact, typically short in duration with minimal horizontal translation, as the impactor rebounds from the surface. Surfaces generating high Ri values are typically ineffective at absorbing energy due to less elastic infill. Surfaces 1 and 3, with the greatest infill, produced the lowest Ri values, likely exposing the skin to the least stress during contact and resulting in minimal injury risk. These surfaces also had longer free pile heights, which elevated Rs. Cork's lower density and elasticity contribute to its lower Impact Resistance. Meanwhile, its particle shape and sphericity also affect infill behaviour, with angular shapes increasing Rs and abrasiveness.

The congruity of the expert panel and the MTI scores provides confidence for incorporating this test method into Regulation 22. World Rugby's commitment to prioritising player welfare will reduce the incidence of skin injuries and foster a more sustainable and long-lasting growth of the sport. With this new technology at their disposal, rugby can confidently embrace artificial pitches, knowing that player safety remains a top priority.

CHAPTER 7

Summary of Findings and Conclusions

SKIN INJURIES

Through interactions during game play in rugby

7.1 Introduction

This chapter concludes the thesis by reviewing each chapter to provide the reader with a summary allowing appreciation of the depth and breadth of the research. Section 7.2 offers a series of abstracts that underscores the novelty and substantial contribution to understanding skin injury risk on artificial turf. The initial aims and objectives were thoroughly evaluated, providing a clear measure of the project's success and instilling a profound sense of accomplishment in the reader. Then, Section 7.3 presents an overview of MTI assessments to demonstrate how the surface system materials and design influenced the device and the MTI metric. Finally, Section 7.4 explores the broader implications of the research, carefully considering, outlining, and extending them beyond the immediate scope of this thesis.

The principal aim of this thesis was to improve the current testing methodology for evaluating the potential skin injury risk associated with artificial turf. To achieve this, the study had the following objectives:

1. Obtain an extensive understanding of skin properties and identify factors contributing to injury risk.
2. Review the literature on artificial turf developments and associated test methodologies to understand current knowledge and identify gaps that must be addressed comprehensively.
3. Develop a set of realistic simulation characteristics describing injurious interactions. This prerequisite will contribute to knowledge gaps in the existing literature, thereby facilitating data-driven rationale and providing confidence in the simulation's motion profile.
4. Develop and critically analyse a series of potential concepts against the desired design specification.
5. Assimilate knowledge from Objectives 1, 2 and 3 to create an injury prediction model.
6. Improve player welfare as a consequence of enhanced understanding of player surface interactions and associated skin injury risk.

7.2 Summary of Findings

Chapter 1 provided a general introduction to the thesis and defined the problem of skin injuries on artificial turf. World Rugby, a leading authority in rugby, had been at the forefront of promoting player safety. As early adopters of artificial grass surfaces as an alternative to natural grass, World Rugby had developed Rugby Turf Performance Specifications to ensure a safe playing environment. However, despite their efforts, the continued prevalence of turf burns implies that the current test method for assessing skin friction must be improved. This thesis aimed to design and develop a new test device to represent a player in motion better, thereby, addressing the limitations of current testing methodologies.

Chapter 2 presented a comprehensive skin review, providing insights into anatomy, skin friction and measurement techniques, mechanical properties, failure conditions, types of friction injuries, skin infections, and skin simulants. This review highlighted that skin is biomechanically complex due to its anisotropic, non-linear elastic, and viscoelastic behaviours **[Objective 1]**.

The review of artificial turf aimed to comprehend the components contributing to skin injury risk **[Objective 1]**. Rugby Turf, the most complex artificial turf system, exhibited non-linear impact attenuation. Key components included shock pads, carpet backing, stabilising infill, performance infill, and fibres. Shock pads, typically made of rubber or foam, reduce injury risk by cushioning impacts. Whether woven or tufted, carpet backing was expected to have negligible impact on injury risk. Stabilising infill, primarily silica sand, provided ballast but could be abrasive. Performance infill, like SBR, improved shock absorption; therefore, systems with larger volumes of performance infill (Rugby Turf) were expected to exhibit lower injury risk than Football Turf. Throughout this thesis, it became apparent that the potential ban on intentionally added microplastics, such as SBR, would be enforced **[Objective 2]**. SBR currently dominates the artificial turf market. Therefore, an alternative must fill the gap when the product is removed. There was a lack of literature about skin injury risk on systems with alternative infills. Therefore, this was an area that required further research. Fibres, particularly monofilament types, offered better durability and performance, though flattened fibres increased skin contact and friction risk. Increased free pile height was expected to increase friction; however, there was no research documenting the effects of turf density on skin injury risk. The presence of spin oil, which was applied to the fibre during the tufting process, was identified to produce favourable Securisport results. Consequently, the FIFA Technical Advisory Group has validated a washing method, making it compulsory to remove excess spin oil before testing **[Objective 2].**

Exploring the main concepts of tribology contributed to a better understanding of friction, wear, lubrication, and contact mechanics. This review highlighted that rugby turf is a non-Hertzian material that exhibits non-linear behaviours due to integration of a mobile granular infill into a lattice network of yarn fibres. Consequently, both the skin and Rugby Turf should not be regarded as adhering to the fundamental principles of friction **[Novel]**.

The Rugby Turf Performance Specification sets a minimum standard to ensure quality products are installed and that players are safe. Only World Rugby-approved synthetic surfaces can be referred to as Rugby Turf. Despite extensive World Rugby testing of artificial turf, the continued prevalence of turf burns implies that the current test method for assessing skin friction needs to be updated. This limitation is associated with the interaction not representing a player's forces in motion **[Objective 2]**. Additionally, the current test methodology analyses the Coefficient of Friction, which has been reported to be a poor indicator of skin abrasion. Additionally, the device's mechanism interacts with the surface, compromising the surface's condition and adversely affecting the results **[Objective 2]**. These issues impact the validity of the current test device, emphasising the potential for low-quality Rugby Turfs to gain accreditation and possibly cause erroneously preventable skin injuries. Consequently, a new device is required.

Five alternative methods for assessing the risk of skin injuries on synthetic turf were identified, each with unique strengths and limitations **[Objective 2]**. The ASTM F1015 method quantified turf abrasiveness but lacked biofidelity and realistic simulation of player impacts. The Modified Securisport better represented player motion but fell short in assessing abrasion. The Ramp and Sliding Tester effectively captured thermal profiles and potential abrasion but lacked detailed data on artificial skin properties. The Biaxial Load Applicator provided comprehensive biomechanical data and realistic conditions but struggled with achieving desired velocities and standardised testing integration. Finally, the Skin Friction Test achieved horizontal velocity insights but lacked the desired natural deceleration and peer review. Among these, the Biaxial Load Applicator offered the most realistic testing conditions, while the ASTM F1015 method was limited by its lack of biofidelity and realistic impact simulation.

The literature review concluded with a section identifying a suitable skin simulant for the new test method. Human skin's biomechanical complexity and variability present ethical and practical challenges for testing with artificial turf **[Objective 1]**. Ex-vivo samples degrade quickly, and although porcine skin is anatomically similar to human skin, ethical concerns limit its use. Skin surrogates, typically silicone elastomers or polyurethanes, are preferred for repeatability but often fail to replicate mechanical and textural properties. FIFA's use of silicone skin has been criticised for its hydrophobic nature, leading to inaccurate friction responses **[Objective 2]**. SynTissue®, while realistic in texture, is unsuitable for friction testing due to fluid loss under pressure. No single material replicates all properties of human skin. However, synthetic leather closely matches human skin's surface roughness and friction behaviour, especially under varying moisture conditions. Therefore, Lorica Soft was selected as the skin simulant for the new test method **[Objective 3]**.

Chapter 3 introduced the prospective cohort study at the 7s tournament, which reported a skin injury rate of 1024 per 1000 hours of player exposure and that the knee was the most vulnerable anatomical location **[Objective 3]**. In 7s, a fast-paced game and the high defensive responsibilities increase the risk of sustaining a skin injury **[Novel]**. Every interaction was unique. Therefore, no clear trends were identified concerning skin injury risk; however, the severity of the injury typically increased with impact speed. The linear regression analysis of SDASI versus impact velocity recommends that the new test device simulate an impact velocity of 5.35 – 6.26 m/s **[Novel]**. However, the previously rationalised impact velocity of 5 m/s was deemed acceptable.

Interactions, where the momentum of two players was involved, emerged as a characteristic which typically generated greater SDASI scores. Therefore, the new test method should simulate this scenario. The study revealed two distinct injury mechanisms through which players could incur skin damage: either through a high rate of energy transfer during impact or a substantial impulse resulting from an extended sliding motion (1.9 – 2.6m) **[Novel]**. The magnitude of impact decelerations and sliding dynamics, such as slide resistance and resulting displacements, should be evaluated to assess injurious interactions comprehensively **[Objective 3]**.

Furthermore, two unique interactions were identified, highlighting that players were more susceptible to severe injuries when exposed to an acceleration during the sliding phase than a natural deceleration. However, this motion profile was deemed undesirable for the new test method as a natural deceleration was more favourable for the simplicity of analysing the Sliding Phase. It appears this is the only data describing skin injuries during rugby gameplay **[Novel]**. The main limitation of this study was utilising broadcast footage to analyse the players. If a follow-up study were conducted, the players would ideally be tracked individually to monitor instantaneous velocities. The findings from this study will be incorporated into the MTI **[Objective 5]**.

The literature review highlighted a lack of essential biomechanical data describing injurious interactions in rugby gameplay. Therefore, a study was conducted to establish appropriate loading conditions during the sliding phase. This investigation reported that players applied 24.6-41.3% of their body weight through one knee during a simulated tackle **[Novel]**. When translating the loading conditions recorded during the simulated tackle to an elite player (108.0 kg & 187.6 cm) [144]. The impactor's mass would be 26.6-44.6kg **[Objective 3]**.

The assessment of Lorica Soft reported a surface roughness of 10.55±0.27 μm, which aligns with the literature **[Contribution]**. Tensile testing reported the material is more robust and less susceptible to strain in the machined direction **[Contribution]**. Consequently, the skin template will be cut, ensuring the testing orientation runs parallel to the machined direction **[Objective 3]**. Non-woven materials are typically poor conductors of heat, which was confirmed during the analysis of Lorica Soft's thermal properties. This outcome raised concerns over the suitability of thermocouples for the new test method.

Chapter 4 presented and critically analysed nine potential design concepts for an apparatus to simulate a realistic player-surface interaction **[Objective 4]**. Considering alternative solutions was essential while developing the new test device to ensure an enhanced final product was produced. The critical review highlighted that propulsion systems that utilise gravity to convert rotational acceleration into linear motion are unsuitable due to the reduced vertical velocity on impact. Consequently, a linear gantry frame and dropping mechanism will be combined to independently generate the horizontal and vertical velocities.

Chapter 5 culminated in the development of the Maxwell Tribo Index (MTI); a multi-faceted classification system **[Objective 5]**. Despite the in-depth review of published literature, the aetiology of 'turf burns' is not yet fully understood. Therefore, the abrasive nature of turf and heat profiles are evaluated to provide insights into the potential injury mechanisms. The Abrasion Severity Index (ASI) was a greyscale thresholding technique which forecasts skin damage when the entire simulation energy was dissipated **[Novel]**. Meanwhile, thermal cameras were utilised to monitor the Heat Profiles during the interaction and record the peak temperatures (T_P). Several ancillary kinematic injury metrics were explored by manipulating accelerometer data to enhance understanding of impact mechanics and sliding characteristics. The final iteration of the MTI monitors global surface resistance by combining Impact and Slide Resistance **[Novel]**.

The research tool developed in this thesis provides a fully functioning solution for evaluating skin injury risk on sports surfaces. The accompanying classification system facilitates an in-depth analysis of artificial turf, enabling manufacturers to optimise their products. Now that this has been achieved it can form a foundation for future design and construction of artificial pitches. Ultimately improving player safety **[Objective 6]**.

7.3 MTI Assessment of Artificial Sports Surfaces

World Rugby's endorsement and commitment to adopting the new test method and classification system underscores the successful achievement of the principal aims. The tribological analysis of artificial turf, performed under standard player-surface contact conditions during gameplay, has yielded novel insights into injurious interactions (Figure 7-1). This knowledge is instrumental for manufacturers aiming to optimise their products to enhance player welfare.

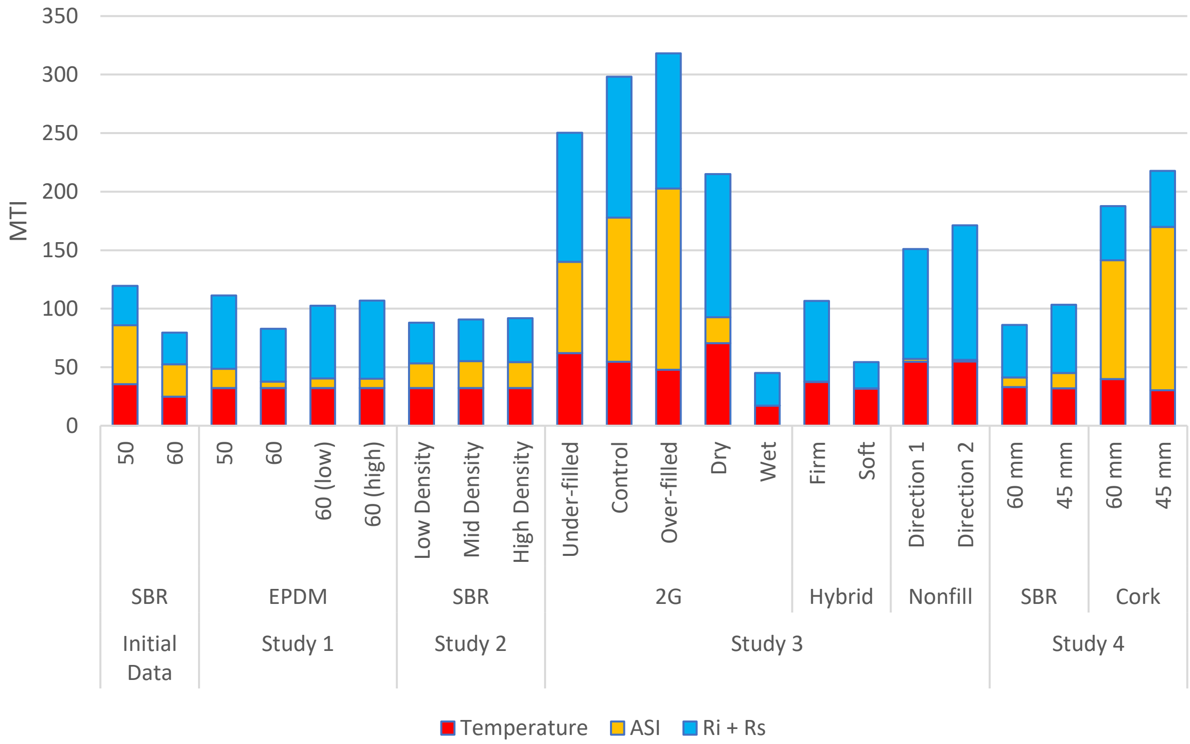

Figure 7-1: Overview of skin injury risk on surfaces assessed throughout this thesis.

The main findings of this research are both novel and significant, particularly in challenging previous assumptions surrounding skin injuries on artificial turf. Insufficient heat to cause burns suggests that injuries are primarily mechanical abrasions rather than thermal damage. Key factors influencing skin injury risk include the ratio of sand to performance infill, turf density, and shock pad density, all of which contribute to surface stiffness. These revelations open new avenues for research and emphasise the importance of SID in validating new alternative infills. This chapter will summarise the practical implications of these findings to demonstrate how the device and the MTI are influenced by the surface system materials and design.

7.3.1 Turf Properties

This section combines data from the initial validation study presented in Chapter 5 with findings from Study 1 detailed in Chapter 6.

Surface Properties

- The performance infill rate was ratiometrically reduced in Sample 1 (50 mm) to produce the same free pile height (15 mm) as Sample 2 (60 mm).
- Surfaces 3 and 4, with 60 mm fibre length, had identical stabilising and performance infill rates to produce a free pile height of 20 mm. This construction was aimed at monitoring the effects of turf density.
- Surfaces 1 and 3 had the highest and lowest turf densities, respectively. Meanwhile, Surfaces 2 and 4 had similar turf densities.
- All samples were tested on a 14 mm shock pad with a force reduction of 58%.

Abrasion Severity Index

- The ASI scores indicated that 50 mm samples caused more skin damage than 60 mm samples.
- EPDM samples caused less discolouration and smoother skin damage than SBR samples, likely due to EPDM's elasticity and fine dust coating.

Peak Temperature

- 50 mm samples generated a greater peak temperature than 60 mm
- The 50 mm had a higher turf density, attributed to this result.
- Unfortunately, no thermal camera data was collected during Study 1; therefore, a standard 25°C was assumed to calculate the MTI for all surfaces.

Impact Resistance

- Surfaces with higher turf densities and lower infill rates produced higher Impact Resistance.
- SBR exhibited lower Impact Resistance than EPDM

Slide Resistance

- Surfaces with higher turf densities produced higher Slide Resistance.
- This result was attributed to increased yarn exposure, which reduced rolling friction and increased sliding friction.
- The relationship between free pile height and turf density exhibited varying Slide Resistance, suggesting a more complex turf response than Tay et al. (2015) proposed.

Maxwell Tribo Index

Previously, the MTI was displayed as a conventional bar chart. When it comes to visualising multidimensional data, radar graphs are clearly superior since they provide a thorough and detailed comparison across all four criteria that affect the likelihood of skin injuries. Utilisation of a radar graph will give manufacturers a diagnostic tool that can identify areas where their products need to be improved and will also help them better grasp the intricate dynamics involved in assessing skin injuries. There are five segmental boundaries on the radar graph, each representing twenty MTI score integrals. A score of 100 indicates a test result equivalent to the normalising coefficient, therefore, as a particular parameter extends toward the outer edge of the radar graph, the risk of skin injury escalates. Any data point that exceeds the outermost boundary indicates a high risk, which could lead World Rugby to consider the injury risk too severe for the sport to be safely played on that surface.

Figure 7-2 demonstrates that a 50-mm sample may not always pose a higher risk than a 60-mm sample, which has significant implications for future testing and injury prevention.

- Sample 1 (50mm) posed the greatest injury risk per the MTI; however, the results were not statistically different from Samples 3 and 4.
- Sample 2 was the safest surface with lower sand content, higher performance infill rates, shorter free pile heights, and a high turf density.

Figure 7-3 illustrates the differences observed in 50- and 60-mm samples filled with SBR and EPDM:

- SBR was more abrasive than EMPD.
- EPDM generated greater Impact and Slide Resistance compared to SBR.

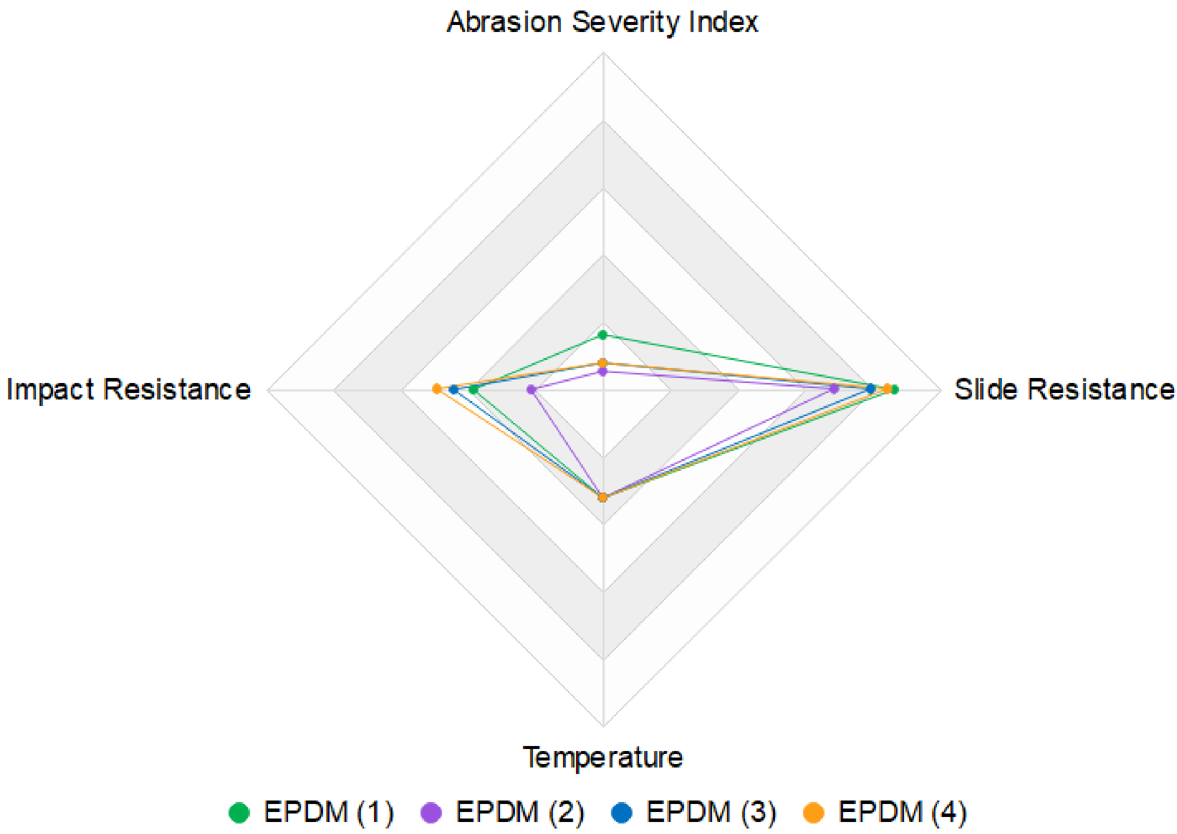

Figure 7-2: MTI Radar Graph comparing carpet with different turf properties filled with EPDM

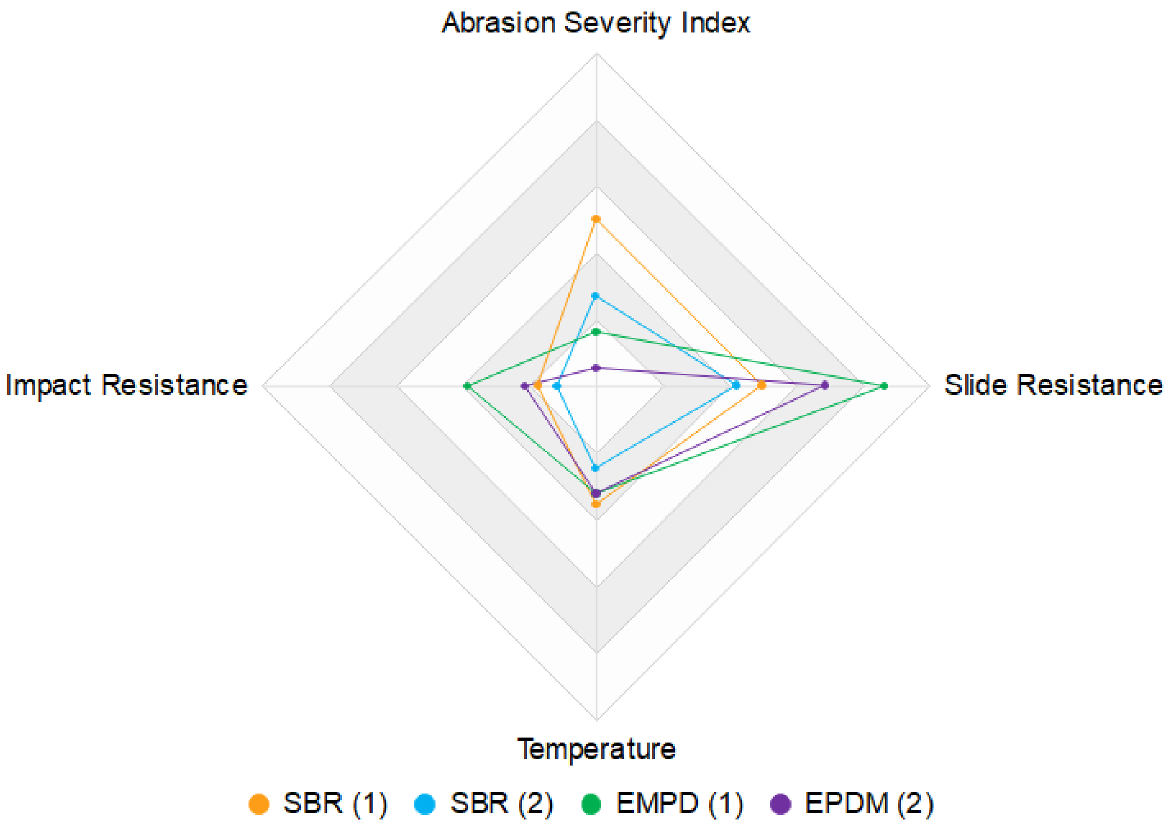

Figure 7-3: MTI Radar Graph comparing SBR and EPDM in a 50- and 60-mm carpet.

7.3.2 Shock Pad

This section evaluated skin injury risk across three identical systems with different shock pads.

Surface Properties

- Three pad densities were selected to monitor the influence of the shock pad on skin injury risk while maintaining a constant thickness (12 mm).
- The three densities were selected to vary the shock-absorbing properties of the pad: 39%, 45%, and 55%, respectively.
- Each system had identical infill ratios, free pile heights, and turf densities.

Abrasion Severity Index

- There were trivial differences between the ASI scores when assessing the influence of a shock pad on skin injury risk.

Peak Temperature

- Unfortunately, no thermal camera data was collected during Study 2; therefore, a standard 25°C was assumed to calculate the MTI for all surfaces.

Impact Resistance

- Shock pads with lower force reduction were expected to produce stiffer surfaces.
- A statistically significant difference in Impact Resistance was observed only between Pads 1 and 3, which had markedly different shock-absorbing properties.

Slide Resistance

- Expected minimal impact from shock pad during Sliding Phase.
- One significant comparison suggested surface preparation affects results.
- Proper sample preparation is crucial for accurate results.

Maxwell Tribo Index

The MTI suggested that the force reduction properties of a shock pad do not significantly influence skin injury risk as illustrated in Figure 7-4.

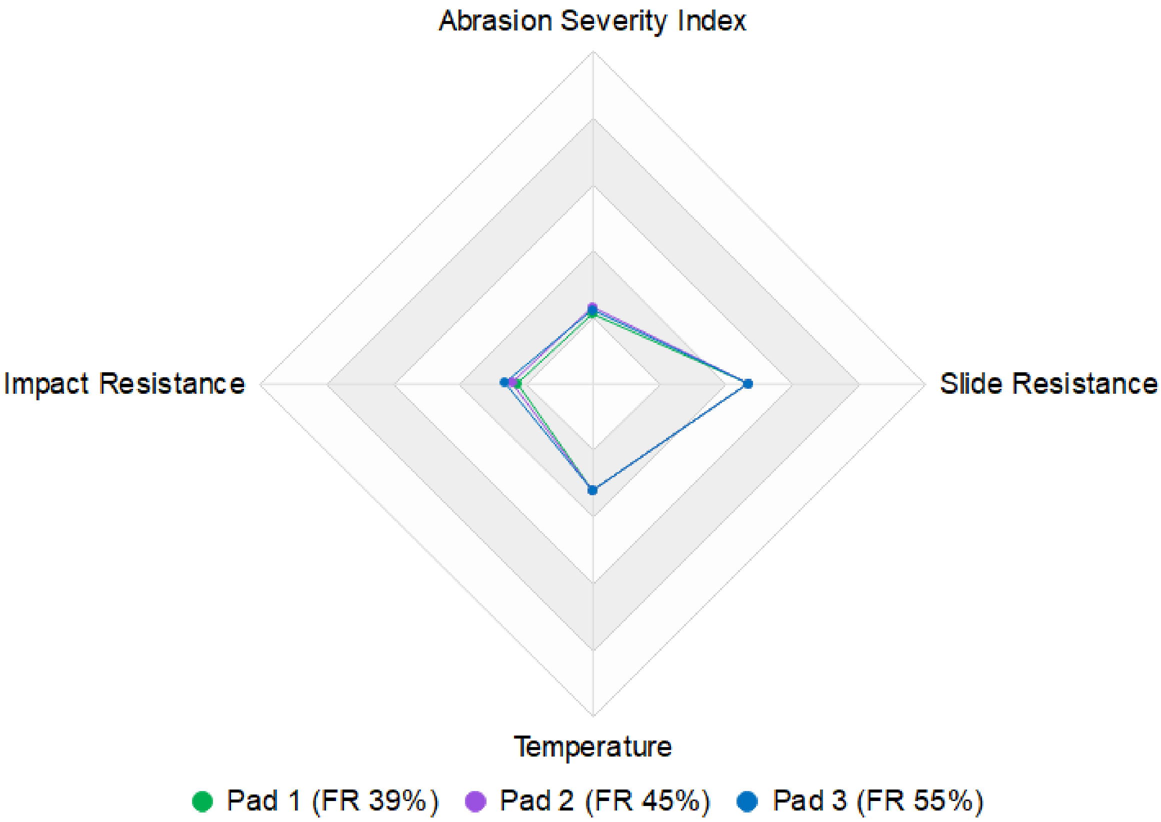

Figure 7-4: MTI Radar Graph comparing the effects of a shock pad's force reduction on skin injury risk.

7.3.3 Alternative Turfs

This section aimed to provide a nuanced overview of skin injury risk on alternative artificial sports surfaces.

Surface Properties

- Second Generation
  - The sand-filled carpet, with a 10 mm pile height, was secured to a 12 mm shock pad and tested at three different infill rates (3, 5, and 7 kg/m^2).
  - The water-based carpet, with a 13 mm pile height, was tested dry and irrigated with 1.25 L/m^2 of water.

- Hybrid
  - A 55-mm tufted grass system with and without an artificial rootzone.
- Non-fill
  - A 28 mm carpet with a texturised thatch attached to a 14 mm shock pad.
  - Skin injury risk was evaluated with and against the grain.

Abrasion Severity Index

- The ASI showed a clear positive relationship with infill quantity on the sand-based 2G.
- The water-based 2G (dry and wet), hybrid, and non-filled systems all generated minimal skin damage
- Therefore, infill material is the turf property associated with generating abrasions.

Peak Temperature

- The observation of temperature increasing with exposed free pile height was attributed to the variation in kinetic energy.
- Infill is mobile and free to move; any force it experiences will be transferred to kinetic energy. In contrast, the yarn is rooted within the carpet backing; therefore, any kinetic energy absorbed will be transferred to heat.
- The results from the water-based surface support this observation as it generated the highest temperatures.
- The firm and dry hybrid generated greater temperatures than the soft and wet surface.
- Orientation of the non-fill did not affect peak temperatures.
- The non-fill generated lower temperatures than the dry water-based 2G surface, which was attributed to the properties of the thatch.
- Kinetic energy was dissipated during the deformation and recovery of the surface, whilst the air within the thatch acts as an insulator, limiting thermal build-up.

Impact Resistance

- On the 2G surface, Impact Resistance increased with sand infill rates until the surface was overfilled, where a trivial decrease was observed. This outcome was attributed to the granular infill reducing friction due to rolling resistance.

- Irrigating the surface significantly reduces Impact Resistance.
- The firm and dry hybrid generated a higher Impact Resistance than the softer surface.
- On a non-fill system, testing against the grain generated a greater Impact Resistance.

Slide Resistance

- Slide resistance decreased with increasing infill rates of sand. This outcome was attributed to rolling friction and the reduced yarn exposure, which reduced sliding friction.
- Irrigating the surface significantly reduces Slide Resistance.
- The firm and dry hybrid generated a higher Slide Resistance than the softer surface.
- On a non-fill system, testing against the grain generated a greater Slide Resistance.

Maxwell Tribo Index

- The sand-based and dry 2G systems yielded MTI scores significantly higher than those of a 3G system.
- Figure 7-5 illustrates that surfaces identified as high risk are those known to cause injuries, giving World Rugby confidence in setting acceptable risk levels.
- Irrigating the surface significantly lowers skin injury risk.
- Dry grass has been reported in the literature to be more harmful than natural turf, a finding that aligns with our MTI scores.
- Figure 7-6 illustrates that non-filled systems generated the greatest Slide Resistance. This outcome was attributed to the lack of granular infill which assists rolling friction.
- Non-filled systems fell between 2G and 3G in MTI scores, suggesting further innovation is required before they can be considered skin-friendly alternative sports surfaces.

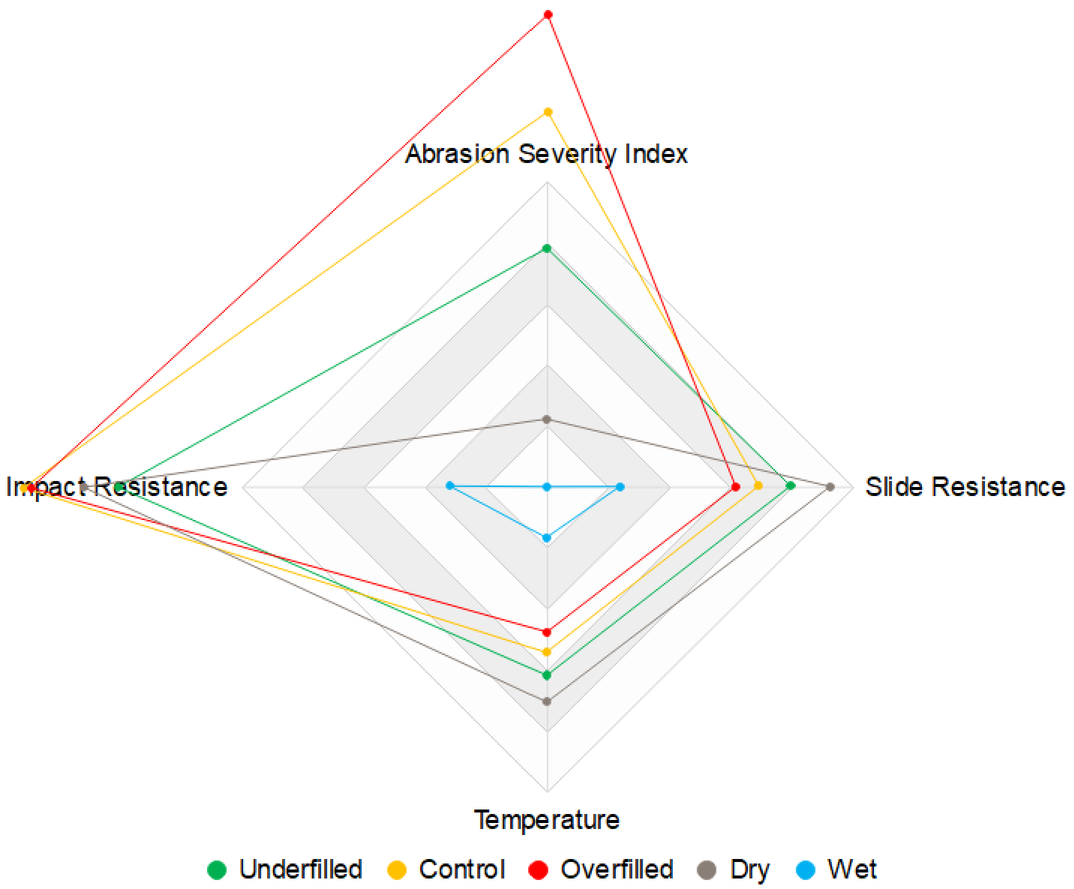

Figure 7-5: MTI Radar Graph evaluating skin injury risk on hockey surfaces.

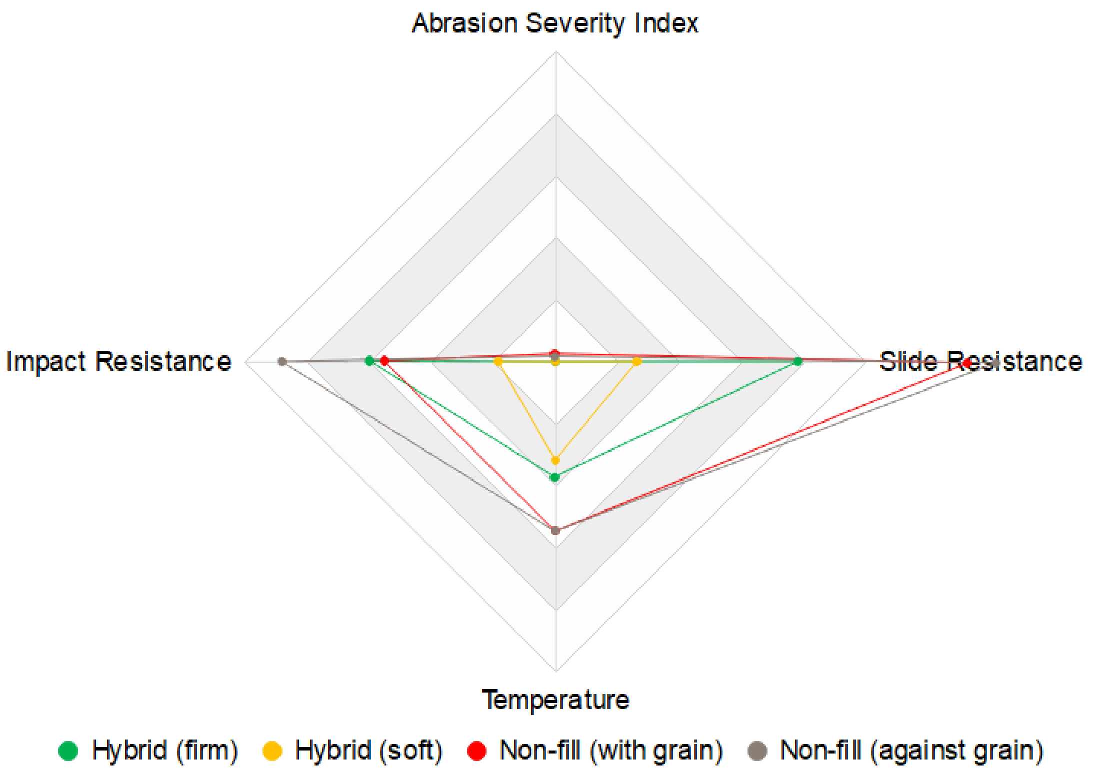

Figure 7-6: MTI Radar Graph evaluating skin injury risk on alternative sports surfaces.

7.3.4 Inter-operator repeatability

This section evaluated the repeatability of different operators assessing rugby and football turf.

Surface Properties

- Two 45 mm and 60 mm carpets were filled with SBR and cork.
- Free pile height was 15 and 18 mm for the 45- and 60-mm, respectively.
- All surfaces were constructed on a 10 mm shock pad.

Abrasion Severity Index

- Cork generated more severe abrasions than SBR
- 45 mm surfaces generated greater ASI scores than 60 mm surfaces; however, the results were trivial.

Peak Temperature

- 60 mm surfaces generated higher temperatures than 45 mm. This outcome was attributed to longer free pile heights.
- Cork exhibits lower compressibility and promotes internal dampening due to its cellular structure of hollow chambers. This internal dissipation converts a proportion of kinetic energy into heat, explaining the higher temperatures than SBR.

Impact Resistance

- 45 mm surfaces generated higher Impact Resistance. This result was attributed to lower volumes of performance infill, which enhanced impact attenuation.
- Higher Impact Resistance was expected to yield greater ASI scores; however, this theory holds true only when comparing surfaces with the same infill material.
- SBR is highly elastic and quickly recovers upon impact. This inherent elasticity contributes significantly to its heightened impact resistance.
- Cork exhibited lower Impact Resistance, which was attributed to lower bulk densities and energy of restitution.

- Lightweight granular infill with reduced energy restitution preserves less energy after a collision, reducing Impact Resistance. When the momentum of the simulated player drives the impactor across the turf sample, a pressure bulb forms at the front of the knee form. The density of the infill influences how this force propagates through the sample and the extent of the resultant infill displacement. Low-density materials will displace more, creating a path of least resistance and reducing Impact Resistance.

Slide Resistance

- Increased yarn exposure has a positive correlation with Slide Resistance.
- 60 mm surfaces exhibited elevated levels of Slide Resistance. This outcome was linked to the longer free pile height.
- The shape of the infill influences how it behaves as the knee slides over it.
- Higher sphericity will enhance rolling friction, diminishing Slide Resistance.
- Cork exhibits low sphericity; therefore, Slide Resistance is elevated compared to SBR.

Maxwell Tribo Index

- Ranking of the MTI aligns with the expert panel's consensus opinion, demonstrating this new methodology's validity. Most of the panel suggested that Surface 1 had the lowest risk of injury while Surface 4 had the highest potential to cause harm.
- Surface 1 was perceived to be the most skin-friendly due to the additional infill, which was attributed to making the system softer.
- In contrast, Surface 4 was linked to being the most harmful due to the reduced infill, making the system firmer, and the “rougher” texture of cork, increasing the likelihood of an abrasion.
- There were conflicting opinions concerning the differences between Surface 2 and 3. The lack of agreement arose from varying perceptions relating to the benefits of additional infill versus the texture of cork.
- The congruity of the expert panel and the MTI scores provides confidence for incorporating this test method into Regulation 22; however, further work is required to define an acceptable level of injury (Figure 7-7).

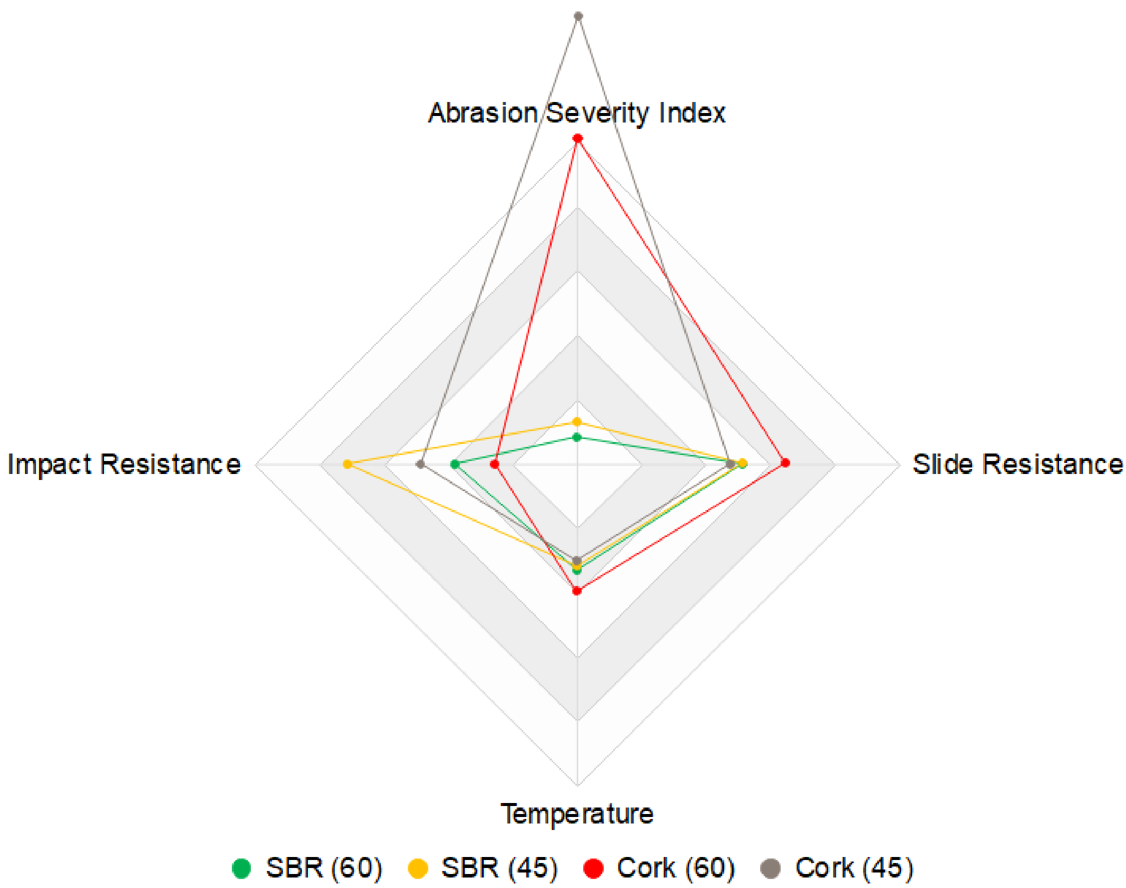

Figure 7-7: MTI Radar Graph evaluating skin injury risk on alternative sports surfaces.

7.4 Future Work

Now that a classification system has been developed; the collaboration between Cardiff University and Sports Labs will continue to help World Rugby set acceptable thresholds for Regulation 22. Throughout this thesis, data has been collected on a wide range of samples. Some results were not included due to the reduced and inadequate sample size. However, the need for further data collection and experimentation is crucial for the advancement of our understanding. Insights from these studies have suggested that post-Lisport samples generated greater Impact and Slide Resistance. It would be helpful to collect more data to better understand the influence accelerated wear has on the ASI and temperatures generated. Additional data collection on alternative infills is also required.

As mentioned previously, a second device has been manufactured. The next step for that project will be to conduct a series of experiments to evaluate the reproducibility between the two devices. Alongside the deployment of the new device, a prospective study should be undertaken to investigate the correlation between skin injury severity and different surface types, aiming to further validate the MTI. This evidence will bolster World Rugby's confidence in the device and facilitate buy-in from other key stakeholders involved in the Rugby Turf Performance Specifications. These devices will be solely laboratory-based; therefore, developing a portable device that can be taken out on-site would be beneficial. Such a device would allow for real-time monitoring of player-surface interactions, potentially leading to immediate adjustments to enhance safety and performance. Furthermore, findings from the 7s tournament highlighted multiple interaction characteristics that contributed to different injuries, which could be explored in greater depth.

Adaptions to the device could also be considered, such as representing a female or child interaction. Alternatively, different body parts could be assessed. On a broader consideration, the impactor could be replaced with, for example, a shoe to monitor different player surface interactions. There are multiple applications where this device could be utilised to extend the safety parameters within alternative sports where player surface interaction knowledge can improve safety or performance.

References

[1] D. Twomey, “Injuries on artificial turf: What do players thinks?,” *J Sci Med Sport*, vol. 22, 2019, doi: 10.1016/j.jsams.2019.08.152.

[2] World Rugby, “Rugby Turf Performance Specification,” pp. 29–30, 2016.

[3] M. Venus, J. Waterman, and I. McNab, “Basic physiology of the skin,” *Surgery (Oxford)*, vol. 28, no. 10, Oct. 2010, doi: 10.1016/j.mpsur.2010.07.011.

[4] Taylor Tim, “Integumentary System,” Innerbody Research. Accessed: Feb. 16, 2021. [Online]. Available: https://www.innerbody.com/anatomy/integumentary

[5] N. K. (Noortje K. Veijgen, “Skin friction : a novel approach to measuring in vivo human skin,” s.n.], 2013.

[6] L. A. Fenton, I. Horsfall, and D. J. Carr, “Skin and skin simulants,” *Australian Journal of Forensic Sciences*, vol. 52, no. 1. 2020. doi: 10.1080/00450618.2018.1450896.

[7] S. Lawton, “Skin 1: the structure and functions of the skin,” *Nurs Times*, vol. 115, no. 12, pp. 30–33, 2019.

[8] R. Seeley, T. Stephens, and P. Tate, *Anatomy and Physiology* . Mosby, St. Louis, 1995.

[9] Schwartz C J, *Friction, Human Body: Skin*. 2013. doi: 10.1007/978-0-387-92897-5.

[10] M. Kwiatkowska, S. E. Franklin, C. P. Hendriks, and K. Kwiatkowski, “Friction and deformation behaviour of human skin,” *Wear*, vol. 267, no. 5–8, Jun. 2009, doi: 10.1016/j.wear.2008.12.030.

[11] K. A. Subhi, A. Tudor, E. K. Hussein, and H. S. Wahad, “The adhesion and hysteresis effect in friction skin with artificial materials,” *IOP Conf Ser Mater Sci Eng*, vol. 174, no. 1, 2017, doi: 10.1088/1757-899X/174/1/012018.

[12] F. Motamen Salehi, A. Neville, and M. Bryant, “Bio-tribology of incontinence management products: additional complexities at the skin–pad interface,” *Tribology - Materials, Surfaces and Interfaces*, vol. 12, no. 4, pp. 193–199, 2018, doi: 10.1080/17515831.2018.1512784.

[13] S. Comaish and E. Bottoms, “The Skin and Friction: Deviations From Amonton’S Laws, and the Effects of Hydration and Lubrication,” *British Journal of Dermatology*, vol. 84, no. 1, pp. 37–43, 1971, doi: 10.1111/j.1365-2133.1971.tb14194.x.

[14] R. K. Sivamani, J. Goodman, N. V Gitis, and H. I. Maibach, “Friction coefficient of skin in real-time,” *Skin Research and Technology*, vol. 9, pp. 235–239, 2003.

[15] M. F. Leyva-Mendivil, J. Lengiewicz, A. Page, N. W. Bressloff, and G. Limbert, “Skin Microstructure is a Key Contributor to Its Friction Behaviour,” *Tribol Lett*, vol. 65, no. 1, p. 12, Mar. 2017, doi: 10.1007/s11249-016-0794-4.

[16] H. Joodaki and M. B. Panzer, “Skin mechanical properties and modeling: A review,” *Proc Inst Mech Eng H*, vol. 232, no. 4, Apr. 2018, doi: 10.1177/0954411918759801.

[17] S. Derler and L. C. Gerhardt, “Tribology of skin: Review and analysis of experimental results for the friction coefficient of human skin,” *Tribol Lett*, vol. 45, no. 1, pp. 1–27, 2012, doi: 10.1007/s11249-011-9854-y.

[18] N. T. Clancy, G. E. Nilsson, C. D. Anderson, and M. J. Leahy, “A new device for assessing changes in skin viscoelasticity using indentation and optical measurement,” *Skin Research and Technology*, vol. 16, no. 2, pp. 210–228, 2010, doi: 10.1111/j.1600-0846.2010.00433.x.

[19] G. P. Seehra and F. H. Silver, “Viscoelastic properties of acid- and alkaline-treated human dermis: a correlation between total surface charge and elastic modulus,” *Skin Research and Technology*, vol. 12, no. 3, Aug. 2006, doi: 10.1111/j.0909-752X.2006.00150.x.

[20] X. Liu, Z. Lu, R. Lewis, M. J. Carré, and S. J. Matcher, “Feasibility of using optical coherence tomography to study the influence of skin structure on finger friction,” in

Tribology International, Elsevier Ltd, Jul. 2013, pp. 34–44. doi: 10.1016/j.triboint.2012.08.020.

[21] M. J. Adams, B. J. Briscoe, and S. A. Johnson, "Friction and lubrication of human skin," *Tribol Lett*, vol. 26, no. 3, pp. 239–253, Jun. 2007, doi: 10.1007/s11249-007-9206-0.

[22] J. Liu, Q. Zhang, and X. Liu, "Understanding handling performance of rugby balls under wet conditions: analysis of finger-ball friction," *Int J Perform Anal Sport*, vol. 20, no. 5, Sep. 2020, doi: 10.1080/24748668.2020.1786299.

[23] T. André, P. Lefèvre, and J. L. Thonnard, "A continuous measure of fingertip friction during precision grip," *J Neurosci Methods*, vol. 179, no. 2, pp. 224–229, May 2009, doi: 10.1016/j.jneumeth.2009.01.031.

[24] S. E. Tomlinson, R. Lewis, X. Liu, C. Texier, and M. J. Carré, "Understanding the friction mechanisms between the human finger and flat contacting surfaces in moist conditions," *Tribol Lett*, vol. 41, no. 1, pp. 283–294, 2011, doi: 10.1007/s11249-010-9709-y.

[25] S. Derler, R. M. Rossi, and G. M. Rotaru, "Understanding the variation of friction coefficients of human skin as a function of skin hydration and interfacial water films," *Proceedings of the Institution of Mechanical Engineers, Part J: Journal of Engineering Tribology*, vol. 229, no. 3, pp. 285–293, Mar. 2015, doi: 10.1177/1350650114527922.

[26] R. Maiti, M. Duan, S. G. Danby, R. Lewis, S. J. Matcher, and M. J. Carré, "Morphological parametric mapping of 21 skin sites throughout the body using optical coherence tomography," *J Mech Behav Biomed Mater*, vol. 102, no. October 2019, 2020, doi: 10.1016/j.jmbbm.2019.103501.

[27] C. J. Boyle *et al.*, "Morphology and composition play distinct and complementary roles in the tolerance of plantar skin to mechanical load," *Sci Adv*, vol. 5, no. 10, pp. 1–14, 2019, doi: 10.1126/sciadv.aay0244.

[28] X. Liu, D. Gad, Z. Lu, R. Lewis, M. J. Carré, and S. J. Matcher, "The contributions of skin structural properties to the friction of human finger-pads," *Proceedings of the*

Institution of Mechanical Engineers, Part J: Journal of Engineering Tribology, vol. 229, no. 3, pp. 294–311, Mar. 2015, doi: 10.1177/1350650114567699.

[29] K. T. Korbeld, M. Klaassen, R. D. Jobanputra, E. G. de Vries, and M. A. Masen, "Effects of sebum properties on skin friction: Investigation using a bench test," *Biosurf Biotribol*, vol. 6, no. 2, pp. 43–47, Jun. 2020, doi: 10.1049/bsbt.2019.0015.

[30] A. S. McIntosh, "Risk compensation, motivation, injuries, and biomechanics in competitive sport," *Br J Sports Med*, vol. 39, no. 1, pp. 2–3, 2005, doi: 10.1136/bjsm.2004.016188.

[31] G. S. Lazarus, M. Diane, D. R. Knighton, J. David, G. Rodeheaver, and M. C. Robson, "Definitions and Guidelines for Assessment of Wounds and Evaluation of Healing," *Arch Dermatol*, vol. 130, pp. 498–493, 1994.

[32] R. S. W. Basler, C. M. Hunzeker, and M. A. Garcia, "Athketic Skin Injuries: Combating Pressure and Friction," *Physician and Sportsmedicine*, vol. 32, no. 5, pp. 33–40, 2004, doi: 10.3810/psm.2004.05.304.

[33] S. Enoch and P. Price, "Key Points Acute (normal) wound healing," *World Wide Woulds*, pp. 1–15, 2004, [Online]. Available: http://www.worldwidewounds.com/2004/august/Enoch/Pathophysiology-Of-Healing

[34] D. T. Foster, L. J. Rowedder, and S. K. Reese, "Management Skin Wounds Sports-Induced," *J Athl Train*, vol. 30, no. 2, pp. 135–140, 1995.

[35] H. C. Korting, C. Schöllmann, and R. J. White, "Management of minor acute cutaneous wounds: Importance of wound healing in a moist environment," *Journal of the European Academy of Dermatology and Venereology*, vol. 25, no. 2, pp. 130–137, 2011, doi: 10.1111/j.1468-3083.2010.03775.x.

[36] W. Potthast, R. Verhelst, M. Hughes, K. Stone, and D. De Clercq, "Football-specific evaluation of player–surface interaction on different football turf systems," *Sports Technology*, vol. 3, no. 1, pp. 5–12, 2010, doi: 10.1080/19346190.2010.504278.

[37] W. van den Eijnde, "Skin injury due to artificial turf," 2017.

[38] L. Cañedo-Dorantes and M. Cañedo-Ayala, "Skin acute wound healing: A comprehensive review," *Int J Inflam*, vol. 2019, 2019, doi: 10.1155/2019/3706315.

[39] R. Shrestha, K. Krishan, and T. Kanchan, "Abrasion," StatPearls - Treasure Island. Accessed: May 26, 2021. [Online]. Available: https://www.ncbi.nlm.nih.gov/books/NBK554465/

[40] Just-Athletic, "Why Do Boxers Use Vaseline?" Accessed: May 26, 2021. [Online]. Available: https://just-athletics.com/why-do-boxers-use-vaseline/

[41] Adidas, "adidas climacool | adidas UK." Accessed: May 26, 2021. [Online]. Available: https://www.adidas.co.uk/climacool

[42] Nike, "What Is Nike Dri-FIT? | Nike Help." Accessed: May 26, 2021. [Online]. Available: https://www.nike.com/gb/help/a/nike-dri-fit

[43] N. Brown, J. White, A. Brasher, and J. Scurr, "An investigation into breast support and sports bra use in female runners of the 2012 London Marathon," *J Sports Sci*, vol. 32, no. 9, pp. 801–809, 2014, doi: 10.1080/02640414.2013.844348.

[44] F. H. Brennan, "Managing blisters in competitive athletes.," *Curr Sports Med Rep*, vol. 1, no. 6, pp. 319–322, 2002, doi: 10.1249/00149619-200212000-00003.

[45] A. R. Moritz and F. C. Henriques, "Studies of Thermal Injury: I. The Conduction of Heat to and through Skin and the Temperatures Attained Therein. A Theoretical and an Experimental Investigation," *Am J Pathol*, vol. 23, no. 4, pp. 530–549, 1947.

[46] N. A. Martin and S. Falder, "A review of the evidence for threshold of burn injury," *Burns*, vol. 43, no. 8. 2017. doi: 10.1016/j.burns.2017.04.003.

[47] J. Hardy, "Thresholds of Pain and Reflex Contraction as Related to Noxious Stimulation," *J Appl Physiol*, vol. 5, no. 12, pp. 725–739, 1953.

[48] J. Hardy, H. Wolff, and H. Goodell, “STUDIES ON PAIN: DISCRIMINATION OF DIFFERENCES IN INTENSITY OF A PAIN STIMULUS AS A BASIS OF A SCALE OF PAIN INTENSITY.,” vol. 25, no. 6, pp. 1152–8, 1947.

[49] A. Stoll and G. Leon, “Relationship between pain and tissue damage due to thermal radiation,” *J Appl Physiol*, vol. 14, no. 3, pp. 373–382, 1959.

[50] A. Stoll, M. A. Chiantam, and J. R. Piergallini, “Thermal conduction effects in human skin,” *Aviat Space Environ Med.*, vol. 50, no. 8, pp. 779–87, 1979.

[51] Henriques. F. Jr., “Studies of thermal injury; the predictability and the significance of thermally induced rate processes leading to irreversible epidermal injury.,” *Arch Pathol*, vol. 43, no. 5, pp. 489–502, 1947.

[52] A. Stoll and M. A. Chiantam, “HEAT TRANSFER THROUGH FABRICS AS RELATED TO THERMAL INJURY,” *Trans N Y Acad Sci*, vol. 33, no. 7, pp. 649–670, 1971.

[53] E. H. Wright, A. L. Harris, and D. Furniss, “Cooling of burns: Mechanisms and models,” *Burns*, vol. 41, no. 5, pp. 882–889, 2015, doi: 10.1016/j.burns.2015.01.004.

[54] Schartz C J, “Friction, Human Body: Skin,” in *Encyclopedia of Tribology*, Boston: Springer US, 2013, pp. 1386–13393.

[55] R. S. W. Basler, M. A. Garcia, K. S. Gooding, and W. O. Roberts, “Immediate steps for treating abrasions,” *Physician and Sportsmedicine*, vol. 29, no. 4, pp. 69–70, 2001, doi: 10.3810/psm.2001.04.744.

[56] R. Verhelst, S. Rambour, P. Verleysen, and J. Degrieck, “Temperature development during sliding on different types of artificial turf for hockey,” *International Conference on Latest Advances in High-Tech Textiles and Textile-Based Materials*, pp. 90–95, 2009, [Online]. Available: https://biblio.ugent.be/input/download?func=downloadFile&recordOId=767613&fileOId=767615

[57] Agrawal A., R. S.C., and V. H.J., “Ann-Burns-and-Fire-Disasters-21-3,” *Ann Burns Fire Disasters*, vol. 21, no. 1, pp. 3–6, 2008.

[58] K. A. Lenehan and D. M. Twomey, “Abrasion testing on synthetic turf: A modified device,” *Proc Inst Mech Eng P J Sport Eng Technol*, vol. 230, no. 4, pp. 280–284, 2016, doi: 10.1177/1754337115612657.

[59] M. M. Hurtado, M. Peppelman, X. Zeng, P. E. J. van Erp, and E. Van Der Heide, “Tribological behaviour of skin equivalents and ex-vivo human skin against the material components of artificial turf in sliding contact,” *Tribol Int*, vol. 102, pp. 103–113, 2016, doi: 10.1016/j.triboint.2016.05.018.

[60] R. S. Deu and M. Khodaee, “Skin and Subcutaneous Tissue,” in *Sports-related Fractures, Dislocations and Trauma: Advanced On- and Off-field Management*, M. Khodaee, A. L. Waterbrook, and M. Gammons, Eds., Cham: Springer International Publishing, 2020, pp. 693–702. doi: 10.1007/978-3-030-36790-9_40.

[61] C.-Y. Hsieh and T.-F. Tsai, “Friction-Induced Skin Disorders—A Review,” *Dermatitis®*, vol. 34, no. 4, pp. 278–286, 2023, doi: 10.1097/DER.0000000000000934.

[62] R. Warby and C. Maani, “Burn Classification,” StatPearls - Treasure Island. Accessed: Feb. 07, 2024. [Online]. Available: https://www.ncbi.nlm.nih.gov/books/NBK539773/

[63] A. Urakov, “What are bruises? Causes, Symptoms, Diagnosis, Treatment, Remedies,” *IP International Journal of Comprehensive and Advanced Pharmacology*, vol. 5, no. 1, pp. 1–5, 2020, doi: 10.18231/j.ijcaap.2020.001.

[64] Stuart Shalat, “Does Playing On Artificial Turf Pose A Health Risk For Your Child,” Online. Accessed: Apr. 02, 2023. [Online]. Available: https://www.washingtonpost.com/national/health-science/does-playing-on-artificial-turf-pose-a-health-risk-for-your-child/2017/03/17/0c61b7b4-0380-11e7-ad5b-d22680e18d10_story.html

[65] WebMD Editorial Contributor, “ Regular Exercise: How It Can Boost Your Health,” Online. Accessed: Apr. 02, 2023. [Online]. Available: https://www.webmd.com/fitness-exercise/health-benefits-exercise

[66] E. M. Begier *et al.*, “A high-morbidity outbreak of methicillin-resistant Staphylococcus aureus among players on a college football team, facilitated by cosmetic body shaving and turf burns,” *Clinical Infectious Diseases*, vol. 39, no. 10, pp. 1446–1453, 2004, doi: 10.1086/425313.

[67] T. J. Serensits, A. S. McNitt, and D. M. Petrunak, “Human health issues on synthetic turf in the USA,” *Proc Inst Mech Eng P J Sport Eng Technol*, vol. 225, no. 3, 2011, doi: 10.1177/1754337111398407.

[68] NHS, “MRSA,” Online. Accessed: Apr. 03, 2023. [Online]. Available: https://www.nhs.uk/conditions/mrsa/

[69] A. S. McNitt, D. M. Petrunak, and T. J. Serensits, “ Survival of Staphylococcus aureus applied to Poa pratensis L. and synthetic turf ,” *Int Turfgrass Soc Res J*, vol. 14, no. 1, 2022, doi: 10.1002/its2.35.

[70] J. R. Jastifer *et al.*, “Synthetic Turf: History, Design, Maintenance, and Athlete Safety,” *Sports Health*, vol. 11, no. 1. 2019. doi: 10.1177/1941738118793378.

[71] S. A. Taylor, P. D. Fabricant, M. M. Khair, A. M. Haleem, and M. C. Drakos, “A review of synthetic playing surfaces, the shoe-surface interface, and lower extremity injuries in athletes,” *Physician and Sportsmedicine*, vol. 40, no. 4, 2012, doi: 10.3810/psm.2012.11.1989.

[72] V. H. Stiles, I. T. James, S. J. Dixon, and I. N. Guisasola, “Natural turf surfaces: The case for continued research,” *Sports Medicine*, vol. 39, no. 1. 2009. doi: 10.2165/00007256-200939010-00005.

[73] P. Fleming, “Artificial turf systems for sport surfaces: Current knowledge and research needs,” *Proc Inst Mech Eng P J Sport Eng Technol*, vol. 225, no. 2, 2011, doi: 10.1177/1754337111401688.

[74] Neo Grass, “The History of Artificial Grass,” Online.

[75] G. Oldenkotte, “Non-filled development doesn’t satisfy FIFA yet,” Online. Accessed: Sep. 23, 2023. [Online]. Available: https://sportsfields.info/non-filled-development-doesnt-satisfy-fifa-yet/

[76] M. R. Shorten and J. a Himmelsbach, “Shock attenuation of sports surfaces,” *The Engineering of Sport IV: Proceedings of the 4th International Conference on the Engineering of Sport*, vol. 4, no. September, 2002.

[77] K. Fujikake, T. Yamamoto, and M. Takemura, “A comparison of the mechanical charatceristics of natural turf and artificial turf football pitches,” *Football Science*, 2007.

[78] World Rugby, “ Shock pad advice: World Rugby.” Accessed: Nov. 13, 2023. [Online]. Available: https://www.world.rugby/the-game/facilities-equipment/surfaces/shock-pads

[79] P. R. Fleming, C. Watts, and S. Forrester, “A new model of third generation artificial turf degradation, maintenance interventions and benefits,” *Proc Inst Mech Eng P J Sport Eng Technol*, vol. 237, no. 1, 2023, doi: 10.1177/1754337120961602.

[80] C. H. Webb, “Mechanical traction behaviour of artificial turf,” Loughborough University, Loughborough , 2017.

[81] David Cole, “Numerical modelling of 3G artificial turf under vertical loading Cite Download (14.96 MB) Share Embed + Collect,” Loughborough University, Loughborough , 2020.

[82] SAPCA, *The SAPCA Code of Practice for the Construction and Maintenance of Synthetic Turf Sports Pitches*. 2009.

[83] E. Scott, “End-of-life Tyre REPORT, European Tyre & Rubber Manufacturers Association, 2015,” *Resour Conserv Recycl*, vol. 3, no. 2, 2015.

[84] A. J. Verschoor, A. van Gelderen, and U. Hofstra, “Fate of recycled tyre granulate used on artificial turf,” *Environmental Sciences Europe*, vol. 33, no. 1. 2021. doi: 10.1186/s12302-021-00459-1.

[85] B. Grynkiewicz-Bylina, B. Rakwic, and B. Słomka-Słupik, “Tests of rubber granules used as artificial turf for football fields in terms of toxicity to human health and the environment,” *Sci Rep*, vol. 12, no. 1, 2022, doi: 10.1038/s41598-022-10691-1.

[86] S. Pfautsch, A. Wujeska-Klause, and J. Walters, “Outdoor playgrounds and climate change: Importance of surface materials and shade to extend play time and prevent burn injuries,” *Build Environ*, vol. 223, 2022, doi: 10.1016/j.buildenv.2022.109500.

[87] J. Gigault *et al.*, “Current opinion: What is a nanoplastic?,” *Environmental Pollution*, vol. 235. 2018. doi: 10.1016/j.envpol.2018.01.024.

[88] T. Schell, A. Rico, and M. Vighi, “Occurrence, Fate and Fluxes of Plastics and Microplastics in Terrestrial and Freshwater Ecosystems,” in *Reviews of Environmental Contamination and Toxicology*, vol. 250, 2020. doi: 10.1007/398_2019_40.

[89] S. S. Muthu, *Microplastic Pollution*. Singapore: Springer Singapore, 2021. doi: 10.1007/978-981-16-0297-9.

[90] Synthetic Turf Council EMEA, “ECHA calls for total ban on plastic infill,” Online. Accessed: Dec. 19, 2023. [Online]. Available: https://www.estc.info/echa-calls-for-total-ban-on-plastic-infill/

[91] Field Turf, “THE GUIDE TO BUYING YOUR FIRST ARTIFICIAL TURF FIELD.” Accessed: Feb. 07, 2024. [Online]. Available: https://fieldturf.com/en/articles/detail/buying-guide-first-artificial-turf-field/

[92] I. James and A. McLeod, “Maintaining Synthetic Turf : Sand Filled Systems,” *The Cranfield - IOG Guidelines*, no. September, 2008.

[93] N. J. McLaren, P. R. Fleming, and S. Forrester, “Artificial grass: A longitudinal study on ball roll and free pile height,” in *Procedia Engineering*, 2014. doi: 10.1016/j.proeng.2014.06.146.

[94] S. P. Tay, P. Fleming, S. Forrester, and X. Hu, “Insights to skin-turf friction as investigated using the Securisport,” in *Procedia Engineering*, 2015. doi: 10.1016/j.proeng.2015.07.252.

[95] G. Oldenkotte, “FIFA makes washing of test samples mandatory,” Online. Accessed: Sep. 17, 2023. [Online]. Available: https://sportsfields.info/fifa-makes-washing-of-test-samples-mandatory/

[96] M. M. Khonsari and E. R. Booser, *Applied tribology: bearing design and lubrication*. John Wiley & Sons., 2017.

[97] R. Lewis, M. J. Carré, and S. E. Tomlinson, “Skin friction at the interface between hands and sports equipment,” in *Procedia Engineering*, Elsevier Ltd, 2014, pp. 611–617. doi: 10.1016/j.proeng.2014.06.064.

[98] Gedeon M., “Introduction to Friction,” 2015, pp. 7–48. doi: 10.1007/978-3-319-20022-4_2.

[99] J. F. Archard, “Wear {Theory} and {Mechanisms},” *Wear {Control} {Handbook}*. 1980.

[100] E. Rabinowicz and R. I. Tanner, “Friction and Wear of Materials,” *J Appl Mech*, vol. 33, no. 2, 1966, doi: 10.1115/1.3625110.

[101] T. M. Laronge and M. A. Ward, “The basics and not so basics of water corrosion processes altered by flow changes,” in *NACE - International Corrosion Conference Series*, 1999.

[102] A. Tsujimoto *et al.*, “Wear of resin composites: Current insights into underlying mechanisms, evaluation methods and influential factors.,” *Jpn Dent Sci Rev*, vol. 54, no. 2, pp. 76–87, May 2018, doi: 10.1016/j.jdsr.2017.11.002.

[103] M. D. Hersey, “The laws of lubrication of horizontal journal bearings,” *Journal of the Washington Academy of Sciences*, vol. 4, no. 19, pp. 542–552, Nov. 1914.

[104] C. Zhang, “Understanding the wear and tribological properties of ceramic matrix composites,” in *Advances in Ceramic Matrix Composites*, 2014. doi: 10.1533/9780857098825.2.312.

[105] J. Sotres and T. Arnebrant, “Experimental investigations of biological lubrication at the nanoscale: The cases of synovial joints and the oral cavity,” *Lubricants*, vol. 1, no. 4, pp. 102–131, 2013, doi: 10.3390/lubricants1040102.

[106] J. de Vicente, J. R. Stokes, and H. A. Spikes, “Rolling and sliding friction in compliant, lubricated contact,” *Proceedings of the Institution of Mechanical Engineers, Part J: Journal of Engineering Tribology*, vol. 220, no. 2, pp. 55–63, 2006, doi: 10.1243/13506501JET90.

[107] E. Ciulli, A. Betti, and P. Forte, “The Applicability of the Hertzian Formulas to Point Contacts of Spheres and Spherical Caps,” *Lubricants*, vol. 10, no. 10, 2022, doi: 10.3390/lubricants10100233.

[108] M. J. Carré, S. E. Tomlinson, J. W. Collins, and R. Lewis, “An assessment of the performance of grip enhancing agents used in sports applications,” *Proceedings of the Institution of Mechanical Engineers, Part J: Journal of Engineering Tribology*, vol. 226, no. 7, pp. 616–625, Jul. 2012, doi: 10.1177/1350650112439647.

[109] T. Yamaguchi, N. Yamakura, S. Murata, T. Fukuda, and D. Nasu, “Effects of Rosin Powder Application on the Frictional Behavior Between a Finger Pad and Baseball,” *Front Sports Act Living*, vol. 2, Apr. 2020, doi: 10.3389/fspor.2020.00030.

[110] S. E. Tomlinson, R. Lewis, S. Ball, A. Yoxall, and M. J. Carré, “Understanding the effect of finger-ball friction on the handling performance of rugby balls,” *Sports Engineering*, vol. 11, no. 3, pp. 109–118, Jun. 2009, doi: 10.1007/s12283-009-0014-7.

[111] R. Lewis, M. J. Carré, A. Abu Bakar, and S. E. Tomlinson, “Effect of surface texture, moisture and wear on handling of rugby balls,” *Tribol Int*, vol. 63, Jul. 2013, doi: 10.1016/j.triboint.2012.07.002.

[112] G. G. Sorbie, P. Darroch, F. M. Grace, Y. Gu, J. S. Baker, and U. C. Ugbolue, “Commercial golf glove effects on golf performance and forearm muscle activity,” *Research in Sports Medicine*, vol. 25, no. 4, pp. 451–461, 2017, doi: 10.1080/15438627.2017.1365291.

[113] M. Lutgendorf, B. Mason, L. van der Woude, and V. L. Goosey-Tolfrey, "Effect of glove type on wheelchair rugby sports performance," *Sports Engineering*, vol. 2, no. 3–4, pp. 121–128, 2009, doi: 10.1002/jst.103.

[114] K. A. Karlson, "Rowing injuries," *Phys Sportsmed*, vol. 28, no. 4, pp. 40–50, 2000, doi: 10.3810/psm.2000.04.837.

[115] S. S. Gardner, "Cauliflower Ear: Symptoms, Causes, and Treatments," WebMD. Accessed: May 26, 2021. [Online]. Available: https://www.webmd.com/skin-problems-and-treatments/cauliflower-ear-symptoms-causes-treatments

[116] LoveRugbyLeague, "NRL ban James Graham using Vaseline | LoveRugbyLeague." Accessed: May 26, 2021. [Online]. Available: https://www.loverugbyleague.com/post/nrl-ban-james-graham-using-vaseline/

[117] ScottishRugbyBlog, "The New Scotland Rugby Kit 2011 - Scottish Rugby Blog." Accessed: May 26, 2021. [Online]. Available: https://www.scottishrugbyblog.co.uk/2011/06/the-new-scotland-2011-rugby-kit/

[118] S. P. Tay, "New strategies towards the next generation of skin-friendly artificial turf surfaces," Nanyang Technological University, 2016.

[119] World Rugby, "A Year In Review 2021 Annual Report," vol. 44, 2021, [Online]. Available: http://publications.worldrugby.org/yearinreview2021/en/2-1

[120] L. Paul *et al.*, "Correction: Quantifying Collision Frequency and Intensity in Rugby Union and Rugby Sevens: A Systematic Review (Sports Medicine - Open, (2022), 8, 1, (12), 10.1186/s40798-021-00398-4)," *Sports Medicine - Open*, vol. 8, no. 1. 2022. doi: 10.1186/s40798-022-00494-z.

[121] A. Bathgate, J. P. Best, G. Craig, and M. Jamieson, "A prospective study of injuries to elite Australian rugby union players," *Br J Sports Med*, vol. 36, no. 4, 2002, doi: 10.1136/bjsm.36.4.265.

[122] S. Williams *et al.*, "Injuries in Elite Men's Rugby Union: An Updated (2012–2020) Meta-Analysis of 11,620 Match and Training Injuries," *Sports Medicine*, vol. 52, no. 5. 2022. doi: 10.1007/s40279-021-01603-w.

[123] H. Rees, U. McCarthy Persson, E. Delahunt, C. Boreham, and C. Blake, "Epidemiology of injuries in senior men's field hockey: A two-season prospective observational injury surveillance study," *J Sports Sci*, vol. 38, no. 24, 2020, doi: 10.1080/02640414.2020.1802094.

[124] J. Ekstrand, M. Hägglund, and C. W. Fuller, "Comparison of injuries sustained on artificial turf and grass by male and female elite football players," *Scand J Med Sci Sports*, vol. 21, no. 6, pp. 824–832, 2011, doi: 10.1111/j.1600-0838.2010.01118.x.

[125] S. Hendricks *et al.*, "Technical determinants of tackle and ruck performance in International rugby union," *J Sports Sci*, vol. 36, no. 5, 2018, doi: 10.1080/02640414.2017.1322216.

[126] G. G. Gosnell, B. A. Gerber, G. P. Guyton, and H. P. Gould, "Playing Surface and Injury Risk: Artificial Turf Vs. Natural Grass," in *Injuries and Sports Medicine*, 2023. doi: 10.5772/intechopen.106615.

[127] L. Sivasundaram *et al.*, "Injury risk among athletes on artificial turf: A review of current literature," *Current Orthopaedic Practice*, vol. 32, no. 5. 2021. doi: 10.1097/BCO.0000000000001021.

[128] M. Peppelman, W. A. J. Van Den Eijnde, A. M. G. Langewouters, M. O. Weghuis, and P. E. J. Van Erp, "The Potential of the Skin as a Readout System to Test Artificial Turf Systems: Clinical and Immunohistological Effects of a Sliding on Natural Grass and Artificial Turf," *Int J Sports Med*, vol. 34, no. 9, 2013, doi: 10.1055/s-0032-1331173.

[129] W. A. J. van den Eijnde, M. Peppelman, E. A. D. Lamers, P. C. M. van de Kerkhof, and P. E. J. van Erp, "Understanding the acute skin injury mechanism caused by player-surface contact during soccer: A survey and systematic review," *Orthop J Sports Med*, vol. 2, no. 5, pp. 1–8, 2014, doi: 10.1177/2325967114533482.

[130] C. W. Fuller, R. W. Dick, J. Corlette, and R. Schmalz, "Comparison of the incidence, nature and cause of injuries sustained on grass and new generation artificial turf by male and female football players. Part 2: Training injuries," *Br J Sports Med*, vol. 41, no. SUPPL. 1, 2007, doi: 10.1136/bjsm.2007.037275.

[131] C. W. Fuller *et al.*, "Consensus statement on injury definitions and data collection procedures for studies of injuries in rugby union," *Clinical Journal of Sport Medicine*, vol. 17, no. 3, 2007, doi: 10.1097/JSM.0b013e31803220b3.

[132] E. Mathewson and R. Grobbelaar, "Tackle-injury epidemiology in *koshuis* rugby players at Stellenbosch University," *South African Journal of Sports Medicine*, vol. 27, no. 3, 2015, doi: 10.7196/sajsm.8091.

[133] B. Y. Oudshoorn, H. Driscoll, K. Kilner, M. Dunn, and D. James, "Prevalence of laceration injuries in professional and amateur rugby union: A systematic review and meta-analysis," *BMJ Open Sport Exerc Med*, vol. 3, no. 1, 2017, doi: 10.1136/bmjsem-2017-000239.

[134] T. Soligard, R. Bahr, and T. E. Andersen, "Injury risk on artificial turf and grass in youth tournament football," *Scand J Med Sci Sports*, vol. 22, no. 3, 2012, doi: 10.1111/j.1600-0838.2010.01174.x.

[135] S. Williams, G. Trewartha, S. P. T. Kemp, R. Michell, K. A. Stokes, and S. Williams, "The influence of an artificial playing surface on injury risk and perceptions of muscle soreness in elite Rugby Union," 2015, doi: 10.1111/sms.12402.

[136] J. Worobets and J. W. Wannop, "Influence of basketball shoe mass, outsole traction, and forefoot bending stiffness on three athletic movements," *Sports Biomech*, vol. 14, no. 3, 2015, doi: 10.1080/14763141.2015.1084031.

[137] G. Luo and D. Stefanyshyn, "Identification of critical traction values for maximum athletic performance," *Footwear Sci*, vol. 3, no. 3, 2011, doi: 10.1080/19424280.2011.639807.

[138] J. W. Wannop, T. Foreman, R. Madden, and D. Stefanyshyn, “Influence of the composition of artificial turf on rotational traction and athlete biomechanics,” *J Sports Sci*, vol. 37, no. 16, 2019, doi: 10.1080/02640414.2019.1598923.

[139] T. Sterzing, C. Müller, E. M. Hennig, and T. L. Milani, “Actual and perceived running performance in soccer shoes: A series of eight studies,” *Footwear Sci*, vol. 1, no. 1, 2009, doi: 10.1080/19424280902915350.

[140] J. R. Roberts, P. Osei-Owusu, A. C. Mears, and A. R. Harland, “Elite Players’ Perceptions of Football Playing Surfaces: A Qualitative Study,” *Res Q Exerc Sport*, vol. 91, no. 2, 2020, doi: 10.1080/02701367.2019.1660757.

[141] R. D. Corzatt, J. L. Groppel, E. Pfautsch, and J. Boscardin, “The biomechanics of head-first versus feet-first sliding,” *Am J Sports Med*, vol. 12, no. 3, 1984, doi: 10.1177/036354658401200312.

[142] C. W. Fuller, G. L. Smith, A. Junge, and J. Dvorak, “The Influence of Tackle Parameters on the Propensity for Injury in International Football,” *American Journal of Sports Medicine*, vol. 32, no. SUPPL. 1, 2004, doi: 10.1177/0363546503261248.

[143] R. G. Hosey and J. C. Puffer, “Baseball and softball sliding injuries. Incidence, and the effect of technique in collegiate baseball and softball players.,” *Am J Sports Med*, vol. 28, no. 3, pp. 360–363, 2000, doi: 10.1177/03635465000280031301.

[144] L. Posthumus, C. Macgregor, P. Winwood, K. Darry, M. Driller, and N. Gill, “Physical and fitness characteristics of elite professional rugby union players,” *Sports*, vol. 8, no. 6, 2020, doi: 10.3390/sports8060085.

[145] Rugby Rucker, “Ranking the top 5 fastest rugby union players in the world,” Online. Accessed: Nov. 13, 2023. [Online]. Available: https://www.ruck.co.uk/ranking-the-top-5-fastest-rugby-union-players-in-the-world/3/

[146] NASA, “ANTHROPOMETRY AND BIOMECHANICS.” [Online]. Available: https://msis.jsc.nasa.gov/sections/section03.htm

[147] M. T. G. Pain, F. Tsui, and S. Cove, "In vivo determination of the effect of shoulder pads on tackling forces in rugby," *J Sports Sci*, vol. 26, no. 8, 2008, doi: 10.1080/02640410801910319.

[148] K. U. Schmitt, M. Schlittler, and P. Boesiger, "Biomechanical loading of the hip during side jumps by soccer goalkeepers," *J Sports Sci*, vol. 28, no. 1, 2010, doi: 10.1080/02640410903369927.

[149] W. Van Den Eijnde, K. Meijer, E. Lamers, M. Peppelman, and P. Van Erp, "Exploring the biomechanical load of a sliding on the skin: Understanding the acute skin injury mechanism of player-surface interaction," *Journal of Sports Medicine and Physical Fitness*, vol. 57, no. 9, 2017, doi: 10.23736/S0022-4707.16.06404-5.

[150] M. C. Drakos, S. A. Taylor, P. D. Fabricant, and A. M. Haleem, "Synthetic playing surfaces and athlete health," *Journal of the American Academy of Orthopaedic Surgeons*, vol. 21, no. 5. 2013. doi: 10.5435/JAAOS-21-05-293.

[151] N. McLaren, P. Fleming, and S. Forrester, "Artificial grass: A conceptual model for degradation in performance," in *Procedia Engineering*, 2012. doi: 10.1016/j.proeng.2012.04.142.

[152] M. C. Meyers, "Incidence, Mechanisms, and Severity of Game-Related High School Football Injuries Across Artificial Turf Systems of Various Infill Weights," *Orthop J Sports Med*, vol. 7, no. 3, 2019, doi: 10.1177/2325967119832878.

[153] K. Fujitaka, A. Taniguchi, T. Kumai, S. Otuki, M. Okubo, and Y. Tanaka, "Effect of changes in artificial turf on sports injuries in male university soccer players," *Orthop J Sports Med*, vol. 5, no. 8, 2017, doi: 10.1177/2325967117719648.

[154] Craig Ingham, " Linear vs. Rotational Skin Friction 'A deductive evaluation of the Securisport tests suitability for the analysis of skin friction on football turf.,'" Strathclyde University, Glasgow, 2013.

[155] S. P. Tay, X. Hu, P. Fleming, and S. Forrester, “Tribological investigation into achieving skin-friendly artificial turf surfaces,” *Mater Des*, vol. 89, 2016, doi: 10.1016/j.matdes.2015.09.033.

[156] W. Van den Eijnde, M. Peppelman, M. O. Weghuis, and P. E. J. Van Erp, “Psychosensorial assessment of skin damage caused by a sliding on artificial turf: The development and validation of a skin damage area and severity index,” *J Sci Med Sport*, vol. 17, no. 1, 2014, doi: 10.1016/j.jsams.2013.03.017.

[157] S. P. Tay, P. Fleming, X. Hu, and S. Forrester, “Skin friction related behaviour of artificial turf systems,” *J Sports Sci*, vol. 35, no. 15, 2017, doi: 10.1080/02640414.2016.1223330.

[158] a. S. McNitt and D. Petrunak, “Evaluation of playing surface characteristics of various in-filled systems,” *Evaluation*, vol. 9, p. 20, 2007, [Online]. Available: http://cropsoil.psu.edu/mcnitt/infill8.cfm%5Cnhttp://www.ci.wellesley.ma.us/Pages/WellesleyMA_SpragueResources/Evaluation of Playing Surface Characteristics.pdf

[159] hockey.nl, “FIH: REVOLUTIONISING HOCKEY – FIH BANNING WATER-BASED PITCHES IN INTERNATIONAL GAMES POST-PARIS 2024,” Hockey World News. Accessed: Oct. 22, 2023. [Online]. Available: https://www.hockeywrldnws.com/fih-revolutionising-hockey-fih-banning-water-based-pitches-in-international-games-post-paris-2024/

[160] Labo Sport, “Skin Injury Test.” Accessed: Nov. 16, 2023. [Online]. Available: https://labosport.com/skin-injury-test/

[161] Fédération Internationale de Football Association, “FIFA Quality Concept for Football Turf: Handbook of Test Methods.,” Online. Accessed: Dec. 20, 2023. [Online]. Available: www.FIFA.com

[162] A. B. Cua, K. P. Wilhelm, and H. I. Maibach, “Frictional properties of human skin: Relation to age, sex and anatomical region, stratum corneum hydration and transepidermal water loss,” *British Journal of Dermatology*, vol. 123, no. 4, 1990, doi: 10.1111/j.1365-2133.1990.tb01452.x.

[163] D. J. Cottenden and A. M. Cottenden, “A study of friction mechanisms between a surrogate skin (lorica soft) and nonwoven fabrics,” *J Mech Behav Biomed Mater*, vol. 28, pp. 410–426, 2013, doi: 10.1016/j.jmbbm.2013.04.024.

[164] A. Summerfield, F. Meurens, and M. E. Ricklin, “The immunology of the porcine skin and its value as a model for human skin,” *Molecular Immunology*, vol. 66, no. 1. 2015. doi: 10.1016/j.molimm.2014.10.023.

[165] S. Shahrokhi, A. Arno, and M. G. Jeschke, “The use of dermal substitutes in burn surgery: Acute phase,” *Wound Repair and Regeneration*, vol. 22, no. 1. 2014. doi: 10.1111/wrr.12119.

[166] R. Neupane, S. H. S. Boddu, J. Renukuntla, R. J. Babu, and A. K. Tiwari, “Alternatives to biological skin in permeation studies: Current trends and possibilities,” *Pharmaceutics*, vol. 12, no. 2. 2020. doi: 10.3390/pharmaceutics12020152.

[167] B. L. Seal, T. C. Otero, and A. Panitch, “Polymeric biomaterials for tissue and organ regeneration,” *Materials Science and Engineering: R: Reports*, vol. 34, no. 4–5. 2001. doi: 10.1016/S0927-796X(01)00035-3.

[168] A. Demir and E. Cevher, “Biopolymers as Wound Healing Materials: Challenges and New Strategies,” in *Biomaterials Applications for Nanomedicine*, 2011. doi: 10.5772/25177.

[169] S. N. A. Mohd Noor and J. Mahmud, “A review on synthetic skin: Materials investigation, experimentation and simulation,” in *Advanced Materials Research*, 2014. doi: 10.4028/www.scientific.net/AMR.915-916.858.

[170] N. K. Veijgen, M. A. Masen, and E. Van Der Heide, “A novel approach to measuring the frictional behaviour of human skin in vivo,” *Tribol Int*, vol. 54, 2012, doi: 10.1016/j.triboint.2012.05.022.

[171] M. R. Cutkosky, J. M. Jourdain, and P. K. Wright, “SKIN MATERIALS FOR ROBOTIC FINGERS.,” 1987. doi: 10.1109/robot.1987.1087913.

[172] J. Jachowicz, R. Mcmullen, and D. Prettypaul, "Indentometric analysis of in vivo skin and comparison with artificial skin models," *Skin Research and Technology*, vol. 13, no. 3, 2007, doi: 10.1111/j.1600-0846.2007.00229.x.

[173] F. Shao, T. H. C. Childs, and B. Henson, "Developing an artificial fingertip with human friction properties," *Tribol Int*, vol. 42, no. 11–12, 2009, doi: 10.1016/j.triboint.2009.02.005.

[174] E. van der Heide, C. M. Lossie, K. J. C. Vanbommel, S. A. F. Reinders, and H. B. M. Lenting, "Experimental investigation of a polymer coating in sliding contact with skin-equivalent silicone rubber in an aqueous environment," *Tribology Transactions*, vol. 53, no. 6, 2010, doi: 10.1080/10402004.2010.496068.

[175] S. Franklin, J. Baranowska, J. Furgala, and J. Piwowarczyk, "Friction of natural human, porcine and synthetic skin," in *Proceedings of the 5th international conference on mechanics of biomaterials and tissues*, Sitges, Dec. 2013.

[176] A. K. Dabrowska *et al.*, "Materials used to simulate physical properties of human skin," *Skin Research and Technology*, vol. 22, no. 1, 2016, doi: 10.1111/srt.12235.

[177] C. P. Hendriks and S. E. Franklin, "Influence of surface roughness, material and climate conditions on the friction of human skin," *Tribol Lett*, vol. 37, no. 2, 2010, doi: 10.1007/s11249-009-9530-7.

[178] SynDaver, " Adult Skin," Online. Accessed: May 23, 2023. [Online]. Available: https://syndaver.com/product/adult-skin/

[179] S. S. Falloon and A. Cottenden, "Friction between a surrogate skin (Lorica Soft) and nonwoven fabrics used in hygiene products," *Surf Topogr*, vol. 4, no. 3, 2016, doi: 10.1088/2051-672X/4/3/034010.

[180] K. P. M. Tang, K. H. Chau, C. W. Kan, and J. T. Fan, "Instrumental Evaluation of Stickiness of Textiles under Wet Skin Surface," *IEEE Access*, vol. 6, 2018, doi: 10.1109/ACCESS.2018.2829151.

[181] I. J. DeBois, E. Agarwal, A. Kapoor, and K. Mathur, "Tribology of the sock-skin Interface – the influence of different fabric parameters on sock friction," *J Foot Ankle Res*, vol. 15, no. 1, 2022, doi: 10.1186/s13047-022-00560-5.

[182] S. Derler, U. Schrade, and L. C. Gerhardt, "Tribology of human skin and mechanical skin equivalents in contact with textiles," *Wear*, vol. 263, no. 7-12 SPEC. ISS., 2007, doi: 10.1016/j.wear.2006.11.031.

[183] J. M. Lagarde, C. Rouvrais, and D. Black, "Topography and anisotropy of the skin surface with ageing," *Skin Research and Technology*, vol. 11, no. 2, 2005, doi: 10.1111/j.1600-0846.2005.00096.x.

[184] L. Li *et al.*, "Age-related changes in skin topography and microcirculation," *Arch Dermatol Res*, vol. 297, no. 9, 2006, doi: 10.1007/s00403-005-0628-y.

[185] M. Klaassen, E. G. de Vries, and M. A. Masen, "Friction in the contact between skin and a soft counter material: Effects of hardness and surface finish," *J Mech Behav Biomed Mater*, vol. 92, 2019, doi: 10.1016/j.jmbbm.2019.01.006.

[186] J. Van Kuilenburg, M. A. Masen, and E. Van Der Heide, "Contact modelling of human skin: What value to use for the modulus of elasticity?," *Proceedings of the Institution of Mechanical Engineers, Part J: Journal of Engineering Tribology*, vol. 227, no. 4, 2013, doi: 10.1177/1350650112463307.

[187] J. Ekstrand and B. M. Nigg, "Surface-Related Injuries in Soccer," *Sports Medicine*, vol. 8, no. 1, 1989, doi: 10.2165/00007256-198908010-00006.

[188] J. L. Dragoo and H. J. Braun, "The effect of playing surface on injury rate: A review of the current literature," *Sports Medicine*, vol. 40, no. 11. 2010. doi: 10.2165/11535910-000000000-00000.

[189] D. M. Twomey, L. A. Petrass, and P. R. Fleming, "Abrasion injuries on artificial turf: A real risk or not?," *South African Journal of Sports Medicine*, vol. 26, no. 3, 2014, doi: 10.7196/sajsm.563.

[190] H. Andersson, B. Ekblom, and P. Krustrup, "Elite football on artificial turf versus natural grass: Movement patterns, technical standards, and player impressions," *J Sports Sci*, vol. 26, no. 2, 2008, doi: 10.1080/02640410701422076.

[191] J. L. Felipe, L. Gallardo, P. Burillo, A. Gallardo, J. Sánchez-Sánchez, and M. Plaza-Carmona, "A qualitative vision of artificial turf football fields: Elite players and coaches," *South African Journal for Research in Sport, Physical Education and Recreation*, vol. 35, no. 2, 2013.

[192] S. Williams, G. Trewartha, S. Kemp, and K. Stokes, "A meta-analysis of injuries in senior men's professional Rugby Union," *Sports Medicine*, vol. 43, no. 10. 2013. doi: 10.1007/s40279-013-0078-1.

[193] I. Cameron, "Super controversial 'waist height tackling' among 6 law changes 'endorsed,'" Online. Accessed: Jun. 03, 2023. [Online]. Available: https://www.rugbypass.com/news/super-controversial-waist-height-tackling-among-6-law-changes-endorsed/

[194] A. Peeters, C. Carling, J. Piscione, and M. Lacome, "In-match physical performance fluctuations in international rugby sevens competition," *J Sports Sci Med*, vol. 18, no. 3, 2019.

[195] H. Yamamoto, M. Takemura, J. Iguchi, M. Tachibana, J. Tsujita, and T. Hojo, "In-match physical demands on elite Japanese rugby union players using a global positioning system," *BMJ Open Sport Exerc Med*, vol. 6, no. 1, 2020, doi: 10.1136/bmjsem-2019-000659.

[196] S. Wang, G. Zhang, H. Meng, and L. Li, "Effect of Exercise-induced sweating on facial sebum, stratum corneum hydration, and skin surface ph in normal population," *Skin Research and Technology*, vol. 19, no. 1, 2013, doi: 10.1111/j.1600-0846.2012.00645.x.

[197] O. Ryosuke and S. Yoshie, "The association between activity levels and skin moisturising function in adults," *Dermatol Reports*, vol. 13, no. 1, 2021, doi: 10.4081/DR.2021.8811.

[198] L. Wolfram, “Friction of skin ,” *J Soc Cosmet Chem*, vol. Soc, no. REF 13, pp. 465–476, 1983.

[199] S. A. Johnson, D. M. Gorman, M. J. Adams, and B. J. Briscoe, “The friction and lubrication of human stratum corneum,” *Tribology Series*, vol. 25, no. C, 1993, doi: 10.1016/S0167-8922(08)70419-X.

[200] P. Kenins, “Influence of Fiber Type and Moisture on Measured Fabric-to-Skin Friction,” *Textile Research Journal*, vol. 64, no. 12, 1994, doi: 10.1177/004051759406401204.

[201] L. C. Gerhardt, N. Mattle, G. U. Schrade, N. D. Spencer, and S. Derler, “Study of skin-fabric interactions of relevance to decubitus: Friction and contact-pressure measurements,” *Skin Research and Technology*, vol. 14, no. 1, pp. 77–88, 2008, doi: 10.1111/j.1600-0846.2007.00264.x.

[202] I. Pereira, P. Severino, A. C. Santos, A. M. Silva, and E. B. Souto, “Linalool bioactive properties and potential applicability in drug delivery systems,” *Colloids and Surfaces B: Biointerfaces*, vol. 171. 2018. doi: 10.1016/j.colsurfb.2018.08.001.

[203] H. Mohammed, N. Sukumar, and B. Seyoum, “Thermal Conductivity & Tensile Properties of Stitch Bonded Nonwoven Fabric Developed Using Reclaimed Cotton and Virgin Acrylic Blend,” *Journal of Natural Fibers*, vol. 19, no. 11, 2022, doi: 10.1080/15440478.2020.1856269.

[204] The Open University, “Systems thinking,” Online. Accessed: Nov. 14, 2023. [Online]. Available: https://www.open.edu/openlearn/digital-computing/systems-thinking-and-practice/content-section-4

[205] Eisenhower, “Professional Services Capability Framework: Planning,” 2023. Accessed: Nov. 14, 2023. [Online]. Available: https://blogs.shu.ac.uk/shupdreviewtoolkit/files/2019/01/Eisenhower-Quadrant.pdf

[206] A. Parr, *Hydraulics and Pneumatics: A Technician’s and Engineer’s Guide*, 3rd Edition. 2011.

[207] ABB, “Technical guide No. 9 - Guide to motion control drives,” 2013. [Online]. Available: https://library.e.abb.com/public/bbc682806eb5be78c125727c0043f50b/Technical_guide_No_9_3AFE68695201_EN_RevB_11_2.pdf

[208] M. Peiyuan, L. Yuguang, and X. Chuanjun, “Research on the technology of fixed stroke lead screw transmission mechanism with self positioning function,” in *Proceedings - 2020 5th International Conference on Mechanical, Control and Computer Engineering, ICMCCE 2020*, 2020. doi: 10.1109/ICMCCE51767.2020.00135.

[209] A. Rahmani Hanzaki, P. V. M. Rao, and S. K. Saha, “Kinematic and sensitivity analysis and optimization of planar rack-and-pinion steering linkages,” *Mech Mach Theory*, vol. 44, no. 1, 2009, doi: 10.1016/j.mechmachtheory.2008.02.014.

[210] K. Stockman, S. Dereyne, P. Defreyne, E. Algoet, and S. Derammelaere, “An efficiency measurement campaign on belt drives,” *Energy efficiency in motor driven systems, Proceedings*, 2015.

[211] R. Palka and K. Woronowicz, “Linear induction motors in transportation systems,” *Energies*, vol. 14, no. 9. 2021. doi: 10.3390/en14092549.

[212] M. Seal and M. Sengupta, “Optimised design, analysis, fabrication and experiments on a tubular linear induction motor prototype,” *Sadhana - Academy Proceedings in Engineering Sciences*, vol. 47, no. 4, 2022, doi: 10.1007/s12046-022-01942-y.

[213] The Editors of Encyclopaedia Britannica, “Lorentz force,” Online. Accessed: Jan. 27, 2023. [Online]. Available: https://www.britannica.com/science/Lorentz-force

[214] HumanShape, “Human Shape,” Online. Accessed: Nov. 14, 2023. [Online]. Available: http://humanshape.org/

[215] John Winter, “Ages Of Professional Rugby Players (2022/23),” Online. Accessed: Jun. 12, 2023. [Online]. Available: https://rugbydome.com/how-old-are-rugby-players/

[216] J. D. Serna and A. Joshi, “Studying springs in series using a single spring,” *Phys Educ*, vol. 46, no. 1, 2011, doi: 10.1088/0031-9120/46/1/003.

[217] D. J. Stefanyshyn and J. W. Wannop, “Biomechanics research and sport equipment development,” *Sports Engineering*, vol. 18, no. 4, 2015, doi: 10.1007/s12283-015-0183-5.

[218] J. Wollaeger, T. J. Puccinelli, W. Brown, C. Link, I. Krause, and S. Ferris, “Dead Blow Hammer in Orthopedics,” Wisconsin, Dec. 2021.

[219] B. Parikh, “How dampers turn WRC cars into high fliers,” Online. Accessed: Nov. 14, 2023. [Online]. Available: https://www.redbull.com/gb-en/how-wrc-cars-do-big-jumps-in-rallies

[220] FOX Academy, “ How To Use Rebound Damping,” Online. Accessed: Nov. 14, 2023. [Online]. Available: https://foxacademy.ridefox.com/2020/11/how-to-use-rebound-damping/

[221] Sports Labs, “Distance Travelled By Sports Labs Lisport XLs ,” *LinkedIn*. 2023. Accessed: Sep. 18, 2023. [Online]. Available: https://www.linkedin.com/posts/sports-labs-ltd_distance-travelled-by-sports-labs-lisport-activity-7051892252003999744-Kkhu/

[222] World Rugby, “Regulation 22. Standard relating to the use of rugby turf,” Online. Accessed: Nov. 14, 2023. [Online]. Available: https://www.world.rugby/organisation/governance/regulations/reg-22

[223] World Rugby, “Player Welfare,” Online. Accessed: Nov. 14, 2023. [Online]. Available: https://www.world.rugby/the-game/player-welfare

[224] M. J. MacFarlane and P. Theobald, “Skin tribology in sport,” *Biosurface and Biotribology*, vol. 7, no. 3. 2021. doi: 10.1049/bsb2.12015.

[225] A. Abdelbary and L. Chang, *Principles of Engineering Tribology: Fundamentals and Applications*. 2023. doi: 10.1016/C2021-0-01365-1.

[226] J. Wu, “A Basic Guide to Thermocouple Measurements,” *Texas Instruments Incorporated*, no. September, 2018.

[227] Reem Malik, "Thermocouple Linearization When Using the AD8494/AD8495/AD8496/AD8497," Norwood, 2023.

[228] A. Szajewska, "Development of the Thermal Imaging Camera (TIC) Technology," in *Procedia Engineering*, 2017. doi: 10.1016/j.proeng.2017.02.164.

[229] S. De Iuliis, R. Dondè, and I. Altman, "On Pyrometry in Particulate-Generating Flames," *Combustion Science and Technology*, vol. 194, no. 9, 2022, doi: 10.1080/00102202.2020.1834391.

[230] World Rugby, "Pile Height Change," Online. Accessed: Nov. 20, 2023. [Online]. Available: https://www.world.rugby/the-game/facilities-equipment/surfaces/50mm

[231] World Rugby, "Rationale for the introduction of a 50mm pile height to the World Rugby Turf Performance Specification," Dublin, Aug. 2020.

[232] Brock USA, "Brock Matters ," Online. Accessed: Nov. 12, 2023. [Online]. Available: https://www.brockusa.com/

[233] F. Kisuka, C.-Y. Wu, and C. Hare, "Friction-induced heat generation between two particles," *EPJ Web Conf*, vol. 249, 2021, doi: 10.1051/epjconf/202124905007.

[234] H. Blok, "The flash temperature concept," *Wear*, vol. 6, no. 6, 1963, doi: 10.1016/0043-1648(63)90283-7.

[235] R. Shrestha, K. Krishan, H. Ishaq, and T. Kanchan, *Abrasion* . Florida: StatPearls, 2023.

[236] R. Udroiu and L. A. Mihail, "Experimental determination of surface roughness of parts obtained by rapid prototyping," *Proceedings of the 8th WSEAS International Conference on Circuits, Systems, Electronics, Control & Signal Processing*, no. January 2015, 2009.

[237] W. Häßler-Grohne, D. Hüser, K. P. Johnsen, C. G. Frase, and H. Bosse, "Current limitations of SEM and AFM metrology for the characterization of 3D nanostructures," *Meas Sci Technol*, vol. 22, no. 9, 2011, doi: 10.1088/0957-0233/22/9/094003.

[238] K. Grochalski, M. Wieczorowski, J. H'Roura, and G. Le Goic, "The Optical Aspect of Errors in Measurements of Surface Asperities Using the Optical Profilometry Method," *Front Mech Eng*, vol. 6, 2020, doi: 10.3389/fmech.2020.00012.

[239] G. S. Larue, A. Rakotonirainy, and A. N. Pettitt, "Driving performance impairments due to hypovigilance on monotonous roads," *Accid Anal Prev*, vol. 43, no. 6, 2011, doi: 10.1016/j.aap.2011.05.023.

[240] MathWorks, "Image Types," Online. Accessed: Feb. 21, 2023. [Online]. Available: https://www.mathworks.com/help/matlab/creating_plots/image-types.html

[241] J. H. Challis, *Experimental Methods in Biomechanics*. 2020. doi: 10.1007/978-3-030-52256-8.

[242] S. Farah, Z. Hamid, G. Birasamy, S. Farah Binti Hussin, and Z. Binti Hamid, "Design of Butterworth Band-Pass Filter," *Politeknik & Kolej Komuniti Journal of Engineering and Technology*, vol. 1, 2016.

[243] A. Kumar and A. K. Verma, "Design of Bessel low-pass filter using DGS for RF/microwave applications," *International Journal of Electronics*, vol. 103, no. 9, 2016, doi: 10.1080/00207217.2015.1126860.

[244] C. S. Bretherton, "Lecture 17: Filter design and Butterworth filters," Bretherton, 2015.

[245] X. Wang, P. R. Fleming, and S. Forrester, "Advanced measurement of sports surface system behaviour under player loading," in *Procedia Engineering*, 2014. doi: 10.1016/j.proeng.2014.06.145.

[246] D. Cole *et al.*, "Comparison of player perceptions to mechanical measurements of third generation synthetic turf football surfaces," *Sports Engineering*, vol. 26, no. 1, 2023, doi: 10.1007/s12283-022-00398-x.

[247] D. Cole, P. Fleming, K. Morrison, and S. Forrester, "Evaluation of the advanced artificial athlete and Hall effect sensors for measuring strain in multi-layer sports surfaces," *SN Appl Sci*, vol. 2, no. 3, 2020, doi: 10.1007/s42452-020-2178-5.

[248] Emerson, “Selection of Numerical Integration Methods Using LabVIEW,” Online. Accessed: Oct. 13, 2023. [Online]. Available: https://forums.ni.com/t5/Example-Code/Selection-of-Numerical-Integration-Methods-Using-LabVIEW/ta-p/3515962#:~:text=When%20it%20comes%20to%20the,the%203%20selections%20presented%20here

[249] Kevin Sweeney, “Factors Affecting Friction Torque in Bearings,” Online. Accessed: Dec. 13, 2023. [Online]. Available: https://pibsales.com/tutorials/factors-affecting-friction-torque-in-bearings/#:~:text=The%20bearing%20load%20and%20speed,leading%20to%20higher%20frictional%20losses

[250] Y. Ando, Y. Ishikawa, and T. Kitahara, “Friction cliaracteristics and adhesion force under low normal load,” *J Tribol*, vol. 117, no. 4, 1995, doi: 10.1115/1.2831515.

[251] D. J. Harper, C. Carling, and J. Kiely, “High-Intensity Acceleration and Deceleration Demands in Elite Team Sports Competitive Match Play: A Systematic Review and Meta-Analysis of Observational Studies,” *Sports Medicine*, vol. 49, no. 12. 2019. doi: 10.1007/s40279-019-01170-1.

[252] K. Hader, A. Mendez-Villanueva, D. Palazzi, S. Ahmaidi, and M. Buchheit, “Metabolic power requirement of change of direction speed in young soccer players: Not all is what it seems,” *PLoS One*, vol. 11, no. 3, 2016, doi: 10.1371/journal.pone.0149839.

[253] T. Dalen, I. JØrgen, E. Gertjan, H. G. Havard, and W. Ulrik, “Player load, acceleration, and deceleration during forty-five competitive matches of elite soccer,” *J Strength Cond Res*, vol. 30, no. 2, 2016, doi: 10.1519/JSC.0000000000001063.

[254] J. Verheul *et al.*, “Biomechanical loading during running: can a two mass-spring-damper model be used to evaluate ground reaction forces for high-intensity tasks?,” *Sports Biomech*, vol. 20, no. 5, 2021, doi: 10.1080/14763141.2019.1584238.

[255] D. J. Harper and J. Kiely, “Damaging nature of decelerations: Do we adequately prepare players?,” *BMJ Open Sport and Exercise Medicine*, vol. 4, no. 1. 2018. doi: 10.1136/bmjsem-2018-000379.

[256] G. V. Mariotti, “Head Injury Criterion: Mini Review,” *Am J Biomed Sci Res*, vol. 5, no. 5, 2019, doi: 10.34297/ajbsr.2019.05.000957.

[257] S. Manikandan, “Measures of central tendency: Median and mode,” *Journal of Pharmacology and Pharmacotherapeutics*, vol. 2, no. 3. 2011. doi: 10.4103/0976-500X.83300.

[258] K. Dickson, J. Sorochan, and W. Strunk, “Impact of Alternative Synthetic Turf Infills on Athlete Performance and Safety,” 2020. doi: 10.3390/proceedings2020049035.

[259] S. E. Forrester and F. Tsui, “Spatial and temporal analysis of surface hardness across a third-generation artificial turf pitch over a year,” *Proc Inst Mech Eng P J Sport Eng Technol*, vol. 228, no. 3, 2014, doi: 10.1177/1754337114523756.

[260] K. H. Dickson, C. M. Straw, A. W. Thoms, T. D. Carson, and J. C. Sorochan, “Impact of third generation synthetic turf athletic field age on surface hardness and infill depth spatial variability,” *Proc Inst Mech Eng P J Sport Eng Technol*, vol. 236, no. 3, 2022, doi: 10.1177/17543371211002947.

[261] G. Oldenkotte, “Non-filled development doesn’t satisfy FIFA yet,” Online. Accessed: Nov. 14, 2023. [Online]. Available: https://sportsfields.info/non-filled-development-doesnt-satisfy-fifa-yet/

[262] T. A. McMahon and P. R. Greene, “Fast running tracks.,” *Sci Am*, vol. 239, no. 6, 1978, doi: 10.1038/scientificamerican1278-148.

[263] T. A. McMahon and P. R. Greene, “The influence of track compliance on running,” *J Biomech*, vol. 12, no. 12, 1979, doi: 10.1016/0021-9290(79)90057-5.

[264] C. R. Firminger, O. L. Bruce, J. W. Wannop, D. J. Stefanyshyn, and W. B. Edwards, “Effect of Shoe and Surface Stiffness on Lower Limb Tendon Strain in Jumping,” *Med Sci Sports Exerc*, vol. 51, no. 9, 2019, doi: 10.1249/MSS.0000000000002004.

[265] T. Liu, J. Yu, H. Wang, Y. Yu, H. Li, and B. Zhou, “Modified Method for Determination of Wear Coefficient of Reciprocating Sliding Wear and Experimental Comparative Study,” *J Mar Sci Eng*, vol. 10, no. 8, 2022, doi: 10.3390/jmse10081014.

[266] R. Bahr and T. Krosshaug, "Understanding injury mechanisms: A key component of preventing injuries in sport," *British Journal of Sports Medicine*, vol. 39, no. 6. 2005. doi: 10.1136/bjsm.2005.018341.

[267] L. Anderson, P. Fleming, and A. Ansarifar, "Recent advances in understanding the behavior of shockpads for outdoor synthetic sports pitches," in *The Engineering of Sport 6*, vol. 3, 2006. doi: 10.1007/978-0-387-45951-6_18.

[268] X. Wang, P. Fleming, and N. Dixon, "Advanced measurement for sports surface system behaviour," in *Procedia Engineering*, 2012. doi: 10.1016/j.proeng.2012.04.141.

[269] N. Leiva-Molano, B. Cappuccilli, and E. A. Nauman, "An experimental analysis of component contributions to shock absorption performance in third generation sport artificial turf," *Proc Inst Mech Eng P J Sport Eng Technol*, 2022, doi: 10.1177/17543371221132098.

[270] P. Burillo, L. Gallardo, J. L. Felipe, and A. M. Gallardo, "Artificial turf surfaces: Perception of safety, sporting feature, satisfaction and preference of football users," *Eur J Sport Sci*, vol. 14, no. SUPPL.1, 2014, doi: 10.1080/17461391.2012.713005.

[271] P. R. Fleming, S. E. Forrester, and N. J. McLaren, "Understanding the effects of decompaction maintenance on the infill state and play performance of third-generation artificial grass pitches," *Proc Inst Mech Eng P J Sport Eng Technol*, vol. 229, no. 3, 2015, doi: 10.1177/1754337114566480.

[272] J. Sánchez-Sánchez, J. García-Unanue, A. M. Gallardo, L. Gallardo, P. Hexaire, and J. L. Felipe, "Effect of structural components, mechanical wear and environmental conditions on the player–surface interaction on artificial turf football pitches," *Mater Des*, vol. 140, 2018, doi: 10.1016/j.matdes.2017.11.066.

[273] D. M. Twomey, L. A. Petrass, P. Fleming, and K. Lenehan, "Abrasion injuries on artificial turf: A systematic review," *Journal of Science and Medicine in Sport*, vol. 22, no. 5. 2019. doi: 10.1016/j.jsams.2018.11.005.

[274] S. Dixon, P. Fleming, I. James, and M. Carré, *The science and engineering of sport surfaces*. 2015. doi: 10.4324/9780203133385.

[275] P. Fleming, M. Ferrandino, and S. Forrester, "Artificial Turf Field-A New Build Case Study," in *Procedia Engineering*, 2016. doi: 10.1016/j.proeng.2016.06.294.

[276] stma.org, "Guide to synthetic infill products," Jan. 2012.

[277] J. Wannop, S. Kowalchuk, M. Esposito, and D. Stefanyshyn, "Influence of artificial turf surface stiffness on athlete performance," *Life*, vol. 10, no. 12, 2020, doi: 10.3390/life10120340.

[278] S. Williams, P. A. Hume, and S. Kara, "A review of football injuries on third and fourth generation artificial turfs compared with natural turf," *Sports Medicine*, vol. 41, no. 11. 2011. doi: 10.2165/11593190-000000000-00000.

[279] A. E. Kerdok, A. A. Biewener, T. A. McMahon, P. G. Weyand, and H. M. Herr, "Energetics and mechanics of human running on surfaces of different stiffnesses," *J Appl Physiol*, vol. 92, no. 2, 2002, doi: 10.1152/japplphysiol.01164.2000.

[280] A. Arampatzis, S. Stafilidis, G. Morey-Klapsing, and G. P. Brüggemann, "Interaction of the Human Body and Surfaces of Different Stiffness during Drop Jumps," *Med Sci Sports Exerc*, vol. 36, no. 3, 2004, doi: 10.1249/01.MSS.0000117166.87736.0A.

[281] H. Qu, S. Zhang, J. C. Sorochan, J. T. Weinhandl, A. W. Thoms, and K. H. Dickson, "Effects of synthetic turf and shock pad on impact attenuation related biomechanics during drop landing," *Sports Biomech*, vol. 21, no. 6, 2022, doi: 10.1080/14763141.2019.1690570.

[282] K. Steffen, T. E. Andersen, and R. Bahr, "Risk of injury on artificial turf and natural grass in young female football players," *Br J Sports Med*, vol. 41, no. SUPPL. 1, 2007, doi: 10.1136/bjsm.2007.036665.

[283] M. C. Meyers, "Incidence, mechanisms, and severity of match-related collegiate women's soccer injuries on FieldTurf and natural grass surfaces: A 5-year prospective

study," *American Journal of Sports Medicine*, vol. 41, no. 10. 2013. doi: 10.1177/0363546513498994.

[284] M. C. Meyers, "Incidence, mechanisms, and severity of game-related college football injuries on FieldTurf versus natural grass: a 3-year prospective study," *Am J Sports Med*, vol. 38, no. 4, 2010.

[285] Kennelly, "Water Management on Greens with Soil Moisture Sensors," Kansas State University. Accessed: Nov. 13, 2023. [Online]. Available: https://blogs.k-state.edu/turf/water-management-on-greens-with-soil-moisture-sensors/#:~:text=General%20guidelines%20for%20the%20volumetric,when%20the%20soil%20is%20rewetted.

[286] Labosport, "SPORT SURFACES RESEARCH AND DEVELOPMENT FRICTION TEMPERATURE ON SYNTHETIC TURFS COMPARATIVE STUDY OF THE INFLUENCE OF INFILL 'COMPARISONS BASED ON TEMPERATURE INCREASE DURING FALL ON THE SURFACE-LABOSPORT FRICTION TEST.,'" 2018. [Online]. Available: www.labosport.com

[287] S. Knapic, V. Oliveira, J. S. Machado, and H. Pereira, "Cork as a building material: a review," *European Journal of Wood and Wood Products*, vol. 74, no. 6, pp. 775–791, 2016, doi: 10.1007/s00107-016-1076-4.

[288] Field Turf, "INFILL Solutions." Accessed: Feb. 07, 2024. [Online]. Available: https://fieldturf.com/en/products/detail/infill-systems-2/

Appendix

Appendix 1: Skin injury report template

Anonymous Player I.D.				
Survey Questions:				
Surface Temp	°C	Playing Conditions		
Player Details	Height	Weight	Position	Number
Body Location of Injury				
Side of body injured	Left	Right	Bilateral	
Was the injury caused by	Overuse ☐	Trauma ☐		
Did the injury occur during	Match ☐	Training ☐		
Did you have any previous injuries on the affected location?				
Scale of 1-10 how bad is the injury?				
When do you think the injury occurred?	First Half ☐	Second Half ☐		
How do you think the injury occurred?	Tackle	Yes ☐	No ☐	
		Tackler ☐	Ball Carrier ☐	
	Scoring	Yes ☐	No ☐	
	Position	Above ☐	Below ☐	
How would you describe the injury?				
Additional Comments which would assist characterise the interaction which caused the injury?				

Number of Boxes	Involved Area	Abrasion	Erythema	Type of Exudation	SDASI
68	6	4	2	1	42

Time (s) [T1 - T2]	Distance (m) [T1 - T2]	Speed (m/s) [T1 - T2]	Distance (m) [T2 - T3]	Abrupt / Smooth	Centre of Mass	Angle Impact Joint	Body Weight
1.23	8.3	6.7	0.8	Abrupt	Above	43.3	100%

Incident 1 – SDASI 42

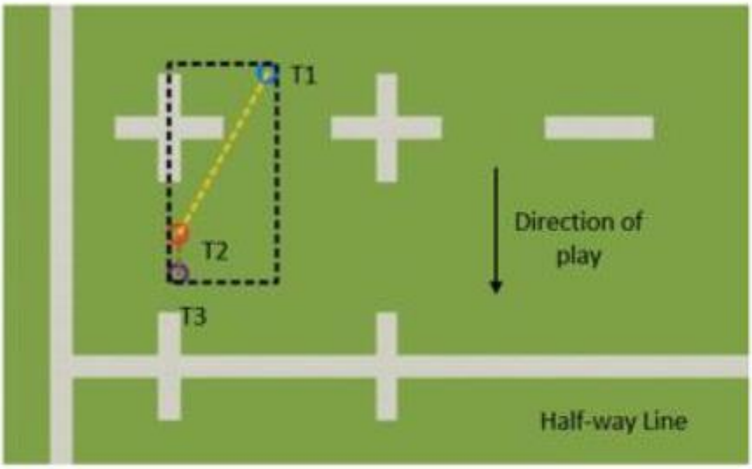

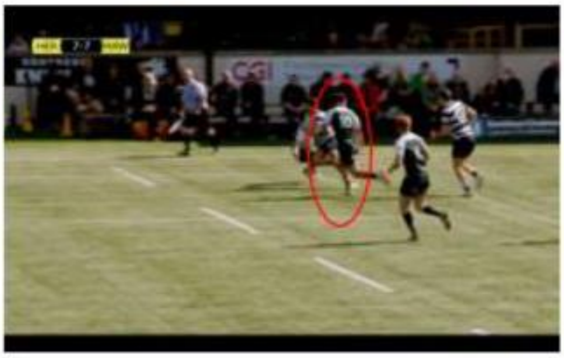

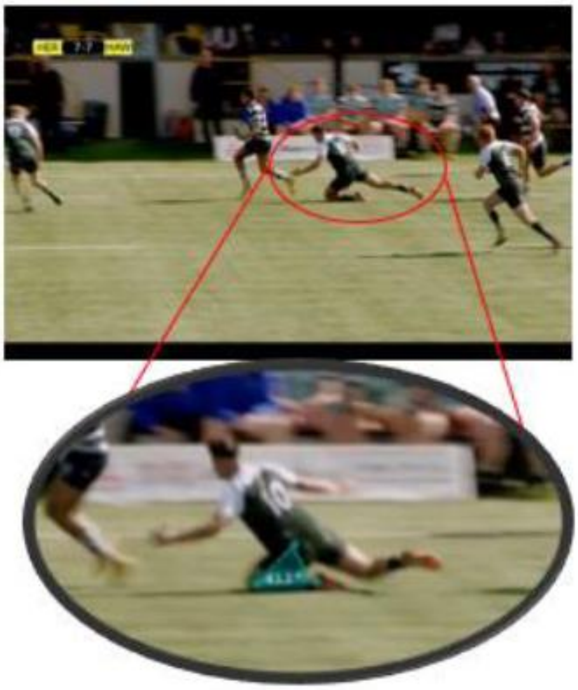

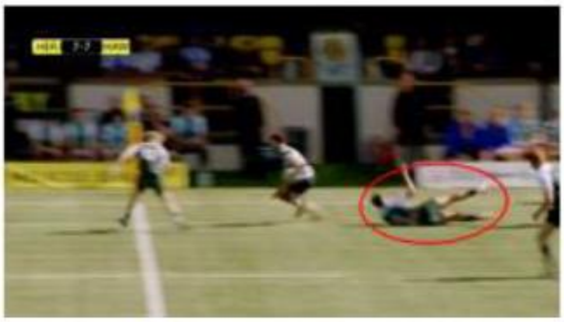

Appendix 3

Number of Boxes	Involved Area	Abrasion	Erythema	Type of Exudation	SDASI
30	4	4	4	2	40

Time (s) [T1 - T2]	Distance (m) [T1 - T2]	Speed (m/s) [T1 - T2]	Distance (m) [T2 - T3]	Abrupt / Smooth	Centre of Mass	Angle Impact Joint	Body Weight
2.4	15.2	6.3	5.4	Smooth	Infront	-	50 %

Incident 3 – SDASI 40

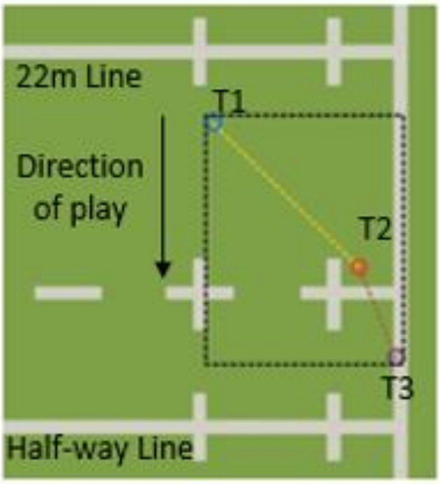

Number of Boxes	Involved Area	Abrasion	Erythema	Type of Exudation	SDASI
50	5	4	2	2	40

Time (s) [T1 - T2]	Distance (m) [T1 - T2]	Speed (m/s) [T1 - T2]	Distance (m) [T2 - T3]	Abrupt / Smooth	Centre of Mass	Angle Impact Joint	Body Weight
1.7	11.0	6.5	2.3	Smooth	Above	44.4	100%

Incident 4 – SDASI 40

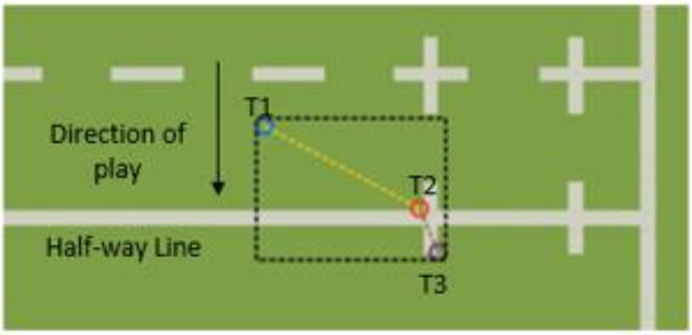

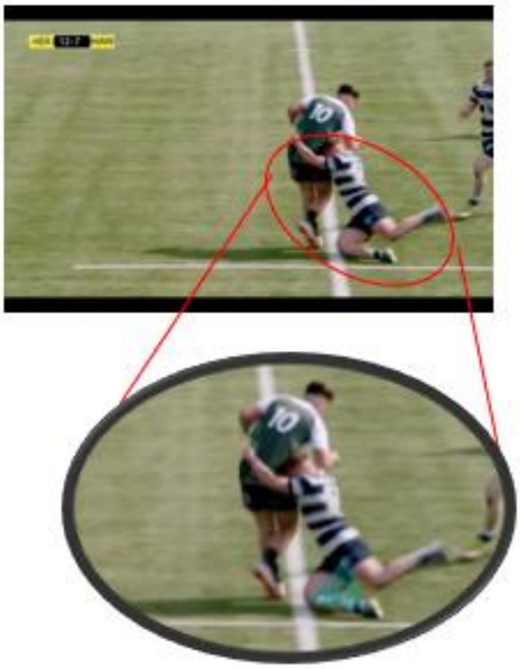

Appendix 5

Number of Boxes	Involved Area	Abrasion	Erythema	Type of Exudation	SDASI
31	4	4	4	2	40

Time (s) [T1 - T2]	Distance (m) [T1 - T2]	Speed (m/s) [T1 - T2]	Distance (m) [T2 - T3]	Abrupt / Smooth	Centre of Mass	Angle Impact Joint	Body Weight
4.13	24.4	5.9	3.7	Smooth	Above	73.1	125%

Incident 5 – SDASI 40

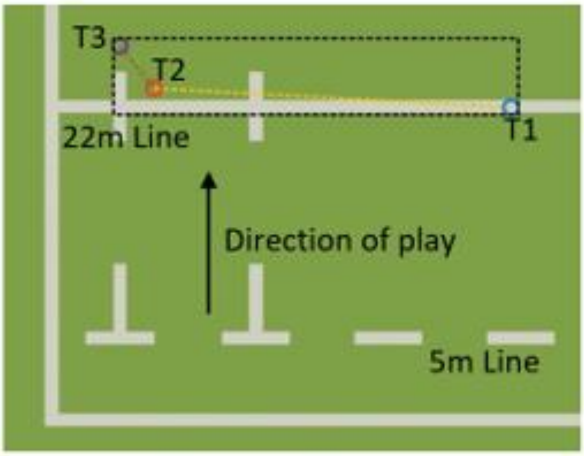

Appendix 6

Number of Boxes	Involved Area	Abrasion	Erythema	Type of Exudation	SDASI
45	4	3	3	1	35

Time (s) [T1 - T2]	Distance (m) [T1 - T2]	Speed (m/s) [T1 - T2]	Distance (m) [T2 - T3]	Abrupt / Smooth	Centre of Mass	Angle Impact Joint	Body Weight
1.8	10.1	5.6	0.9	Abrupt	Above	-	125%

Incident 8 – SDASI 35

Appendix 7

Number of Boxes	Involved Area	Abrasion	Erythema	Type of Exudation	SDASI
22	3	4	4	2	30

Time (s) [T1 - T2]	Distance (m) [T1 - T2]	Speed (m/s) [T1 - T2]	Distance (m) [T2 - T3]	Abrupt / Smooth	Centre of Mass	Angle Impact Joint	Body Weight
2.87	16.2	5.7	0.9	Abrupt	In front	44.2	100%

Incident 12 – SDASI 30

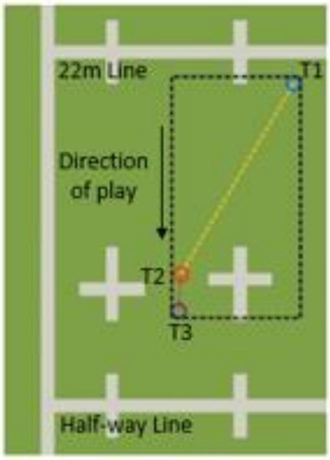

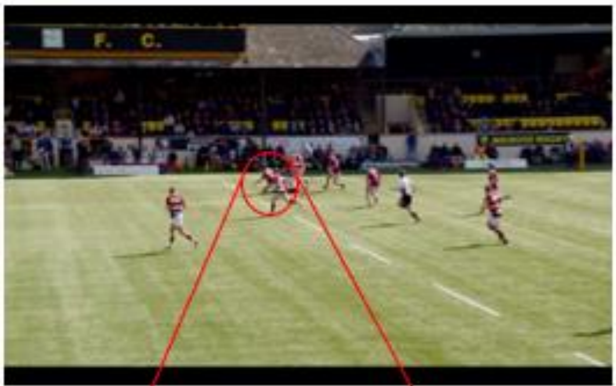

Number of Boxes	Involved Area	Abrasion	Erythema	Type of Exudation	SDASI
28	3	4	4	2	30

Time (s) [T1 - T2]	Distance (m) [T1 - T2]	Speed (m/s) [T1 - T2]	Distance (m) [T2 - T3]	Abrupt / Smooth	Centre of Mass	Angle Impact Joint	Body Weight
2.37	16.2	5.7	0.9	Abrupt	Above	82.2	125%

Incident 13 – SDASI 30

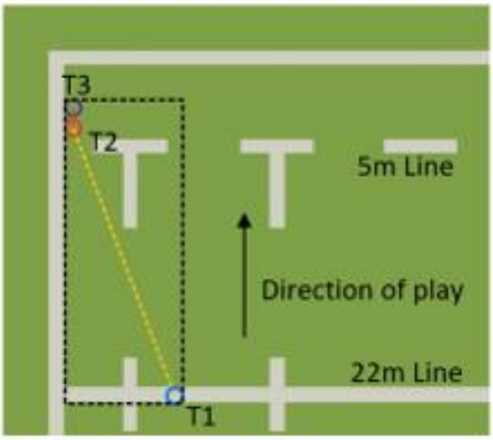

Appendix 9

Number of Boxes	Involved Area	Abrasion	Erythema	Type of Exudation	SDASI
19	3	3	4	2	27

Time (s) [T1 - T2]	Distance (m) [T1 - T2]	Speed (m/s) [T1 - T2]	Distance (m) [T2 - T3]	Abrupt / Smooth	Centre of Mass	Angle Impact Joint	Body Weight
3.47	18.9	5.5	3.7	Smooth	Above	34.7	125%

Incident 17 – SDASI 27

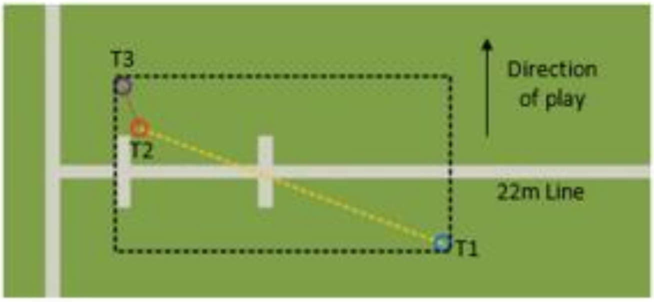

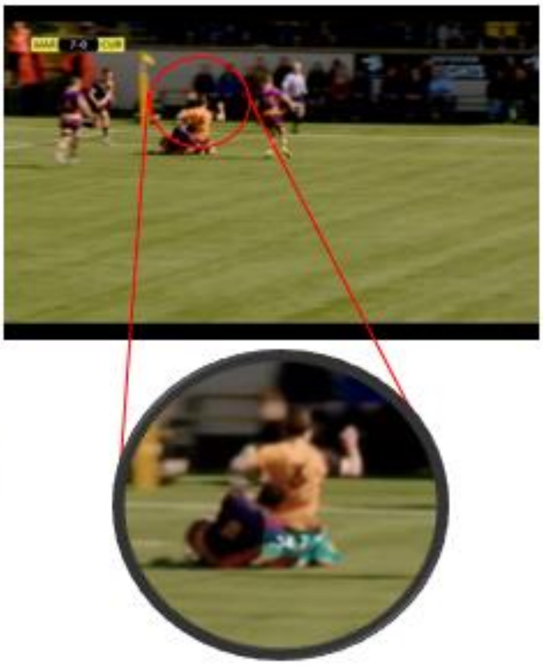

Number of Boxes	Involved Area	Abrasion	Erythema	Type of Exudation	SDASI
37	4	3	2	1	24

Time (s) [T1 - T2]	Distance (m) [T1 - T2]	Speed (m/s) [T1 - T2]	Distance (m) [T2 - T3]	Abrupt / Smooth	Centre of Mass	Angle Impact Joint	Body Weight
0.97	5.1	5.3	0.7	Abrupt	Above	53.4	100%

Incident 20 – SDASI 24

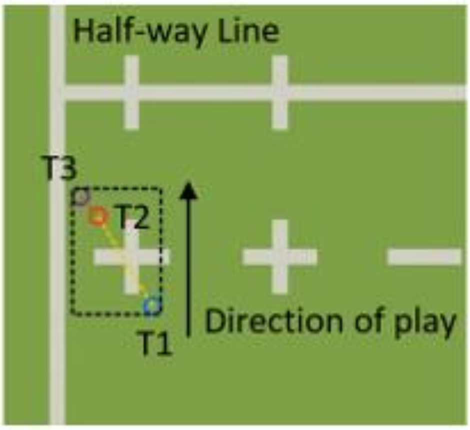

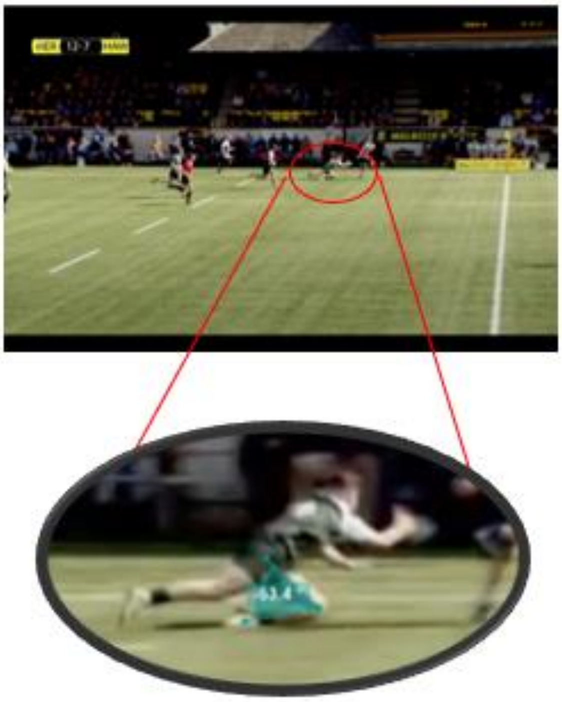

Appendix 11

Number of Boxes	Involved Area	Abrasion	Erythema	Type of Exudation	SDASI
23	3	3	3	2	24
25	3	2	3	2	21

Time (s) [T1 - T2]	Distance (m) [T1 - T2]	Speed (m/s) [T1 - T2]	Distance (m) [T2 - T3]	Abrupt / Smooth	Centre of Mass	Angle Impact Joint	Body Weight
2.97	15.2	5.1	2.8	Smooth	In front	141	25%
2.97	15.2	5.1	2.8	Smooth	In front		25%

Incident 21 – SDASI 24

Incident 26 – SDASI 21

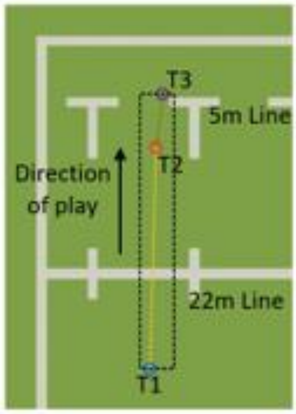

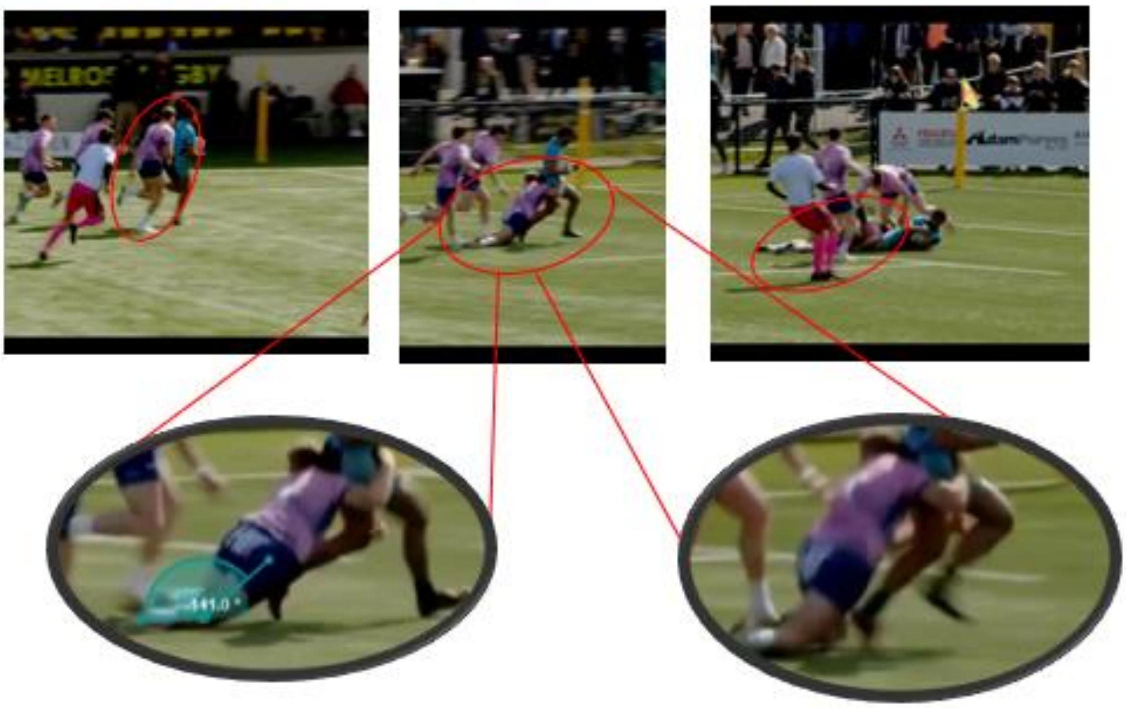

Appendix 12

Number of Boxes	Involved Area	Abrasion	Erythema	Type of Exudation	SDASI
20	3	3	3	2	24
19	3	1	1	2	12

Time (s) [T1 - T2]	Distance (m) [T1 - T2]	Speed (m/s) [T1 - T2]	Distance (m) [T2 - T3]	Abrupt / Smooth	Centre of Mass	Angle Impact Joint	Body Weight
1.73	13.1	7.6	3.0	Smooth	Behind	-	25%
1.73	13.1	7.6	3.0	Smooth	Above	122.6	50%

Incident 22 – SDASI 24

Incident 57 – SDASI 12

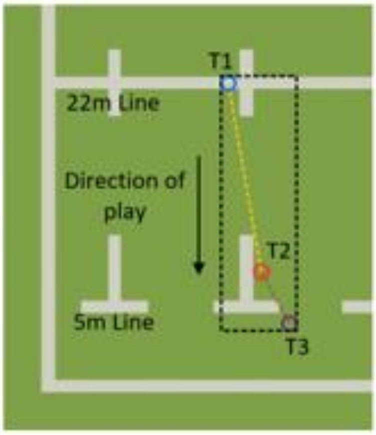

Number of Boxes	Involved Area	Abrasion	Erythema	Type of Exudation	SDASI
22	3	3	3	2	24
25	3	2	3	2	21

Time (s) [T1 - T2]	Distance (m) [T1 - T2]	Speed (m/s) [T1 - T2]	Distance (m) [T2 - T3]	Abrupt / Smooth	Centre of Mass	Angle Impact Joint	Body Weight
2.53	16.7	6.6	1.6	Smooth	Above	180	25%
2.43	16.5	6.8	0.5	Smooth	Behind	-	50%

Incident 23 – SDASI 24 Incident 28 – SDASI 21

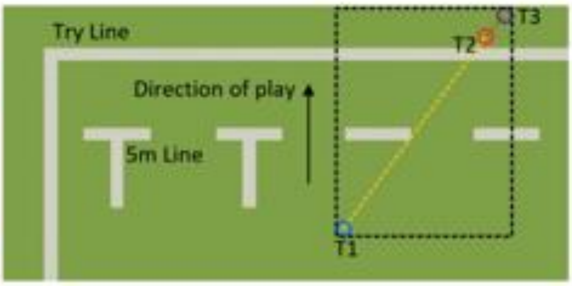

Number of Boxes	Involved Area	Abrasion	Erythema	Type of Exudation	SDASI
39	4	3	2	0	20

Time (s) [T1 - T2]	Distance (m) [T1 - T2]	Speed (m/s) [T1 - T2]	Distance (m) [T2 - T3]	Abrupt / Smooth	Centre of Mass	Angle Impact Joint	Body Weight
0.73	4.1	5.6	2.4	Smooth	Above	-	25%

Incident 26 – SDASI 20

Number of Boxes	Involved Area	Abrasion	Erythema	Type of Exudation	SDASI
10	2	4	4	2	20
11	2	3	3	2	16

Time (s) [T1 - T2]	Distance (m) [T1 - T2]	Speed (m/s) [T1 - T2]	Distance (m) [T2 - T3]	Abrupt / Smooth	Centre of Mass	Angle Impact Joint	Body Weight
2.23	8.4	3.8	1.6	Smooth	In front	122.4	50%
2.23	8.4	3.8	1.6	Smooth	In front	121.9	50%

Incident 29 – SDASI 20

Incident 44 – SDASI 16

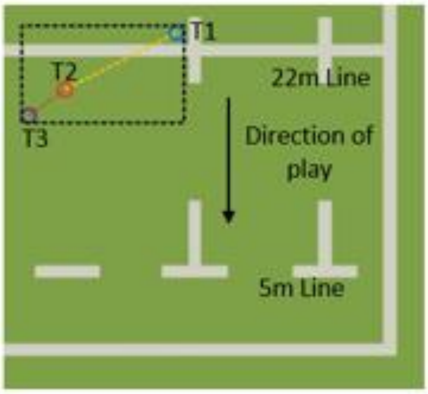

Number of Boxes	Involved Area	Abrasion	Erythema	Type of Exudation	SDASI
15	2	4	4	2	20

Time (s) [T1 - T2]	Distance (m) [T1 - T2]	Speed (m/s) [T1 - T2]	Distance (m) [T2 - T3]	Abrupt / Smooth	Centre of Mass	Angle Impact Joint	Body Weight
2.9	13.2	4.6	0.6	Abrupt	Behind	78	25%

Incident 30 – SDASI 20

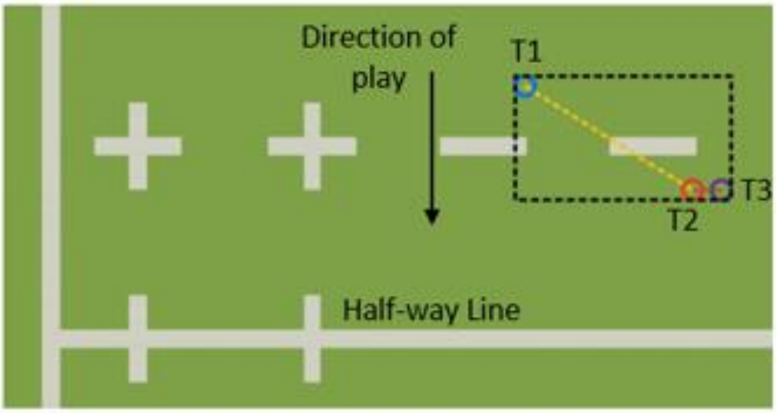

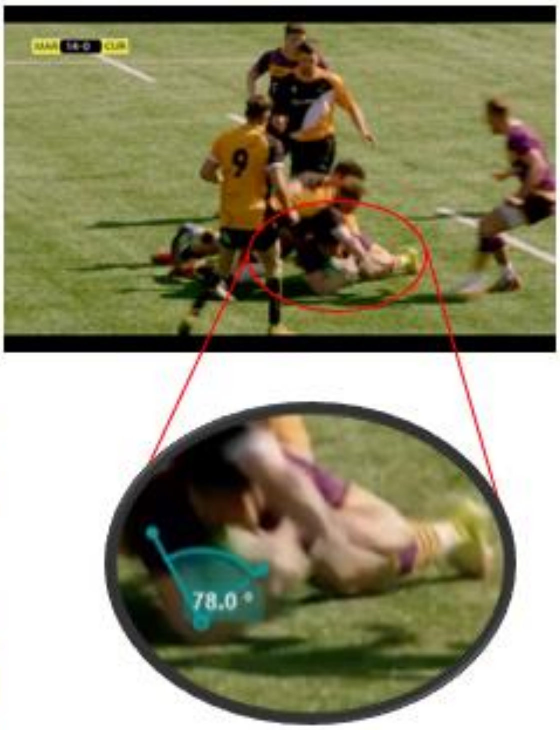

Number of Boxes	Involved Area	Abrasion	Erythema	Type of Exudation	SDASI
27	3	2	3	1	18

Time (s) [T1 - T2]	Distance (m) [T1 - T2]	Speed (m/s) [T1 - T2]	Distance (m) [T2 - T3]	Abrupt / Smooth	Centre of Mass	Angle Impact Joint	Body Weight
0.9	4.3	4.8	3.8	Smooth	In front	116.8	50%

Incident 33 – SDASI 18

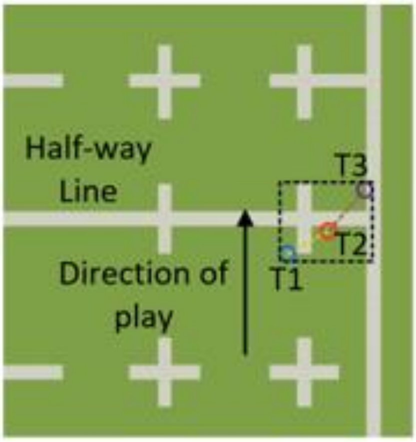

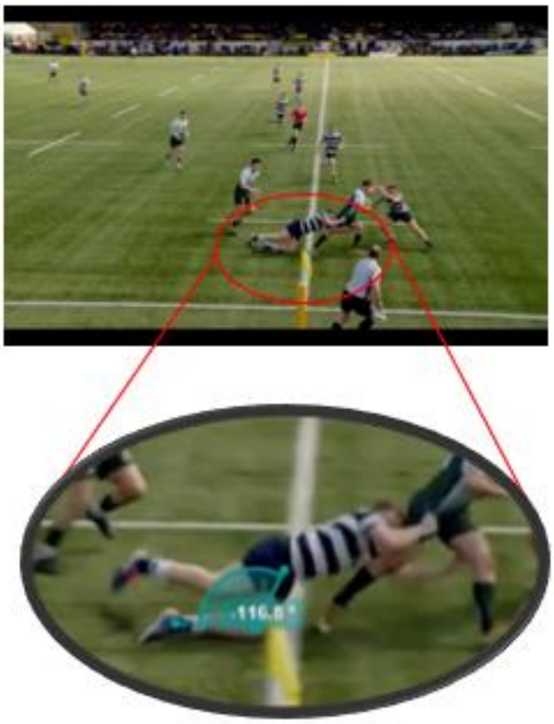

Number of Boxes	Involved Area	Abrasion	Erythema	Type of Exudation	SDASI
17	2	3	3	2	16

Time (s) [T1 - T2]	Distance (m) [T1 - T2]	Speed (m/s) [T1 - T2]	Distance (m) [T2 - T3]	Abrupt / Smooth	Centre of Mass	Angle Impact Joint	Body Weight
2.37	11.9	5.0	1.7	Smooth	Above	61.8	50%

Incident 41 – SDASI 16

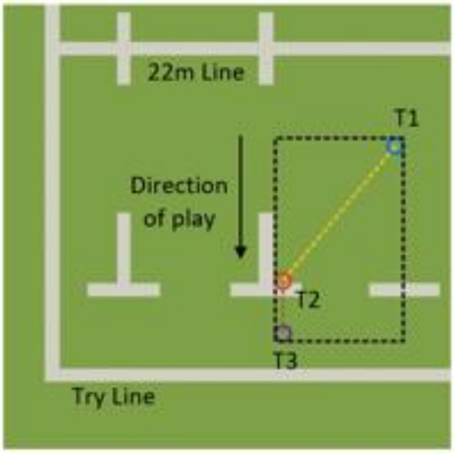

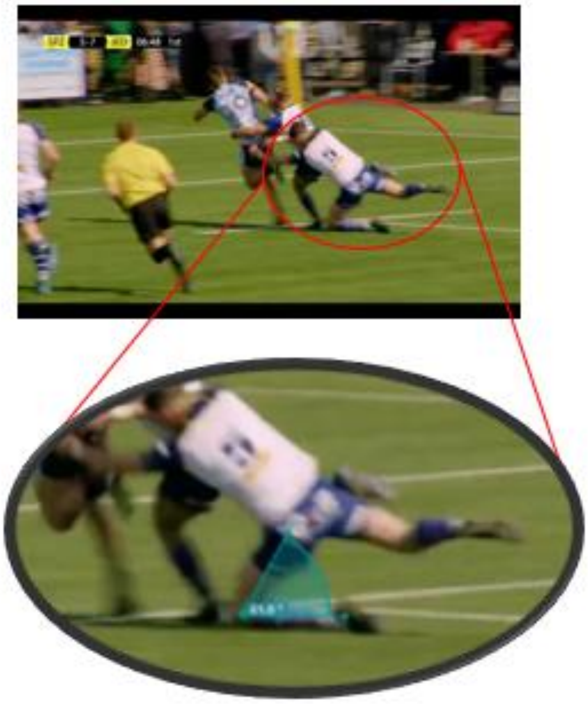

Appendix 19

Number of Boxes	Involved Area	Abrasion	Erythema	Type of Exudation	SDASI
16	2	3	3	2	16

Time (s) [T1 - T2]	Distance (m) [T1 - T2]	Speed (m/s) [T1 - T2]	Distance (m) [T2 - T3]	Abrupt / Smooth	Centre of Mass	Angle Impact Joint	Body Weight
0.4	2.3	5.8	0.5	Abrupt	Above		50%

Incident 42 – SDASI 16

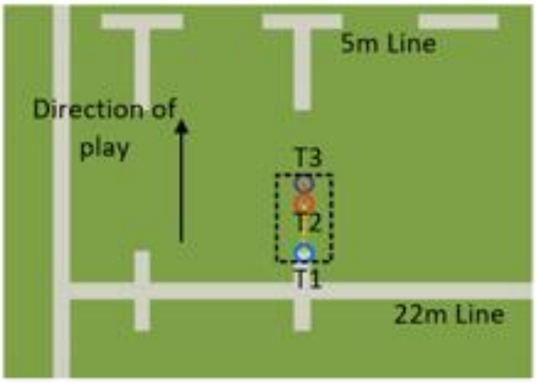

Number of Boxes	Involved Area	Abrasion	Erythema	Type of Exudation	SDASI
17	2	3	3	2	16

Time (s) [T1 - T2]	Distance (m) [T1 - T2]	Speed (m/s) [T1 - T2]	Distance (m) [T2 - T3]	Abrupt / Smooth	Centre of Mass	Angle Impact Joint	Body Weight
1.17	5.3	4.5	0.7	Abrupt	Above	46.8	50%

Incident 43 – SDASI 16

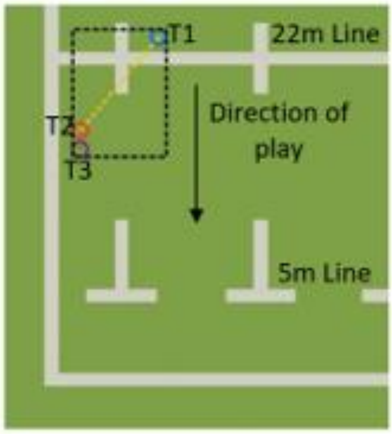

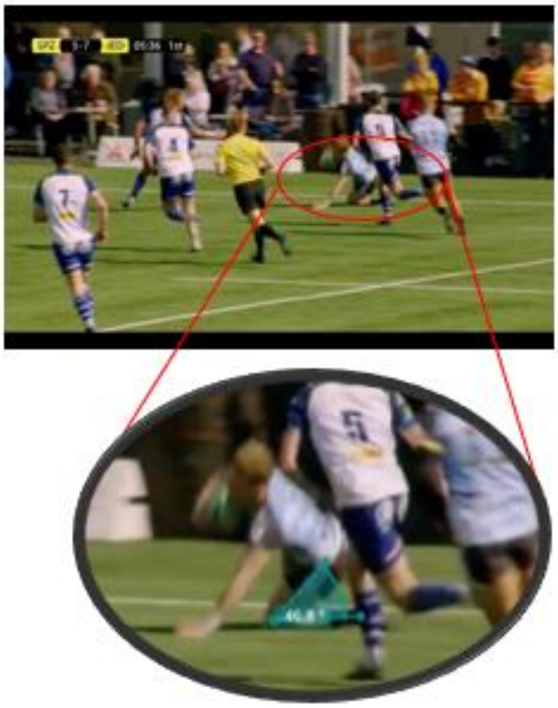

Number of Boxes	Involved Area	Abrasion	Erythema	Type of Exudation	SDASI
15	2	2	3	2	14

Time (s) [T1 - T2]	Distance (m) [T1 - T2]	Speed (m/s) [T1 - T2]	Distance (m) [T2 - T3]	Abrupt / Smooth	Centre of Mass	Angle Impact Joint	Body Weight
0.4	2.1	5.3	1.3	Abrupt	Above	25.7	100%

Incident 54 – SDASI 14

Number of Boxes	Involved Area	Abrasion	Erythema	Type of Exudation	SDASI
4	1	3	3	2	8

Time (s) [T1 - T2]	Distance (m) [T1 - T2]	Speed (m/s) [T1 - T2]	Distance (m) [T2 - T3]	Abrupt / Smooth	Centre of Mass	Angle Impact Joint	Body Weight
1.4	7.8	5.6	0.3	Abrupt	Above	83.8	50%

Incident 73 – SDASI 8

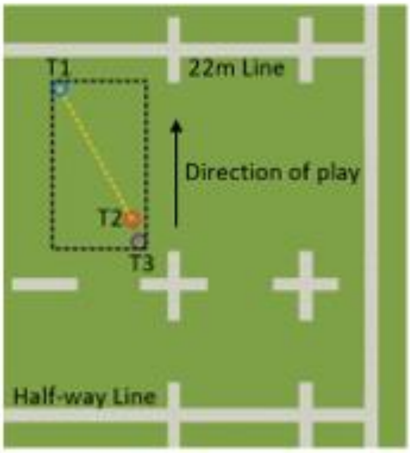

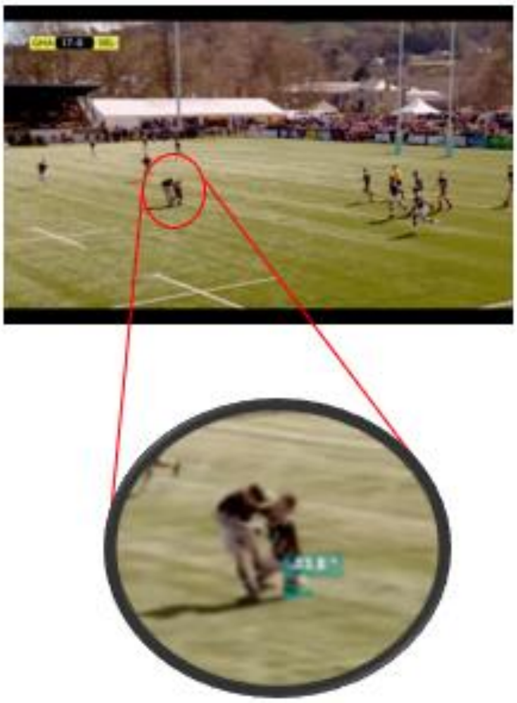

Appendix 23: Skin Damage and Severity Index

Incident No.	No. of Boxes	IA	A	E	TE	SDASI	Image
1	68	6	4	2	1	42	
2	64	6	4	2	1	42	
3	30	4	4	4	2	40	
4	50	5	4	2	2	40	
5	31	4	4	4	2	40	

Incident No.	No. of Boxes	IA	A	E	TE	SDASI	Image
6	46	5	4	2	2	40	
7	38	4	4	3	2	36	
8	45	5	3	3	1	35	
9	39	5	4	2	1	35	
10	35	4	3	3	2	32	

Incident No.	No. of Boxes	IA	A	E	TE	SDASI	Image
11	36	4	3	3	2	32	
12	22	3	4	4	2	30	
13	28	3	4	4	2	30	
14	28	3	4	4	2	30	
15	21	3	4	4	2	30	

Incident No.	No. of Boxes	IA	A	E	TE	SDASI	Image
16	38	4	3	2	2	28	
17	19	3	3	4	2	27	
18	20	3	4	3	2	27	
19	44	5	3	1	1	25	
20	37	4	3	2	1	24	

Incident No.	No. of Boxes	IA	A	E	TE	SDASI	Image
21	23	3	3	3	2	24	
22	20	3	3	3	2	24	
23	22	3	3	3	2	24	
24	29	3	2	4	2	24	
25	25	3	2	3	2	21	

Incident No.	No. of Boxes	IA	A	E	TE	SDASI	Image
26	24	3	2	3	2	21	
27	21	3	2	3	2	21	
28	39	4	3	2	0	20	
29	10	2	4	4	2	20	
30	15	2	4	4	2	20	

Incident No.	No. of Boxes	IA	A	E	TE	SDASI	Image
31	13	2	4	4	2	20	
32	14	2	4	4	2	20	
33	27	3	2	3	1	18	
34	27	3	2	2	2	18	
35	20	3	3	2	1	18	

Incident No.	No. of Boxes	IA	A	E	TE	SDASI	Image
36	24	3	1	3	2	18	
37	24	3	2	2	2	18	
38	20	3	2	2	2	18	
39	24	3	2	2	2	18	
40	12	2	4	3	2	18	

Incident No.	No. of Boxes	IA	A	E	TE	SDASI	Image
41	17	2	3	3	2	16	
42	16	2	3	3	2	16	
43	17	2	3	3	2	16	
44	11	2	3	3	2	16	
45	15	2	3	3	2	16	

Incident No.	No. of Boxes	IA	A	E	TE	SDASI	Image
46	33	4	2	1	1	16	
47	14	2	3	3	2	16	
48	10	2	3	3	2	16	
49	16	2	3	3	2	16	
50	16	2	3	3	2	16	

Incident No.	No. of Boxes	IA	A	E	TE	SDASI	Image
51	16	2	3	3	2	16	
52	44	5	1	1	1	15	
53	28	3	2	2	1	15	
54	15	2	2	3	2	14	
55	17	2	3	2	2	14	

Incident No.	No. of Boxes	IA	A	E	TE	SDASI	Image
56	7	2	3	2	2	14	
57	19	3	1	1	2	12	
58	15	2	3	2	1	12	
59	40	4	2	1	0	12	
60	14	2	2	2	2	12	

Incident No.	No. of Boxes	IA	A	E	TE	SDASI	Image
61	36	4	2	1	0	12	
62	16	2	2	2	2	12	
63	10	2	2	2	2	12	
64	18	3	1	2	1	12	
65	14	2	2	2	2	12	

Incident No.	No. of Boxes	IA	A	E	TE	SDASI	Image
66	10	2	2	2	1	10	
67	8	2	2	2	1	10	
68	6	2	2	2	1	10	
69	10	2	1	2	2	10	
70	14	2	2	2	1	10	

Incident No.	No. of Boxes	IA	A	E	TE	SDASI	Image
71	6	2	2	2	1	10	
72	8	2	1	2	2	10	
73	2	1	3	3	2	8	
74	14	2	1	3	0	8	
75	17	2	1	1	2	8	

Incident No.	No. of Boxes	IA	A	E	TE	SDASI	Image
76	6	2	1	2	1	8	
77	38	4	1	1	0	8	
78	8	2	2	1	1	8	
79	17	2	1	1	1	6	
80	10	2	1	1	1	6	

Incident No.	No. of Boxes	IA	A	E	TE	SDASI	Image
81	5	1	2	2	1	5	
82	11	2	1	1	0	4	
83	5	1	1	1	1	3	

Appendix 24: Study 1 - 50 mm EPDM

Test	Skin Damage	Abrasion Zone Image	AZ	ASI
1			566	961
2		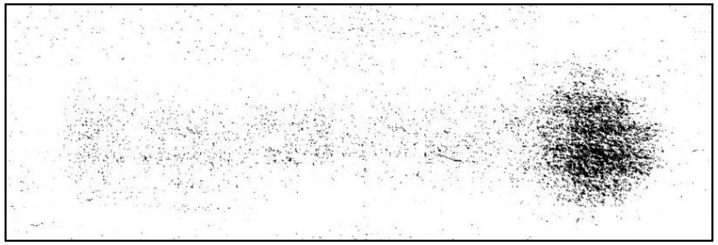	502	817
3		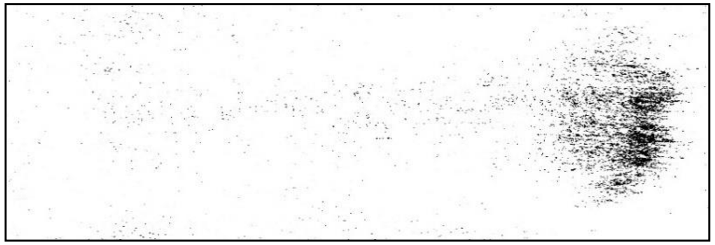	330	668
4		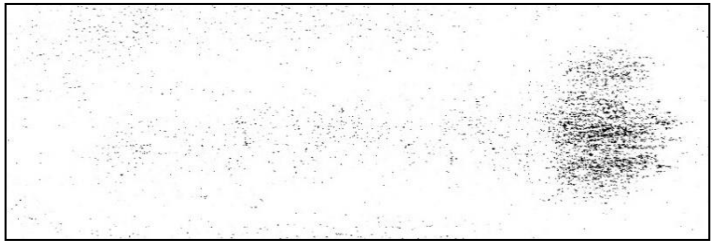	241	387

Appendix 25: Study 1 - 60 mm EPDM

Test	Skin Damage	Abrasion Zone Image	AZ	ASI
1		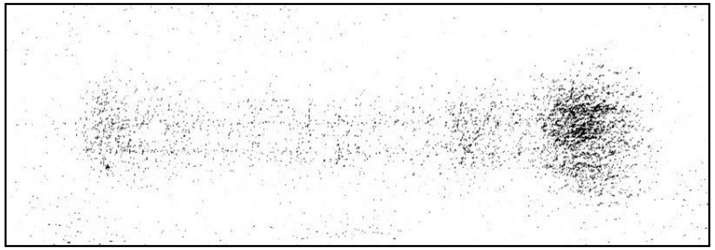	295	428
2			292	449
3		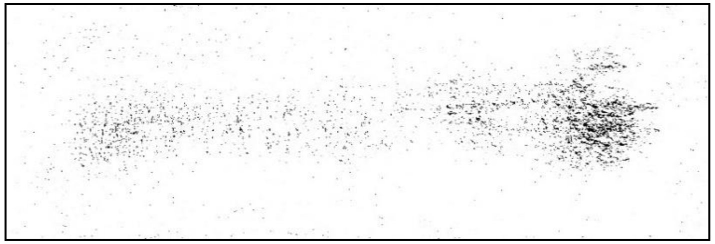	228	329
4		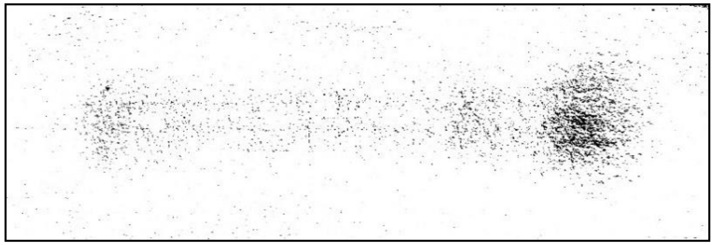	289	428

Appendix 26: Study 1 - 60 mm – Low Density Turf & EPDM

Test	Skin Damage	Abrasion Zone Image	AZ	ASI
1		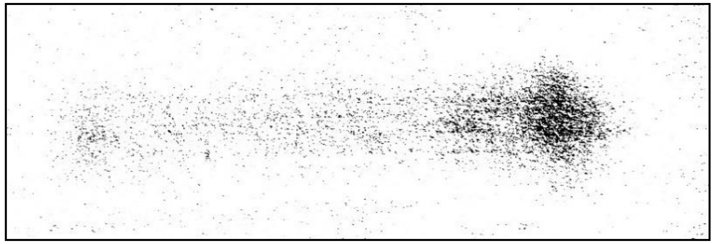	448	666
2			447	664
3			326	460
4		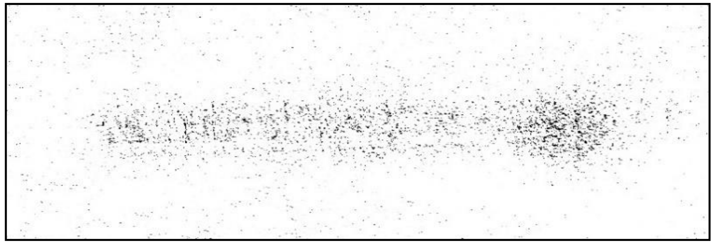	142	207

Appendix 27: Study 1 - 60 mm – High Density Turf & EPDM

Test	Skin Damage	Abrasion Zone Image	AZ	ASI
1	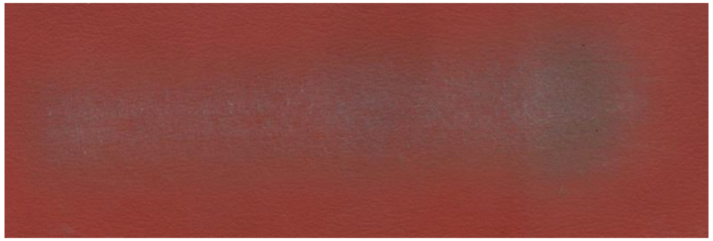		136	210
2			282	456
3	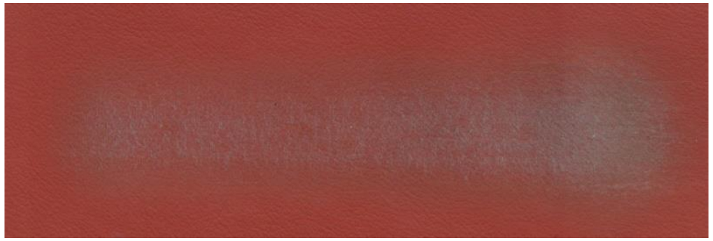	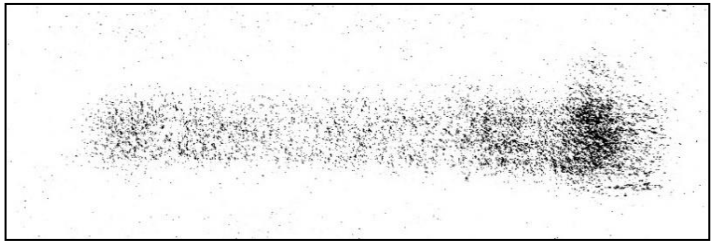	582	871
4			289	421

Test	Skin Damage	Abrasion Zone Image	AZ	ASI
1		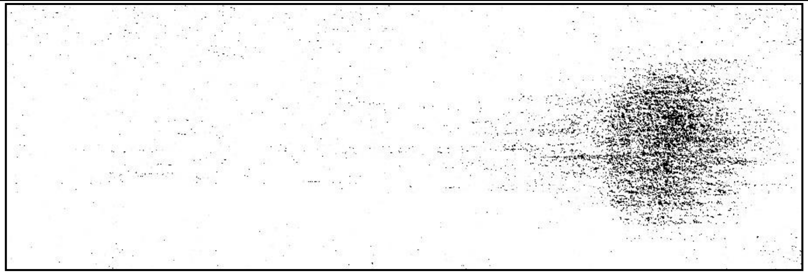	482	687
2		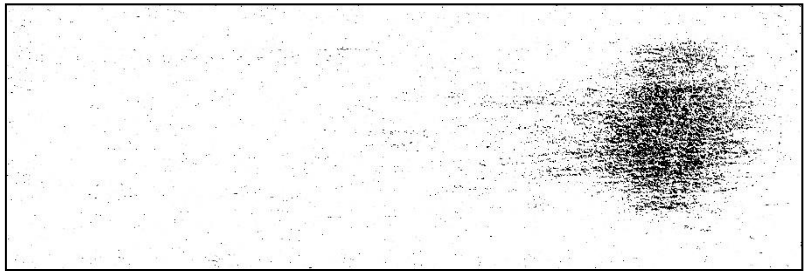	588	828
3		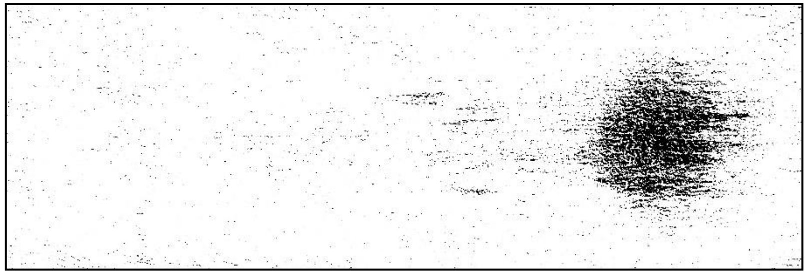	636	876

Appendix 29: Study 2 - Mid Density Pad

Test	Skin Damage	Abrasion Zone Image	AZ	ASI
1		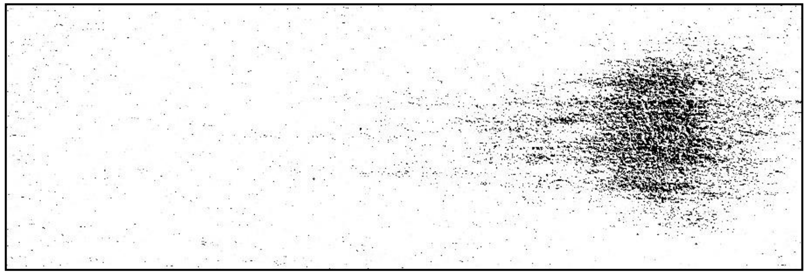	630	872
2			596	862
3	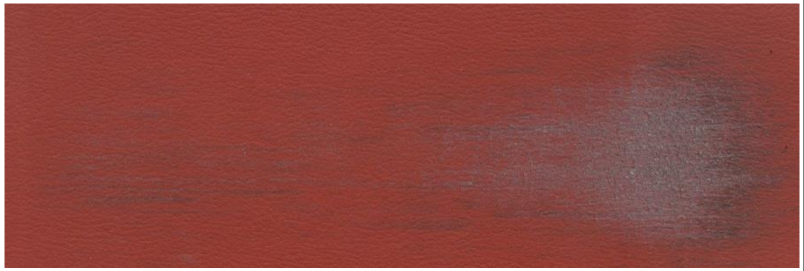	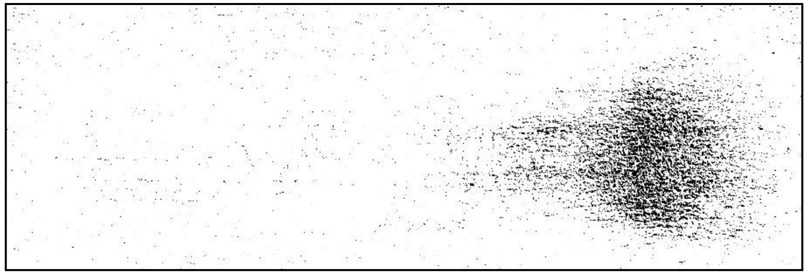	556	783

Appendix 30: Study 2 - Low Density Pad

Test	Skin Damage	Abrasion Zone Image	AZ	ASI
1			498	736
2			700	999
3		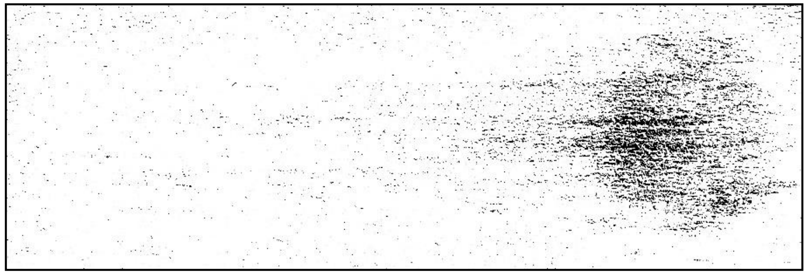	494	704

Test	Skin Damage	Abrasion Zone Image	AZ	ASI
S1		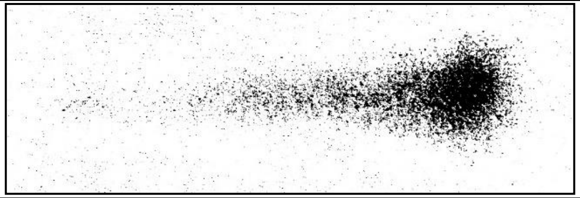	1039	1547
S2			1428	1941
S3		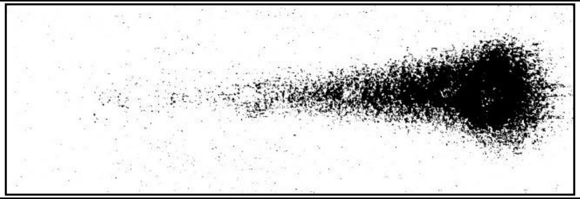	1610	2178
W1		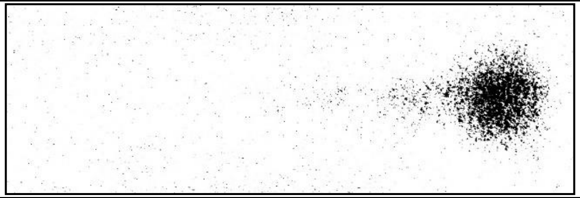	510	823
W2		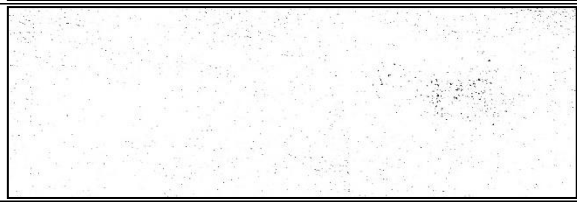	50	58

Appendix 33: Study 3 – Hybrid – without root zone

Test	Skin Damage	Abrasion Zone Image	AZ	ASI
1		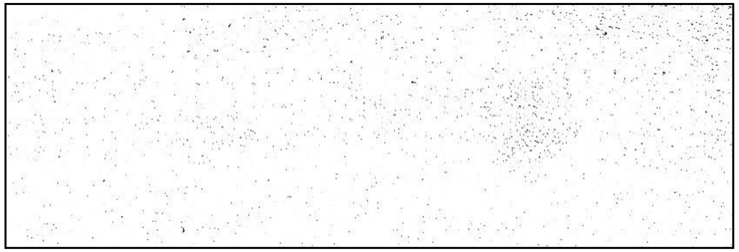	91	121
2	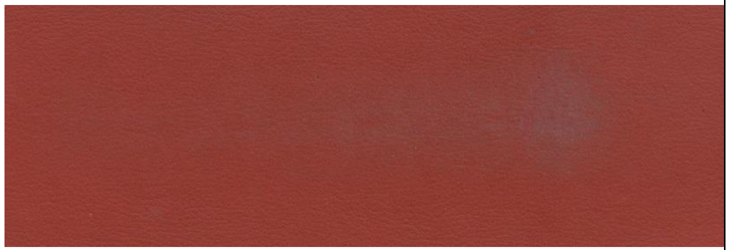		78	106
3			98	137

Appendix 34: Study 3 – Hybrid – with root zone

Test	Skin Damage	Abrasion Zone Image	AZ	ASI
1		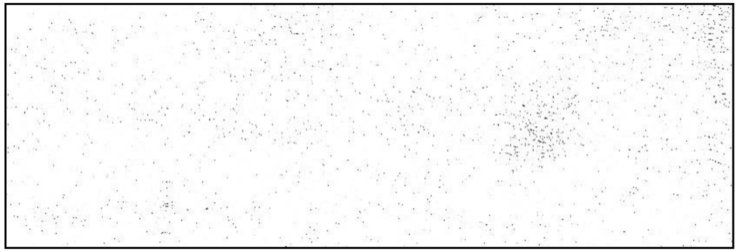	72	86
2		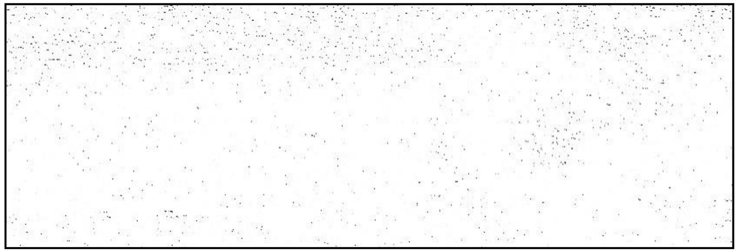	67	77
3		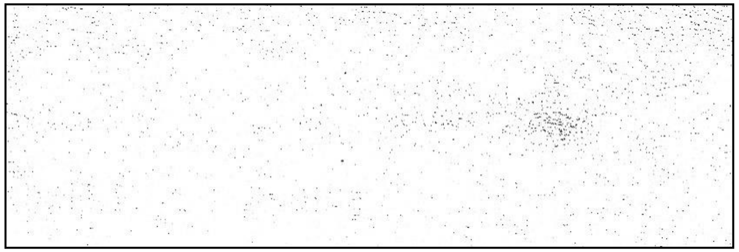	91	105

Test	Skin Damage	Abrasion Zone Image	AZ	ASI
1			154	369
2	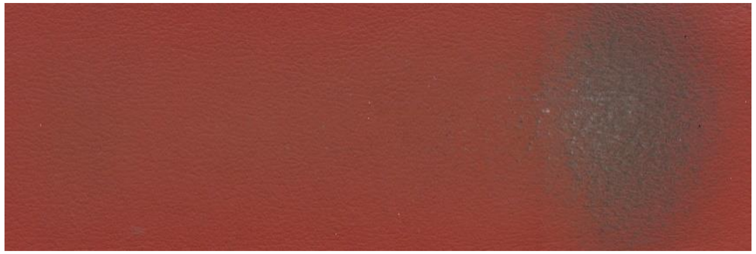		88	182
3		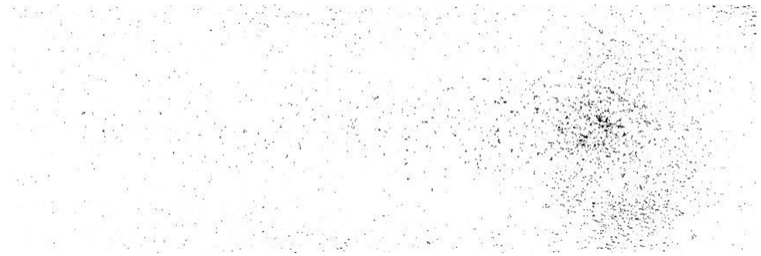	118	237
4			88	187

Appendix 35: Study 3 – Non-fill

Test	Skin Damage	Abrasion Zone Image	AZ	ASI
1		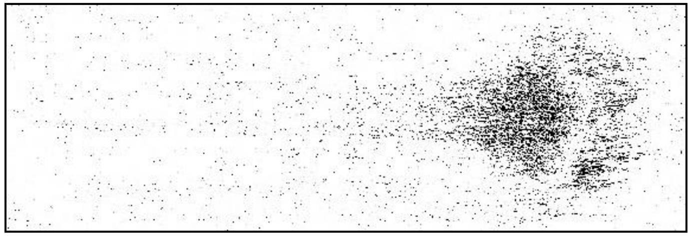	426	825
2		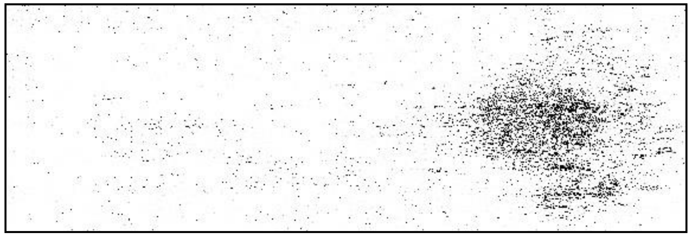	356	547
3		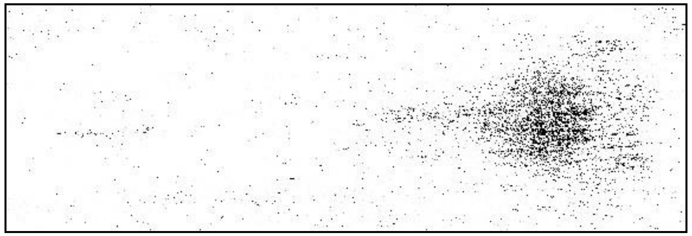	314	643
4		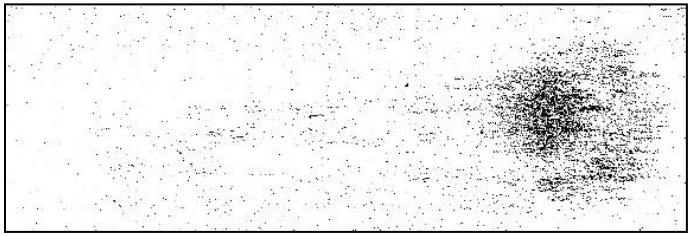	369	709

Appendix 36: Study 4 – SBR 60

Lab	Skin Damage	Abrasion Zone Image	AZ	ASI
1			550	892
2			495	826
3		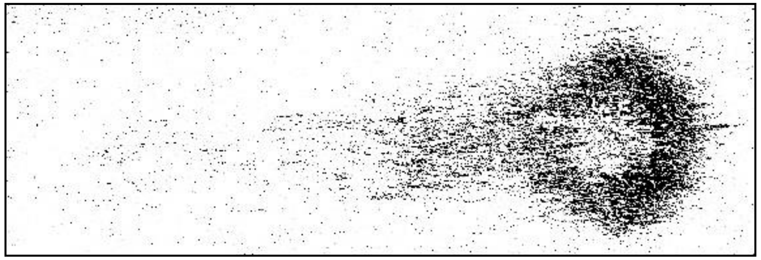	414	712
4		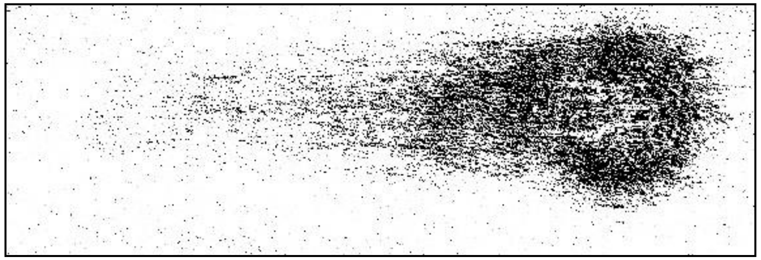	504	774

Appendix 37: Study 4 – SBR 60

Appendix 38: Study 4 – Cork 60

Test	Skin Damage	Abrasion Zone Image	AZ	ASI
1		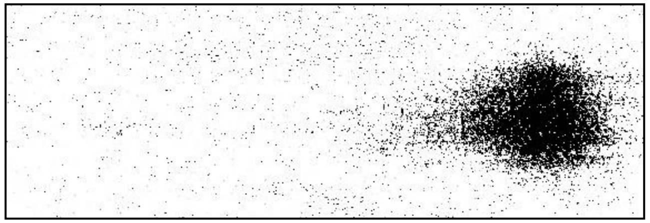	999	1191
2		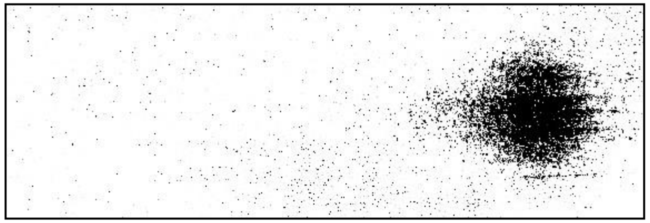	875	957
3		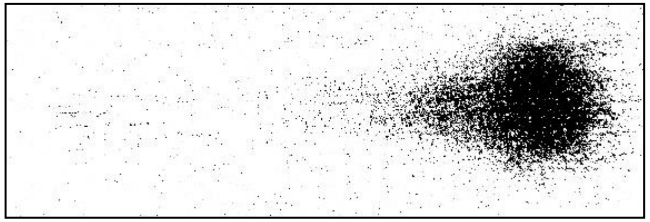	1009	1430
4		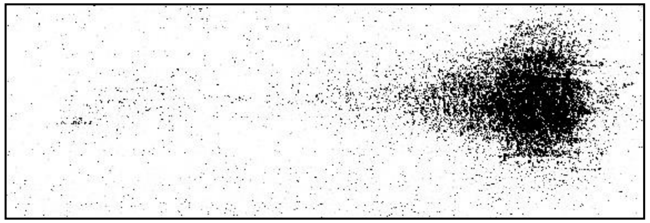	931	1190

Lab	Skin Damage	Abrasion Zone Image	AZ	ASI
1		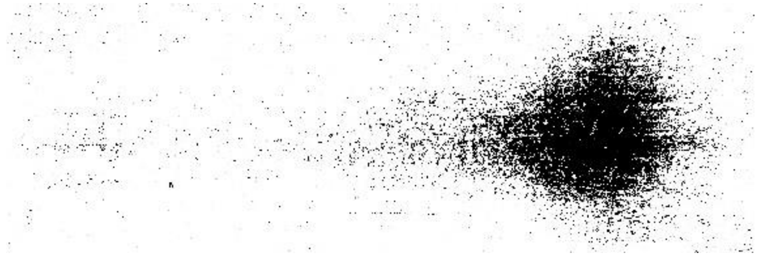	819	1435
2		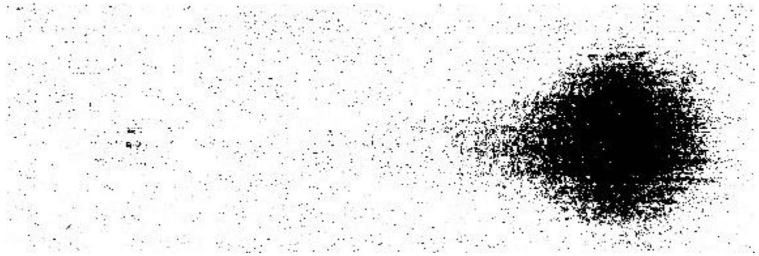	804	1590
3		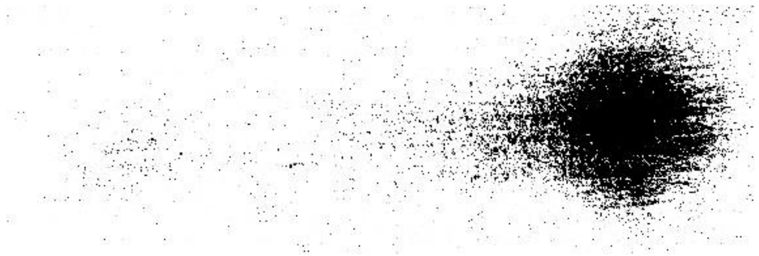	1626	773
4		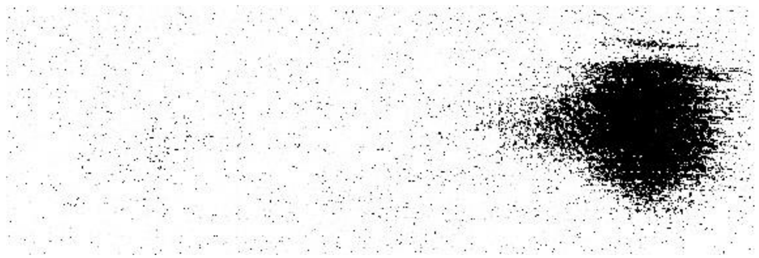	709	1403

Appendix 39: Study 4 – Cork 45

Datasheet 1

TESTING TECHNOLOGY FOR SPORT

Sand

PARTICLE SIZE DISTRIBUTION PAQXOS 5.0.4 **CHORD_MIN**, sphere(CHORD_MIN), ISO

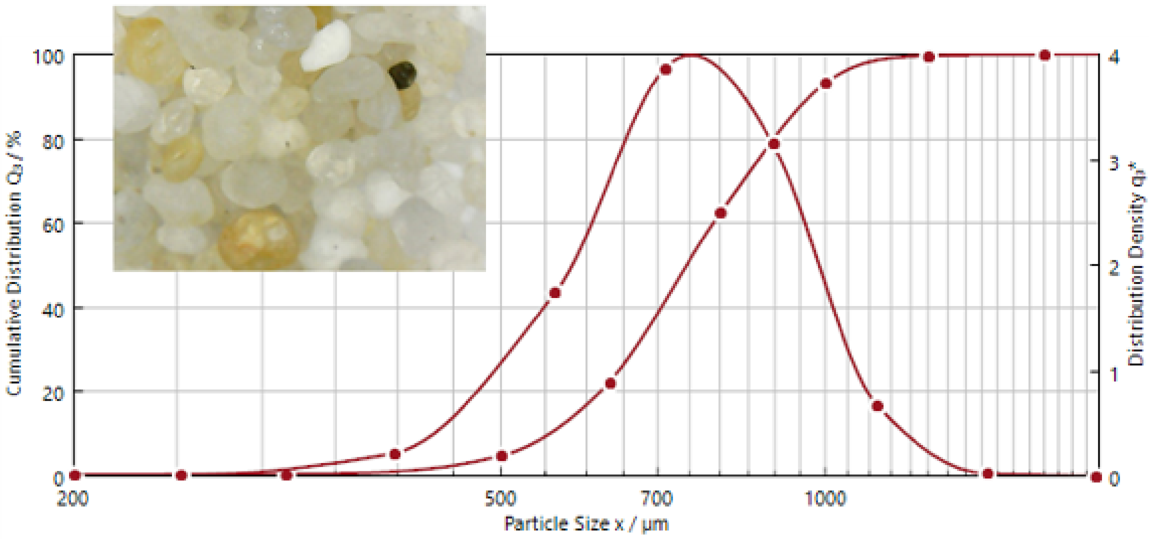

CUMULATIVE DISTRIBUTION

x_0 / µm	Q_3 / %	x_0 / µm	Q_3 / %
18.62	0.00	630.00	22.42
63.00	0.05	800.00	62.60
100.00	0.19	1000.00	93.18
150.00	0.30	1250.00	99.73
200.00	0.36	1600.00	100.00
315.00	0.53	2000.00	100.00
500.00	4.94		

13.17	0.000	561.25	1.742
34.25	0.001	709.93	3.872
79.37	0.007	894.43	3.156
122.47	0.006	1118.03	0.675
173.21	0.005	1414.21	0.025
251.00	0.008	1788.85	0.000
396.86	0.220		

Datasheet 2

EPDM

PARTICLE SIZE DISTRIBUTION PAQXOS 5.0.4 **CHORD_MIN**, sphere(CHORD_MIN), ISO

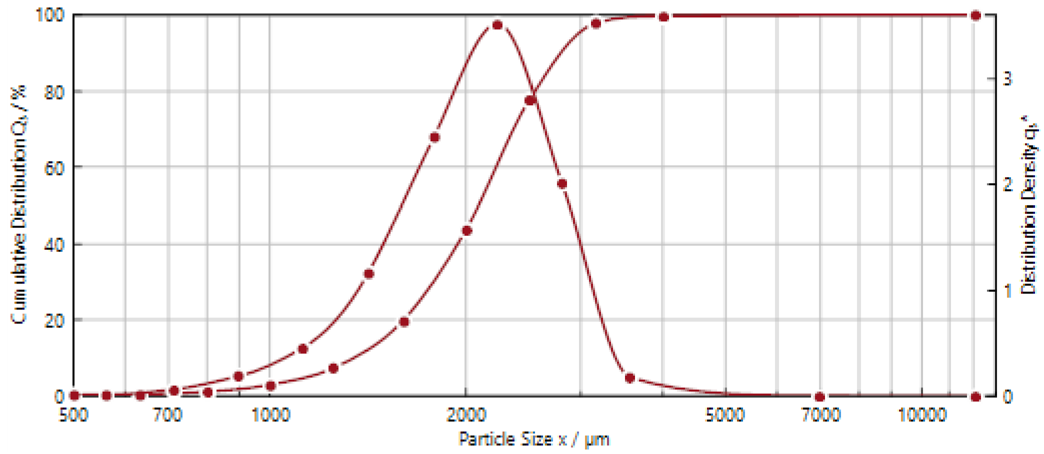

CUMULATIVE DISTRIBUTION

x_o / µm	Q_3 / %	x_o / µm	Q_3 / %				
18.62	0.01	1000.00	3.05	13.17	0.000	894.43	0.190
63.00	0.13	1250.00	7.41	34.25	0.002	1118.03	0.449
100.00	0.24	1600.00	19.82	79.37	0.005	1414.21	1.158
150.00	0.29	2000.00	43.59	122.47	0.003	1788.85	2.453
200.00	0.33	2500.00	77.67	173.21	0.003	2236.07	3.517
315.00	0.39	3150.00	97.79	251.00	0.003	2806.24	2.005
500.00	0.43	4000.00	99.69	396.86	0.002	3549.65	0.183
630.00	0.55	12057.82	100.00	561.25	0.012	6944.88	0.007
800.00	1.21			709.93	0.064		

Datasheet 3

SBR

PARTICLE SIZE DISTRIBUTION PAQXOS 5.0.4 **CHORD_MIN**, sphere(CHORD_MIN), ISO

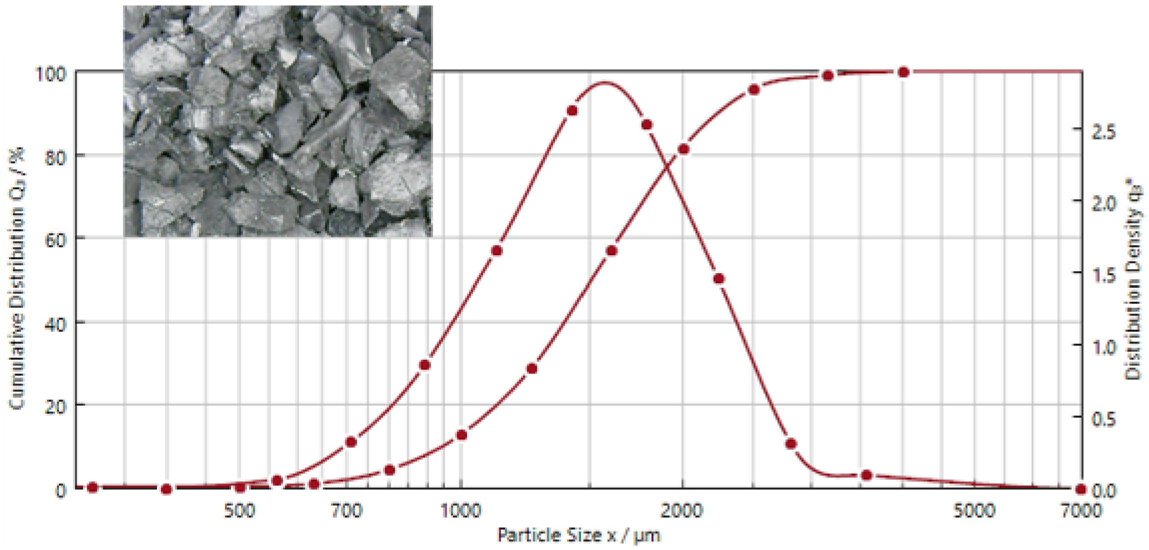

CUMULATIVE DISTRIBUTION

x_0 / µm	Q_3 / %	x_0 / µm	Q_3 / %
18.62	0.01	1000.00	12.85
63.00	0.15	1250.00	28.90
100.00	0.31	1600.00	57.11
150.00	0.36	2000.00	81.62
200.00	0.38	2500.00	95.82
315.00	0.44	3150.00	99.02
500.00	0.52	4000.00	100.00
630.00	1.15	12057.82	100.00
800.00	4.52		

13.17	0.000	894.43	0.860
34.25	0.003	1118.03	1.656
79.37	0.008	1414.21	2.631
122.47	0.003	1788.85	2.529
173.21	0.002	2236.07	1.465
251.00	0.003	2806.24	0.319
396.86	0.004	3549.65	0.094
561.25	0.062	6944.88	0.000
709.93	0.325		

Datasheet 4

TESTING TECHNOLOGY FOR SPORT

Cork

WARNING: Number dropped frames >= 5%.

PARTICLE SIZE DISTRIBUTION PAQXOS 5.0.4 **CHORD_MIN**, sphere(CHORD_MIN), ISO

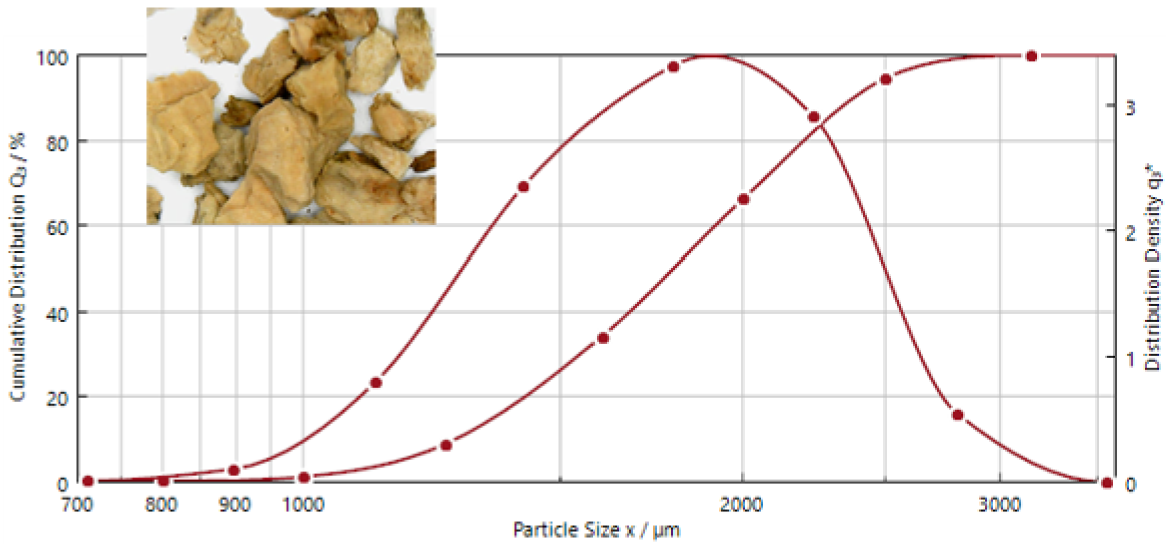

CUMULATIVE DISTRIBUTION

x_o / µm	Q_3 / %	x_o / µm	Q_3 / %				
18.62	0.00	800.00	0.26	13.17	0.000	709.93	0.009
63.00	0.04	1000.00	1.27	34.25	0.001	894.43	0.105
100.00	0.08	1250.00	8.97	79.37	0.002	1118.03	0.795
150.00	0.10	1600.00	34.21	122.47	0.002	1414.21	2.354
200.00	0.13	2000.00	66.35	173.21	0.002	1788.85	3.316
315.00	0.14	2500.00	94.54	251.00	0.001	2236.07	2.909
500.00	0.16	3150.00	100.00	396.86	0.001	2806.24	0.544
630.00	0.17	4000.00	100.00	561.25	0.001	3549.65	0.000

Datasheet 5

Study 1 – Sample 1			
Tuft pattern	Straight		
Pile yarns	Yarn A	Yarn B	**Standard Test Method**
Pile yarn profile	Propeller	Propeller	_
Pile thickness [μm]	380	380	–
Pile colour [RAL]	Turf Green 6003	Bright Green 6025	–
Pile width [mm]	1.2		–
Pile length [mm]	50		ISO 2549
No of tufts/m²	10,710		ISO1773
Pile weight [g/m²]	1,361		ISO 8543
Pile yarn characterization	PE		_
Pile yarn dtex	6,000		_
minimum tuft withdrawal force [N]	40		–
Carpet mass per unit area [g/m²]	2,161		–

Datasheet 6

Study 1 – Sample 2			
Tuft pattern	Straight		
Pile yarns	Yarn A	Yarn B	**Standard Test Method**
Pile yarn profile	Propeller	Propeller	_
Pile thickness [μm]	380	380	–
Pile colour [RAL]	Turf Green 6003	Bright Green 6025	–
Pile width [mm]	1.2		–
Pile length [mm]	60		ISO 2549
No of tufts/m²	9,842		ISO1773
Pile weight [g/m²]	1,618		ISO 8543
Pile yarn characterization	PE		_
Pile yarn dtex	6,000		_
minimum tuft withdrawal force [N]	30		–
Carpet mass per unit area [g/m²]	2,434		–

Datasheet 7

Study 1 – Sample 3			
Tuft pattern	Straight		
Pile yarns	Yarn A	Yarn B	**Standard Test Method**
Pile yarn profile	Diamond	Diamond	–
Pile thickness [μm]	360	360	–
Pile colour [RAL]	6013	6025	–
Pile width [mm]	1.1		–
Pile length [mm]	60		ISO 2549
No of tufts/m²	7,560		ISO1773
Pile weight [g/m²]	1,187		ISO 8543
Pile yarn characterization	PE		–
Pile yarn dtex	13,300 / 7		–
minimum tuft withdrawal force [N]	>40		–
Carpet mass per unit area [g/m²]	2100		–

Datasheet 8

Study 1 – Sample 4			
Tuft pattern	Straight		
Pile yarns	Yarn A	Yarn B	**Standard Test Method**
Pile yarn profile	Diamond	Diamond	_
Pile thickness [μm]	360	360	–
Pile colour [RAL]	6013	6025	–
Pile width [mm]	1.1		–
Pile length [mm]	60		ISO 2549
No of tufts/m²	9,652		ISO1773
Pile weight [g/m²]	1,187		ISO 8543
Pile yarn characterization	PE		_
Pile yarn dtex	13,300 / 7		_
minimum tuft withdrawal force [N]	>40		–
Carpet mass per unit area [g/m²]	2650		–

Datasheet 9

Study 2			
Tuft pattern	Straight		
Pile yarns	Yarn A	Yarn B	**Standard Test Method**
Pile yarn profile	Diamond	Diamond	_
Pile thickness [μm]	360	360	–
Pile colour [RAL]	6013	6025	–
Pile width [mm]	1.1		–
Pile length [mm]	60		ISO 2549
No of tufts/m²	9,852		ISO1773
Pile weight [g/m²]	1,507		ISO 8543
Pile yarn characterization	PE		_
Pile yarn dtex	13,300 / 7		_
minimum tuft withdrawal force [N]	>40		–
Carpet mass per unit area [g/m²]	2620		–

Datasheet 10

Technical Characteristics

Type	Tufted hybrid grass on Special Backing	
Pile content	100% Omega Shaped 1,7mm wide polyethylene monofilament, U.V.-resistant, 18.000/6 dtex- 430mic	
Primary backing	80% Porous, PE Special fabric containing prefabricated voids for grass roots penetration. Primary backing weight approximately 200 g/m²	
Secondary backing	PE Fusion with dissolvable woodpulp (No Latex/ No PU/No Glue) Aprox 200gr/m2	
Pile height	55 mm	+/- 5%
Total Pile Lenght	118 mm	+/- 5%
Stitch rate per 100cm (width)	Min.52 Stitches	
Stitch rate per 100cm (length)	Min. 100 Stitches	
Number of stiches/m²	5.200 Stitches	+/- 5%
Number of filaments/m²	62.400 filaments/m²	+/- 10%
Face weight	± 1.500 g/m²	+/- 10%
Weight primary backing	± 200 g/m²	+/- 10%
Total weight	± 1.700 g/m²	+/- 10%
Roll width	400 cm	+/- 10%
Roll length	As required	
Pile anchoring (Tuft Withdrawal Force)	50 N (+/- 10%)	
Water permeability	> 1.000 l/m²/min (unfilled) and > 1.000 l/m²/min at 300mm tension once filled with specified rootzone mix.	
Color fastness	grey-scale>4	

Color

Duo tone green; lime green and field green

Installation Method

Loose laid on specific rootzone mixture to HYBRIDGRASS specification, sewn seams or stripe glued

Infill (Required)

35 - 40 mm of dried rootzone mixture to HYBRIDGRASS specification approximately 60 kg per m²

Product Application

Football & Rugby Fields

Datasheet 11

Study 4 - Surface 1 & 3			
Tuft pattern		Straight	
Pile yarns		Yarn A	**Standard Test Method**
Pile yarn profile		Diamond	_
Pile thickness [μm]		365	–
Pile colour [RAL]	**1**	Field (120 40 30)	–
	2	Lime-Green (110 40 40)	
Pile width [mm]		1.05	–
Pile length [mm]		60	ISO 2549
No of tufts/m²		8820	ISO1773
Pile weight [g/m²]		1,488	ISO 8543
Pile yarn characterization		PE	_
Pile yarn dtex		13,200 / 6	–
minimum tuft withdrawal force [N]		>40	–
Carpet mass per unit area [g/m²]		2,345	–

Datasheet 12

Study 4 - Surface 2 & 4			
Tuft pattern		A-tuft	
Pile yarns		Yarn A	**Standard Test Method**
Pile yarn profile		Star	–
Pile thickness [μm]		435	–
Pile colour [RAL]	**1**	Field	–
	2	Lime-Green	
Pile width [mm]		1.25	–
Pile length [mm]		45	ISO 2549
No of tufts/m²		8850	ISO1773
Pile weight [g/m²]		1,275	ISO 8543
Pile yarn characterization		PE	_
Pile yarn dtex		14,600	–
minimum tuft withdrawal force [N]		50	–
Carpet mass per unit area [g/m²]		2,175	–